AFRL-ML-TY-TR-2004-4531

Evaluation Of Elastomeric Polymers Used For External Reinforcement Of Masonry Walls Subjected To Blast.

A Thesis
Submitted to the graduate faculty of The University of Alabama at Birmingham, in partial fulfillment of the requirements for the degree of Master of Science in Civil Engineering, Birmingham, Alabama, 2004

By

Danica Leigh Thornburg

Approved for Public Release; Distribution Unlimited

AIR FORCE RESEARCH LABORATORY
MATERIALS & MANUFACTURING DIRECTORATE
AIR BASE TECHNOLOGIES DIVISION
139 BARNES DRIVE, STE 2
TYNDALL AFB FL 32403-5323

BEST AVAILABLE COPY

20040709 018

NOTICES

USING GOVERNMENT DRAWINGS, SPECIFICATIONS, OR OTHER DATA INCLUDED IN THIS DOCUMENT FOR ANY PURPOSE OTHER THAN GOVERNMENT PROCUREMENT DOES NOT IN ANY WAY OBLIGATE THE US GOVERNMENT. THE FACT THAT THE GOVERNMENT FORMULATED OR SUPPLIED THE DRAWINGS, SPECIFICATIONS, OR OTHER DATA DOES NOT LICENSE THE HOLDER OR ANY OTHER PERSON OR CORPORATION; OR CONVEY ANY RIGHTS OR PERMISSION TO MANUFACTURE, USE, OR SELL ANY PATENTED INVENTION THAT MAY RELATE TO THEM.

THIS REPORT IS RELEASABLE TO THE NATIONAL TECHNICAL INFORMATION SERVICE
5285 PORT ROYAL RD.
SPRINGFIELD VA 22 161
TELEPHONE 703 487 4650; 703 4874639 (TDD for the hearing-impaired)
E-MAIL orders@ntis.fedworld.gov
WWW http://www.ntis.gov/index.html

AT NTIS, IT WILL BE AVAILABLE TO THE GENERAL PUBLIC, INCLUDING FOREIGN NATIONS.

THIS TECHNICAL REPORT HAS BEEN REVIEWED AND IS APPROVED FOR PUBLICATION.

/s/
Robert J. Dinan
Program Manager

/s/
Jimmy L. Pollard, Colonel, USAF
Chief, Airbase Technologies Division

Do not return copies of this report unless contractual obligations or notice on a specific document requires its return.

REPORT DOCUMENTATION PAGE

Form Approved
OMB No. 0704-0188

Public reporting burden for this collection of information is estimated to average 1 hour per response, including the time for reviewing instructions, searching existing data sources, gathering and maintaining the data needed, and completing and reviewing this collection of information. Send comments regarding this burden estimate or any other aspect of this collection of information, including suggestions for reducing this burden to Department of Defense, Washington Headquarters Services, Directorate for Information Operations and Reports (0704-0188), 1215 Jefferson Davis Highway, Suite 1204, Arlington, VA 22202-4302. Respondents should be aware that notwithstanding any other provision of law, no person shall be subject to any penalty for failing to comply with a collection of information if it does not display a currently valid OMB control number. **PLEASE DO NOT RETURN YOUR FORM TO THE ABOVE ADDRESS.**

1. REPORT DATE *(DD-MM-YYYY)*	2. REPORT TYPE	3. DATES COVERED *(From - To)*
2004	Thesis	2004 - 2004

4. TITLE AND SUBTITLE
Evaluation Of Elastomeric Polymers Used For External Reinforcement Of Masonry Walls Subjected To Blast

5a. CONTRACT NUMBER

5b. GRANT NUMBER

5c. PROGRAM ELEMENT NUMBER

6. AUTHOR(S)
Danica Leigh Thornburg

5d. PROJECT NUMBER
4915F23D

5e. TASK NUMBER

5f. WORK UNIT NUMBER

7. PERFORMING ORGANIZATION NAME(S) AND ADDRESS(ES)
University of Alabama
Birmingham, Alabama

8. PERFORMING ORGANIZATION REPORT NUMBER

9. SPONSORING / MONITORING AGENCY NAME(S) AND ADDRESS(ES)
Air Force Research Laboratory
Materials & Manufacturing Directorate
Air Base Technologies Division
139 Barnes Drive, Suite 2
Tyndall AFB FL 32403-5323

10. SPONSOR/MONITOR'S ACRONYM(S)

11. SPONSOR/MONITOR'S REPORT NUMBER(S)

12. DISTRIBUTION / AVAILABILITY STATEMENT "A"

Approved for Public Release; Distribution Unlimited

13. SUPPLEMENTARY NOTES

14. ABSTRACT

Terrorist attacks have become increasingly common and severe. The weapon of choice is the easily and cheaply made bomb. Most injuries and deaths occurring in bomb attacks are caused by flying debris due to the fragmentation of walls and windows. Many buildings in use today are comprised of unreinforced masonry walls that cannot withstand the load produced by even small explosive devices. Therefore, a critical need has arisen to strengthen walls in a timely and cost-efficient manner.

15. SUBJECT TERMS

16. SECURITY CLASSIFICATION OF: "A" Public Release – Distribution Unlimited			17. LIMITATION OF ABSTRACT	18. NUMBER OF PAGES	19a. NAME OF RESPONSIBLE PERSON
a. REPORT	b. ABSTRACT	c. THIS PAGE	Unclassified		Robert J. Dinan
					19b. TELEPHONE NUMBER *(include area code)*

AFRL-ML-TY-TR-2004-4531

EVALUATION OF ELASTOMERIC POLYMERS USED FOR EXTERNAL REINFORCEMENT OF MASONRY WALLS SUBJECTED TO BLAST

by

DANICA LEIGH THORNBURG

A THESIS

Submitted to the graduate faculty of The University of Alabama at Birmingham,
in partial fulfillment of the requirements for the degree of
Master of Science in Civil Engineering

BIRMINGHAM, ALABAMA

2004

ABSTRACT OF THESIS
GRADUATE SCHOOL, UNIVERSITY OF ALABAMA AT BIRMINGHAM

Degree M.S.C.E. Program Civil Engineering

Name of Candidate Danica Leigh Thornburg

Committee Chair James S. Davidson

Title Evaluation of Elastomeric Polymer Used for External Reinforcement of Masonry Walls Subjected to Blast

Terrorist attacks have become increasingly common and severe. The weapon of choice is the easily and cheaply made bomb. Most injuries and deaths occurring in bomb attacks are caused by flying debris due to the fragmentation of walls and windows. Many buildings in use today are comprised of unreinforced masonry walls that cannot withstand the load produced by even small explosive devices. Therefore, a critical need has arisen to strengthen walls in a timely and cost-efficient manner.

The Air Force Research Laboratory (AFRL) at Tyndall Air Force Base, Florida, conducted full-scale explosive tests to evaluate the effectiveness of an elastomeric polymer for blast reinforcement. This document summarizes the results of seven full-scale explosive tests that demonstrated that a thin coating of a low stiffness, high elongation polymer can be effective in reducing wall deflection and fracture of unreinforced non-load-bearing masonry walls.

The success of the explosive tests implies an opportunity for other advanced materials to be designed and optimized for blast reinforcement purposes. Uniaxial tension test results on 53 blast reinforcement candidate polymeric and composite materials that were submitted to the AFRL are summarized. These tests illustrate the

wide range of static mechanical properties that can be designed into a blast reinforcement concept.

The enormous expense of explosive tests prohibits the evaluation of a broad survey of blast reinforcement candidate materials using full-scale methodology. Therefore, structural evaluation equipment, a gas gun facility, and a drop tower facility at the University of Alabama at Birmingham were the non-explosive methods used to evaluate the potential of a material for blast reinforcement purposes. The laboratory tests included a static flexural test, a drop tower puncture test, and a gas gun test. The static flexural test identified bond failure mechanisms between the polymer and concrete substrate, as well as the tension capacity of candidate materials. The drop tower puncture test and gas gun test revealed the energy absorption capacity and failure mechanism in dynamic shear of candidate materials. The effectiveness of these tests and recommendations for laboratory evaluation of candidate blast reinforcement materials is summarized.

ACKNOWLEDGMENTS

I wish to thank the entire team at the Air Force Research Laboratory at Tyndall Air Force Base, Florida, for the opportunity to participate in this project. I wish to thank Drs. James S. Davidson, my committee chair, and Jon Porter, Uday Vaidya, and Fouad Fouad, for serving on my thesis research committee.

I thank Dr. Vaidya specifically for the use of his lab and equipment. Thanks also to Shane Bartus for help with the gas gun, Tim Hartness for expert advice, and Dan Connell for help in preparing this document.

TABLE OF CONTENTS

Page

ABSTRACT ii

ACKNOWLEDGMENTS iv

LIST OF TABLES viii

LIST OF FIGURES x

LIST OF ABBREVIATIONS xxiii

CHAPTER

1 INTRODUCTION 1

1.1 Objectives 3
1.2 Scope/Methodology 3
1.3 Thesis Organization 3

2 LITERATURE REVIEW 5

2.1 Recent Terrorist Attacks 5
2.2 Retrofit Testing 11

3 EXPLOSIVE TESTS 17

3.1 Introduction 17
3.2 Wall Test 1 18
3.2.1 Construction 18
3.2.2 Instrumentation 26
3.2.3 Results 30
3.3 Wall Test 2 42
3.3.1 Construction 43
3.3.2 Instrumentation 49
3.3.3 Results 54
3.4 Wall Test 3 64
3.4.1 Construction 65
3.4.2 Instrumentation 72

TABLE OF CONTENTS (Continued)

Page

CHAPTER

3.4.3 Results....76
3.5 Wall Test 9....89
3.5.1 Construction....89
3.5.2 Instrumentation....97
3.5.3 Results....100
3.6 Wall Test 10....109
3.6.1 Construction....109
3.6.2 Instrumentation....115
3.6.3 Results....117
3.7 Wall Test 11....127
3.7.1 Construction....129
3.7.2 Instrumentation....141
3.7.3 Results....147
3.8 Wall Test 12....158
3.8.1 Construction....160
3.8.2 Instrumentation....167
3.8.3 Results....171
3.9 Explosive Testing Summary Analysis and Conclusions....180
3.9.1 Wall Test 1....186
3.9.2 Wall Test 2....186
3.9.3 Wall Test 3....187
3.9.4 Wall Test 9....188
3.9.5 Wall Test 10....189
3.9.6 Wall Test 11....189
3.9.7 Wall Test 12....190

4 LABORATORY TESTING....191

4.1 Introduction....191
4.2 Static Flexural Test....192
4.2.1 Material Selection....192
4.2.2 Preparation of Blocks....193
4.2.3 Application of Material....194
4.2.4 Introduction....204
4.2.5 Test Methodology....204
4.2.6 Results....209
4.2.7 Conclusions....214
4.3 Drop Tower Impact Test....214
4.3.1 Introduction....214
4.3.2 Test Methodology....215

TABLE OF CONTENTS (Continued)

Page

CHAPTER

4.3.3 Results 223
4.3.4 Conclusions 230
4.4 Gas Gun Tests 231
4.4.1 Introduction 231
4.4.2 Gas Gun Test 1 Methodology 232
4.4.3 Gas Gun Test 1 Results 241
4.4.4 Gas Gun Test 2 Methodology 242
4.4.5 Gas Gun Test 2 Results 250
4.4.6 Conclusions 250
4.5 MTS Tensile Test 251
4.5.1 Introduction 251
4.5.2 Test Methodology 251
4.5.3 Results 254
4.5.4 Conclusions 254
4.6 Exploratory Testing Conclusions 256

5 CONCLUSIONS 260

5.1 Summary and Conclusions 260
5.2 Recommendations and Suggested Research 262

LIST OF REFERENCES 264

APPENDIX: UNIAXIAL TENSION TEST MATERIAL DATA 267

LIST OF TABLES

Table		*Page*
1	Test 1, Gauge Predictions	31
2	Test 1, Predicted vs. Recorded Data	39
3	Test 2, Gauge Predictions	55
4	Test 2, Predicted vs. Recorded Data	59
5	Test 3, Gauge Predictions	77
6	Test 3, Predicted vs. Recorded Data	82
7	Test 9, Gauge Predictions	100
8	Test 9, Predicted vs. Recorded Data	104
9	Test 10, Gauge Predictions	117
10	Test 10, Predicted vs. Recorded Data	121
11	Test 11, Gauge Predictions	148
12	Test 11, Predicted vs. Recorded Data	155
13	Test 12, Gauge Predictions	171
14	Test 12, Predicted vs. Recorded Data	175
15	Typical Properties of Primer	195
16	Pot Life of Primer	196
17	Applicable Conditions of Primer	196
18	Cure Time of Primer	196
19	Typical Properties of Geothane 520	200

LIST OF TABLES (Continued)

Table		*Page*
20	Specification Data of Geothane 520	200
21	Pot Life of Geothane 520	200
22	Application Conditions of Geothane 520	201
23	Cure Time of Geothane 520	201
24	Elastomeric Polymer	210
25	Polypropylene/Polypropylene Woven Material	211
26	Polyester Thermoplastic Polyurethane	211
27	Drop Tower Impact Test, Sample Thickness Measurements	217
28	Drop Tower Impact Test, Polymer 1 Data	224
29	Drop Tower Impact Test, Polymer 3 Data	225
30	Drop Tower Impact Test, Polymer 4 Data	226
31	Drop Tower Impact Test, Polymer 5 Data	227
32	Drop Tower Impact Test, Polypropylene 1 Data	228
33	Drop Tower Impact Test, Polypropylene 2 Data	229
34	Drop Tower Impact Test, Data Summary	230
35	Gas Gun Test 1 Specimens	234
36	Gas Gun Test 1 Results	241
37	Gas Gun Test 2, Notch Data	242
38	Gas Gun Test 2 Results	250
39	Uniaxial Tension Test, Material Averages	258

LIST OF FIGURES

Figure		*Page*
1	Test 1 Layout	19
2	Reaction Structure Construction	19
3	Reaction Structure, Roofing and Cladding	20
4	Reaction Structure, Center I-Beam	21
5	Reaction Structure, Center I-Beam Installed	21
6	Reaction Structure, Foam Insulation Board	22
7	Test 1, CMU Construction	23
8	Test 1, Angle Irons and Steel Cladding	24
9	Test 1, Constructed Walls	25
10	Test 1, Blast Door	25
11	Test 1, Gauge Locations	26
12	Test 1, Gauge Details	27
13	Test 1, Reflected Pressure Gauges	28
14	Test 1, Deflection Gauge	28
15	Test 1, Interior Camera Target Areas	29
16	Test 1, Low Speed Camera	30
17	Test 1, High Speed Cameras	30
18	Test 1, Gauge R1	33
19	Test 1, Gauge R2	33

LIST OF FIGURES (Continued)

Figure		*Page*
20	Test 1, Gauge R3	34
21	Test 1, Gauge F1	34
22	Test 1, Gauge F2	35
23	Test 1, Gauge L1	35
24	Test 1, Gauge L2	36
25	Test 1, Acceleration and Velocity (A1)	36
26	Test 1, Acceleration and Displacement (A1)	37
27	Test 1, Acceleration and Velocity (A2)	37
28	Test 1, Velocity and Displacement (A2)	38
29	Test 1, Acceleration and Velocity (A3)	38
30	Test 1, Acceleration and Displacement (A3)	39
31	Test 1, Post Test Reaction Structure	40
32	Test 1, Defacing of Retrofit Wall	40
33	Test 1, Collapsed Control Wall	41
34	Test 1, Mid-Height Failure, Control Wall (High Speed Image)	41
35	Test 1, Mortar Failure and Defacing	42
36	Test 2 Layout	43
37	Test 2, Top Cladding Modifications	45
38	Test 2, Foam Insulation Board	46
39	Test 2, Wall Panel Construction	47
40	Test 2, Angle, Cladding, and Polymer Locations	48

LIST OF FIGURES (Continued)

Figure		*Page*
41	Test 2, Roof Cladding and Angle Iron	48
42	Test 2, Gauge Locations	49
43	Test 2, Gauge Details	50
44	Test 2, Reflected Pressure Gauges	51
45	Test 2, Laser Gauge L1	51
46	Test 2, Laser Deflection Gauge L2	52
47	Test 2, Interior Camera Target Locations	53
48	Test 2, Cameras	53
49	Test 2, Lighting Fixtures	54
50	Test 2, Gauge R1	56
51	Test 2, Gauge R2	56
52	Test 2, Gauge R3	57
53	Test 2, Gauge R4	57
54	Test 2, Gauge F1	58
55	Test 2, Gauge F2	58
56	Test 2, Post-test Structure	60
57	Test 2, Bent I-Beam	61
58	Test 2, Unretrofitted Wall Debris	61
59	Test 2, Retrofitted Wall Debris	62
60	Test 2, Bending of Retrofit Wall	62
61	Test 2, Post-test Retrofit Material	63

LIST OF FIGURES (Continued)

Figure		*Page*
62	Test 3 Layout	64
63	Test 3, Constructed Test Structure	66
64	Test 3, Individual Cubicles	66
65	Test 3, Center Divider	67
66	Test 3, Roof Connection Modifications	68
67	Test 3, Roof Connection Modifications Installed	69
68	Test 3, Roof Cladding	69
69	Test 3, Roof Connections	70
70	Test 3, Polymer Application	71
71	Test 3, Walls A and B, Ready for Testing	71
72	Test 3, Wall B Floor Overlap	72
73	Test 3, Gauge Locations	73
74	Test 3, Gauge Details	74
75	Test 3, Scratch Gauge	75
76	Test 3, Interior Camera Target Areas	76
77	Test 3, Gauge R1	79
78	Test 3, Gauge R2	79
79	Test 3, Gauge R3	80
80	Test 3, Gauge R4	80
81	Test 3, Gauge R5	81
82	Test 3, Gauge F1	81

LIST OF FIGURES (Continued)

Figure		*Page*
83	Test 3, Walls A and B, Damage	83
84	Test 3, Walls A and B, Top Exterior	83
85	Test 3, Wall A, Left Bottom Interior	84
86	Test 3, Wall A, Left Top Interior	85
87	Test 3, Wall B, Right Interior	85
88	Test 3, Wall B, Close Up	86
89	Test 3, Walls C and D	86
90	Test 3, Wall C	87
91	Test 3, Mid Wall C	87
92	Test 3, Wall D	88
93	Test 3, Wall D Bottom	88
94	Test 9 Layout	90
95	Test 9, Steel Divider	91
96	Test 9, Door Installation	92
97	Test 9, New Angle Locations	93
98	Test 9, Newly Installed Angle	94
99	Test 9, Wall with Door	94
100	Test 9, Wall with Window	95
101	Test 9, Paper Wrapping	95
102	Test 9, Coating Process	96
103	Test 9, Wall with Door Completed	96

LIST OF FIGURES (Continued)

Figure		*Page*
104	Test 9, Wall with Window Completed	97
105	Test 9, Gauge Locations	98
106	Test 9, Interior Camera Target Areas	99
107	Test 9, Lighting System	99
108	Test 9, Gauge R1	101
109	Test 9, Gauge R2	101
110	Test 9, Gauge R3	102
111	Test 9, Gauge F1	102
112	Test 9, Gauge I1	103
113	Test 9, Gauge D1	103
114	Test 9, Posttest Door	105
115	Test 9, Posttest Window	106
116	Test 9, Top Left Wall Defacing	107
117	Test 9, Bottom Left Wall Defacing	108
118	Test 9, Right Wall Cracks	108
119	Test 10 Layout	111
120	Test 10, Interior and Exterior Door	112
121	Test 10, Ceiling Overlap	113
122	Test 10, Floor Overlap	113
123	Test 10, Constructed Wall	114
124	Test 10, Test Cubicle	114

LIST OF FIGURES (Continued)

Figure *Page*

125 Test 10, Gauge Locations 115

126 Test 10, Interior Camera Target Areas 116

127 Test 10, Gauge R1....118

128 Test 10, Gauge R2....118

129 Test 10, Gauge F1....119

130 Test 10, Gauge I1....119

131 Test 10, Gauge D1....120

132 Test 10, Gauge D2....120

133 Test 10, Posttest Test Cubicle....122

134 Test 10, Posttest Test Structure....123

135 Test 10, Shear Cracks, Left Side....124

136 Test 10, Left Side Interior Tear....124

137 Test 10, Protruded Block, Left Side....125

138 Test 10, Shear Cracks, Right Side....125

139 Test 10, Right Side Interior Tear....126

140 Test 10, Steel Door, Post Test....126

141 Test 11 Layout....128

142 Test 11, Window Cross-Section....130

143 Test 11, Complete Window....131

144 Test 11, Blocks Beneath Window....132

145 Test 11, Wooden Stand-in Frame....133

LIST OF FIGURES (Continued)

Figure *Page*

146 Test 11, Empty Lintel Blocks 133

147 Test 11, Lintel Blocks with Rebar 134

148 Test 11, Complete Lintels 134

149 Test 11, Completing the Construction 135

150 Test 11, Completed Wall 135

151 Test 11, Window Installation Plan 137

152 Test 11, Window Adhesive 138

153 Test 11, Overpressure Escape Holes 138

154 Test 11, Installed Window 139

155 Test 11, Complete Structure 140

156 Test 11, Retrofitted Window Frame 140

157 Test 11, Gauge Locations 141

158 Test 11, Reflected Pressure Gauges 142

159 Test 11, Pressure Gauges, Windows 143

160 Test 11, Interior Pressure Gauge 144

161 Test 11, Left Deflection Gauge, Laser 145

162 Test 11, Right Deflection Gauge (Gear and Yo-Yo) 145

163 Test 11, Interior Camera Target Areas 146

164 Test 11, Lighting 147

165 Test 11, Gauge R1 149

166 Test 11, Gauge R2 149

LIST OF FIGURES (Continued)

Figure		*Page*
167	Test 11, Gauge WIS (Window)	150
168	Test 11, Gauge WIB (Window)	150
169	Test 11, Gauge WVS (Window)	151
170	Test 11, Gauge WVB (Window)	151
171	Test 11, Gauge F1	152
172	Test 11, Gauge I1	152
173	Test 11, Gauge D1	153
174	Test 11, Gauge D2	153
175	Test 11, Test Structure, Posttest	156
176	Test 11, Front Defacing	156
177	Test 11, Right Side Rips	156
178	Test 11, Left Side Deflection	157
179	Test 11, Posttest Window	158
180	Test 12 Layout	159
181	Test 12, Right Wall, Bottom Course Leveling	160
182	Test 12, Right Wall, Top Course Leveling	161
183	Test 12, Left Wall, Top Course Leveling	161
184	Test 12, Left Wall Inside, Plastic Covering	162
185	Test 12, Drawing Details	163
186	Test 12, Fiberglass Scrim Fabric	164
187	Test 12, Wall A with Retrofit	165

LIST OF FIGURES (Continued)

Figure		*Page*
188	Test 12, Wall B with Retrofit	166
189	Test 12, Completed Structure	167
190	Test 12, Gauge Locations	168
191	Test 12, Deflection Gauge	169
192	Test 12, Interior Camera Target Areas	170
193	Test 12, Gauge R1	172
194	Test 12, Gauge R2	172
195	Test 12, Gauge R3	173
196	Test 12, Gauge F1	173
197	Test 12, Gauge D1	174
198	Test 12, Gauge D2	174
199	Test 12, Posttest Structure	176
200	Test 12, Left Wall, Posttest	176
201	Test 12, Right Wall, Top	177
202	Test 12, Right Wall, Bottom	178
203	Test 12, Right Wall, Bubbles and Right Tear	179
204	Test 12, Right Wall, Left Tear	180
205	Test 12, Right Wall, Both Tears	180
206	Concrete Saw	193
207	Notched Pavers	193
208	Priming Mixture and Clayed Blocks	197

LIST OF FIGURES (Continued)

Figure		*Page*
209	Priming Process	198
210	Primed Blocks	198
211	Geothane Mixing Process	202
212	Coating Process	203
213	Coated Blocks	203
214	General Test Setup	204
215	Geothane Test Setup	205
216	Elastomeric Polymer, Before Failure	206
217	Elastomeric Polymer after Tearing	207
218	Polyester Thermoplastic Polyurethane	208
219	Load-Deflection Curve	212
220	Normalized Load-Deflection Curve	213
221	Drop Tower Machine	216
222	Drop Tower Impact Test, Thickness Measurement Locations	216
223	Drop Tower Impact Test, Polymer Samples	217
224	Drop Tower Supports	218
225	Drop Tower Impact Test, Polymer 1	218
226	Drop Tower Impact Test, Polymer 2	219
227	Drop Tower Impact Test, Polymer 3	219
228	Drop Tower Impact Test, Polymer 4, Open	220
229	Drop Tower Impact Test, Polymer 4, Closed	220

LIST OF FIGURES (Continued)

Figure		*Page*
230	Drop Tower Impact Test, Polymer 4 Bottom View	221
231	Drop Tower Impact Test, Polymer 5 Top View	221
232	Drop Tower Impact Test, Polymer 5 Side View	222
233	Drop Tower Impact Test, Polypropylene Samples Top View	222
234	Drop Tower Impact Test, Polypropylene Samples Side View	223
235	Drop Tower Impact Test, Polypropylene Samples Bottom View	223
236	Drop Tower Impact Test, Polymer 1 Graph	224
237	Drop Tower Impact Test, Polymer 3 Graph	225
238	Drop Tower Impact Test, Polymer 4 Graph	226
239	Drop Tower Impact Test, Polymer 5 Graph	227
240	Drop Tower Impact Test, Polypropylene 1 Graph	228
241	Drop Tower Impact Test, Polypropylene 2 Graph	229
242	Gas Gun, Gas Chamber	231
243	Gas Gun	232
244	Gas Gun Test 1, Thickness Measurement Locations	233
245	Gas Gun Test 1 Setup Specimen	234
246	Gas Gun Test 1, Specimen One	235
247	Gas Gun Test 1, Specimen Two	235
248	Gas Gun Test 1, Specimen Three	236
249	Gas Gun Test 1, Specimen Four Top View	236
250	Gas Gun Test 1, Specimen Four Side View	237

LIST OF FIGURES (Continued)

Figure		*Page*
251	Gas Gun Test 1, Specimen Five	237
252	Gas Gun Test 1, Specimen Six Top View	238
253	Gas Gun Test 1, Specimen Six Bottom View	238
254	Gas Gun Test 1, Specimen Seven Top View	239
255	Gas Gun Test 1, Specimen Seven Left Side View	239
256	Gas Gun Test 1, Specimen Seven Right Side View	240
257	Gas Gun Test 2, Notched Block	243
258	Gas Gun Test 2, Standing Block	243
259	Gas Gun Test 2, Sample 1 Side View	244
260	Gas Gun Test 2, Sample 1	245
261	Gas Gun Test 2, Sample 2	246
262	Gas Gun Test 2, Sample 2 Side View	246
263	Gas Gun Test 2, Sample 2	246
264	Gas Gun Test 2, Sample 3	247
265	Gas Gun Test 2, Sample 4	248
266	Gas Gun Test 2, Sample 5 Setup	249
267	Gas Gun Test 2, Sample 5	249

LIST OF ABBREVIATIONS

AFB	Air Force Base
AFRL	Air Force Research Laboratory
CFRP	Carbon Fiber Reinforced Plastic
CMU	Concrete Masonry Unit
CONWEP	Conventional Weapon Effect
MTS	Mechanical Testing and Simulation
TCCMAR	Technical Coordinating Committee for Masonry Research
UHMWPE	Ultra High Molecular Weight Polyethylene
URM	Unreinforced Masonry
WAC	Wall Analysis Code
WTC	World Trade Center

CHAPTER 1

INTRODUCTION

The world we live in has become a violent place. Terrorist attacks happen somewhere in the world nearly every day. These attacks occur for different reasons, but often they are carried out by political and religious extremists. Complicating matters more is a new class of terrorists that deem it an honor to die in the blast. This makes preventing bomb attacks extremely difficult.

Bombs are cheaply and easily made. They can be placed in small places and are often undetected. They can be equipped with timers or triggered by cell phones, allowing the bomber to be miles from the scene at detonation. It is unlikely that all terrorist acts will ever be stopped, so something more must be done to protect the civilian population.

Although there is some loss of life from fire, smoke inhalation, and direct pressure from the bomb, victims in a blast are usually killed by secondary fragmentation. Secondary fragmentation occurs when the blast shatters walls and other components of a structure. These fragments are often massive. They become airborne, and people in their path may be killed or severely injured.

Many structures in use today are constructed from concrete masonry units (CMUs). Prior to 1970, these types of structures were rarely reinforced. CMU walls are unable to withstand effects from a blast load and collapse within only milliseconds of the occurrence of the blast. Since demolishing and rebuilding all unreinforced masonry

structures is not an option, buildings can be made safer through a technique called retrofitting.

Retrofitting is the process of using materials to strengthen existing structures. Adding mass can reduce the blast vulnerability of many types of structures; however, the addition of mass is often not an option for practical reasons such as cost, space limitations, and weight limitations on the structural frame. Therefore, the Air Force Research Laboratory (AFRL) has begun seeking alternative materials. A lightweight, relatively inexpensive, and easily applied polymer has been investigated. This polymer has been applied to unreinforced CMU walls and subjected to blast in full-scale wall tests.

The wall tests that have been performed have been valuable in understanding the effectiveness of the polymer reinforcement. High-speed cameras have been used to catch the response of the walls. Thus far, the polymer has been very effective in reducing wall deflections, preventing collapse, and preventing debris from entering the structure.

As the mission of the AFRL has become more widely known, material manufacturers throughout the United States have submitted polymer and composite materials to be considered for blast reinforcement purposes. However, wall tests are extremely expensive and time consuming. In fact, only a small number of them can be completed in a year. For this reason, a need has arisen for non-explosive laboratory methodology that can evaluate the potential of a material for blast reinforcement purposes. These tests could promote or eliminate material candidates with little time, money, and effort. Since retrofitting has been proven to work, finding appropriate materials is the next step in the process.

1.1 Objectives

The overall objectives of this project were to evaluate the effectiveness of an elastomeric polymer for reducing deflection and fragmentation of unreinforced masonry walls subjected to blast and to investigate laboratory methods that can be used to predict the potential effectiveness of a blast reinforcement candidate.

1.2 Scope/Methodology

Explosive tests were planned and conducted by AFRL engineers at Tyndall Air Force Base (AFB), Florida. The walls in each explosive test were equipped with gauges to provide data on pressure, acceleration, and deflection. Each test was wired with digital still and high-speed photography. The results from each test were thoroughly analyzed and are summarized in this report.

Several exploratory laboratory tests were conducted to investigate tests that may aid in material selection. A static flexural test, a drop tower puncture test, and a gas gun test were performed. In addition, this report summarizes uniaxial tension tests performed at Tyndall AFB on over 50 materials submitted to AFRL as blast reinforcement materials.

1.3 Thesis Organization

This thesis is organized into five chapters. Chapter 1 is an introductory chapter that identifies the objectives, scope, methodology, and organization of the document. Chapter 2 provides a literature review that covers recent bombings, the need for retrofit, reinforcement techniques, and other wall reinforcement research. Chapter 3 presents the review of seven full-scale explosive tests performed by the AFRL at Tyndall AFB. This

chapter provides a parallel layout that includes construction methods, results, and conclusions. Chapter 4 contains a summary of a trial material tested in the laboratory and the investigation of three laboratory test approaches that may be used to evaluate the effectiveness of a material for the blast reinforcement purpose. Also in this chapter is a discussion on a uniaxial tension test of 53 materials submitted to the AFRL. Material recommendations are made based on results of the test. Chapter 5 provides a summary of the testing program, laboratory tests, and material selection. Recommendations for further research are also made. Finally, the appendix includes the data from the uniaxial tension test.

CHAPTER 2

LITERATURE REVIEW

2.1 Recent Terrorist Attacks

Terrorist threats are becoming more common and more severe. Terrorism, however, is not a new phenomenon. Over the past years, there have been many structures destroyed by blast. In each of these, innocent people have lost their lives. These cowardly acts bring much attention to the design of buildings, and safer construction approaches are being sought. However, before one can begin to find a solution to the problem, one must understand it. Studying the recent bombings can give us insights as to which parts of buildings need to be improved or changed. A brief history of bombings directed toward the United States in the last decade follows.

On February 26, 1993, Islamic extremist groups bombed the World Trade Center (WTC) in New York City. The blast was detonated on the second floor of the WTC basement. The result was a crater approximately 150 ft in diameter and five stories deep (Williams 1998).

According to officials, the materials used in the terrorist act were collected for two months prior to the event (Terrorism 2004). Using a large van, the bombers drove the 1500-lb urea-nitrate bomb into the basement of the world trade center (Terrorism 2004). They set the timer and fled the scene. Upon exploding, the bomb killed six people and injured over 1,000 others. The blast caused $600 million in property damage (Wilkens 2000).

On April 19, 1995, a "home-grown terrorist" parked a rented truck loaded with explosives outside the Alfred P. Murrah Government Building (Terrorism 2004). Two minutes later, the bomb exploded, collapsing the north face of the nine-story concrete building. The blast killed 168 people and injured over 500 more (Oklahoma 1996). At the time of the bombing, it was the worst terrorist attack on U.S. soil.

The bomb used in this attack caused severe wall failure on the front side of the building that faced the blast and partial collapse of the building. Could the front wall failure have been prevented, many lives could have been saved. Mild wall failure occurred on the sides of the building, but no fragments entered the structure. This side defacing occurred mainly at the bottom of the structure, and is similar to results from wall tests that are presented in Chapter 3. There was no fragmentation of the back of the building (opposite the blast).

On the evening of June 25, 1996, Saudi Arabian Hezbollah members parked a tanker truck near the Khobar Tower apartment buildings. Security personnel realized there was a bomb threat and began evacuations. The bomb exploded before the building was fully evacuated, killing 19 servicemen and wounding hundreds of others (Terrorism 2004).

The Khobar Towers sustained full front wall failure. The building frame, however, did not fail, and the building remained intact. Front wall failure of this structure exposed the occupants. Once defacing occurs, occupants are not protected. Results are often as detrimental as total collapse.

A network of terrorists coordinated an attack on two U.S. embassies, Kenya and Tanzania, on August 7, 1998. A refrigeration truck housing a bomb was parked outside

of the embassy located in Tanzania. Upon exploding, the bomb killed 11 people and injured 86 others, none of whom were Americans (Terrorism 2004). The Kenyan bombing killed 247 people and injured over 5000 (McLaughlin 1998). Of those killed, 12 were Americans (Terrorism 2004). Again in these attacks, severe front wall failure caused most of the casualties. There was collapse of a small structure adjacent to the Kenyan embassy (McLaughlin 1998).

At the Port of Aden in Yemen on October 12, 2000, a small craft boarded by two suicide bombers pulled alongside the U.S.S. Cole and detonated a bomb while the ship was refueling offshore, leaving a 40-ft hole in the side of the ship. The attack killed 17 sailors and wounded 39 more (Attack 2004).

On September 11, 2001, a network of terrorists hijacked four commercial jet planes and attempted to fly them into various U.S. targets. One of the planes crashed into Tower One of the World Trade Center in New York City. Another plane crashed into Tower Two several minutes later. A third plane crashed into the Pentagon in Washington, D.C. Finally, a fourth plane crashed in a field in Pennsylvania. The two World Trade towers both collapsed, killing nearly 3,000 people. Other people were killed in the Pentagon (189 total) and on United Airlines Flight 93 that crashed in the Pennsylvania field (Terrorism 2004).

Failure patterns for these bombings were much more severe than front wall failure. In the attacks, jet planes actually entered the buildings, which destroyed major structural components. Also, fire resulted from the jet fuel. The combination led to the collapse of both of the World Trade Towers. The damage done to the Pentagon was confined to the area in which the plane crashed.

Bomb attacks such as those described above have become a mark of modern times, not only in the United States, but all around the world. Bombing has long been the most common weapon used by terrorists. Bombings account for nearly half of all terrorist attacks worldwide (Committee 1995). In the United States, however, bombings are even more common. The Federal Bureau of Investigation reports that between 1982 and 1992, 77.5% of terrorist attacks in America were in the form of bombs. Of those, 36% targeted commercial buildings, 20% targeted military personnel and facilities, 19% targeted government office buildings/property, 11% targeted private residences, 10% targeted diplomatic establishments, and 4% targeted educational facilities (Committee 1995).

Bombs are easily made, yet the results are dramatic and deadly. Materials used to make bombs are readily available and easily obtained. Once made, planting of the device is easy and, except in the case of a suicide bomber, often risk-free, as the bomber can easily be miles away from the bomb when it explodes. Building a device is not only easy, but also cheap. The bomb that struck the World Trade Center in 1993 cost less than $400 to make (Committee 1995). Simple homemade devices fabricated by amateurs can be just as deadly as sophisticated weapons made by those with extensive knowledge and experience.

"A bomb explosion within or immediately nearby a building can have catastrophic effects, destroying or severely damaging portions of the building's external and internal structural framework, collapsing walls, blowing out large expanses of windows, and shutting down critical fire- and life-safety systems, such as fire detection and suppression, ventilation, light, water, sewage, and power" (Committee 1995).

Personal injuries and loss of life can occur from different things in an explosive blast. They can occur from blast pressure, collapse of structural members, fire, smoke inhalation, and various other causes. Although many deaths are caused by smoke inhalation, the primary cause of death in an explosion is flying debris.

The events that have unfolded over the past decade have generated concern over the ability of the United States to protect structures and their occupants from the bombings and other direct physical attacks (Committee 1995). Ensuring structural integrity from explosive blasts is an important issue. Concerns arose in the days of World War II, continued through the Cold War, and are at an all-time high due to worldwide threats of terrorism.

There are three methods to minimize deaths from explosives. The first of these is to increase the difficulty of placing a bomb close enough to a structure to damage it. Another method is to strengthen the structure so that the effects of the blast are minimized. A final approach is to take measures to ensure the survival and rescue of building occupants present during an explosive blast (Committee 1995).

In the history of structures, masonry has been widely used. There are some properties of masonry that are important to understand. Masonry, like concrete, has a low resistance to tension. Reinforcement is often used to offset the effects of tensile forces. Masonry structures are also subject to time-dependent dimensional variations that are (MacGregor and Luse 1978). Creep, shrinkage, and swelling due to rehydration of masonry units are a few worth noting. Furthermore, quality of a well-built masonry wall varies with the level of workmanship and quality control.

Codes require consideration of dead loads, live loads, earthquake forces, wind forces, and other forces, which usually include those due to shrinkage, creep, and temperature. However, codes used for common structures do not require consideration of blast loads. Some federal government buildings are required to be designed for blast loads, but commercial buildings usually are not. They are usually designed for earthquake loads, which in some ways are similar to blast loads.

When a structure moves during an earthquake, an inertial force is imposed on a unit volume of material. The magnitude of the force equals the mass of the material multiplied by its acceleration. If a structure had no mass, it would have no forces acting on it during an earthquake (Englekirk and Hart 1982). The more mass a structure has the more severe the earthquake loads will be. The motion in the ground during an earthquake is not regular. Therefore, inertial forces on masonry walls are also irregular. Like blast loads, but not to the same magnitude, earthquakes occur quickly, making it difficult for engineers to understand all of the combined affects that cause damage or failure.

In-plane loading is generally predictable to masonry walls, and the walls usually perform quite adequately for this particular type of load. However, retrofitting is often used to account for weaknesses in out-of-plane loading. Earthquakes are just one type of this loading. Wind loads are another, but are not usually as severe, due in part to the fast accelerations involved in earthquakes. Blast loading is yet another type of out-of-plane loading. It is severe because of the accelerations involved. Blast loads occur in only milliseconds. Unlike earthquake loads, the ground does not move during blast loads. Still, blast loads can be extremely deadly.

The structural components that transfer loads to the ground in an earthquake may be much the same as in a blast load. Some of those components are floor diaphragms, frames, and shear walls. Since the ground moves during an earthquake, each mass of the structure experiences acceleration. An earthquake force is developed on the roof due to its mass multiplied by its acceleration (Englekirk and Hart 1982). This force must be transmitted down the structure by the lateral-force-resisting elements between the floors. When these forces reach the floor, they must be added to any additional forces and the total must be transferred through the shear walls to the ground level. The foundation transmits the forces to the ground (Englekirk and Hart 1982).

Masonry walls are not designed to withstand large lateral forces. Masonry walls can be designed in one of two ways: load bearing or non-load bearing. Load bearing walls are generally designed to transmit compressive forces. Non-load-bearing walls define structural space, comparable to sheetrock.

There are two types of masonry walls: unreinforced and reinforced. Reinforced masonry walls react better to tensile forces. However, many of the older buildings were designed with unreinforced construction. For this reason, retrofitting has been a practice that has gained much attention. It is not practical to reconstruct old buildings. It is, however, practical to retrofit these buildings to make them stronger and, as a result, safer.

2.2 Retrofit Testing

It has been estimated that about 90% of masonry buildings worldwide are made of brick without steel reinforcement (Clark 1997). Most masonry and reinforced concrete buildings built in the United States prior to 1970 are not properly reinforced. These

buildings are very brittle. To help make the buildings safer in areas where lateral loads could be significant, such as seismic areas, these buildings are retrofitted.

Retrofitting is a relatively cheap and easy way of protecting buildings from damage or total destruction. The process is similar to wallpapering a wall. A fabric woven from fine fibers of composite materials is saturated with an epoxy adhesive and is applied to walls, creating reinforcement as strong as six inches of reinforced concrete (Clark 1997).

Carbon overlays have been investigated as a repair and retrofit technique for masonry during tests of single-story masonry walls. The overlays were used to enhance shear and flexural strength. The test results indicated a significant increase in strength and deformation resistance (Laursen et al. 1995).

Individual structural components have also been experimentally tested with retrofit. Circular and rectangular bridge columns were retrofitted with composite jackets of glass fiber reinforcement and resin (Seible and Karbhari 1996). These composite jackets were found to be just as effective as steel jackets in improving deformation resistance of columns subjected to blast loads.

Concrete beams were retrofitted and tested in a 1994 study by C. Allen Ross. This study investigated the hardening and rehabilitation of concrete structures using carbon fiber-reinforced plastics (CFRP). CFRP was applied to the tension side of beams. It greatly increased the maximum load carrying capacity of beams with less than 1% of steel reinforcement. Beams with higher amounts of reinforcement experienced delamination of the CFRP panels due to low bond strength between the panels and adhesive (Ross et al. 1994).

Many small components have been tested with retrofits, and they work very well. Retrofit has also been applied to full-scale structures. The Technical Coordinating Committee for Masonry Research (TCCMAR) constructed a five-story building. Simulated seismic loads were applied to the structure. Retrofit was applied to the damaged and undamaged components of the structure. Carbon fiber overlays, polymer-concrete repairs, and epoxy injection techniques were used to enhance the shear transfer in the walls, beams, and floor panels. The repaired building was seismically loaded. Results were compared to results of the initial loading. The repaired building had an increased load carrying capacity and resistance against deformation (Weeks et al. 1994).

Retrofitting is a relatively cheap and easy way of protecting buildings from damage, or worse, total destruction. Retrofitting has long been researched in areas with seismic activity, but it can be beneficial in other applications too. Retrofitting is now being studied for protection against blasts, as masonry walls are particularly vulnerable to terrorist bombs, especially walls that are either lightly reinforced or unreinforced (Crawford, Bogosian, et al. 1997). The failure of just a few outer support columns can cause the collapse of even a reinforced concrete structure. Blast loads tend to make the columns fail in shear, usually near the supports (Crawford, Malvar, et al. 1997).

In 1994, the United States participated in a composite retrofit material study with the Israeli Home Front Command. The purpose of the study was to learn more about blast loads and their effects on concrete and masonry structures retrofitted with composite materials. Dynamic testing Tyndall AFB led to the selection of two retrofit materials for the first phase of the study. The first was an autoclaved 3-ply carbon fiber composite laminate, and the second was a knitted biaxial fiberglass fabric (Purcell et al. 1995).

Phase I of the test series consisted of full-scale explosive tests of structures retrofitted with the chosen composite materials.

Israeli engineers constructed the structures used for the test. Each structure had 8-in.-thick wall panels that were reinforced with 3/8-in. rebar spaced 12 in. from center to center. Retrofitting was bonded to the wall surfaces after they had been cleaned and primed. The carbon fiber laminate and the knitted fiberglass fabric were bonded to the wall panels with HYSOL 9460 epoxy adhesive (Purcell et al. 1995).

A standoff distance of TNT was calculated with Conventional Weapon Effect (CONWEP) software to ensure breaching of the wall panels. The charge was detonated from the calculated distance. Results showed that the retrofit had a significant effect on the amount of wall displacement caused by the blast. The carbon fiber composite used in the test was only minimally effective, due in part to the poor bond between the material and the concrete that resulted in delamination. The knitted fiberglass fabric performed better than the carbon fiber. Results from the test resulted in a recommendation for development of a finite element analysis to predict wall response to explosive charge.

In 1995, Eglin AFB, Florida, conducted a blast response experiment on a three-story building. The purpose of this test was to evaluate the effectiveness of externally applied reinforcement. A 40 ft wide x 40 ft deep x 30 ft tall building was constructed. It had 10-in.-thick center walls and nine 14 in. x 14 in. square sectioned columns. The exterior walls were 7.2 ft wide, 8.5 ft tall, and 6 in. thick. They contained #4 rebar spaced 18 in. on center. A Kevlar fabric was used to retrofit the interior side of the four wall panels facing the explosive charge. The fabric was applied to the walls in the same manner as the previous test. An explosive charge of TNT was detonated. Three of the

four retrofitted walls failed completely. It was recommended that more work be done on optimizing the fiber orientation of the retrofit materials used.

In 1996, explosive tests were done to evaluate retrofit measures for conventional concrete masonry unit buildings. The tests were performed on a five-story building and two additional test cubicles. The U.S. Army Engineer Waterways Experiment Station produced a paper concentrating on the two test cubicles and the retrofit techniques (Whiting and Coltharp 1996). The test cubicles were constructed with load-bearing CMU frames with the assumption that the walls were part of a generic two-story building. The CMU walls were constructed with post-tensioned steel bars in CMU void spaces. This was done to add the weight that would be present in a two-story structure. Several mechanical and retrofit techniques previously tested for seismic retrofit were selected and evaluated for effectiveness in the blast loads. Pilasters, shotcrete, and knee bracing were used during the test.

During this test and the one before it, finite element models were used to predict damage done to the walls. The first test predictions were not accurate. Models predicted much less damage. However, predictions for the second test were very accurate (Whiting et al. 1996). It was concluded that finite element code was the most accurate means of predicting the damage during a blast.

In the fall of 1999, researchers of the Air Force Research Laboratory (AFRL) at Tyndall AFB, Florida, began searching for retrofit methods to increase blast resistance of common exterior walls. Priorities included finding a retrofit with an easy application process and a low cost. There was also a need for a lighter weight solution (as opposed to strengthening with mass) that would introduce ductility and resilience into walls (Knox

et al. 2000). A spray-on elastomeric polymer with a polyurea base was chosen based on the results of polymer testing at the AFRL. The material was easily applied to interior and exterior walls while maintaining consistency in application thickness. Proof of concept tests showed that masonry and lightweight structure walls experienced large deflections without breaching. No debris entered the structure. However, the structure experienced severe crushing of the ceiling, which needed to be mitigated.

The success of the spray-on retrofit led to the development of the lightweight structures program. Three explosive tests were performed on structures retrofitted with the polymer material. The first test consisted of two lightweight constructed wall panels (Knox et al. 2000). This test was used to study the strain rates of the retrofit when subjected to a blast. The next two tests consisted of small trailers (Knox et al. 2000). A steel frame was implemented in the trailer tests to reduce ceiling crushing. A higher charge was used in this test.

Results of the tests showed that the polymer retrofit was very effective in reducing fragmentation. The lightweight wall panels and structures sustained severe damage, but very little debris entered the structure. The higher charge of the trailer tests resulted in numerous tears in the retrofit that were significant enough to allow debris to enter (Knox et al. 2000). Based on the results of the tests, the research team concluded that the polymer retrofit technique would be an effective addition to a comprehensive security program (Knox et al. 2000). This led the AFRL to continue testing the polymer retrofit. However, the focus was shifted to unreinforced concrete masonry walls. An overview of Tests 1, 2, 3, 9, 10, 11, and 12 is presented in the next chapter of this document. Tests 4 through 8 were omitted because they were not masonry wall tests.

CHAPTER 3

EXPLOSIVE TESTS

3.1 Introduction

In 2001, AFRL began a testing program at Tyndall AFB, Florida, to evaluate the effectiveness of reinforcing walls for blast using spray-on polymer coatings. Twelve explosive tests were conducted. Seven of those involved testing of masonry walls and are reported in this chapter: Wall Test 1, Wall Test 2, Wall Test 3, Wall Test 9, Wall Test 10, Wall Test 11, and Wall Test 12. Tests 4 through 8 did not involve masonry walls and therefore are not reviewed in this document. Test numbering used in this document was kept consistent with the numbering scheme used by AFRL.

Unreinforced masonry (URM) walls were constructed for each test. Some walls were coated with the polymer, while others were used as controls. After effectiveness of the polymer on masonry walls was established, some tests did not involve control walls. Bonding techniques, doors, and windows were tested as reported throughout this chapter.

The reaction structures were equipped with gauges to measure pressures, deflections, and accelerations. Predictions were made for each gauge in each test and compared to recorded data. High-speed and digital still photography were used to aid in analysis.

The objectives of the wall tests were to determine the effectiveness of an elastomeric polymer coating as retrofit for URM walls subjected to blast loads. Specific objectives for each test were to measure deflections at critical wall locations, measure

internal and external pressures created by the blast, and determine differences in failure modes.

3.2 Wall Test 1

Wall Test 1 involved an explosive test on two URM walls, one reinforced with an elastomeric polymer coating on the inside of the wall, and one control wall without the polymer coating. The key objectives of Wall Test 1 were to (1) evaluate the application process for the polymer coating; (2) measure the deflection of key wall elements; and (3) evaluate the failure modes of retrofitted and unretrofitted masonry walls. The layout of Test 1 is shown in Fig. 1.

3.2.1 Construction

A reinforced concrete reaction structure was constructed at the site where tests were to be conducted. The housing structure was a rectangular building in which the back wall and two sidewalls were permanently constructed from steel and concrete. The rear and the sidewalls of the permanent structure were heavily reinforced. The exposed back wall is shown in Fig. 2. This image was taken during early construction. The rebar can be seen in this image. The reaction structure was designed to house temporary CMU walls used for testing. It was also designed to withstand the loads of repeated blast testing. New unreinforced masonry walls could quickly be rebuilt on its front face, saving material costs and expediting the next test.

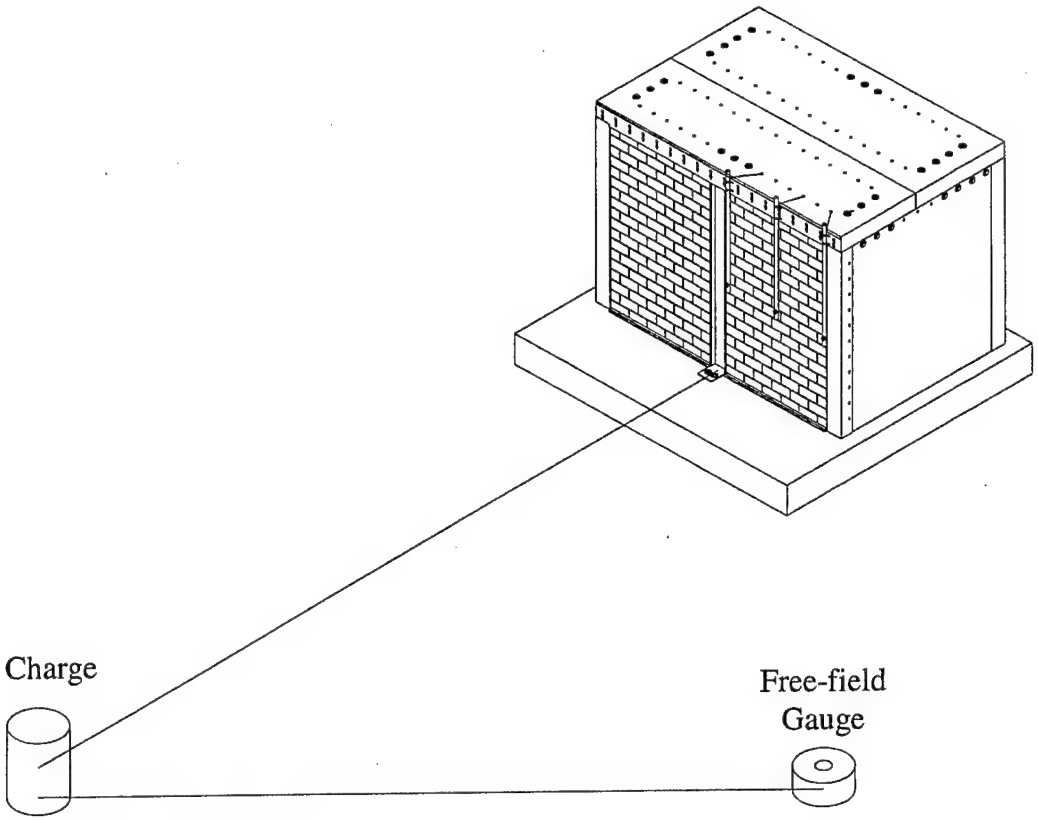

FIG. 1. Test 1 Layout

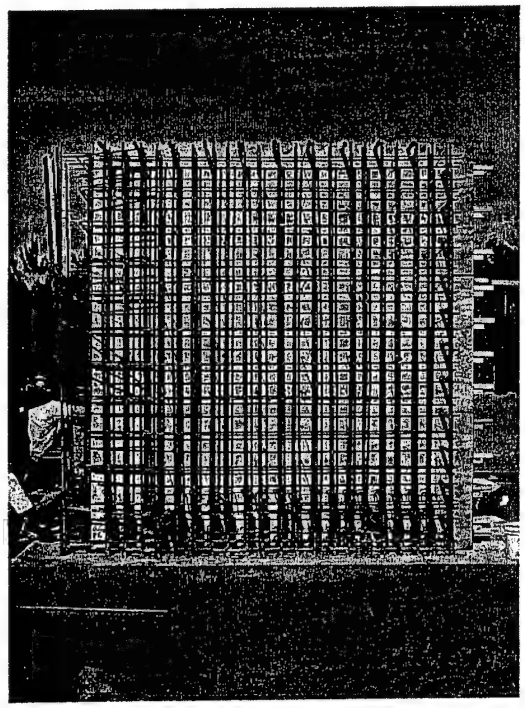

FIG. 2. Reaction Structure Construction

The roof of the test structure consisted of panels connected by a 6 in. x 6 in. x ½ in. angle. The roof angle had holes drilled in it to match up to those in the panels. It was attached with nuts and bolts. To protect the front faces of the sidewalls, ¼-in. flat steel cladding was implemented. The cladding was cut as necessary, and holes were drilled to match those in the sidewalls. Round stock was cut and welded in every other hole in order to secure cladding to sidewalls. A diagram of the roofing and cladding is shown in Fig. 3.

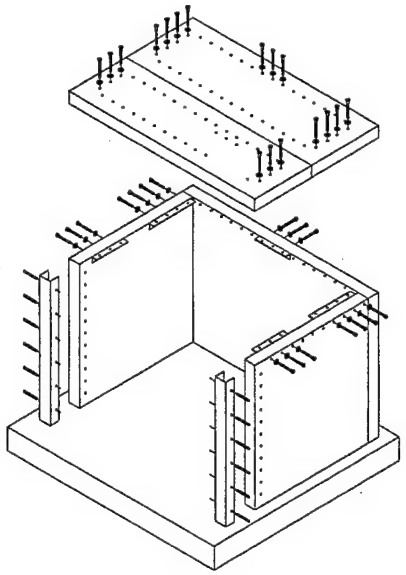

FIG. 3. Reaction Structure, Roofing and Cladding

Test 1 consisted of a retrofitted wall and a control wall. These walls were separated with a W12x35 steel I-beam with a plate welded to the top and bottom of the beam to secure it. The bottom plate was secured to the structure with anchor bolts. The top plate was secured to the roof slab with nuts and bolts. A diagram and the installed center I-beam can be seen in Figs. 4 and 5.

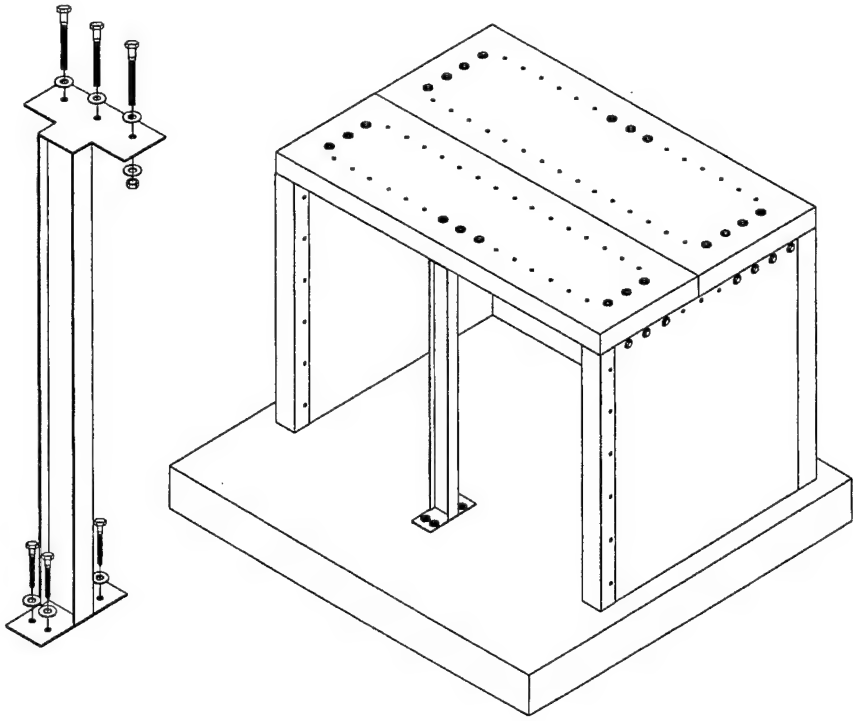

FIG. 4. Reaction Structure, Center I-Beam

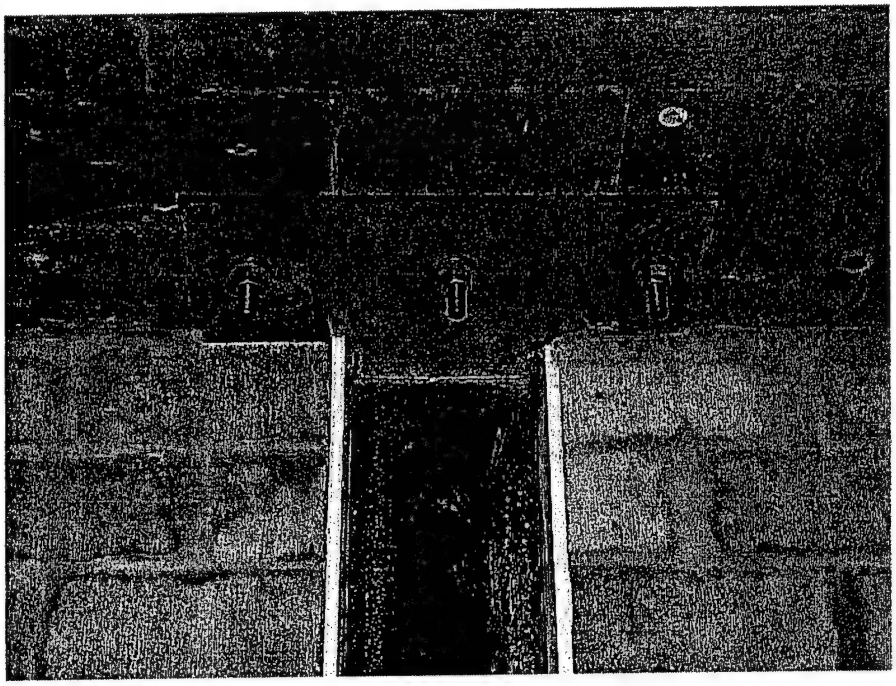

FIG. 5. Reaction Structure, Center I-Beam Installed

After the walls and roof were constructed, the test structure was prepared for the URM wall. The interior walls, floor, and roof slab were scrubbed with a muratic acid and water mixture. This removed all latents from the structure. This cleaning was in addition to other preparatory work.

After preparatory work and the initial cleaning, 8-in. strips of ¾-in. foam insulation board were placed on the sidewalls, as well as on the sides of the I-beam, in order to isolate the masonry walls from the reaction structure. This foam was adhered with construction adhesive. The locations of foam are illustrated in Fig. 6.

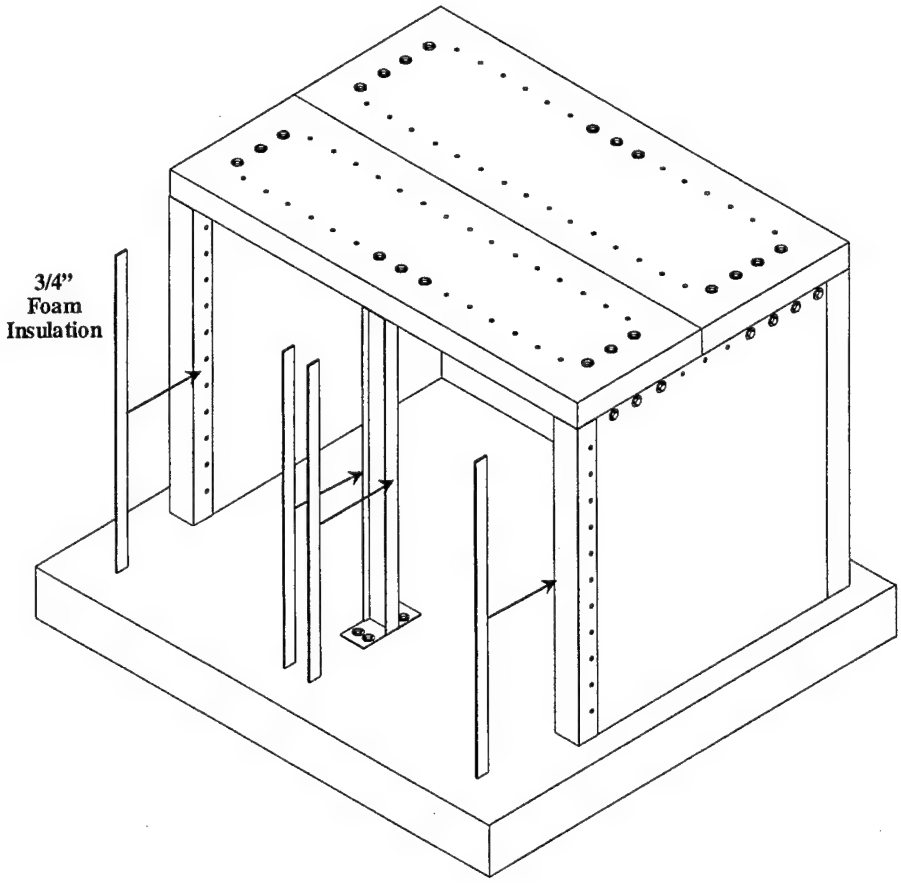

FIG. 6. Reaction Structure, Foam Insulation Board

With the cleaning of the structure and installation of the insulation foam, the structure was ready for the URM walls. Two wall panels were constructed as shown in Fig 7.

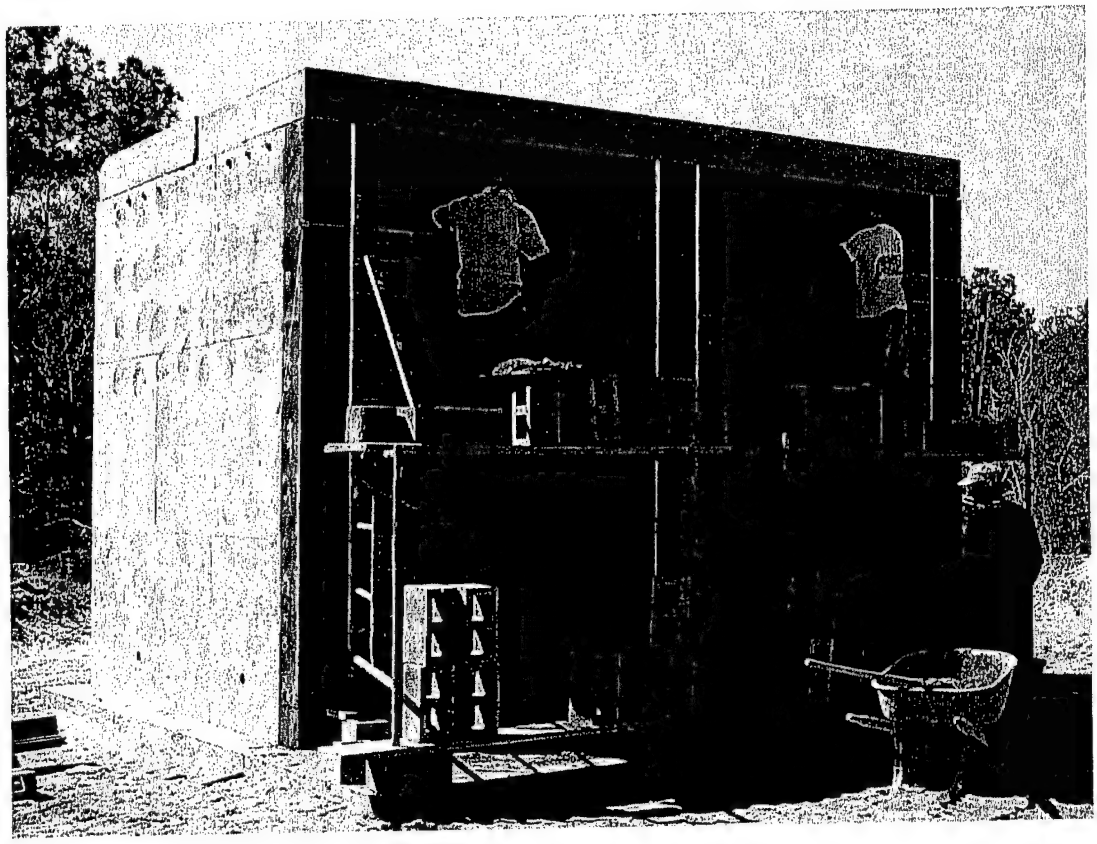

FIG. 7. Test 1, CMU Construction

The walls measured 7 ft 6 in. in width and were separated by the W12x35 steel I-beam and the insulating foam. The walls were secured to the structure with 3 in. x 4 in. x ¼-in-thick angle irons. These angles were secured with bolts to the interior and exterior bottom and interior top of the panels. The exterior top of the wall panels was locked in with a 16 ft x 1 ft x ¼ in. steel plate. This steel plates doubled by also protecting the roof slab. Angle iron supports and flat steel cladding are shown in Fig. 8.

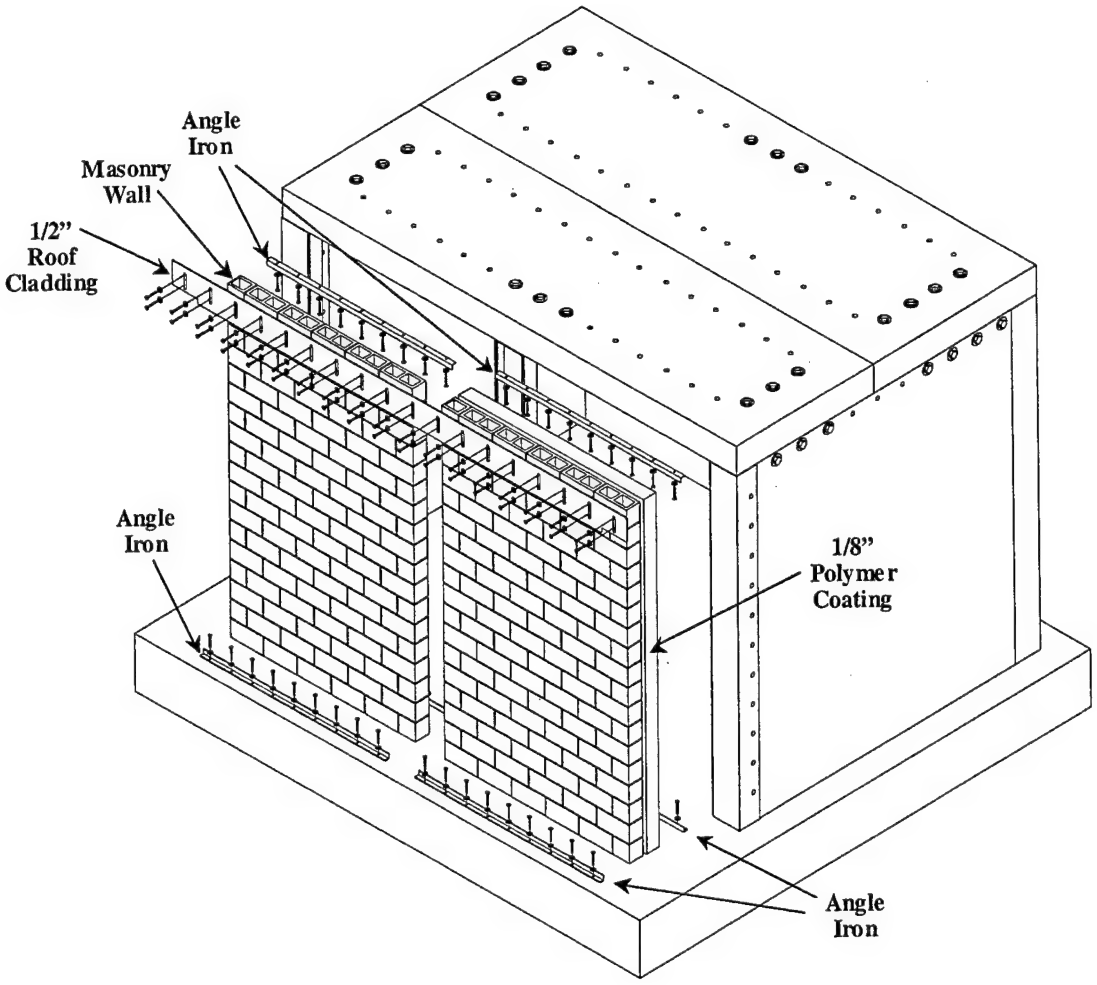

FIG. 8. Test 1, Angle Irons and Steel Cladding

The right wall was coated with a layer of polymer approximately 1/8 in. thick. The polymer was overlapped onto the wall, roof, floor, and front-center I-beam by approximately 6 in. The left wall panel was a control wall and therefore had no polymer coating. An image of the outside of the constructed walls is shown in Fig. 9.

A ½ in.-steel blast-proof door was installed on the rear side of the reaction structure. This allowed the structure to be enclosed while maintaining access to the inside. A diagram of the blast door can be seen in Fig. 10.

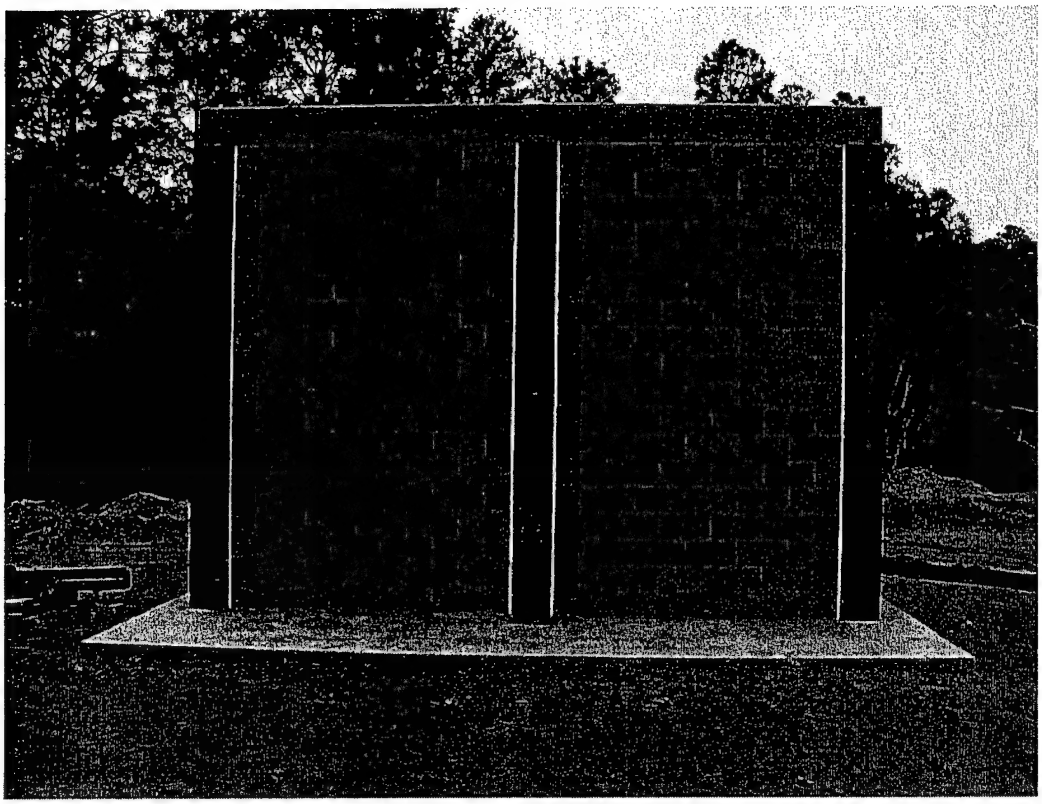

FIG. 9. Test 1, Constructed Walls

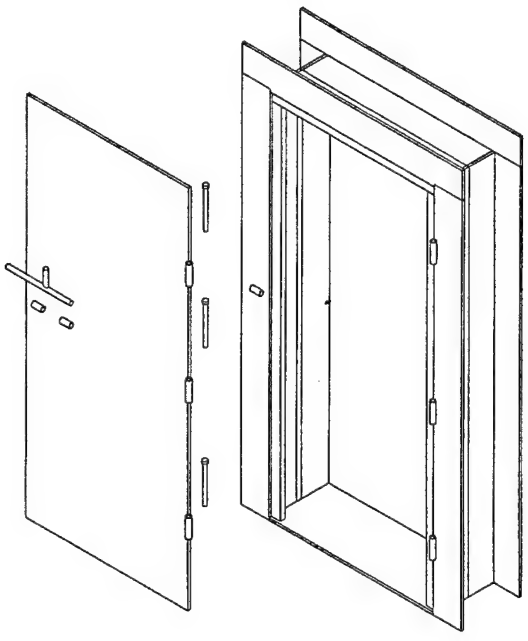

FIG. 10. Test 1, Blast Door

3.2.2 Instrumentation

Gauge instrumentation used in Wall Test 1 included three reflected pressure gauges (R1, R2, R3), one free-field pressure gauge (F1), one interior pressure gauge (F2), five single-axis accelerometers (A1, A2, A3, A4, A5), and two laser deflection gauges (L1, L2).

The reflected pressure gauges were pipe mounted and suspended from the top of the building. The laser gauges were mounted at the center of each CMU wall. The accelerometers were mounted to the interior face of the retrofitted wall. The instrumentation locations are illustrated in Fig. 11. The instrumentation details follow in Fig. 12. The pipe-mounted pressure gauges are shown in Fig. 13. The deflection gauges are shown in Fig. 14.

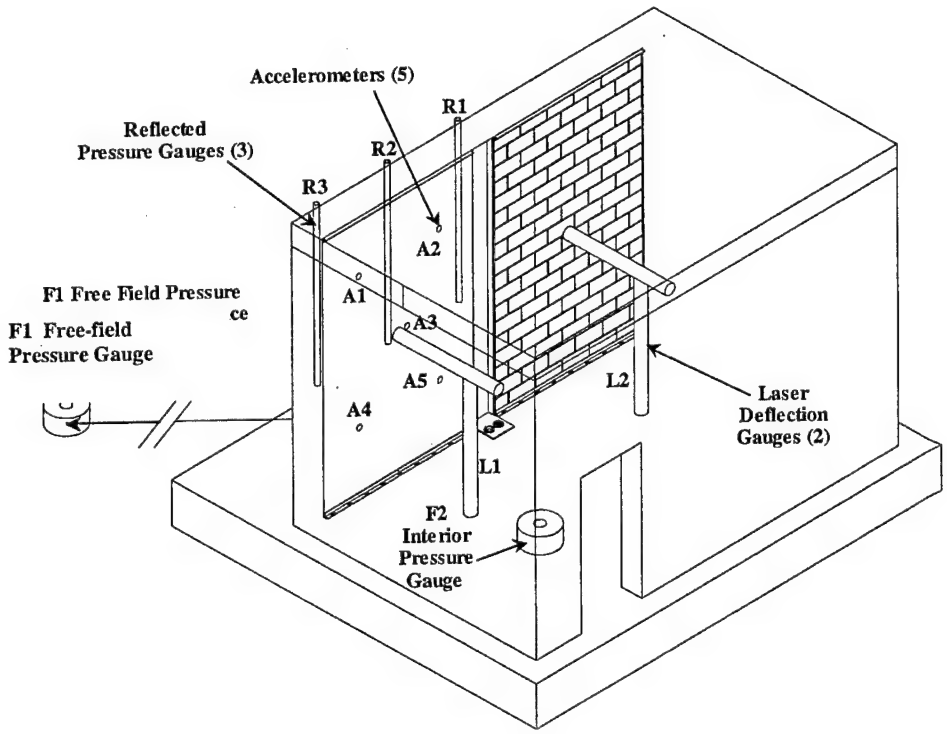

FIG. 11. Test 1, Gauge Locations

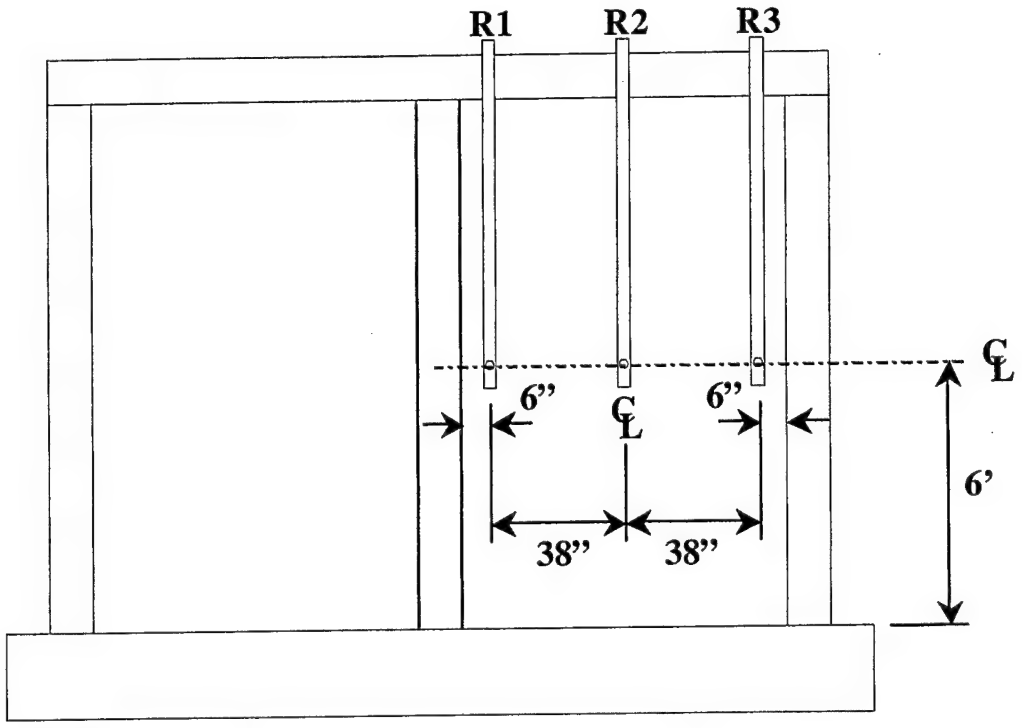

Reflected Pressure Gauges (Exterior View)

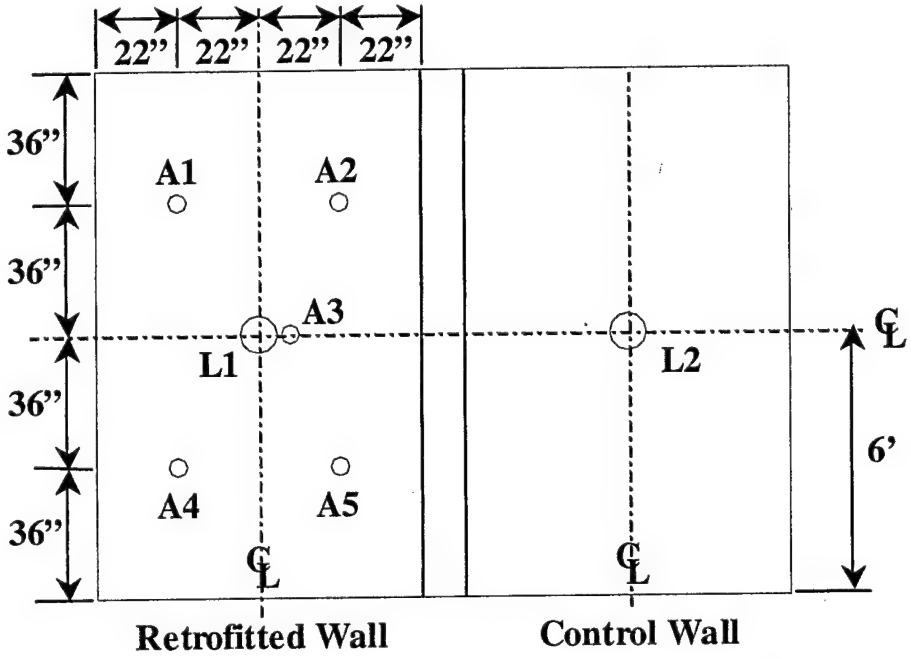

Accelerometers and Laser Gauges (Interior View)

FIG. 12. Test 1, Gauge Details

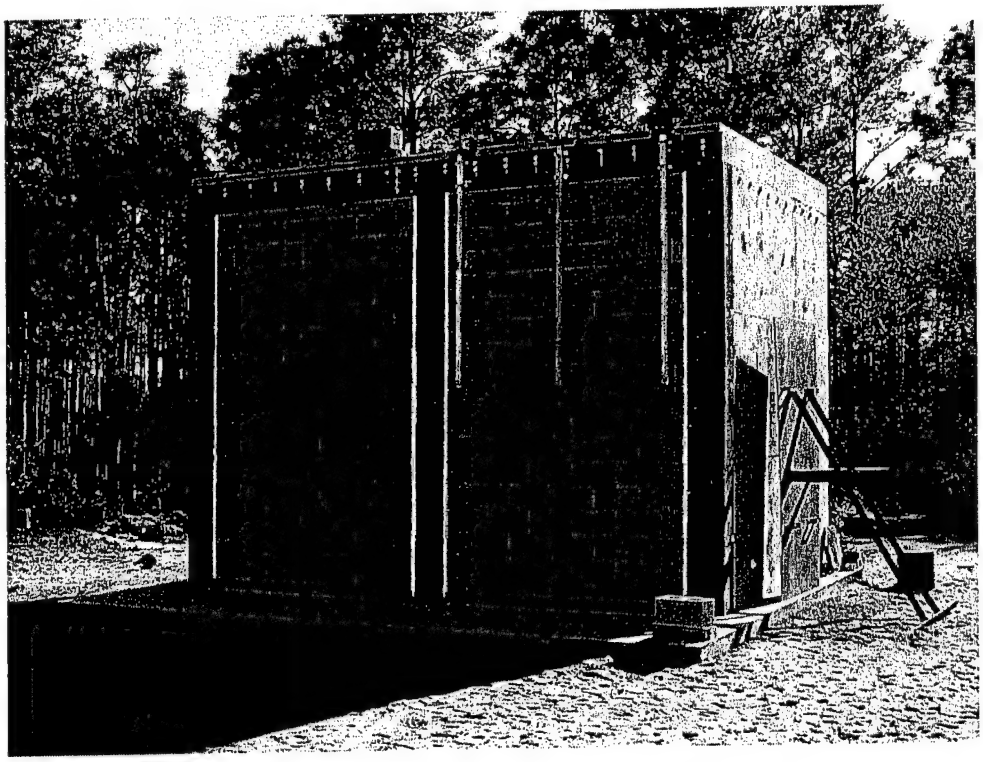

FIG. 13. Test 1, Reflected Pressure Gauges

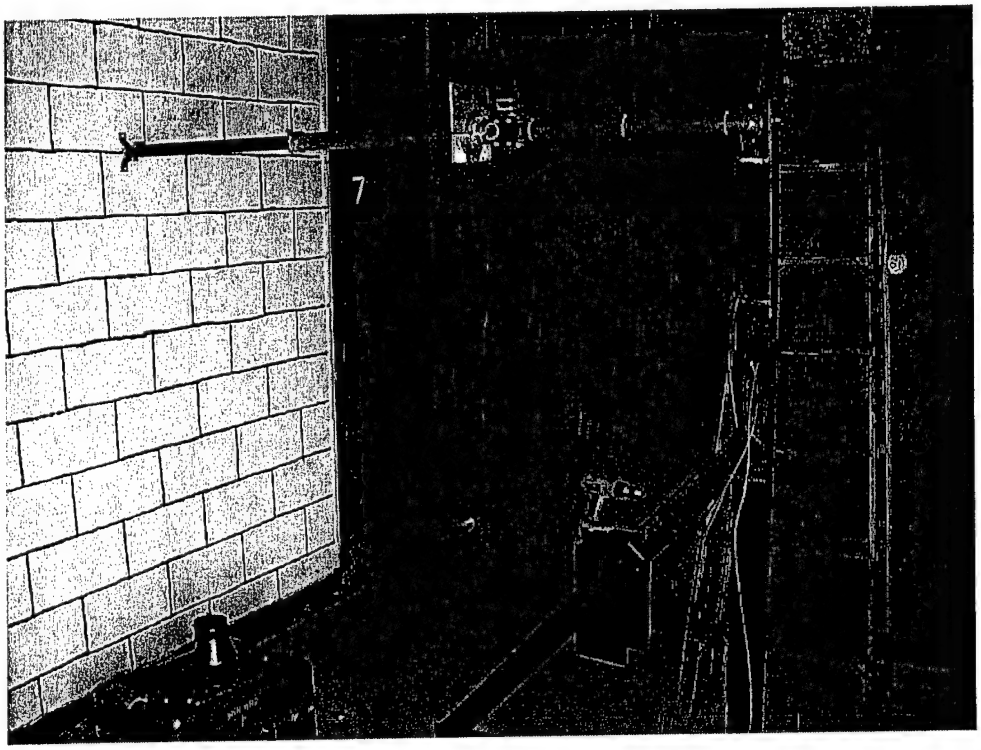

FIG. 14. Test 1, Deflection Gauge

Photography instrumentation consisted of pre- and post-test still photography and high-speed photography of the wall deflection. Two high-speed 16 mm cameras were mounted to catch the top and center of the unretrofitted wall at 1000 frames per second. A LOCAM camera (200 frames per second) was directed at the center of the retrofitted wall. A digital high-speed camera was also located outside the wall to capture the response of the structure (at 1000 frames per second). Camera target areas are illustrated below in Fig. 15. A low speed camera is shown in Fig. 16. The high-speed cameras are shown in Fig. 17.

Lighting for Test 1 consisted of two separate panels, each with four lights. The lights used in the test were similar to flood lights. The lights were necessary for photography.

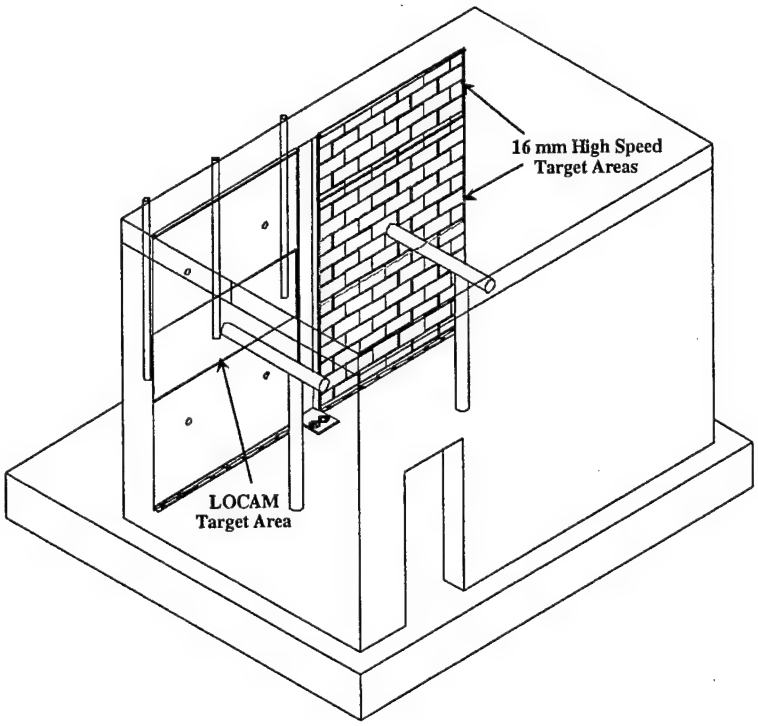

FIG. 15. Test 1, Interior Camera Target Areas

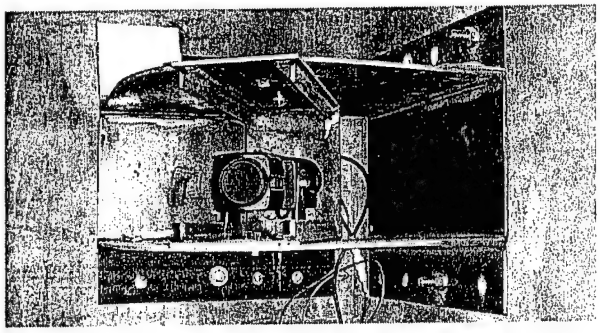

FIG. 16. Test 1, Low Speed Camera

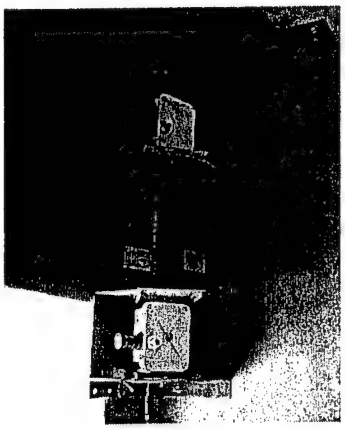

FIG. 17. Test 1, High Speed Cameras

3.2.3 Results

WAC (Wall Analysis Code) software was used to predict the pressures, impulse, and response of the walls during the explosive test. WAC was developed by the Army Corp of Engineers and uses a single-degree-of-freedom model developed for a variety of wall structures. In essence, the user provides the type of wall (reinforced concrete, unreinforced concrete, unreinforced masonry, etc.), geometric parameters (height, width, thickness, etc.), material properties, and load parameters (type of explosive, standoff distance, and charge size). The model uses nonlinear resistance functions to predict

rotation, deflection, and failure of the wall structure. Pressures, deflections, and accelerations predicted for each gauge are provided in Table 1.

Table 1. Test 1, Gauge Predictions

Gauge ID	Type	Location	Prediction
R1	Reflected Pressure	Center of Structure	66 psi
R2	Reflected Pressure	Center of Retrofitted Wall	66 psi
R3	Reflected Pressure	Edge of Structure	50 psi
F1	Free-field Pressure	Outside Structure	22 psi
F2	Free-field Pressure	Inside Structure	22 psi
L1	Laser Deflection	Center Polymer Wall	8 in. inward, 3 in. outward
L2	Laser Deflection	Center Control Wall	Failure – all inward
A1	Accelerometer	Upper Left Polymer Wall	1000 g's
A2	Accelerometer	Upper Right Polymer Wall	1000 g's
A3	Accelerometer	Center Polymer Wall	1000 g's
A4	Accelerometer	Lower Left Polymer Wall	1000 g's
A5	Accelerometer	Lower Right Polymer Wall	1000 g's

Twelve gauges were placed on, behind, or near the walls to collect data from the explosive charge. R1, R2, and R3 recorded reflective pressure. The data collected from the devices is shown in Figs. 18 through 20. Free-field pressure gauge F1 and interior pressure gauge F2 recorded data, as shown in Figs. 21 through 22. Laser deflection gauges L1 (retrofitted) and L2 (control) recorded data, as shown in Figs. 23 through 24.

Five accelerometers were placed on one wall, as shown in Figs. 11 through 12. The gauges A1, A2, and A3 recorded data, as shown in Figs. 25 through 30. Acceleration gauges A4 and A5 failed. For each accelerometer, two graphs are shown.

The first is for acceleration plotted with velocity; the second is for velocity plotted with displacement.

The graphs show data through the most significant time period of the blast. Table 2 summarizes the predicted data and the recorded data of Wall Test 1.

A post-test image of both walls is shown in Fig. 31. Defacing of the right wall is shown in Fig. 32. The control wall collapsed, as shown in Fig. 33. The polymer retrofit prevented the right wall from collapsing and prevented intrusion of wall fragments. Significant defacing of the CMUs near the top of the wall occurred.

A high-speed camera image of the unretrofitted wall, illustrating tension separation at the mortar joints, is shown in Fig. 34. The right (retrofitted) wall had significantly less deflection than the left (unretrofitted) wall. Generally, when a masonry wall deflection exceeds wall thickness, gravity collapse occurs. The mortar failures in the retrofitted wall are shown in Fig. 35.

The interior of the right (west) wall was retrofitted. The left (east) wall was painted (but not retrofitted), and the blocks were outlined. Both of the wall panels sustained major damage. The mortar layers at mid-height experienced the highest bending stresses and failed in tension. There was significant defacing of CMUs on the retrofitted wall. No debris entered the reaction structure through this wall.

The maximum pressures recorded by the pressure gauges were (R1) 57 psi at 15.5 msec, (R2) 52.5 psi at 16.7 msec, and (R3) 44 psi at 17.3 msec. The maximum pressures recorded by the pressure gauges were (F1) 27 psi at 15.4 msec and (F2) 0.7 psi at 50 msec. The maximum deflections recorded by the laser gauges were (L1) 7.3 in. at 49 msec and (L2) 7.3 in. at 1.0 msec.

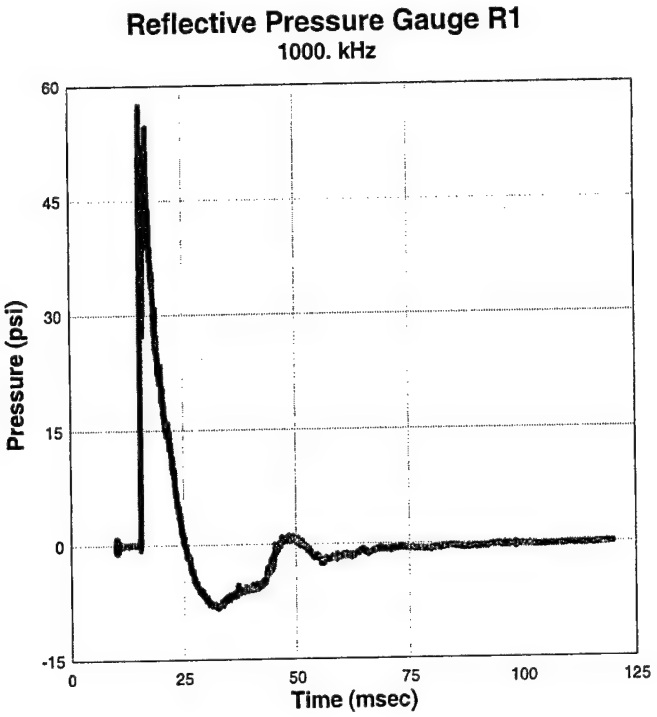

FIG. 18. Test 1, Gauge R1

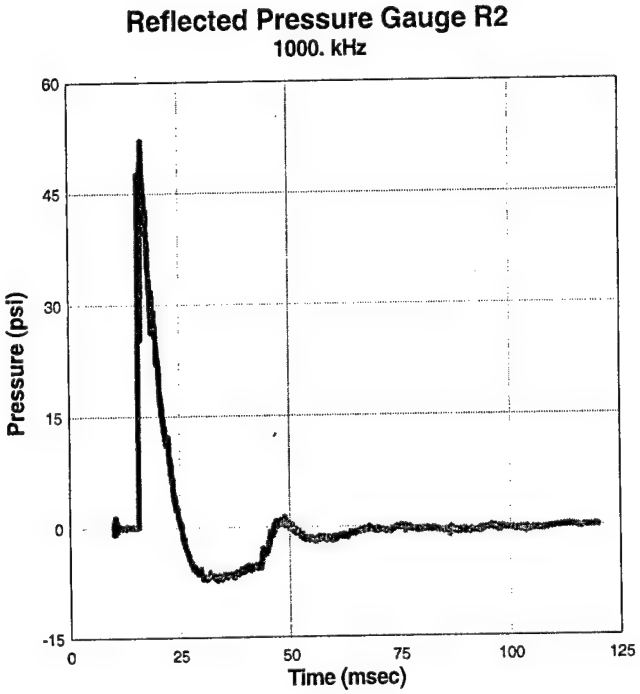

FIG. 19. Test 1, Gauge R2

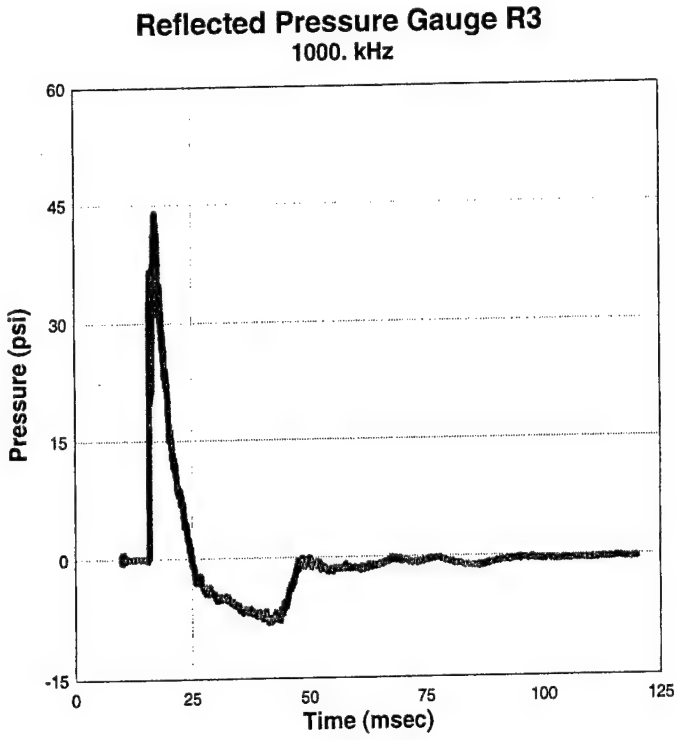

FIG. 20. Test 1, Gauge R3

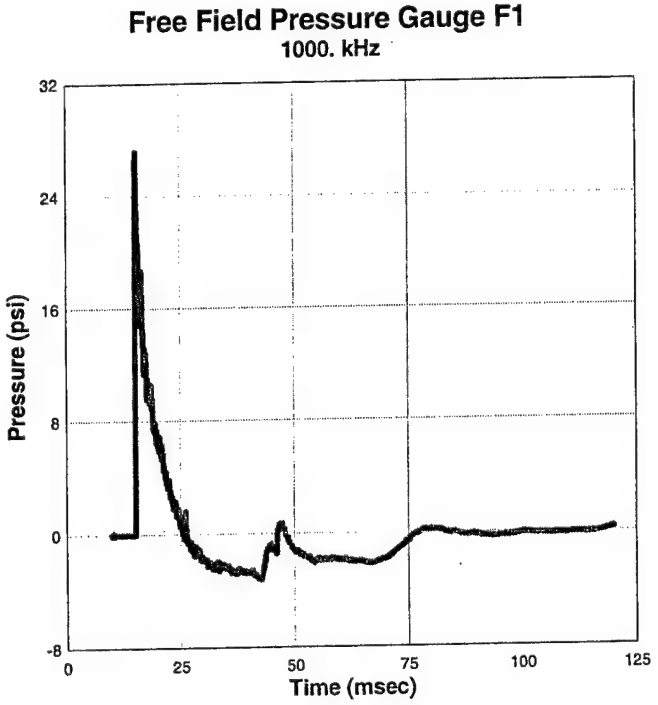

FIG. 21. Test 1, Gauge F1

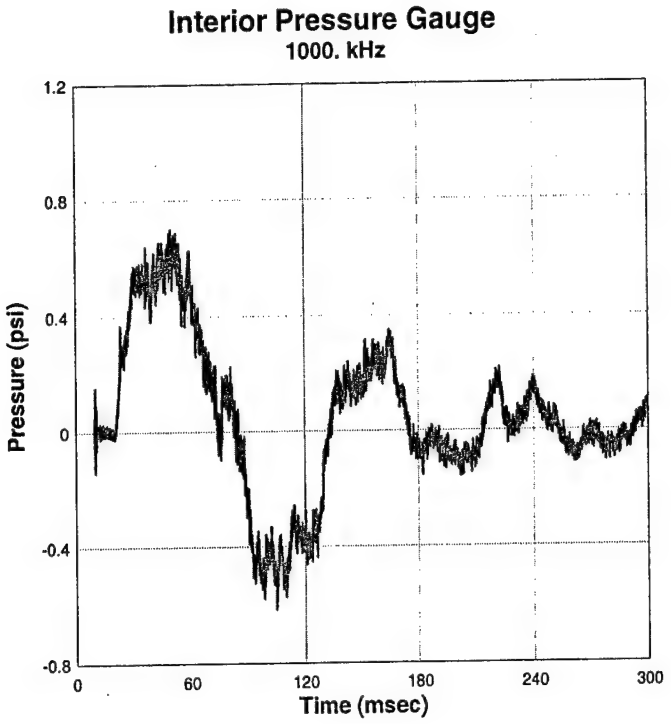

FIG. 22. Test 1, Gauge F2

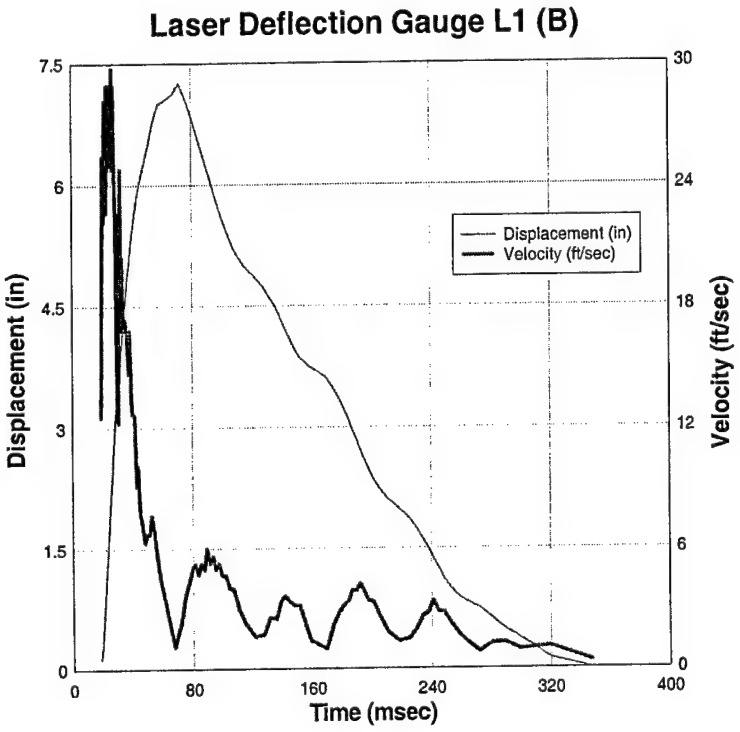

FIG. 23. Test 1, Gauge L1

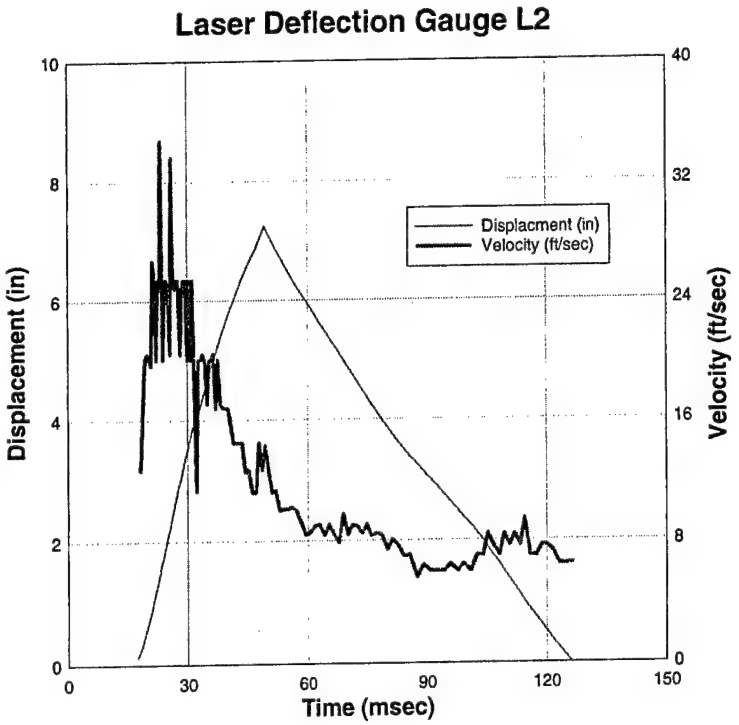

FIG. 24. Test 1, Gauge L2

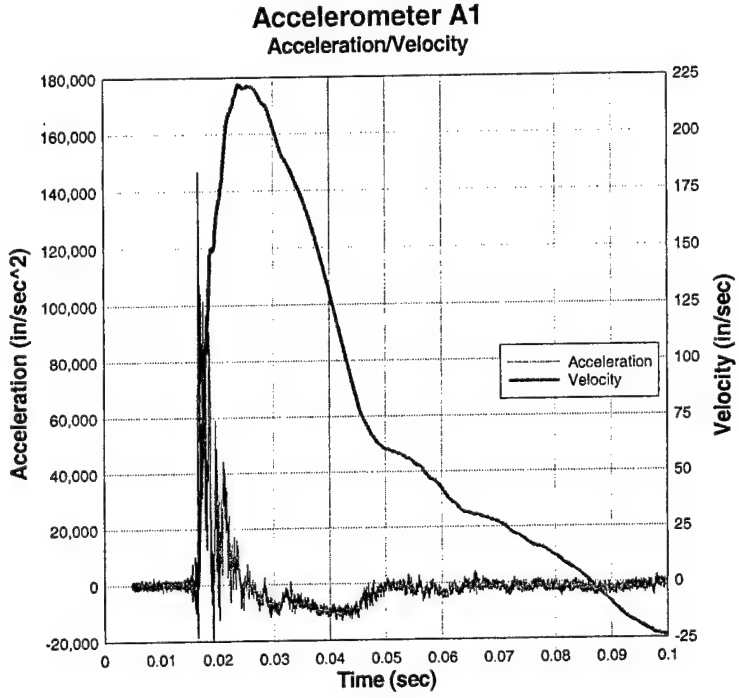

FIG. 25. Test 1, Acceleration and Velocity (A1)

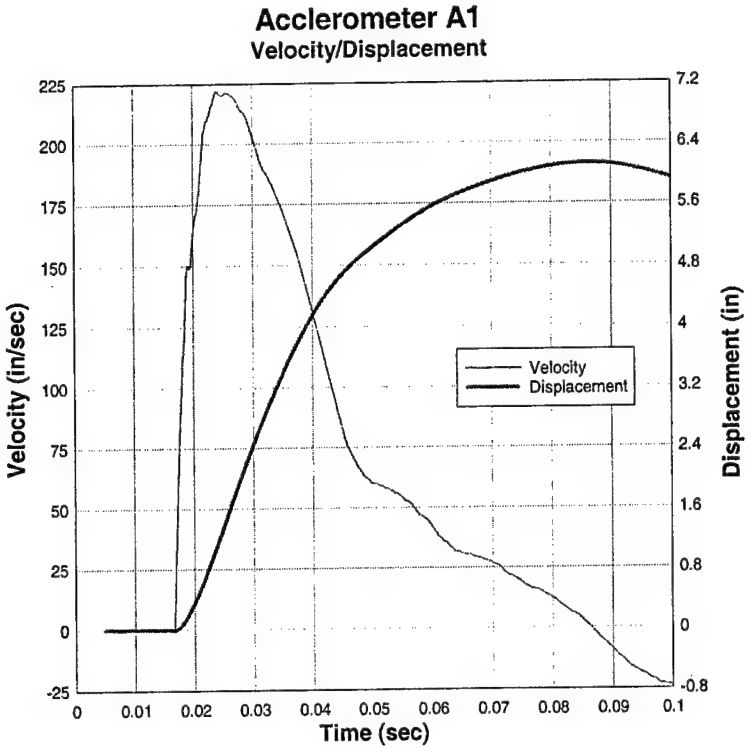

FIG. 26. Test 1, Acceleration and Displacement (A1)

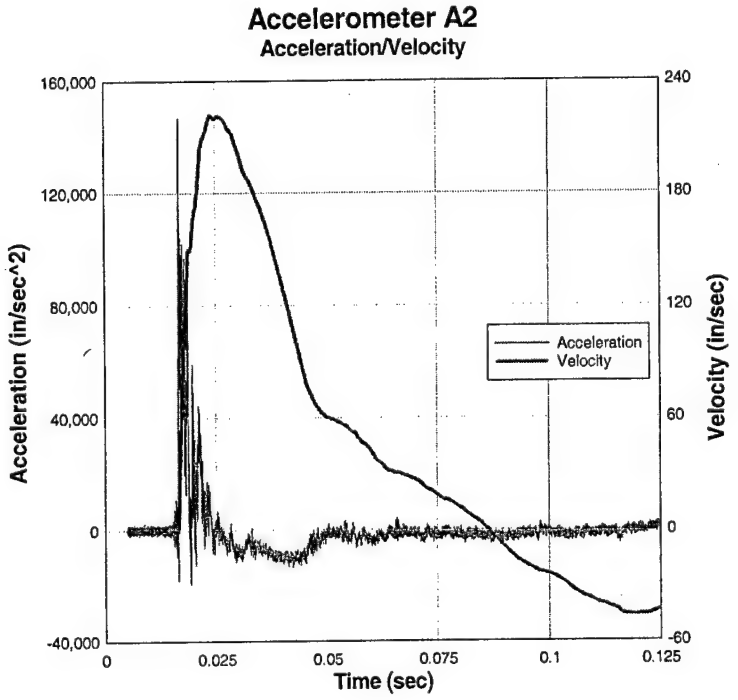

FIG. 27. Test 1, Acceleration and Velocity (A2)

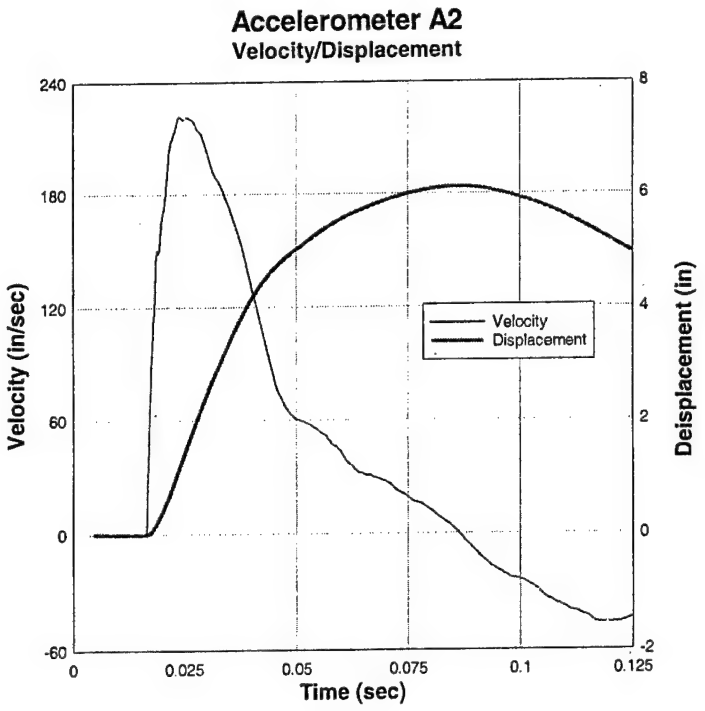

FIG. 28. Test 1, Velocity and Displacement (A2)

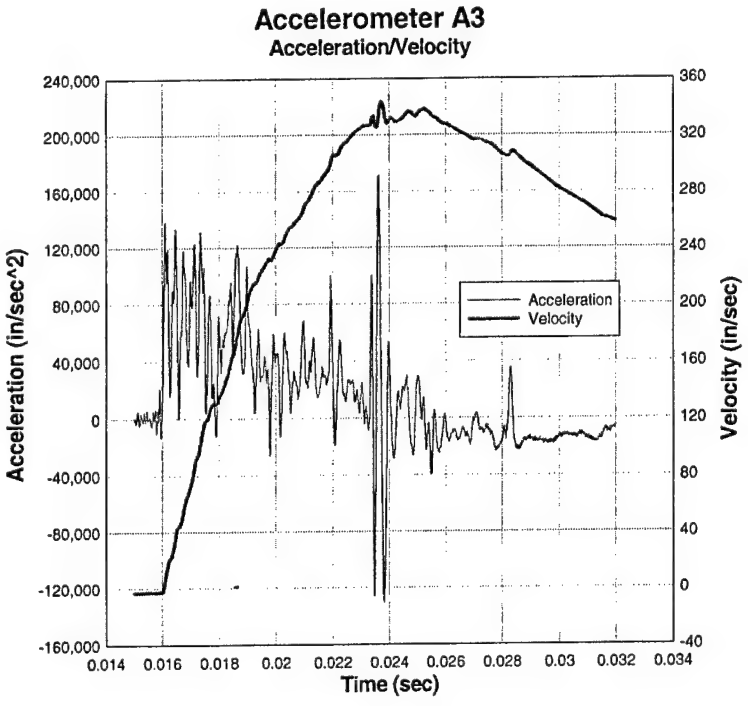

FIG. 29. Test 1, Acceleration and Velocity (A3)

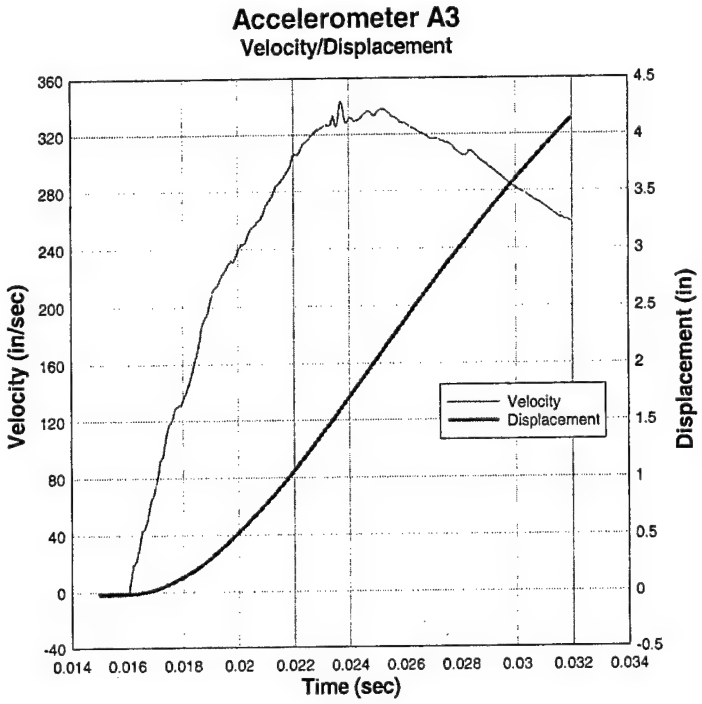

FIG. 30. Test 1, Acceleration and Displacement (A3)

TABLE 2. Test 1, Predicted vs. Recorded Data

Gauge ID	Type	Prediction	Actual
R1	Reflected pressure	66 psi	57 psi
R2	Reflected pressure	66 psi	52.5 psi
R3	Reflected pressure	50 psi	44 psi
F1	Free-field pressure	22 psi	27 psi
F2	Free-field pressure	22 psi	0.7 psi
L1	Laser deflection	8 in. inward / 3 in. out	7.25 in. inward
L2	Laser deflection	Failure - all inward	7.25 in. inward
A1	Accelerometer	1000 g's	379 g's
A2	Accelerometer	1000 g's	379 g's
A3	Accelerometer	1000 g's	444 g's
A4	Accelerometer	1000 g's	Gauge Failure
A5	Accelerometer	1000 g's	Gauge Failure

FIG. 31. Test 1, Post Test Reaction Structure

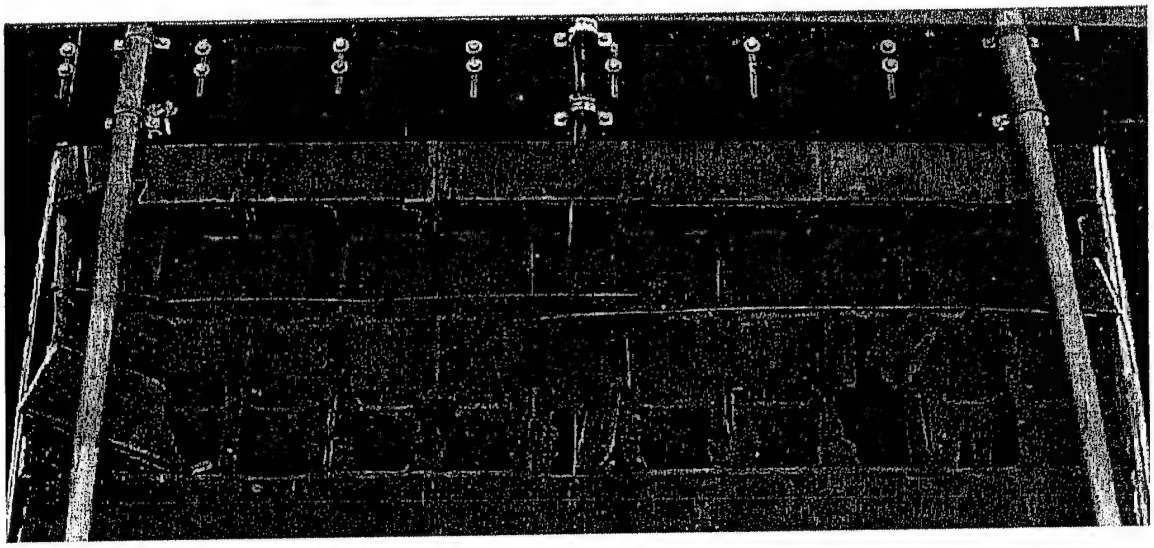

FIG. 32. Test 1, Defacing of Retrofit Wall

FIG. 33. Test 1, Collapsed Control Wall

FIG. 34. Test 1, Mid-Height Failure, Control Wall (High Speed Image)

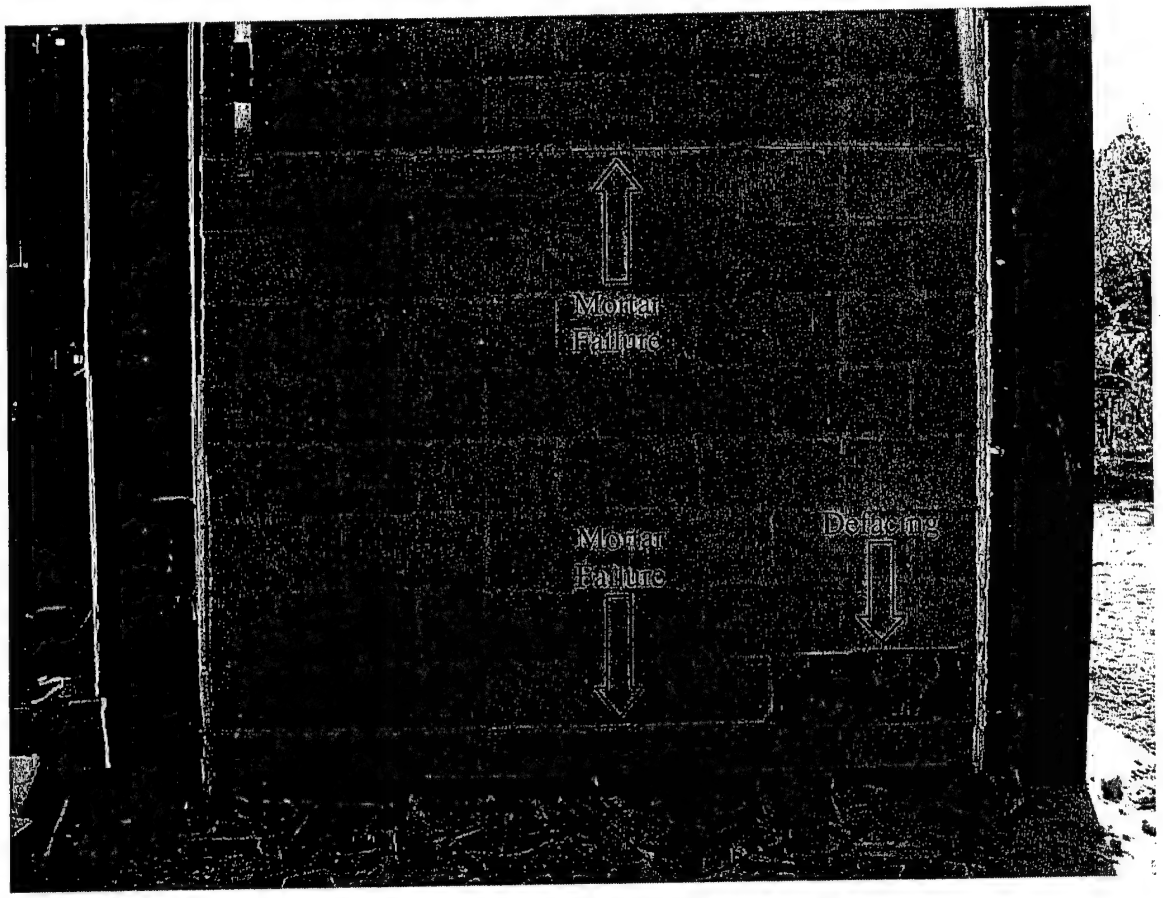

FIG 35. Test 1, Mortar Failure and Defacing

3.3 Wall Test 2

Wall Test 2 involved an explosive test on two 16 ft x 12 ft masonry walls, one retrofitted with a 1/8-in. interior elastomeric polymer coating and the other a control wall without the polymer coating. The key objectives of Wall Test 2 were to (1) evaluate the application process for the polymer coating; (2) measure the deflection of key wall elements and internal pressures; (3) evaluate the failure modes of retrofitted and unretrofitted masonry walls; (4) identify connection failure points on retrofitted wall; and (5) validate the bending response of the unretrofitted wall at higher pressures.

A layout of Test 2 is shown in Fig. 36. Since Test 1 did not appear to reach the capacity of the polymer-reinforced wall, the charge size used in Test 2 was doubled from that used in Wall Test 1, and the distance between the reaction structure and the explosive charge was decreased, resulting in significantly increased loading over Test 1.

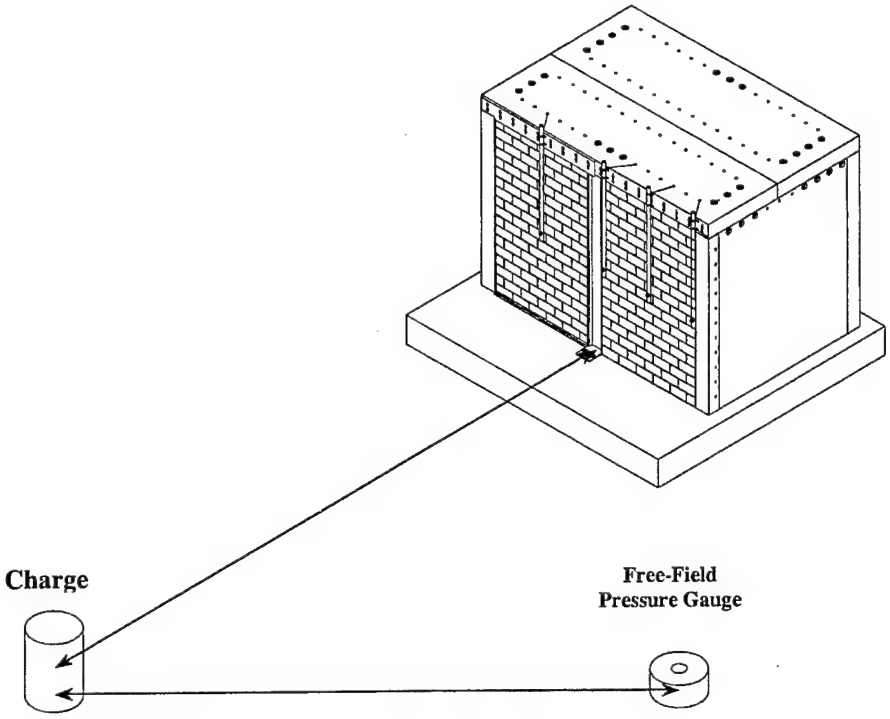

FIG. 36. Test 2 Layout

3.3.1 Construction

The test articles in Wall Test 2 were two standard unreinforced masonry block walls with 3/8-in. mortar joints. The two walls were separated by a W12x35 I-beam. The top and bottom of the left wall (control wall) were clamped with a 3 in. x 4 in. x 1/4 in. angle iron. The top and bottom of the right wall (retrofit wall) were secured with a 6 in.

overlay of 1/8 in. polymer coating. Both walls were allowed to move freely on the sides to approximate a one-way flexural response.

Several tasks were completed after Wall Test 1 in order to proceed to Wall Test #2: (1) masonry debris from Wall Test #1 was removed; (2) a blast door was installed; (3) top front roof cladding was moved to the highest position; (4) center section top roof cladding was cut; and (5) an additional 6 in. x 6 in. x ½ in. angle was installed on the roof.

Masonry debris from the left wall was removed. Fracture patterns of the individual masonry blocks were documented. Because most of the right wall was still intact and representative samples of the polymer were needed for thickness verification, a sledgehammer was used in the demolition of the right wall. The 3 in. x 4 in. x 1/4 in. angle iron (top and bottom) and the attachment bolts were removed from the right wall and stored. All residue from the adhesive used to attach the foam insulation board was removed. The test structure was thoroughly cleaned.

Bolts holding the top front cladding were loosened and moved up. It was drilled and tapped in place to accommodate an additional pipe-mounted reflected pressure gauge. The welding shop cut the center section in half so the cladding over each wall panel could move independently. The section over the left wall was moved down after the construction of the masonry walls. A diagram of the changes is illustrated in Fig. 37.

To insure one-way flexure, ¾-in.-thick, 8-in.-wide foam insulation board was attached with construction adhesive. An image of this foam insulation is shown in Fig. 38. The foam was applied to each side of each masonry wall constructed for the test.

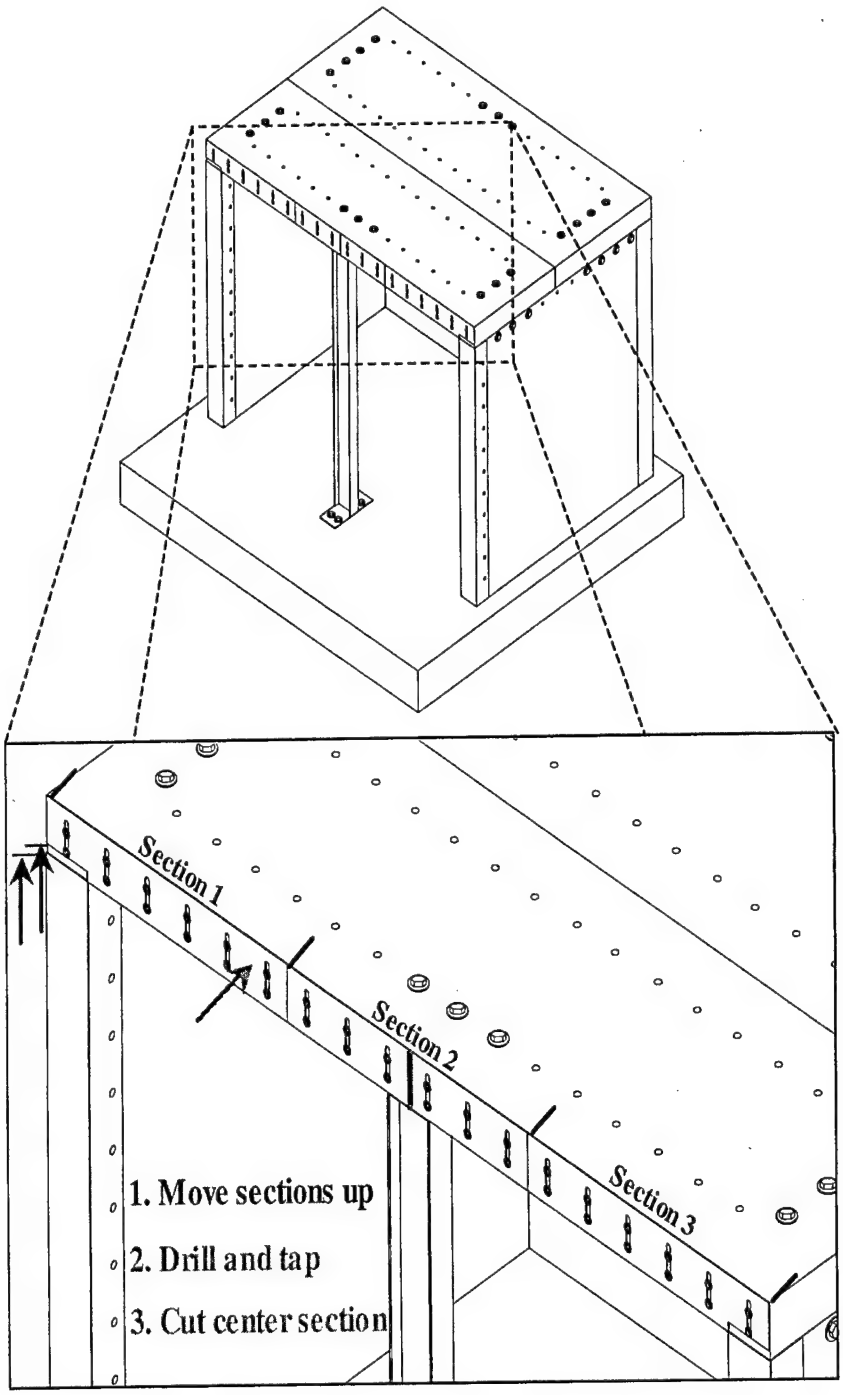

FIG. 37. Test 2, Top Cladding Modifications

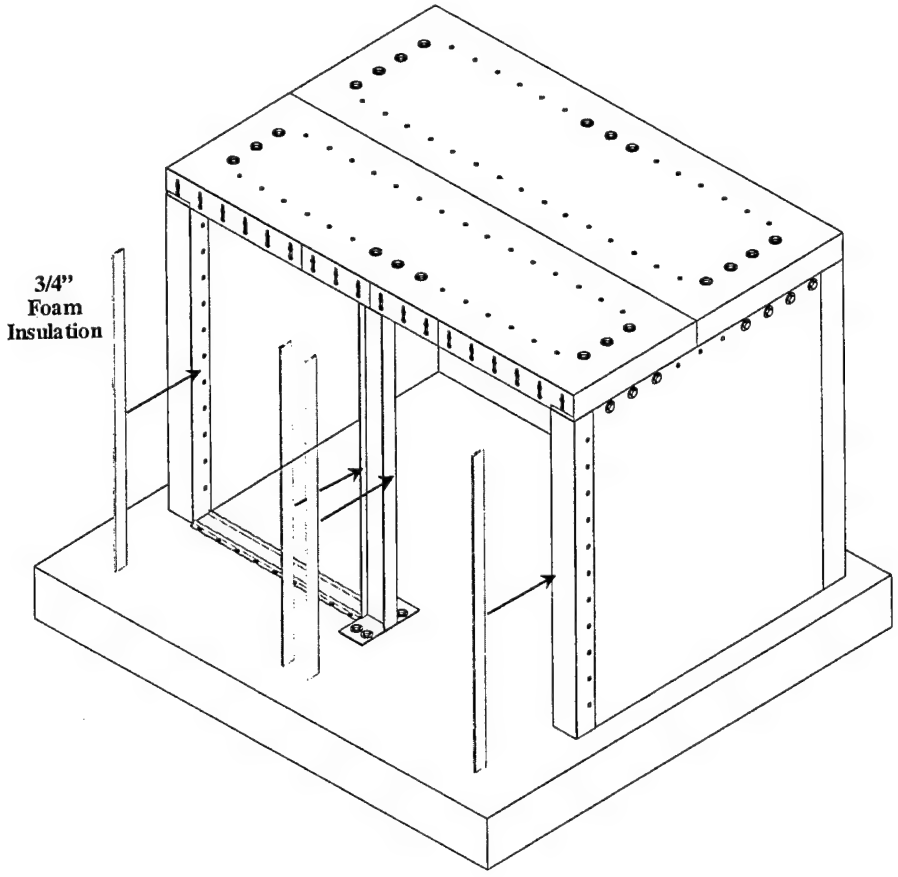

FIG. 38. Test 2, Foam Insulation Board

As in Test 1, two unreinforced masonry walls were constructed in the reaction structure. The walls measured approximately 7 ft 6 in. x 12 ft and were separated by a W12x35 I-beam and ¾-in. foam insulation board on both sides of the wall panels. An existing 3 in. x 4 in. x ¼ in. angle iron locked the top and exterior side of the wall panel. There was a slight gap between the left masonry wall and the angle iron, and it was filled by wood shims. Caulking was applied between the masonry wall and foam insulation board to prevent dust from entering the structure. An image of the wall construction is shown in Fig. 39.

FIG. 39. Test 2, Wall Panel Construction

To insure that the polymer would adhere to the wall, the test structure was thoroughly cleaned prior to application. The interior walls, floor, and roof were cleaned with a 5:1 muratic acid and water solution.

After all preparation work was completed, the right wall panel was coated with a 1/8-in. layer of polymer. The polymer overlapped onto the reaction structure floor and roof by 6 in. Caulking was then applied to insure a smooth bond between the masonry wall and test structure. Masking was applied to maintain a 6 in. overlap and to allow free movement on the sides. A drawing of the reaction structure with angle, cladding, and polymer locations is shown in Fig. 40. The constructed walls are shown in Fig. 41.

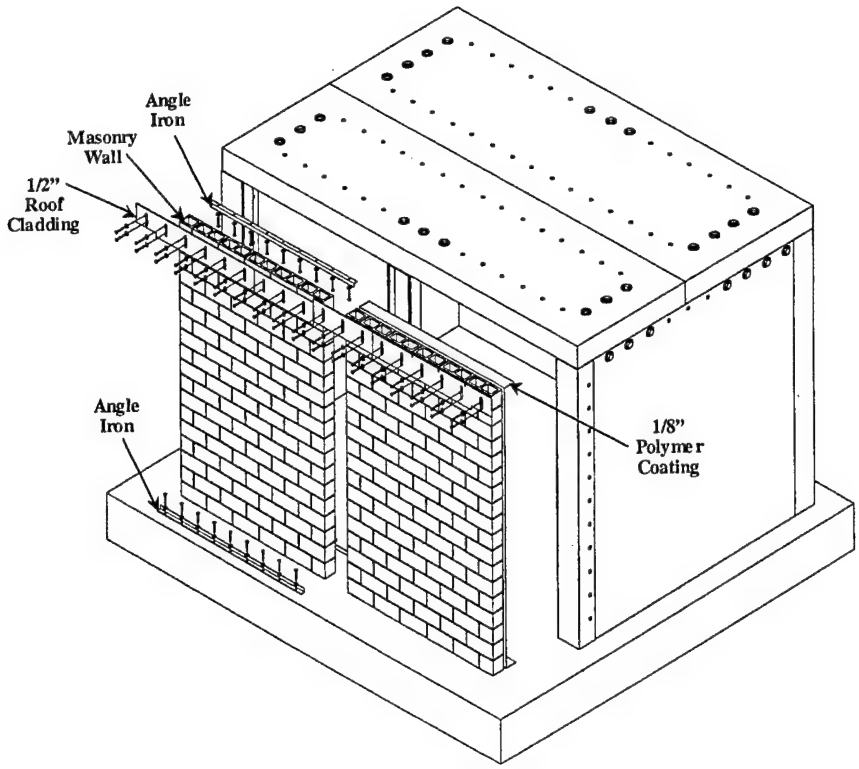

FIG. 40. Test 2, Angle, Cladding, and Polymer Locations

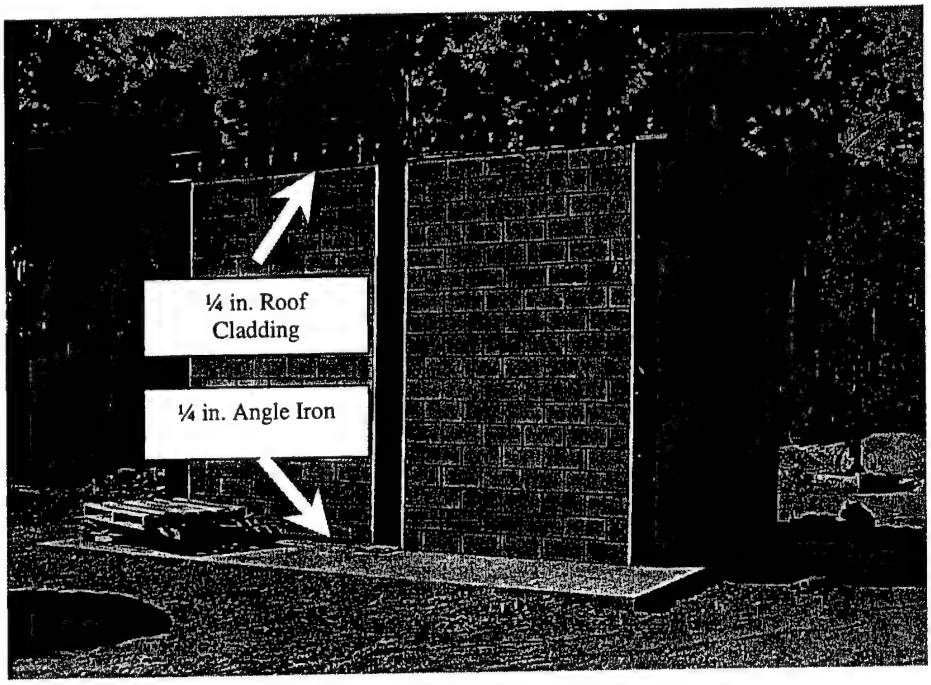

FIG. 41. Test 2, Roof Cladding and Angle Iron

3.3.2 Instrumentation

Gauge instrumentation used in Wall Test 2 included four reflected pressure gauges (R1, R2, R3, R4), one free-field pressure gauge (F1), one interior pressure gauge (F2), four single-axis accelerometers (A1, A2, A3, A4), and two laser deflection gauges (L1, L2). The reflected pressure gauges were pipe mounted and suspended from the top of the building. The pipe was held in place by two mounts per pipe and secured to the roof cladding and bearing on Styrofoam to reduce ringing. The accelerometers were mounted to the interior face of the polymer wall. Locations of the above-mentioned gauges are shown in Fig. 42. Instrumentation details are shown in Fig. 43. Reflected pressure gauges and laser gauges are shown in Figs. 44 to 46.

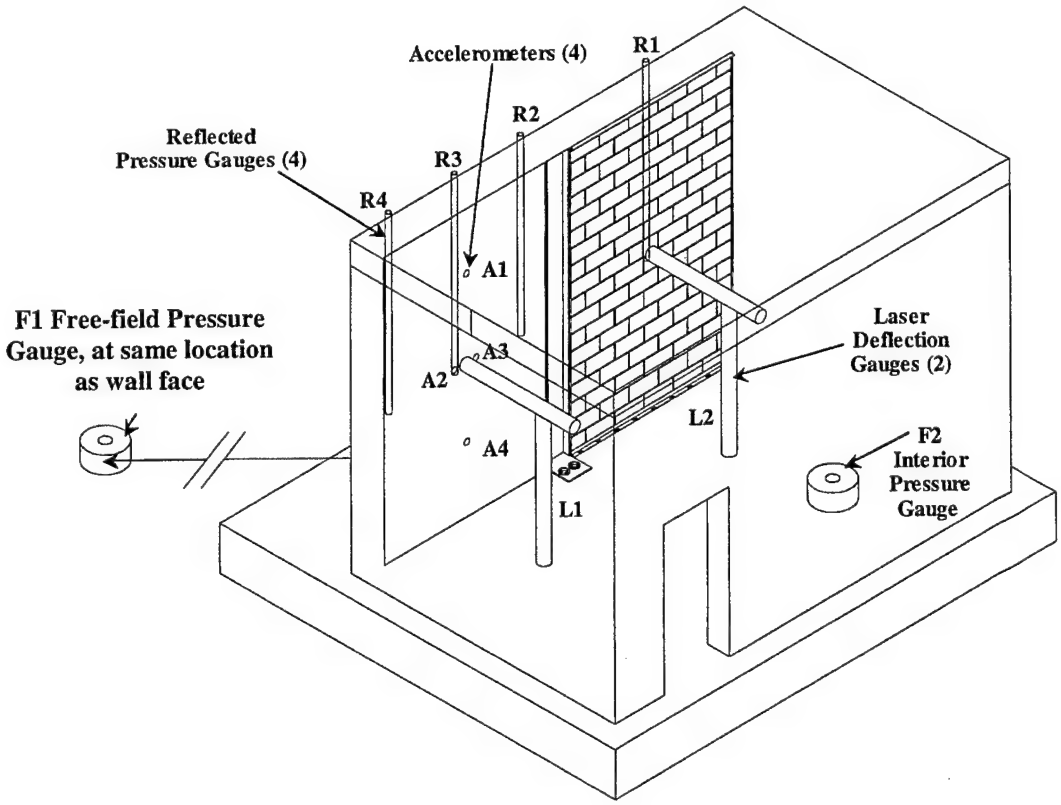

FIG. 42. Test 2, Gauge Locations

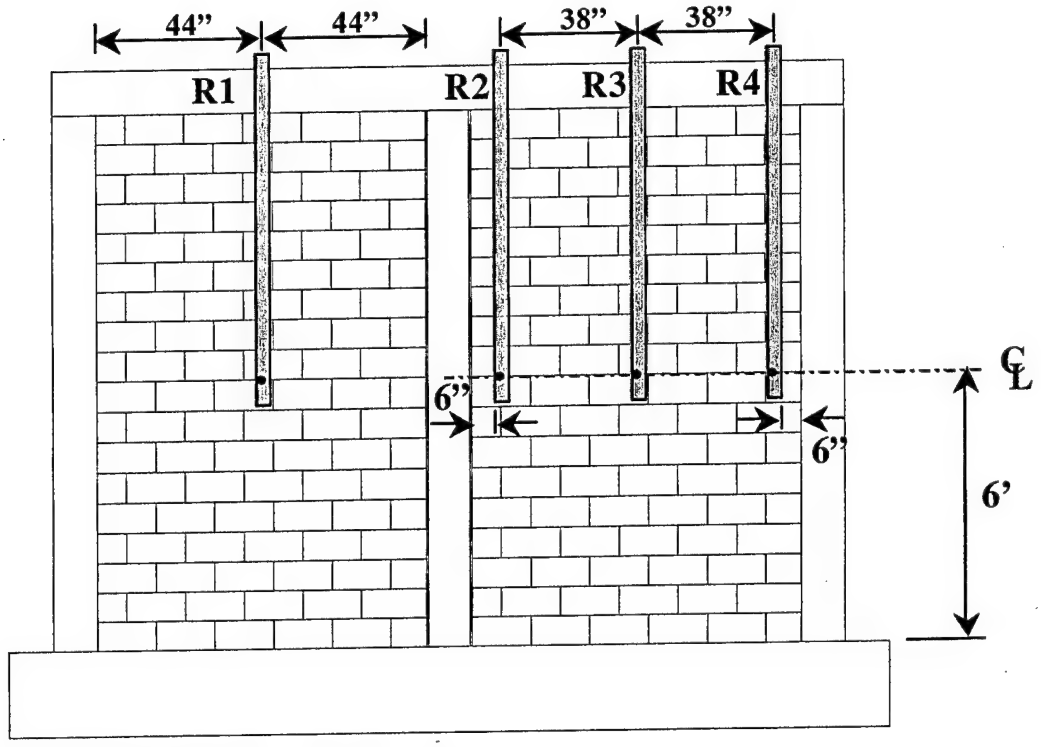

Reflected Pressure Gauges (Exterior View)

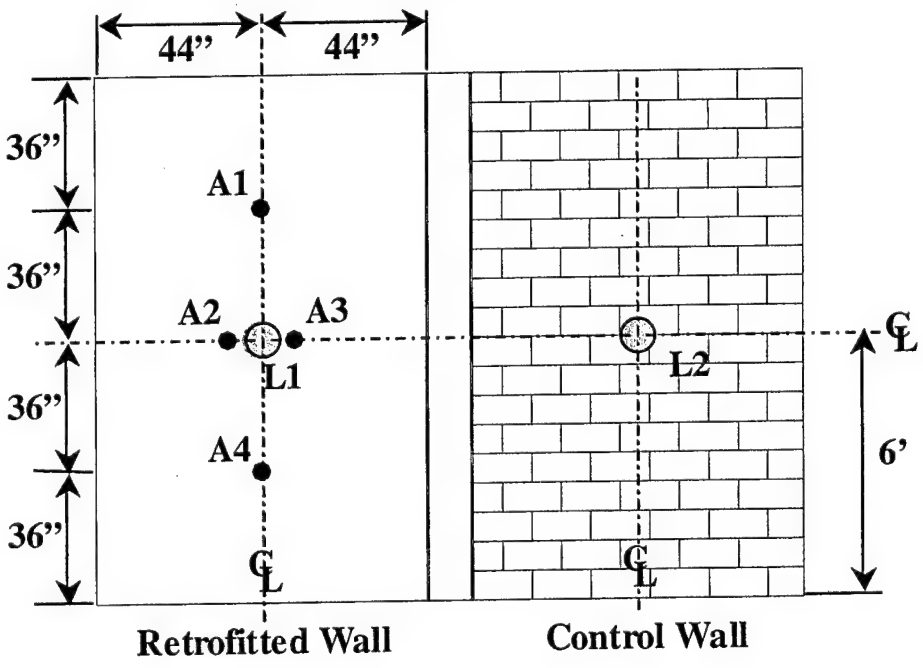

FIG. 43. Test 2, Gauge Details

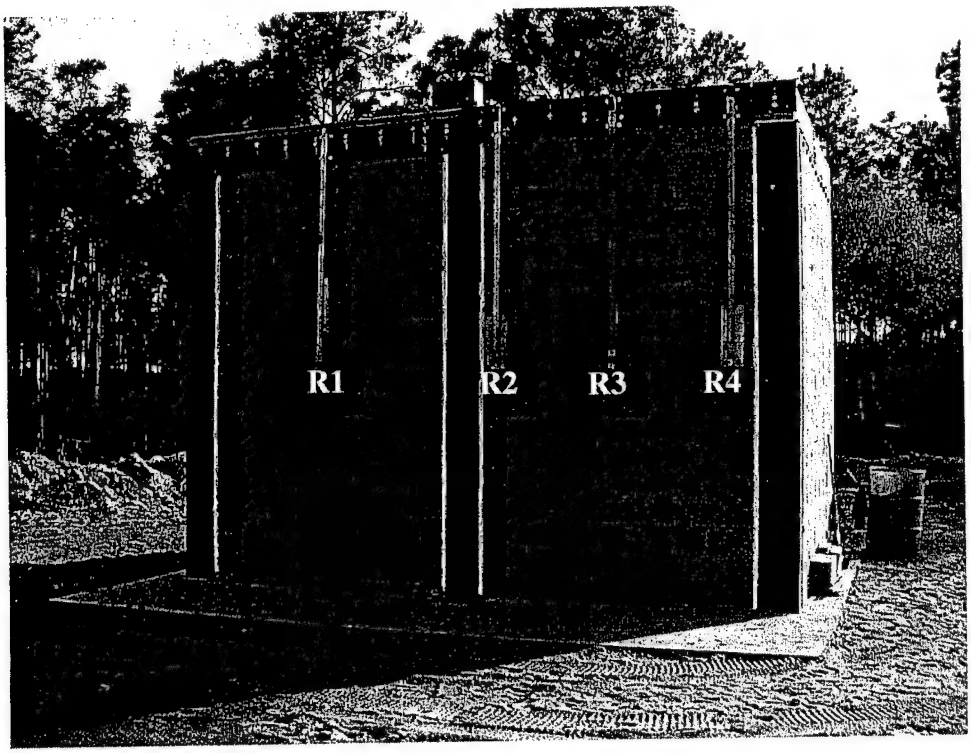

FIG. 44. Test 2, Reflected Pressure Gauges

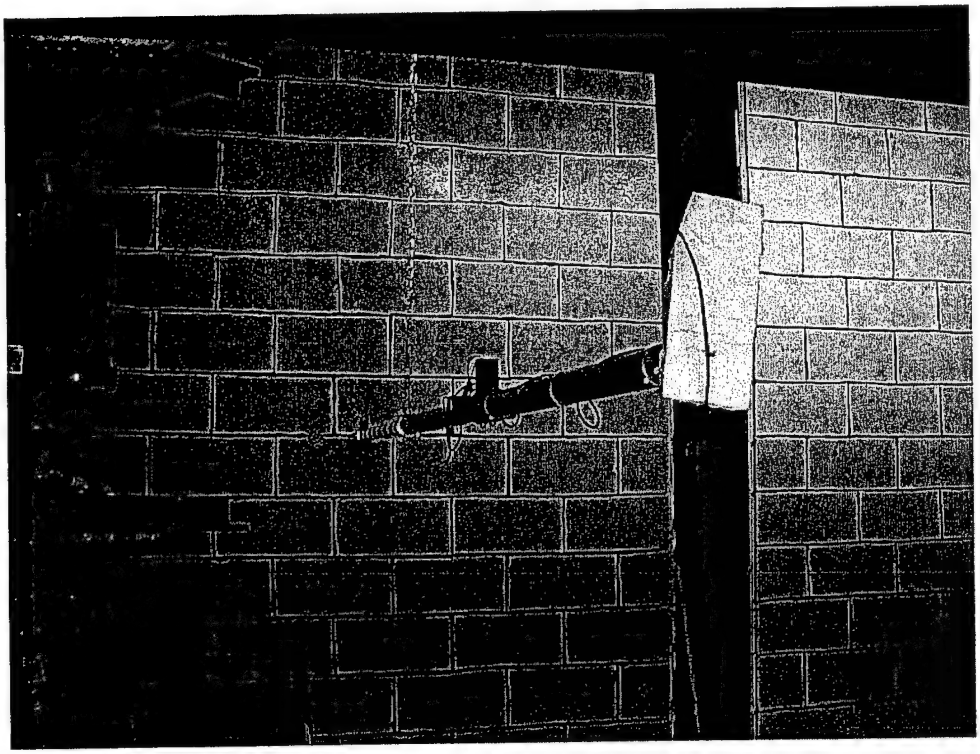

FIG. 45. Test 2, Laser Gauge L1

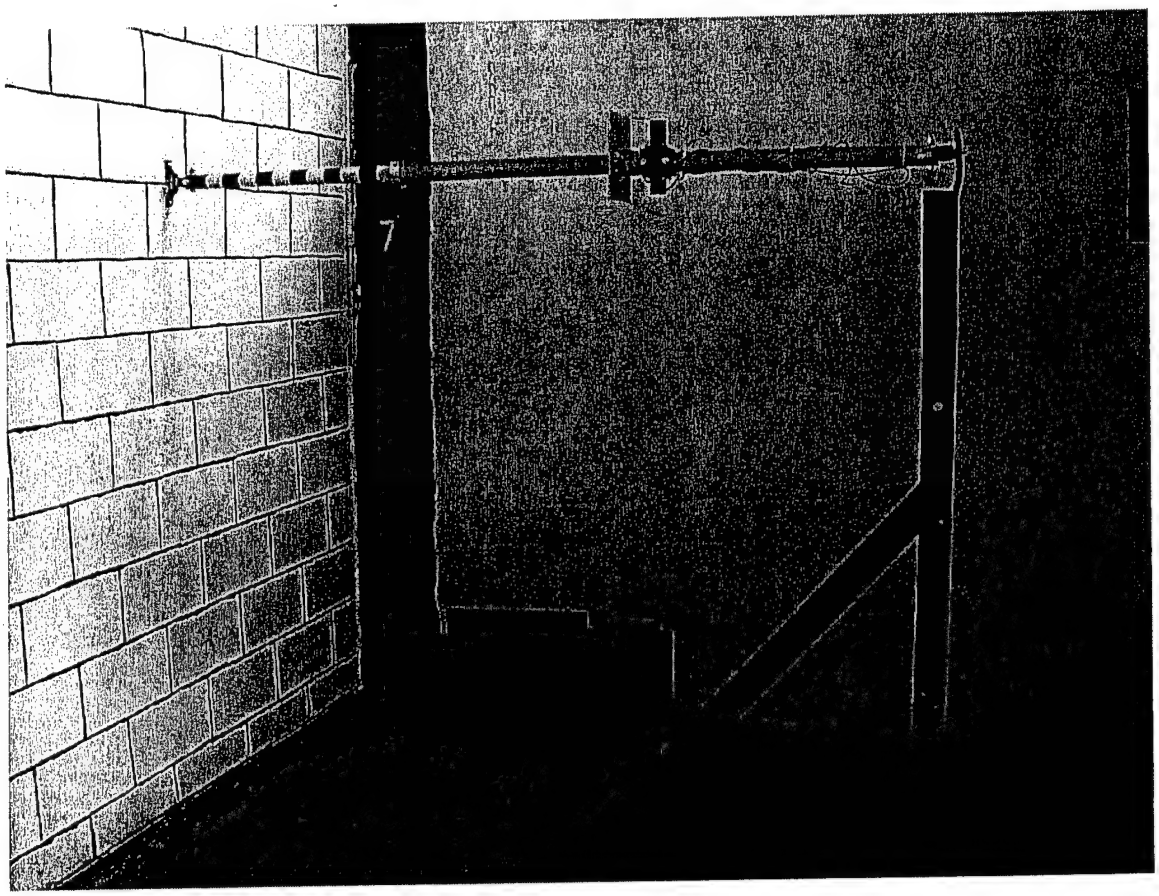

FIG. 46. Test 2, Laser Deflection Gauge L2

Photography instrumentation included pre- and post-test still photography and high-speed photography of the wall deflection. Two high-speed 16 mm cameras were mounted to capture the top and center of the unretrofitted wall at 1000 frames per second. Two spy cameras were directed at the center of each wall. The digital high-speed camera was located outside the structure to capture the response of both test walls at 1000 frames per second. Interior camera targets are shown in Fig. 47. The low speed camera and spy camera are shown in Fig. 48.

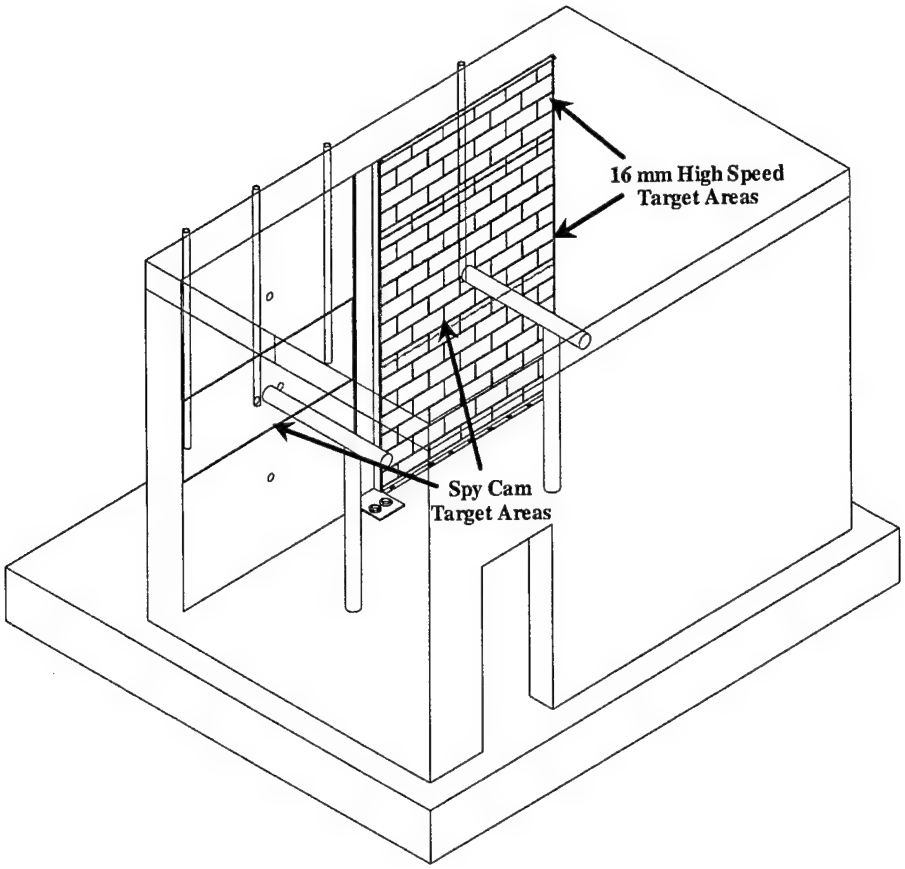

FIG. 47. Test 2, Interior Camera Target Locations

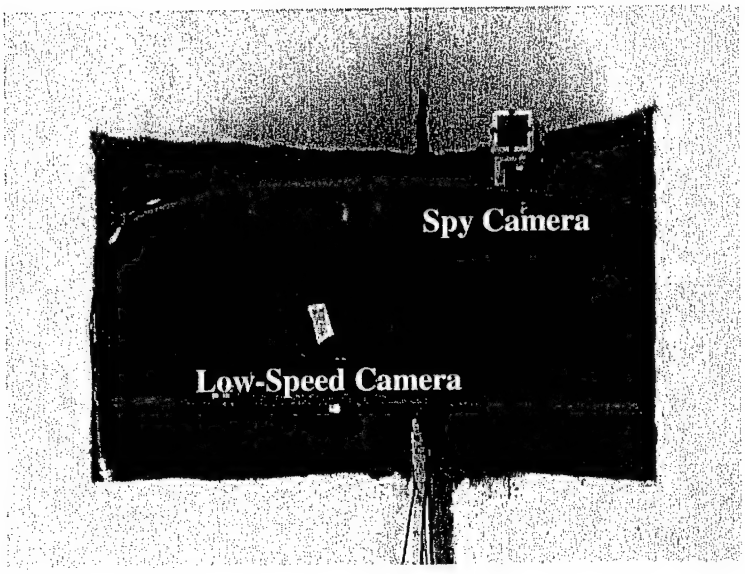

FIG. 48. Test 2, Cameras

The lighting system from Wall Test 1 was evaluated. The two panels from Wall Test 1 were used in this test. A lighting strip of twelve floodlights was added. The increased light increased the quality of images from the cameras. A picture of the new light strip is shown in Fig. 49. The square box with four holes in it is the original lighting system used in Wall Test 1. New bulbs were placed in the device for use in Wall Test 2.

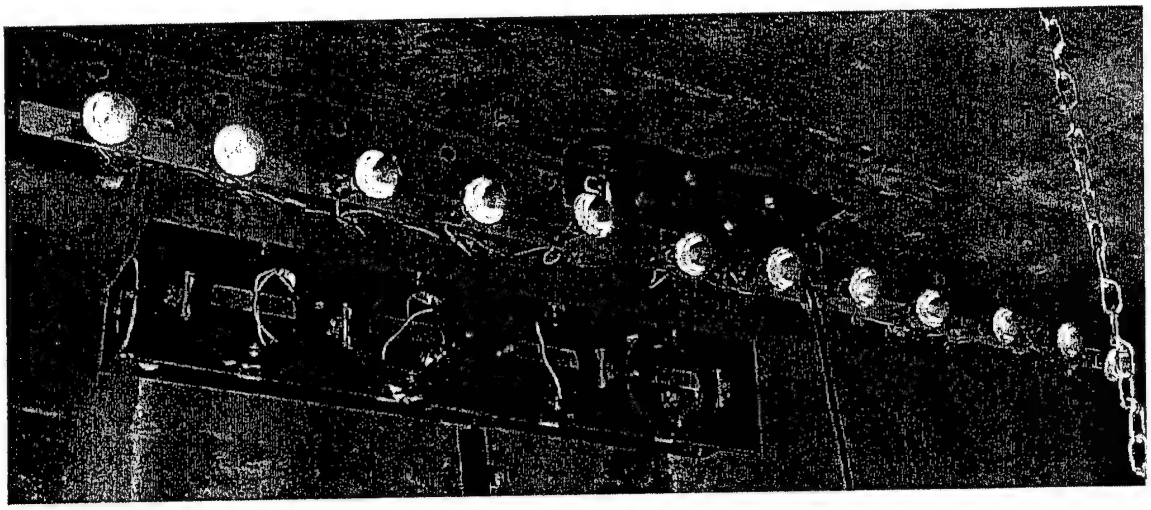

FIG. 49. Test 2, Lighting Fixtures

3.3.3 Results

Gauge predictions were calculated using the WAC software. These predictions are shown in Table 3. There are four reflected pressure gauge predictions, two free-field pressure gauge predictions, two laser deflection gauge predictions, and four accelerometer gauge predictions.

TABLE 3. Test 2, Gauge Predictions

Gauge ID	Type	Location	Prediction
R1	Reflected Pressure	Center of Left Wall	180 psi
R2	Reflected Pressure	Center of Structure	186 psi
R3	Reflected Pressure	Center of Retrofitted Wall	180 psi
R4	Reflected Pressure	Edge of Structure	180 psi
F1	Free-field Pressure	Outside Structure	51 psi
F2	Free-field Pressure	Inside Structure	4 psi
L1	Laser Deflection	Center Polymer Wall	20 in. inward, 12 inward. out
L2	Laser Deflection	Center Control Wall	20 in. inward, 2 in. outward
A1	Accelerometer	Upper Polymer Wall	704 g's
A2	Accelerometer	Center Left Polymer Wall	704 g's
A3	Accelerometer	Center Right Polymer Wall	704 g's
A4	Accelerometer	Lower Polymer Wall	704 g's

Both the control wall and retrofit wall panels collapsed in this test. Mortar layers at mid-height of the wall experienced the highest stresses and failed in tension. The steel beam separating the walls was bent. In addition to the walls being destroyed, there was damage to the reaction structure.

Due to the increased explosive charge in this test, some of the gauges were damaged and did not function properly. The laser deflection gauges did not record data. The accelerometers also failed. Results from the reflected pressures gauges are shown below in Figs. 50 through 53. Results from free-field pressure gauges follow in Figs. 54 and Fig. 55.

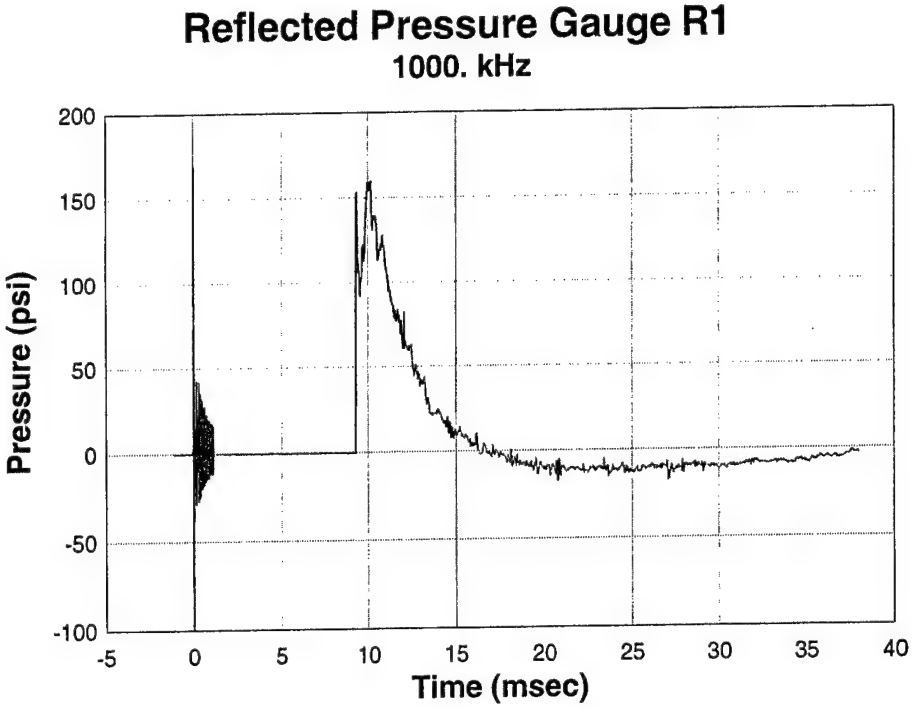

FIG. 50. Test 2, Gauge R1

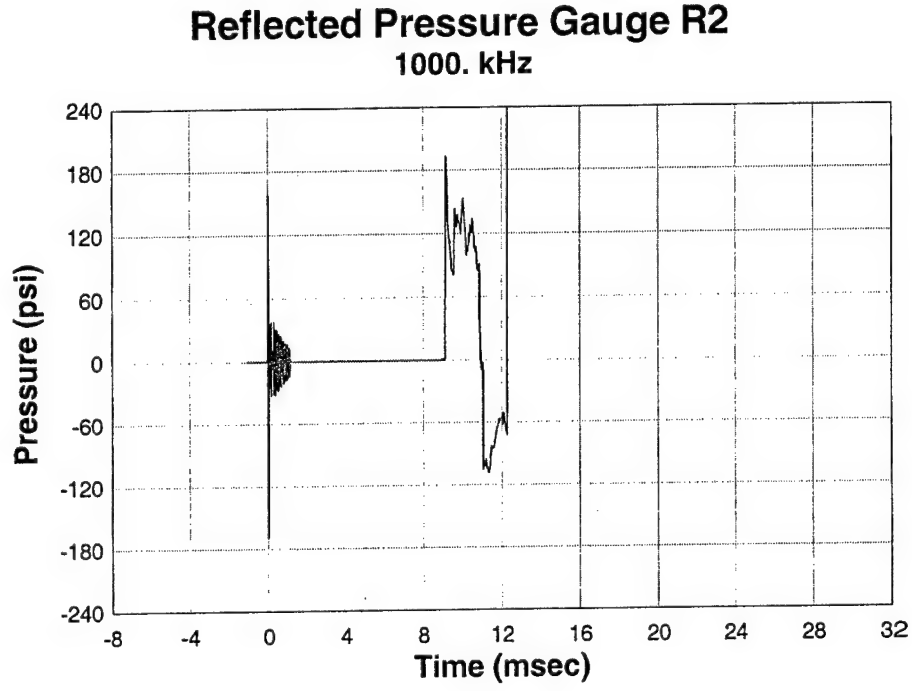

FIG. 51. Test 2, Gauge R2

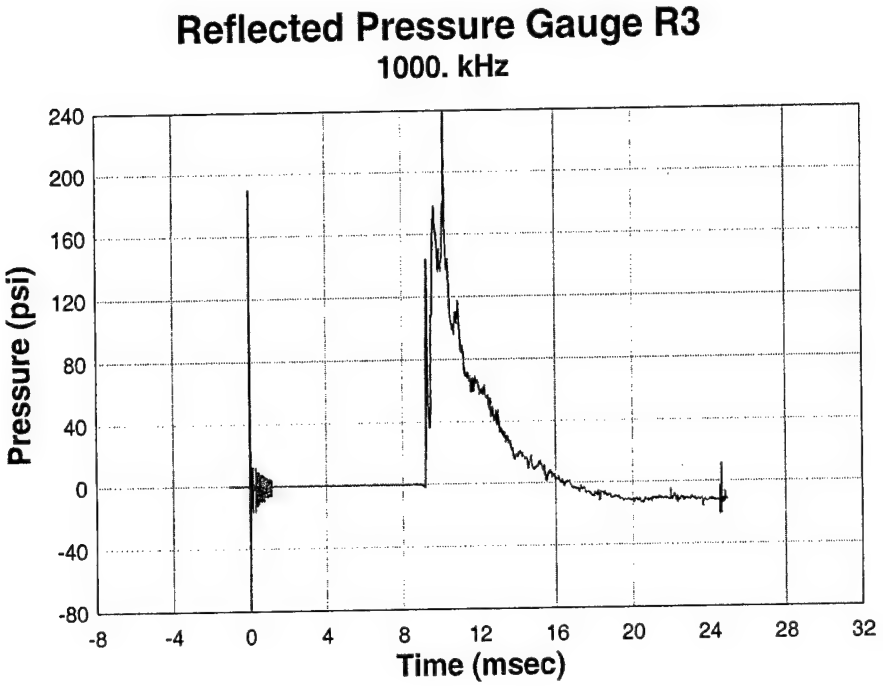

FIG. 52. Test 2, Gauge R3

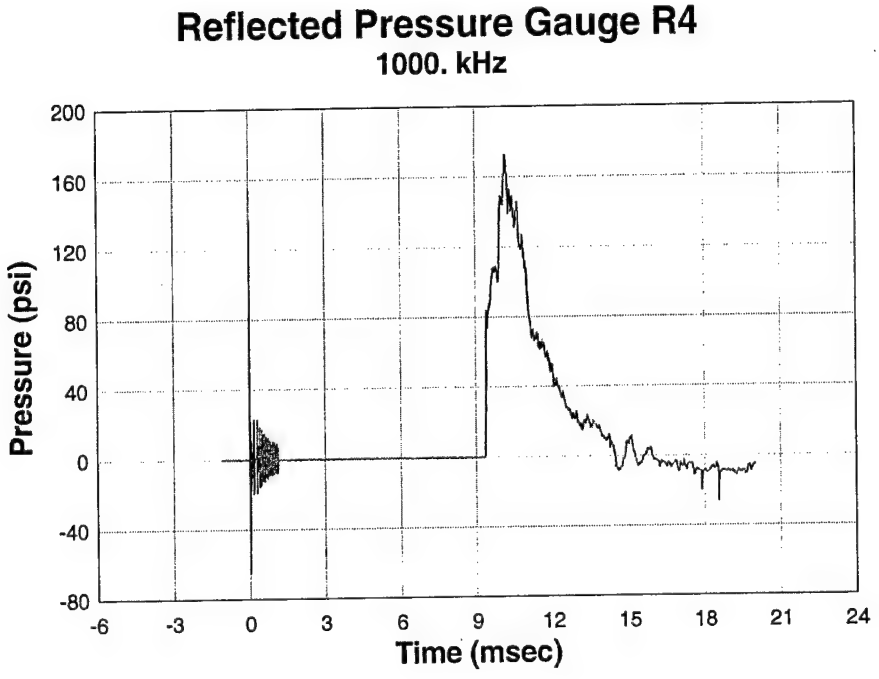

FIG. 53. Test 2, Gauge R4

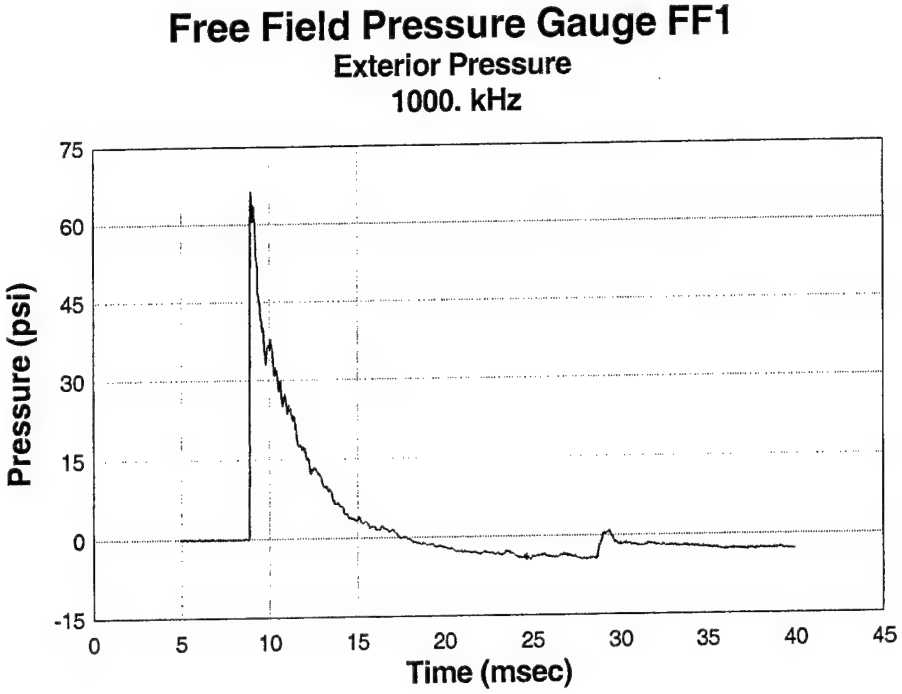

FIG. 54. Test 2, Gauge F1

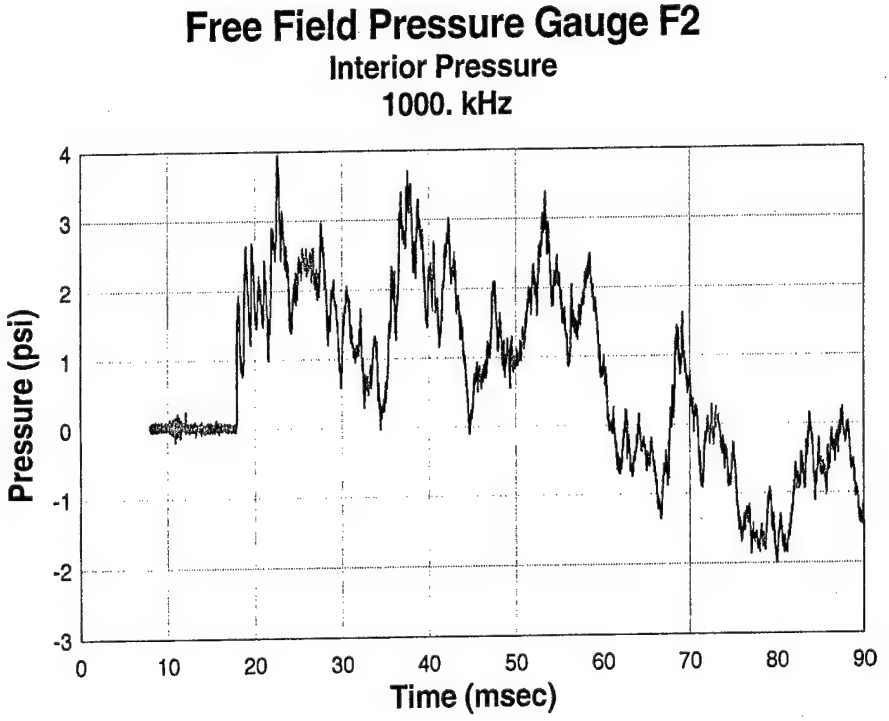

FIG. 55. Test 2, Gauge F2

The maximum pressures recorded by the pressure gauges were (R1) 159 psi at 10.0 msec, (R2) 192 psi at 9.2 msec, (R3) 238 psi at 10.3 msec, and (R4) 174 psi at 10.2 msec. The maximum pressures recorded by the pressure gauges were (F1) 66 psi at 8.9 msec and (F2) 4.0 psi at 22.7 msec. The laser deflection gauges and accelerometers failed in the test. Table 4 compares all of the predicted gauge measurements to actual gauge readings.

TABLE 4. Test 2, Predicted vs. Recorded Data

Gauge ID	Type	Prediction	Actual
R1	Reflected pressure	180 psi	159 psi
R2	Reflected pressure	186 psi	192 psi
R3	Reflected pressure	180 psi	238 psi
R4	Reflected pressure	180 psi	174 psi
F1	Free-field pressure	51 psi	66 psi
F2	Free-field pressure	4 psi	4 psi
L1	Laser deflection	20 in. inward, 12 in. outward	Gauge Failure
L2	Laser deflection	20 in. inward, 12 in. outward	Gauge Failure
A1	Accelerometer	704 g's	Gauge Failure
A2	Accelerometer	704 g's	Gauge Failure
A3	Accelerometer	704 g's	Gauge Failure
A4	Accelerometer	704 g's	Gauge Failure

Fig. 56 shows the post-test reaction structure. The damage to the reaction structure is evident. Fig. 57 shows a side view of the reaction structure. Fig. 58 shows the debris of the control wall, while Fig. 59 shows the debris of the retrofitted wall. Many of the retrofitted blocks were held together by the polymer coating. Fig. 60 shows how the blocks failed in tension. The large cracks where the blocks debonded are shown. Fig. 61 shows the piece of retrofit material after debris was removed. This image shows where the retrofit failed.

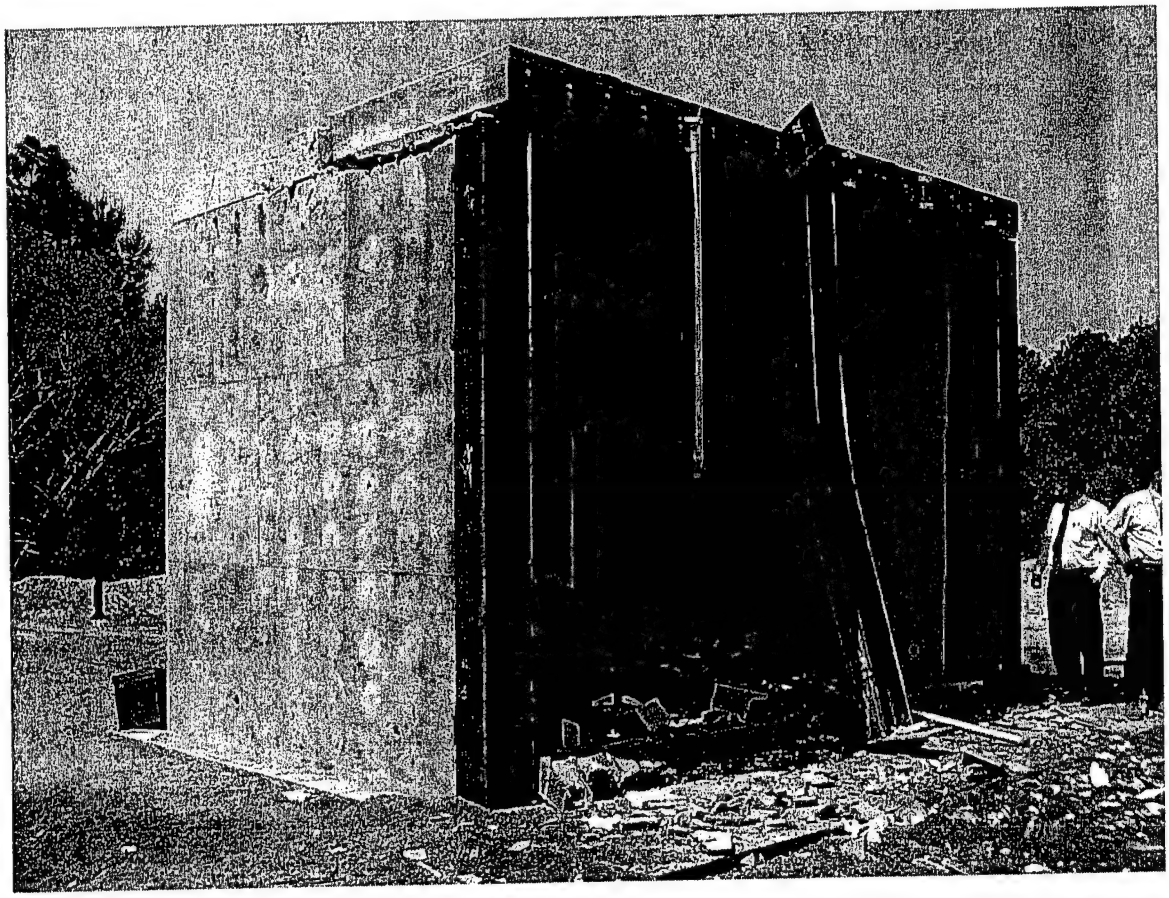

FIG. 56. Test 2, Post-Test Structure

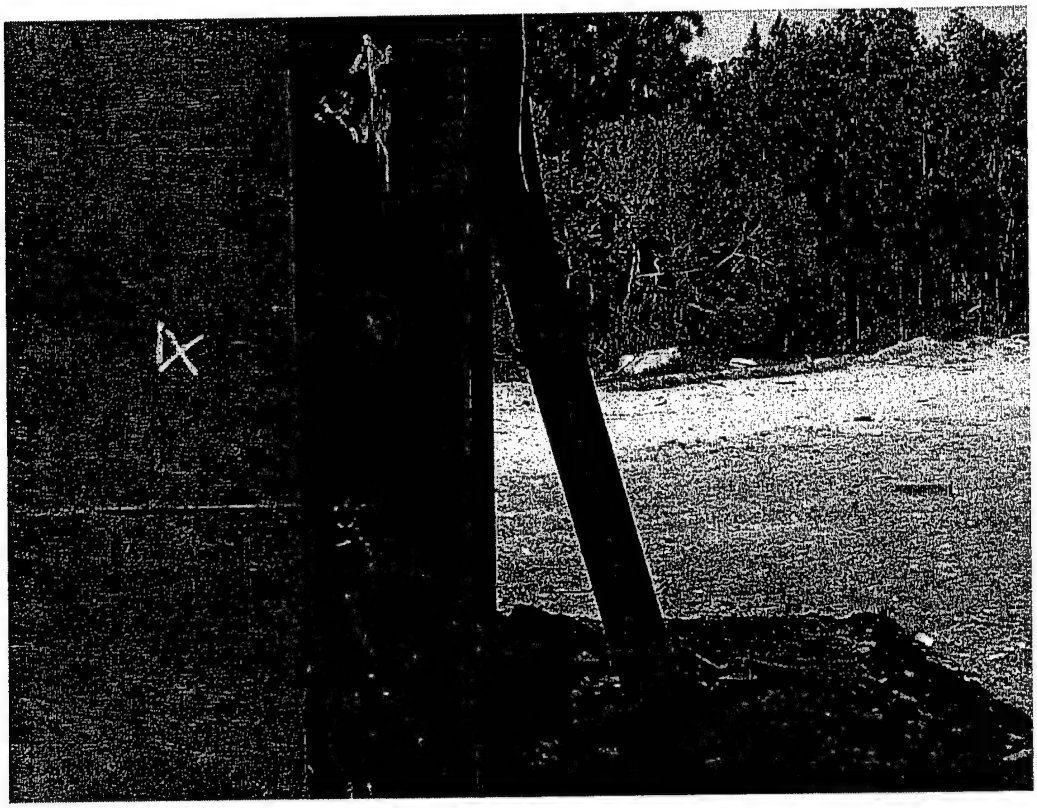

FIG. 57. Test 2, Bent I-Beam

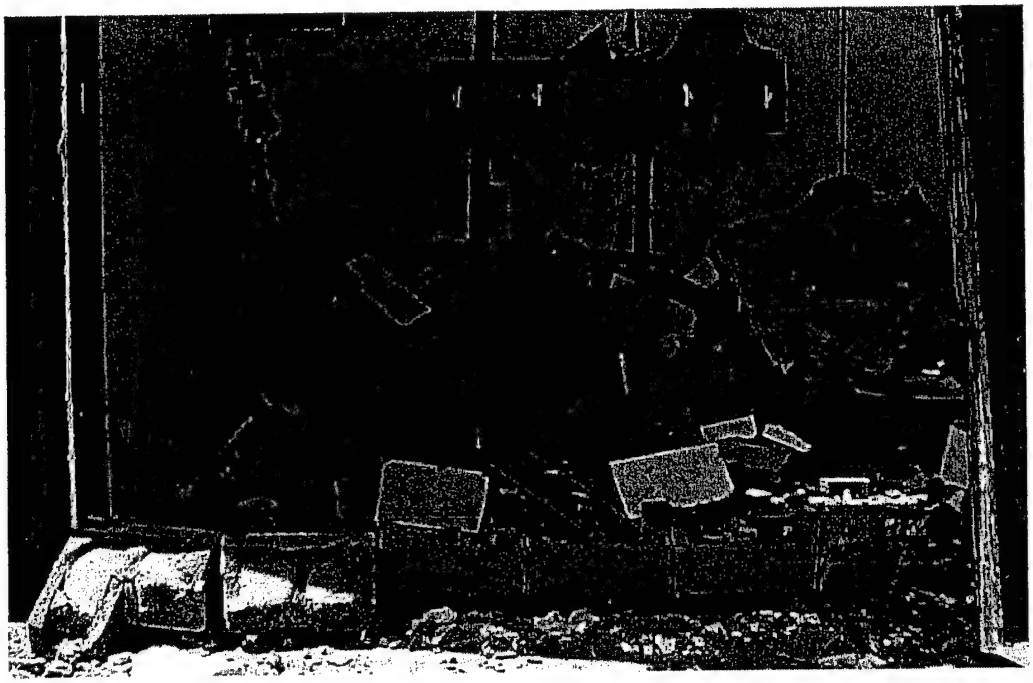

FIG. 58. Test 2, Unretrofitted Wall Debris

FIG. 59. Test 2, Retrofitted Wall Debris

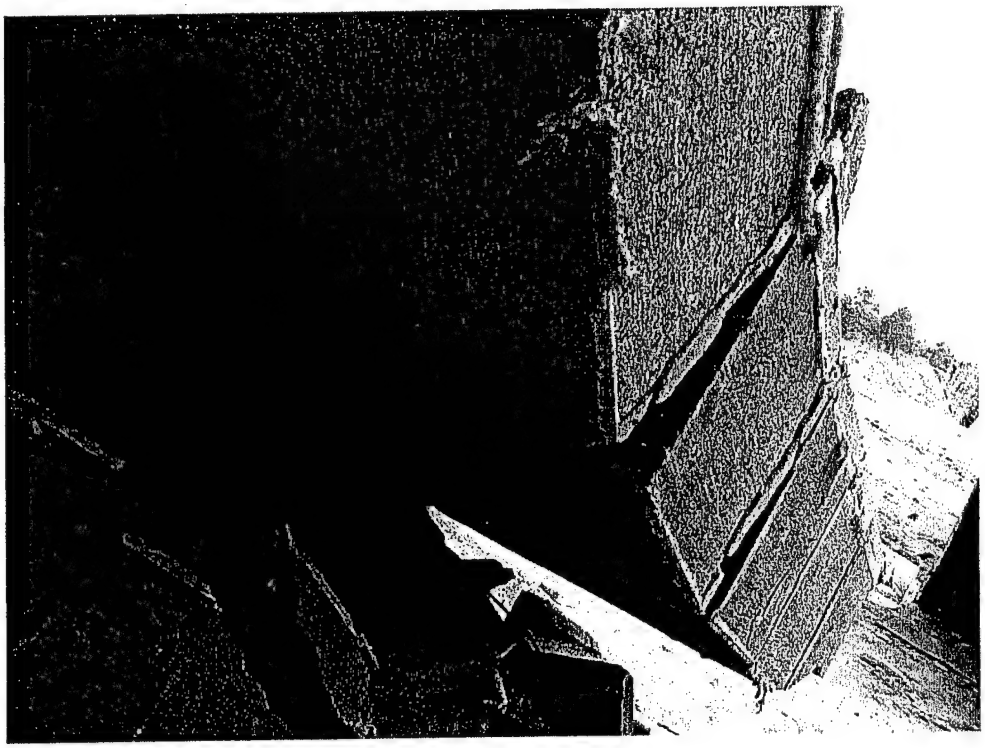

FIG. 60. Test 2, Bending of Retrofit Wall

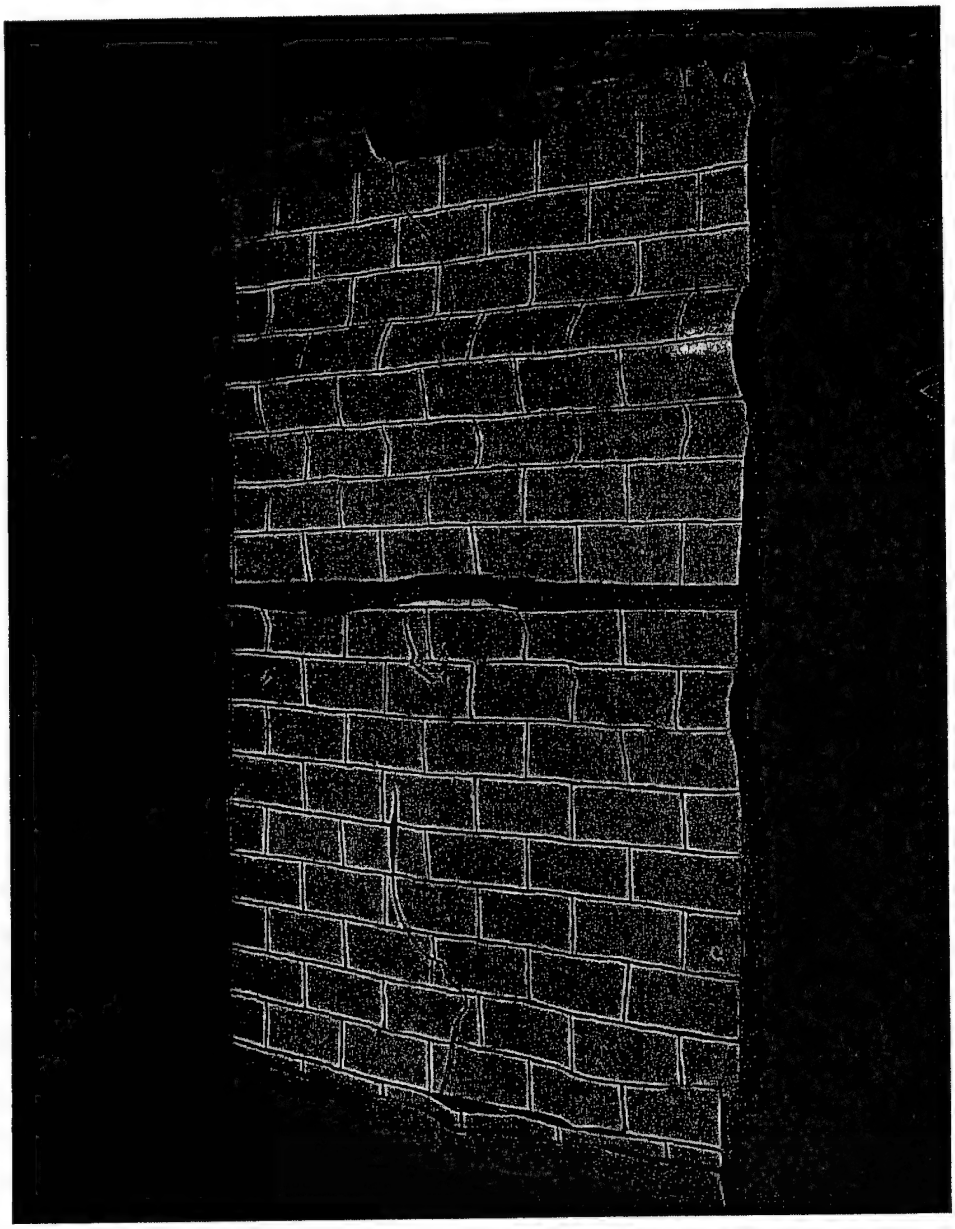

FIG. 61. Test 2, Post-Test Retrofit Material

The interior of the right (west) wall was retrofitted. The left (east) wall was painted, and the blocks were outlined. Both of the wall panels were destroyed. In addition, the reaction structure and many of its components were damaged. Although the polymer did not prevent collapse, it kept many pieces of the debris together.

3.4 Wall Test 3

Wall Test 3 involved an explosive test on four URM walls retrofitted with an elastomeric polymer coating using different application thicknesses and connection overlaps. The key objectives of Wall Test 3 were to (1) evaluate the application process for the polymer coating; (2) measure the deflection of key wall elements; (3) evaluate the failure modes for the four test walls; (4) evaluate influence of polymer application to one versus two sides; and (5) evaluate responses from the two aspect ratios, larger walls vs. smaller cubicles. The test layout can be seen in Fig. 62.

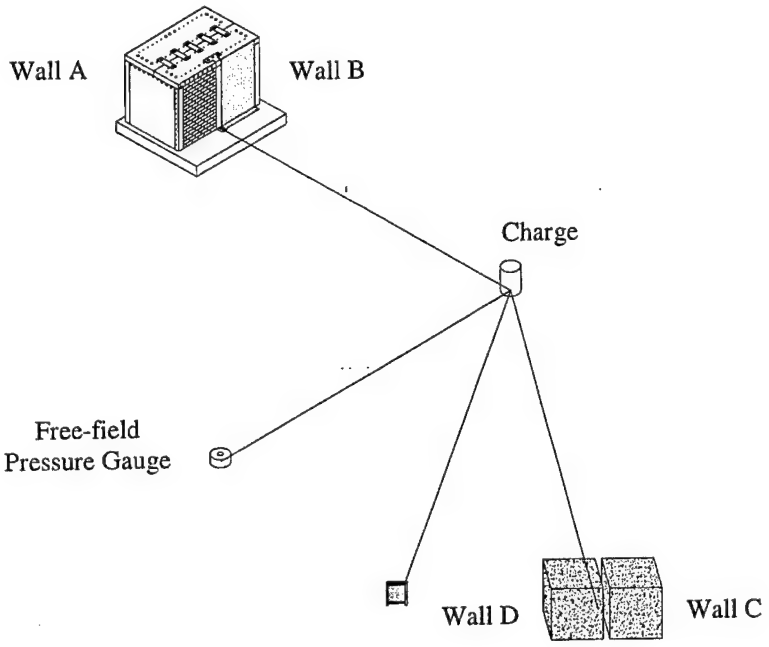

FIG. 62. Test 3 Layout

Test 3 included three reaction structures. The permanent reaction structure contained two walls. Two additional walls were constructed in mobile reaction structures. The charge size was the same as that of Test 2, but the standoff distance was increased so that the walls were subjected to a loading between that of Test 1 and Test 2

Several tasks were completed after Wall Test 2 to proceed to Wall Test #3: (1) masonry debris from Wall Test 2 was removed; (2) the center I-beam, roof cladding, and roof and floor angle on the unretrofitted wall were removed; (3) the roof slab was removed from the test structure side wall; (4) side walls were repaired; (5) the front roof slab was reinstalled; and (6) the damaged light frames were removed.

3.4.1 Construction

Walls A and B: The two walls constructed in the first structure were 7 ft 6 in. by 12 ft and were separated by a 12 in. x 12 in. x 1/2 in. steel tube (Fig. 63). The interior of Wall A was retrofitted with ¼-in. elastomeric coating that overlapped the roof and floor slabs 12 in. Wall B was retrofitted with 1/8-in. elastomeric coating on its interior and exterior. The thinner coating overlapped the roof and floor slabs by 12 in. Both walls were allowed to move freely on the sides to approximate a one-way flexural response.

Walls C and D: Two additional 10 ft x 10 ft cubicles each had an 8 ft x 8 ft wall constructed within (Fig. 64). The standoff distance from the blast to Walls C and D was the same as the distance to Walls A and B. Both walls in the cubicles were retrofitted with 1/8 in. elastomeric coating. Wall C had a 6 in. overlap onto the roof and floor slabs, while Wall D was overlapped 12 in. Both cubicle walls were constructed to approximate a one-way flexural response.

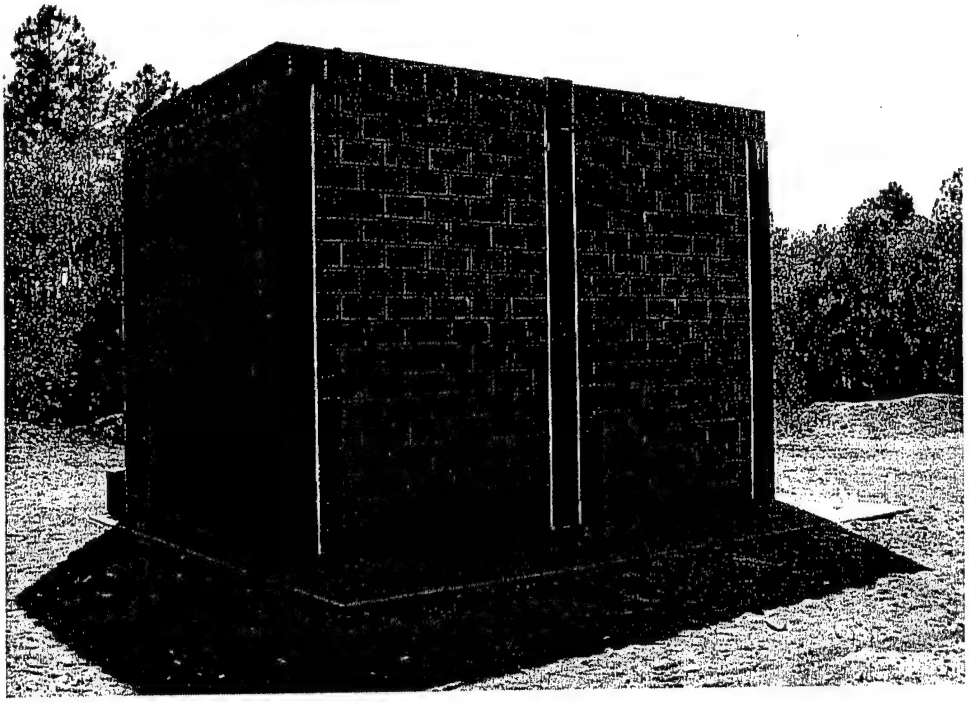

FIG. 63. Test 3, Constructed Test Structure

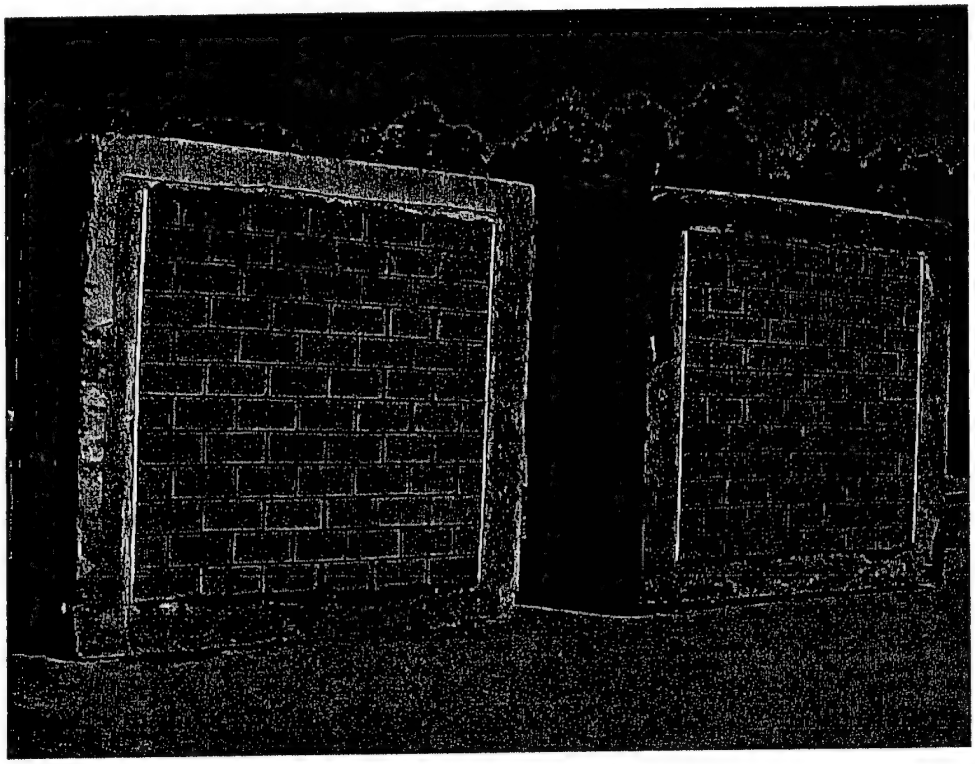

FIG. 64. Test 3, Individual Cubicles

Permanent Structure: A center divider was fabricated for the test structure. It consisted of a 12 in. x 12 in. x 1/2 in. steel tube and a ½-in. piece of flat steel. The center divider had a welded top base that overlapped onto the front roof slab. The top was secured using original holes and bolts. The bottom base of the center divider was also welded to the steel tube and was secured to the floor slab with anchor bolts. The divider was complete with pre-drilled holes for pressure gauges on the outside and gauge installation on the inside. This center divider is shown as a drawing in Fig. 65 and installed in Fig. 63.

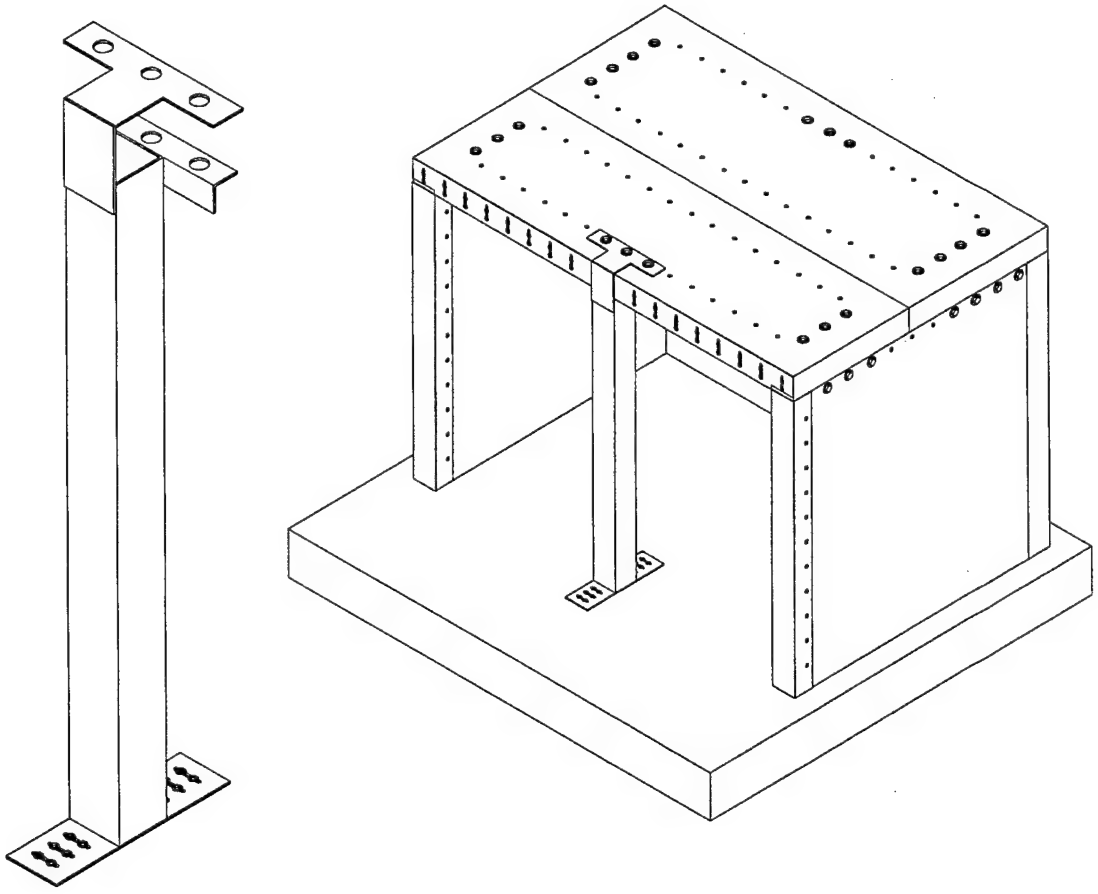

FIG. 65. Test 3, Center Divider

Foam insulation board insured that the URM walls were separated from the test structure. Residue from adhesive used to attach foam board in Wall Test 2 was removed. The test structure was thoroughly cleaned. New ¾-in. foam insulation board was installed on both side walls, on the sides of the center divider of Walls A and B, and also on both side walls of Walls C and D. Caulking was applied between the structures and the foam insulation board to prevent the entering of dust. A thorough cleaning after construction also helped reduce dust during testing. (Control of dust is important for photography during tests.)

A piece of pre-drilled, flat steel was welded to the bottom of the existing angle connecting the roof to the side wall. This was done to eliminate cracks near the bolt holes close to the edge of the structure. A 6 in. x 6 in. x 1/2 in. angle was welded between the angles connecting the roof to side walls as illustrated in Fig. 66 and Fig. 67.

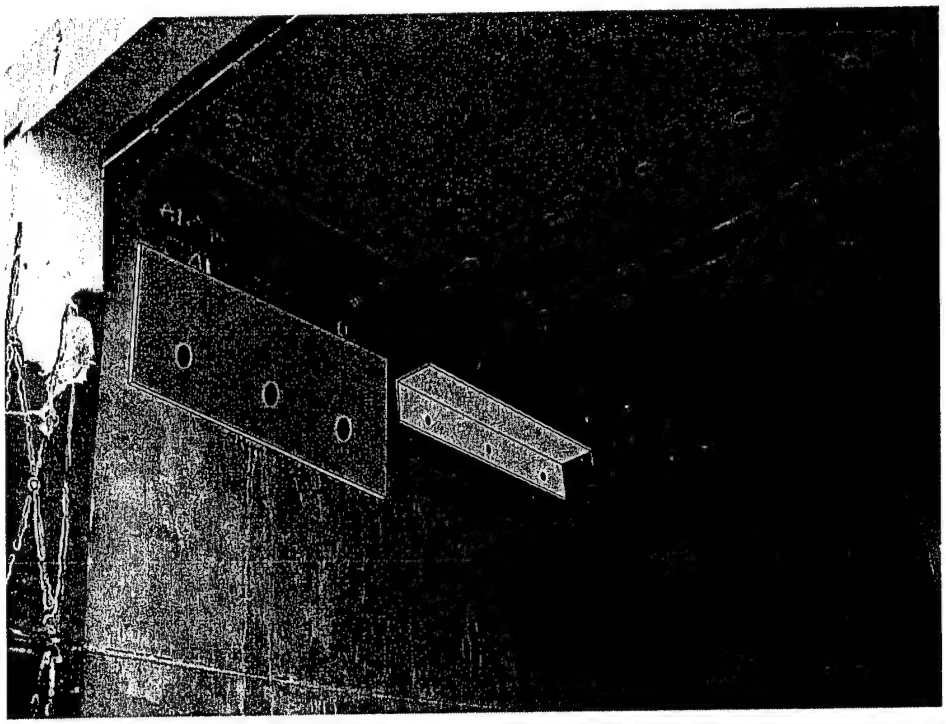

FIG. 66. Test 3, Roof Connection Modifications

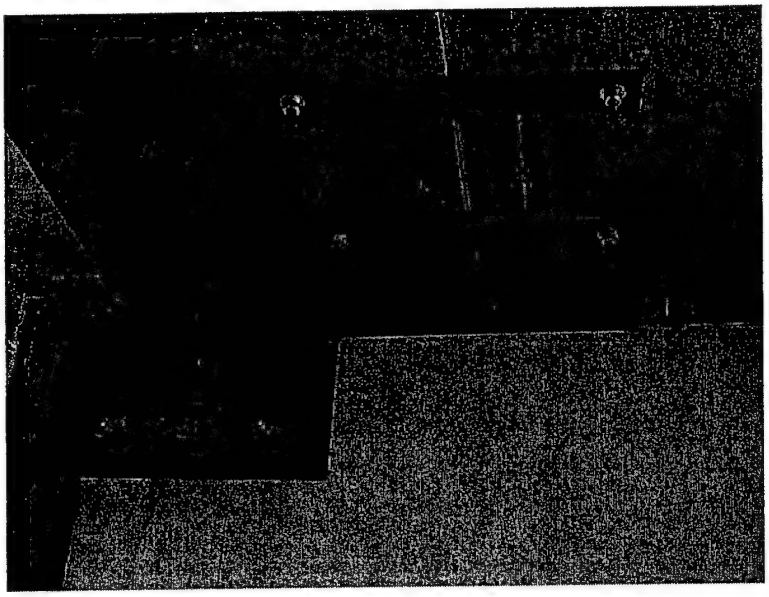

FIG. 67. Test 3, Roof Connection Modifications Installed

Roof cladding was damaged in Wall Test #2. New cladding was fabricated to strengthen the structure. The new cladding was similar to the original design. Cladding above Wall B was not installed because polymer was applied to the outside of the wall and overlapped the roof slab by 12 in. An image of the new cladding is shown in Fig. 68. Top roof slabs were joined with ¼ in. pre-drilled flat steel strips. These strips and their locations on the roof are shown in Fig. 69.

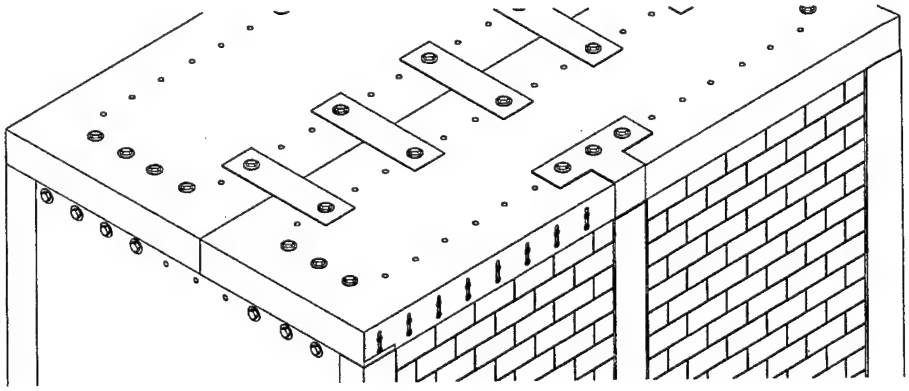

FIG. 68. Test 3, Roof Cladding

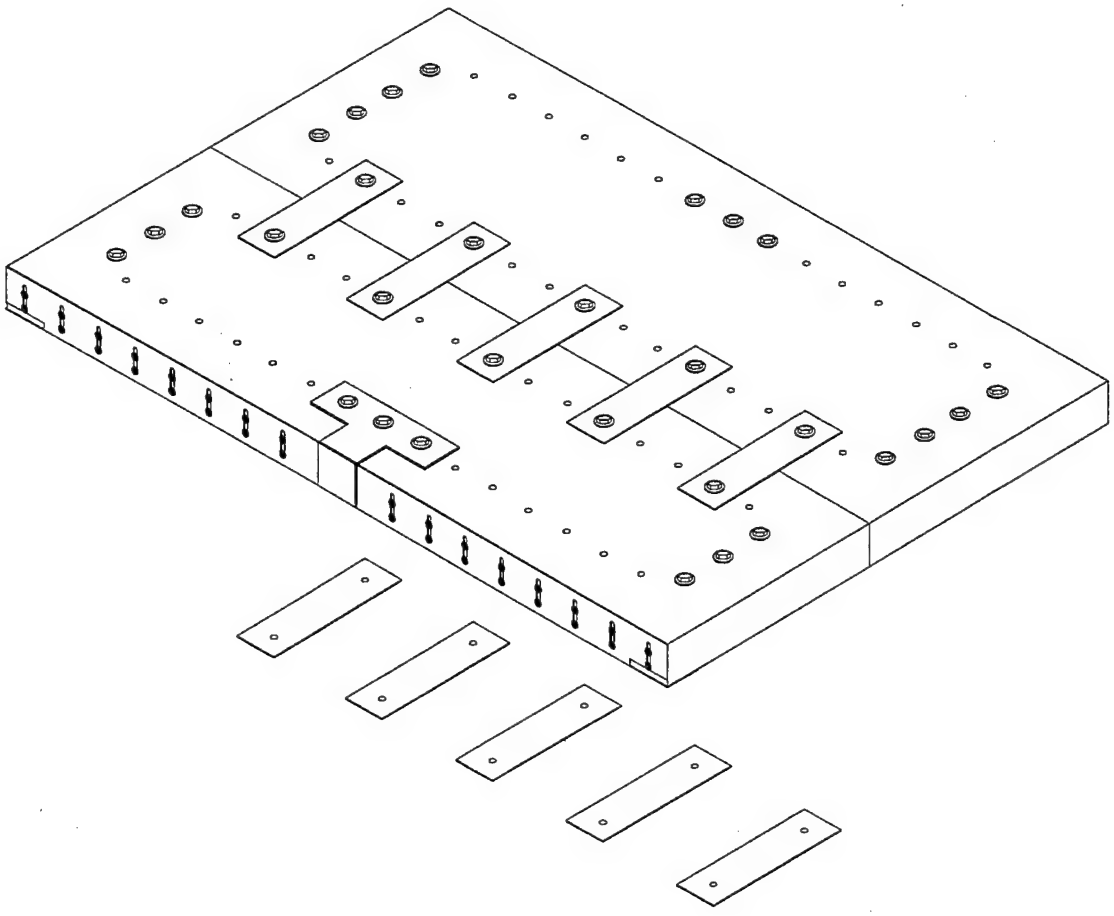

FIG. 69. Test 3, Roof Connections

To insure a strong bond between the walls and the retrofit, the test structure and cubicles were thoroughly cleaned with a solution of muratic acid and water. The cleaning with the muratic acid did not eliminate the need for preparation work as required for proper adhesion of materials used during construction. After the cleaning and the preparation work were complete, the polymer coating was applied. The application process is shown in Fig. 70. The polymer-coated structure is shown in Fig. 71. The floor overlap of the polymer is shown in Fig. 72.

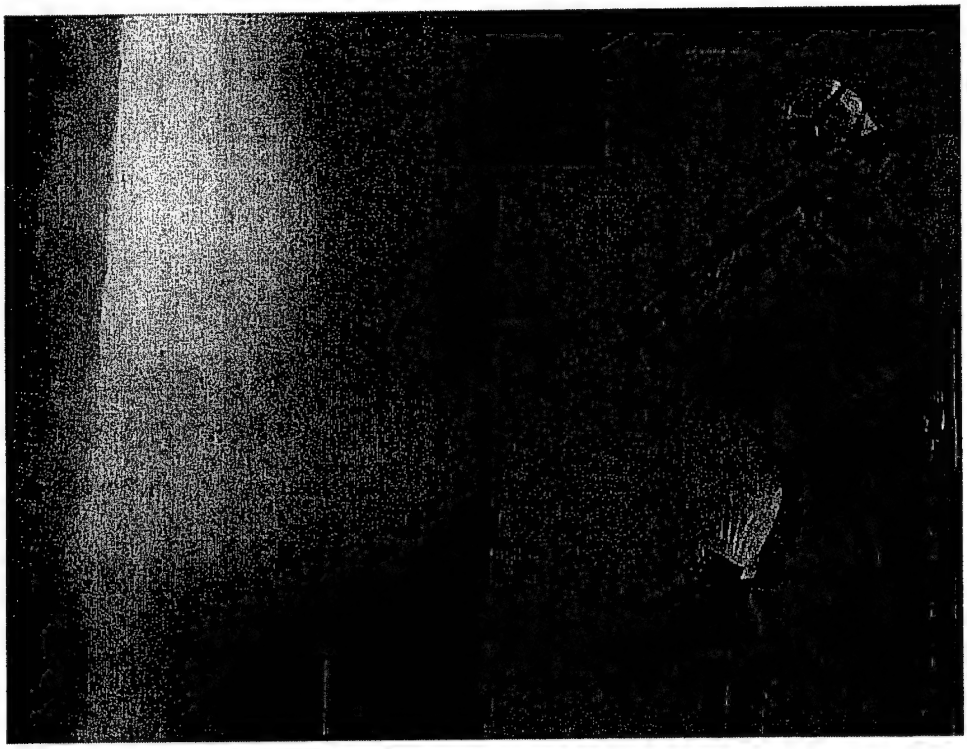

FIG. 70. Test 3, Polymer Application

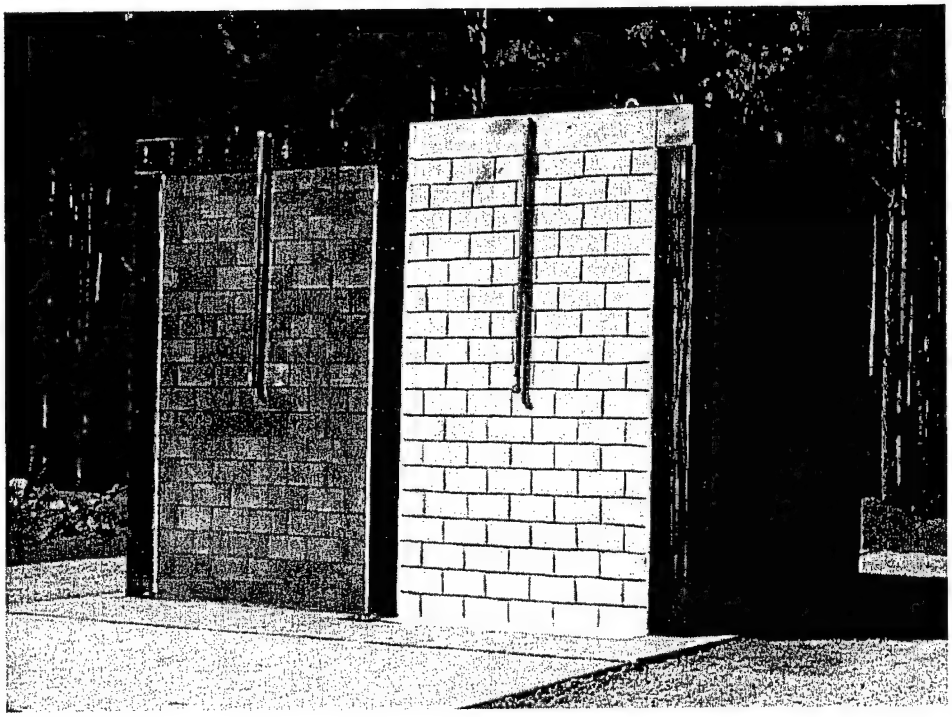

FIG. 71. Test 3, Walls A and B, Ready for Testing

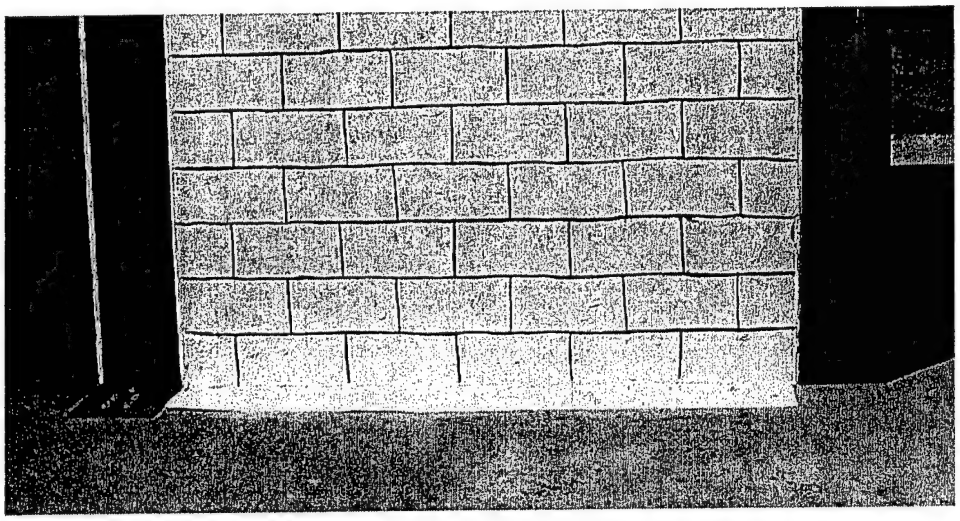

FIG. 72. Test 3, Wall B Floor Overlap

3.4.2 Instrumentation

Gauge instrumentation used in Wall Test 3 included five reflected pressure gauges (R1, R2, R3, R4, R5), one free-field pressure gauge (F1), one accelerometer (A1), and four laser deflection gauges (L1, L2, L3, L4). Gauge layouts and locations are shown in Figs. 73 and 74.

The permanent test structure contained three of the five reflected pressure gauges (R1 through R3). One was located in the center of the steel divider, 6 ft off the ground. The other two were encased in pipes suspended from the top of the test structure, one in the center of each URM wall, 6 ft off the ground. The other two reflected pressure gauges (R4 through R5) were pipe mounted in the two test cubicles, one in the center of each URM wall, 5 ft off the ground. Pipes used to encase the pressure gauges were held in place by pipe mounts (two per pipe). On the permanent test structure, these pipe mounts were secured to the roof cladding. On the test cubicles, the mounts were secured to anchor bolts and Styrofoam (to reduce ringing).

One free-field pressure gauge (F1) was located out from the charge at the same distance the test structures were located. The accelerometer (A1) was located in a polymer-covered steel structure. Placement of the pressure gauge and accelerometer is shown in Figs. 73 and 74.

There were two laser gauges located in the permanent test structure (L1 and L2), and one in each of the two cubicles (L3 and L4). The location of the laser gauges is shown in Figs. 73 and 74 below. An image of a scratch gauge, used to measure deflection in case the laser gauge was destroyed, is shown in Fig. 75.

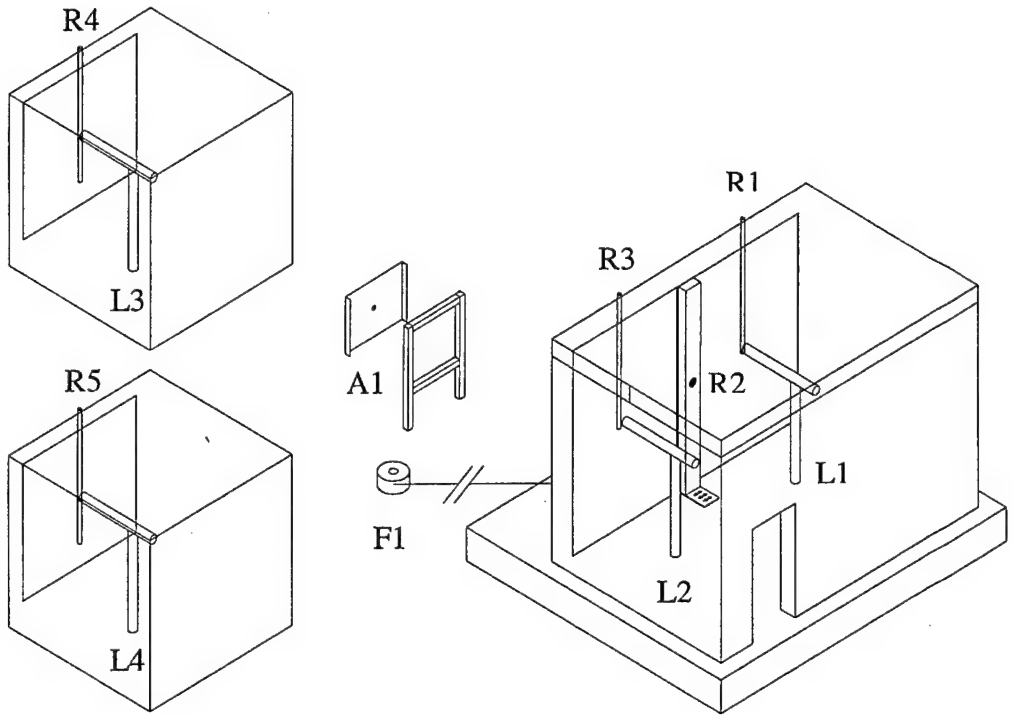

FIG. 73. Test 3, Gauge Locations

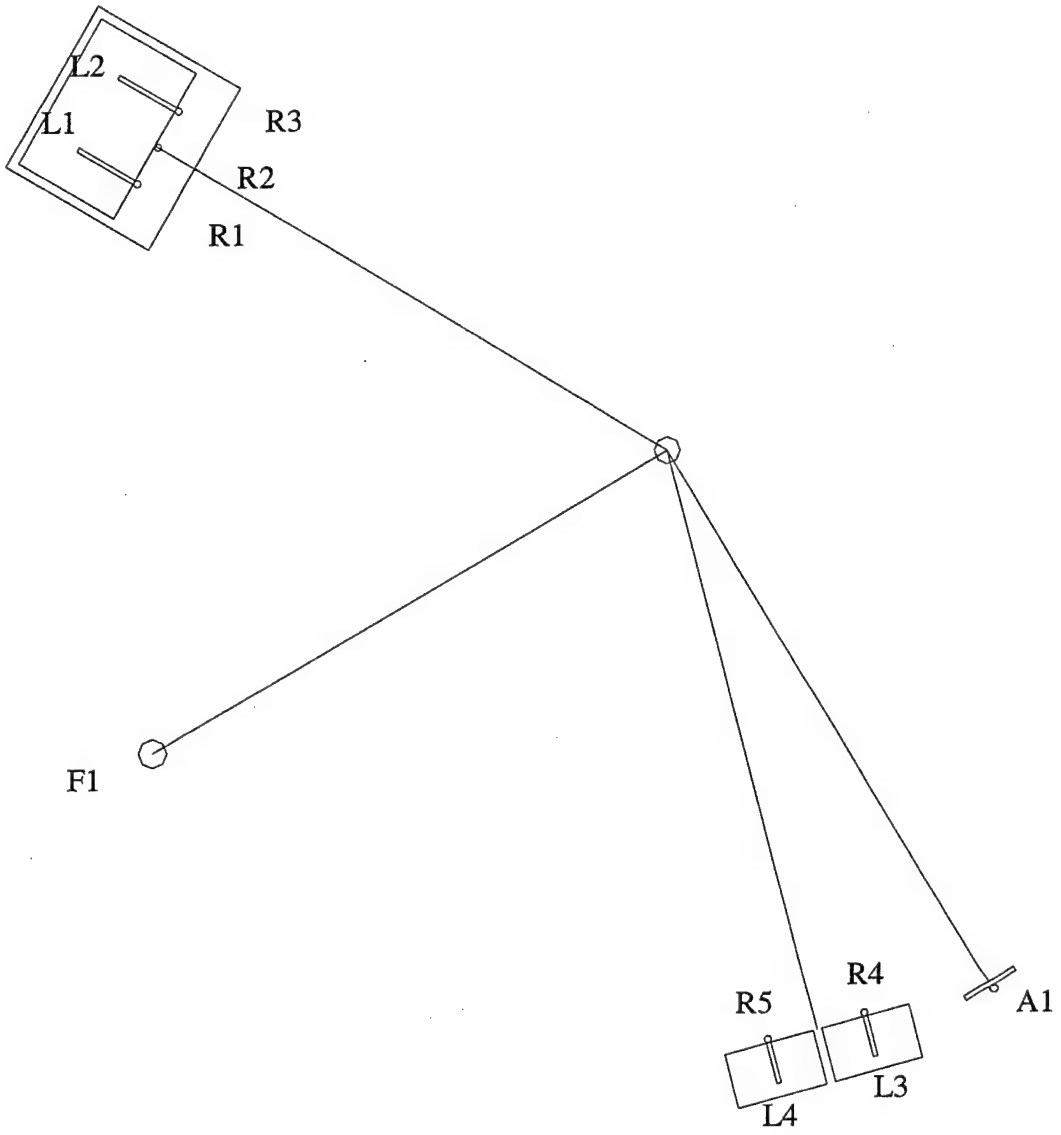

FIG. 74. Test 3, Gauge Details

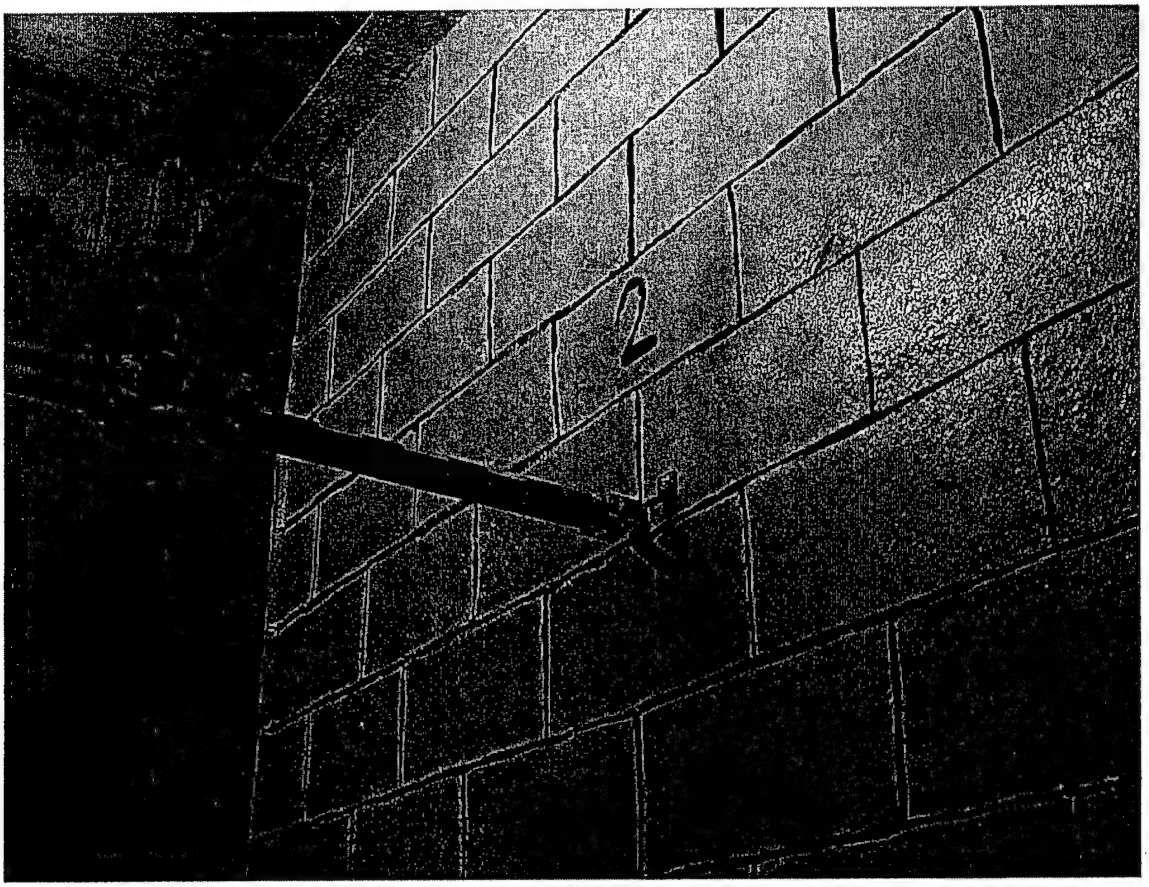

FIG. 75. Test 3, Scratch Gauge

Photography support included pre- and post-test still photography and high-speed photography of the wall deflection. To capture the deflection of each wall, a spy camera was mounted in each back corner of the test structure and in a back corner in each test cubicle. Each of these cameras was directed at the center of a wall. A shielded spy camera was positioned outside the test structure and test cubicles to capture deflection of the walls. A new lighting system was implemented for Wall Test 3 to aid in photography. Camera target locations are illustrated below in Fig. 76.

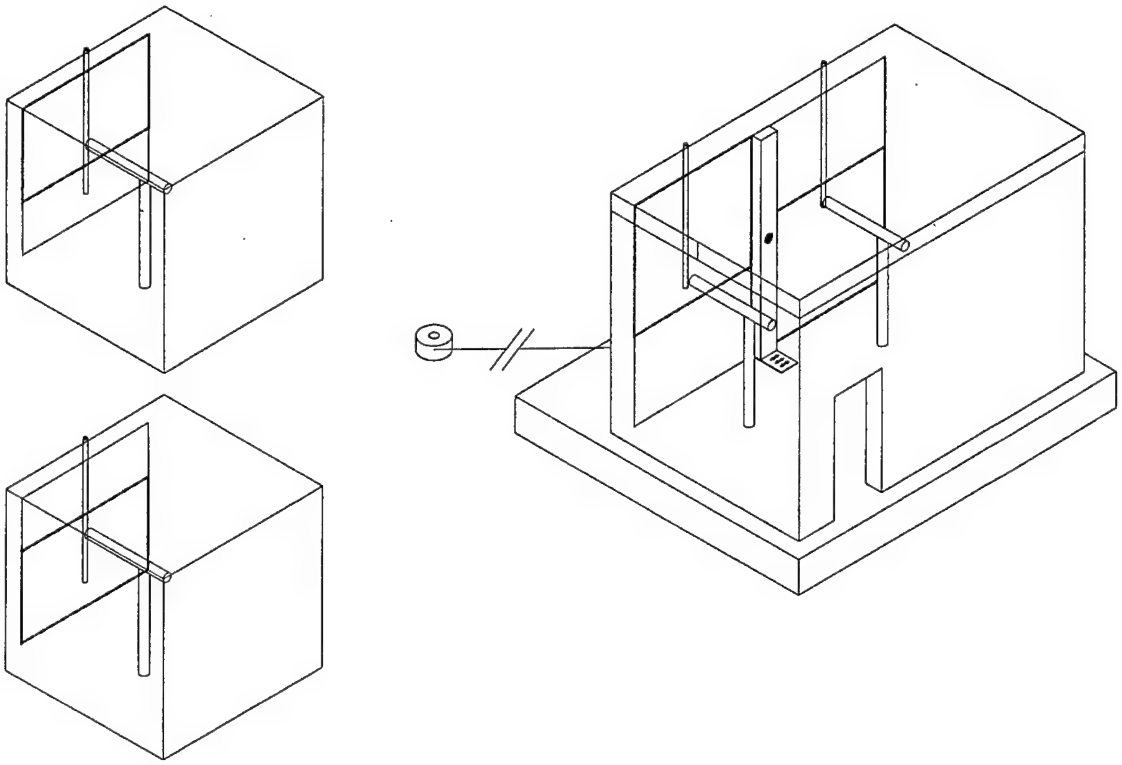

FIG. 76. Test 3, Interior Camera Target Areas

3.4.3 Results

Similar to previous tests, gauge predictions were calculated using the WAC software. The predictions for Wall Test 3 are shown in Table 5. There are predictions for each of the gauges noted above.

TABLE 5. Test 3, Gauge Predictions

Gauge ID	Type	Location	Prediction
R1	Reflected Pressure	Center of Left Wall	60 psi
R2	Reflected Pressure	Center of Divider	60 psi
R3	Reflected Pressure	Center of Right Wall	60 psi
R4	Reflected Pressure	Center of Left Cubicle	61 psi
R5	Reflected Pressure	Center of Right Cubicle	61 psi
F1	Free-field Pressure	Outside Structure	Unable to Predict
L1	Laser Deflection	Center of Left Wall	10.2 in. inward
L2	Laser Deflection	Center of Right Wall	10.2 in. inward
L3	Laser Deflection	Center of Left Cubicle	10.6 in. inward
L4	Laser Deflection	Center of Right Cubicle	10.6 in. inward

There was no control wall in Wall Test 3. All four walls in this test were coated with polymer. Differences were polymer thickness and polymer locations (1/4-in. interior on Wall A; 1/8 in.-interior and exterior on Wall B.) For Wall C and Wall D, polymer coatings were of the same thickness (1/8 in.) but their overlap onto the floor varied.

None of the walls in this test collapsed. Damage occurred on the outside of the walls. No debris entered the structures, indicating again that the polymer was effective in preventing intrusion of wall fragments.

Laser deflection gauges and accelerometers failed. Other data was near predicted values. Results from the reflected pressure gauges are shown in Figs. 77 through 81. Results from free-field pressure gauge are shown in Fig. 82.

All laser gauges and the accelerometer failed to record data. Data from scratch gauges was used to determine deflections. Table 6 shows the predicted data compared to the recorded data. Figs. 83 through 93 show damage done from the blast.

Both Wall A and Wall B survived the blast without collapse. This test demonstrated that applying polymer to the exterior of a wall does not significantly increase its effectiveness and therefore the added cost and effort is not justified. Polymer on the walls prevented debris from entering the structure. The wall with polymer on the outside had less damage on its exterior. For the loading considered in Test 3, the-1/8 in.-thick polymer offered the same level of protection as the ¼-in.-thick polymer coating.

There was defacing on both Wall C and Wall D. The defacing was located across the top and across the bottom. There was also significant defacing on the top of Wall A.

Wall B had less damage than the singly retrofitted wall. Both were successful in preventing flying debris. Wall A had a polymer tear on the inside due to high shear at a mortar joint.

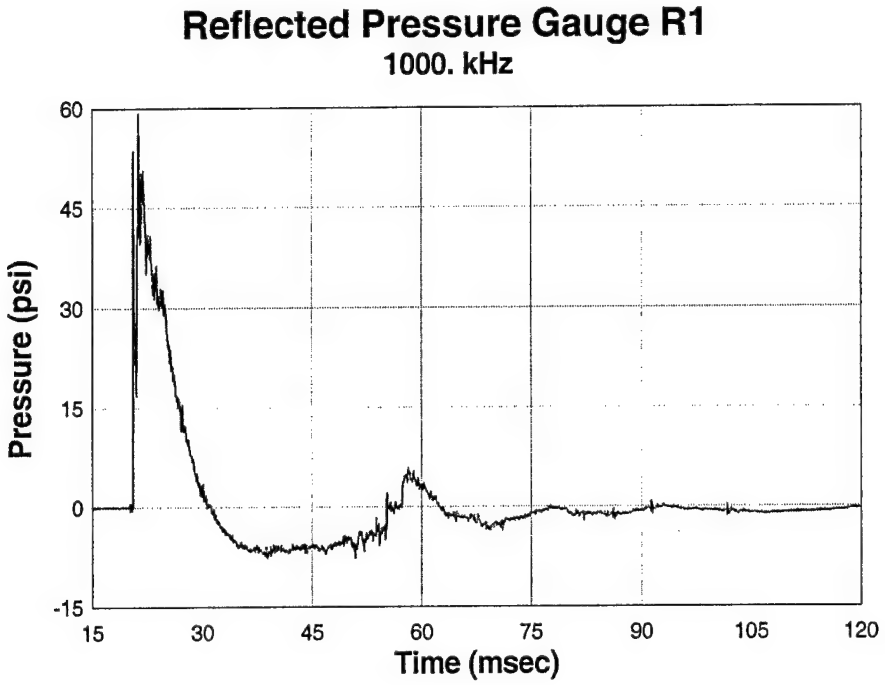

FIG. 77. Test 3, Gauge R1

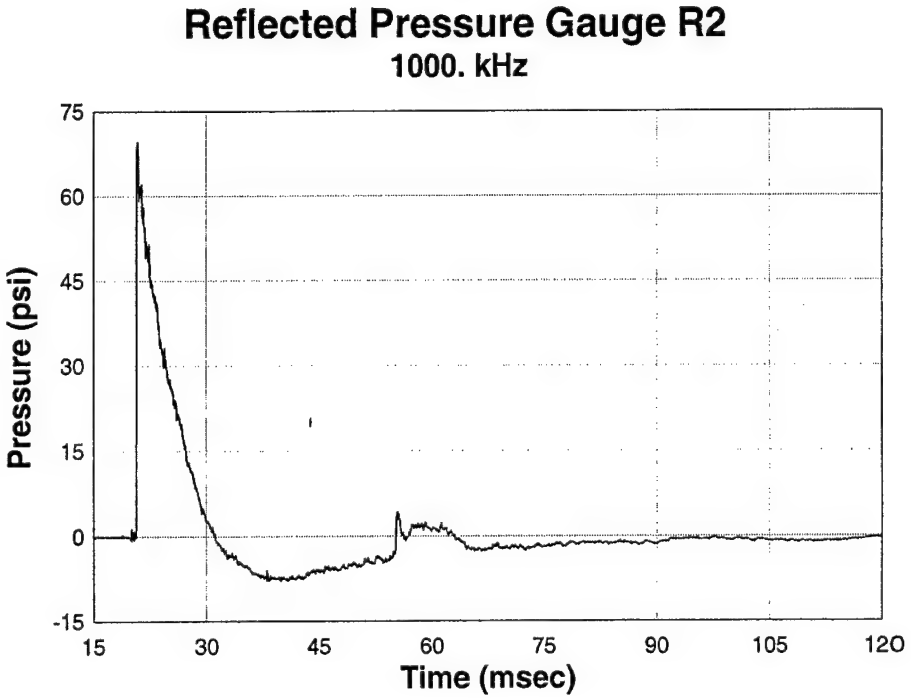

FIG. 78. Test 3, Gauge R2

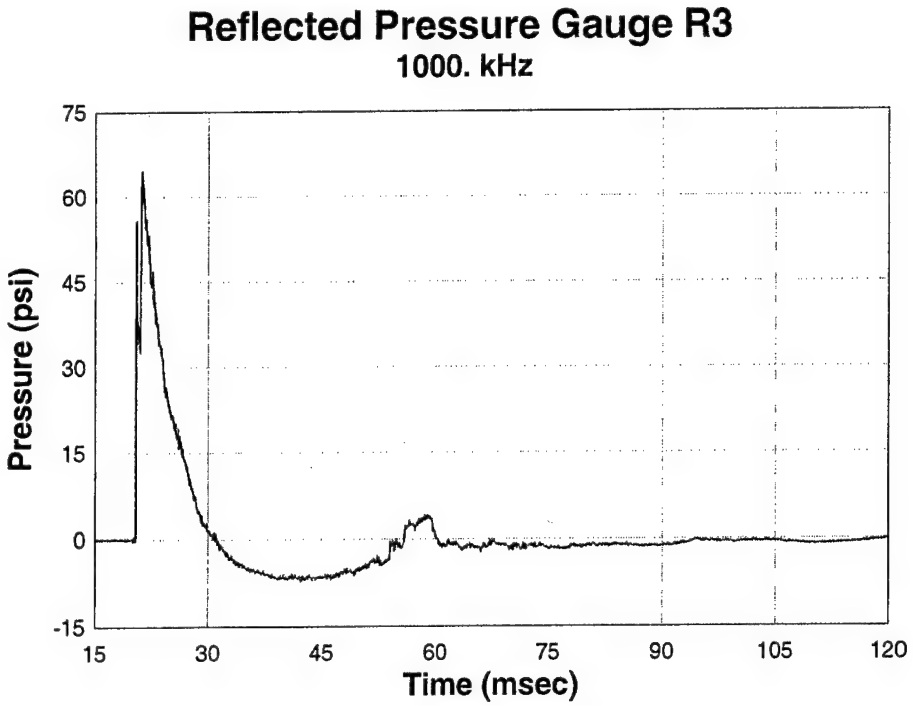

FIG. 79. Test 3, Gauge R3

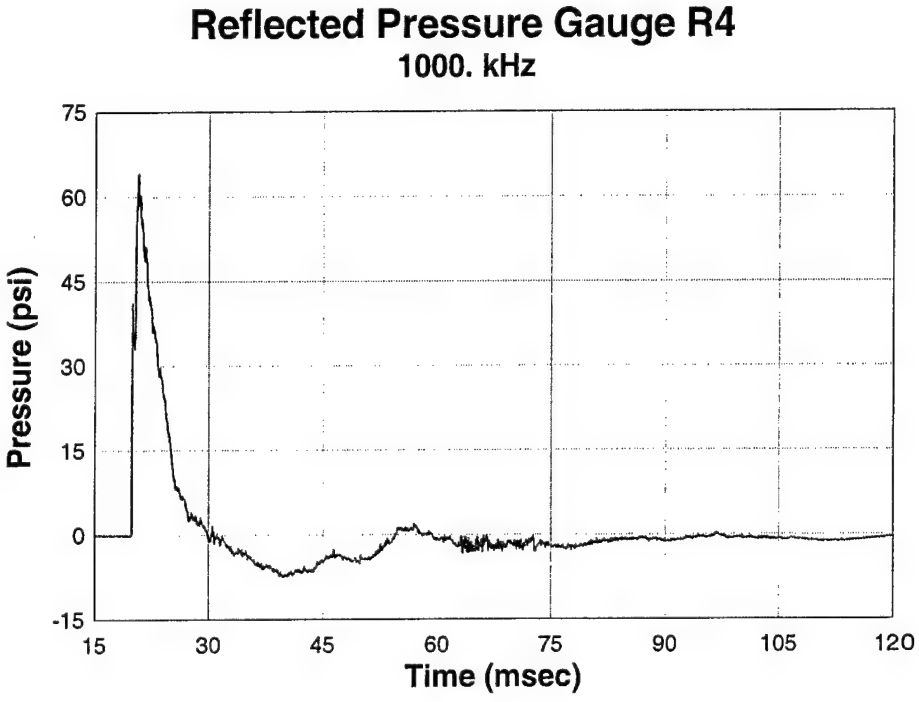

FIG. 80. Test 3, Gauge R4

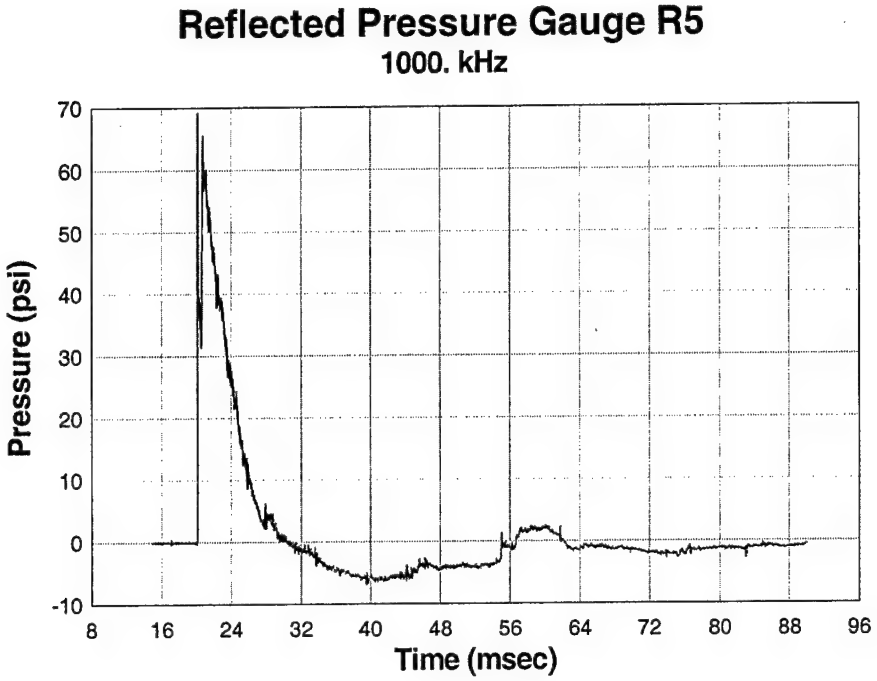

FIG. 81. Test 3, Gauge R5

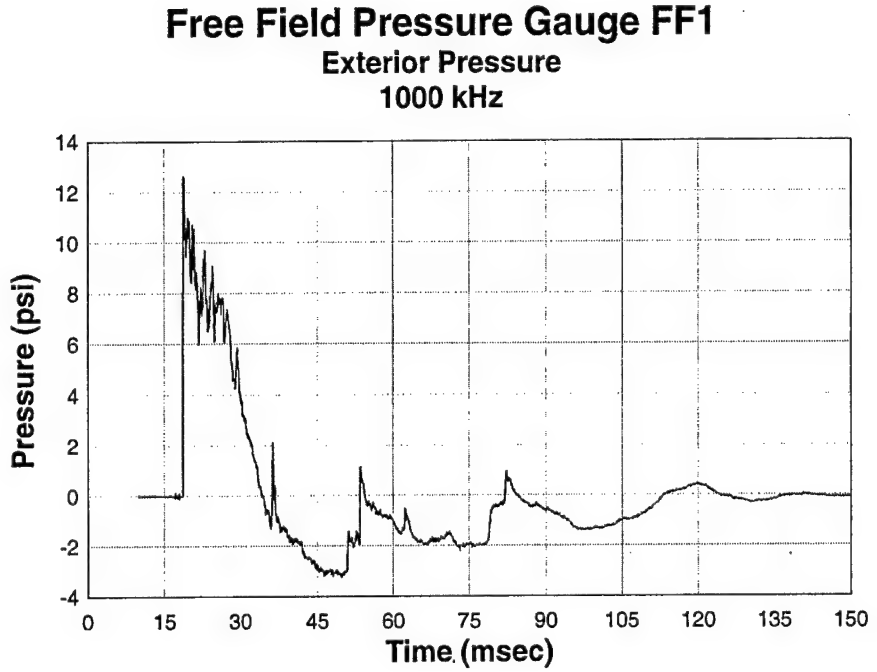

FIG. 82. Test 3, Gauge F1

The maximum pressures recorded by the pressure gauges were (R1) 59.4 psi at 21.3 msec, (R2) 69.5 psi at 20.8 msec, (R3) 64.8 psi at 21.2 msec, (R4) 64.2 psi at 20.7 msec, and (R5) 69.1 psi at 20.3 msec. The maximum pressure recorded by the free-field pressure gauge was (F1) 12.7 psi at 18.7 msec. All laser gauges failed in this test. However, scratch gauges were able to measure maximum deflections. They are shown in Table 6 below.

TABLE 6. Test 3, Predicted vs. Recorded Data

Gauge ID	Type	Prediction	Actual
R1	Reflected pressure	60 psi	59.4 psi
R2	Reflected pressure	60 psi	69.5 psi
R3	Reflected pressure	60 psi	64.8 psi
R4	Reflected pressure	61 psi	64.2 psi
R5	Reflected pressure	61 psi	69.1 psi
F1	Free-field pressure	Unable to predict	12.7 psi
L1	Laser deflection	10.2 in. inward	9.4 in. (scratch gauge)
L2	Laser deflection	10.2 in. inward	7.8 in. (scratch gauge)
L3	Laser deflection	10.6 in. inward	4.9 in. (scratch gauge)
L4	Laser deflection	10.6 in. inward	5.9 in. (scratch gauge)

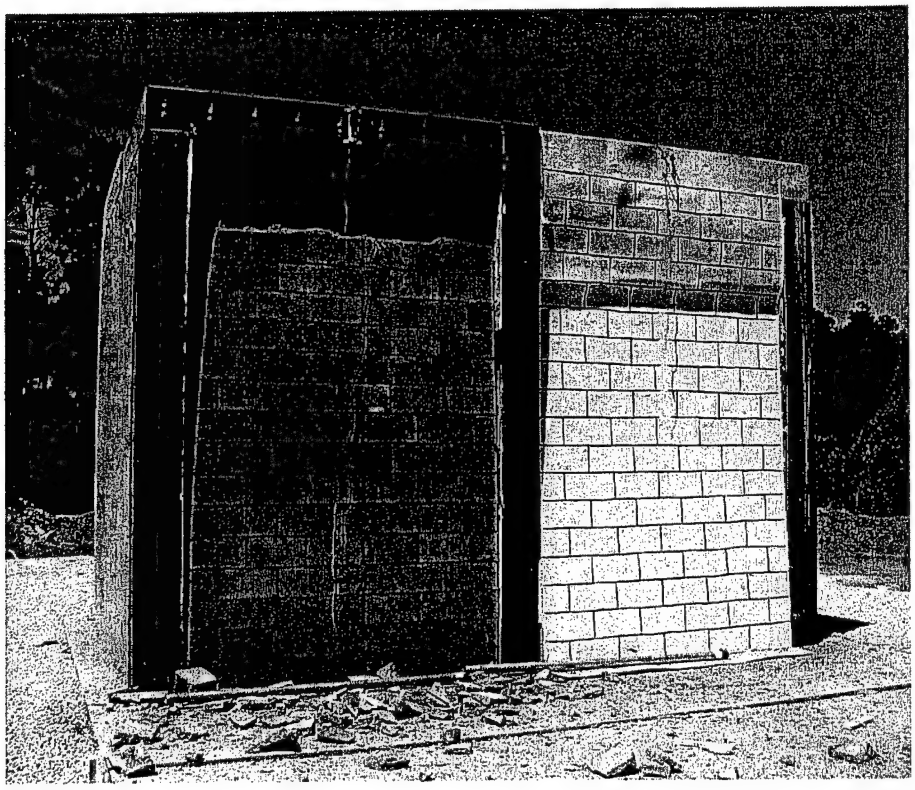

FIG. 83. Test 3, Walls A and B, Damage

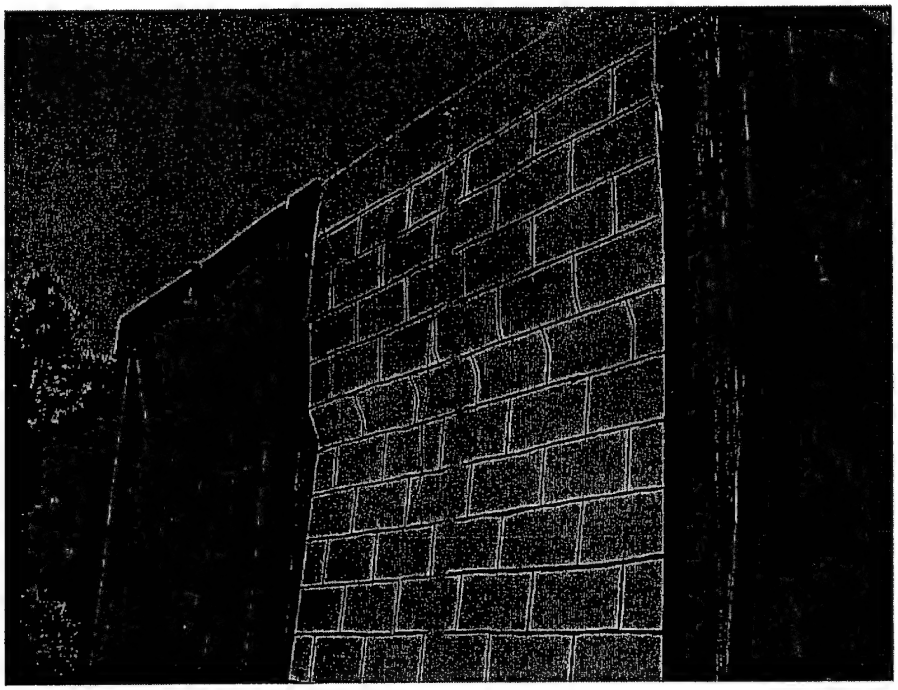

FIG. 84. Test 3, Walls A and B, Top Exterior

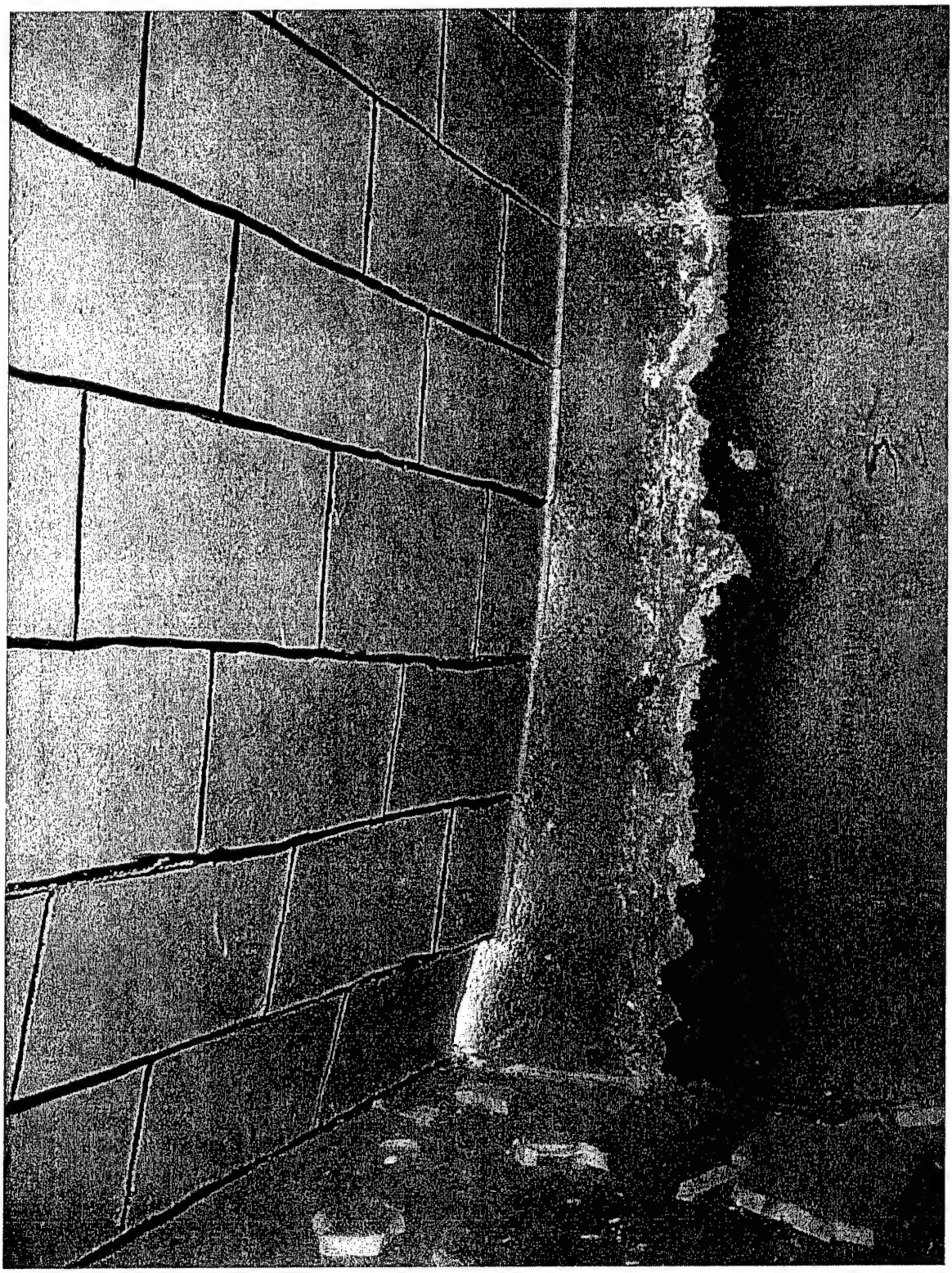

FIG. 85. Test 3, Wall A, Left Bottom Interior

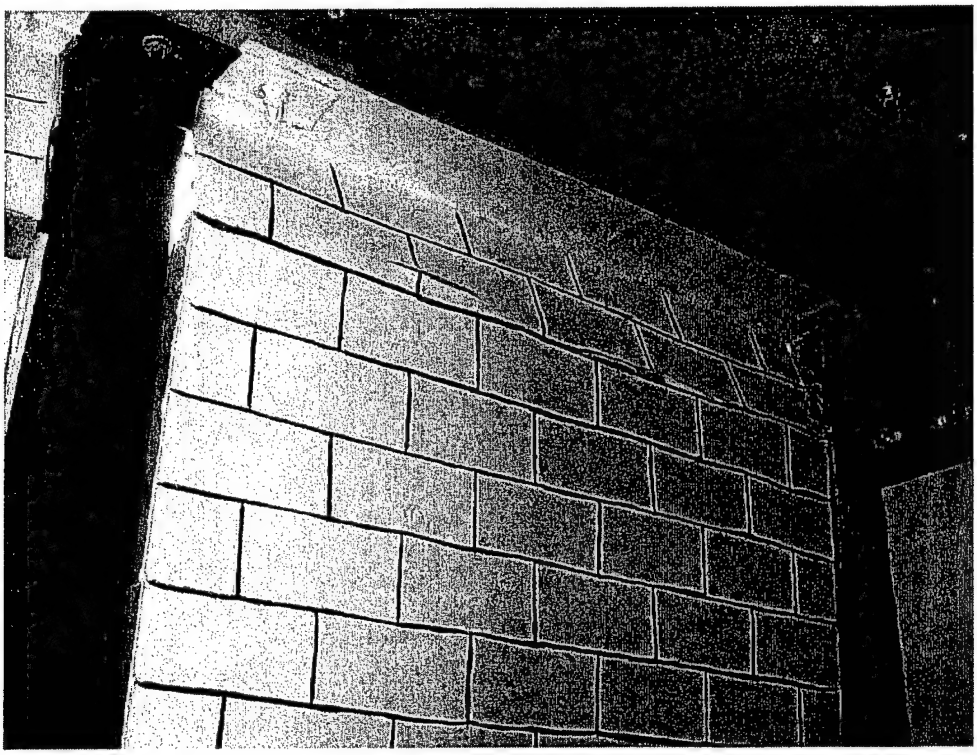

FIG. 86. Test 3, Wall A, Left Top Interior

FIG. 87. Test 3, Wall B, Right Interior

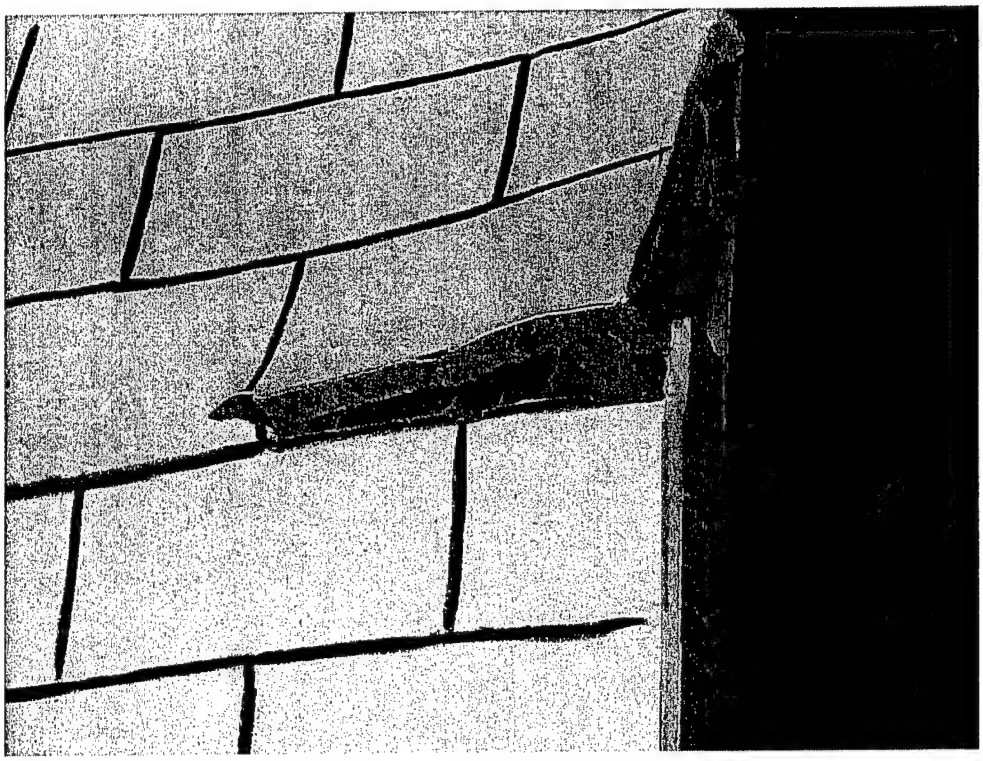

FIG. 88. Test 3, Wall B, Close Up

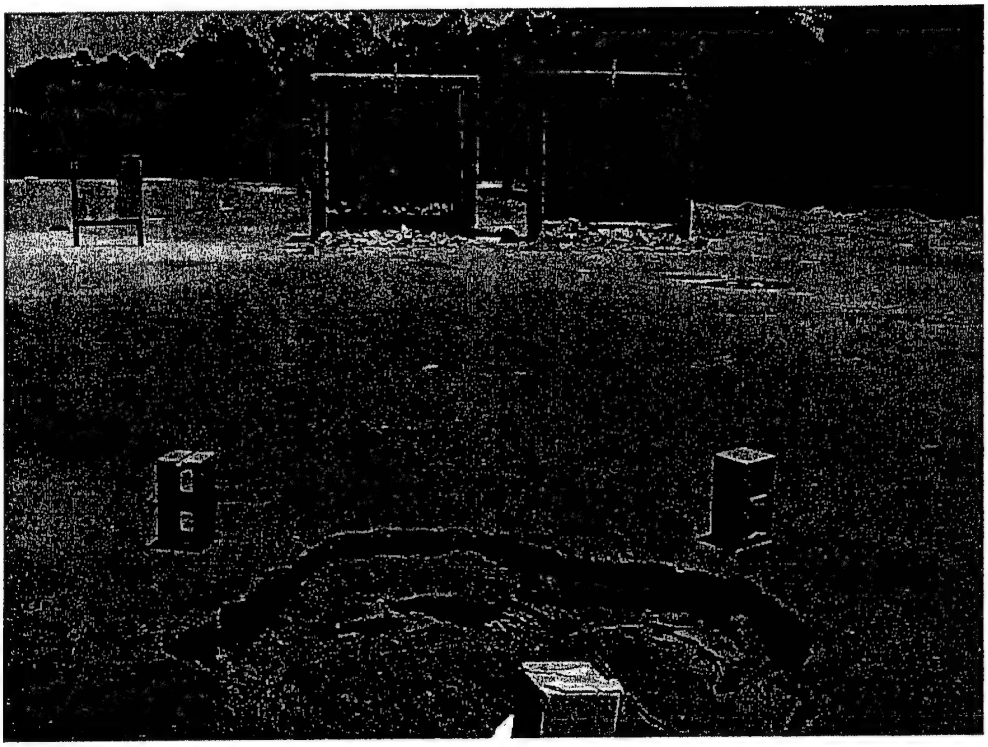

FIG. 89. Test 3, Walls C and D

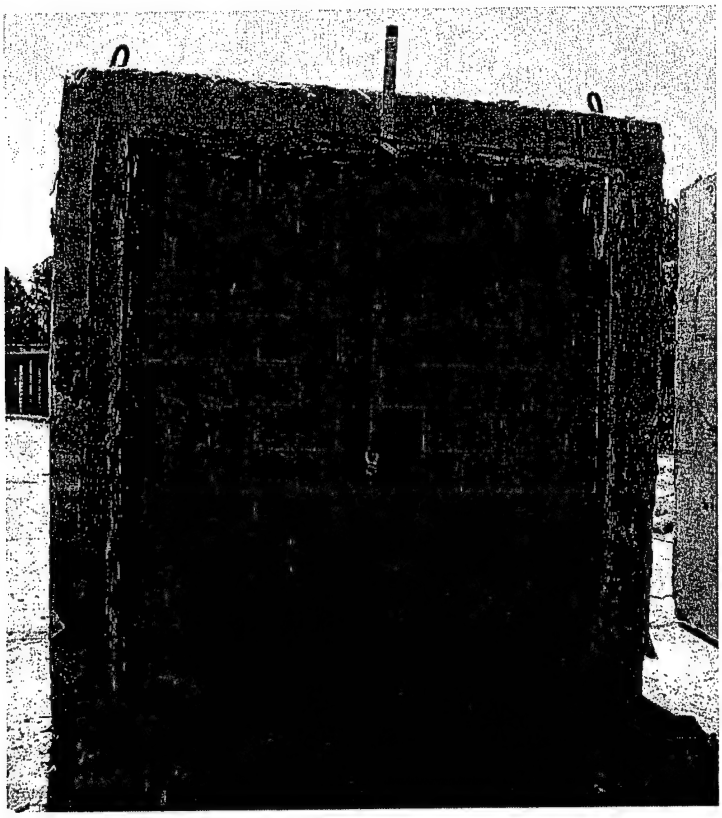

FIG. 90. Test 3, Wall C

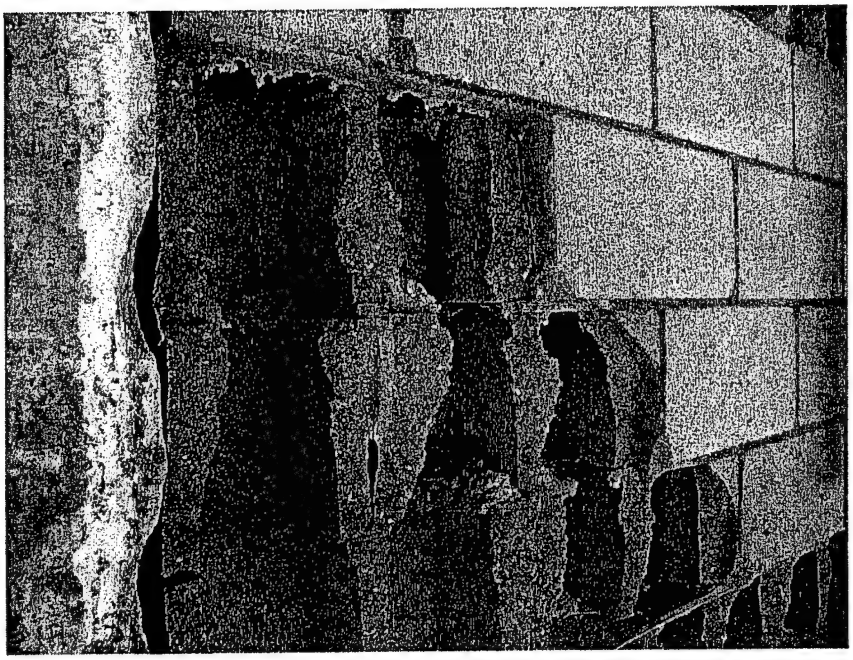

FIG. 91. Test 3, Mid Wall C

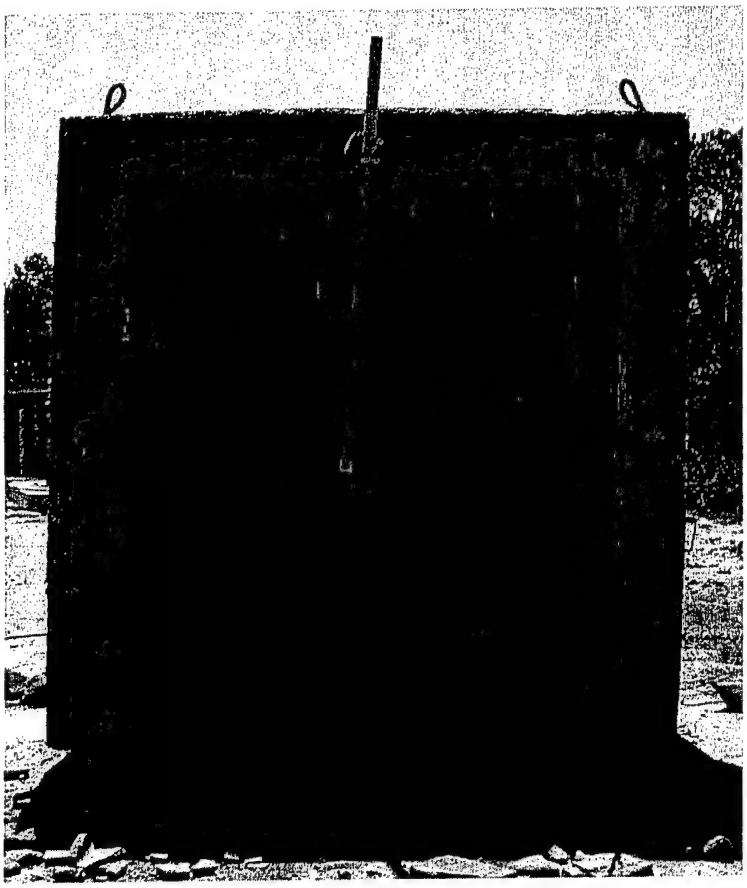

FIG. 92. Test 3, Wall D

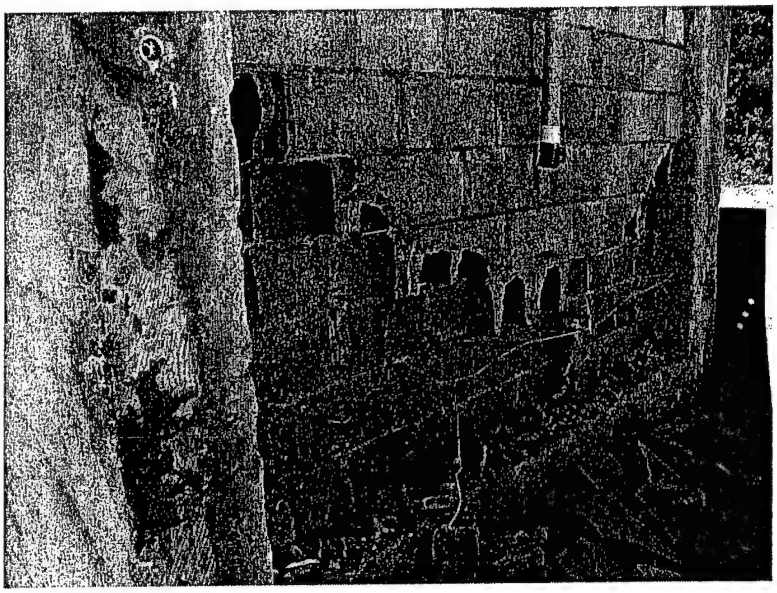

FIG. 93. Test 3, Wall D Bottom

3.5 Wall Test #9

Wall Test 9 involved two 7 ft 6 in. wide by 10-ft-tall CMU walls retrofitted on the interior with a 1/8-in. elastomeric polymer coating. One of the walls contained a standard steel door. The other wall contained an aluminum window. A 6-mil film was coated on the window. No additional retrofitting was done to the door or window. The purpose of Wall Test 9 was not to test the door or the window, but rather to investigate the effects the openings would have on the effectiveness of the polymer coating. The key objectives of Wall Test 9 were to (1) measure the deflection of key wall elements; (2) evaluate failure modes created by the door and window openings; and (3) identify connection failure points at openings. The layout for Wall Test 9 is shown in Fig. 94.

The test articles consisted of two standard unreinforced masonry block walls. They were separated by a 12 in. x 12 in. x ½ in. square steel tube (Fig. 95). Both walls had ¾ in. foam insulation board on both sides. Both walls were coated on their interior with a 1/8 in. layer of elastomeric coating that overlapped the roof and floor slabs and tapered to 24 in. The walls were allowed by move freely on the sides to approximate a one-way response. The charge size and standoff distance was the same as Test 3.

3.5.1 Construction

The doorframe was placed, spaced, and plumbed in the test structure before construction of the walls began. The wall was then constructed around the doorframe. As the wall was built, the hollow steel jam of the door was filled with mortar. A header was formed using solid bottom lintel blocks. After the wall cured, the door was hung. An image of the wall being constructed around the doorframe is shown in Fig. 96.

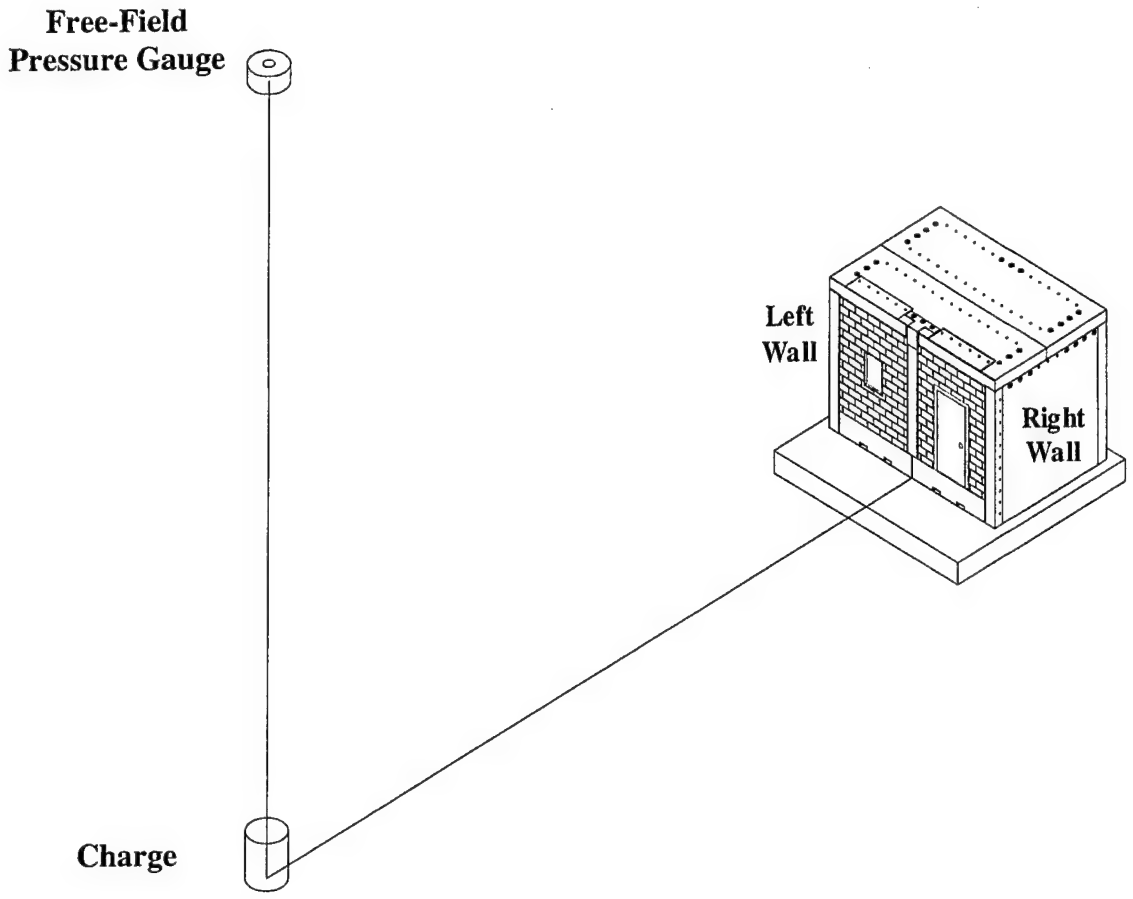

FIG. 94. Test 9 Layout

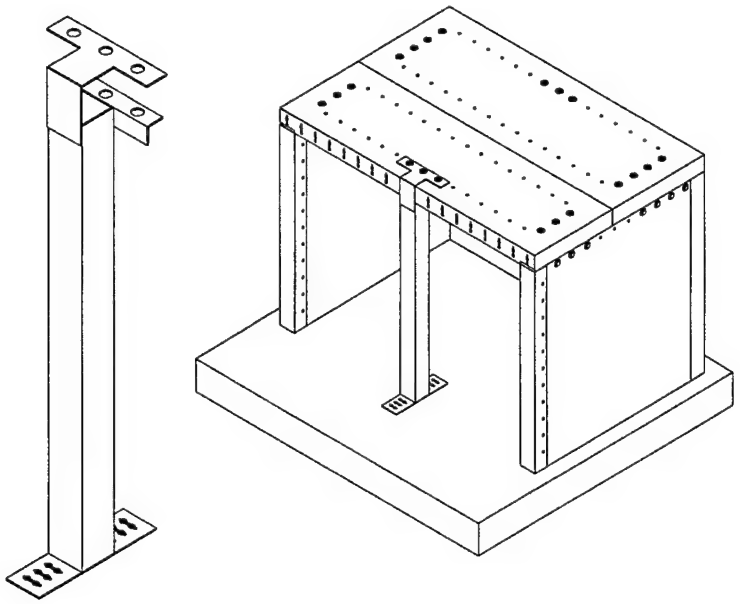

FIG. 95. Test 9, Steel Divider

As the wall was being constructed, a wooden frame was inserted in the wall where the window would be installed. The opening accounted for the total outside dimensions of the window, including the flange. A sill was formed using a solid half block that was mortared in place. A header was formed using solid bottom lintel blocks. During the wall construction, the uninstalled window was coated with a 6-mil (30 ply) Mylar film to allow for the recommended four-day cure time. Once the wall cured, the window was installed.

Installation of the window required several steps. First, the window opening was furred out. The furring was placed so one edge was flush with the interior of the wall. The furring strips were installed using concrete screws and/or cut nails. After the furring strips were in place, the window was set in the opening. The flange of the window rested on the furring strips while the window filled the opening. The window was then fastened to the wall and was ready for weatherproofing.

FIG. 96. Test 9, Door Installation

After the walls were constructed and the door and window were in place, a 2 in. x 2 in. x 7.5 ft steel angle was welded to the existing 1-in. steel plate at the top and bottom of the two openings in the test structure. These angles locked the top and bottom course of CMU blocks. The angles are shown in Fig. 97 and in Fig. 98. In the latter image, the angle is difficult to see. Notice the smaller angle that is installed at the bottom of the larger angle that was already in place.

Primer was applied to the concrete and metal surfaces to insure proper bonding. Separate bonding agents were used for the concrete and metal. Both products were allowed to cure based on the manufacturer's instructions.

Fig. 99 shows the constructed wall with the door. Fig. 100 shows the window. Paper wrapping used to protect elements from polymer during spraying is shown in Fig. 101. Fig. 102 shows the coating process. The retrofitted walls are shown in Figs. 103 and 104.

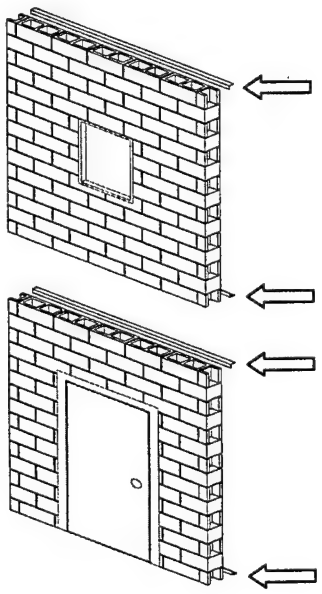

FIG. 97. Test 9, New Angle Locations

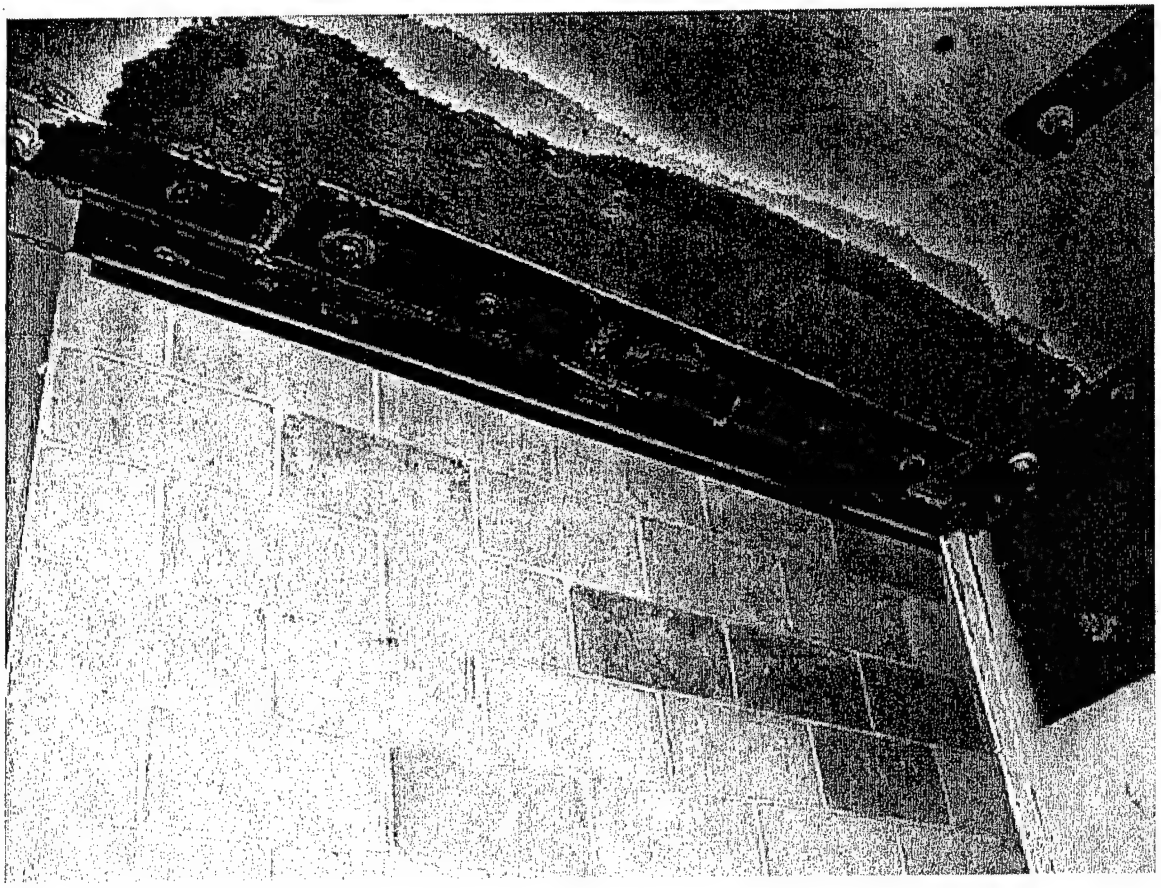

FIG. 98. Test 9, Newly Installed Angle

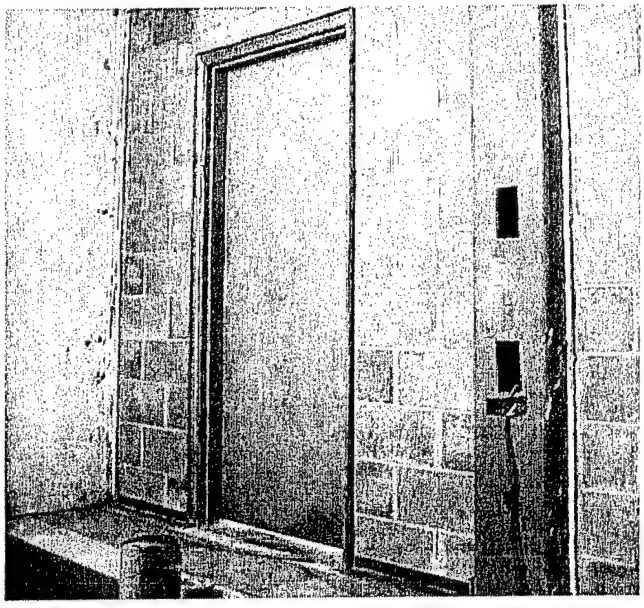

FIG. 99. Test 9, Wall with Door

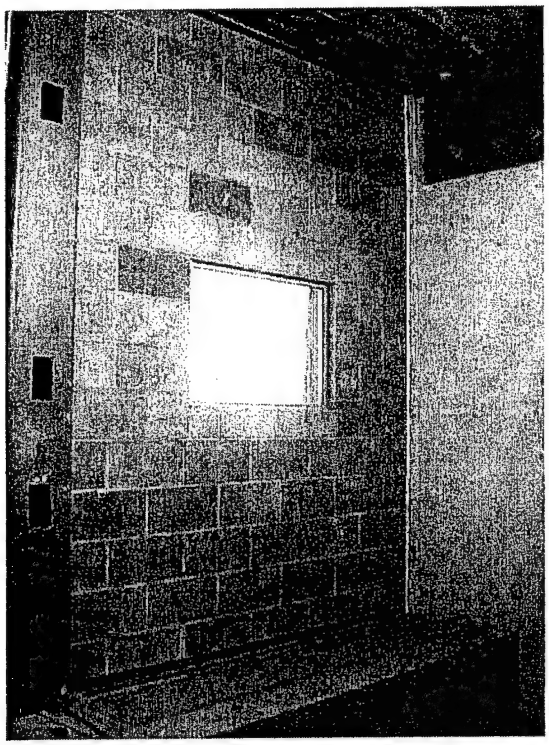

FIG. 100. Test 9, Wall with Window

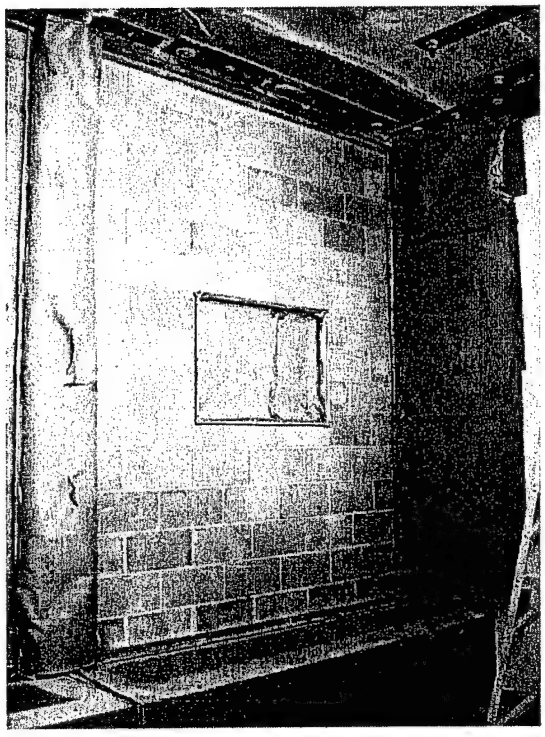

FIG. 101. Test 9, Paper Wrapping

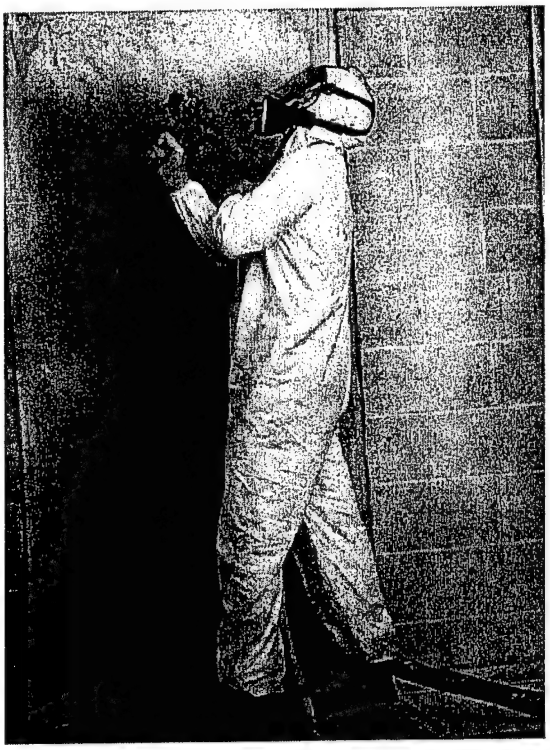

FIG. 102. Test 9, Coating Process

FIG. 103. Test 9, Wall with Door Completed

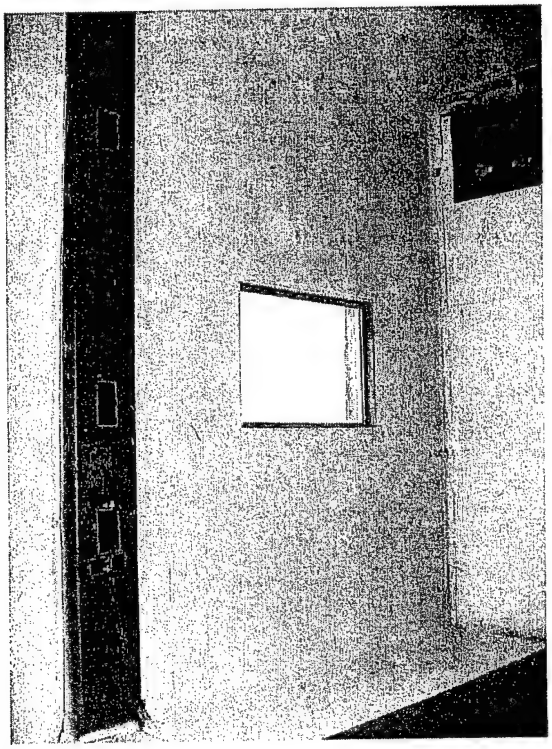

FIG. 104. Test 9, Wall with Window Completed

3.5.2 Instrumentation

Gauge instrumentation used in Wall Test 9 included three reflected pressure gauges (R1, R2, R3), two free-field pressure gauges (F1, I1), and two deflection gauges (D1, L1). All three reflected pressure gauges were mounted in the center of the steel tube divider. One gauge was positioned 5 ft off the top of the 2-ft slab. The other two were positioned 2.5 ft above and below the center gauge. One free-field gauge was placed outside the structure several feet away. The other pressure gauge was placed inside the structure. A deflection gauge was mounted on each wall. One deflection gauge used a laser to measure velocity and deflection to 1/8 in. accuracy. The other deflection gauge was a gear-driven gauge that measured displacement with a rotational position transducer. Locations of all the gauges are shown in Fig. 105.

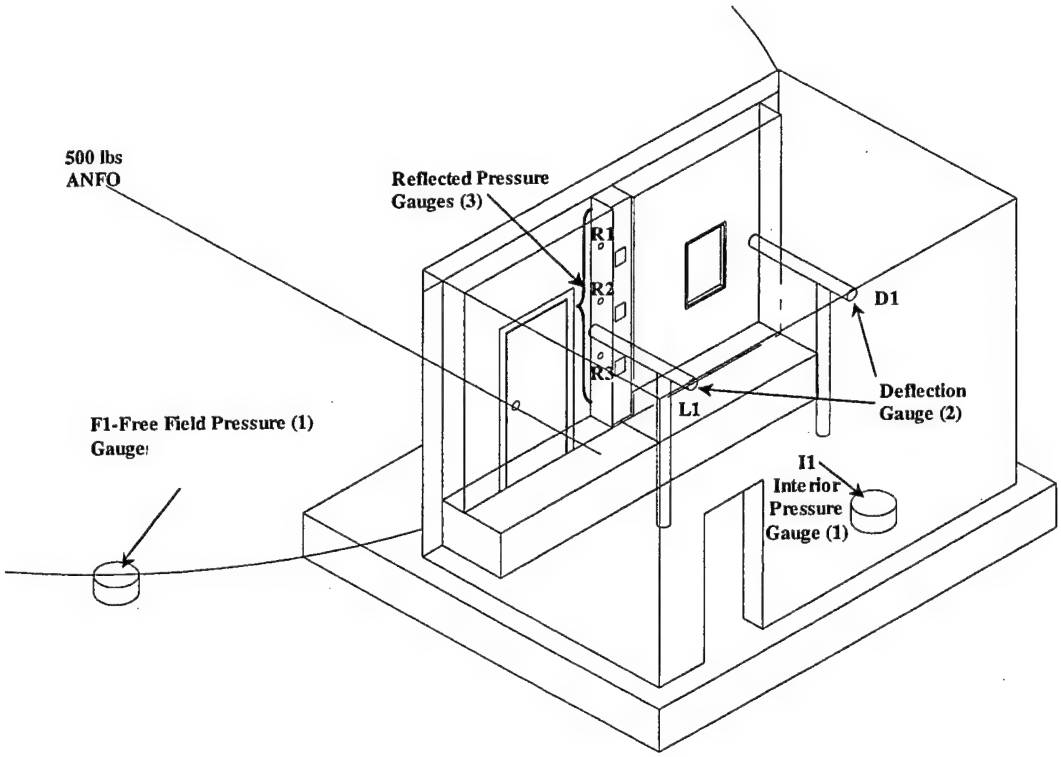

FIG. 105. Test 9, Gauge Locations

The gauges mentioned above were important in capturing numeric data for the wall tests. However, photography is critical for data collection. The high-speed spy cameras that were used in each test reveal much information about the response of the wall. Still photography was taken pre- and post-test. High-speed photography was used to capture the response of the wall. Two spy cameras were mounted inside the back corners of the test structure and directed at the center of the upper wall on the opposite side. A third spy camera was mounted to capture the operation of the new gear driven deflection gauge. A high-speed digital camera was positioned outside the test structure to capture the deflection. The camera targets are shown below in Fig. 106. The targets include the low-middle to top area of both walls, high-middle to bottom area of both walls, and the entire two-wall area (as captured by the outside camera).

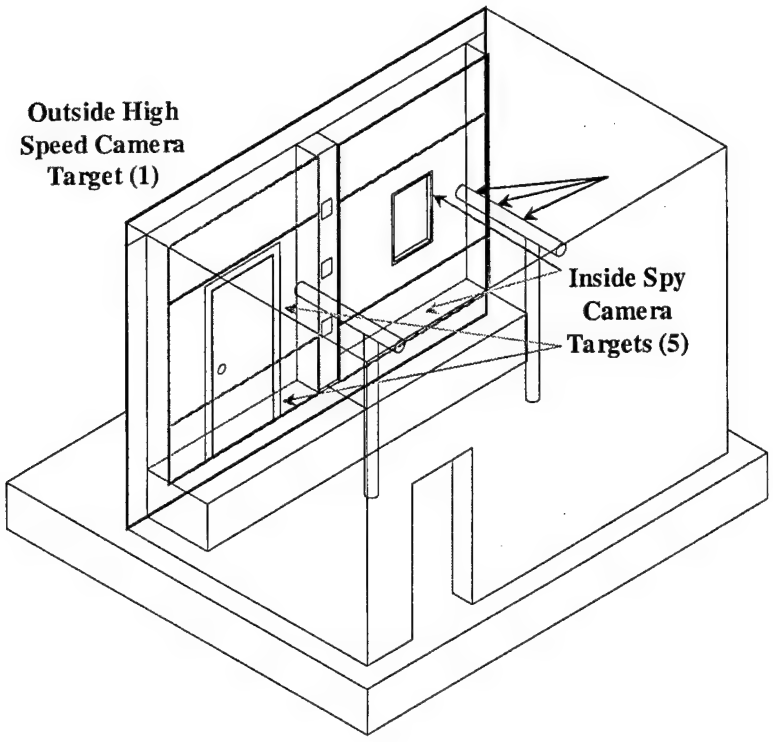

FIG. 106. Test 9, Interior Camera Target Areas

The same lighting system that was used in Wall Test 3 was used in Wall Test 9. It is shown in Fig. 107. One of the corner cameras is also shown in this figure.

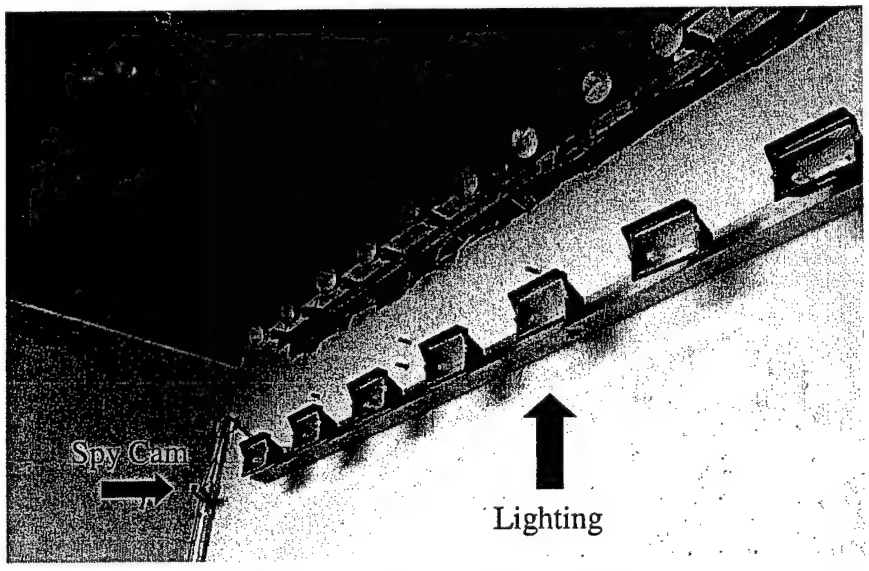

FIG. 107. Test 9, Lighting System

Gauge predictions were made with the WAC software for the gauges used in Wall Test 9. Predictions were made for each of the three reflected pressure gauges, two free-field gauges, and two deflection gauges. The predictions are shown in Table 7.

TABLE 7. Test 9, Gauge Predictions

Gauge ID	Type	Location	Prediction
R1	Reflected Pressure	Center Steel Support, 7.5 ft from bottom of wall, outside	66 psi
R2	Reflected Pressure	Center Steel Support, 5 ft from bottom of wall, outside	66 psi
R3	Reflected Pressure	Center Steel Support, 2.5 ft from bottom of wall, outside	66 psi
F1	Free-field Pressure	Outside Structure	22 psi
I1	Free-field Pressure	Inside Structure	5 psi
D1	Deflection	Left Wall, inside	12 in.
L1	Deflection	Right Wall, inside	12 in.

3.5.3 Results

Walls in this test did not collapse. However, there was extensive mortar joint cracking in both of the walls. The wall with the door had most cracks above the door. The frame of the door was shifted on one side. The polymer tore at the bottom. The wall with the window remained intact. However, there were cracks and defacing on the exterior.

Reflective pressure data is shown in Figs. 108 through 110. Free-field data is shown in Figs. 111 through 112. One deflection gauge failed. The other deflection gauge data is shown in Fig. 113.

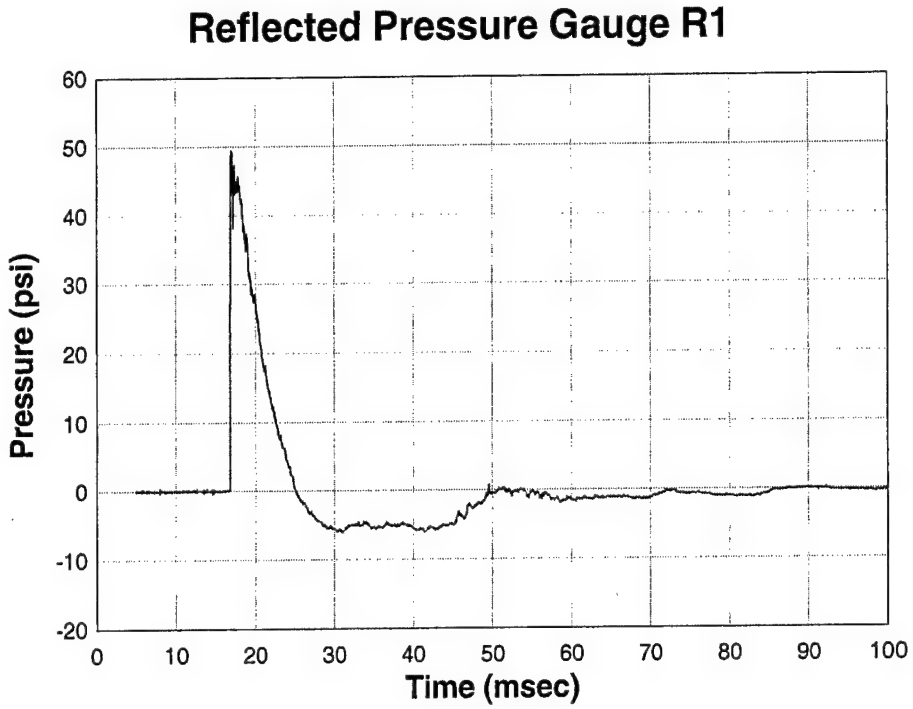

FIG. 108. Test 9, Gauge R1

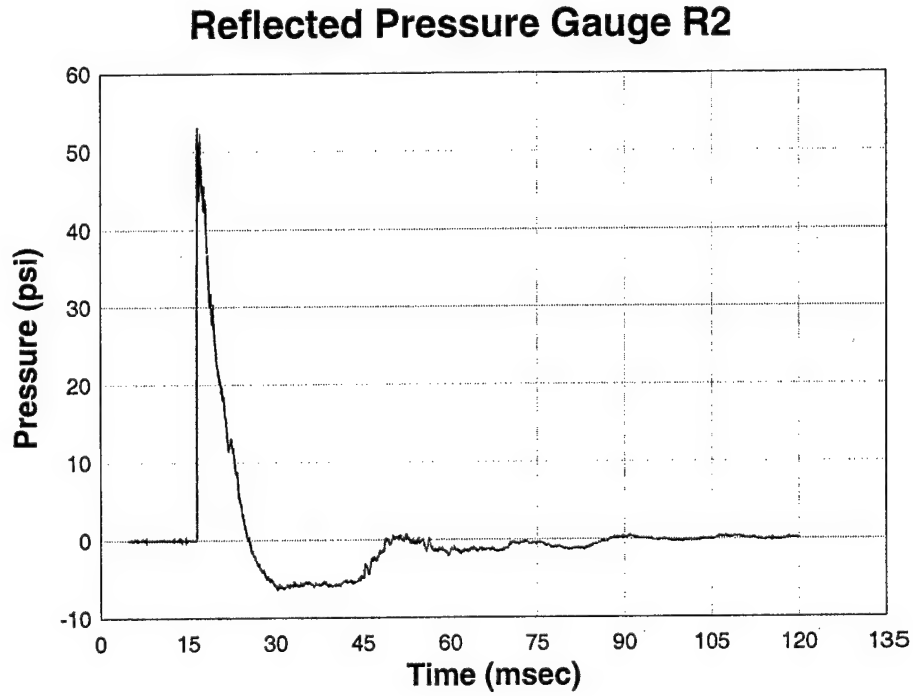

FIG. 109. Test 9, Gauge R2

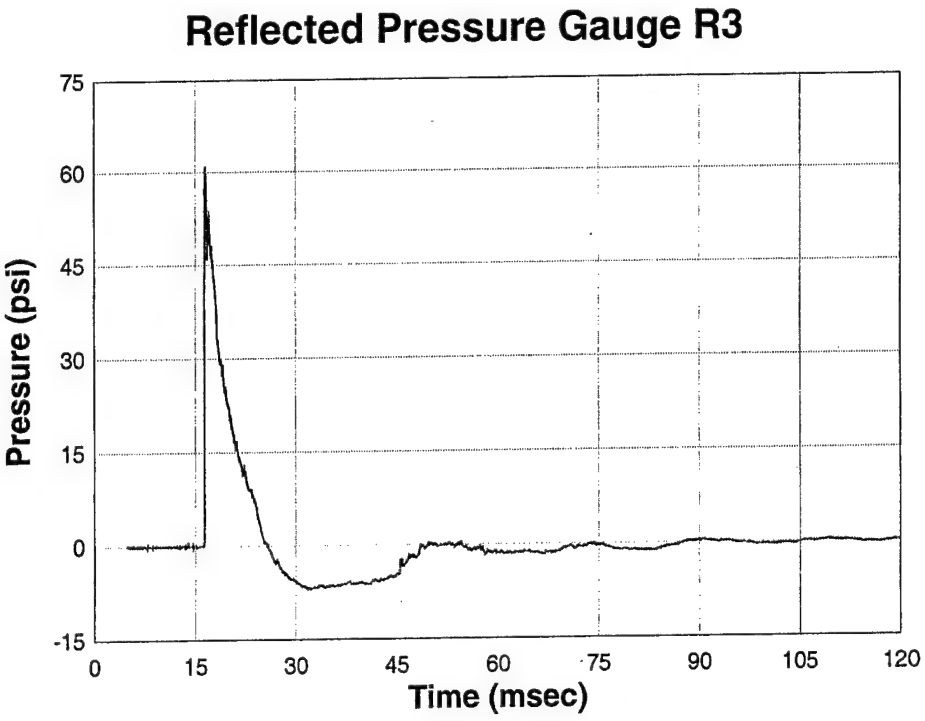

FIG. 110. Test 9, Gauge R3

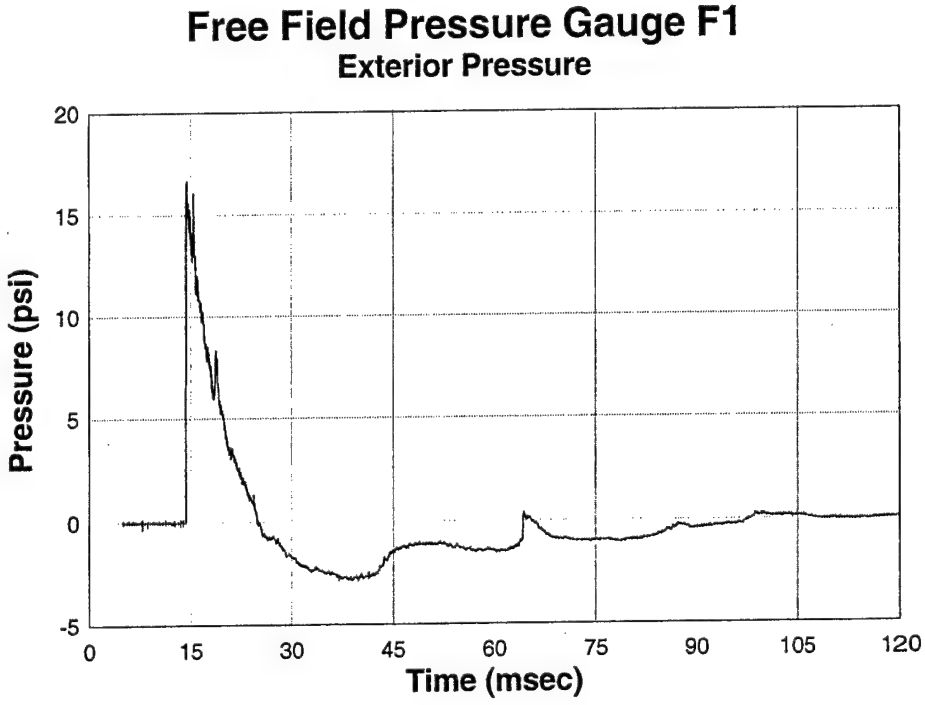

FIG. 111. Test 9, Gauge F1

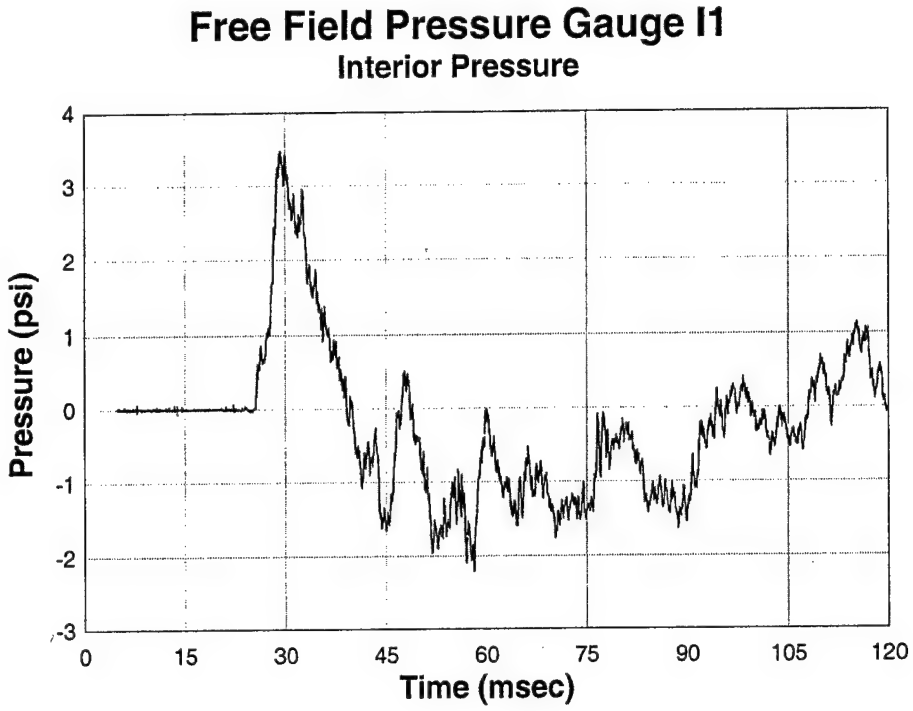

FIG. 112. Test 9, Gauge I1

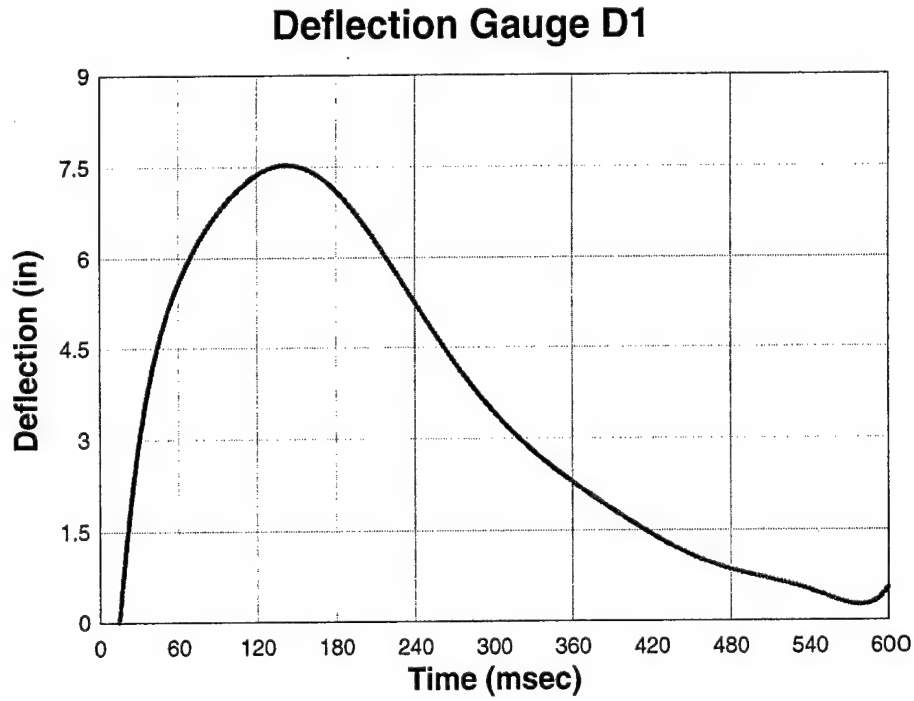

FIG. 113. Test 9, Gauge D1

The maximum pressures recorded by the pressure gauges were (R1) 49.5 psi at 17.0 msec, (R2) 53.1 psi at 16.6 msec, and (R3) 61.1 psi at 16.4 msec. The maximum pressures recorded by the gauges were (F1) 16.7 psi at 14.5 msec and (I2) 3.5 at 29.3 msec. The maximum deflections recorded by the deflection gauges were (D1) 7.7 in. at 121 msec and (L1) 5.6 in. This information is summarized in Table 8.

An image of the door and window are shown in Figs. 114 and 115. The cracks are outlined with paint. The right wall contained the door. The left wall contained the window. Both of the walls survived the blast without collapse. The front face fracture for these walls covered more area than in other tests. In addition, there were cracks at many mortar joints. The doorframe was shifted and bent during the test. However, it resulted in no additional flying debris. Debris did enter the structure through the bottom of the wall containing the door.

TABLE 8. Test 9, Predicted vs. Recorded Data

Gauge ID	Type	Location	Prediction	Measured
R1	Reflected Pressure	Center Steel Support, 7-1/2 ft from bottom of wall, outside	66 psi	49.5 psi
R2	Reflected Pressure	Center Steel Support, 5 ft from bottom of wall, outside	66 psi	53.1 psi
R3	Reflected Pressure	Center Steel Support, 2-1/2 ft from bottom of wall, outside	66 psi	61.1 psi
F1	Free-field Pressure	Outside Structure	22 psi	16.7 psi
I1	Free-field Pressure	Inside Structure	5 psi	3.5 psi
D1	Deflection	Left Wall, Inside	12 in.	7.7 in.
L1	Deflection	Right Wall, Inside	12 in.	5.6 in.

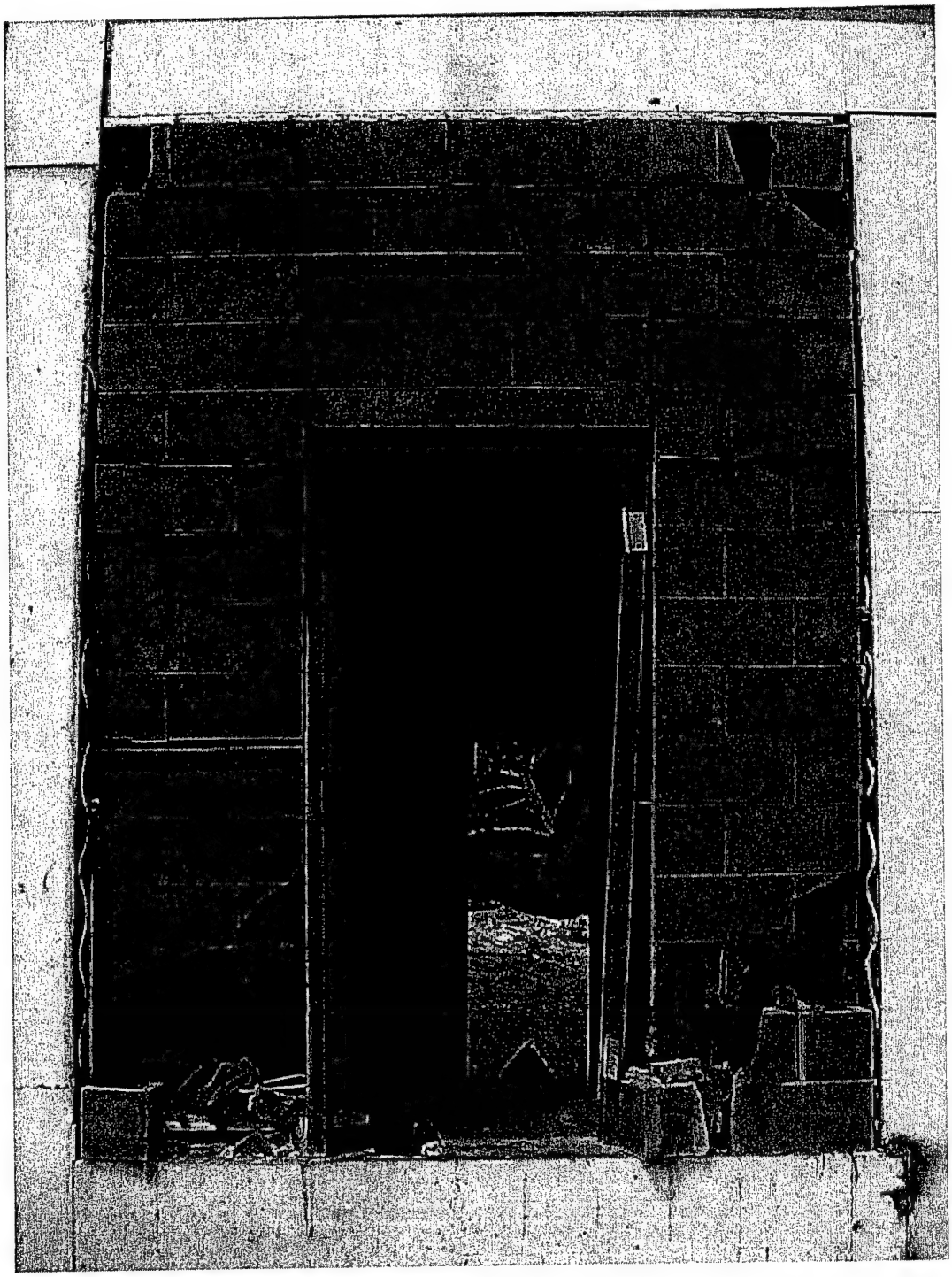

FIG. 114. Test 9, Posttest Door

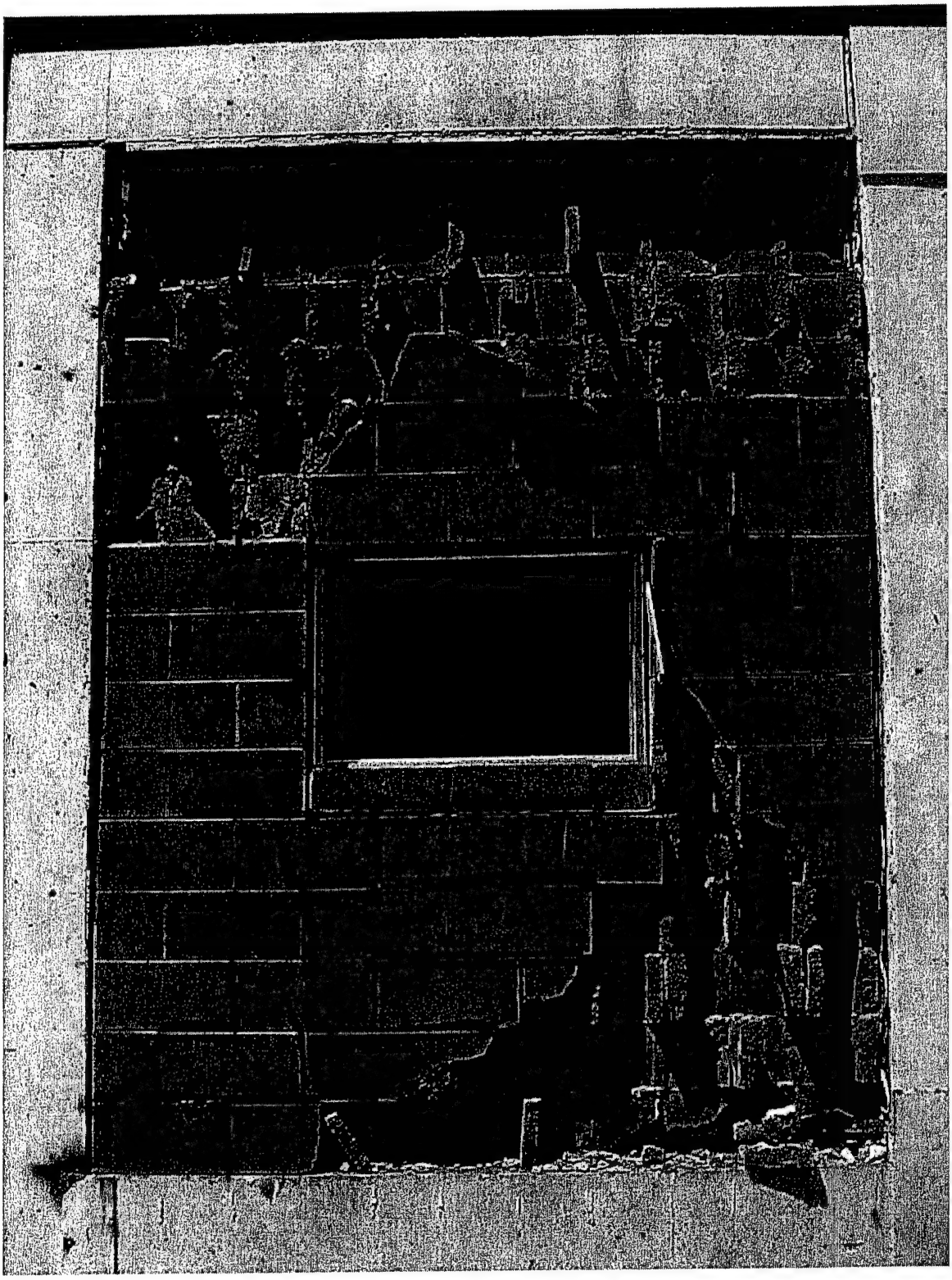

FIG. 115. Test 9, Posttest Window

The mortar bond between the blocks is weak in tension. When the blast load reaches the structure, the shock wave fractures some of the front faces of the blocks and breaks some of the mortar bonds. The wall then flexes inward causing high shear in the upper and lower mortar joints followed by tension failure at the inside center of the wall. The negative phase of the blast loading then pulls the wall back outward. During these movements, mortar joints in the walls fail. This causes cracking throughout the lateral mortar joints.

The front face and mortar failures occur in the first few milliseconds after the blast is detonated. Close-up images of mortar and front face failures are shown in Figs. 116 through 118. Also shown in these images are large cracks, resulting from tension in the walls caused by flexure.

FIG. 116. Test 9, Top Left Wall Defacing

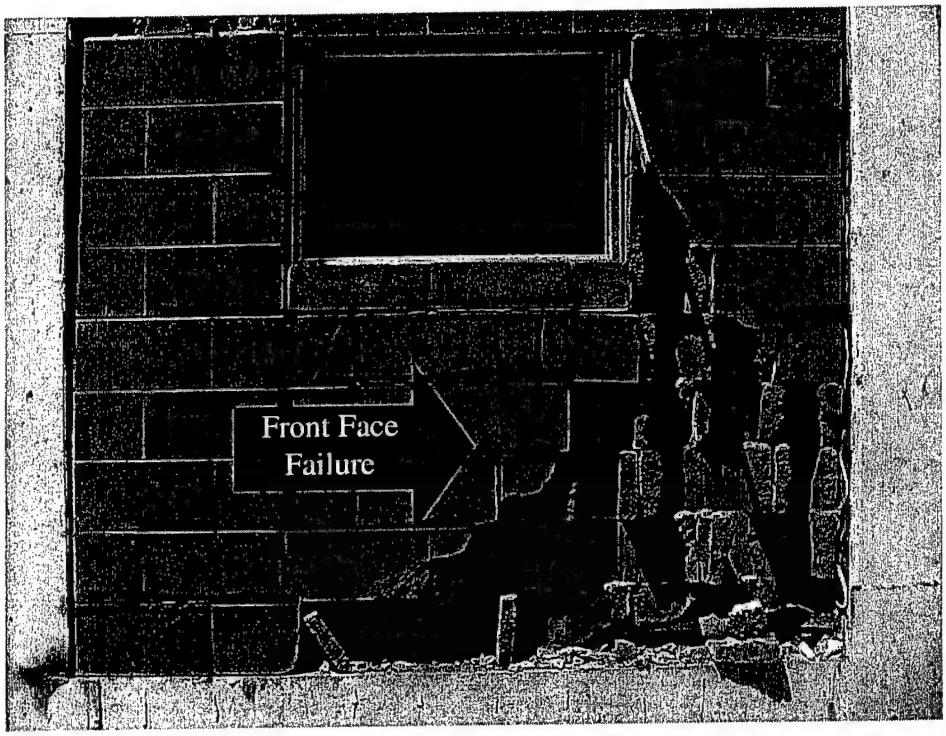

FIG. 117. Test 9, Bottom Left Wall Defacing

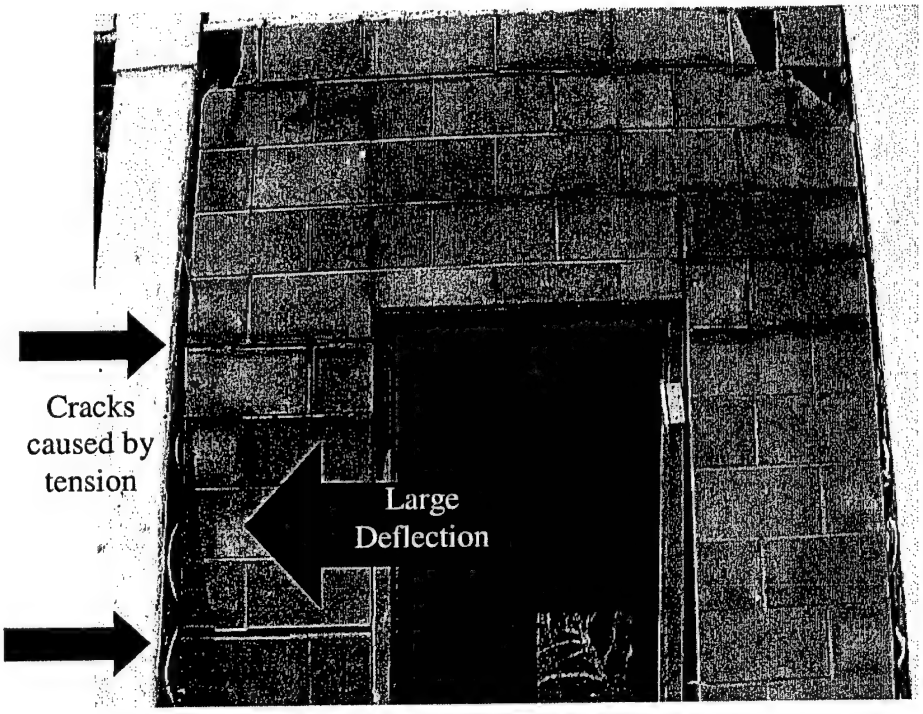

FIG. 118. Test 9, Right Wall Cracks

3.6 Wall Test 10

Wall Test 10 involved an explosive test on a 16 ft wide x 12 ft tall CMU wall and an 8 ft x 8 ft CMU control wall. The larger wall housed a reinforced steel door and doorframe and was retrofitted on its interior with a 1/8-in.-thick elastomeric polymer coating. The control wall was constructed and tested to demonstrate the damage incurred by an unretrofitted CMU wall.

The objective of Wall Test 10 was to test the effects of the door opening on the performance of the polymer coating and how the door challenged polymer application. The key objectives for Wall Test 10 were to (1) measure the deflection of key wall elements; (2) evaluate failure modes created by door/window openings; and (3) identify connection failure points at openings. The layout for Test 10 is shown in Fig. 119.

The test articles for Wall Test 10 were a 16 ft x 12 ft standard unreinforced masonry block wall housing a reinforced steel door and an 8 ft x 8 ft CMU wall constructed inside a portable test cubicle. The interior of the 16 ft x 12 ft wall was retrofitted with a 1/8-in.-thick elastomeric coating that overlapped the roof and floor slabs tapered to 24 in. To isolate the masonry wall from the reaction structure, ¾-in. foam insulation board was installed with adhesive caulk on all sides of each CMU wall. Walls were allowed to move freely to approximate a one-way flexural response.

3.6.1 Construction

The 12 in. x 12 in. x 10 ft steel center divider used in previous tests was removed for Wall Test 10. The 7.5 ft x 2 ft x 3 ft concrete platform used in Wall Test 9 was also

removed. The mobile testing structure was placed the same distance from the charge as the permanent test structure before construction of the walls began.

The doorframe was installed before the walls were constructed. When the doorframe was in place, the CMU walls were built in the testing structures. The door was installed after the walls were completed.

The doorframe was properly placed, spaced, and plumbed, and the wall was then constructed around the frame. Clips (three per side) were hooked into the door jam and laid between the block. As the wall was constructed, the hollow steel jam of the door was filled with mortar. When the wall reached the top of the door, a header was formed using solid bottom lintel blocks. After the wall cured, the door was hung in place.

The door jam was widened with 2 in. x 3 in. x 1/8 in. steel tubing. The tubing was welded in place after installation in order to guarantee proper closing of the door. Two pieces of siding were used at the door handle to keep it functioning properly and to allow the door to close.

The door was reinforced with ¼-in. flat steel plate on the outside and 2 in. x 3 in. x 1/8 in. steel tubing on the inside. The door was sandwiched between the steel plate and tubing with bolts. Tubing was welded together before installation.

The front of the doorframe was secured to the front of the CMU wall with ¼ in. steel plate that was approximately 6 in. wide. It was bent to fit the front of the doorframe and then welded. Steel plate was attached to the front of the CMU wall with concrete screws. Reinforcement is shown in the exterior and interior views of the door in Fig. 120.

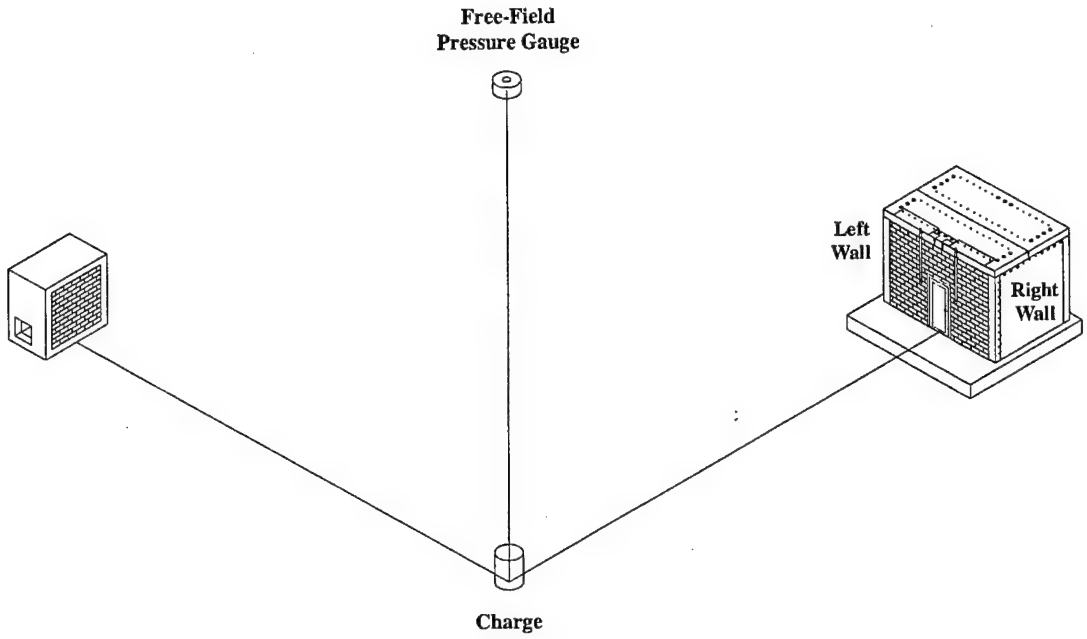

FIG. 119. Test 10 Layout

Cleaning and priming were completed to ensure a strong bond between the wall and the polymer. In Wall Test 10, several parts of the structure were sandblasted: the masonry wall roof, masonry wall floor, metal doorframe, and roof cladding. After sandblasting, concrete and metal surfaces were primed with two different primers, one primer specific to each material. A smooth transition was made between the roof and wall, between the floor and wall, and between the door jam and wall with an open weave fiberglass scrim fabric and epoxy. This weave allowed the polymer to fill the openings while reducing the amount of material required.

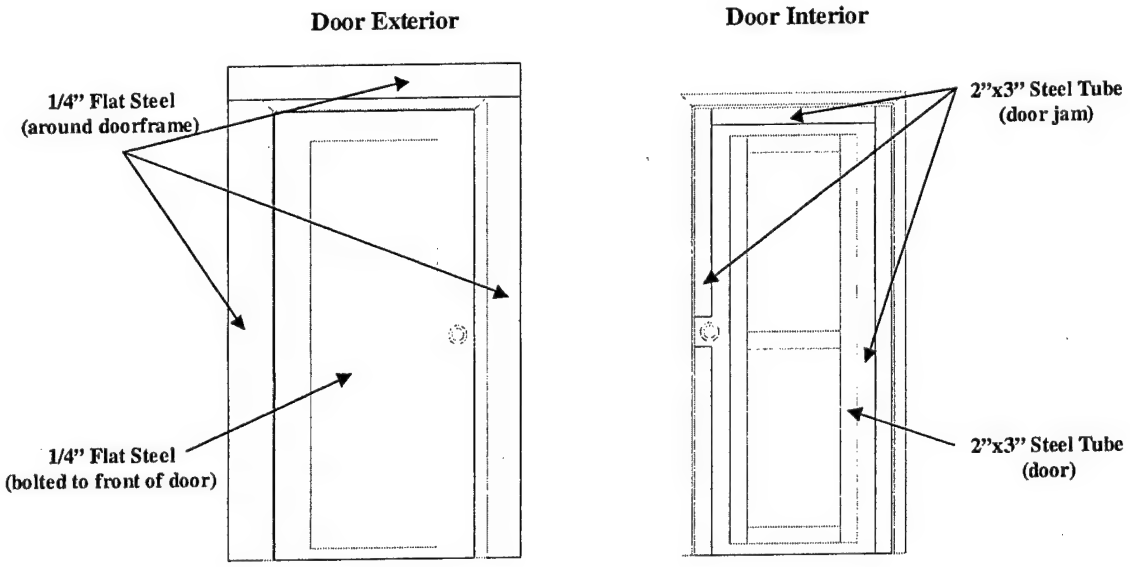

FIG. 120. Test 10, Interior and Exterior Door

After all cleaning and priming were completed, the walls were coated with a 1/8-in.-thick layer of polymer. The polymer overlapped the floor and roof of the reaction structure by 12 in. and tapered out to 24 in. The polymer was also applied to the doorframe. It stopped where the door jam met the closed door. To maintain a consistent overlap and also to allow free movement on all sides, masking was applied before spraying of the polymer began. Ceiling and floor overlaps are shown in Figs. 121 and 122. The wall constructed in the permanent reaction structure is shown in Fig. 123. The finished wall inside the cubicle is shown in Fig. 124.

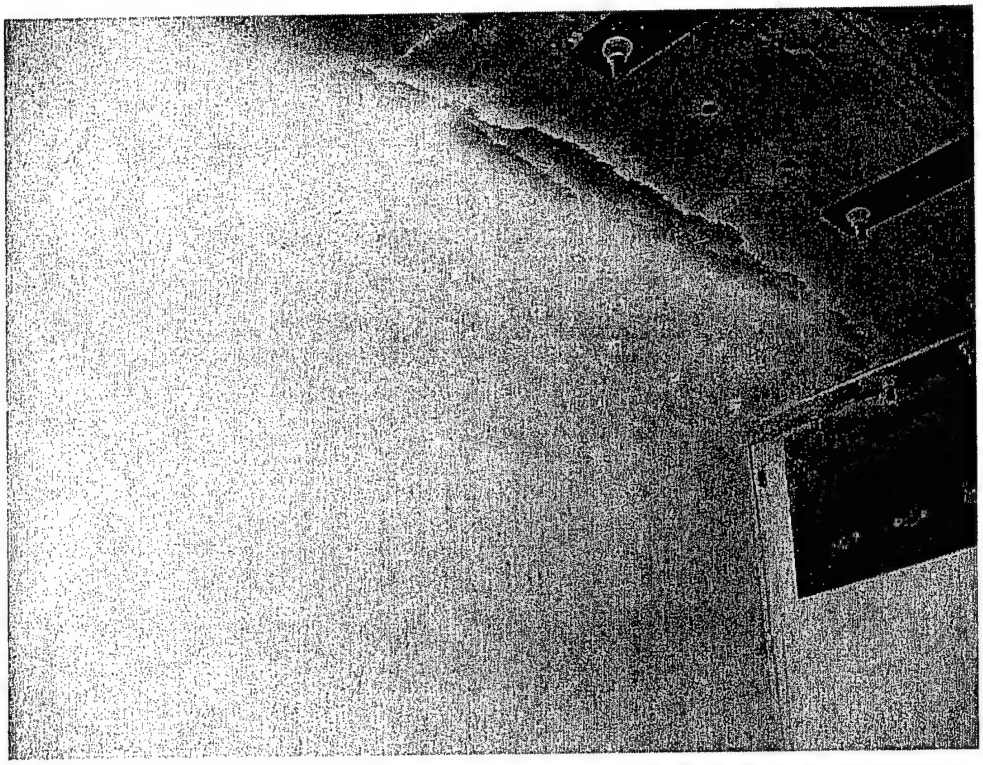

FIG. 121. Test 10, Ceiling Overlap

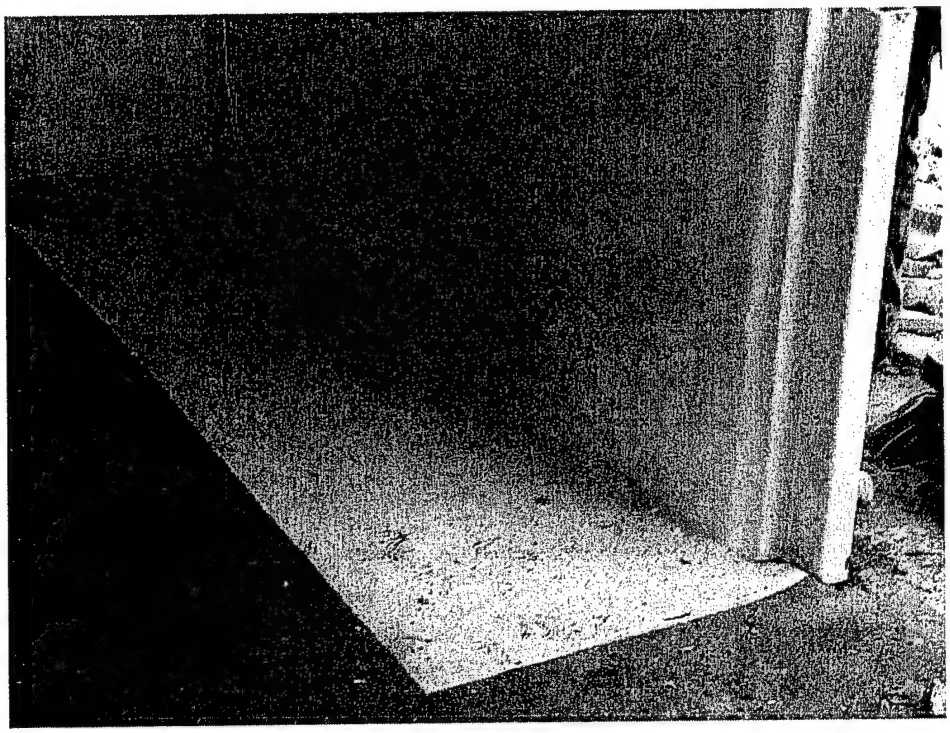

FIG. 122. Test 10, Floor Overlap

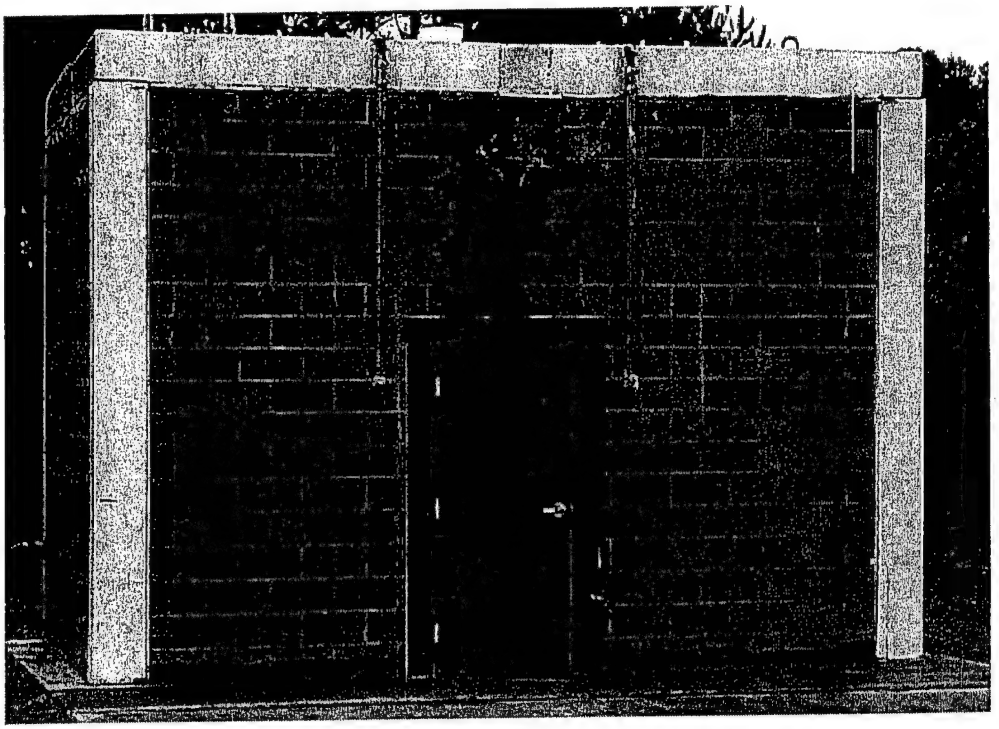

FIG. 123. Test 10, Constructed Wall

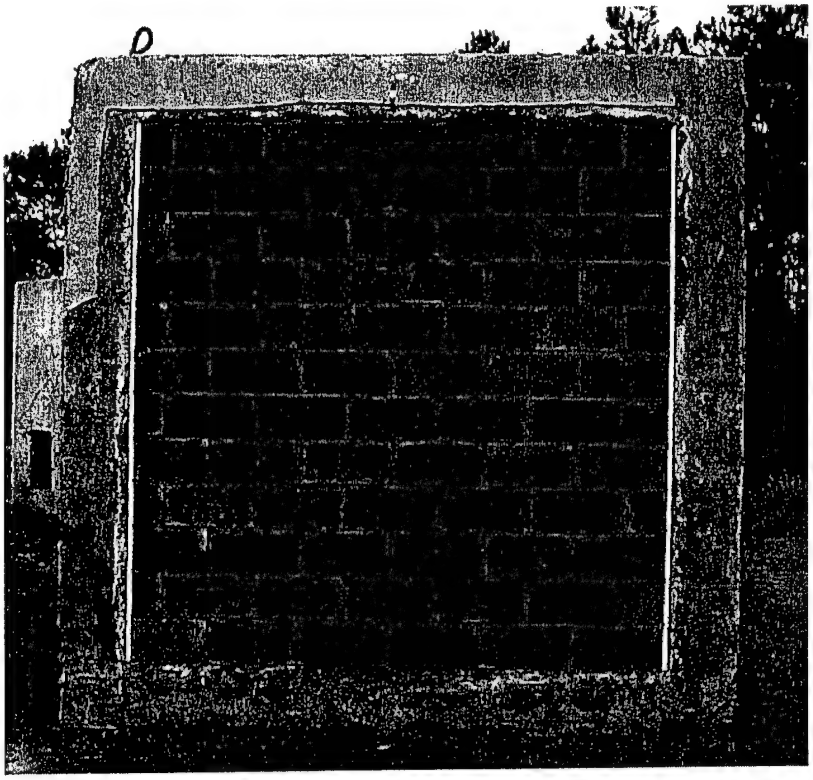

FIG. 124. Test 10, Test Cubicle

3.6.2 Instrumentation

Gauge instrumentation used in Wall Test 10 included two reflected pressure gauges (R1, R2, R3), two free-field pressure gauges (F1, I1), and three deflection gauges (D1, D2, L1). The reflected pressure gauges were installed in pipes suspended on the front of the test structure. One free-field pressure gauge was placed at a standoff distance that was equal to the distance from the explosive charge to the testing structures, but in a different direction. The other free-field pressure gauge was placed inside the permanent test structure. A laser deflection gauge was mounted on the left wall. A gear and a yo-yo gauge were mounted on the right wall. The gear-driven gauge measured displacement with a rotational position transducer. Fig. 125 shows the locations of all the gauges. No gauges were placed inside the small test cubicle.

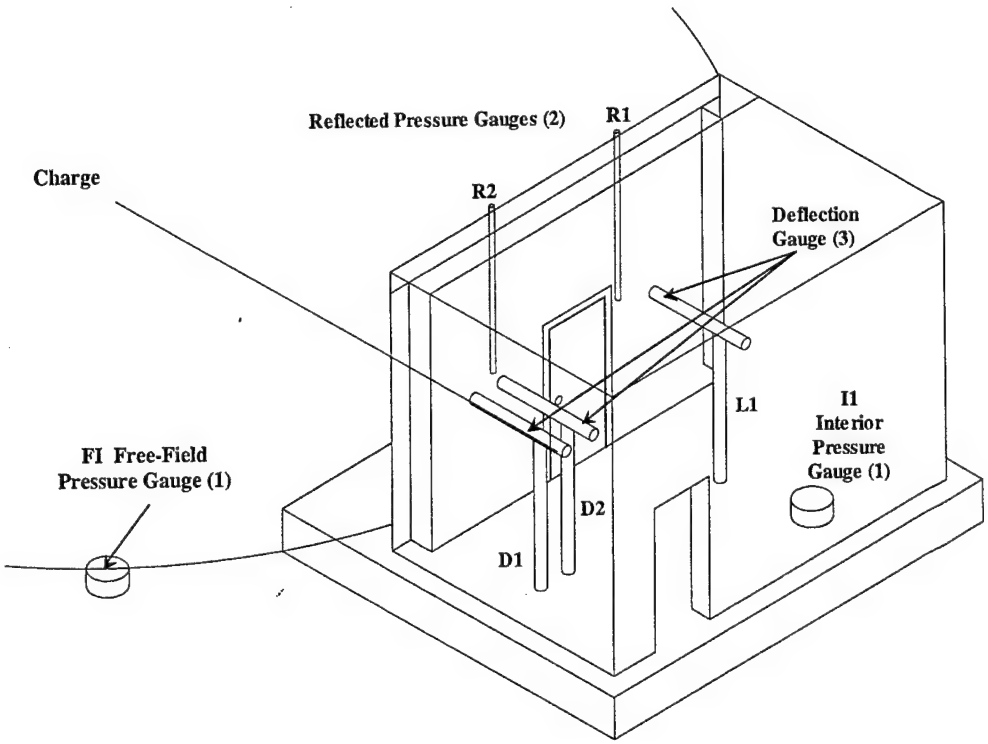

FIG. 125 Test 10, Gauge Locations

Photography support included pre- and post-test digital still photography and high-speed photography taken during the blast. Spy cameras were mounted in each inside back corner of the test structure to capture the deflection of each wall. The camera on the left was directed toward the right wall. The camera on the right was directed toward the right wall. A high-speed digital camera was positioned outside the test structure to capture deflection from an outside view. There were five areas targeted by the inside spy cameras, including the top and bottom of each half of the wall (total of four) and one around the door (Fig. 126).

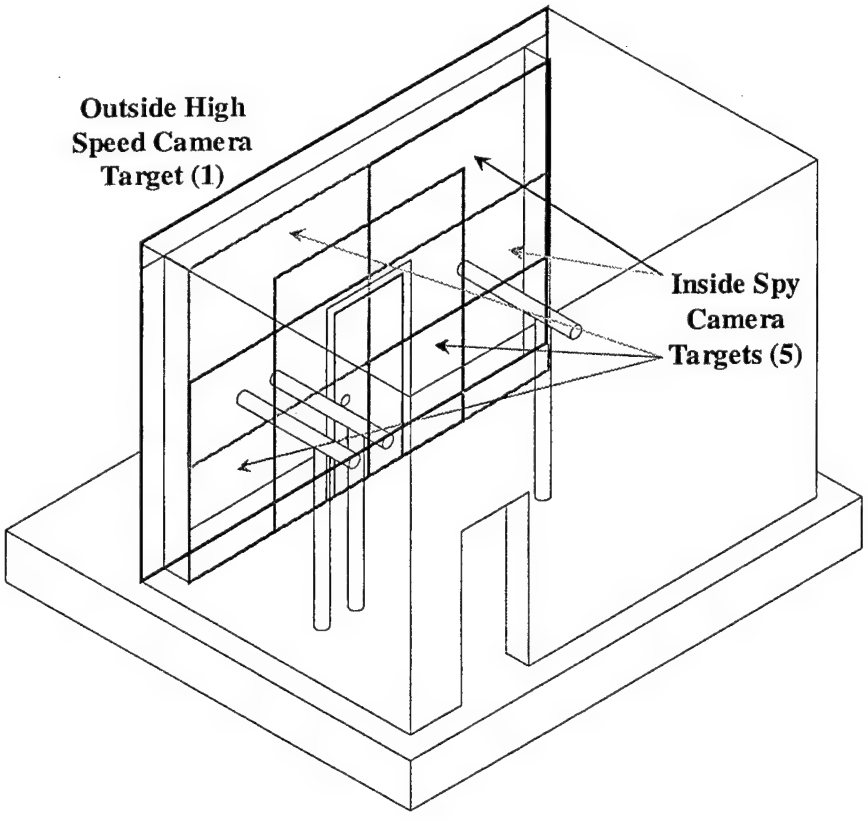

FIG. 126. Test 10, Interior Camera Target Areas

Gauge predictions were made with the WAC software and are provided in Table 9. Instrumentation for Wall Test 10 included seven gauges. Predictions for each gauge are shown in the table.

TABLE 9. Test 10, Gauge Predictions

Gauge ID	Type	Location	Prediction
R1	Reflected Pressure	Center Steel Support, 7.5 ft from bottom of wall, outside	41 psi
R2	Reflected Pressure	Center Steel Support, 5 ft from bottom of wall, outside	41 psi
F1	Free-field Pressure	Outside Structure	15 psi
I1	Free-field Pressure	Inside Structure	3 psi
L1	Laser Deflection	Left Wall, Inside	12 in.
D1	Yo-Yo Deflection	Right Wall, Inside	12 in.
D2	Gear-Driven Deflection	Right Wall, Inside	12 in.

3.6.3 Results

Two walls were tested in Wall Test 10, one with polymer retrofit and one without retrofit. The wall without retrofit collapsed. The retrofitted wall did not collapse. Defacing occurred at the bottom and the top of the retrofitted wall that contained the door.

With the exception of L1, all gauges from Wall Test 10 recorded data. Data is shown in Figs. 127 through 132. Figs. 127 and 128 show reflected pressure data. Figs. 129 and 130 show free-field pressure. Figs. 131 and 132 show deflection data.

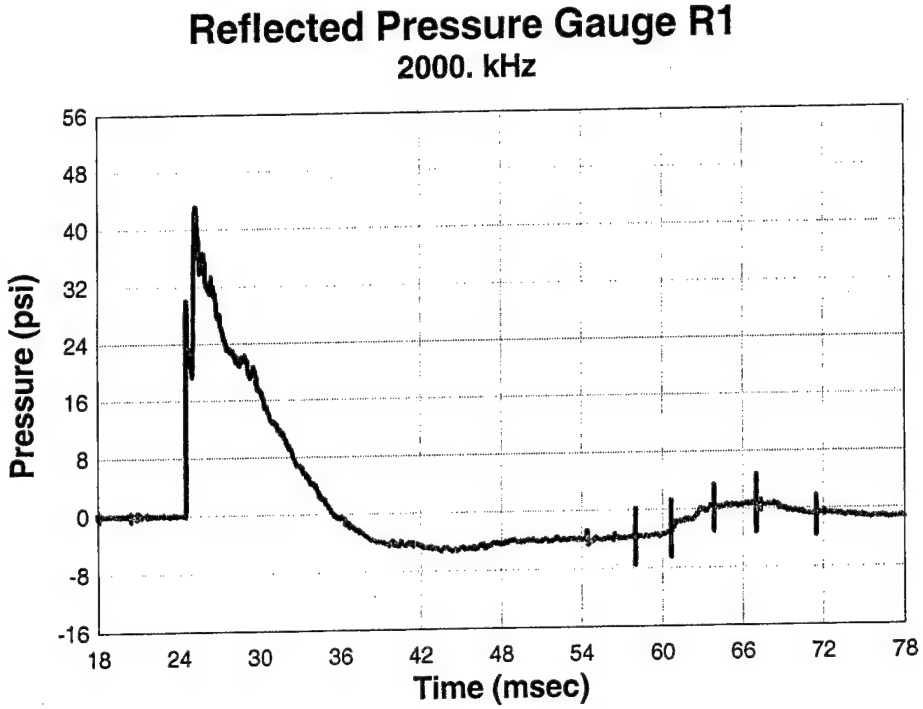

FIG. 127. Test 10, Gauge R1

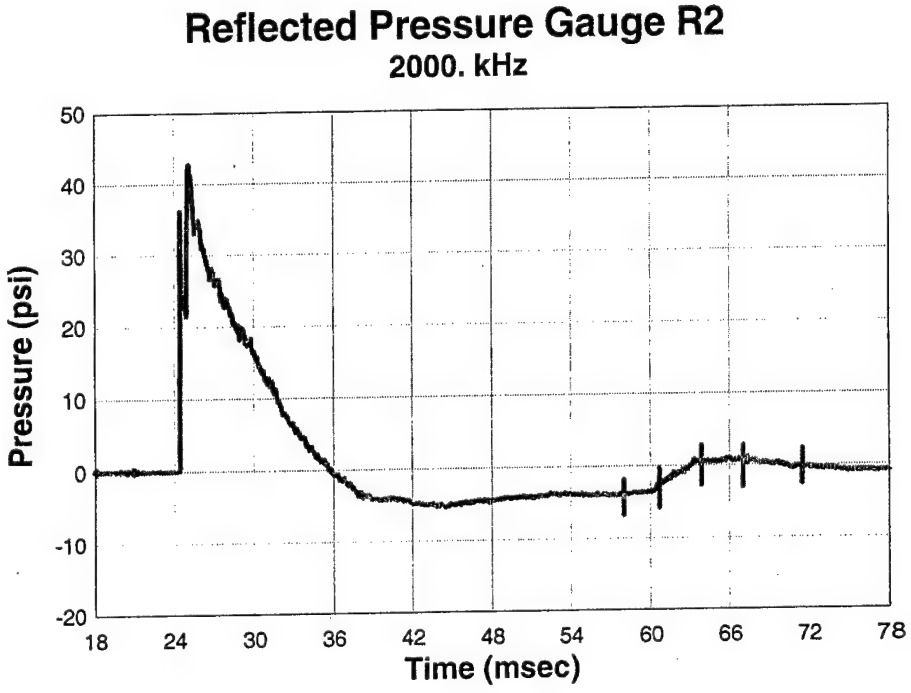

FIG. 128. Test 10, Gauge R2

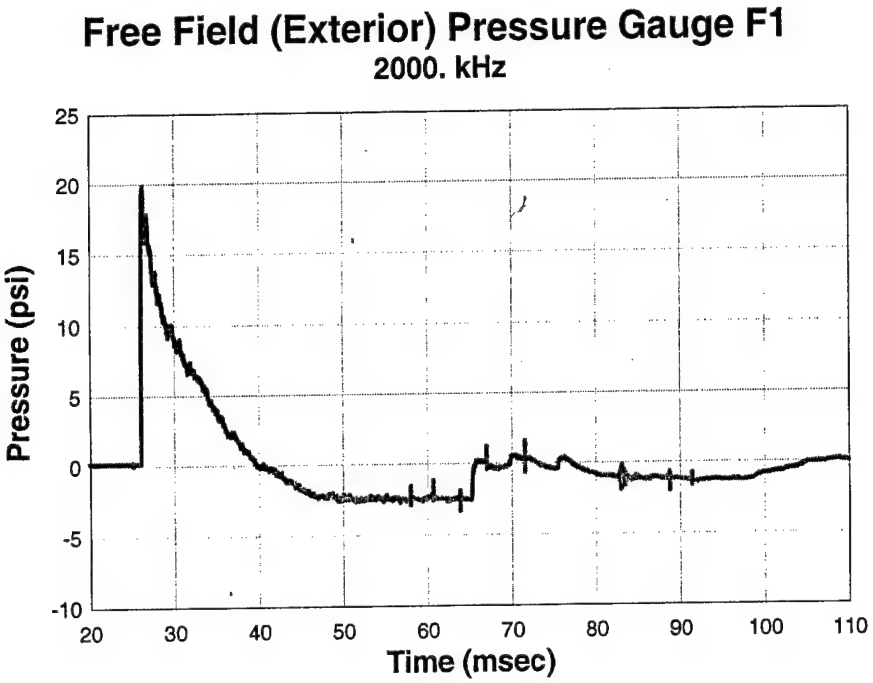

FIG. 129. Test 10, Gauge F1

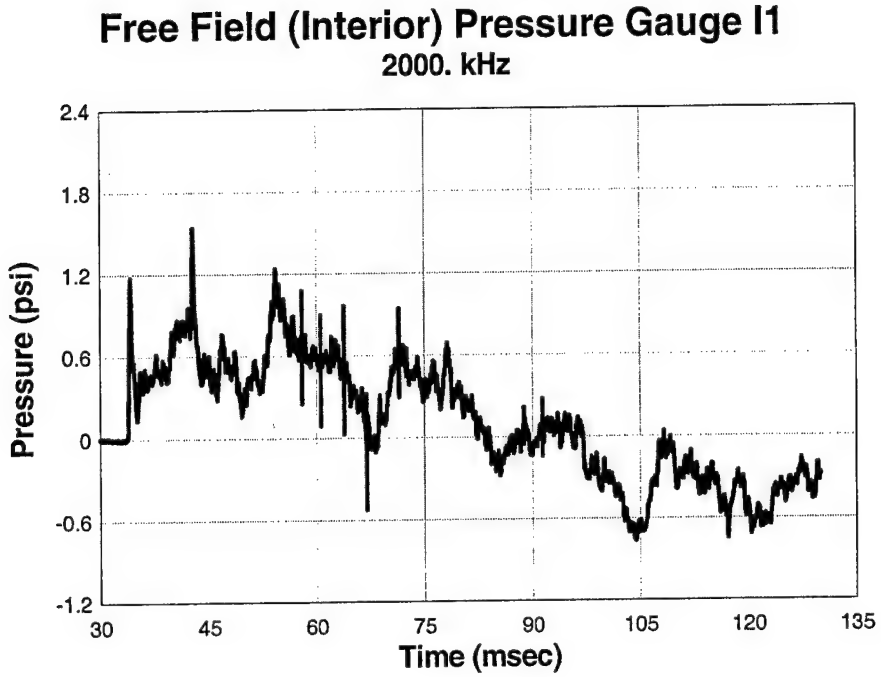

FIG. 130. Test 10, Gauge I1

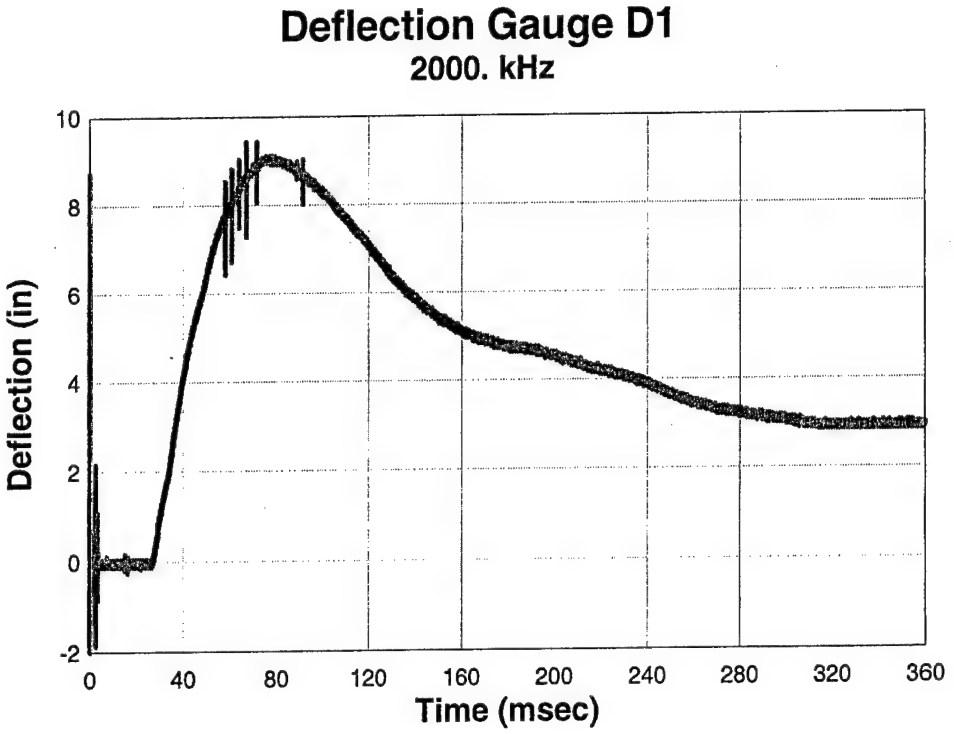

FIG. 131. Test 10, Gauge D1

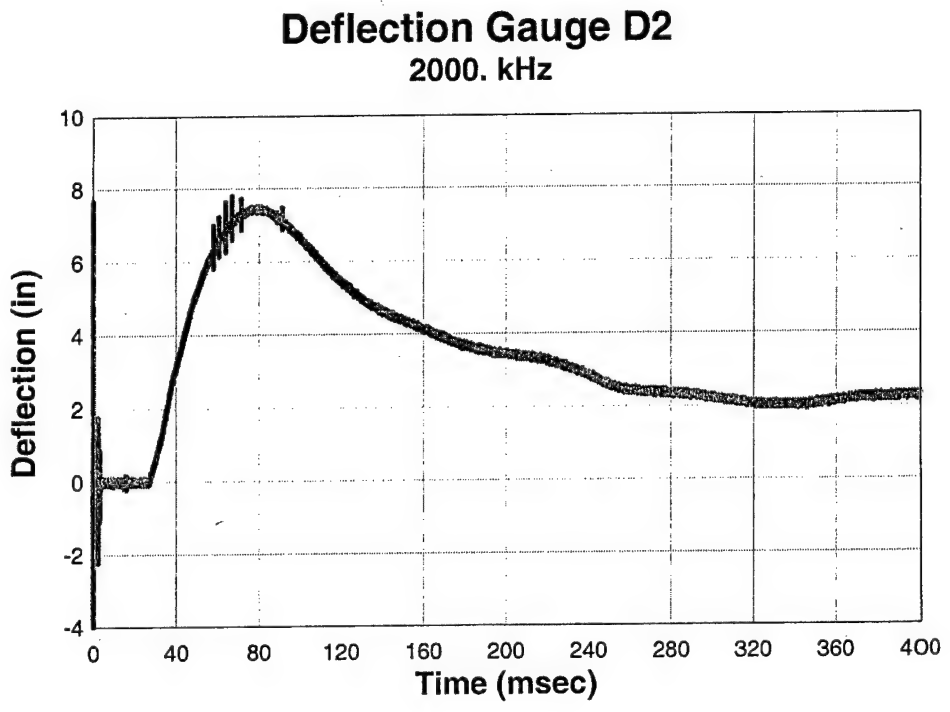

FIG. 132. Test 10, Gauge D2

The maximum pressures experienced by the walls in this test were (R1) 43.4 psi at 25.3 msec and (R2) 42.8 psi at 25.0 msec. The maximum pressures recorded by the free-field pressure gauges were (F1) 20.0 psi at 26.2 msec and (I1) 1.5 psi at 42.8 msec. The maximum measures of deflection recorded by the deflection gauges were (D1) 9.1 in. at 76.7 msec and (D2) 7.6 in. at 79.0 msec. The L1 deflection gauge failed. Table 10 summarizes the predicted and actual measurements for Wall Test 10.

TABLE 10. Test 10, Predicted vs. Recorded Data

Gauge ID	Type	Prediction	Actual
R1	Reflected Pressure	41 psi	43.4 psi
R2	Reflected Pressure	41 psi	42.8 psi
F1	Free-field Pressure	15 psi	20.0 psi
I1	Free-field Pressure	3 psi	1.5 psi
L1	Laser Deflection	12 in.	Gauge Failure
D1	Yo-Yo Deflection	12 in.	9.1 in.
D2	Gear-Driven Deflection	12 in.	7.6 in.

The wall with the door sustained damage. There was defacing at the top and bottom of the wall. The door connections failed. There were mortar bond cracks at

approximately mid-height of the wall. Figs. 133 and 134 show the damage to the two structures.

The purpose of Wall Test 10 was to test the effects of the door opening. The opening did not result in failure of the polymer coating technique. Defacing of the blocks and mortar joint failures have been seen in every test, regardless of openings.

The polymer coating on the interior of the wall experienced a tear due to shear from mortar joint failure. A tear easily propagates once initiated. Mortar joint failure and consequent tears in the polymer are shown in Figs. 135 through 139. The steel door is shown in Fig. 140.

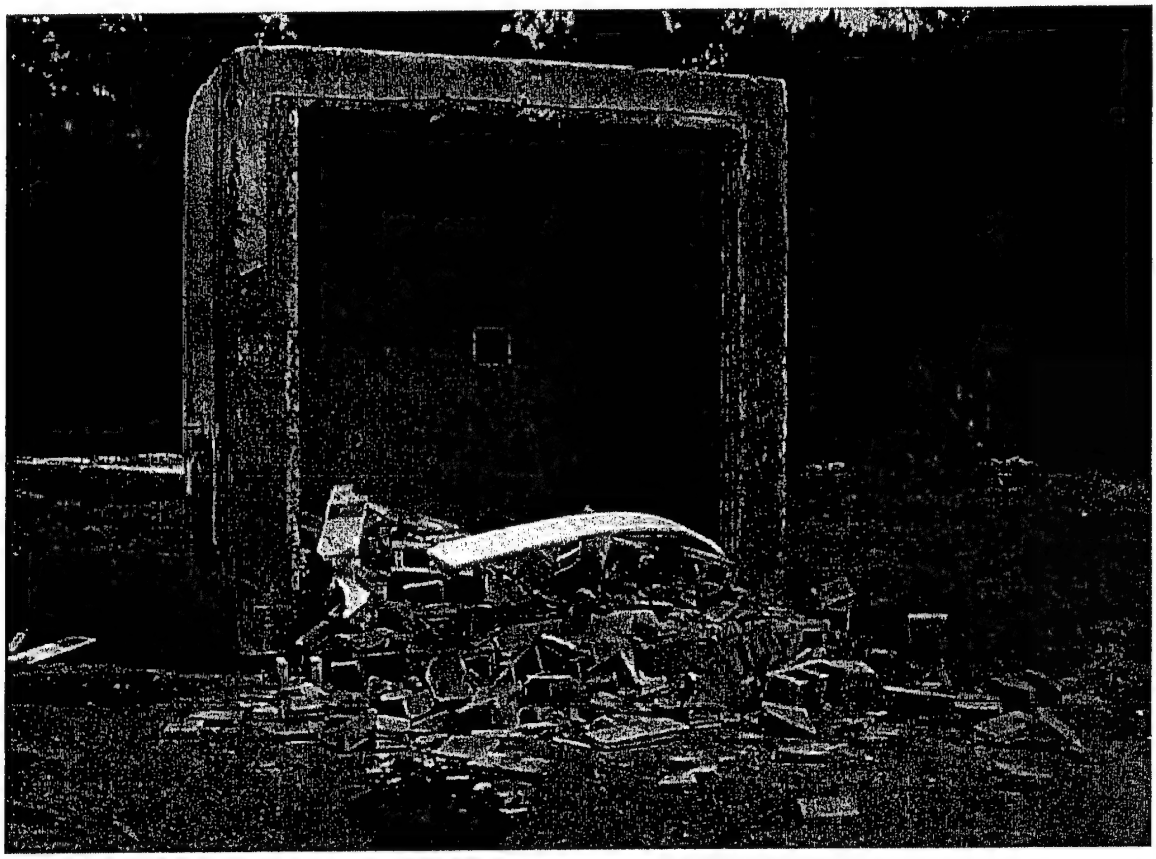

FIG. 133. Test 10, Posttest Test Cubicle

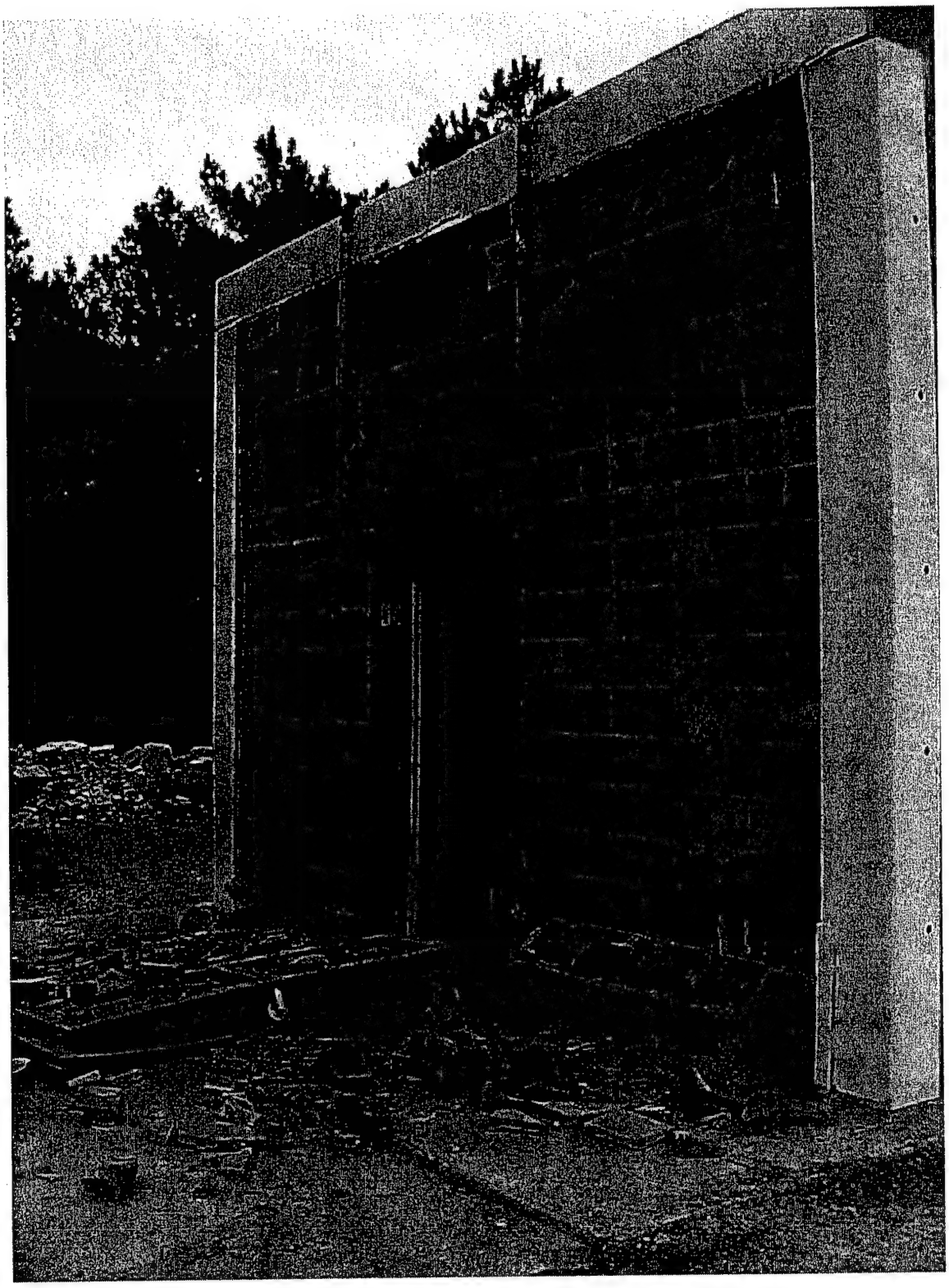

FIG. 134. Test 10, Posttest Test Structure

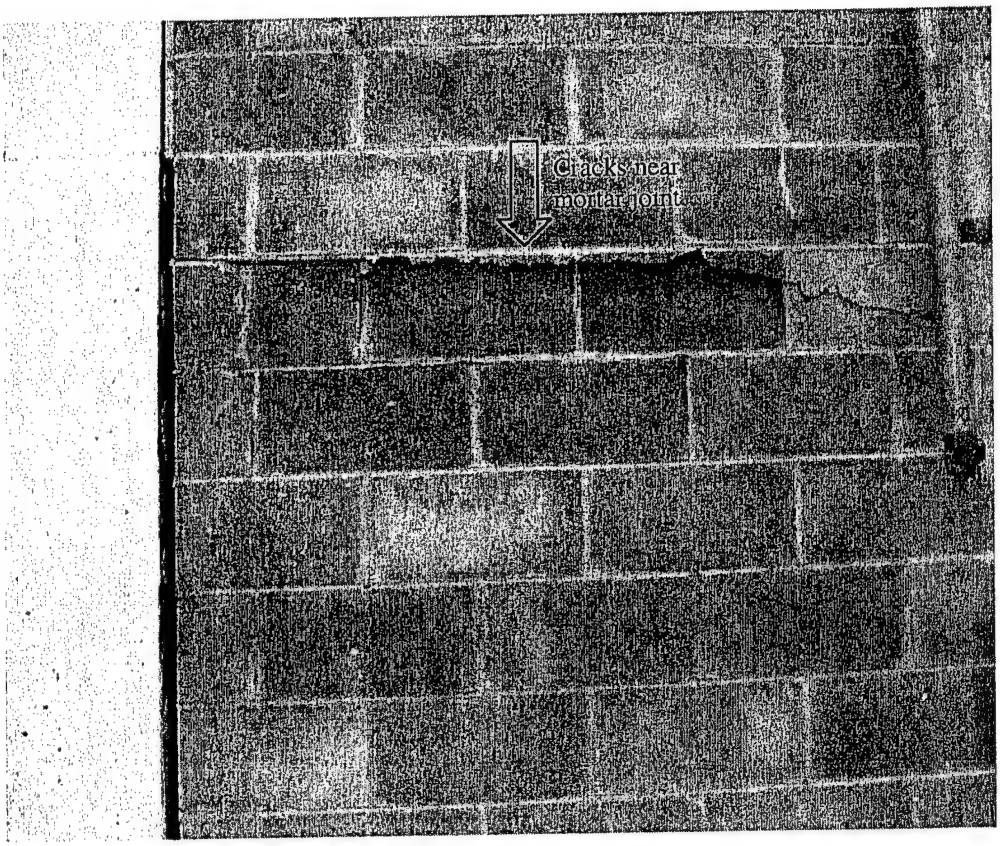

FIG. 135. Test 10, Shear Cracks, Left Side

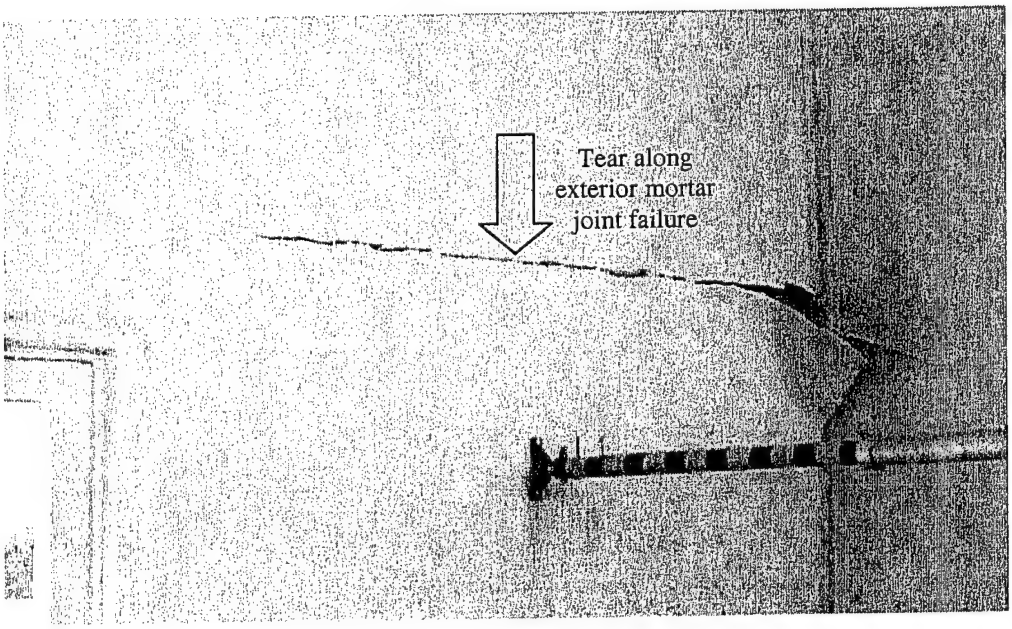

FIG. 136. Test 10, Left Side Interior Tear

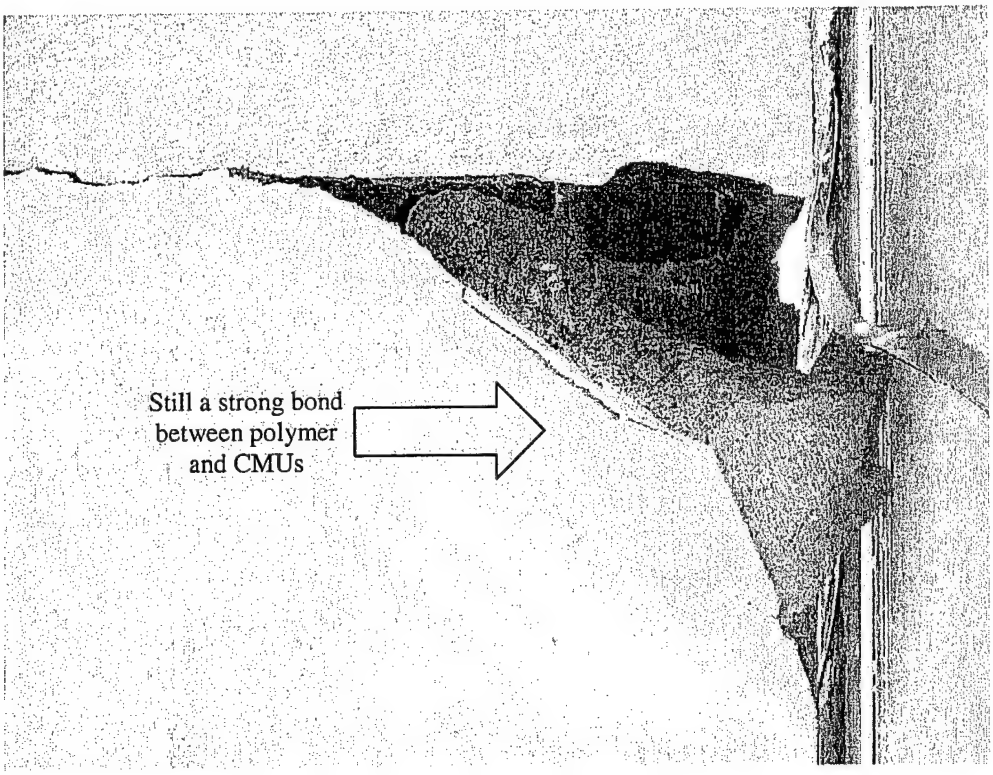

FIG. 137. Test 10, Protruded Block, Left Side

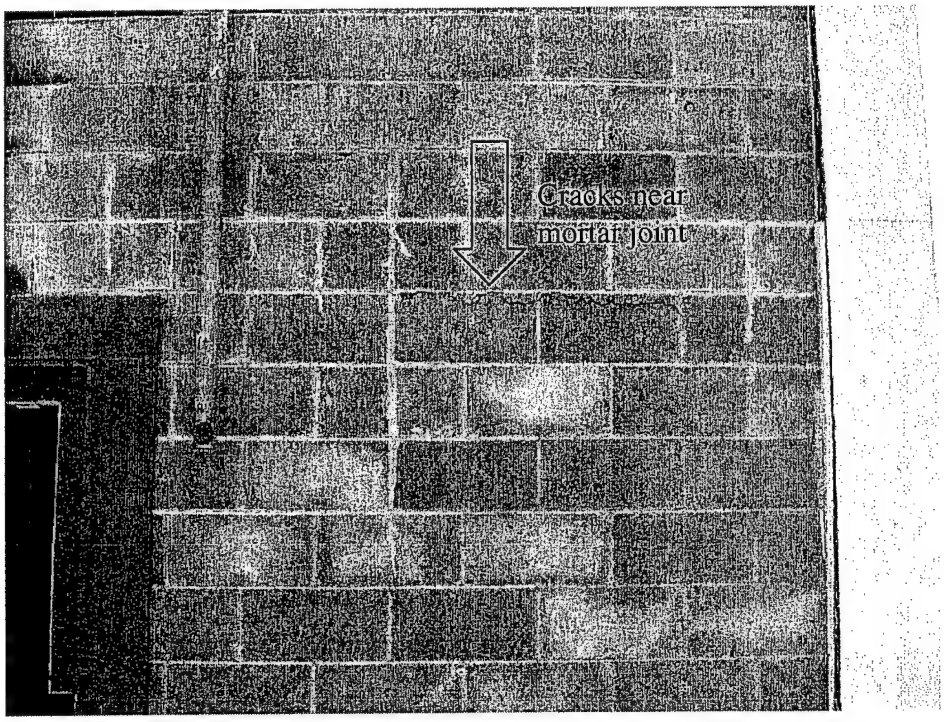

FIG. 138. Test 10, Shear Cracks, Right Side

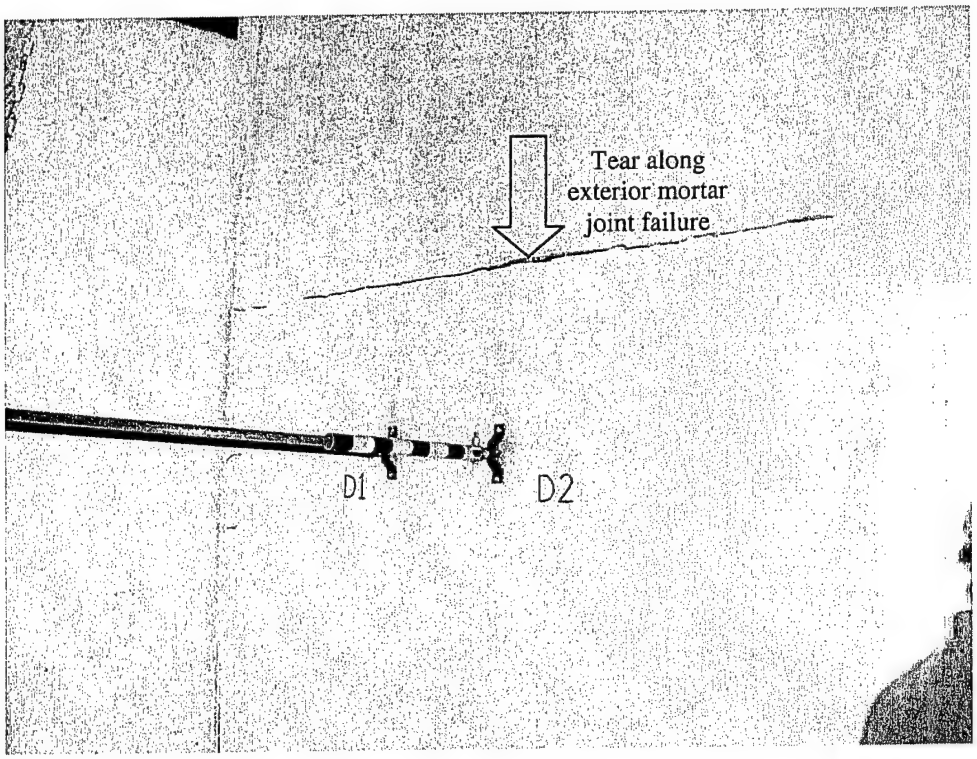

FIG. 139. Test 10, Right Side Interior Tear

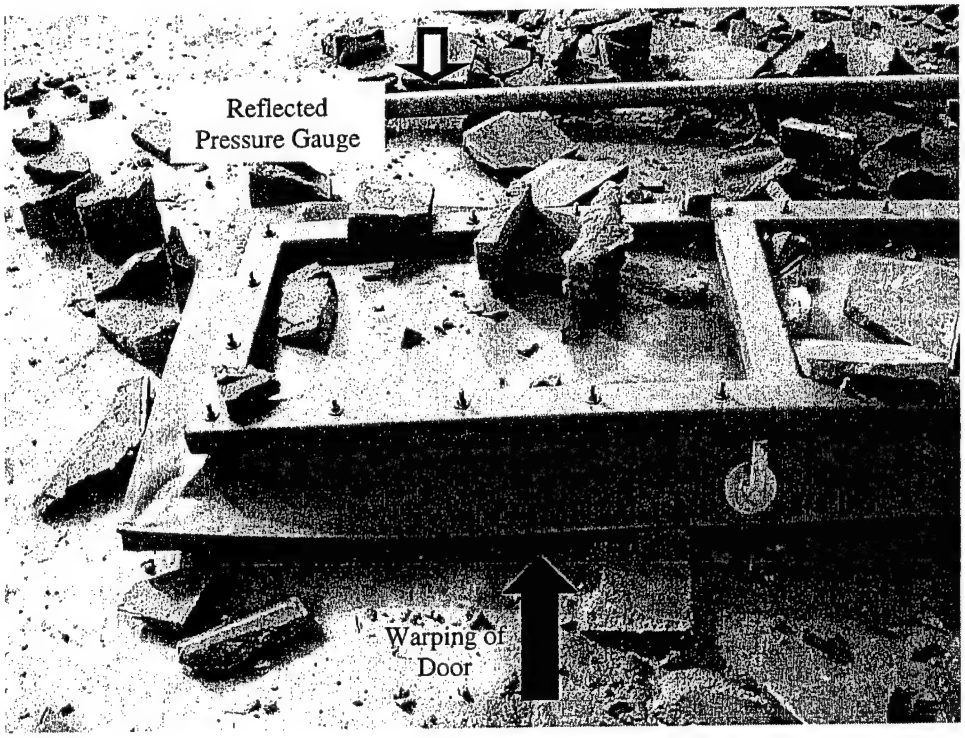

FIG. 140. Test 10, Steel Door, Post Test

3.7 Wall Test 11

Wall Test 11 involved an explosive test on a 16 ft wide x 12 ft tall CMU wall that contained a 3 ft x 4 ft steel frame window. The inside of the wall was coated with a 1/8-in.-thick elastomeric polymer coating. The polymer overlapped the window frame, but did not cover the window. A clear film was applied to the window glass to keep the window intact. Also included in Wall Test 11 were two steel-framed windows mounted inside 8 ft x 8 ft frames and a single, instrumented CMU block placed at a specific distance in the test range, both of which are beyond the scope of this document. The objective of Wall Test 11 was to evaluate the performance of the polymer coating as structural reinforcement to the wall and window frame. Other key objectives were to (1) measure deflection of wall elements; (2) evaluate failure modes created by the window opening; (3) identify connection failure points at opening; and (4) measure the pressure on the front face of a single CMU block.

A layout for Wall Test 11 is shown in Fig. 141. The CMU wall, the individual window walls, the single CMU block, two free-field pressure gauges, and the explosive charge are all illustrated in the figure.

The test article was one 16 ft wide x 12 ft tall unreinforced masonry wall. Foam insulation board was used to separate the wall from the test structure to approximate a one-way flexural response. The insulation board was applied to the interior sidewalls of the structure with an adhesive caulk.

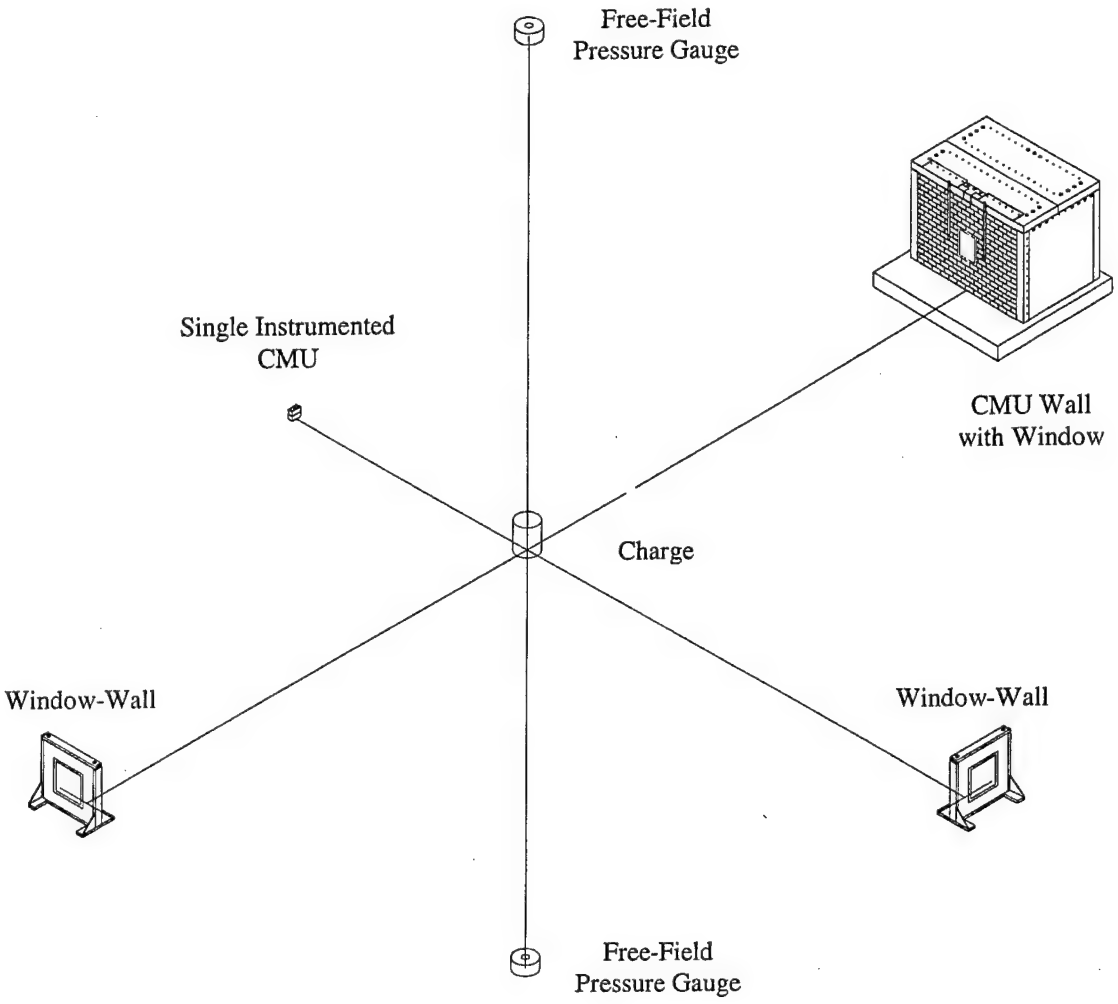

FIG. 141. Test 11 Layout

3.7.1 Construction

Window Frame Construction: The window frame used for this test was fabricated by the AFRL using a 1/8-in. steel plate. Flat steel was bent into a 2 in. x 8 in. x 6 in. C-channel. The corners were cut at 45 degrees. The 2-in. section was placed inside the window opening so that a 2-in. air gap was maintained around the glass. The 8-in. side was punched with 2-in. diameter holes to allow overpressure to vent into the air gap during the blast. Corresponding holes were drilled into the CMUs to allow for additional venting.

Holes were drilled in the 2 in. and 6 in. sides of the C-channel to attach the front and back flanges of the frame. The front flange contained holes to allow the frame to be attached to the CMU wall with toggle bolts. The interior flange was punched with 1¼-in. diameter holes spaced ¼ in. apart across the entire surface of the flange. This was done to allow the polymer coating to adhere to the underlying CMU block as well as to hold the frame to the wall. An image of the cross-section of the window is shown in Fig. 142. A drawing of the complete frame is shown in Fig. 143. Images of wall construction are shown in Figs. 144 through 149. The completed wall is shown in Fig. 150.

The window fabrication could not be completed until the wall was constructed. A 2 in. x 4 in. wooden frame was placed in the wall to "stand in" as the wall was built. The opening of the window was placed near the center of the wall. The window was located 75 in. from the left wall, 80 in. from the right wall, and 31 in. above the floor slab. The insides of the masonry blocks below the window were filled with grout. Blocks on the sides of the window were left unfilled. 4.8-in. sections of 5/8-in. diameter rebar were

placed in four lintel blocks located just above the window. The blocks were then filled with mortar.

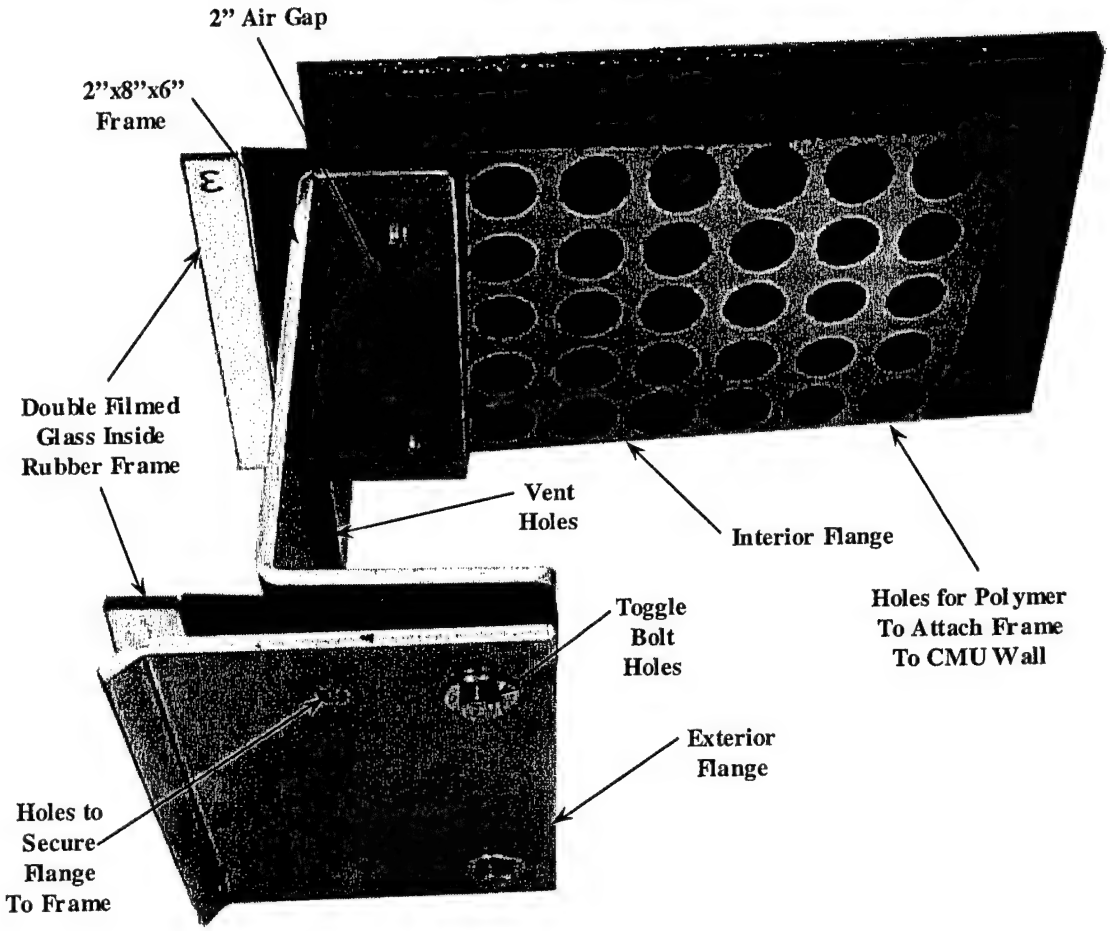

FIG. 142. Test 11, Window Cross-Section

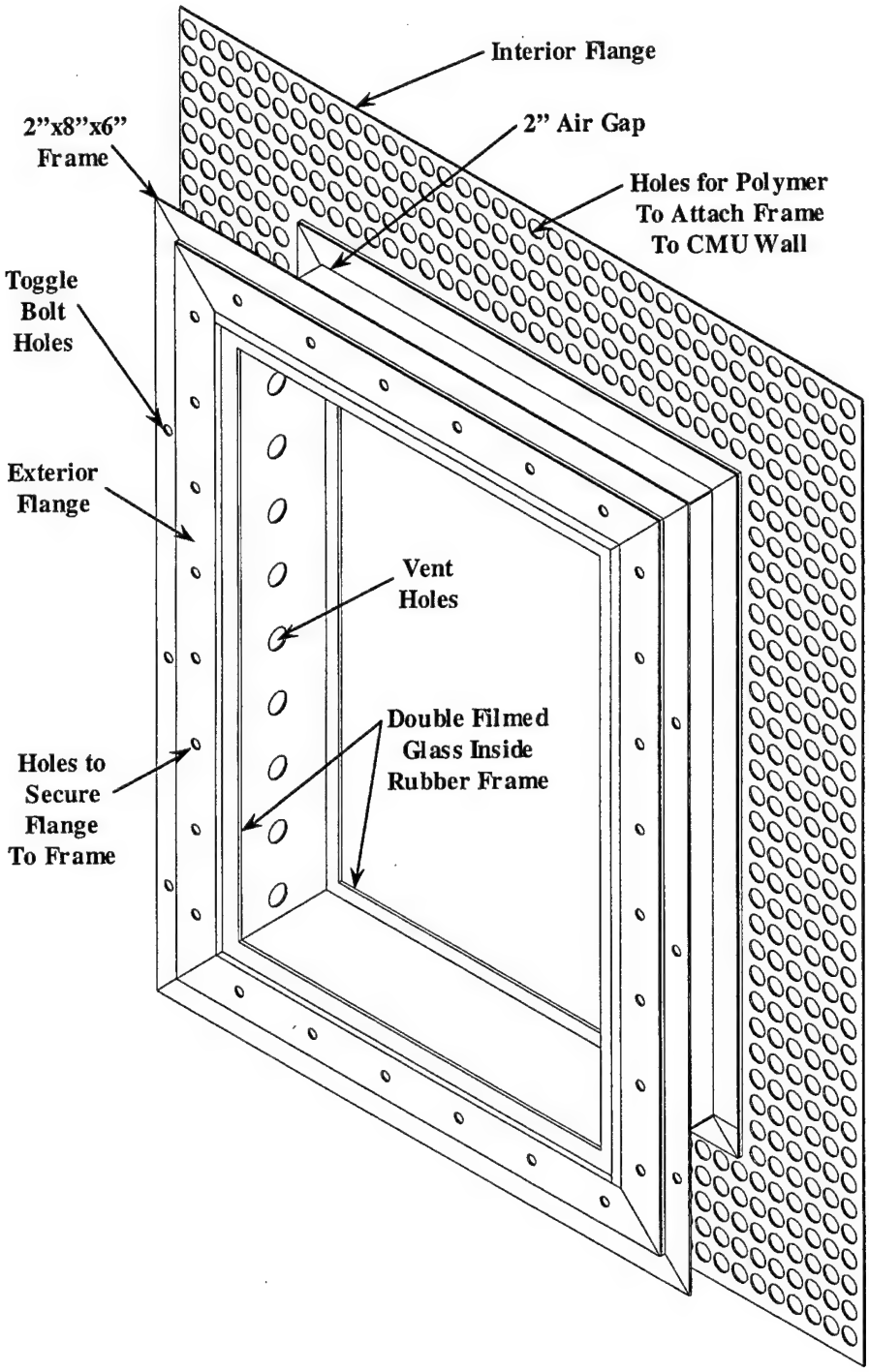

FIG. 143. Test 11, Complete Window

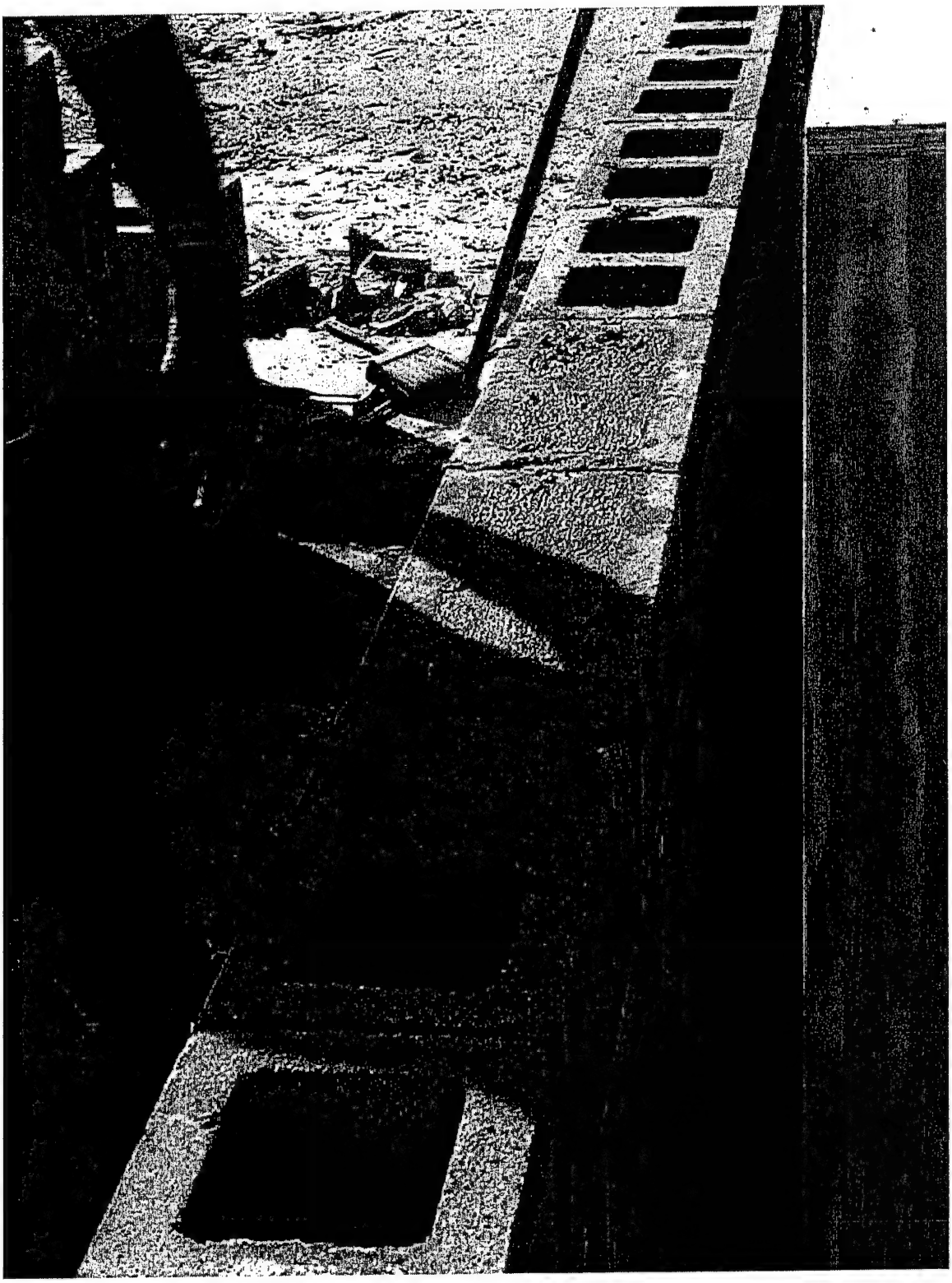

FIG. 144. Test 11, Blocks Beneath Window

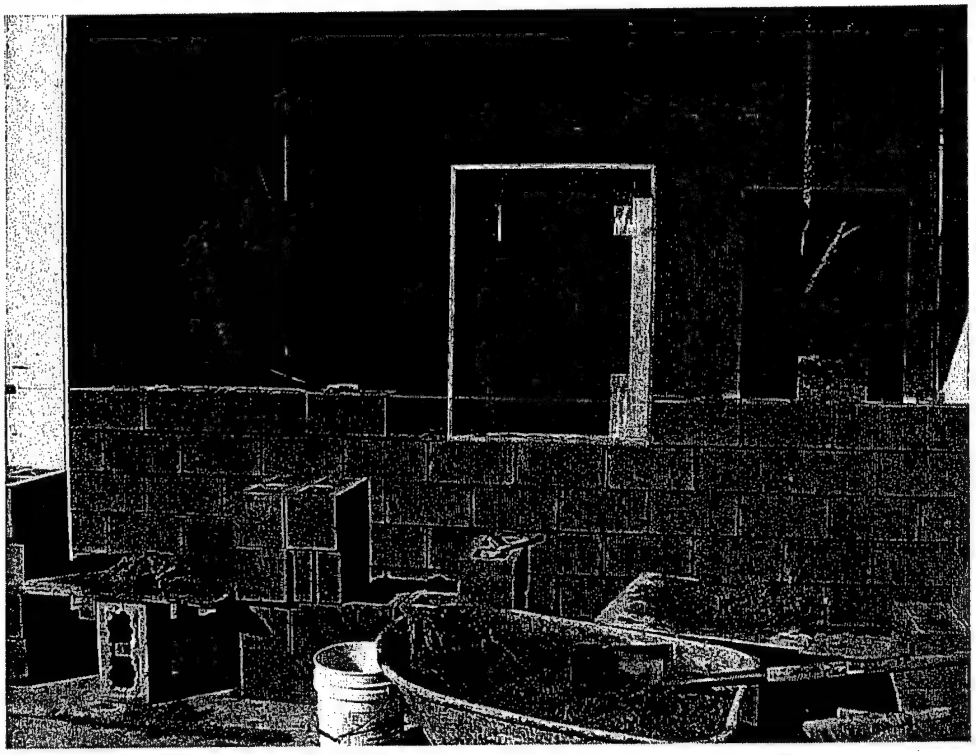

FIG. 145. Test 11, Wooden Stand-in Frame

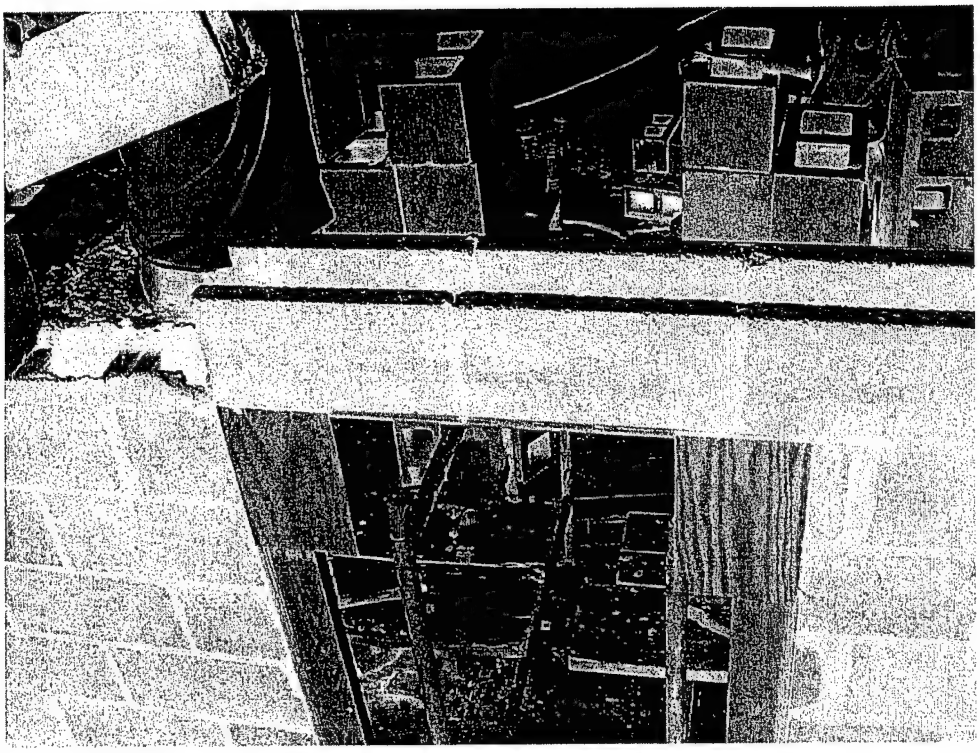

FIG. 146. Test 11, Empty Lintel Blocks

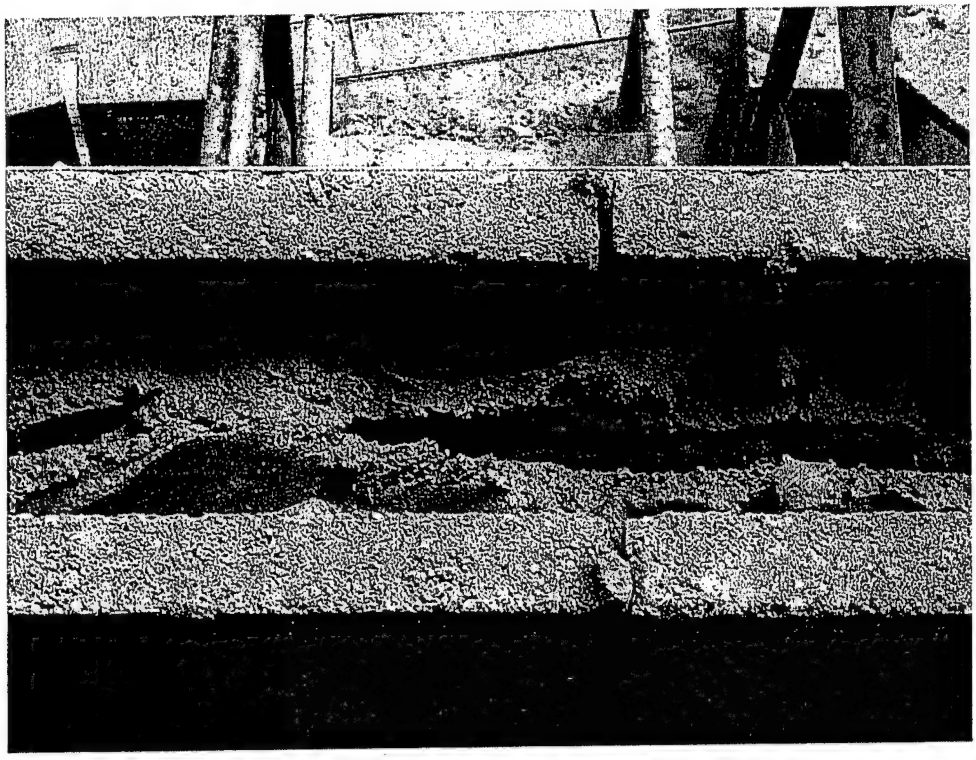

FIG. 147. Test 11, Lintel Blocks with Rebar

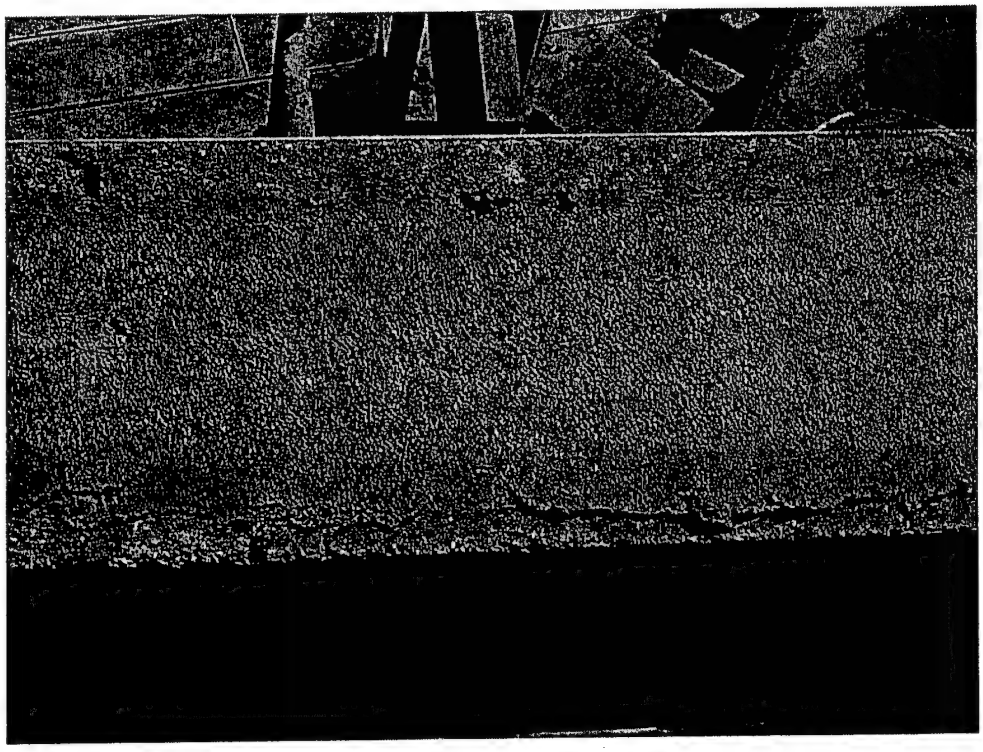

FIG. 148. Test 11, Complete Lintels

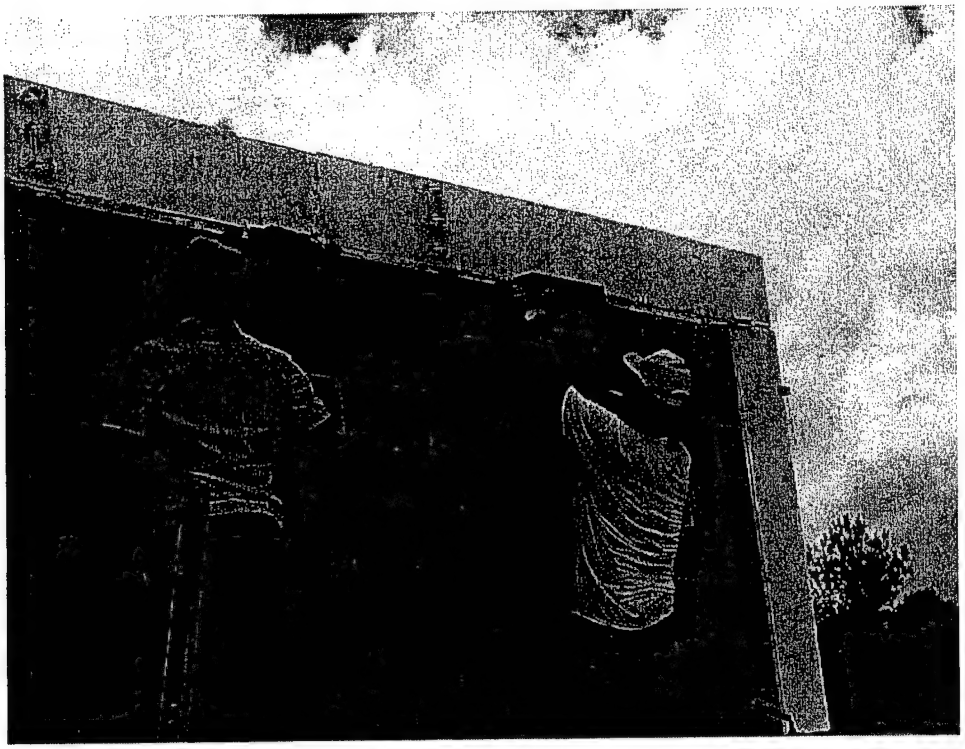

FIG. 149. Test 11, Completing the Construction

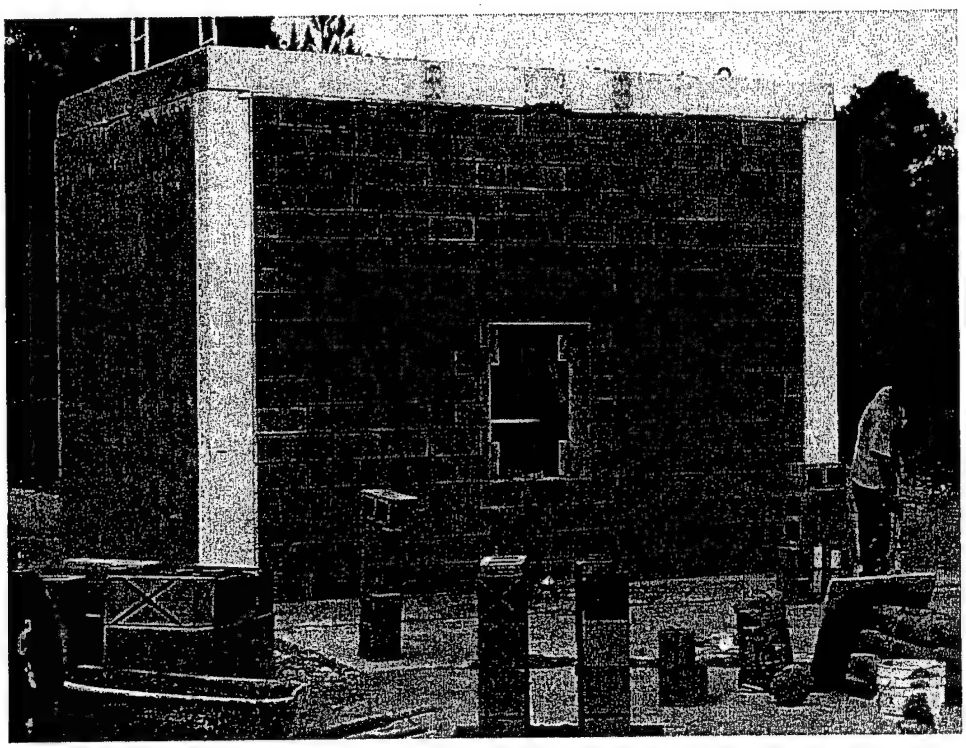

FIG. 150. Test 11, Completed Wall

After the wall was completely constructed, the temporary wooden window frame was removed to allow placement of the permanent window frame. A layer of black window adhesive was then applied to the exterior block around the window opening to allow the frame to be cinched up to the outside wall without any gaps. Holes were drilled in the sides of the CMU blocks on the sides of the windows to allow their hollow insides to vent overpressure. Holes were drilled on the outside of the structure to line up with the holes in the window frame. Using toggle bolts, the frame and window were attached to the structure. The interior flange was bolted to the frame. A drawing of the complete window installation plan is shown in Fig. 151. The installation and adhesive is shown in Fig. 152. The holes drilled in the windows to vent pressure are shown in Fig. 153. The completed window is shown in Fig. 154.

After the window was installed, the walls were cleaned and primed. The masonry wall roof, floor, metal window frame, and roof cladding were all cleaned with a wire brush. A different primer was applied to the concrete and metal surfaces. The instructions provided by the manufacturer were followed for each of the primers.

At the 90-degree joints between the roof and wall, floor and wall, and window frame and wall, an open weave fiberglass scrim fabric was applied with an epoxy bonding adhesive to create a smooth transition between the joints. The fabric reduced the amount of polymer needed to fill a corner and make a smooth transition.

After all preparation work was completed, the interior of the CMU walls and the interior window frame were coated with 1/8-in. thick polymer. The polymer overlapped onto the roof and floor of the reaction structure 12 in., tapering out to 24 in. The polymer also overlapped the interior of the window frame. The polymer stopped where the

interior flange met the rubber window frame. Masking was applied to maintain a consistent overlap while allowing free movement on the sides.

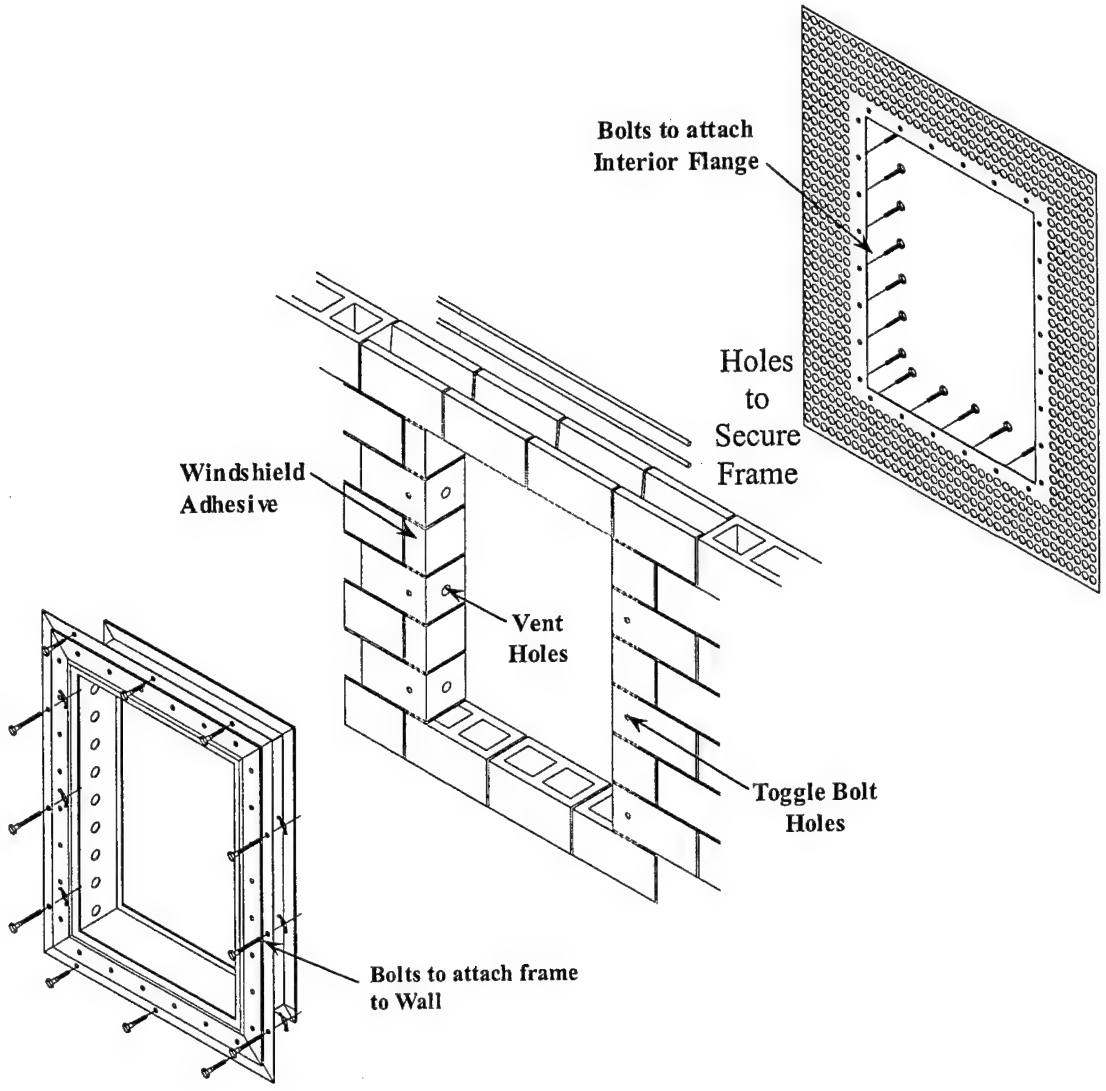

FIG. 151. Test 11, Window Installation Plan

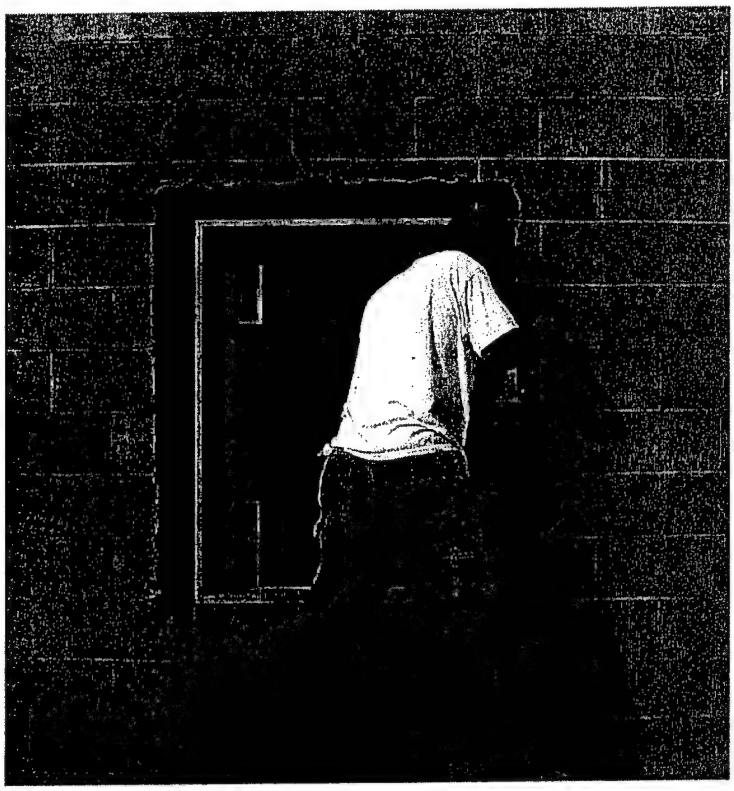

FIG. 152. Test 11, Window Adhesive

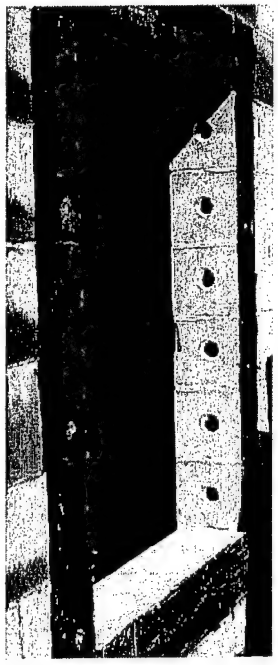

FIG. 153. Test 11, Overpressure Escape Holes

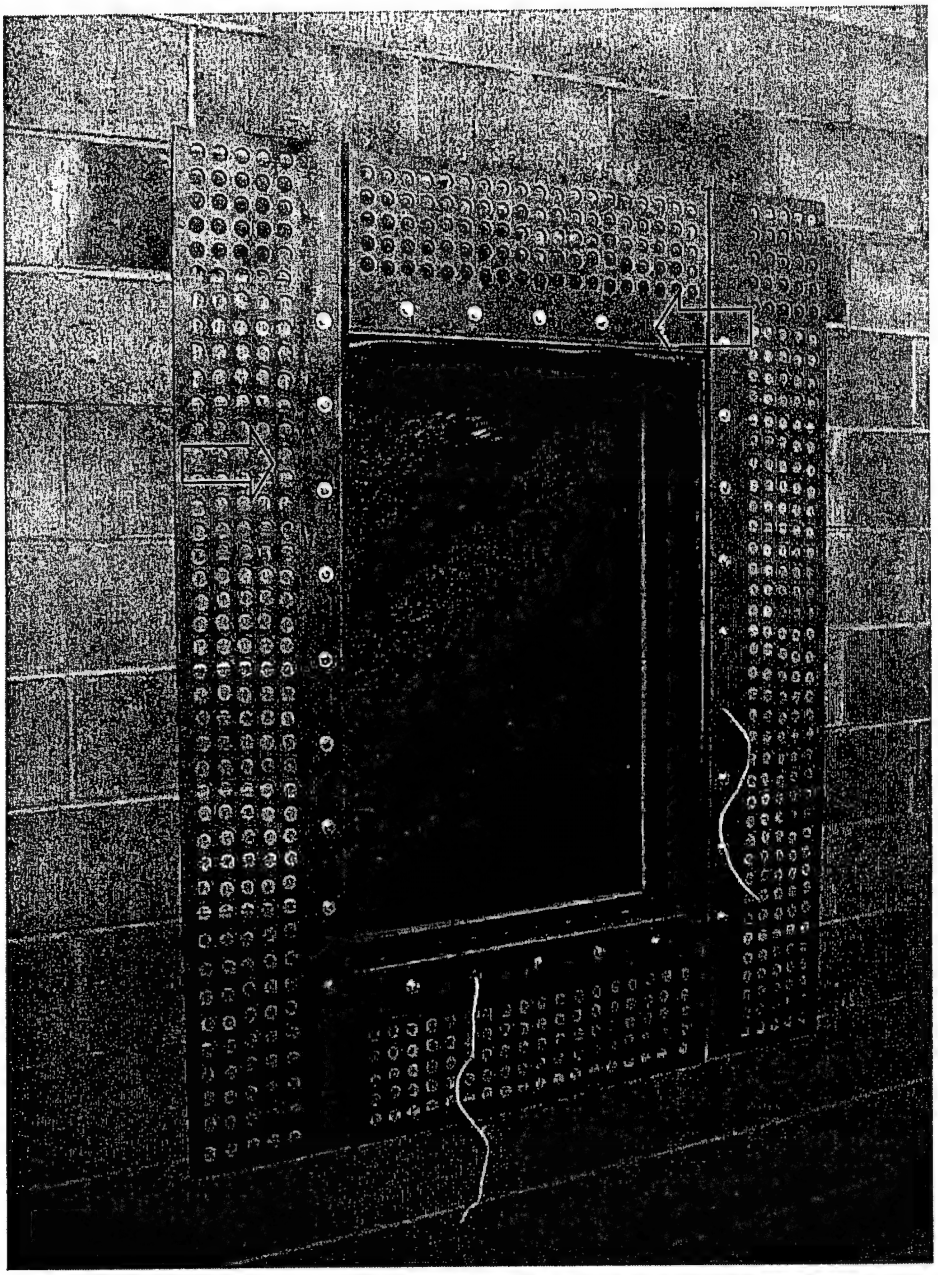

FIG. 154. Test 11, Installed Window

The front face of the wall was painted white and was not coated with polymer. This white paint helped re-piece the fragmented blocks after the test. The finished wall, complete with polymer and paint, is shown in Figs. 155 through 156.

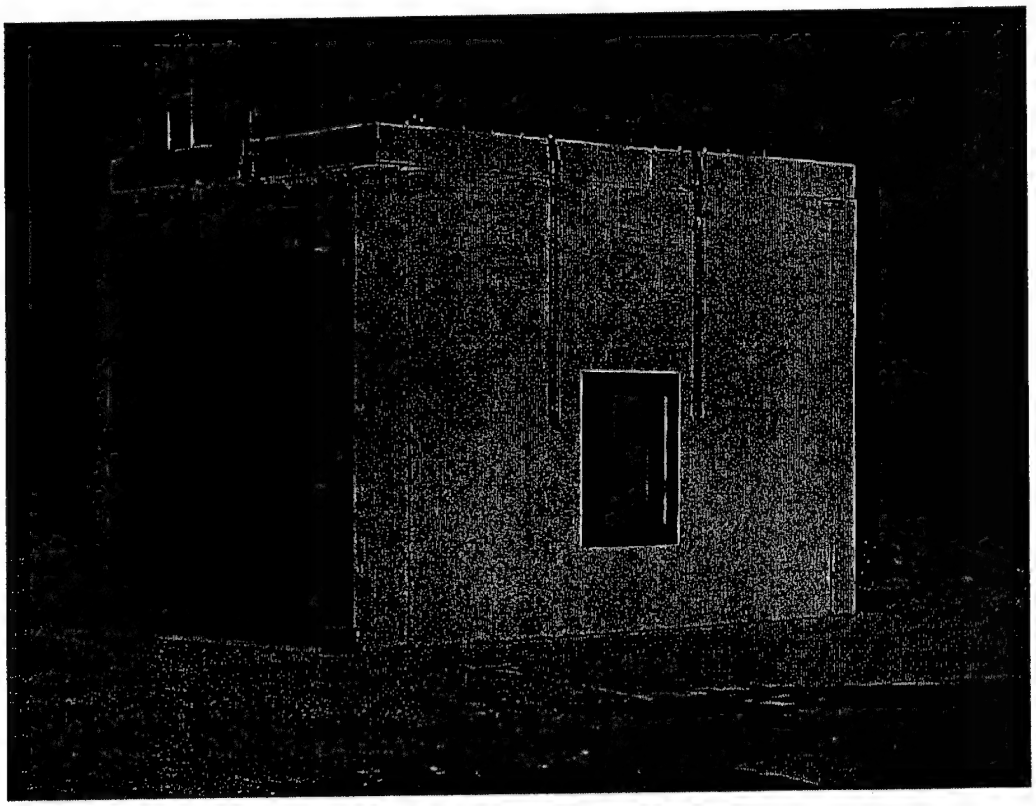

FIG. 155. Test 11, Complete Structure

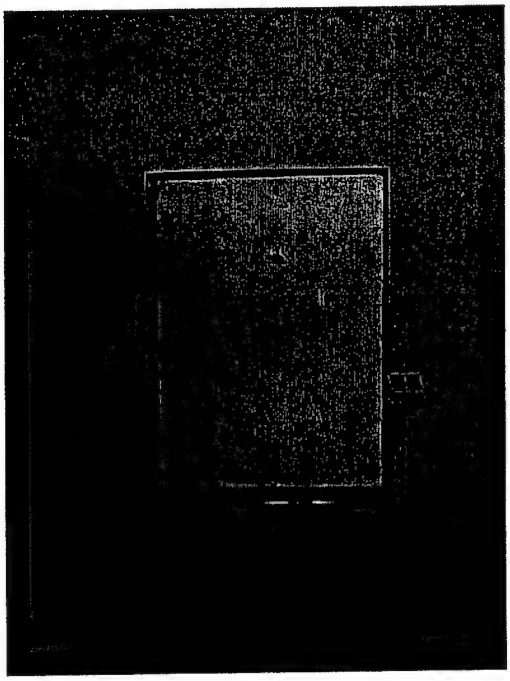

FIG. 156. Test 11, Retrofitted Window Frame

3.7.2 Instrumentation

Gauge instrumentation used in Test 11 included two pipe-mounted reflected pressure gauges (R1, R2) and four pressure gauges used inside the window mounting (WIS, WVS, WIB, WVB). Other gauges included one free-field pressure gauge (F1), one interior pressure gauge (I1), and three deflection gauges (D1, L1, L2). There were additional pressure gauges used on other elements in the test, but these are beyond the scope of this document. The gauges are shown in Fig. 157.

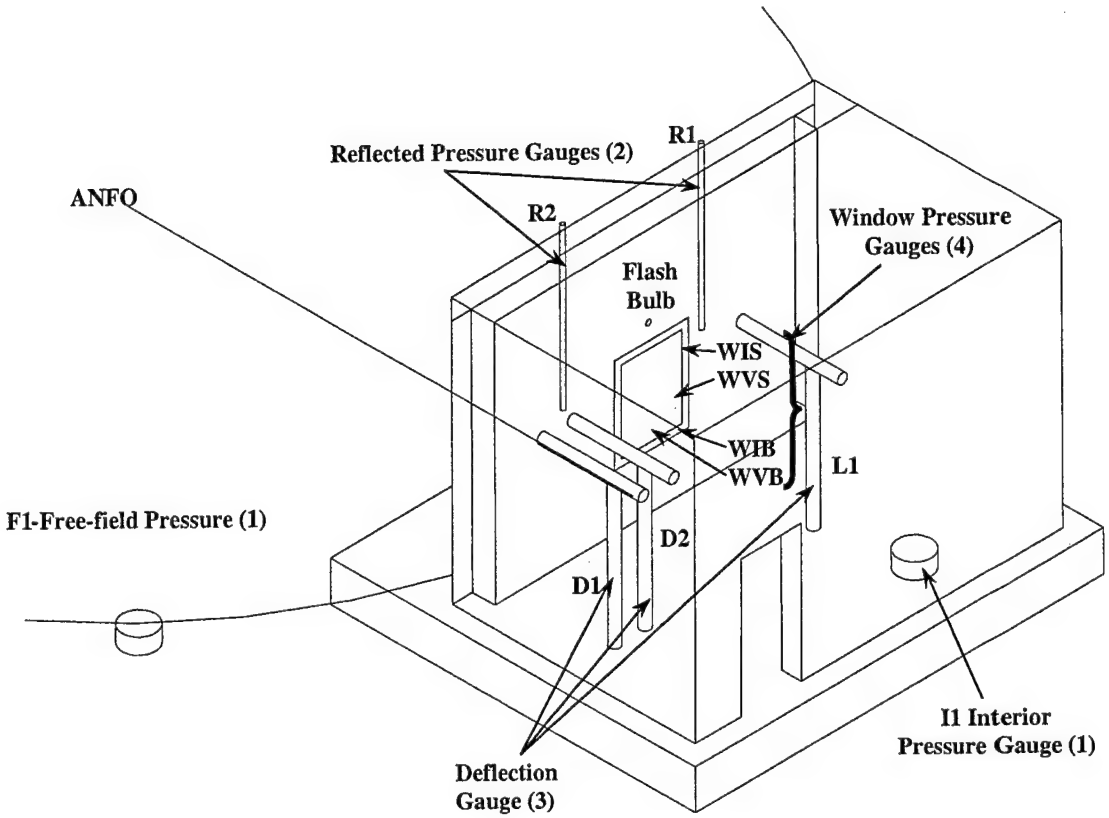

FIG. 157. Test 11, Gauge Locations

Reflected pressure gauges were suspended on the front of the permanent test structure. One was located approximately 1 ft to the left of the window. The other was located approximately 1 ft to the right of the window. These gauges were labeled R1 and R2 (Fig. 158).

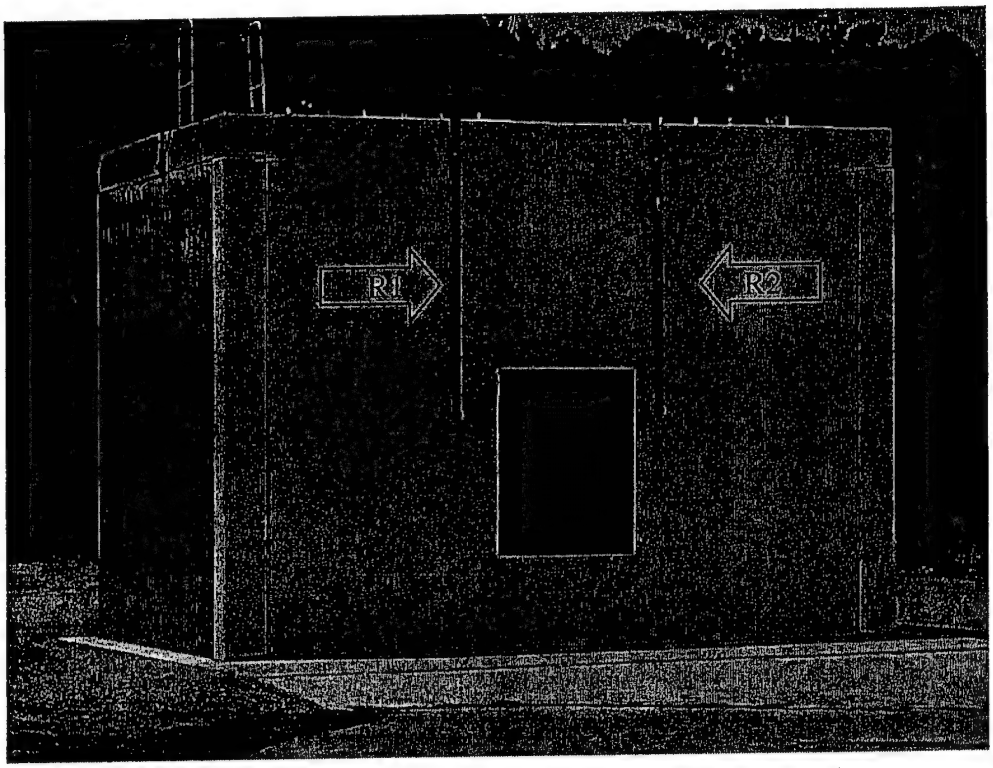

FIG. 158. Test 11, Reflected Pressure Gauges

Four pressure gauges were used inside the permanent test structure to measure pressure on and near the enclosed window. WIS was placed on the interior of the window, on the side and between the panes. WIB was placed on the bottom, between the panes. WVS was mounted in the 2-in. air gap on the side of window. WVB was located in the air gap at the bottom (Fig. 159). The gauges were placed inside when the window was installed.

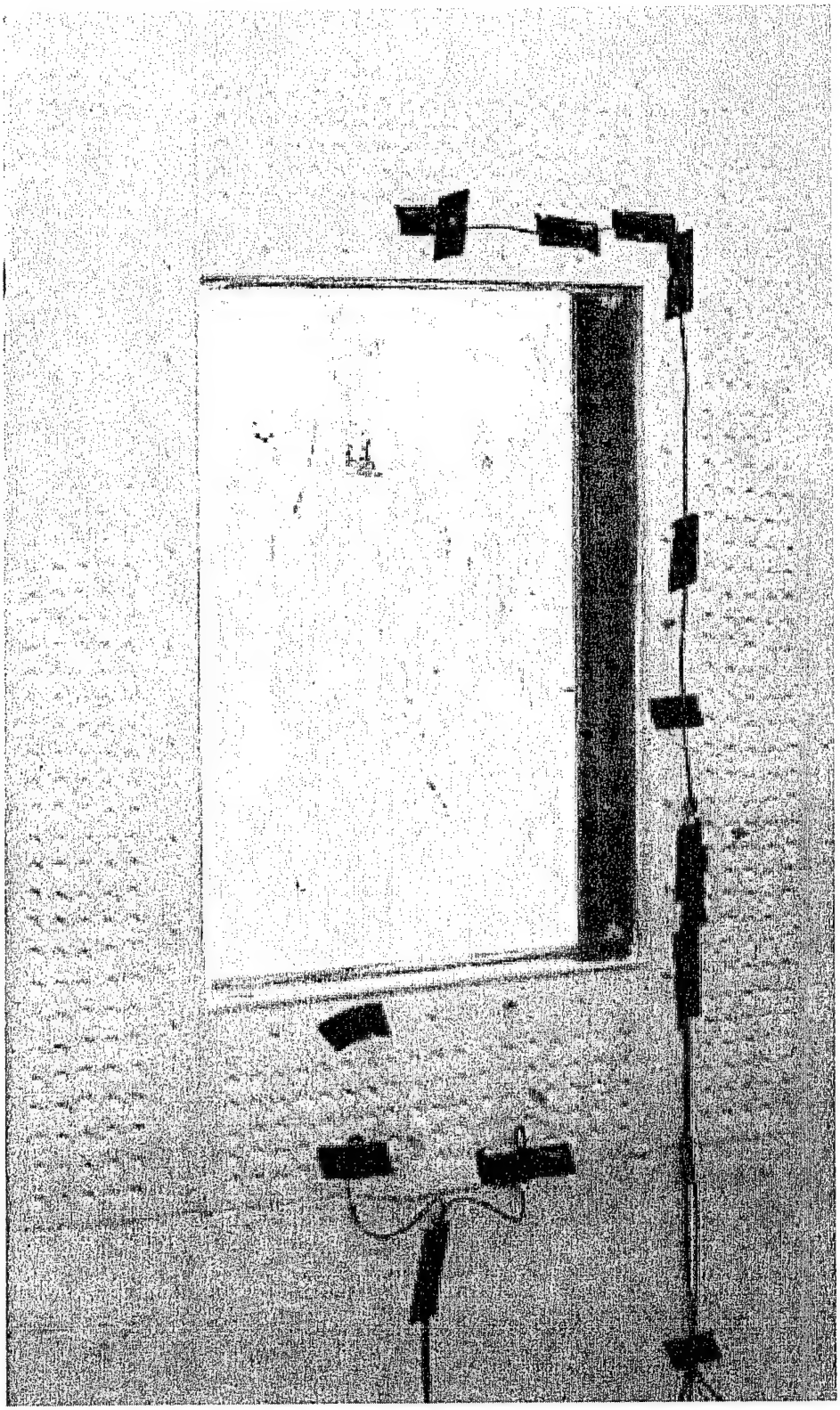

FIG. 159. Test 11, Pressure Gauges, Windows

Two free-field pressure gauges were used in this test. F1 was placed at the same distance from the permanent test structure as the charge. The other, F2, was placed near the steel frames with windows. The interior pressure gauge was located inside the test structure. The interior pressure gauge is shown below in Fig. 160.

Six additional pressure gauges were mounted on the steel frames containing the windows. These were W1F1, W1R1, W1I1, W2F1, W2R2, and W2I2. One additional gauge, FSB1, was mounted on the base of the single CMU block.

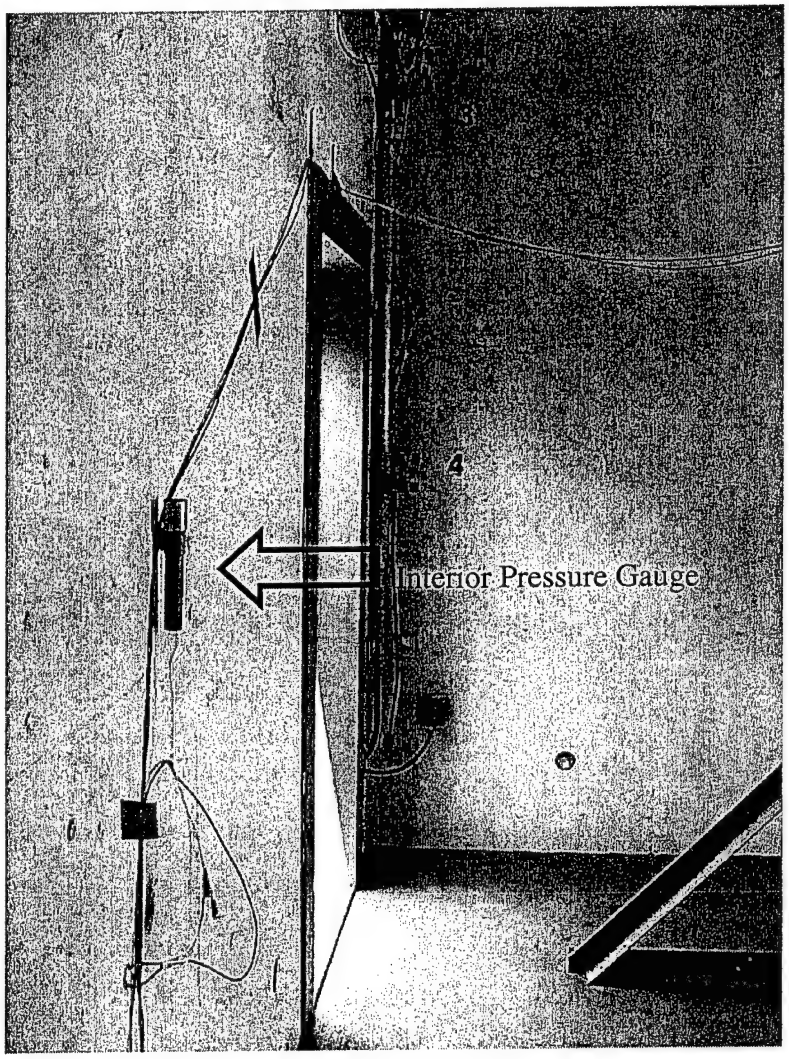

FIG. 160. Test 11, Interior Pressure Gauge

Three deflection gauges were used in Wall Test 11. L1 was mounted on the left of the wall structure. One mount containing both a gear (D1) and yo-yo (D2) gauge was mounted on the right wall of the structure. The deflection gauges are shown in Figs. 161 and 162.

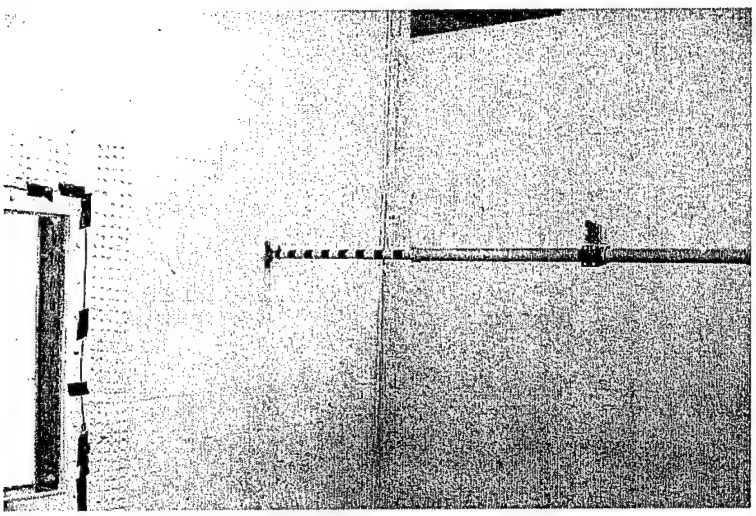

FIG. 161. Test 11, Left Deflection Gauge, Laser

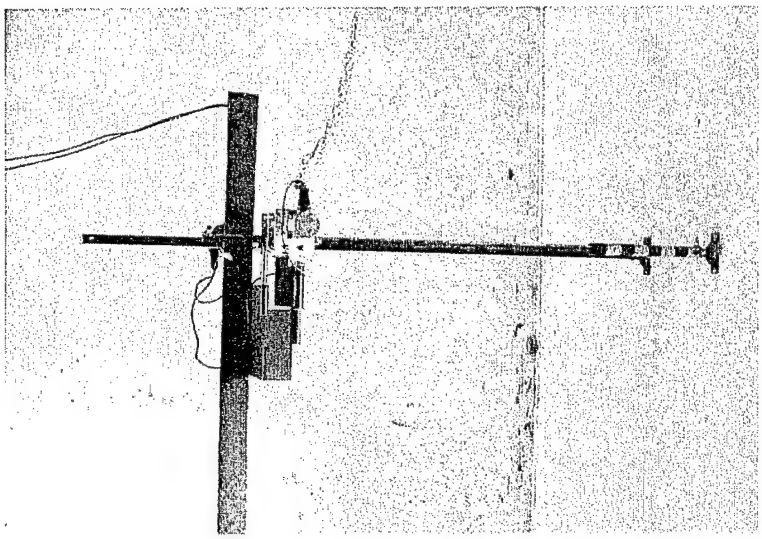

FIG. 162. Test 11, Right Deflection Gauge (Gear and Yo-Yo)

Photography support included digital still and high-speed photography, pre- and post-test. Two spy cameras were mounted in the back corners on each wall inside the test structure. The cameras from each corner were directed at the opposite wall, one toward the top area and one toward the bottom. One spy camera was located in the back center of the test structure to capture the response of the window. Two high-speed cameras were used, one located on the outside of the structure to capture deflection of the wall and window, and one directed toward the steel frames containing larger windows. An image of the camera targets is shown in Fig. 163.

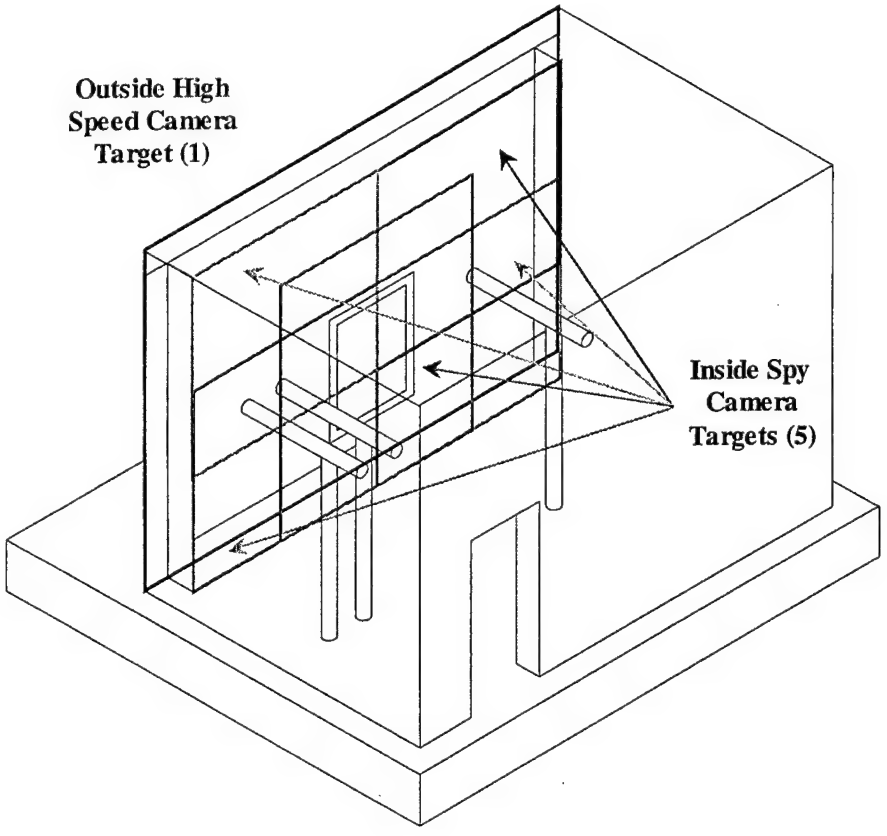

FIG. 163. Test 11, Interior Camera Target Areas

Lighting in Wall Test 11 was the same lighting used in previous tests. An image of the lighting is shown below in Fig. 164.

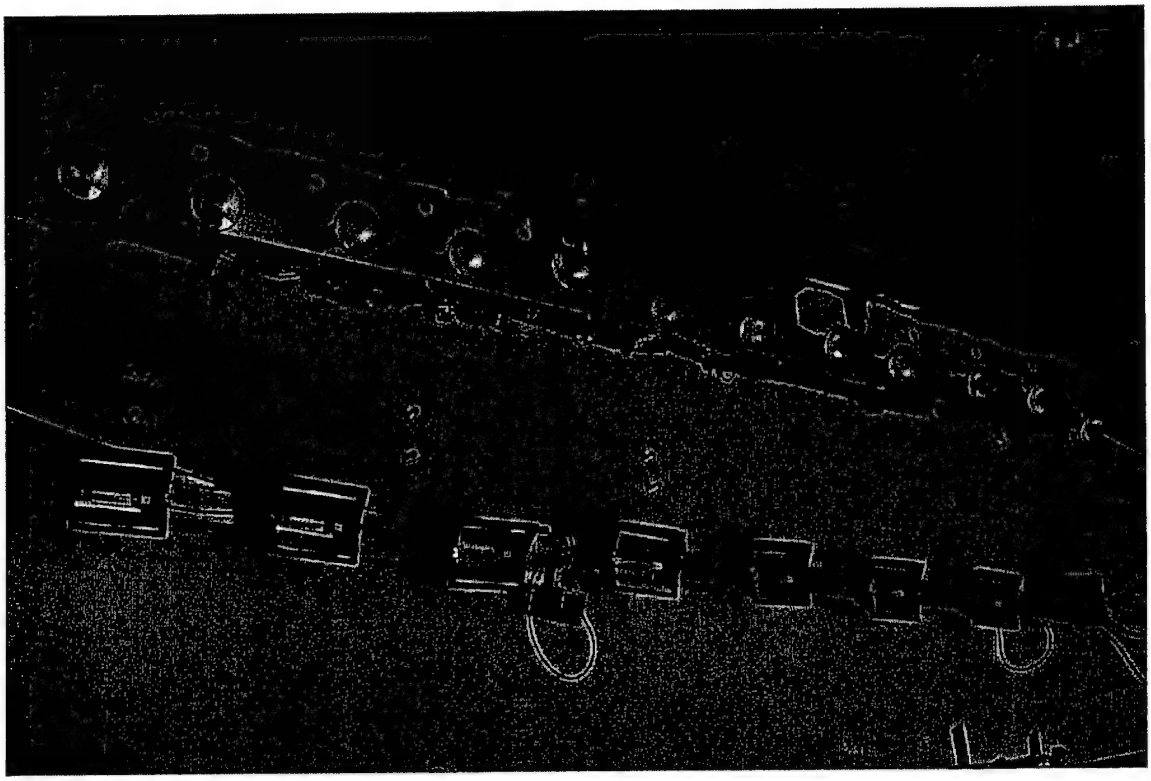

FIG. 164. Test 11, Lighting

3.7.3 Results

Gauge predictions were made for Wall Test 11 using WAC software. The predictions are provided in Table 11 for two reflected pressure gauges, four pressure gauges used in the window, one free-field pressure gauge, one interior pressure gauge, and three deflection gauges. Predictions for the steel structures with windows and the single CMU block are not relevant to the polymer effectiveness effort.

TABLE 11. Test 11, Gauge Predictions

Gauge ID	Type	Location	Prediction
R1	Reflected Pressure	Front Outside, 1ft left of window	42 psi
R2	Reflected Pressure	Front Outside, 1 ft right of window	42 psi
WIS	Reflected Pressure	Between Panes, Interior Side	100 psi
WIB	Reflected Pressure	Between Panes, Interior Bottom	100 psi
WVS	Reflected Pressure	Air Gap, Side	100 psi
WVB	Reflected Pressure	Air Gap, Bottom	100 psi
F1	Free-Field Pressure	Outside Structure	15 psi
I1	Interior Pressure	Inside Structure	5 psi
L1	Laser Deflection	Left Wall, Inside	12 in.
D1	Gear Deflection	Right Wall, Inside	12 in.
D2	Yo-Yo Deflection	Right Wall, Inside	12 in.

Eleven gauges were used in Wall Test 11. Graphs of the data produced from those gauges are provided as follows. Reflected pressure data is shown in Fig. 165 and Fig. 166. Reflected pressure of the windows is shown in Figs. 167 through 170. Free-field pressure is shown in Fig. 171. Interior pressure is shown in Fig. 172. Deflection gauge data is shown in Figs. 173 and 174.

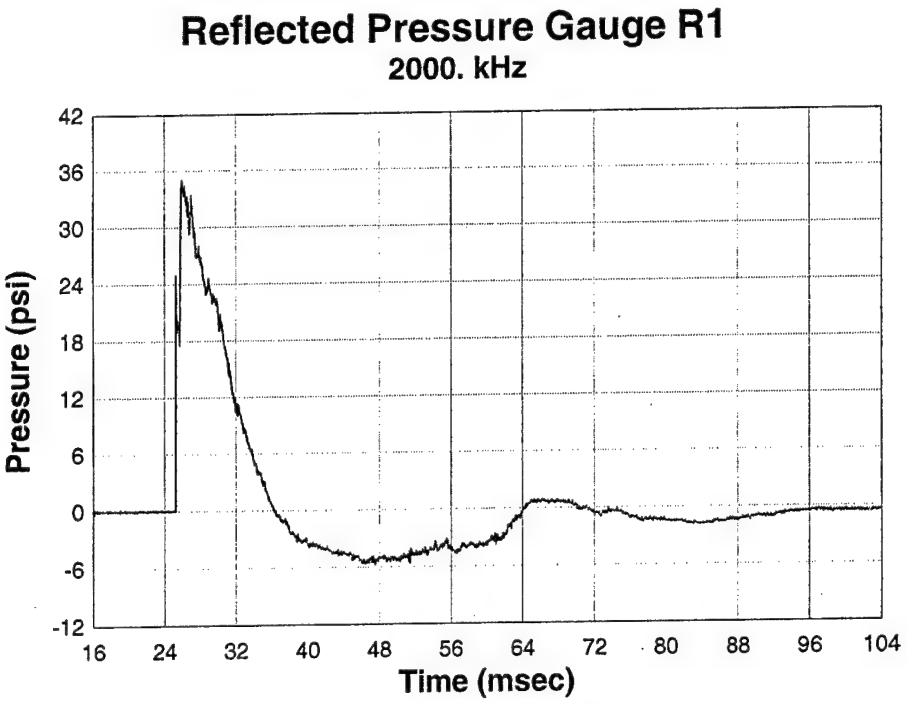

FIG. 165. Test 11, Gauge R1

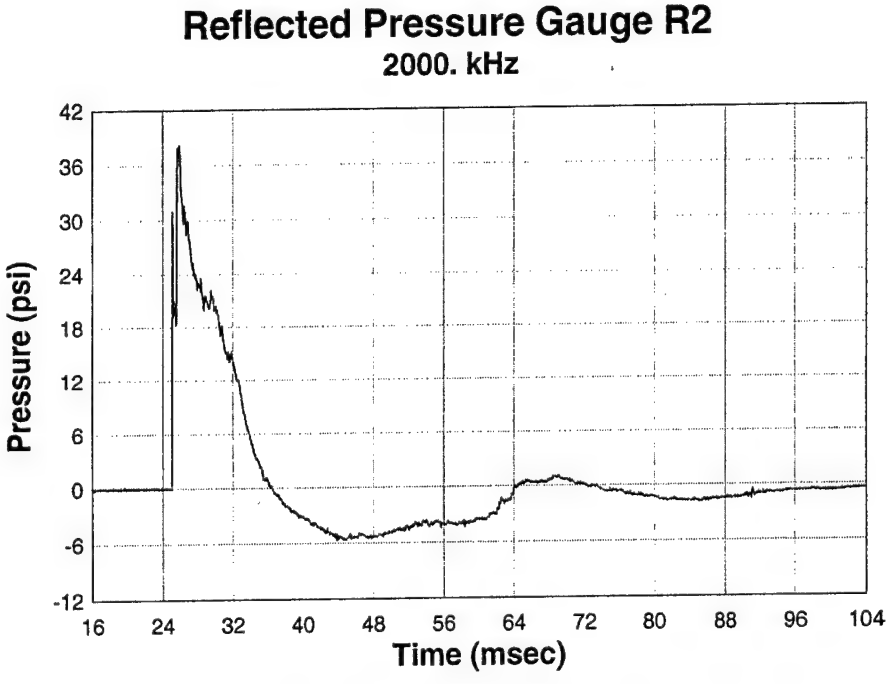

FIG. 166. Test 11, Gauge R2

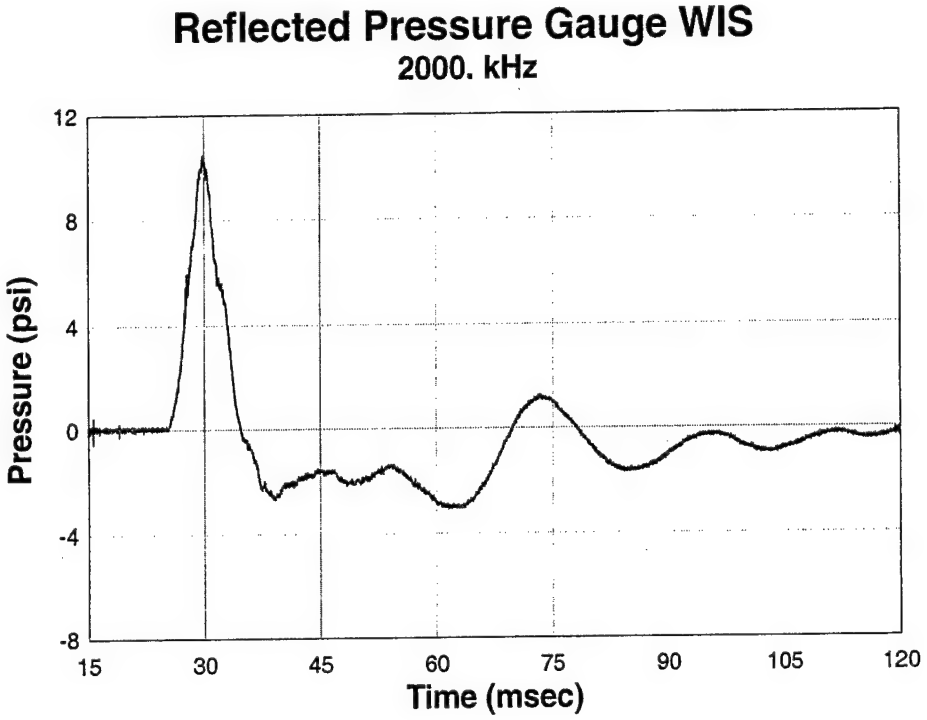

FIG. 167. Test 11, Gauge WIS (Window)

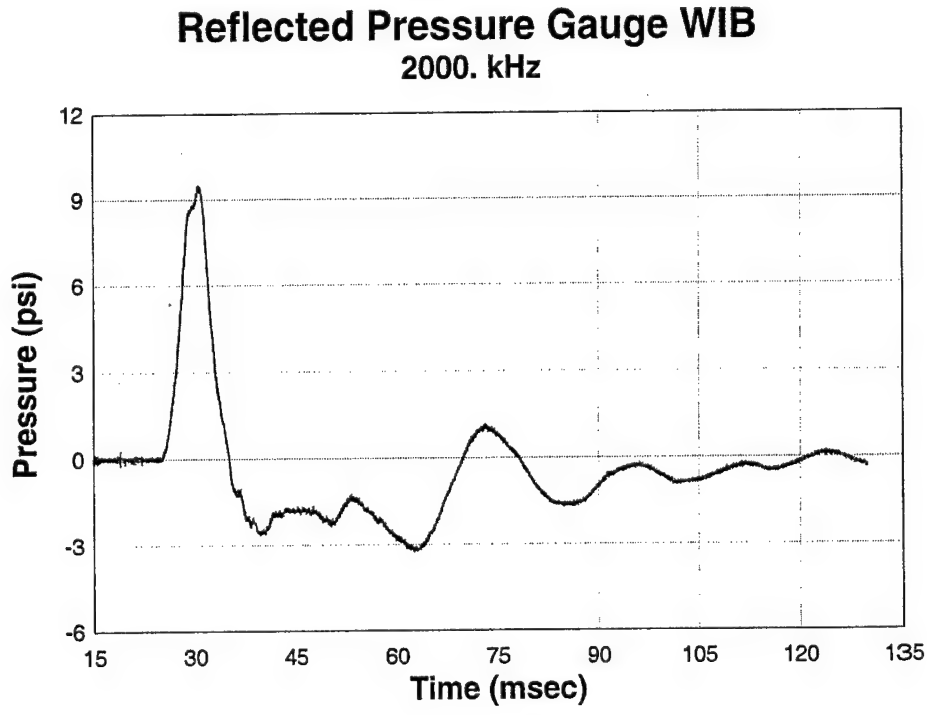

FIG. 168. Test 11, Gauge WIB (Window)

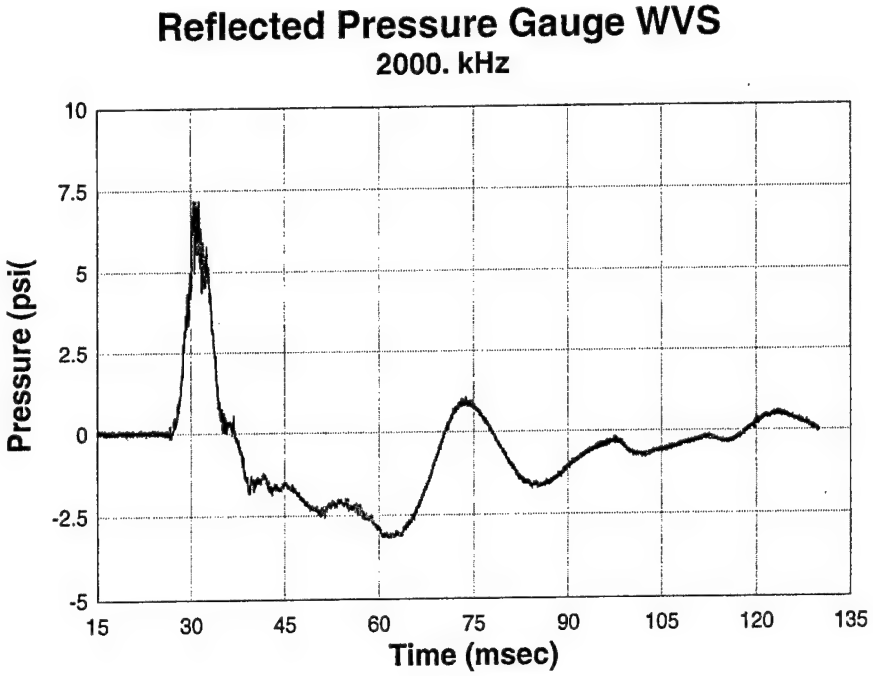

FIG. 169. Test 11, Gauge WVS (Window)

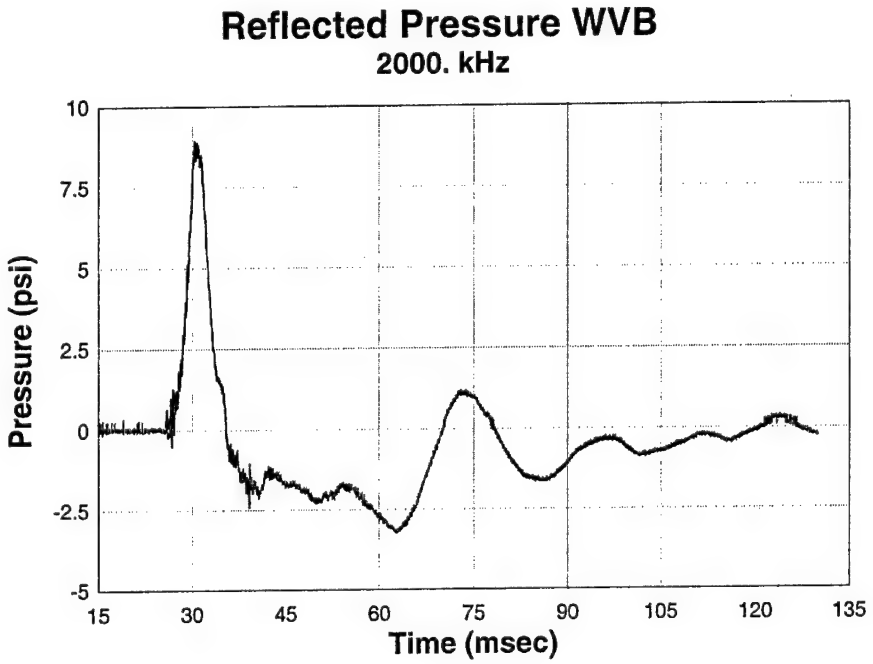

FIG. 170. Test 11, Gauge WVB (Window)

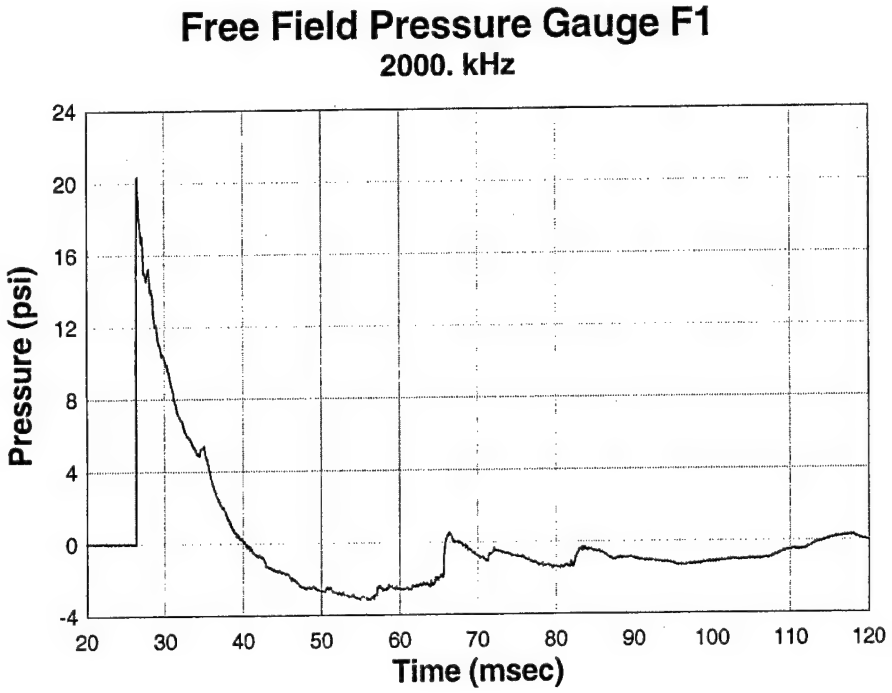

FIG. 171. Test 11, Gauge F1

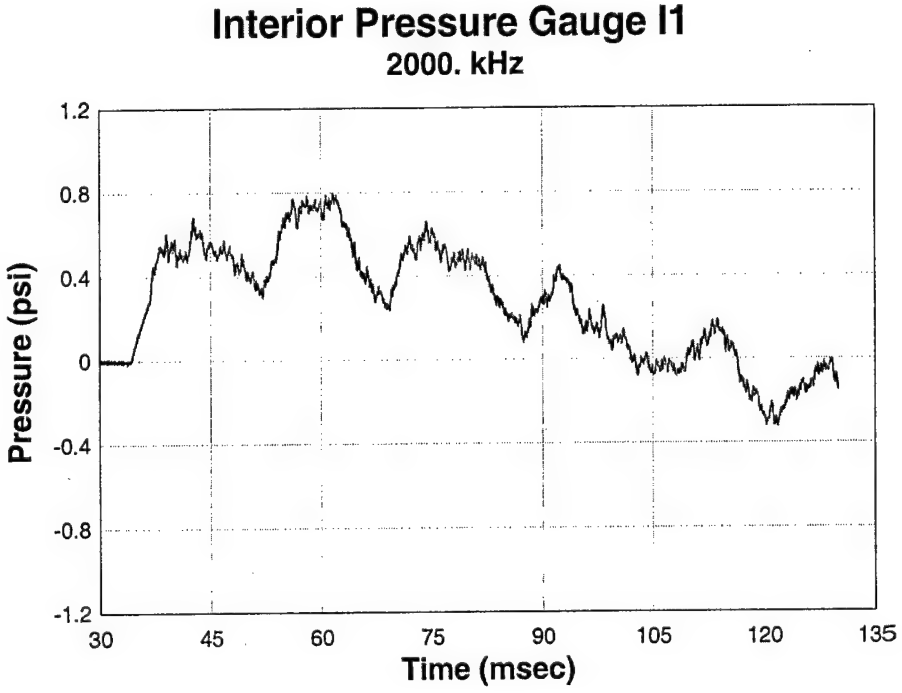

FIG. 172. Test 11, Gauge I1

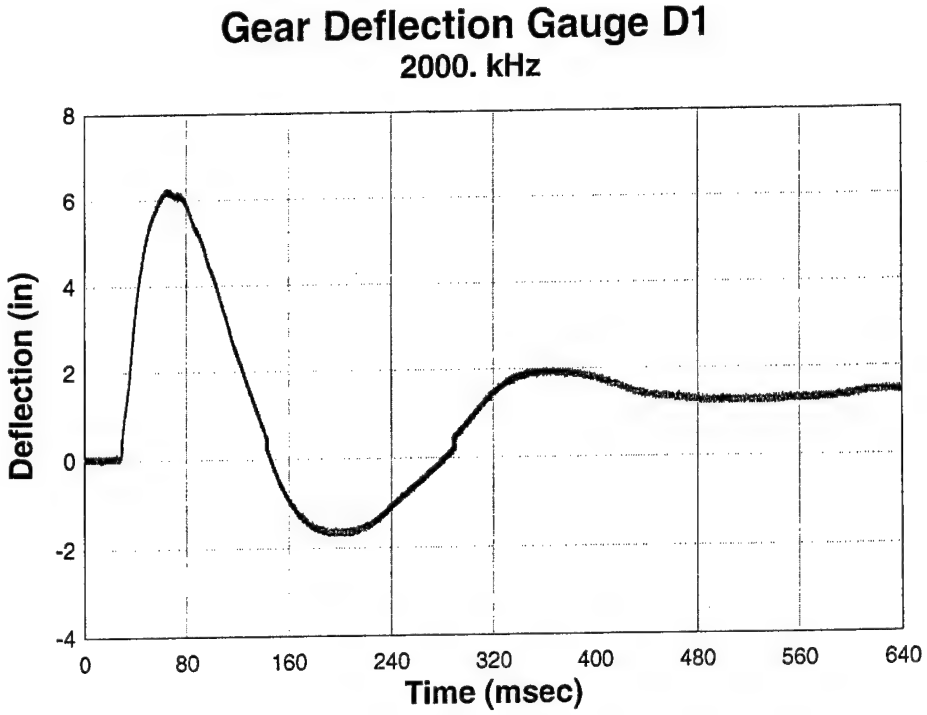

FIG. 173. Test 11, Gauge D1

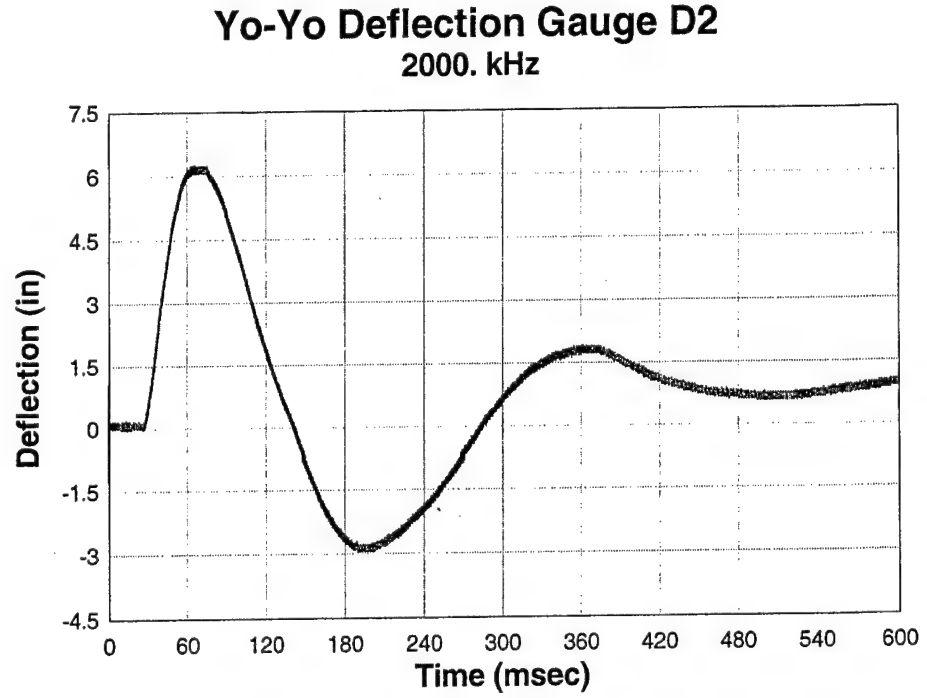

FIG. 174. Test 11, Gauge D2

The maximum pressures recorded by the gauges were (R1) 35.0 psi at 25.8 msec and (R2) 38.1 psi at 25.8 msec. The maximum pressures recorded in and around the windows were (WIS) 10.4 psi at 30.0 msec, (WIB) 9.5 psi at 30.6 msec, (WVS) 7.2 psi at 30.5 msec, and (WVB) 8.9 psi at 30.6 msec. The maximum pressure recorded by the free-field pressure gauge was (F1) 20.4 psi at 26.6 msec. The maximum value recorded by the interior pressure gauge was (I1) 0.8 psi at 61.6 msec. The maximum values recorded by the deflection gauges were (D1) 6.2 in. at 65.3 msec and (D2) 6.2 psi at 68.0 msec.

Figs. 165 through 174 show data for the most significant time period in the blast. The laser deflection gauge failed. Table 12 summarizes the predicted data and the recorded data.

The blast load in Wall Test 11 damaged the test structure. The majority of the damage occurred on the outside of the building. There was defacing of the blocks on the front face of the wall. Defacing typically occurs around edges and corners. One theory for this phenomenon is that the stiffness of the boundary conditions encourages a front face fracture. Another plausible explanation is that the compression thrust highest near the supports causes fracture as flexural arching occurs. An image of the structure is shown in Fig. 175. A close-up of the left wall defacing is shown in Fig. 176.

The polymer coating prevented collapse of the wall. Tears occurred in the polymer on the inside bottom of the right wall. All of the tears were along the same joint line (Fig. 177). There were no polymer tears on the left side of the wall. However, there was permanent deformation. The left wall is shown in Fig. 178.

TABLE 12. Test 11, Predicted vs. Recorded Data

Gauge ID	Type	Prediction	Actual
R1	Reflected Pressure	42 psi	35.0 psi
R2	Reflected Pressure	42 psi	38.1 psi
WIS	Reflected Pressure	100 psi	10.4 psi
WIB	Reflected Pressure	100 psi	9.5 psi
WVS	Reflected Pressure	100 psi	7.2 psi
WVB	Reflected Pressure	100 psi	8.9 psi
F1	Free-field Pressure	15 psi	20.4 psi
I1	Interior Pressure	5 psi	0.8 psi
L1	Laser Deflection	12 in.	Gauge Failure
D1	Gear Deflection	12 in.	6.2 in.
D2	Yo-Yo Deflection	12 in.	6.2 in.

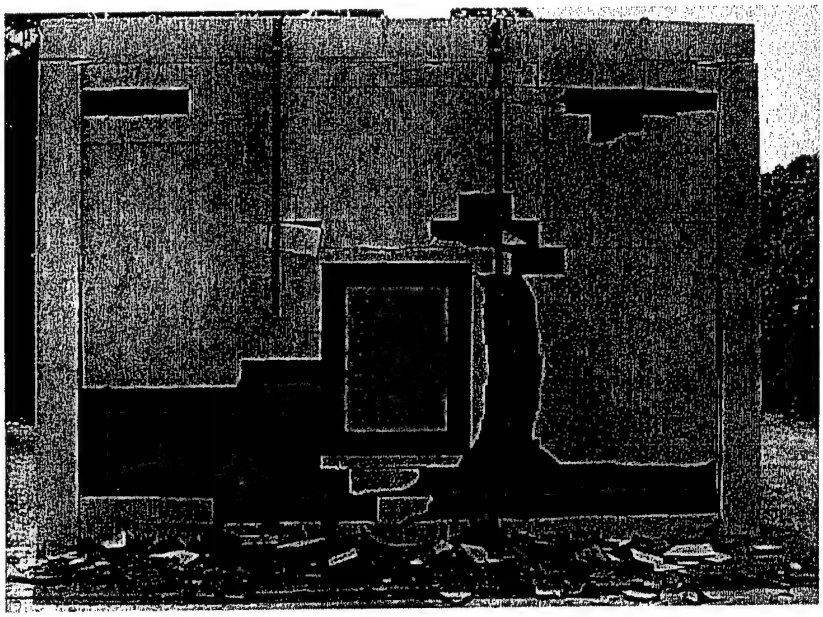

FIG. 175. Test 11, Test Structure, Post-Test

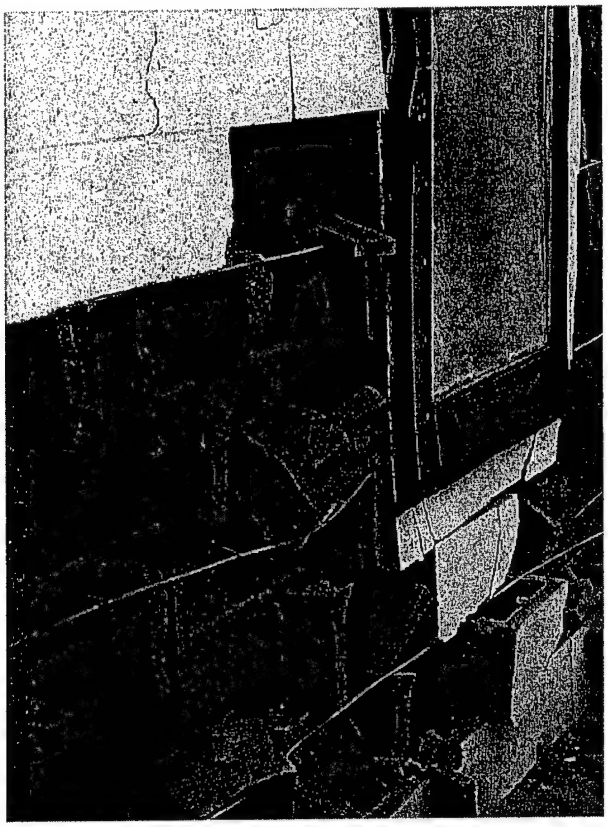

FIG. 176. Test 11, Front Defacing

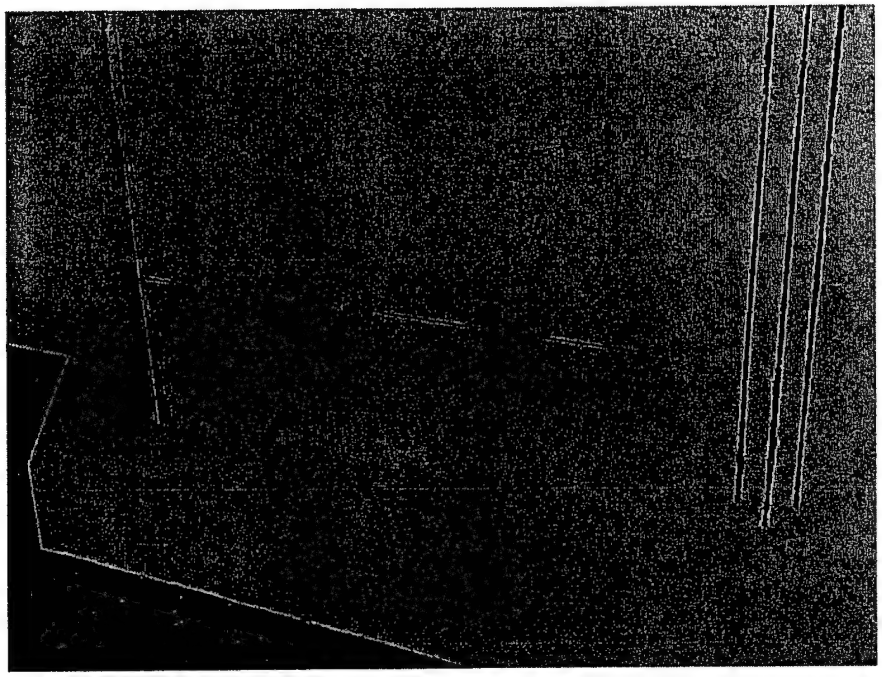

FIG. 177. Test 11, Right Side Rips

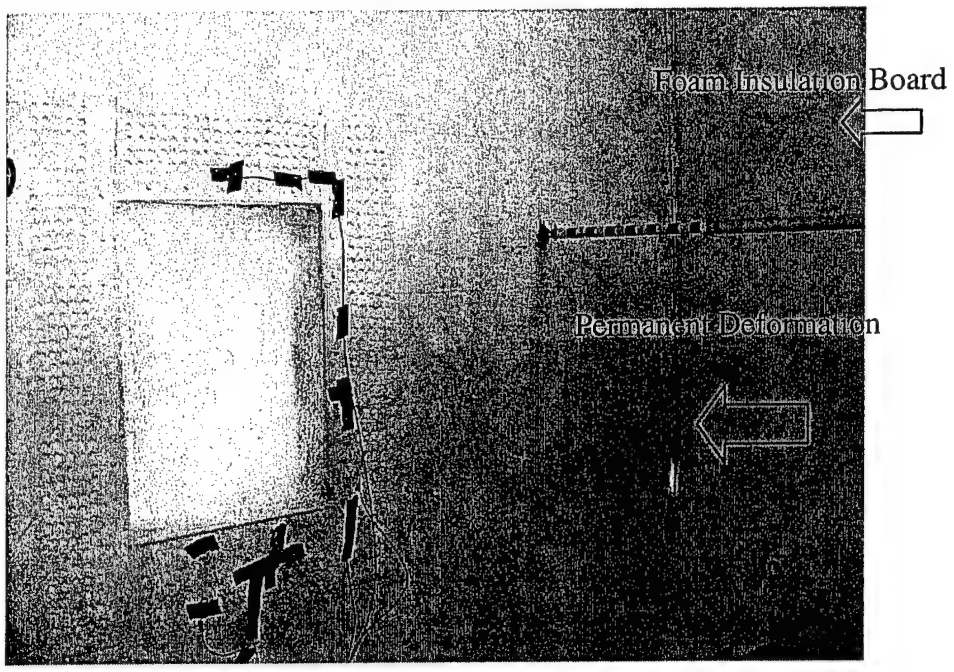

FIG. 178. Test 11, Left Side Deflection

The deflection of the structure was largest at approximately mid-height. It is likely that even if the tear in the retrofit had been completely across the joint line, the wall probably would have not collapsed because the deflection at the bottom was low. If the retrofit had torn from the top of the blocks (at the 90 degree angle), the wall may have collapsed. Securing the retrofit at the top and bottom is critical. The retrofit may prevent fragmentation, but failure of the retrofit at the top of the wall would lead to collapse.

The window glass was shattered in the test, but the film that was applied kept it intact. Reflected pressure gauges were placed inside the double windowpanes. Reflected pressure outside the window averaged 37 psi. Pressure just inside the window, however, averaged only 9 psi. This reduction was due to the windowpane and the air gaps that were placed there to dissipate pressure. The inside image of the window is shown in Fig. 179.

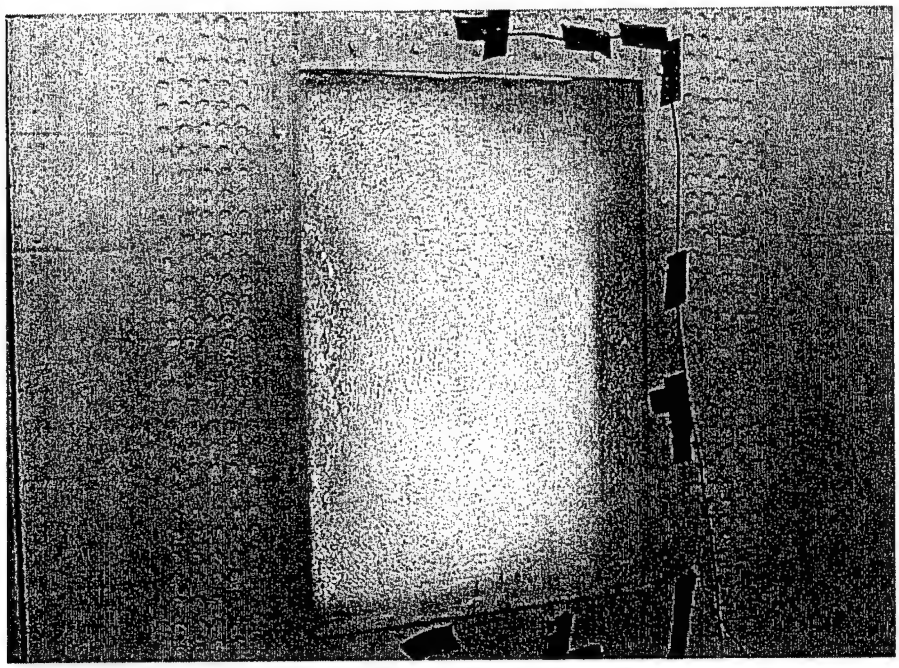

FIG. 179. Test 11, Post-Test Window

3.8 Wall Test 12

Wall Test 12 involved an explosive test on two 8 ft x 12 ft mortarless, unreinforced masonry walls with different polymer applications. One of the walls was sprayed directly with polymer, creating a strong bond between the masonry and the polymer coating. The other wall had a plastic membrane between the wall and the polymer so that the reinforcement was not bonded to the wall. Also in Wall Test 12, performance of four newly designed pressure gauge mounts and a miniature pressure transducer were evaluated for possible use in later testing. The key objectives of Wall Test 12 were to (1) measure the deflection of wall elements; (2) evaluate the performance of the CMU wall without mortar; (3) evaluate the performance of the polymer bond to the CMU wall; (4) evaluate four pressure gauge mounts; and (5) evaluate the performance of

a miniature pressure transducer. In addition to the CMU walls being tested, Wall Test 12 also included door and window tests that are not discussed in this document.

The layout for Wall Test 12 is shown in Fig. 180. Also shown are four pressure gauges in four different mounts, a tent which houses pressure gauges, four steel frames housing three windows and one door, and the permanent testing structure. Only the results of the permanent test structure with the masonry walls are discussed within this document.

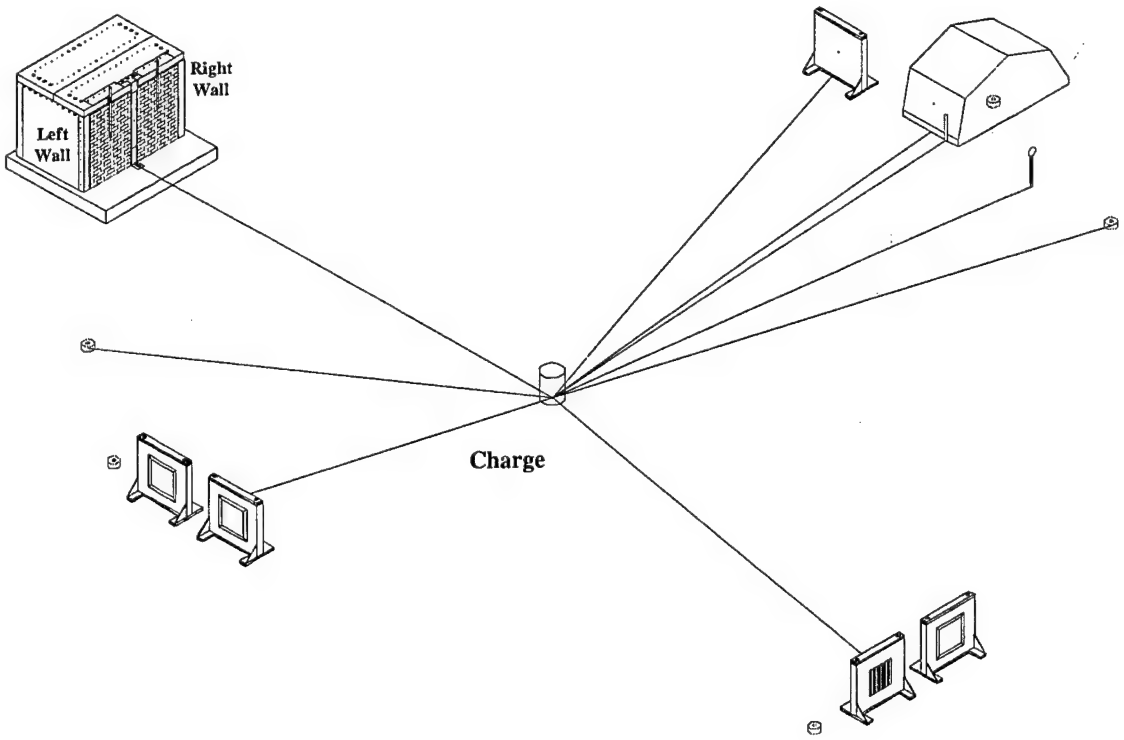

FIG. 180. Test 12 Layout

3.8.1 Construction

Several tasks were completed before construction was begun on the mortarless walls. First, the test structure and the steel center support were sandblasted to remove rust and residue from previous tests. Second, ¾ in. foam insulation board was attached to the interior sides and the steel center support of the structure to allow a one-way flexural response. The foam insulation was attached using an adhesive caulk.

After the walls were clean and the foam insulation board installed, the walls were constructed. The only mortar used in the test was at the bottom of the walls to insure that the first course was level, and at the top of the walls to fill gaps between the top course and the permanent roof of the testing structure. Because the height of CMU blocks can vary ± 1/16 in., leveling problems can arise when not using mortar. Roof felt paper was used to maintain a level course in the blocks. Bottom course leveling is shown in Fig. 181. Top course leveling is shown in Fig. 182.

FIG. 181. Test 12, Right Wall, Bottom Course Leveling

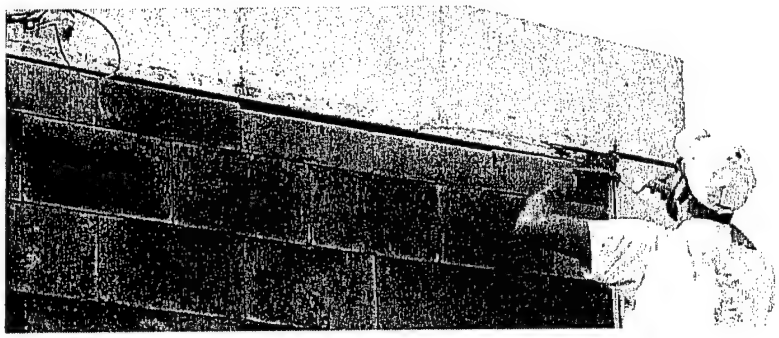

FIG. 182. Test 12, Right Wall, Top Course Leveling

The left wall had a plastic membrane applied to its interior to prevent bonding between the CMU wall and the polymer. This membrane was installed before the mortar could be placed at the top of the left wall. The plastic was fed through the gap and left to drape the inside wall. The mortar was then troweled into the gaps (Fig. 183).

After the mortar dried, the plastic was trimmed to fit the wall. It was attached to the wall with double-sided tape. Creases were eliminated as the plastic was taped. The trimmed and taped plastic is shown from the inside in Fig. 184. A drawing of the walls, plastic, and retrofit is shown in Fig. 185.

FIG. 183. Test 12, Left Wall, Top Course Leveling

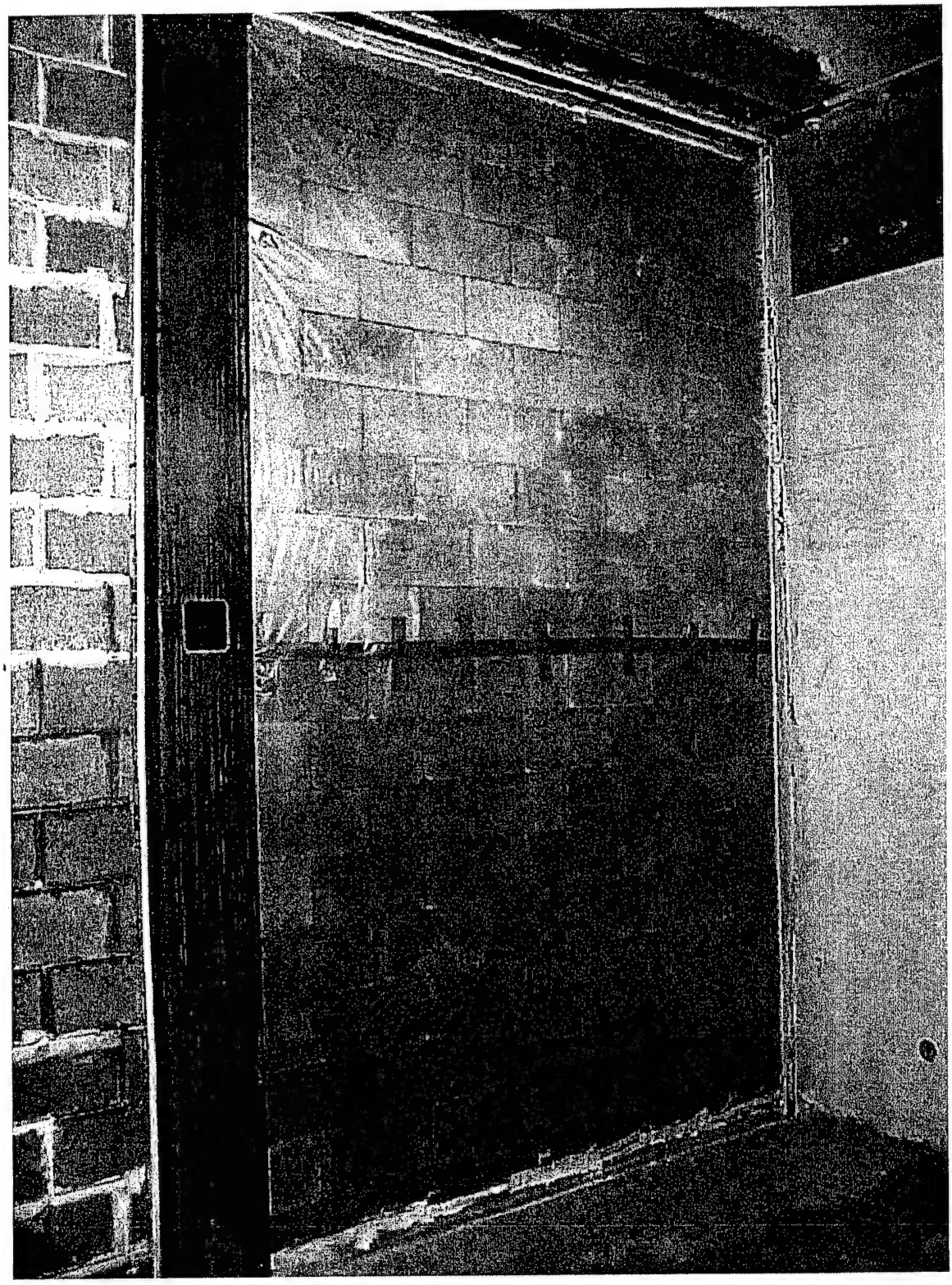

FIG. 184. Test 12, Left Wall Inside, Plastic Covering

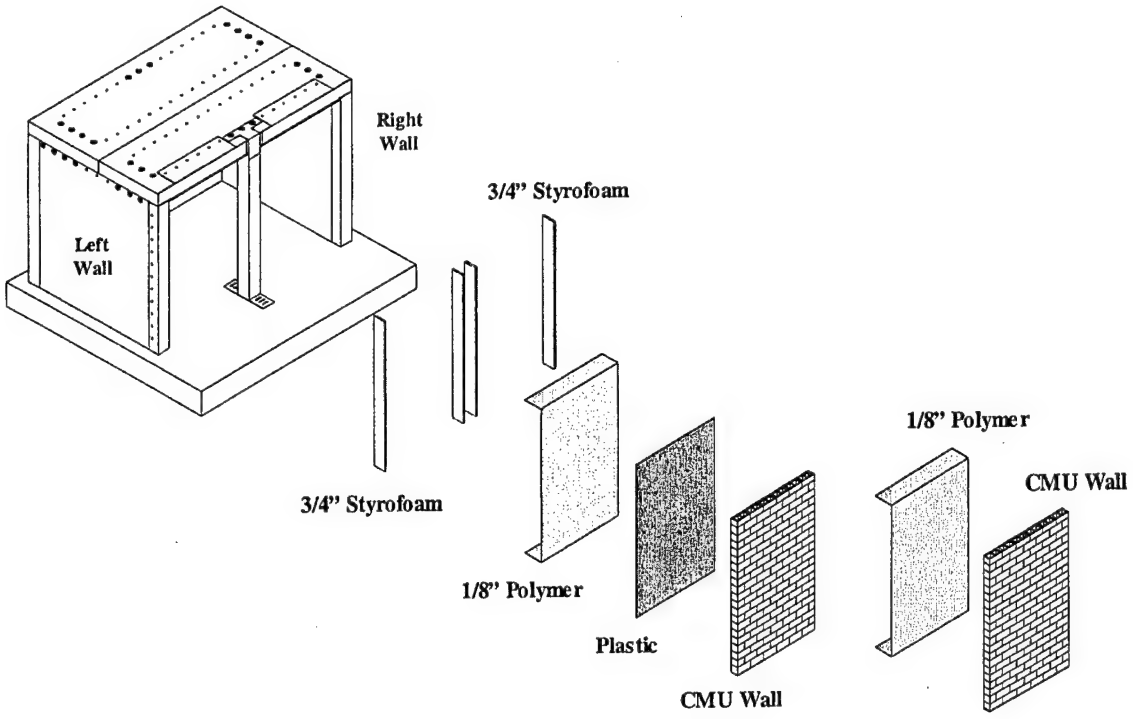

FIG. 185. Test 12, Drawing Details

The bond strength of the polymer to the concrete walls is an important parameter in the wall tests. To insure a strong bond, the appropriate primer was applied to the concrete roof, concrete floor, and metal roof cladding. Both products were applied and cured according to specifications supplied by the manufacturer.

At the 90-degree joints at the roof and floor, an open weave fiberglass scrim fabric was applied with an epoxy bonding to reduce polymer material and create a smooth transition between the roof and wall and the floor and wall. The fiberglass weave is shown in Fig. 186.

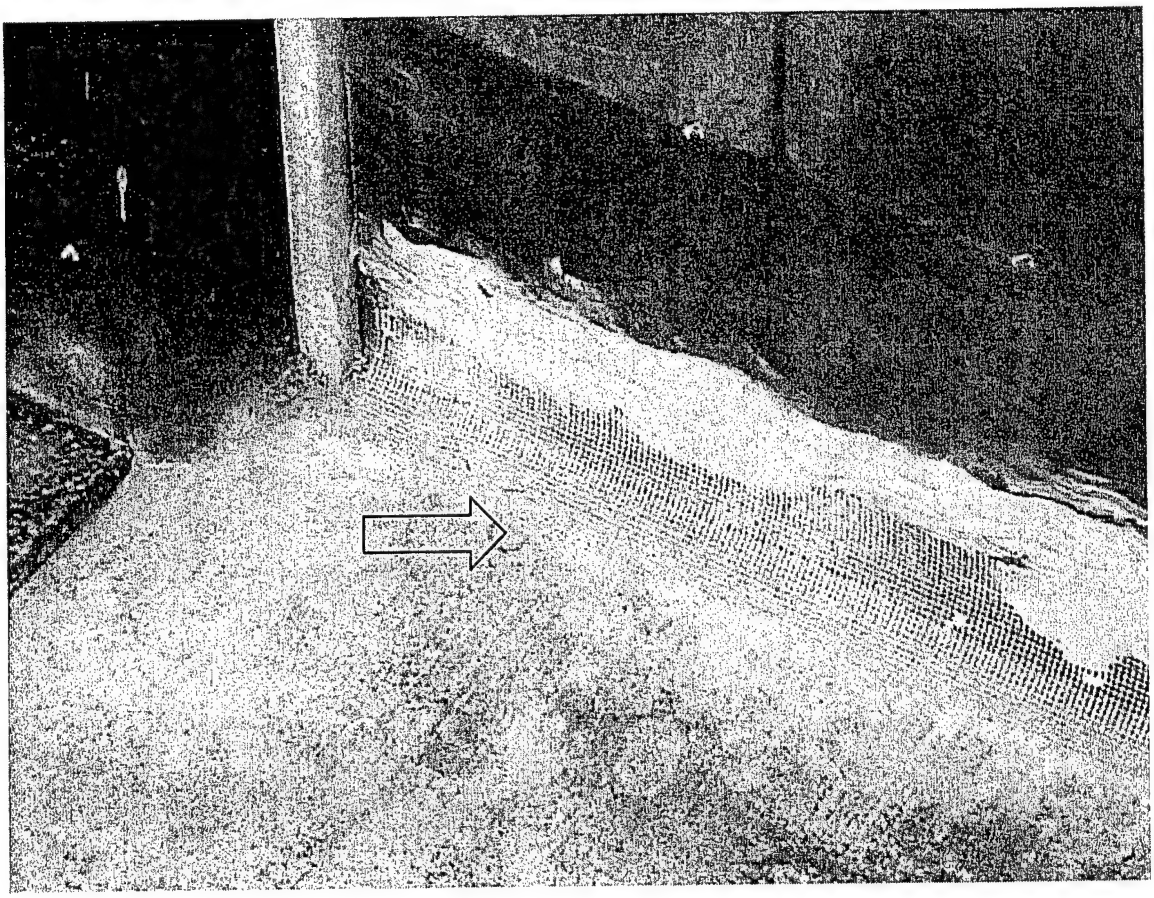

FIG. 186. Test 12, Fiberglass Scrim Fabric

After all cleaning and preparation work were complete, the interior of the CMU walls were coated with a 1/8-in.-thick layer of polymer. It overlapped onto the reaction structure roof by 12 in. and then tapered out to 24 in. Masking was used to maintain a consistent overlap and to allow free movement on the sides. The coated right wall is shown in Fig. 187. The coated left wall is shown in Fig. 188. Although the left wall appears wrinkled, the polymer was very firm. The wrinkling shown was caused by the plastic sheeting beneath the polymer. The completed structure is shown from the outside in Fig. 189.

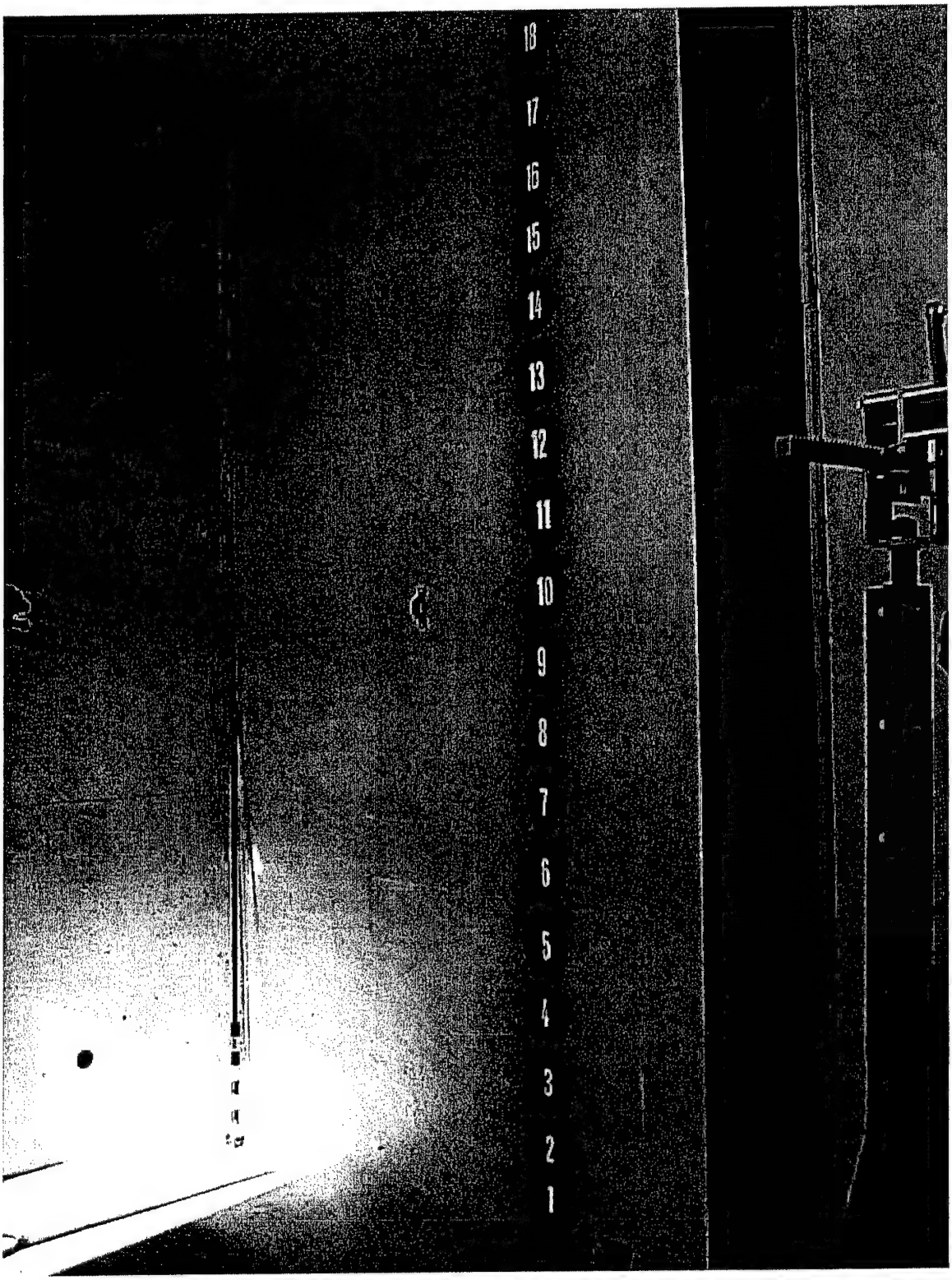

FIG. 187. Test 12, Wall A with Retrofit

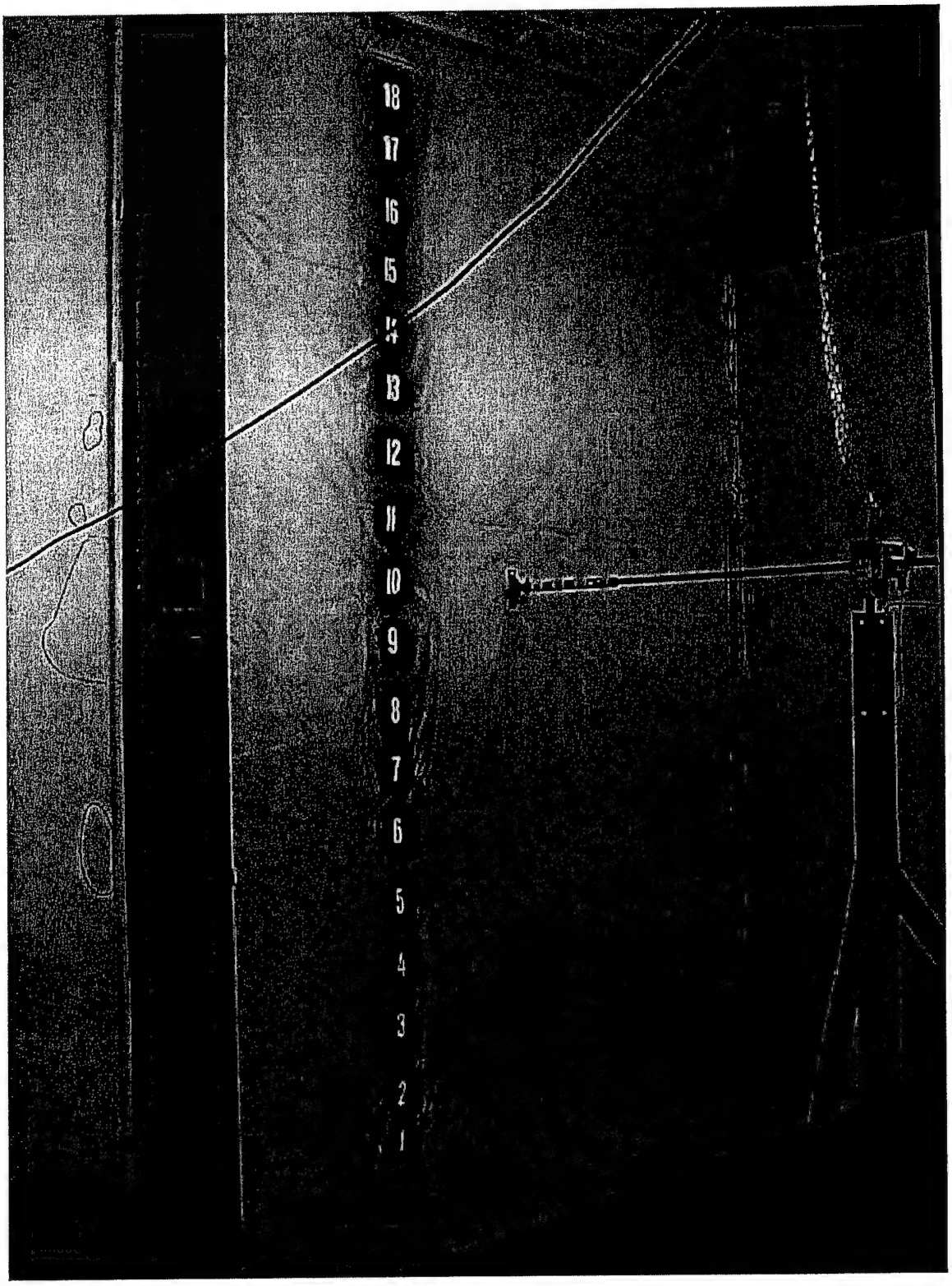

FIG. 188. Test 12, Wall B with Retrofit

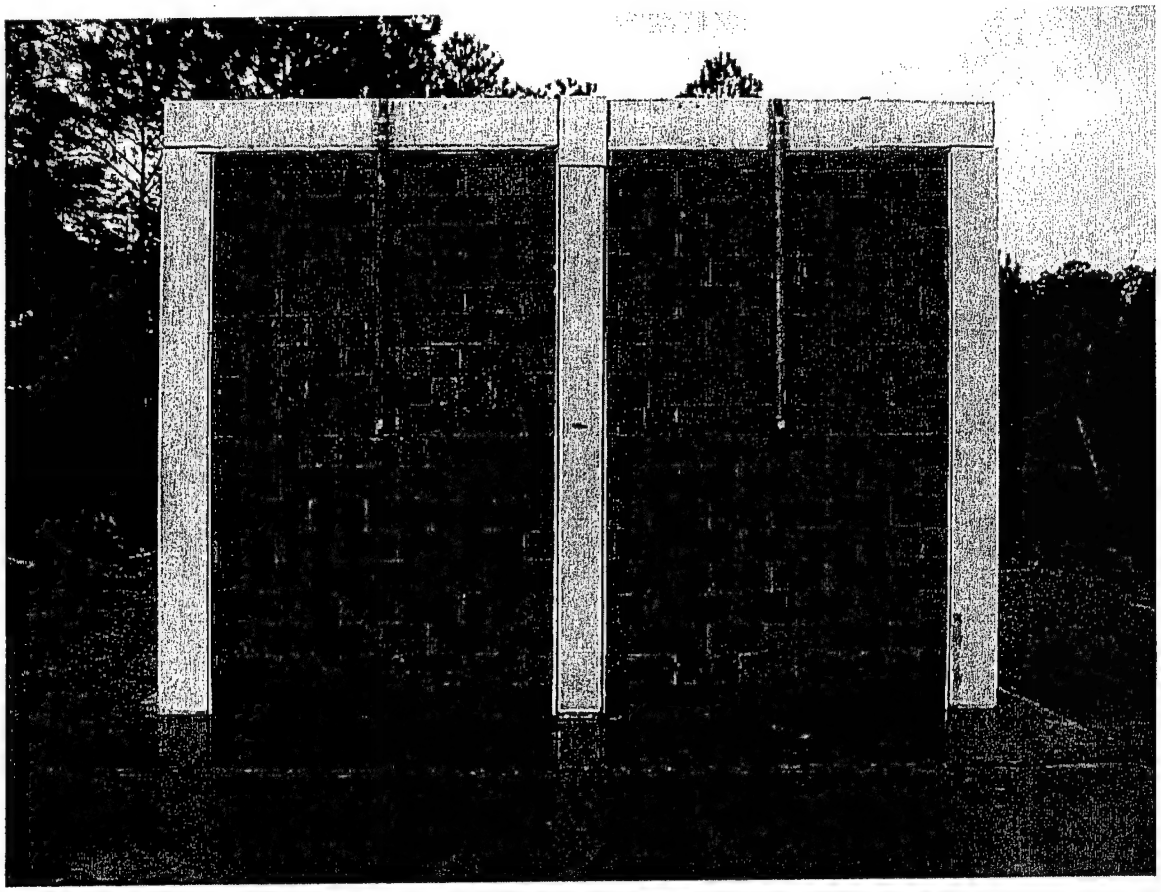

FIG. 189. Test 12, Completed Structure

3.8.2 Instrumentation

Gauge instrumentation used in Wall Test 12 consisted of six reflected pressure gauges, five free-field pressure gauges, two interior pressure gauges, two deflection gauges, and six pressure gauges on the doors and windows in the small steel structures. The instrumentation that was used exclusively for the masonry walls included three reflected pressure gauges (R1, R2, R3), one free-field pressure gauge (F1), one interior pressure gauge (I1), and two deflection gauges (D1, D2). An illustration of the gauge locations is shown in Fig. 190.

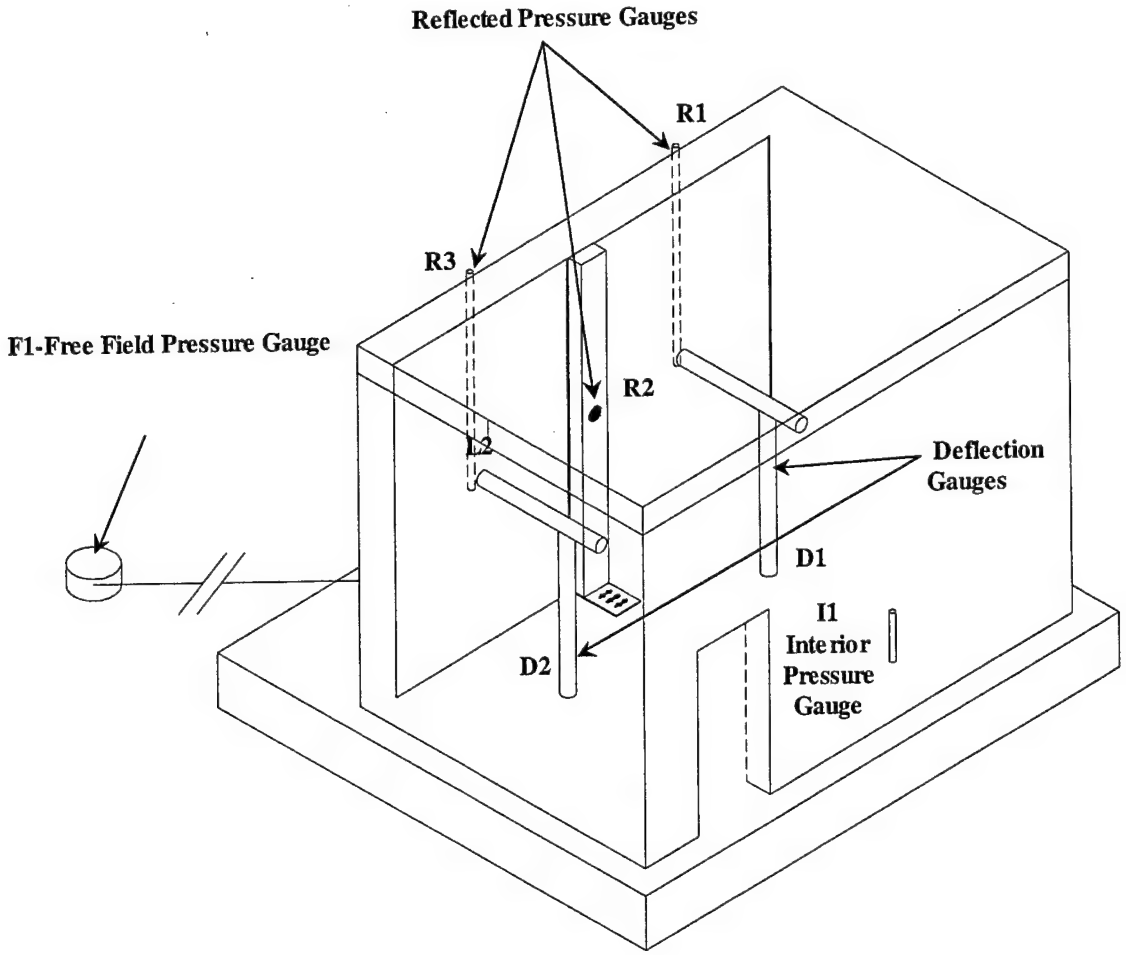

FIG. 190. Test 12, Gauge Locations

Reflected pressure gauges measure the pressure reflected from the wall. Two reflected pressure gauges (R1 and R3) were suspended from the roof onto the front of the test structure. R1 was centered on the left wall, and R3 was centered on the right wall. Reflected pressure gauge R2 was centered on the steel center support on the outside of the testing structure.

F1 was located to the left of the test structure at the same distance from the blast as the wall.

I1 was mounted on the inside back wall of the test structure.

The deflection gauges used in this test were gear-driven gauges that measured displacement with a rotational position transducer. D1 was used on the left wall. D2 was used on the right, and D1 is shown in Fig. 191.

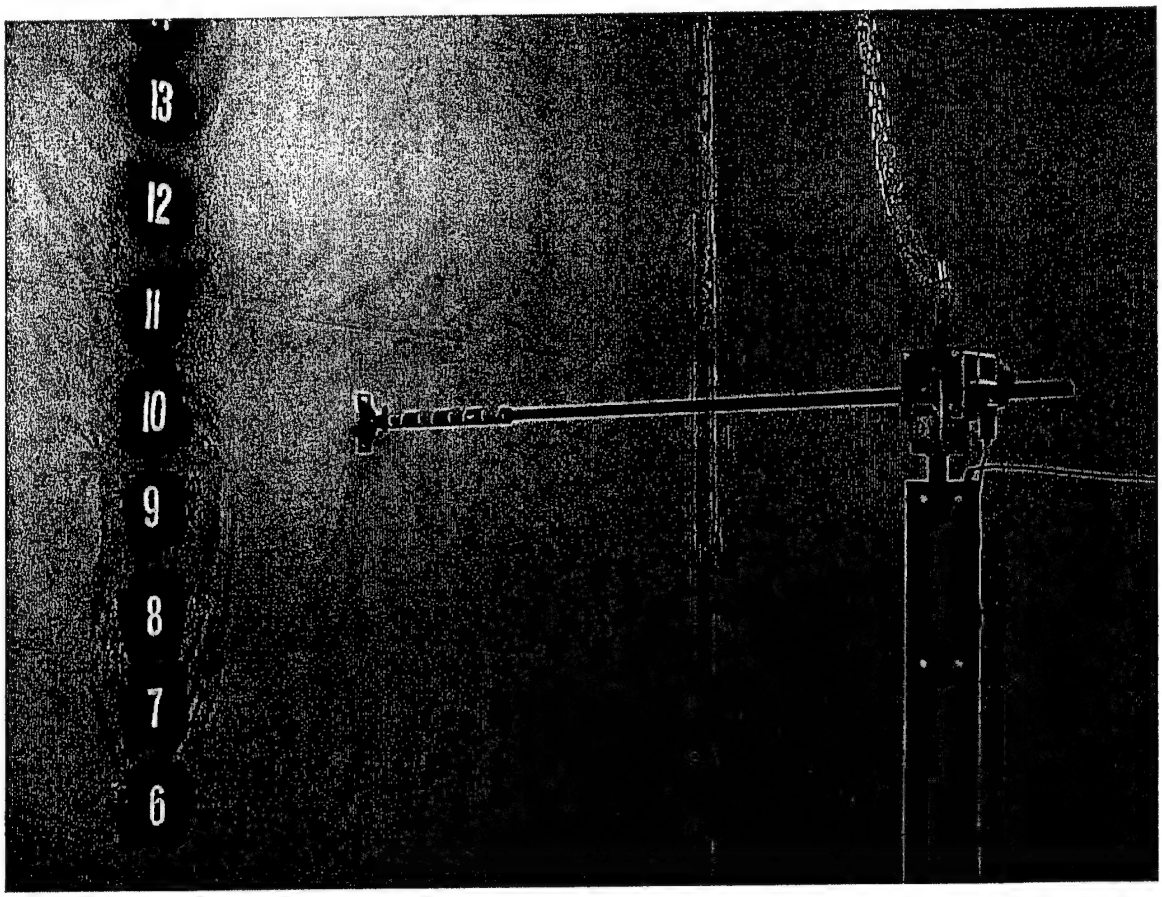

FIG. 191. Test 12, Deflection Gauge

Photography instrumentation included pre- and post-test digital still photography. High-speed digital photography was captured during the test. Two spy cameras were mounted inside each back corner of the test structure (a total of four cameras) and directed toward the center of the opposite wall. One spy camera with a wide-angle lens was mounted in the center of the back wall to capture the reaction of both walls in the

same shot. A high-speed digital camera and another spy camera were positioned outside the test structure to capture the deflection of the walls. Fig. 192 shows the camera targets.

The lighting system used in Wall Test 11 was not damaged during testing. This same lighting system was used for Wall Test 12.

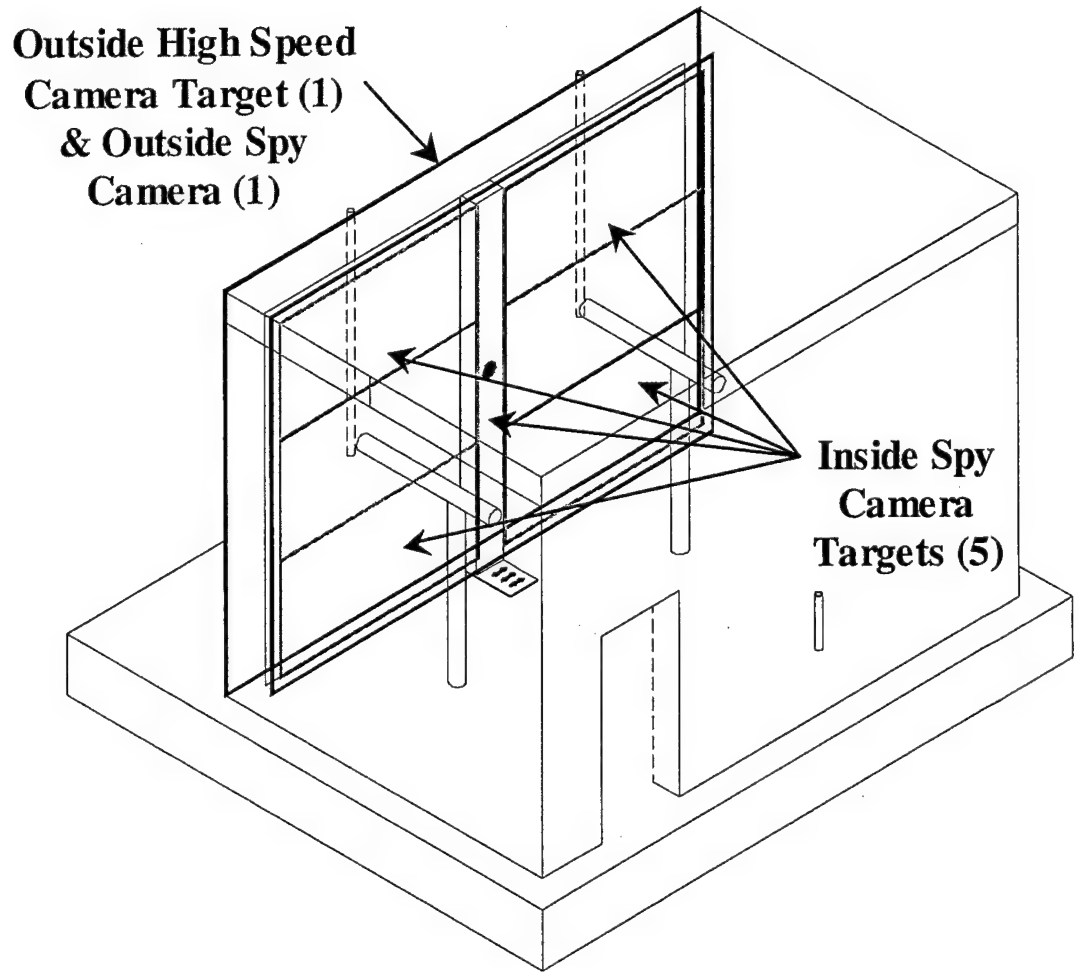

FIG. 192. Test 12, Interior Camera Target Areas

3.8.3 Results

WAC was used to predict data from the explosive test. Pressures and deflections were predicted for each of the gauges and are provided in Table 13. It was predicted that the left wall would fail. When the deflection of the wall exceeds wall thickness, the wall is expected to collapse due to gravity.

TABLE 13. Test 12, Gauge Predictions

Gauge ID	Type	Location	Prediction
R1	Reflected Pressure	Center CMU Wall, Left Side	41.2 psi
R2	Reflected Pressure	Center Steel Support	41.2 psi
R3	Reflected Pressure	Center CMU Wall, Right Side	41.2 psi
F1	Free-Field Pressure	Outside Structure	14.9 psi
I1	Free-Field Pressure	Inside Structure	5 psi
D1	Gear-Driven Deflection	Left Wall, Inside	14 in. (Fail)
D2	Gear-Driven Deflection	Right Wall, Inside	8 in.

The data recorded from Wall Test 12 follows. Gauge R1 is shown in Fig. 193. Gauge R2 is shown in Fig. 194. Gauge R3 is shown in Fig. 195. Free-field pressure is shown in Fig. 196. The interior pressure gauge failed. Deflection gauge data is provided in Figs. 197 and 198.

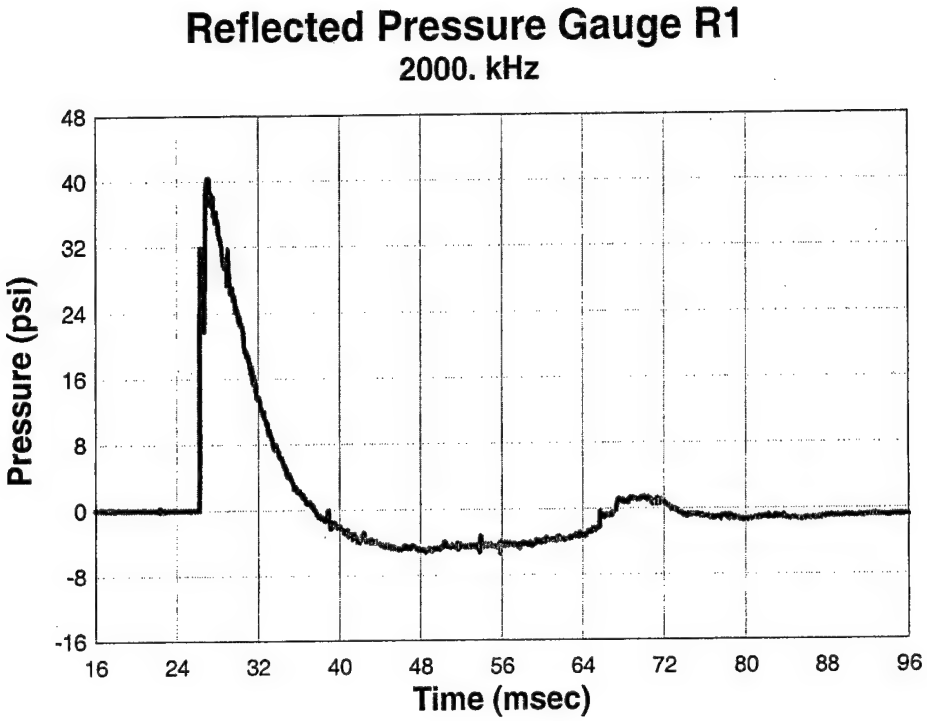

FIG. 193. Test 12, Gauge R1

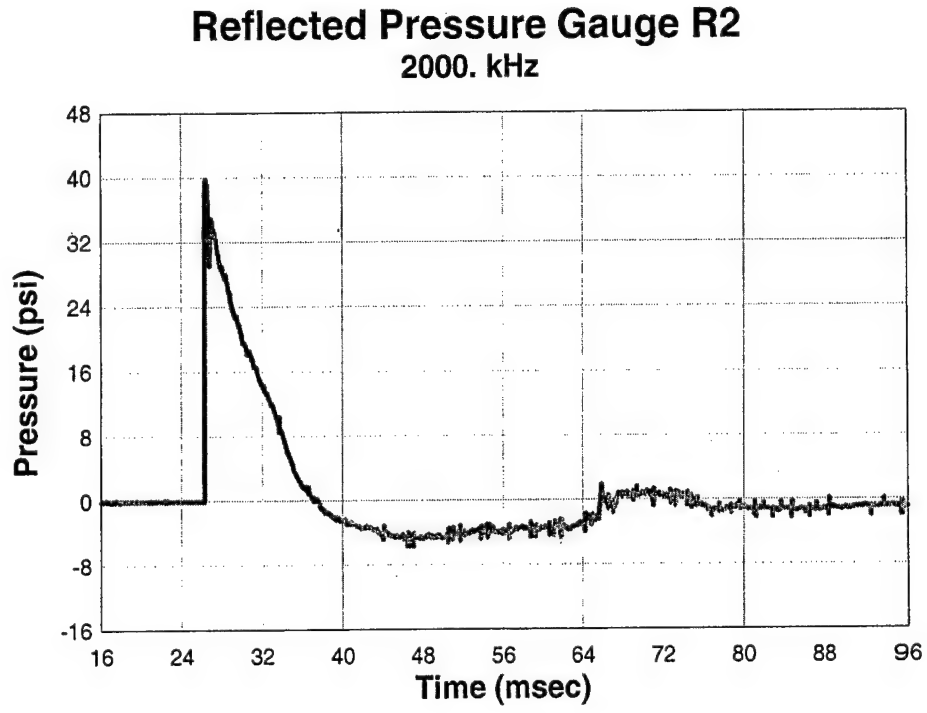

FIG. 194. Test 12, Gauge R2

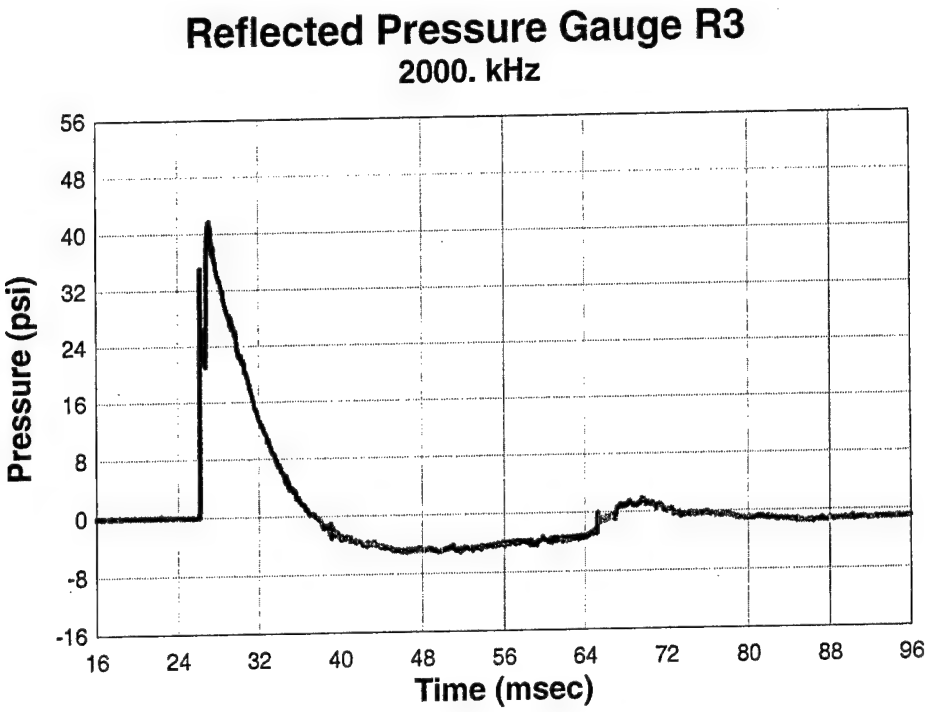

FIG. 195. Test 12, Gauge R3

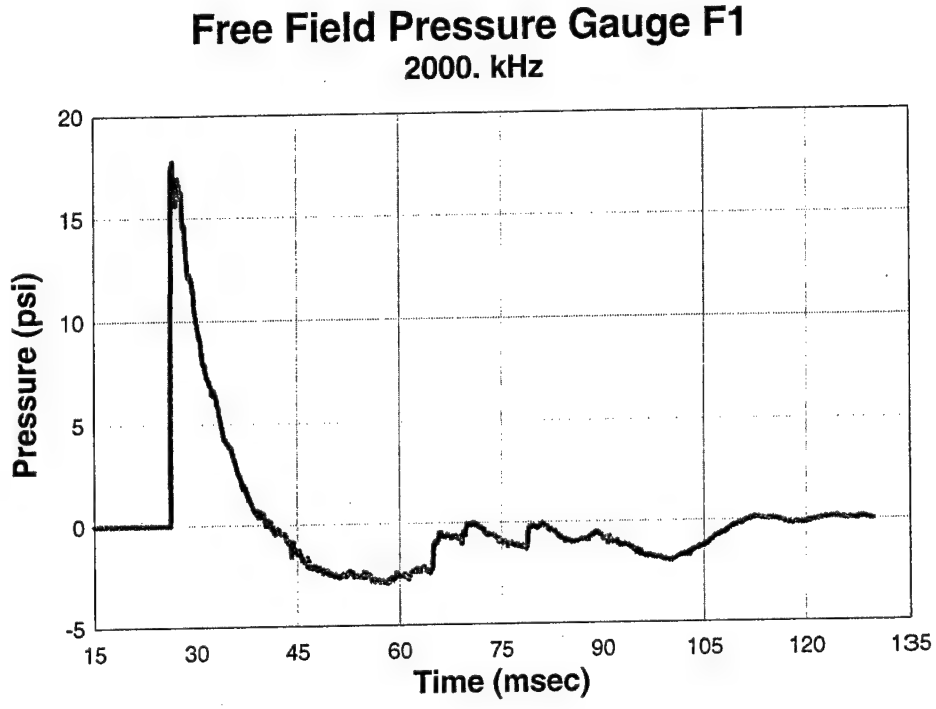

FIG. 196. Test 12, Gauge F1

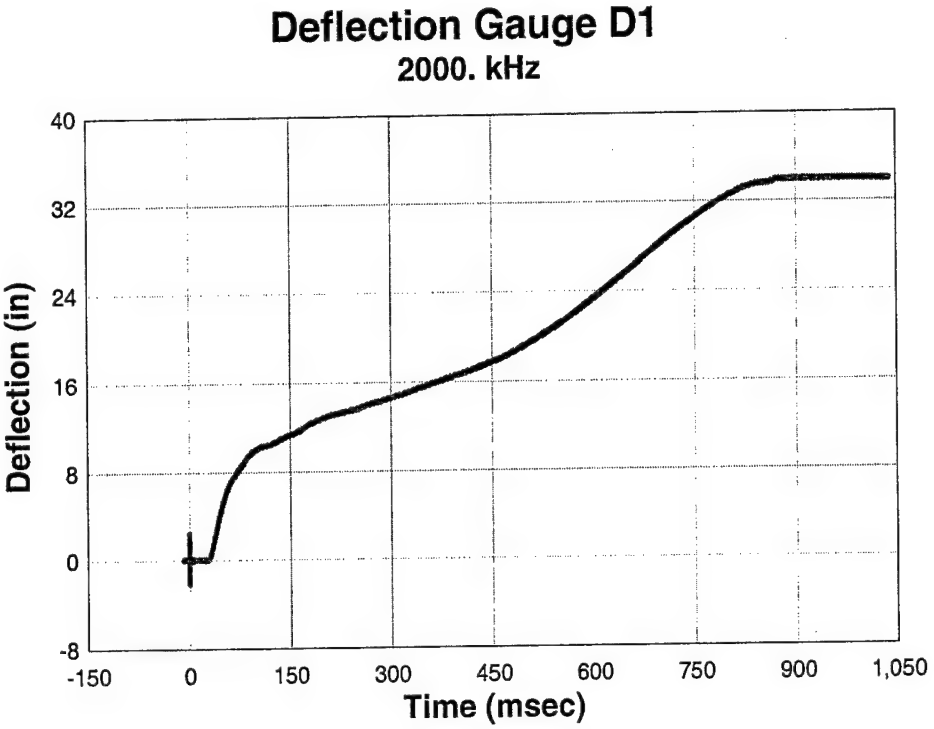

FIG. 197. Test 12, Gauge D1

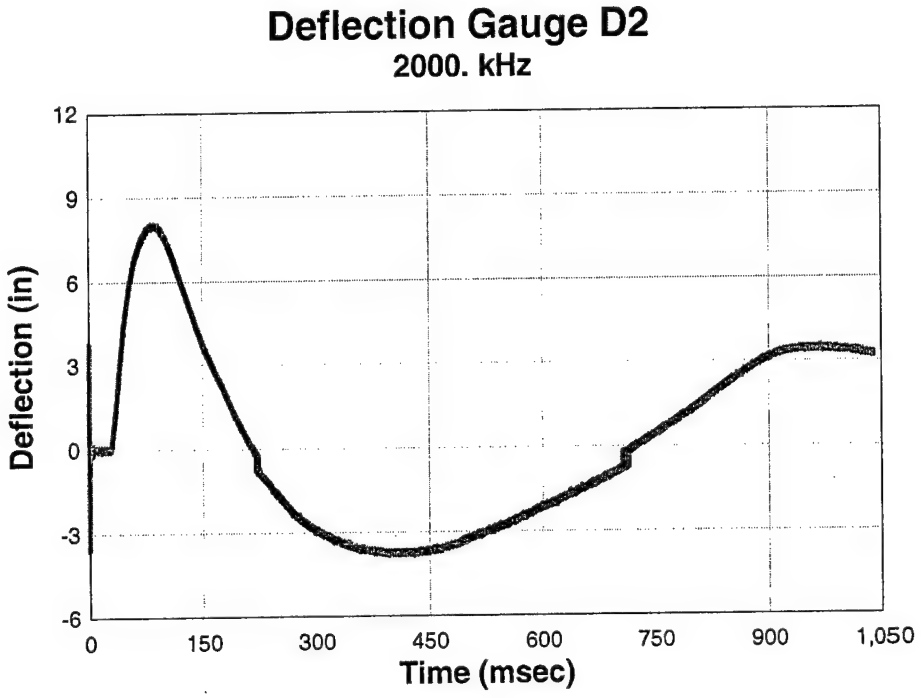

FIG. 198. Test 12, Gauge D2

The maximum pressures recorded by pressure gauges R1, R2, and R3 were (R1) 40.5 psi at 27.0 msec, (R2) 40.0 psi at 26.3 msec, and (R3) 41.6 psi at 27.0 msec. The maximum free-field pressure detected was (F1) 17.8 psi at 26.7 msec. The maximum deflection measured was (D2) 8.1 in. at 85.5 msec. The left wall failed, so deflection gauge D1 could not record a maximum deflection.

The left wall in Wall Test 12 collapsed. The deflection gauge recorded data until collapse occurred. For this reason, the deflection curve rose and then stopped. It did not indicate that the wall flexed back outward. Table 14 compares the predicted and actual data for each gauge used in Wall Test 12.

TABLE 14. Test 12, Predicted vs. Recorded Data

Gauge ID	Type	Prediction	Actual
R1	Reflected Pressure	41.2 psi	40.5 psi
R2	Reflected Pressure	41.2 psi	40.0 psi
R3	Reflected Pressure	41.2 psi	41.6 psi
F1	Free-field Pressure	14.9 psi	17.8 psi
I1	Free-field Pressure	5 psi	Gauge Failure
D1	Gear Driven Deflection	14 in. (Fail)	Failure
D2	Gear Driven Deflection	8 in.	8.1 in.

The result of Test 12 is shown in Fig. 199. The left wall collapsed fully. The polymer reinforcement failed at the top connection due to high shear stress. Since the blocks were not mortared together, there were no sections that remained intact, as there had been in other walls. Debris filled the left side of the test structure. A close-up image of the collapsed left wall is shown in Fig. 200.

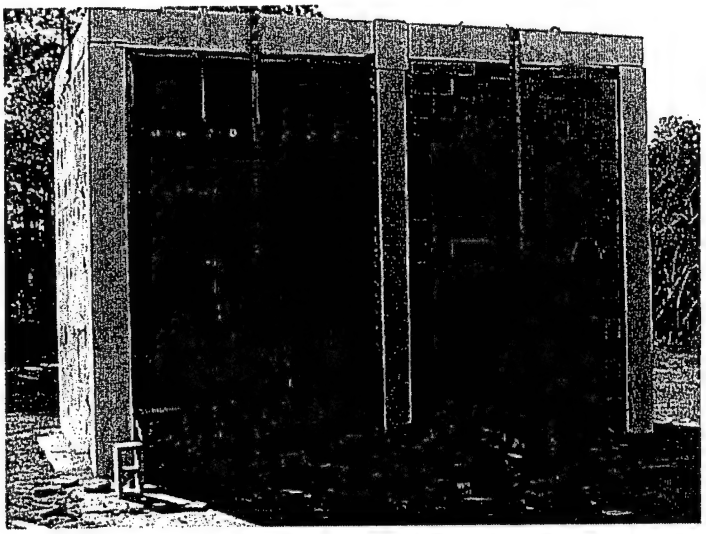

FIG. 199. Test 12, Posttest Structure

FIG. 200. Test 12, Left Wall, Post-Test

The polymer succeeded in preventing collapse of the right wall. Front face failure occurred primarily at the bottom. There were random blocks with defacing in the middle of the wall, which differed from other tests.

The lack of mortar on the walls did not prevent the polymer retrofit from being effective. Deflection data from D2 shows that the wall deflected inward approximately 8 in. and then outward about 4 in. Even deflecting outward, the polymer held the wall together. Some of the top row blocks sheared out. Furthermore, there appeared to be great arching forces due to the lack of mortar. Gravity collapse is predicted when the deflection of the wall equals the thickness of the wall and the right wall deflected more than its thickness. With the application of the polymer, however, the wall can deflect more without collapse. Images of the right wall are shown in Figs. 201 through 205.

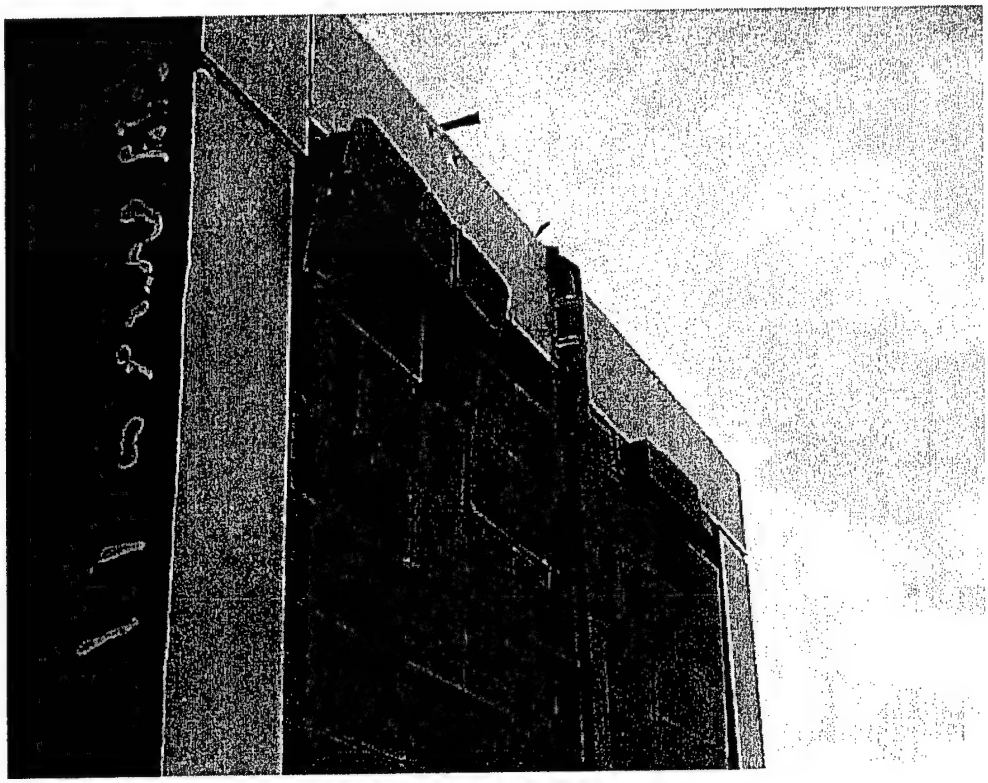

FIG. 201. Test 12, Right Wall, Top

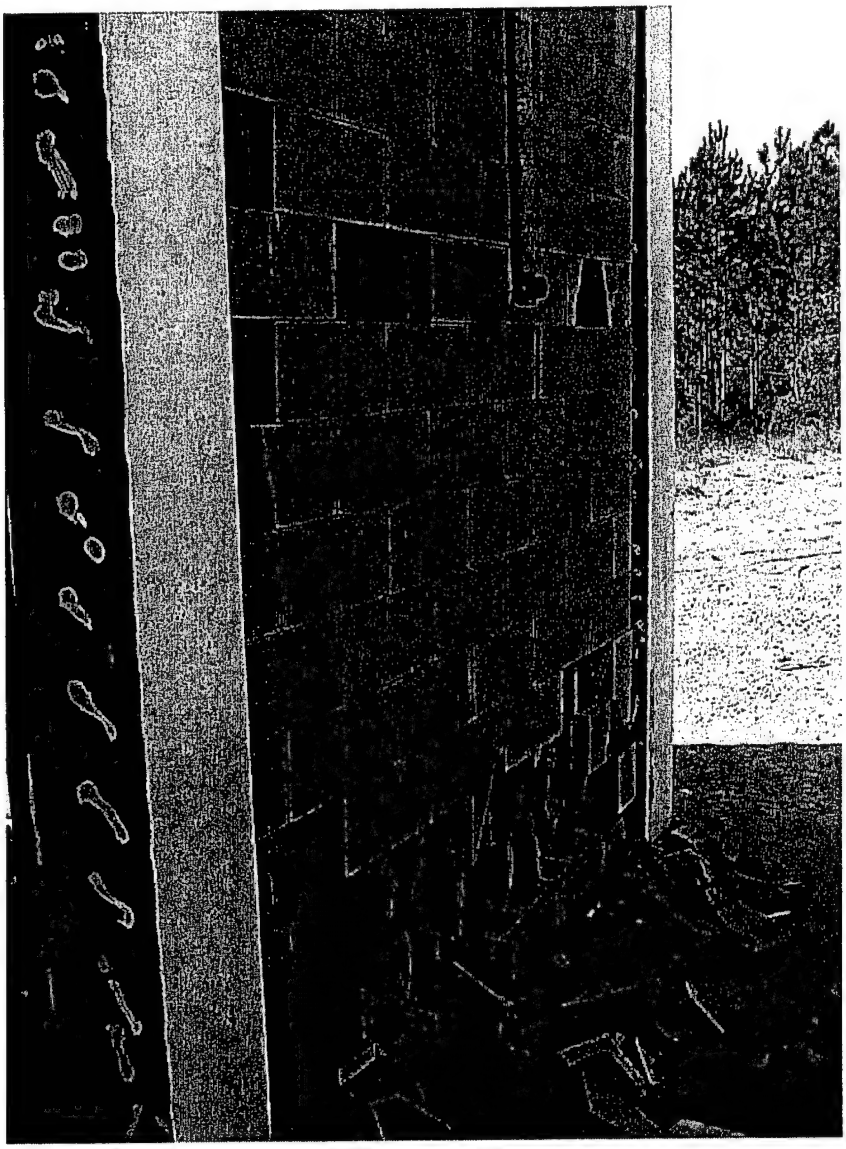

FIG. 202. Test 12, Right Wall, Bottom

When the polymer was applied to the right wall, the temperature was at the limit of the application range. This caused some pockets of air to form in the polymer on the wall. Although there were some tears in the polymer, they were unrelated to the air pockets. The air pockets in the polymer were outlined with a black marker and are shown in Fig. 203. A tear in the polymer is also shown in the figure. The tear was mid-height, which was the part of the wall that experienced the highest flexure stresses. Fig.

204 shows a tear in the polymer on the other side of the right wall. The tears on the left and right sides were in the same course of the blocks. The tears, however, were not connected. This was a direct result of the deflection mid-height of the structure.

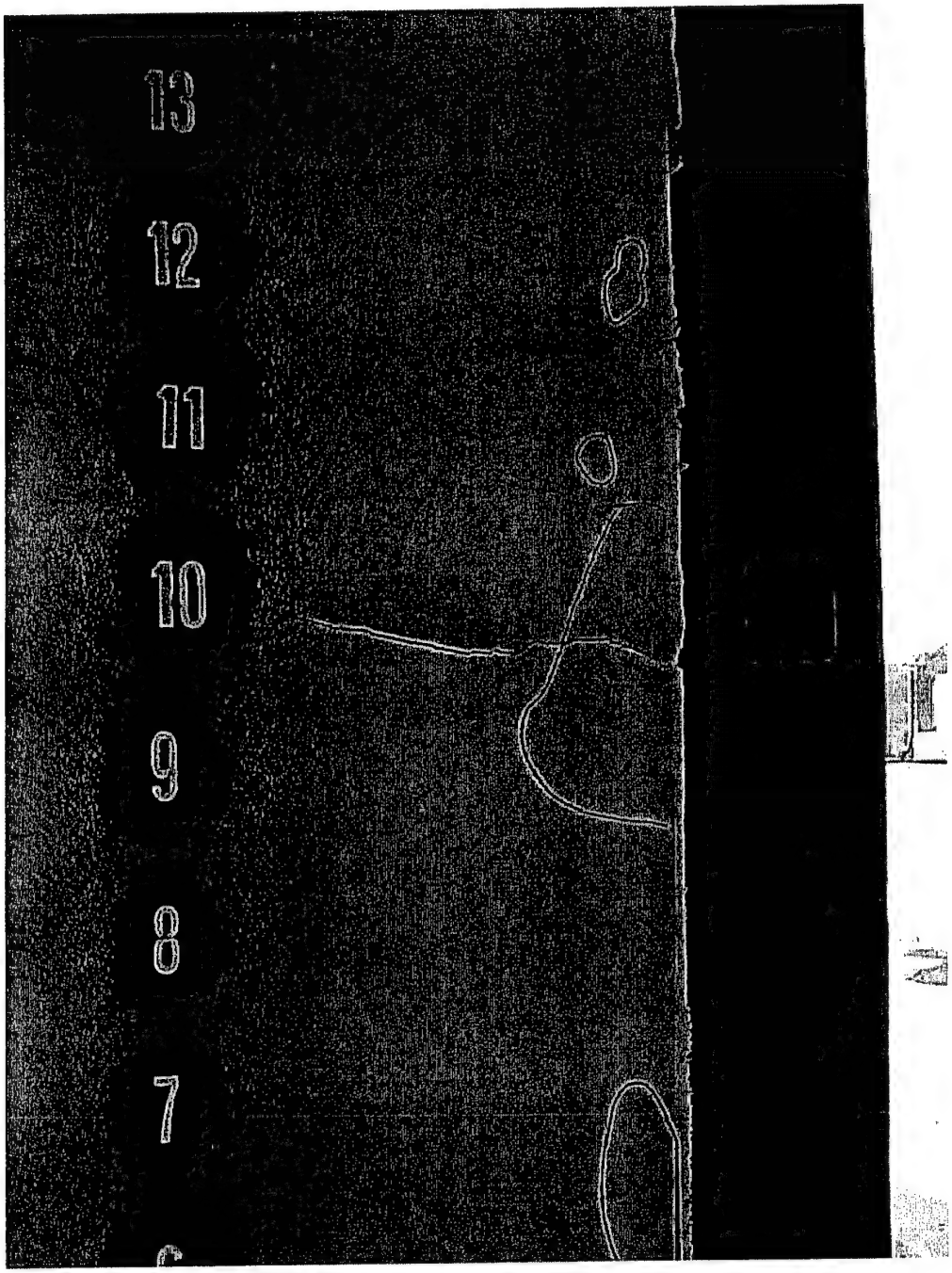

FIG. 203. Test 12, Right Wall, Bubbles and Right Tear

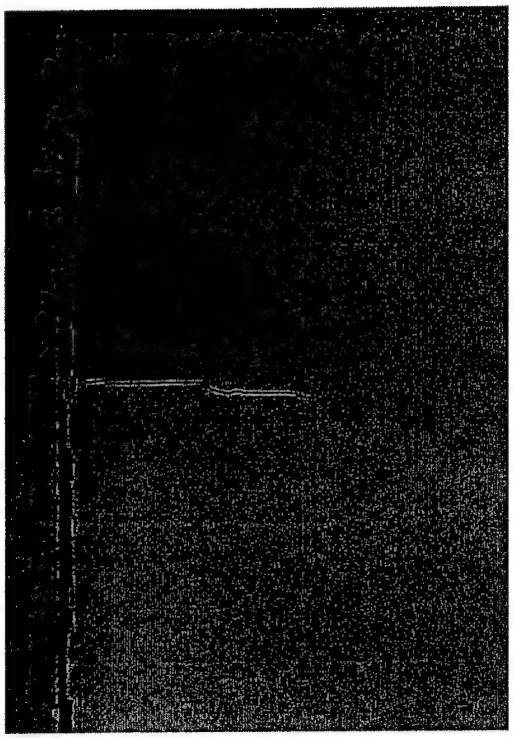

FIG. 204. Test 12, Right Wall, Left Tear

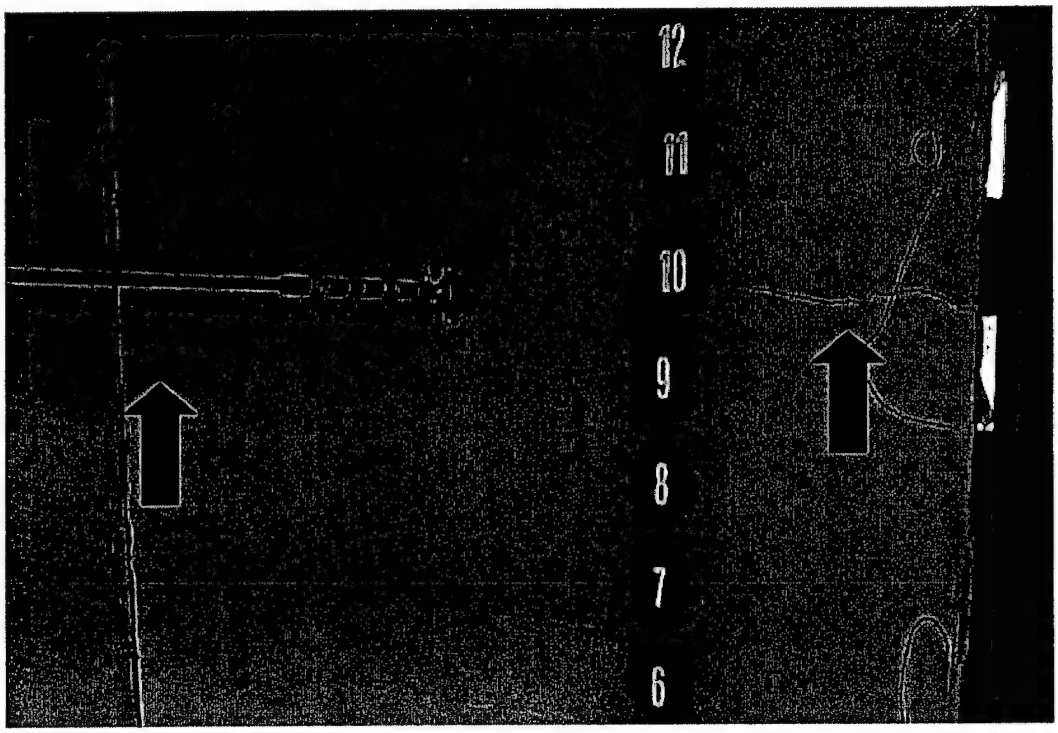

FIG. 205. Test 12, Right Wall, Both Tears

3.9 Explosive Testing Summary Analysis and Conclusions

The masonry wall tests conducted by the Air Force Research Laboratory at Tyndall AFB clearly indicate that a polymer reinforcement approach is effective in reducing the vulnerability of unreinforced, non-load bearing CMU walls subjected to blast loading. The application options are not overly burdensome and the explosive tests indicate that a 10-fold increase in peak pressures can be resisted by polymer reinforced one-way flexure walls compared to unreinforced concrete masonry walls. Although the reinforced walls are of little economic value after the blast event, they reduce the risk to building inhabitants, and therefore save lives.

Failure description of the system is very complex and is highly sensitive to the loading (peak pressure and impulse) and support conditions. It is crucial, however, to develop an engineering description of the resistance to lateral pressure provided by the wall system up to its ultimate load carrying capacity so that design and analysis methodology can be developed for the use of polymer reinforcement. Traditional beam and yield line methods used for static analysis of unreinforced CMU walls for out-of-plane loads give conservative results for walls subjected to low pressures. However, the engineering basis for these methods disappears as components of the wall fail and the overall geometry breaks down. Walls failing in flexure can develop additional resistance through arching mechanisms if the necessary boundary conditions exist and the shear capacity is not exceeded. Another level of complexity is added to the analysis when the out-of-plane loading is the result of blast reflective pressure and impulse. It is difficult to precisely control an explosive test event. Furthermore, predicting the lateral pressure that can be resisted by a polymer reinforced wall is complicated by (1) the variability in

mortar joint flexural bond and shear strength, (2) inconsistencies in polymer thickness or continuity over surface irregularities, and (3) fracture of the front face of the masonry blocks.

Overall, the behavior of the polymer reinforced masonry wall subjected to blast is characterized by (1) a stress wave that may weaken parts of the system such as block/mortar bond, (2) high localized shear at the block/mortar interfaces closest to the supports, which may result in shearing of the polymer coating, (3) fracture of the front face of some of the blocks due to high local stresses from peak pressure or due to flexural compression of the front face of the wall, (4) tearing of the polymer reinforcement in tension as the wall flexes, and (5) tearing or loss of adhesion of the polymer at the connection to the host structure that results in collapse of the system. All control walls failed catastrophically and provided little additional failure mechanism data.

The spray-on polymer treatment demonstrated an excellent bond between the polymer and the masonry. The length of polymer being strained increases as the blocks separate. It is important to realize that the tensile bond between the mortar and the masonry is weak (50-150 psi). Once the polymer begins to strain, the length of polymer involved extends across the mortar joint for slightly more than half of the block height in each direction. The bond between block and polymer is stronger in shear than the tensile strength of the concrete. Consequently, the polymer cracks the concrete as strain progresses.

For the charge sizes and distances considered in this investigation, the forward pressure on the wall (positive phase) resulting from the test explosions lasts only about 10 msec. Although the peak pressure varied between tests, the shape and duration of the

load curve did not vary substantially. Some damage may result from the initial stress wave that travels through the depth of the masonry. However, due to the mass involved, the flexural response of the system is spread over a broader timeframe (approximately 60 msec) and a velocity of approximately 300 in/sec is imparted to the wall.

Front face fracture of the masonry units has been consistently observed. The block is often broken into several pieces, but sometimes the front face shears from the webs and survives as one piece. A causation and timing description of this phenomenon is important, because it reduces the stiffness of the system as the wall flexes inward, and affects the ultimate capacity of the wall. The fracture tends to be concentrated closest to the supporting edges. It has also been observed that the fracture point within the block is deepest nearest to the supports. There are two plausible explanations for the front face fracture phenomenon: (1) the front face is fractured by the peak pressure in the first few milliseconds of the loading, or (2) fracture results from compression of the front side of the wall as flexure occurs. The masonry blocks with the most lateral resistance will have a greater tendency for front face fracture. Combining single block dynamic behavior with an increased lateral stiffness provided by the supports provides a reasonable explanation of why blocks nearest to the support edges experience a higher rate of block face failures. Shock wave propagation in the front face also creates tension and possibly spalling on the interior free surface, which would also weaken the front face.

This approach, however, does not fully explain all front face failure conditions observed from full-scale explosive tests of polymer-reinforced walls. A close look reveals significant evidence that arching is developed. The existence of intact front face pieces is evidence that something more than independent block behavior is occurring. It

is not possible to observe the front face block fracture during the explosive test due to the short time duration and debris carried by the blast wave. It is only revealed if the wall remains standing. Consequently, block face failures have only been verified on polymer reinforced walls. In general, the point of fracture within the web measured from the front face appears to be related to the slope of the deflected shape during blast response.

Wall Test 12 was conducted to address some of the failure mechanism questions. The walls of Test 12 were constructed without mortar, i.e., the blocks were simply stacked on top of each other in a typical running bond pattern. At the top of the wall the thin gap between block and structure was tuck pointed with mortar. A polymer coating was applied directly to the interior of the wall in the same way as the other tests for one wall, while the polymer coating was sprayed onto a plastic membrane liner on the inside of the other wall so that there was no bond between the masonry and the polymer reinforcement.

The wall coated directly withstood the blast without collapse. Front face fracture occurred over the lower three courses of block and was sporadically distributed over several other blocks. Polymer tearing initiated for several inches from both sides at approximately the height-wise center of the wall. Also, it appears from careful post-test analysis of the reaction frame and high-speed videos that flexural rotation lifted the roof of the reaction frame. This indicates dramatic increase in the arching forces as compared to a standard mortared wall. The polymer of the second wall (polymer sprayed onto the membrane) tore at the top support attachment and the wall collapsed. The lack of an integrated masonry-polymer system (no bond between the blocks and polymer) resulted in the polymer coating acting as a "catcher" membrane and thus resulted in a higher

concentration of force at the connection of the polymer to the reaction frame. Although collapse occurred, the rubble was contained to the forward part of the structure and, compared to a masonry wall without polymer reinforcement, a high level of occupant protection would have been provided.

Wall Tests 9, 10, and 11 involved window and door openings. The overall objectives of these tests were to examine the influence of typical window and door frame openings on polymer reinforcement effectiveness and failure mechanisms. These tests also involved a 1/8 in. coating with a 12 in. overlap onto the reaction structure. Walls of Test 9 did not include overlap of the polymer coating onto the window or door frame. Walls in Tests 10 and 11 involved a wider wall structure than the other walls (16 ft vs. 7.5 ft) to eliminate edge condition effects on walls with openings. Wall Test 11 involved a heavily anchored window frame with polymer overlap onto the frame.

Overall, the polymer provided the same level of effectiveness for walls with the openings as walls without openings. Front face fracture occurred, with an evident tendency for fracture around the stiff window or door frames. There was evidence of increased tendency for mortar joint cracking compared to walls of the same test and construction parameters without door or window openings. A large lower portion of Wall Test 9 (containing a door frame) was breached. There was also evidence of a tendency for tear initiation of the polymer coating at the corners of the window frames.

Flexural wall response dissipates as cross sectional structural integrity is lost. The two primary causes for the loss of structural integrity under blast loads are (1) mortar joint separation due to bond, flexure, or shear failure, and (2) failure of the front face of individual blocks. In some of the tests, large areas maintained integrity with mortar

failure limited to three or less joints. Careful post-test analyses reveal that wall behavior involves several mechanisms at different stages of the wall response. The order of these failure mechanisms can vary. If slope change at the critical stress area is severe, then shear may develop in the polymer coating at rough block edges. The polymer tears sooner in these situations than in those where the polymer is predominantly subjected to tension. The following sections summarize additional observations of each test.

3.9.1 Wall Test 1

Retrofitted Wall: The top courses of the block experienced front face failures. Some of the webs in these courses were fractured. There was defacing at the bottom of the CMU wall. Cracks in the mortar joints were visible at the bottom and mid-height. On the inside of the wall, there was a polymer tear at the mid-height mortar joint crack. The top and bottom courses were held in place by angles and were not damaged. The retrofit was successful in preventing debris from entering the structure. Maximum reflected pressure measured 57 psi. Maximum displacement measured 7.2 in.

Unretrofitted Wall: The unretrofitted wall collapsed.

3.9.2 Wall Test 2

The higher charge in this wall test greatly exceeded the lateral load capacity of the walls, as both the retrofitted and unretrofitted walls collapsed. A tear occurred at mid-height of the polymer and extended across the entire width of the right wall. Maximum reflected pressure measured 238 psi. Collapse prevented measurement of maximum displacement.

3.9.3 Wall Test 3

¼-in.-Thick Interior Retrofitted Wall: The top courses in this wall experienced front face failures, and web shear occurred in these courses. Mortar joints at mid-height experienced visible cracks across the entire width of the wall. In the interior, there was significant tearing of the polymer near the top of the wall. The poor bond that was observed between the polymer and the floor had minimal effects on the performance of the polymer. Displacement was highest at the top of the wall. There was minimal deflection at the bottom of the wall. Overall, the polymer was successful in preventing fragments from entering the reaction structure. Maximum reflected pressure measured in this test was 59.4 psi. The maximum deflection measured 9.4 in.

1/8-in.-Thick Interior/Exterior Retrofitted Wall: The posttest polymer membrane shape did not match the interior residual shape. Front face failure and polymer separation were the primary explanations. It appeared that the polymer coating pulled apart and took the bonded block fragments with it. The polymer remained bonded to the majority of the wall. There was a 4-in. tear in the polymer near the top exterior. On the interior of the wall, there was an 18-in. tear and protruding block faces. Deflection in this wall was highest at courses 16 and 17. Deflections above this line were curved; those below the line were linear. Joint 16 through 17 appeared to be the weakest joint in the wall. Maximum reflected pressure measured 64.8 psi. Maximum deflection measured 7.8 in.

Left Retrofitted Cubicle (6-in. Overlap): Several of the top and bottom courses suffered complete defacing. The polymer on the inside of the structure was undamaged. The shorter wall had less deflection, preserving the integrity of the polymer. Nearly 70% of the wall experienced front face failure. However, the polymer was successful in

keeping debris out of the reaction structure. Maximum reflected pressure measured 64.2 psi. Maximum displacement measured 4.9 in.

Right Retrofitted Cubicle (12-in. Overlap): The bottom three and top two courses experienced complete exterior defacing. Nearly 60% of the wall experienced full or partial front face failure. Interior mortar joints were unaffected. The deflection of the wall was greatest at courses 10 and 11. On the interior, there was a 4 in. tear in the polymer near the top of the wall and there was a 2-ft tear at the bottom. Nonetheless, the polymer was successful in preventing wall fragments from entering the reaction structure. Maximum reflected pressure measured 69.1 psi. Maximum deflection measured 5.9 in.

3.9.4 Wall Test 9

Wall with Door: Bottom courses on both sides of the doors and blocks near the top experienced front face failure. There were wide cracks in mortar joints mid-height. Tearing of the polymer occurred along the entire width of the wall at course 2 and 3. There was also a small tear at the upper left corner of the top of the door. The polymer failed late in the wall response at the bottom left of the door. This allowed some block fragments to barely enter the structure. The door hinges failed and the door entered the structure. Maximum reflected pressure measured 61.1 psi. Maximum deflection measured 5.6 in.

Wall with Window: The top three courses experienced complete front face failure. Many other blocks in this wall experienced partial front face failure. There was significant and sporadic mortar joint cracks throughout the wall. There was a 2-n. tear at the lower left corner of the window and a ½-in. tear near the upper right corner. The

polymer was successful in preventing wall fragments from entering the structure. However, the window glazing and the wooden perimeter around the window frame, which were not protected by the polymer, entered the structure. Maximum reflected pressure measured 61.1 psi. Maximum displacement measured 7.7 in.

3.9.5 Wall Test 10

Wall with Door: Front face failure occurred on the right side of the wall near the bottom of the door. There was also defacing across the top of the structure. There were some cracks, indicative of shear failure, near the top of the door. There was a significant polymer tear on the interior of the wall at joints 11 and 12. There were smaller mid-height tears. A single block at the back of the wall protruded into the structure; however, it remained bonded to the polymer and did not break away from the wall. The door was torn from its hinges but did not enter the structure. The polymer was successful in preventing entrance of flying debris. The strength of the center wall strip containing the door frame appears to have prevented the wall from collapsing. Maximum reflected pressure measured 43.4 psi. Maximum deflection measured 9.1 in.

Cubicle: The cubicle test in Wall Test 10 collapsed. The cubicle was not wired with gauges.

3.9.6 Wall Test 11

There was significant front face failure in many courses of the wall. There were mortar failures in a step-like fashion from the window to the top of the wall. Several small tears occurred in the interior polymer near the bottom. The polymer used on the

wall was successful in preventing secondary fragmentation. Maximum reflected pressure measured 38.1 psi. Maximum deflection measured 6.2 in.

3.9.7 Wall Test 12

Bonded Retrofit Mortarless Wall: Front face failure occurred mostly at the bottom of the wall, although there was sporadic defacing throughout. Blocks near the top of the wall dislodged outwardly. There were problems with the polymer due to temperature conditions when it was applied. The cure time of the polymer was approximately twice as long as on a warmer day, which caused air pockets between layers of the polymer. There were some tears in the polymer both through the air pockets and otherwise. The retrofit was still successful in preventing flying debris. Maximum reflected pressure measured 41.6 psi. Maximum displacement measured 8.1 in.

Unbonded Retrofit, Mortarless Wall: The wall with the polymer separated by a plastic membrane sheared at the top attachment and collapsed. This confirms that the bonding of the polymer is an important parameter in effectiveness. The tears in the polymer were considered to be caused by the collapse of the wall. Maximum reflected pressure measured 40.5 psi. Wall collapse prevented measuring maximum displacement.

CHAPTER 4

EXPLORATORY TESTING

4.1 Introduction

The wall tests described in Chapter Three were performed using a single polymer. This material was chosen primarily due to its availability and ease in application. The explosive tests demonstrated that the polymeric spray-on coating can greatly enhance the resistance to collapse and secondary fragmentation of unreinforced masonry walls. However, the polymer used was an off-the-shelf material that was not designed for blast reinforcement. Better materials may be found or developed that would further enhance the ability of wall structures to resist blast loads, while also addressing other issues, such as cost, constructability, and flammability.

Material manufacturers have learned of the success of the masonry wall blast reinforcement project and have submitted many materials to the AFRL as reinforcement candidates. All of the materials cannot be tested in full-scale wall tests due to the high cost and time limitations. Because there is such an enormous range of advanced materials that may be suitable for the blast reinforcement purpose, it is imperative to find a way to evaluate the reinforcement candidates in the laboratory. Furthermore, minimum performance standards of polymer materials for blast retrofit purposes have not yet been defined and are needed by material manufacturers. Materials could then be designed specifically for the purpose of reinforcing walls for protecting building occupants during blast loads.

As part of this project, exploratory laboratory work was conducted with a limited number of polymeric materials. The purpose of this work was not to determine other materials that could be suitable for blast reinforcement, but rather to explore the use of inexpensive tests that might be useful in selecting materials. Therefore, comprehensive background reviews have not yet been conducted and all conclusions must be viewed as preliminary. This chapter considers a static flexural test, a drop tower test, and a gas gun test.

4.2 Static Flexural Test

4.2.1 Material Selection

The first laboratory test that was explored was the static flexural test. Five materials were initially chosen for evaluation. The first material obtained for testing was the spray-on elastomeric polymer used in the full-scale wall testing, as it was proven to be effective for blast reinforcement and could be used to compare to other materials. Two materials investigated were a polypropylene/polypropylene woven material and a thermoplastic polyurethane. Both were supplied in thin sheets and were applied in multiple layers to obtain a 1/8-in. thickness. These were bonded to the blocks with adhesives. The fourth material considered was Sta-Kool 780. This material was a readily available polymeric material with high elongation properties that is primarily used as a roofing sealant. Specifications for this material reported elongation up to 350%. The fifth material obtained was a paint-on product, directly applied with no adhesives. This material, known as Geothane, was chosen because it was relatively easily applied in the laboratory.

4.2.2 Preparation of Blocks

Ten 16 in. x 8 in. x 2 in. concrete pavers were obtained and checked carefully for cracks and other defects. A small notch was cut across the width of the blocks so that their behavior would be analogous to the fracture of mortar joints in the full-scale walls. A concrete saw was used to cut a 1/16-in. notch across the width of the block, dividing the 16 in. length into two 8 in. lengths (Figs. 206 and 207). To ensure that the polymer was of uniform thickness and the material did not seep into the notch, clay was used to fill the notch. A different color of clay was used in each block to differentiate the blocks. The clay was allowed to dry before any further work was done.

FIG. 206. Concrete Saw

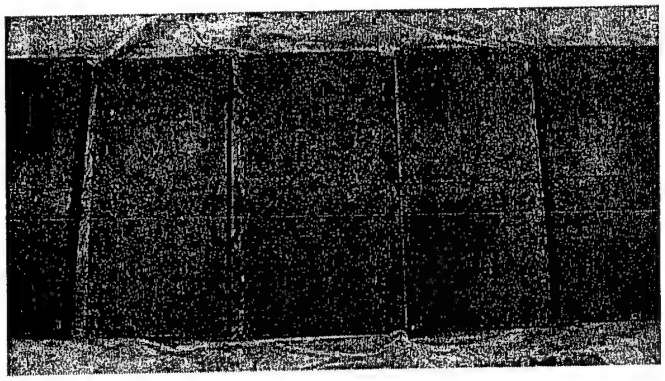

FIG. 207. Notched Pavers

4.2.3 Application of Material

The elastomeric polymer used in blast testing was applied to the blocks by a spray-on process. Upon drying, a strong bond formed between the polymer and the block.

The polypropylene/polypropylene woven material and the thermoplastic polyurethane were bonded using an adhesive. The adhesive required that the blocks be warm for application. The blocks were placed in an oven at 250 degrees for 15 min. Then the adhesive was placed on the blocks and the polypropylene/polypropylene woven material and the thermoplastic polyurethane material was applied. The block was held under a constant pressure while setting.

Before coating any blocks with Sta-Kool, a quick test was done to determine how the material might behave. A square, plastic pan was sprayed with a polymer-releasing agent called Loctite 700-NC Frekote. After the pan was cleaned and coated with Frekote, the Sta-Kool was poured into the pan and allowed to dry for several days. It took over a week for the material to dry enough to be removed from the pan. Although it did elongate as per specifications, the material was deemed inappropriate for blast reinforcement, as it had very little stiffness. The material was eliminated from further testing.

Geothane 520 is a modified urethane elastomer used with a water-borne epoxy primer, Future-Bond 415. Futura Coatings, Inc. technical data specifications state that Geothane 520 "forms a tough, monolithic, seamless, highly elastic membrane with excellent water and chemical resistance" (Futura 2002b). Geothane 520 is a paint-on material and does not require spraying equipment. This material was applied directly to

concrete blocks and tested in the laboratory for strength and elongation characteristics. Applying the Geothane to the blocks was a lengthy process. To ensure proper bonding of the polymer to the concrete, the blocks were primed with Futura Coatings Futura-Bond 415. This primer consisted of two components: Futura-Bond 415A and Futura-Bond 415B. Futura-Bond primer is "a two component, water-borne epoxy primer with outstanding adhesion to most concrete, masonry, metal and wood surfaces, including damp concrete" (Futura 2002a). Some features specified by the manufacturer include (1) convenient 1:1 mixing ratio, (2) high solids, (3) low VOC, (4) low odor, (5) water borne technology, (6) exceptional adhesion to damp concrete and masonry, and (7) spray and/or roller application. Typical properties, pot life, applicable conditions, and cure time of the Futura-Bond 415 primer can be found in Tables 15 through 18.

Table 15. Typical Properties of Primer

Solids by Volume	70%
Solids by Weight	77%
Volatile Organic Compounds	0.9 lb/gal
Theoretical Coverage	1123 ft^2 at 1 mil
Recommend DFT	2-5 mils
Number of Coats	Normally 1
Mix Ratio (by volume)	1 "A":1 "B"
Flash Point (PMCC)	Part A 53°F Part B >200°F
Shelf Life at 60-90°F	12 months
Color	Yellow (only)

Table 16. Pot Life of Primer

Material Temperature	Pot Life
60°F	2 hrs
75°F	80 min
90°F	30 min

Table 17. Applicable Conditions of Primer

	Normal	Minimum	Maximum
Material	75-90°F	65°F	100°F
Surface	75-90°F	45°F	110°F
Ambient	75-90°F	45°F	110°F
Humidity	30-50%	0%	85%

Table 18. Cure Time of Primer

	Surface Temperature		
	50-60°F	70-80°F	90-100°F
Surface Dry	7 hrs	3.5 hrs	2 hrs
Hard Film	24 hrs	8 hrs	5 hrs
Recoat (min)	20 hrs	6 hrs	4.5 hrs
Recoat (max)	2 days	1 day	16 hrs
Full cure	6 days	3 days	2 days

The two components of the Futura-Bond primer were mixed individually in separate containers, then mixed together at a 1:1 ratio in the paint tray. This was done using a small kitchen mixer. The process is shown in Fig. 208. The clayed blocks are also shown.

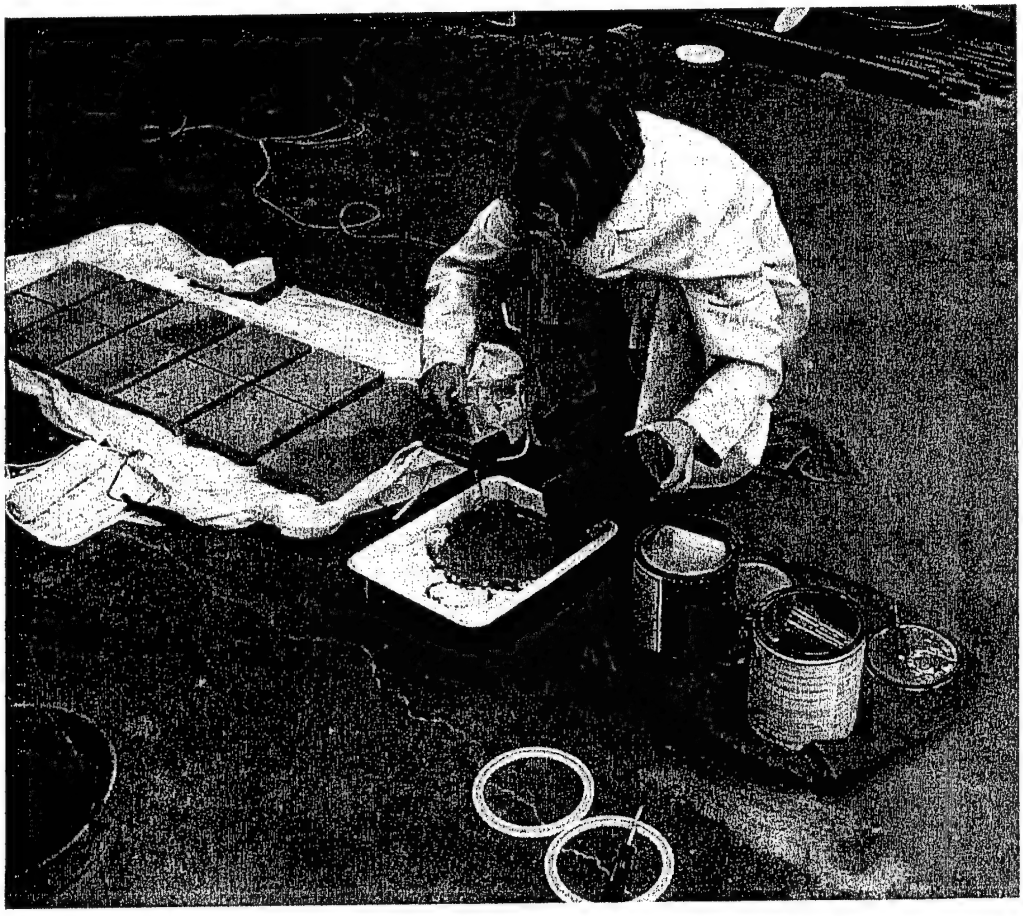

FIG. 208. Priming Mixture and Clayed Blocks

Once mixed, the primer was applied with a paint roller to all six of the concrete blocks. It was allowed several days to dry before any additional work was done. The process is shown in Fig. 209. The primed blocks are shown in Fig. 210.

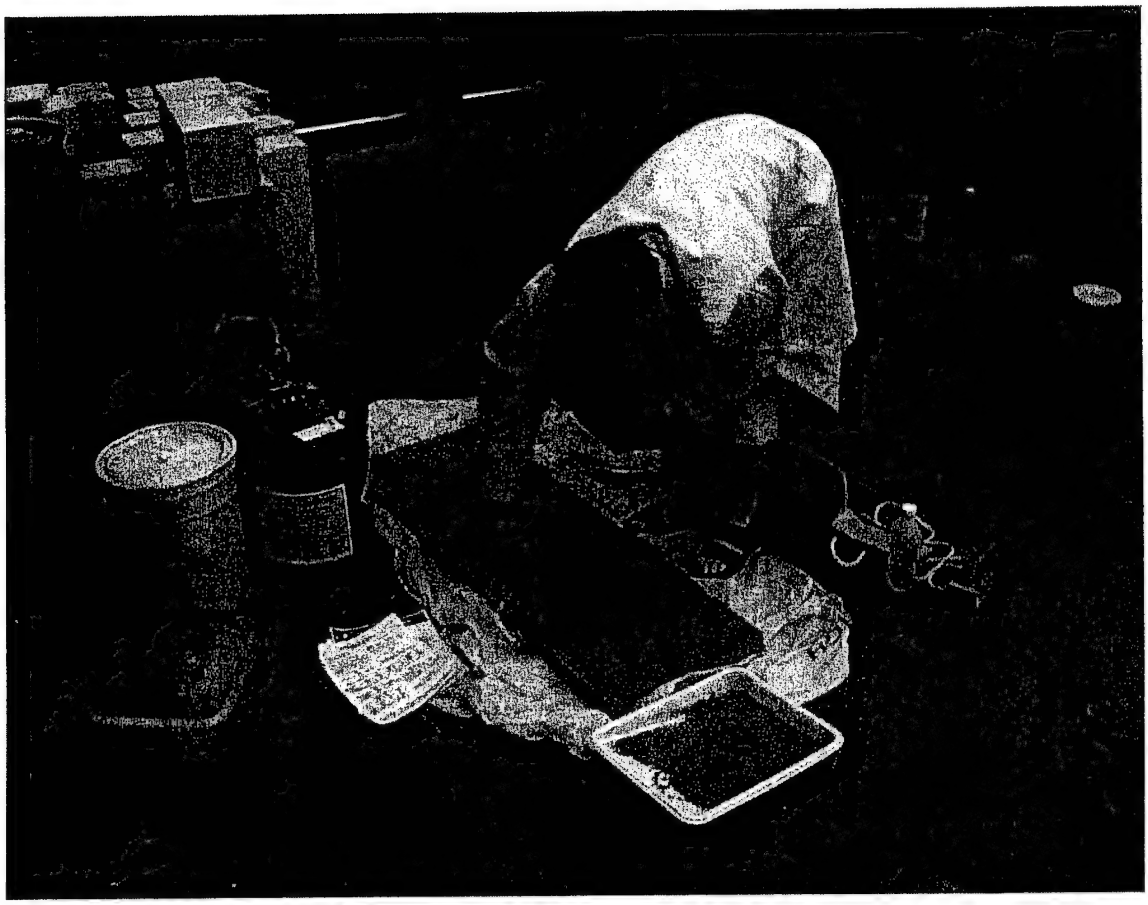

FIG. 209. Priming Process

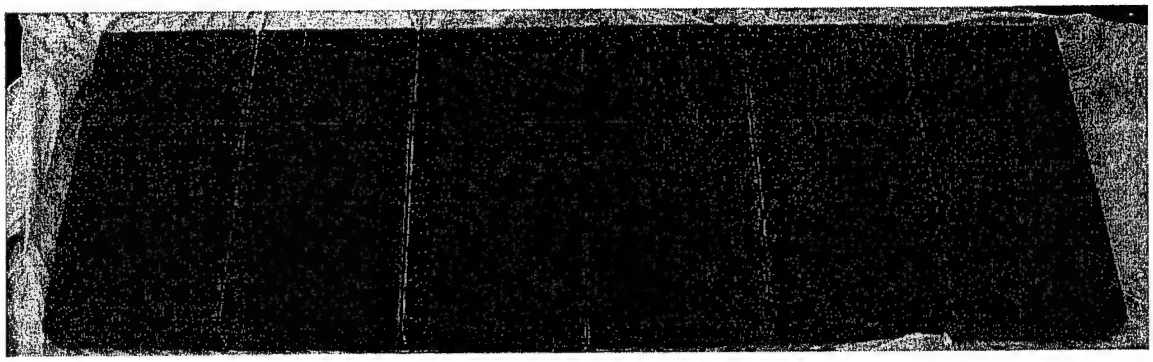

FIG. 210. Primed Blocks

After priming, the blocks were ready to be coated with polymer. The polymer used was Geothane 520, a modified urethane elastomer. The manufacturer describes the material as follows: "A 100% solids, standard cure, two component modified urethane elastomer. It forms a tough, monolithic and chemical resistance. [It] does not require plural component spray system" (Futura 2002b). Some key features of this product include (1) up to 300% elongation, (2) high build—up to 30 mils per coat, (3) usable over geotextile fabric, (4) spray and/or roller application, and (5) good resistance to UV degradation.

The technical specifications for this product read as follows:

> Recommended Uses: As a Primary or Secondary Containment lining on concrete, steel or geotextile fabric surfaces to contain leaks and spills of wastewater, fuels, and a wide range of chemicals. It is excellent as a landfill cap or environmental cover to control leaching and wind erosion. It is also excellent as a repair material for existing pond liners and torn or failed seams in plastic sheet linings and for repairs to GEOTHANE 5020.

Geothane 520 can be used on many materials. The priming agent to be used depends on the material. For concrete applications, Geothane 520 is used with the Futura-Bond 415 Primer. For application to steel, Futura-Bond 610 primer is required.

Use of the primer and material were simple. Care was taken to follow directions given on mixing, application, and cure time. The properties, specification data, pot life, application conditions, and cure time are provided in Tables 19 through 23.

Table 19. Typical Properties of Geothane 520

Solids by Volume	100%
Solids by Weight	100%
Volatile Organic Compounds	0.0 lb/gal
Theoretical Coverage	1604 ft^2 at 1mil
Recommend DFT	20-100 mils
Number of Coats	Normally 2
Mix Ratio (by volume)	1 "A":1 "B"
Flash Point (PMCC)	>200°F
Shelf Life at 60-90°F	9 months
Color Standard	Black and Tan

Table 20. Specification Data of Geothane 520

Property	Test	Value
Elongation	ASTM D 412	300%
Tensile Strength	ASTM D 412	900 psi
Abrasion Resistance	ASTM D 4060 CS 17 / 1000 g / 1000 cycles	23 mg loss
Hardness	ASTM D 2240	65 Shore "A"
Flexibility	ASTM D 1737	-55°F Passes 1/2" mandrel bend
Tear Resistance	ASTM D 4533	240-370 pli
Permeability	ASTM E 96 Procedure B - 50mils dft	.12 perms

Table 21. Pot Life of Geothane 520

Material Temperature	Pot Life
50-60°F	45-60 min
70-80°F	40-50 min
90-100°F	25-35 min

Table 22. Application Conditions of Geothane 520

	Normal	Minimum	Maximum
Material	75-90°F	65°F	150°F
Surface	75-90°F	45°F	110°F
Ambient	75-90°F	45°F	110°F
Humidity	30-50%	0%	85%

Table 23. Cure Time of Geothane 520

	Surface Temperature		
	50-60°F	70-80°F	90-100°F
Surface Dry	7 hrs	3 hrs	2 hrs
Hard Film	30 hrs	16 hrs	9 hrs
Recoat (min)	10 hrs	4 hrs	3 hrs
Recoat (max)	4 days	3 days	30 hrs
Full cure	10 days	6 days	4 days

Geothane 520 consisted of two components that were mixed together. Each component was power mixed individually, and then the two were mixed together to a smooth consistency with a drill mixer. The ratio of components was one "A" to one "B" by volume. The mixing procedure can be seen in Fig. 211.

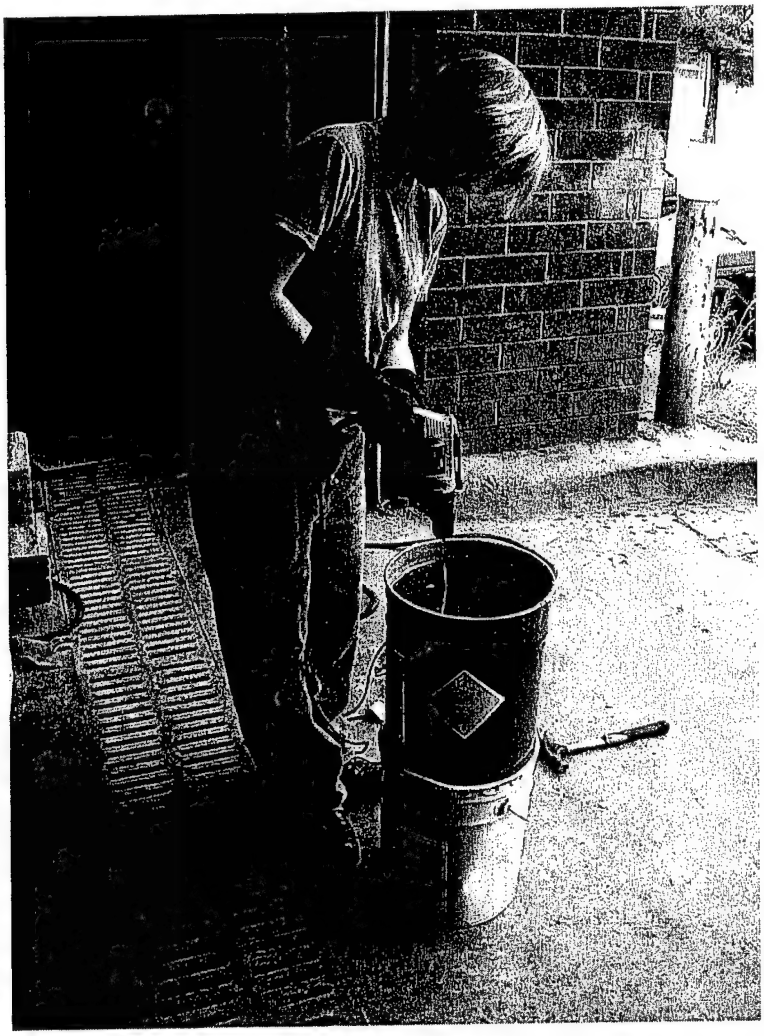

FIG. 211. Geothane Mixing Process

Once the components were thoroughly mixed, the material was applied to the primed blocks with a paint roller. Each coat was kept very thin, as specified by the manufacturer. The desired thickness of material on the blocks was 1/8 in. This required many cycles of mixing and coating. Between each coating, the material was allowed at least 24 hours to dry. A picture of the Geothane 520 being applied to the blocks is shown in Fig. 212. An image of the final blocks is shown in Fig. 213.

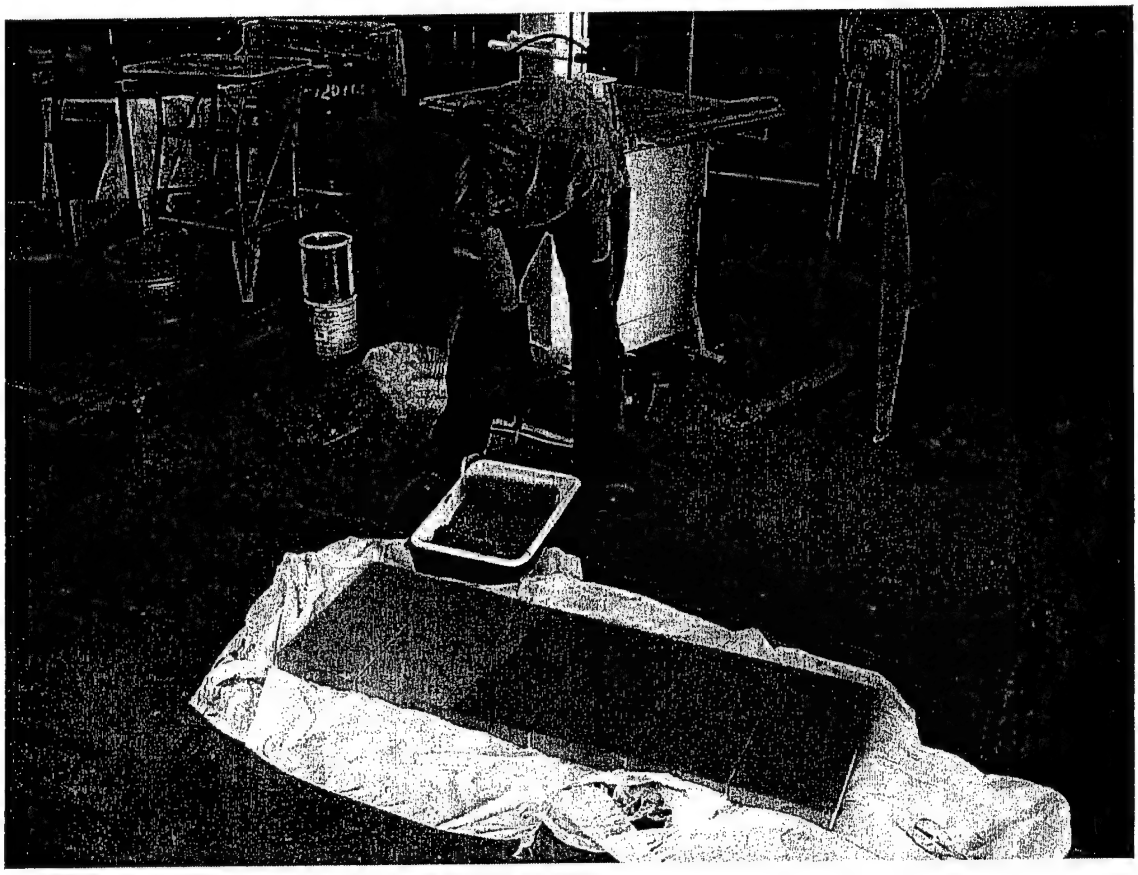

FIG. 212. Coating Process

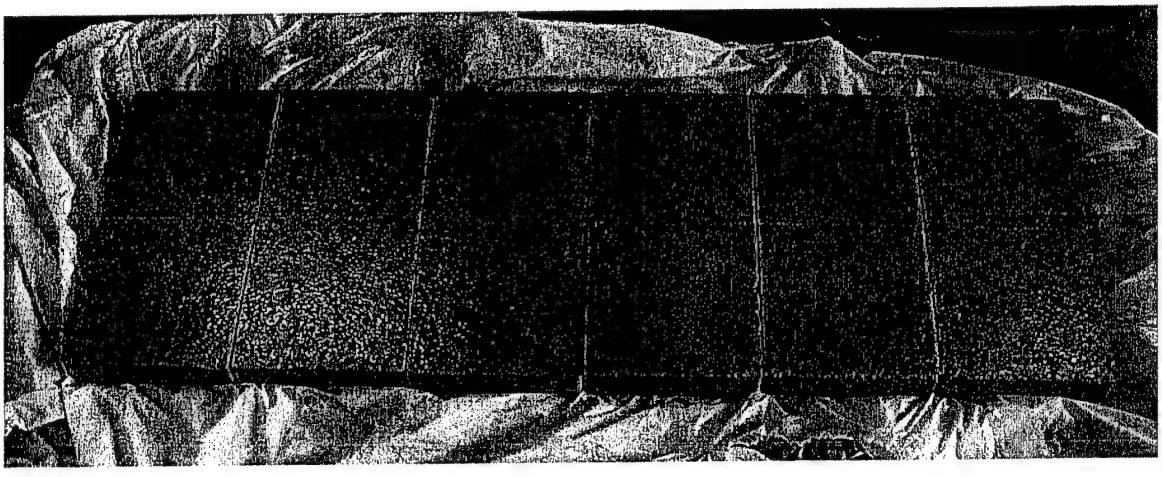

FIG. 213. Coated Blocks

4.2.4 Introduction

The coated blocks were first tested in the static flexural test. Five blocks were evaluated. The static flexural test provides a means of evaluating tensile strength, elongation, bond strength between the materials and blocks tested, and failure mechanisms.

4.2.5 Test Methodology

The five blocks tested included one concrete (no coating), one coated with Geothane, one coated with polyester-based thermoplastic polyurethane (blue), one coated with polypropylene/polypropylene woven material (black), and one coated with the elastomeric polymer used in explosive tests. The setup for the blocks consisted of two round steel supports that stretched the entire width of the concrete blocks. A load head applied the force at the center of each block, resulting in flexure. A basic set-up of the block is shown in Fig. 214.

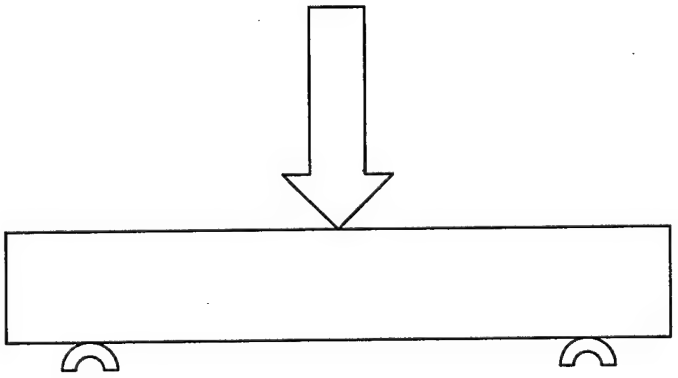

FIG. 214. General Test Setup

A deflectometer was carefully placed in the machine in a position that would be undisturbed during testing. The plain concrete block was placed in the machine. The load head was lowered slowly to 780 lb, where the block failed. The deflectometer registered 0.0 in. at the time of failure.

The next block tested was the concrete block coated with Geothane. Two small pieces of plastic material were put under the block at the supports to ensure that the Geothane was not compressing, causing the deflectometer to have a zero reading. The blocked failed with no measurable deflection, similar to the plain concrete block, at a load of 648 lb. A picture of the test setup and the plastic blocks at the supports is shown in Fig. 215.

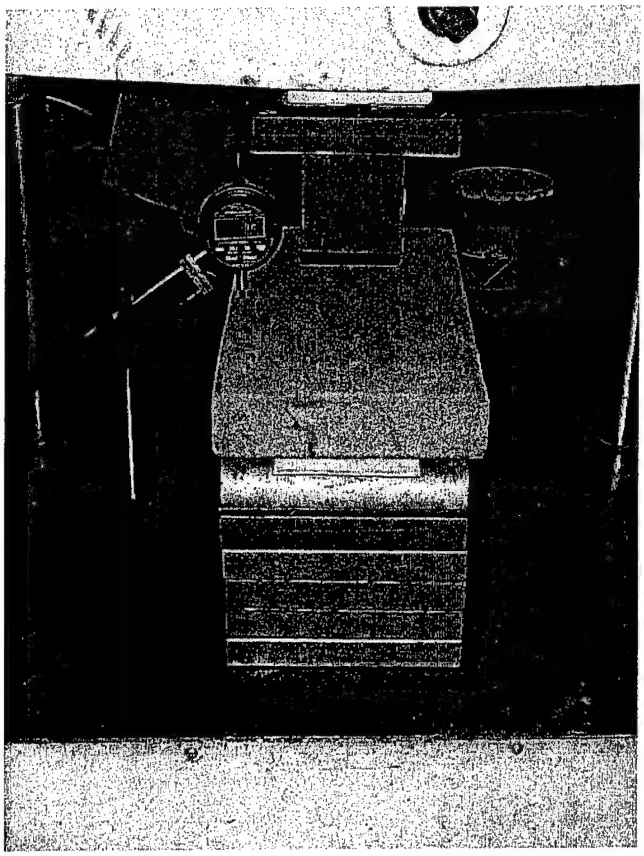

FIG. 215. Geothane Test Setup

The next block tested was the elastomeric polymer used in the blast tests. The block was accidentally loaded to 700 lb at a fast load rate. No visible damage was done to the block. The load was removed and the test reinitiated. The load rate for the elastomeric polymer block was approximately 100 lb every 3 sec. As the block started to crack, the polymer continued to stretch as the crack in the concrete block widened. Before any tears were observed in the elastomeric polymer, the 0.06-in. gap had widened to 0.79 in. Fig. 216 shows the maximum stretch the elastomeric polymer successfully withstood before tearing.

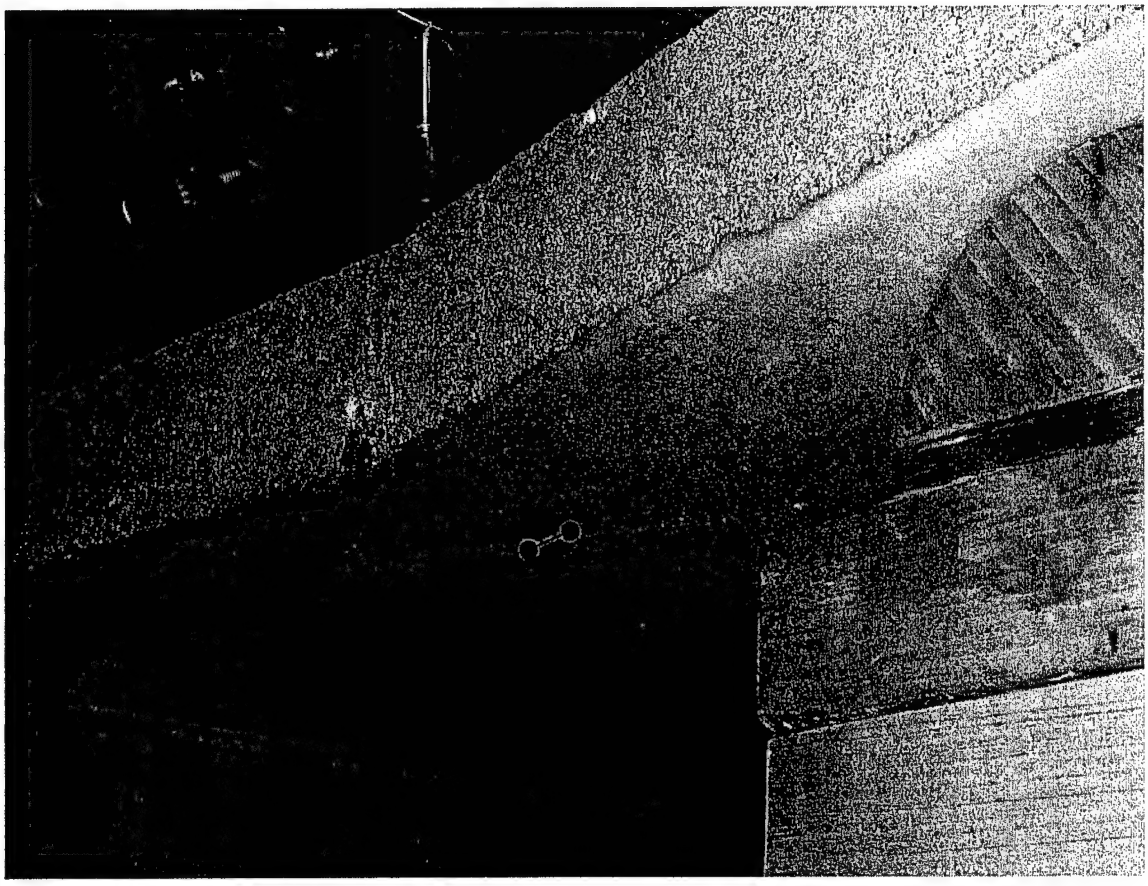

FIG. 216. Elastomeric Polymer, Before Failure

At approximately 900 lb, the elastomeric polymer started to tear. However, the polymer was still resisting load. When the applied load reached 1100 lb, the deflectometer was removed in anticipation of the collapse of the block onto the data collection equipment. The block collapsed at a load of 1160 lb. Fig. 217 shows the tear in the polymer as well as the size of the crack in the concrete.

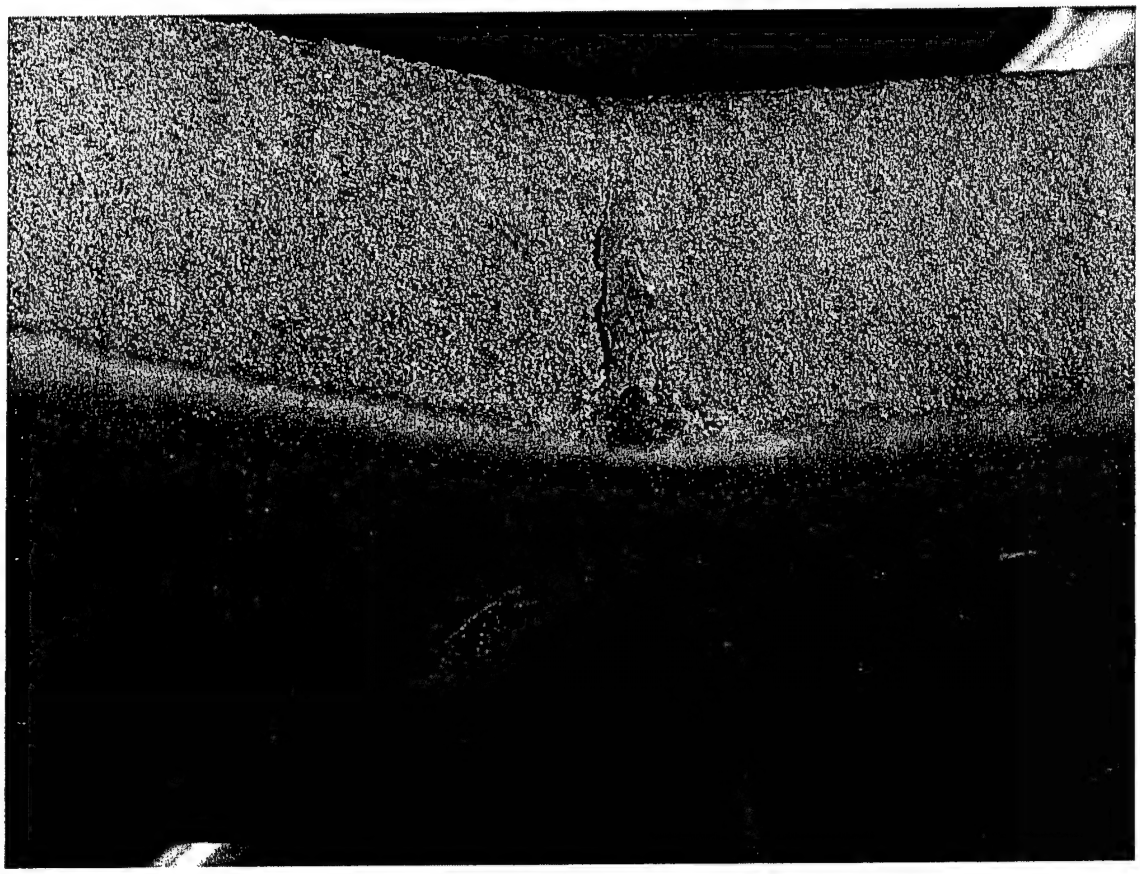

FIG. 217. Elastomeric Polymer after Tearing

Two additional materials were tested to compare to the elastomeric polymer used in full-scale testing. The first of these materials was a black polypropylene/

polypropylene woven material. This material is stiffer than the elastomeric polymer used in the blast tests. It was bonded to the concrete block with an adhesive film. The adhesive was heated upon application. The concrete block was placed in an oven and heated to 250° for approximately 20 min. The block was removed, and the polypropylene/polypropylene woven material was placed on top of the adhesive. The material was heated with a heat gun, and then pressure was applied across the block for bonding. The block remained under pressure for approximately 3 days.

The block was put in the testing machine and loaded at a rate of 100 lb per 3 sec. Cracks were noted in the concrete at 750 lb. At 900 lb, the laminate debonded and testing stopped. At 900 lb, the block had deflected 0.04 in. At 920 lb, almost immediately after debonding, the block fractured and collapsed.

The final block tested was the polyester-based thermoplastic polyurethane. This material exhibits high strength and elongation characteristics, but it was predicted that finding a bonding agent strong enough to bond the material to the concrete would be difficult.

The polyester thermoplastic polyurethane was placed in the testing machine in the same manner as the black polypropylene/polypropylene woven material. The block was loaded. Deflection was recorded at 100-lb increments. After 400 lb, the polyurethane lost bond with the block and took no additional load. However, the material kept the block from collapsing, allowing it to deflect to 0.35 in. An image of the block and the polyester thermoplastic polyurethane can be seen in Fig. 218.

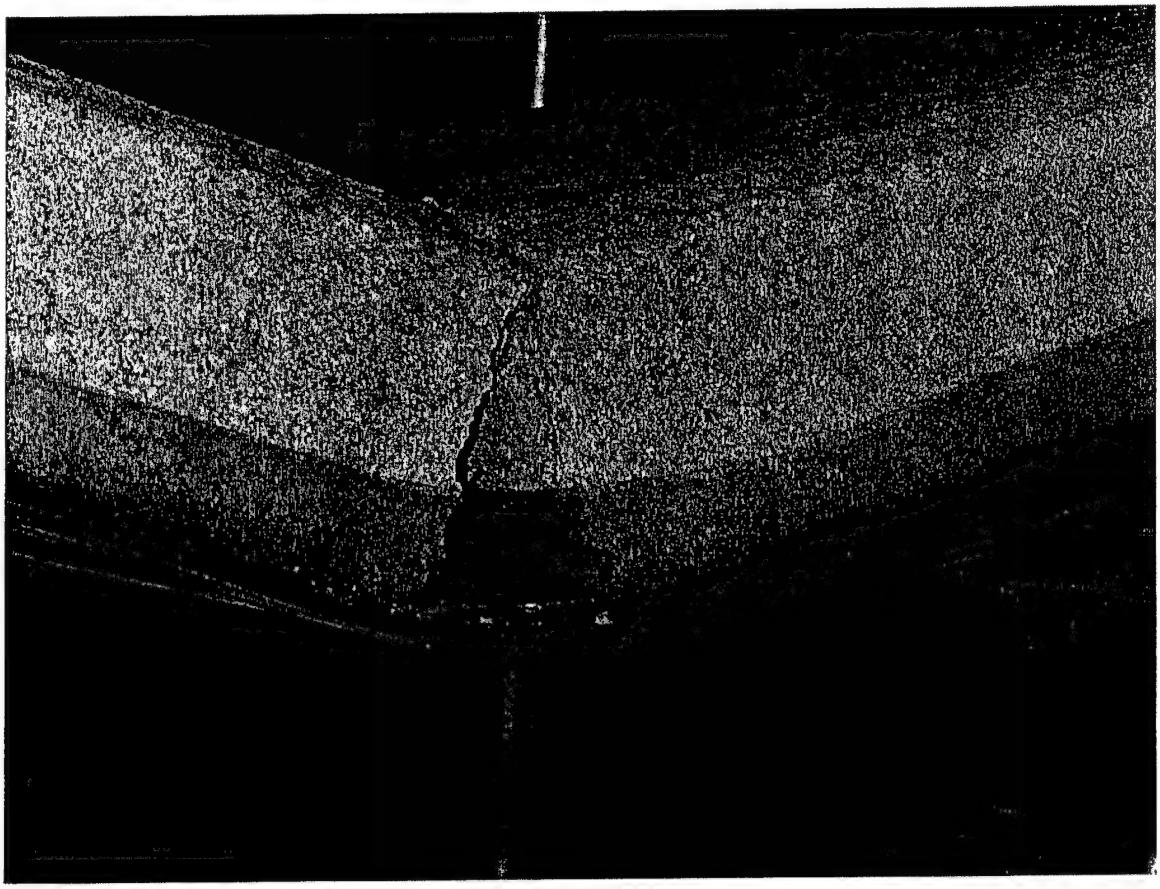

FIG. 218. Polyester Thermoplastic Polyurethane

4.2.6 Results

The overall behavior of the five static flexural tests was described in the previous sections. Because the thickness of the polymeric materials varied, the load-displacement results cannot be compared directly. To address this issue, the load taken by the material was divided by the average thickness of each material. Data from the tests can be seen in Tables 24 through 26 below. Plots of the data can be seen in Figs. 226 and 227. The bare block and the Geothane-coated block failed before a deflection could be recorded.

Table 24. Elastomeric Polymer

Load (lb)	Normalized Load (lb)	Deflection (in.)
100	600	0.01
200	1300	0.01
300	1900	0.02
400	2500	0.02
500	3200	0.02
600	3800	0.03
700	4500	0.03
800	5100	0.05
900	5700	0.07
950	6100	0.13
1030	6600	0.21
1036	6600	0.26
1040	6600	0.27
1050	6700	0.31
1060	6800	0.34
1070	6800	0.37
1080	6900	0.44
1090	6900	0.50
1100	7000	0.56
1160	7400	Failure

Table 25. Polypropylene/Polypropylene Woven Material

Load (lb)	Normalized Load (lb)	Deflection (in.)
100	800	0.01
200	1600	0.01
300	2400	0.02
400	3200	0.01
500	4000	0.02
600	4800	0.02
700	5600	0.02
800	6400	0.03
900	7200	0.04
920	7400	Failure

Table 26. Polyester Thermoplastic Polyurethane

Load (lb)	Normalized Load (lb)	Deflection (in.)
100	800	0.00
200	1600	0.00
300	2400	0.01
400	3200	0.01
500	4000	Failure

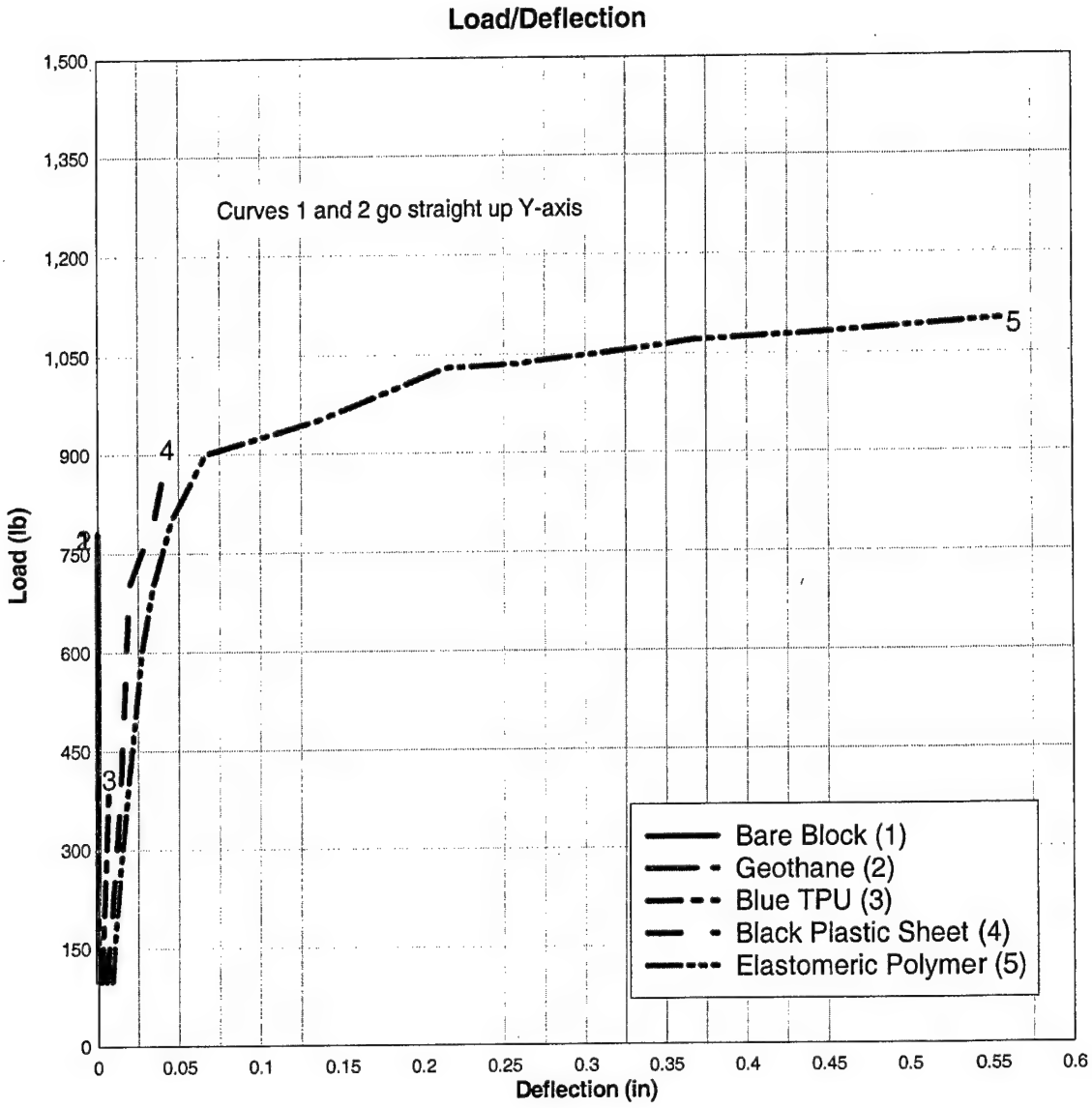

FIG. 219. Load-Deflection Curve

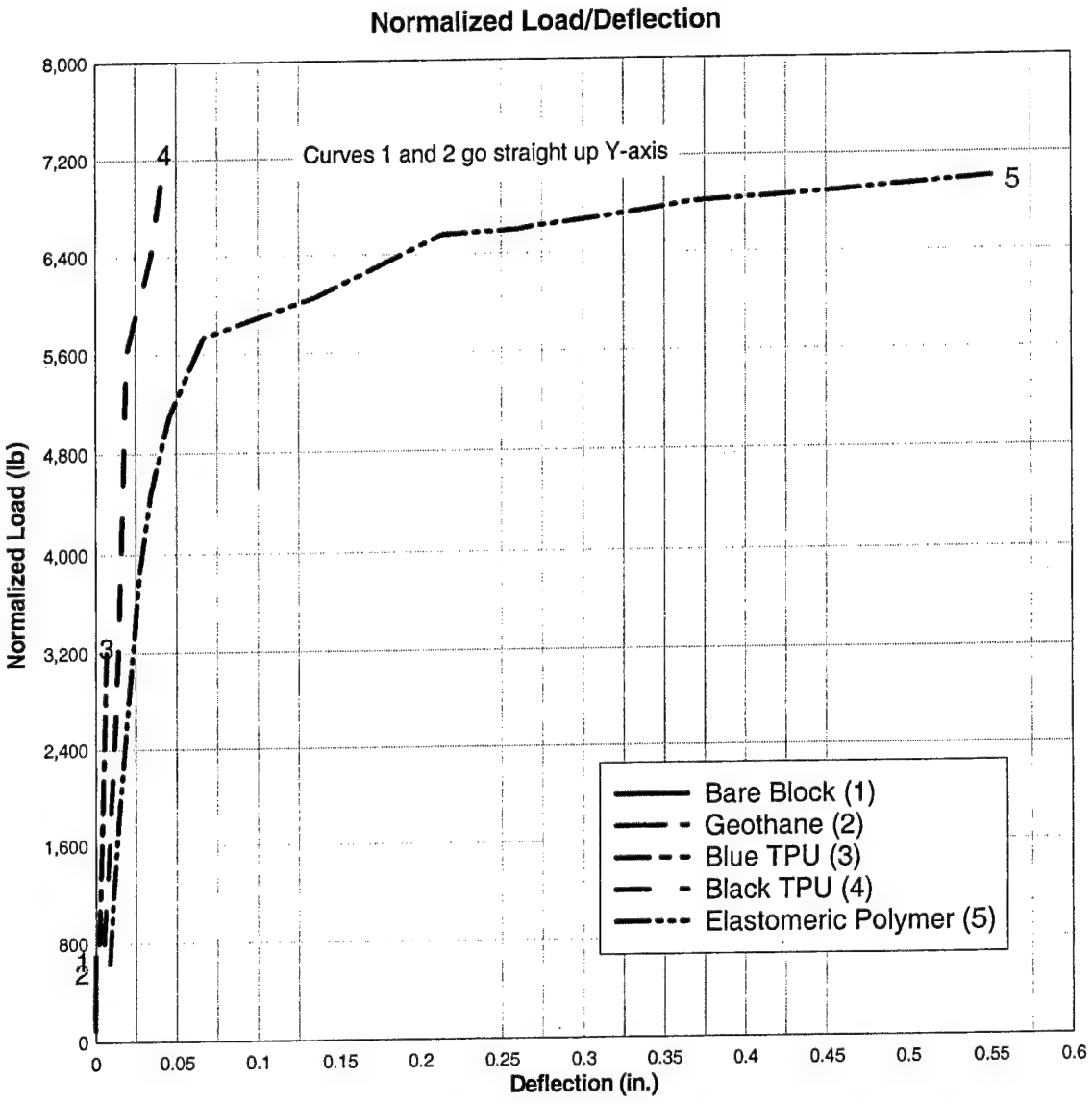

FIG. 220. Normalized Load-Deflection Curve

4.2.7 Conclusions

This test has proven valuable in illustrating the balance required between the stiffness, strength, elongation, and bonding effectiveness of reinforcement materials applied to a concrete substrate. It provides a useful and cost-effective view of the potential failure mechanism of a given externally applied reinforcement. A higher-strength material, such as the polyester-based thermoplastic polyurethane, may not be effective if the bond between it and the concrete is weak. This approach may be useful in evaluating candidacy for a material as a retrofit by indicating tensile strength and elongation characteristics of materials. It could also be used to evaluate the interaction between bonding and flexural strain.

In the static flexural test, the elastomeric polyurea outperformed the other materials. This material took the highest load and had the strongest bond. The other materials should not be disqualified from retrofit candidacy, but perhaps a different bonding technique must first be found before these materials are tested further.

4.3 Drop Tower Impact Test

4.3.1 Introduction

The drop tower test is an effective way to test mechanical properties and failure mechanisms of various materials in a dynamic load environment. The drop tower consists of a drop mass, a load cell, and an aluminum impactor. The equipment also houses a horizontal linear impactor that uses an air compressor to control the velocity of the projectile. Software records various parameters, such as impact velocity, peak load,

deflection, and energy. This test is useful to measure the strain energy absorption ability of a material in a laboratory setting.

4.3.2 Test Methodology

A Dynatup 8250 Drop Tower Testing Machine (Fig. 221) was used to test two materials for properties of energy absorption. The drop tower uses a pneumatic rebound brake system to impact specimens. The manufacturer of the machine supplied a computer-based data acquisition system that is triggered by a photo diode detector just prior to impacting (Schoeppner and Abrate 2000). ASTM D3763 was referenced for this test. This standard was designed to provide impact load and energy vs. striker displacement response of polymers in the form of flat test specimens (Duan, Saigal, et al. et al. 2003).

Five samples of the elastomeric polymer used in the blast and two polypropylene/polypropylene woven samples were tested. Each sample was clamped with sufficient pressure to prevent slippage of the material (ASTM 2000a). For each sample, the impactor was dropped with no initial velocity and accelerated by gravity only. The purpose of the drop tower test was to quantify the strain energy absorbed by the materials and to investigate whether the data could provide insight into which materials might be blast reinforcement candidates.

The two materials tested in the drop tower were the elastomeric polymer used for full-scale wall testing in the explosive tests and the polypropylene/polypropylene woven material, both of which were also evaluated in the static flexural test. Four samples of the elastomeric polymer were cut into 4 in. x 4 in. squares. The thickness of each of the

squares was measured in four locations with a micrometer. The stars in Fig. 222 illustrate the locations where measurements were taken.

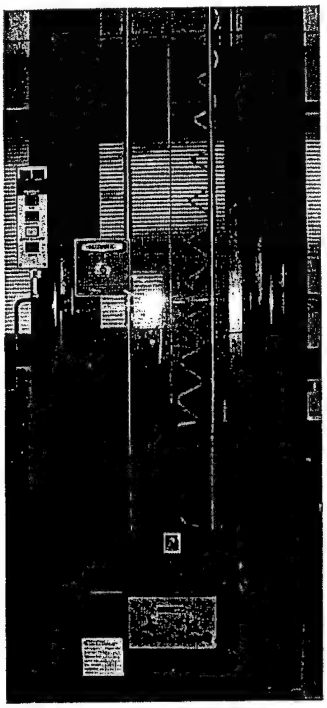

FIG. 221. Drop Tower Machine

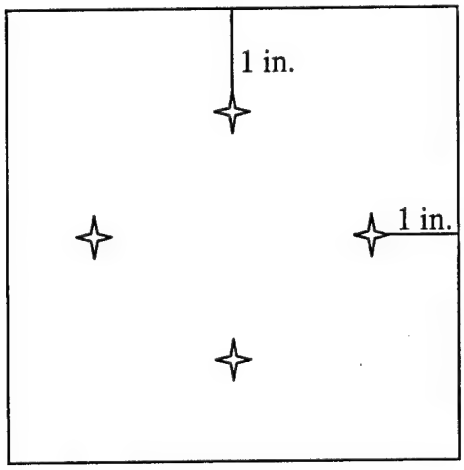

FIG. 222. Drop Tower Impact Test, Thickness Measurement Locations

The elastomeric polymer samples that were used in this test varied in thickness. This was due in part to the application methods of the material. To obtain samples for this test, the elastomeric polymer was sprayed onto a metal sheet and peeled off after curing. Because the material was sprayed by hand, there was little control for uniformity. The polypropylene/polypropylene woven material was uniform in thickness due to a controlled manufacturing process. Thickness measurements are recorded in Table 27. The four samples are shown in Fig. 223.

Table 27. Drop Tower Impact Test, Sample Thickness Measurements

Sample	Thickness 1 (in.)	Thickness 2 (in.)	Thickness 3 (in.)	Thickness 4 (in.)	Average Thickness (in.)
Polymer 1	0.19	0.16	0.15	0.17	0.17
Polymer 2	0.19	0.20	0.17	0.19	0.19
Polymer 3	0.16	0.13	0.11	0.14	0.14
Polymer 4	0.18	0.16	0.13	0.13	0.15
Polymer 5	0.20	0.23	0.26	0.22	0.23
P/P Woven 1	0.09	0.09	0.09	0.09	0.09
P/P Woven 2	0.09	0.09	0.09	0.09	0.09

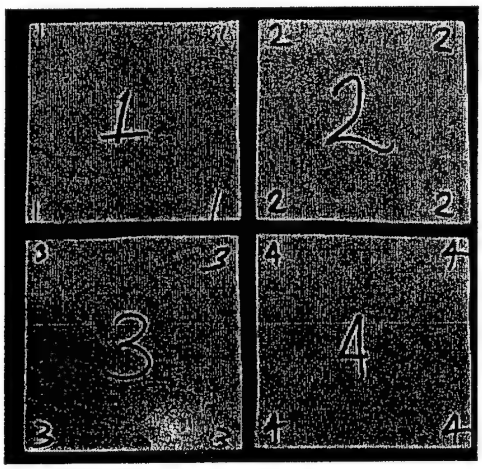

FIG. 223. Drop Tower Impact Test, Polymer Samples

The supports consisted of two thin plates with screws to compress the sample in the supports. An image of the supports is shown in Fig. 224.

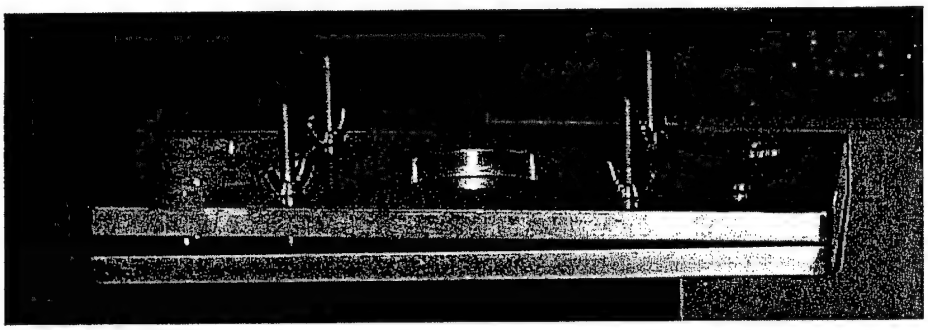

FIG. 224. Drop Tower Supports

Polymer Sample 1 was placed in the testing machine. An aluminum projectile with a diameter of approximately ½ in. and a mass of 7.35 lb was dropped from the top of the tower. The material was not punctured, and very little permanent strain was evident. An image of Polymer 1 is provided in Fig. 225.

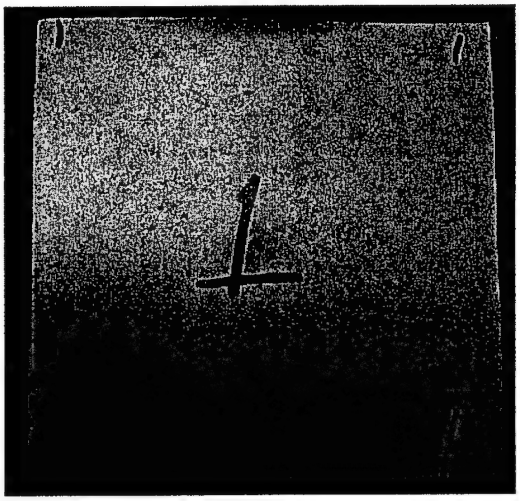

FIG. 225. Drop Tower Impact Test, Polymer 1

The mass of the projectile used for Polymer 2 was increased to 13.56 lb. The machine was fired before the data equipment was ready to record; therefore, no numerical data was obtained for Polymer 2. Fig. 226 shows the extent of rupture of Polymer 2. The material breached but the projectile did not completely penetrate it.

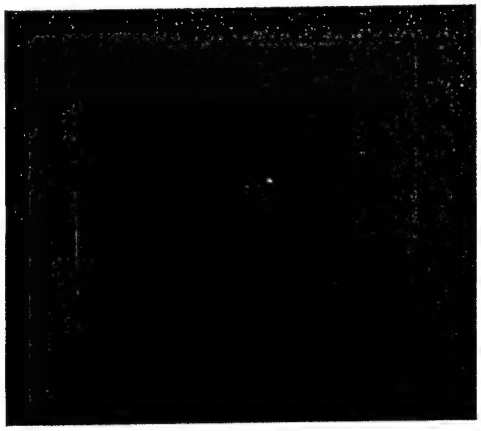

FIG. 226. Drop Tower Impact Test, Polymer 2

The projectile mass for Polymer 3 was 7.35 lb. Polymer 3 was not punctured. However, it exhibited greater permanent deformation than Polymer 1 (Fig. 227).

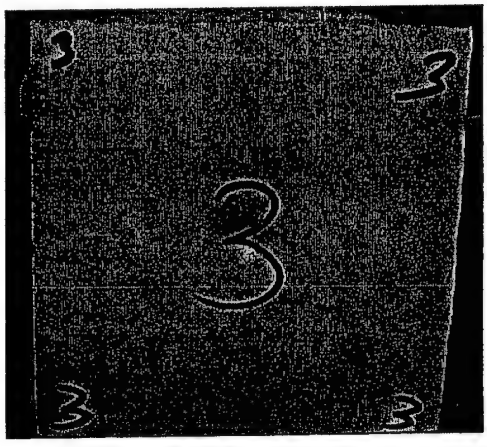

FIG. 227. Drop Tower Impact Test, Polymer 3

Polymer 4 was impacted with the 13.56-lb projectile and was punctured. This sample displayed the elastic properties of the elastomeric polyurea material. Minutes after the testing of Polymer 4, the hole closed back together. Images of Polymer 4 with the hole open and closed are shown in Figs. 228 through 230.

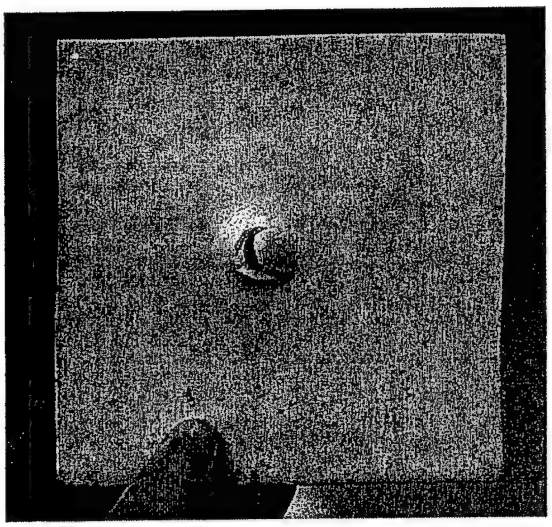

Fig. 228. Drop Tower Impact Test, Polymer 4, Open

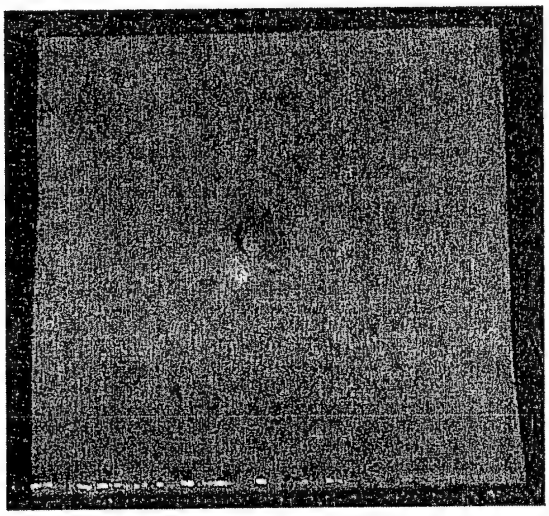

FIG. 229. Drop Tower Impact Test, Polymer 4, Closed

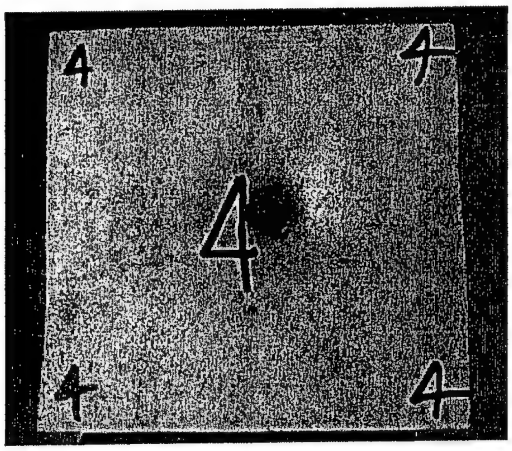

FIG. 230. Drop Tower Impact Test, Polymer 4 Bottom View

The initial test plan did not include Polymer 5, because its thickness was extremely nonuniform, and it was also much thicker than the other samples tested. However, because data was needed for four samples and Sample 2 misfired, Polymer 5 was tested. The 13.56-lb mass was used for testing Polymer 5. It was dropped from the full height of the machine, approximately 3.8 ft. Polymer 5 did not puncture, and was only slightly deformed. Images of Polymer 5 after testing are shown in Figs. 231 and 232.

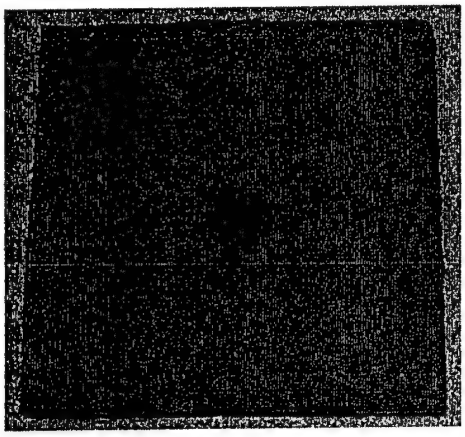

FIG. 231. Drop Tower Impact Test, Polymer 5 Top View

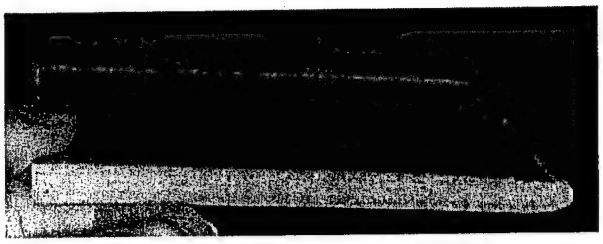

FIG. 232. Drop Tower Impact Test, Polymer 5 Side View

After the five spray-on polymer samples were tested, two of the polypropylene/polypropylene woven samples were tested. These samples were named Polypropylene 1 and Polypropylene 2. They have a lower rupture strain than the spray-on polymers. They were black in color and uniform in thickness.

Polypropylenes 1 and 2 were placed in the supports and then in the testing machine. The 7.35-lb mass was used for both samples. Images of the polypropylene/polypropylene woven samples are shown in Figs 233 through 235. Sample 1 is on the left; Sample 2 is on the right.

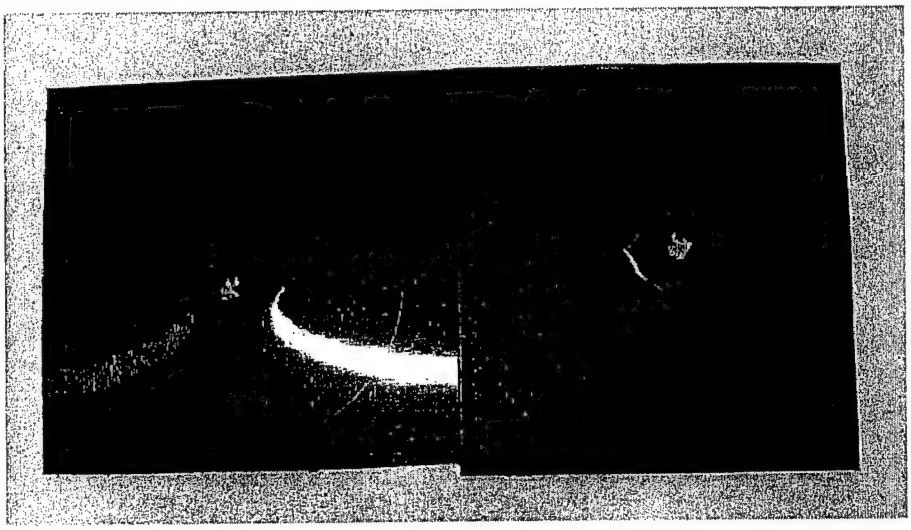

FIG. 233. Drop Tower Impact Test, Polypropylene Samples Top View

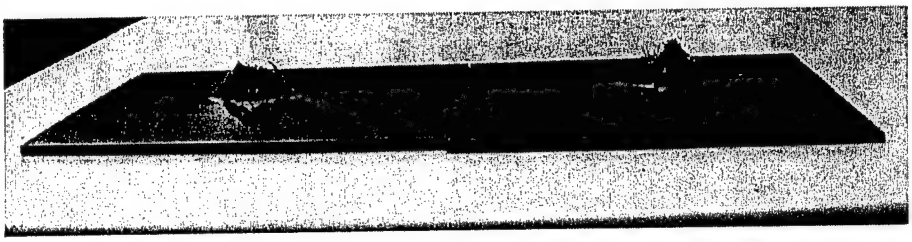

FIG. 234. Drop Tower Impact Test, Polypropylene Samples Side View

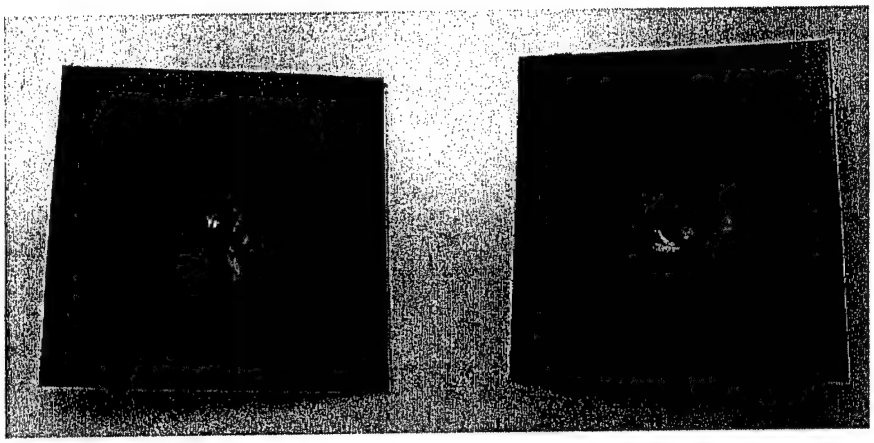

FIG. 235. Drop Tower Impact Test, Polypropylene Samples Bottom View

4.3.3 Results

Results from the drop tower test produced data on velocity, time to impact, and maximum load. The projectile energy was calculated. Polymer Samples 4 and 5 absorbed more energy than the other samples. The Dynatup testing machine output all results. Energy was calculated using $E = \frac{1}{2} mv^2$. A summary is provided in Table 36. The area under the load vs. time curve is related to the strength and elasticity of a material. Data for the elastomeric polymer and polypropylene/polypropylene samples are shown in Tables 28 through 34. Graphs for the materials tested are shown in Figs. 236 through 241. Testing of Polymer 2 produced no data.

Table 28. Drop Tower Impact Test, Polymer 1 Data

Impact energy	27.7 ft*lb
Energy to max load	25.7 ft*lb
Total energy	25.7 ft*lb
Energy to yield	7.5 ft*lb
Energy to failure	25.7 ft*lb
Impact velocity	15.6 ft/sec
Velocity slow down	118 %
Maximum load	1170 lb
Load at yield	400 lb
Load at failure	-150 lb

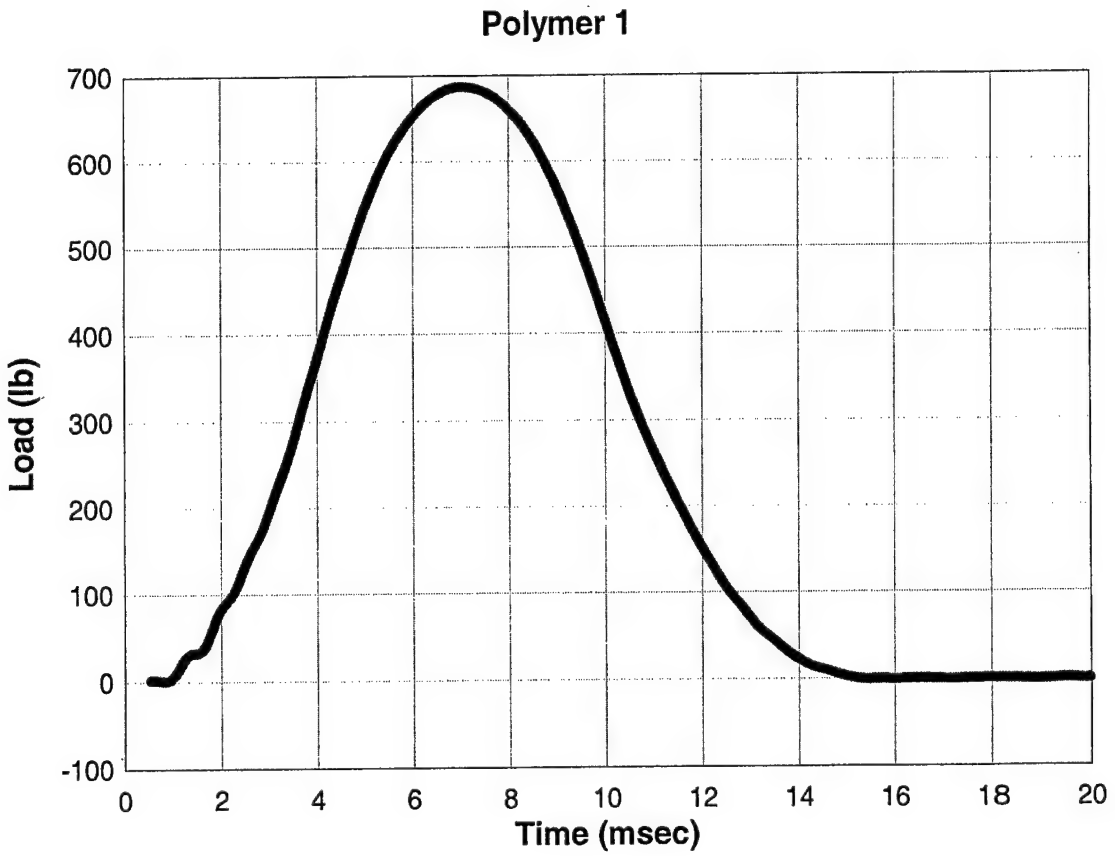

FIG. 236. Drop Tower Impact Test, Polymer 1 Graph

Table 29. Drop Tower Impact Test, Polymer 3 Data

Impact energy	27.4 lb*ft
Energy to max load	26.3 lb*ft
Total energy	26.3 lb*ft
Energy to yield	7.6 lb*ft
Energy to failure	26.3 lb*ft
Impact velocity	15.5 ft/sec
Velocity slow down	112 %
Maximum load	640 lb
Load at yield	400 lb
Load at failure	83 lb

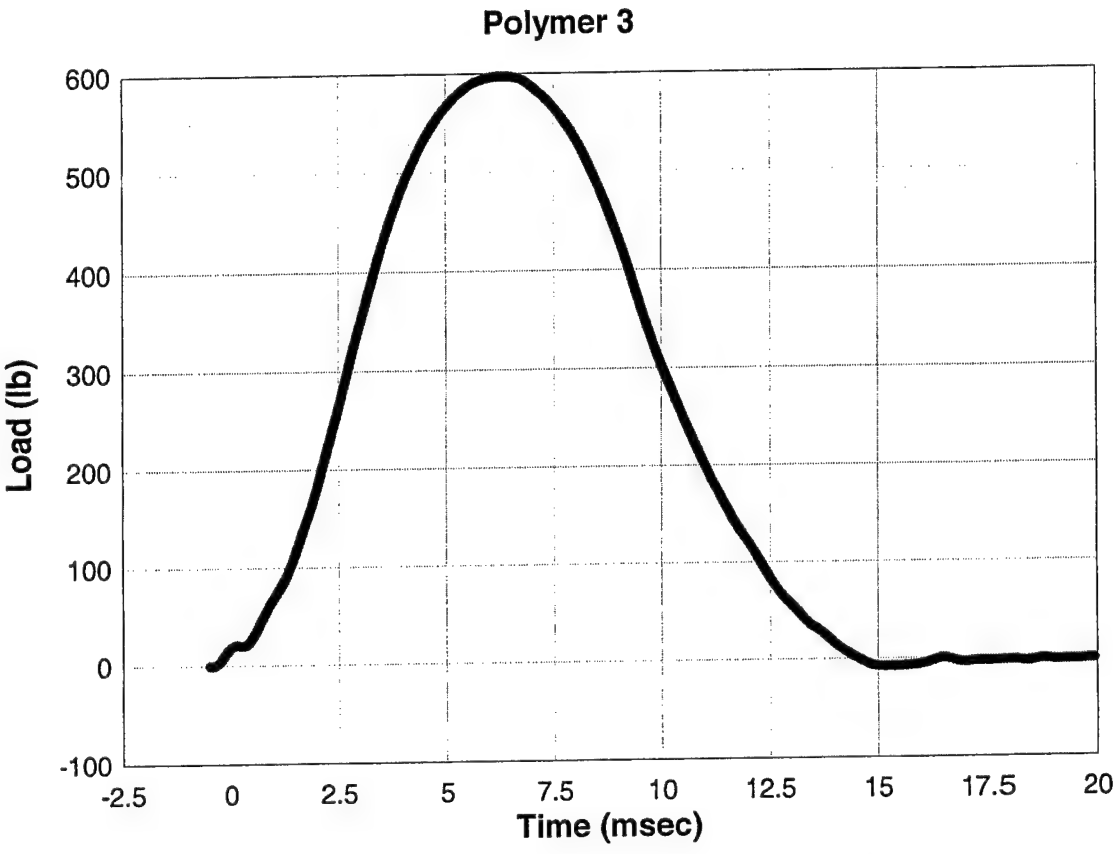

FIG. 237. Drop Tower Impact Test, Polymer 3 Graph

Table 30. Drop Tower Impact Test, Polymer 4 Data

Impact energy	50.9 lb*ft
Energy to max load	42.8 lb*ft
Total energy	43.0 lb*ft
Energy to yield	20.6 lb*ft
Energy to failure	43.0 lb*ft
Impact velocity	15.5 ft/sec
Velocity slow down	55.26 %
Maximum load	1060 lb
Load at yield	670 lb
Load at failure	-40 lb

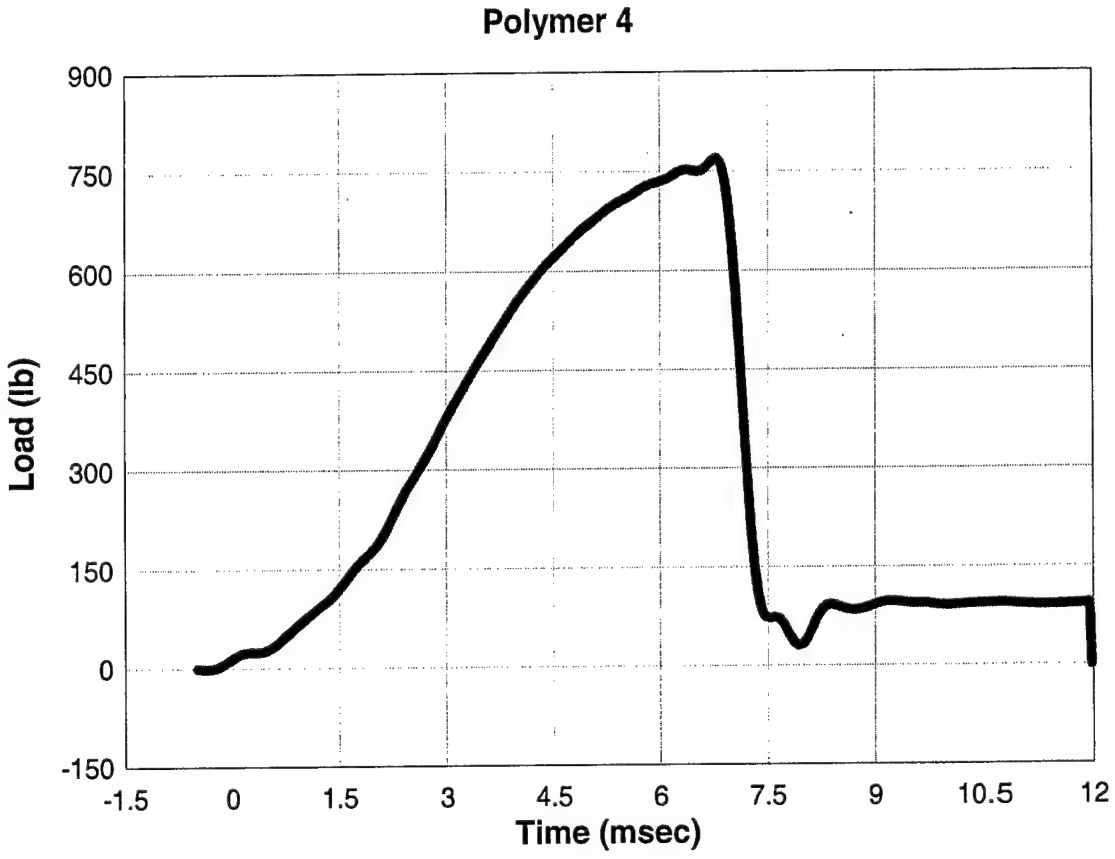

FIG. 238. Drop Tower Impact Test, Polymer 4 Graph

Table 31. Drop Tower Impact Test, Polymer 5 Data

Impact energy	50.8 lb*ft
Energy to max load)	45.1 lb*ft
Total energy	47.7 lb*ft
Energy to yield	34.1 lb*ft
Energy to failure	48.5 lb*ft
Impact velocity	15.5 ft/sec
Velocity slow down	63 %
Maximum load	1010 lb
Load at yield	950 lb
Load at failure	200 lb

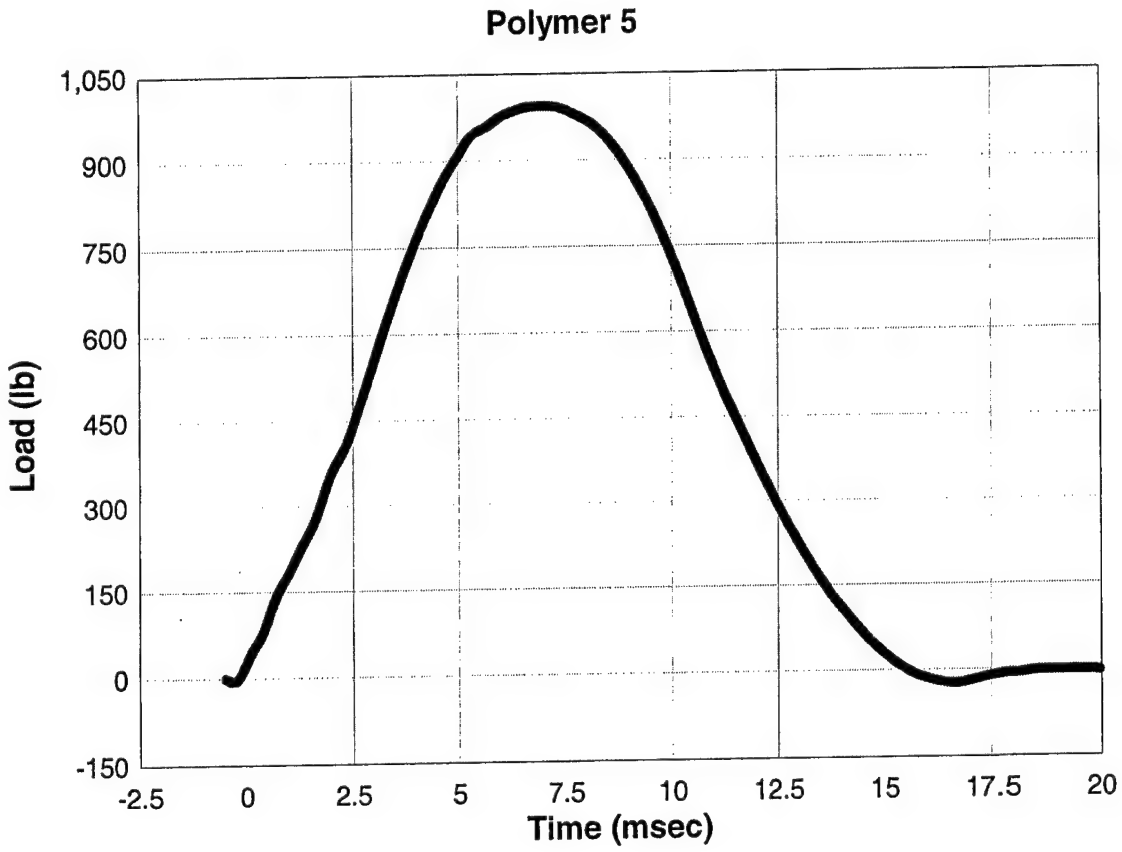

FIG. 239. Drop Tower Impact Test, Polymer 5 Graph

Table 32. Drop Tower Impact Test, Polypropylene 1 Data

Impact energy	28.3 ft*lb
Energy to max load	16.2 ft*lb
Total energy	29.8 ft*lb
Energy to yield	0 ft*lb
Energy to failure	17.7 ft*lb
Impact velocity	15.7 ft/sec
Velocity slow down	34 %
Maximum load	820 lb
Load at yield	10 lb
Load at failure	60 lb

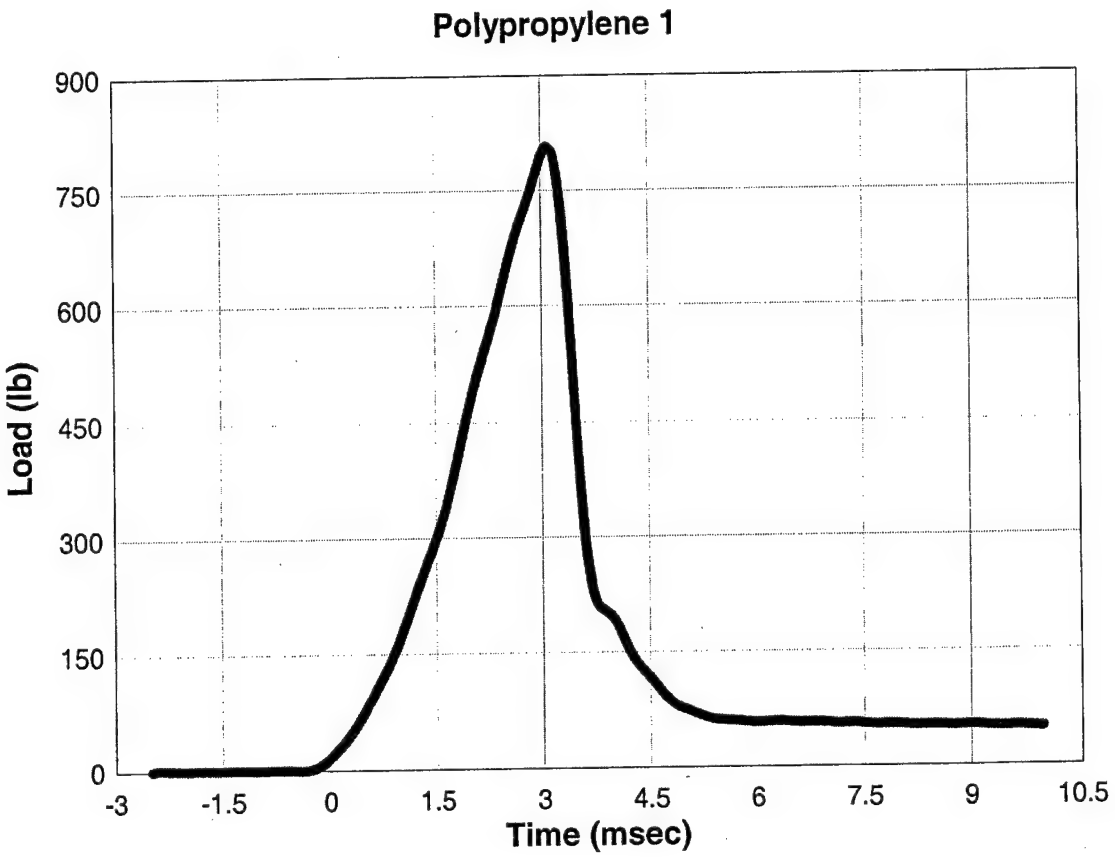

FIG. 240. Drop Tower Impact Test, Polypropylene 1 Graph

Table 33. Drop Tower Impact Test, Polypropylene 2 Data

Impact energy	28.2 ft*lb
Energy to max load	16.2 ft*lb
Total energy	24.1 ft*lb
Energy to yield	0 ft*lb
Energy to failure	18.7 ft*lb
Impact velocity	15.7 ft/sec
Velocity slow down	34 %
Maximum load	850 lb
Load at yield	5 lb
Load at failure	150 lb

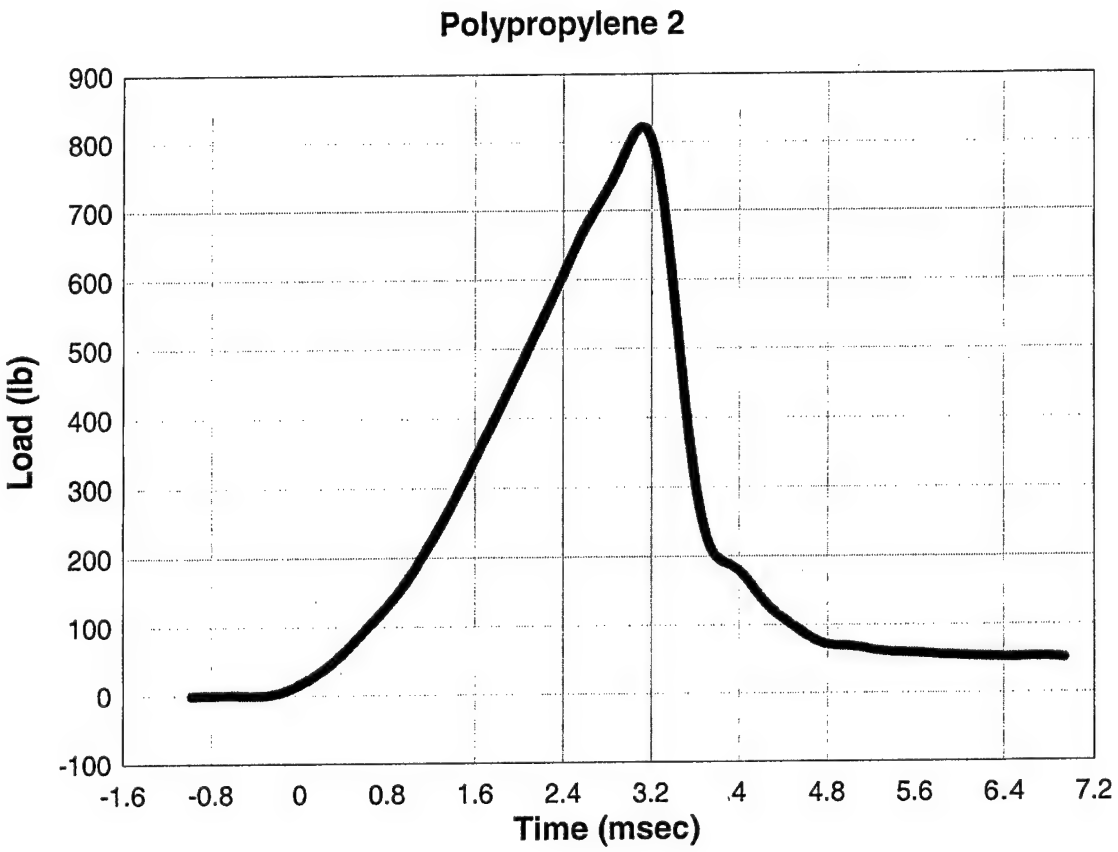

FIG. 241. Drop Tower Impact Test, Polypropylene 2 Graph

TABLE 34. Drop Tower Impact Test, Data Summary

Sample	Impact energy (ft*lb)	Energy to max load (ft*lb)	Energy to failure (ft*lb)	Velocity slow down (%)
Polymer 1	27.7	42.8	25.7	118
Polymer 3	50.9	26.3	26.3	112
Polymer 4	50.9	42.8	42.9	55
Polymer 5	50.8	45.1	48.5	63
Polypropylene 1	28.3	16.2	17.7	34
Polypropylene 2	28.2	16.2	18.7	34

4.3.4 Conclusions

The polypropylene/polypropylene material was thought to be a very good candidate for wall retrofitting. The impact energy absorbed by the polypropylene/polypropylene material was less than the energy for the elastomeric polymer used in full-scale wall testing. The impact energies for Polymer 1, Polypropylene 1, and Polypropylene 2 were smaller, because a lighter projectile was used. The lighter projectile ruptured the polypropylene samples and barely dented the polymer samples. However, a direct comparison cannot be made in this case due to the differences in thicknesses.

This test is valuable in determining the energy absorption capabilities of a material in a dynamic shear puncture environment. The objective of the material in this test is to prevent the mass from exiting upon impact. The energy just before the projectile impacts the material can be calculated. If the material stops the mass, the amount of energy the material absorbed can be calculated.

4.4 Gas Gun Tests

4.4.1 Introduction

The gas gun facility of the Department of Materials Engineering at the University of Alabama at Birmingham was used to perform projectile impact testing. The gas gun approach can investigate the energy absorption capabilities of materials in a dynamic load environment, but at higher rates of strain than the drop tower test. The gas gun is shown in Fig. 242 and Fig. 245.

In the gas gun test, projectiles are launched with an initial velocity induced by compressed gas. High impact velocities can be achieved. The goal of the gas gun test is to calculate energy absorption based on the ballistic limit of the material. Exit velocities can be detected, however, only if velocities exceed 49 ft/sec. If the ballistic limit is reached, the energy absorbed can be calculated by $E = \frac{1}{2} mv^2$.

Two series of gas gun tests were conducted. The only polymeric material used was the spray-on polymer used in the explosive tests. The first test involved only the polymer. The second test involved the polymer bonded to concrete to simulate a concrete masonry unit in a full-scale wall.

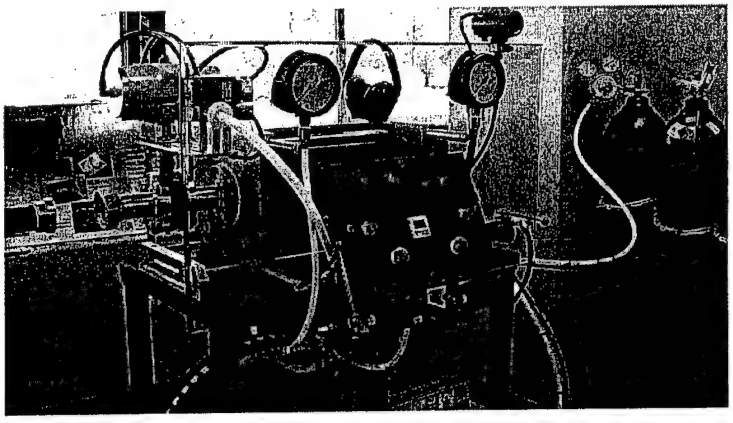

FIG. 242. Gas Gun, Gas Chamber

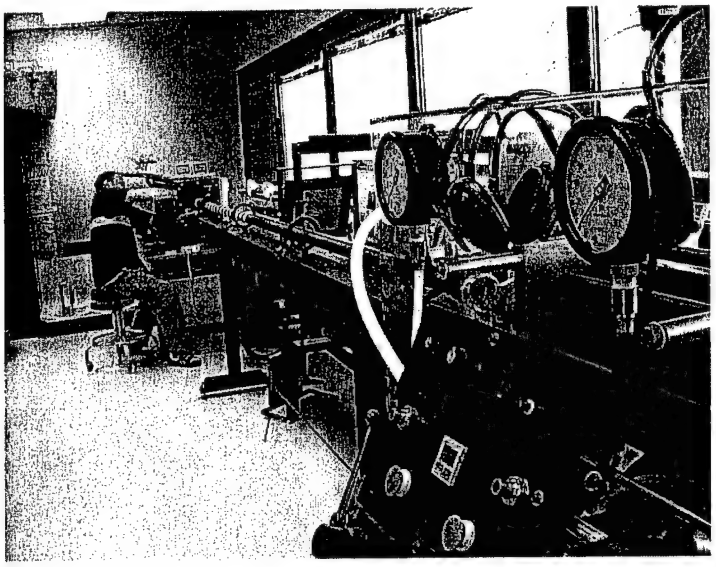

FIG. 243. Gas Gun

4.4.2 Gas Gun Test 1 Methodology

The elastomeric polymer used in the explosive tests was cut into 8 in. x 8 in. squares. 14 specimens were made from two sprayings of the polymer, one nearly white in color and one orange in color. The orange-colored material was slightly thicker than the white material and less stiff. For each specimen, a thickness measurement was taken along each of the four sides. The mass of each specimen was recorded. The thicknesses of the material specimens were taken as illustrated in Fig. 244. The data is provided in Table 35.

The specimens were attached inside the gas gun by clamping the top and bottom. This yielded a simply supported specimen with supports 3.9 in. apart. An aluminum, cylindrical-shaped projectile with mass of 0.24 lb was selected for the first part of the test.

A scrap piece of polymer was used to determine how much pressure was needed to puncture, but not exit, the material. Nitrogen gas filled the tank of the gun until the

pressure inside reached 35 psig, and the first projectile was launched. The projectile struck the sample at 285 ft/sec and became embedded in the material. The ballistic limit was reached on the first attempt. A pressure of 35 psig was used for subsequent shots, and adjustments were made according to the thickness of each specimen. An image of the material and the projectile used for the set-up is shown in Fig. 245.

After the initial pressures were determined, the first specimen, Blunt Object 1 (BO1), was fired and completely penetrated the sample and exited with a significant velocity due to the difference in thickness of the thicker trial specimen compared to the thinner setup specimen. For the second specimen (BO2), the pressure was reduced to 27 psig. Even with the reduced pressure, the projectile still exited the specimen. For the third specimen (BO3), the pressure was reduced to 13.5 psig. This projectile did not penetrate the polymer sample. With the first two specimens, an entrance velocity reading was acquired. With the third, however, no data was obtained since the projectile did not penetrate the polymer. Images of the first, second, and third specimens are shown in Figures 246 through 248.

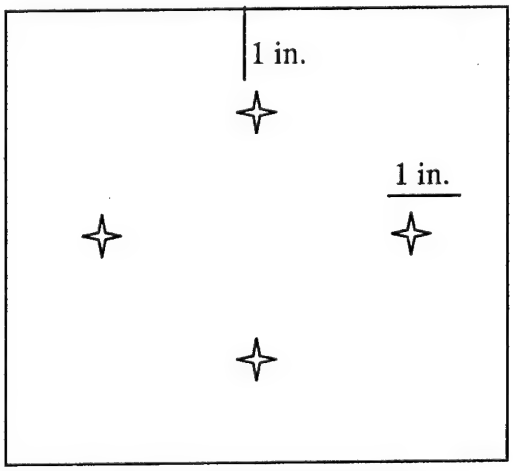

FIG. 244. Gas Gun Test 1, Thickness Measurement Locations

TABLE 35. Gas Gun Test 1 Specimens

Specimen	Thickness 1 (in.)	Thickness 2 (in.)	Thickness 3 (in.)	Thickness 4 (in.)	Average Thickness (in.)	Mass (lb)
BO1	.23	.20	.15	.19	.19	.42
BO2	.15	.21	.21	.18	.19	.41
BO3	.14	.18	.19	.15	.16	.36
BO4	.19	.15	.22	.24	.20	.44
BO5	.19	.21	.24	.17	.20	.45
BO6	.18	.19	.24	.21	.21	.45
BO7	.24	.21	.19	.22	.21	.48
BO8	.24	.17	.22	.26	.22	.49
BO9	.29	.29	.25	.28	.28	.60
BO10	.28	.26	.26	.26	.26	.59
BO11	.27	.23	.24	.32	.26	.63
BO12	.25	.26	.21	.19	.23	.50
BO13	.17	.19	.25	.17	.19	.42
BO14	.27	.26	.26	.26	.26	.60

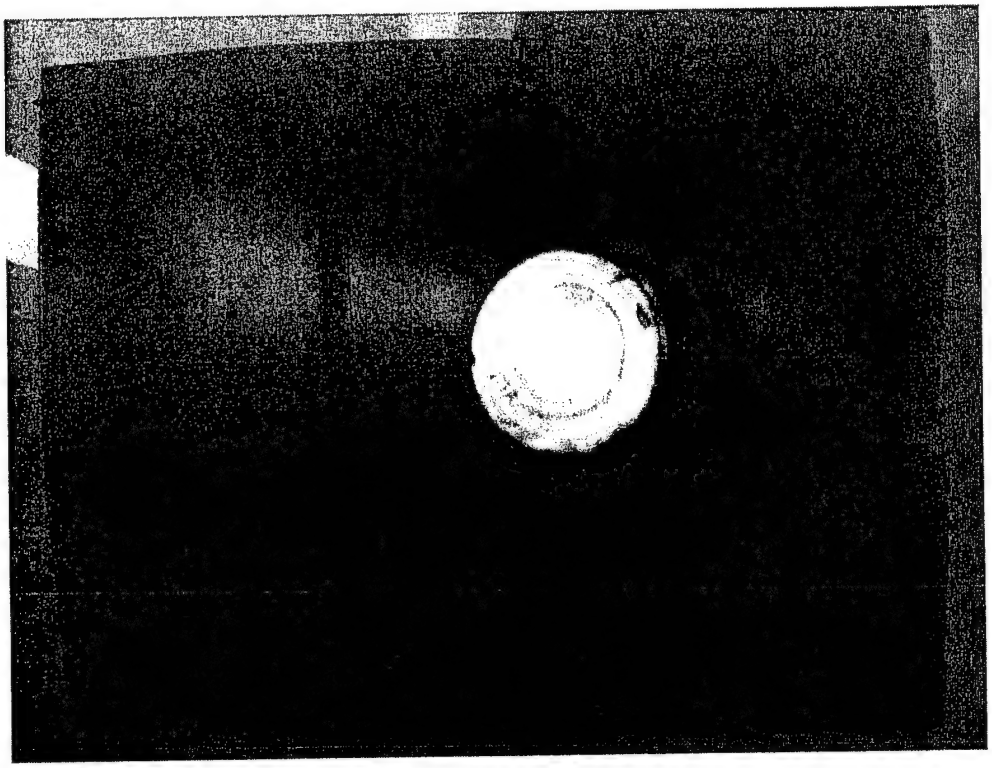

FIG. 245. Gas Gun Test 1 Setup Specimen

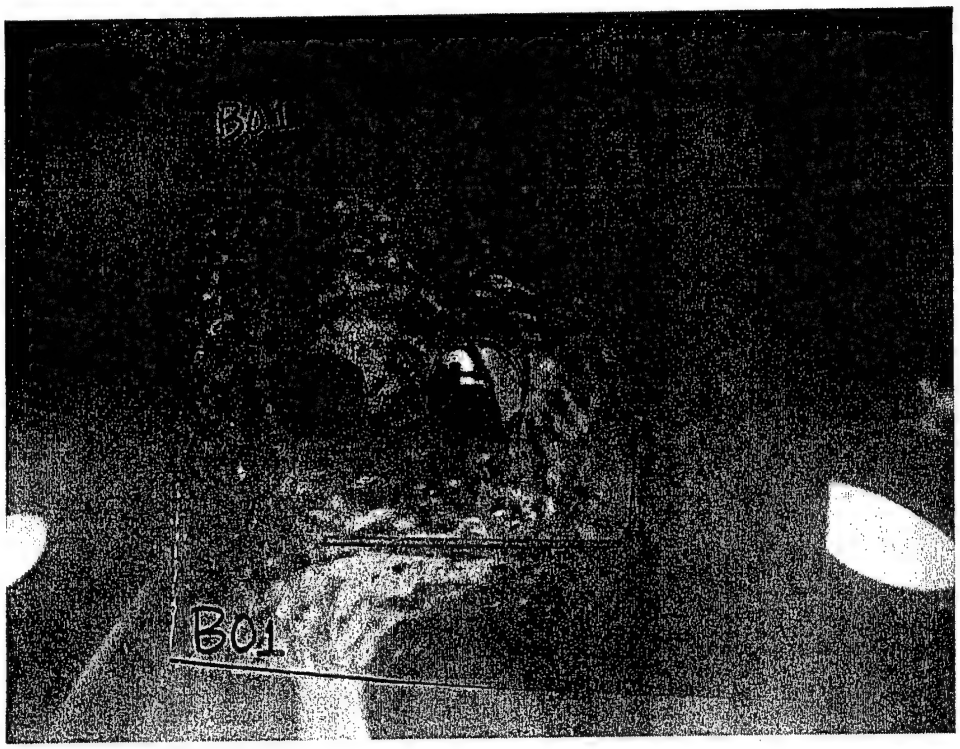

FIG. 246. Gas Gun Test 1, Specimen One

FIG. 247. Gas Gun Test 1, Specimen Two

FIG. 248. Gas Gun Test 1, Specimen Three

The ballistic limit was reached on BO4, with a pressure of 24.6 psig and an entrance velocity of 234 ft/sec. The projectile penetrated and exited BO5 but the exit velocity was not recorded. The ballistic limit was reached for specimens six and seven. Images of specimens four, five, six, and seven are shown in Figures 249 through 256.

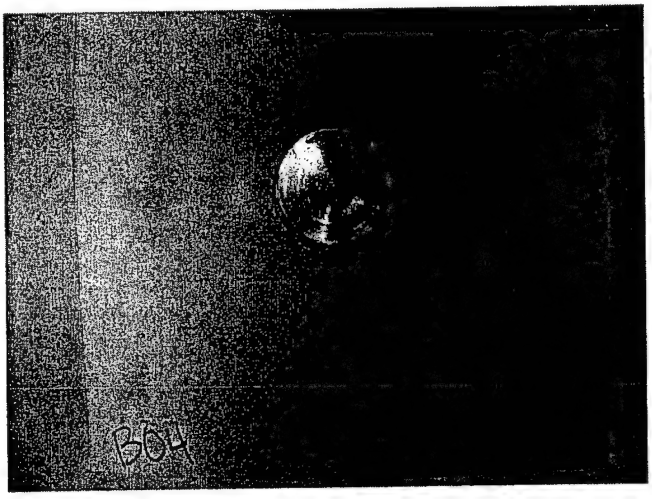

FIG. 249. Gas Gun Test 1, Specimen Four Top View

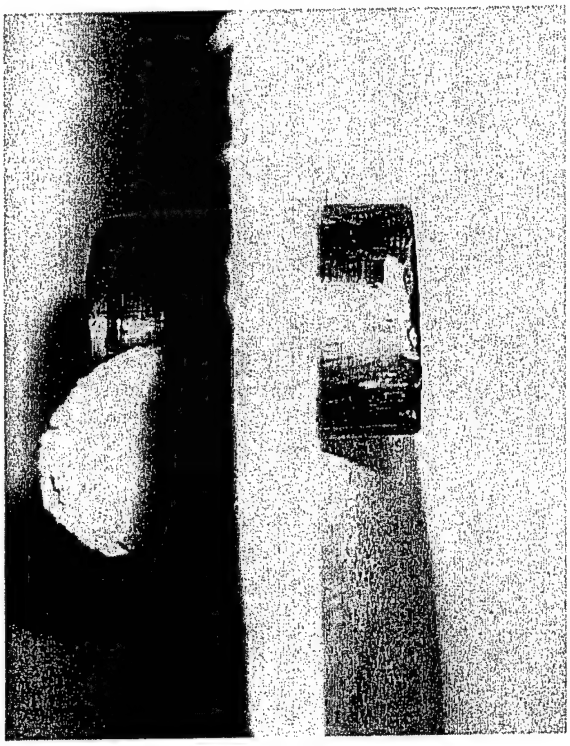

FIG. 250. Gas Gun Test 1, Specimen Four Side View

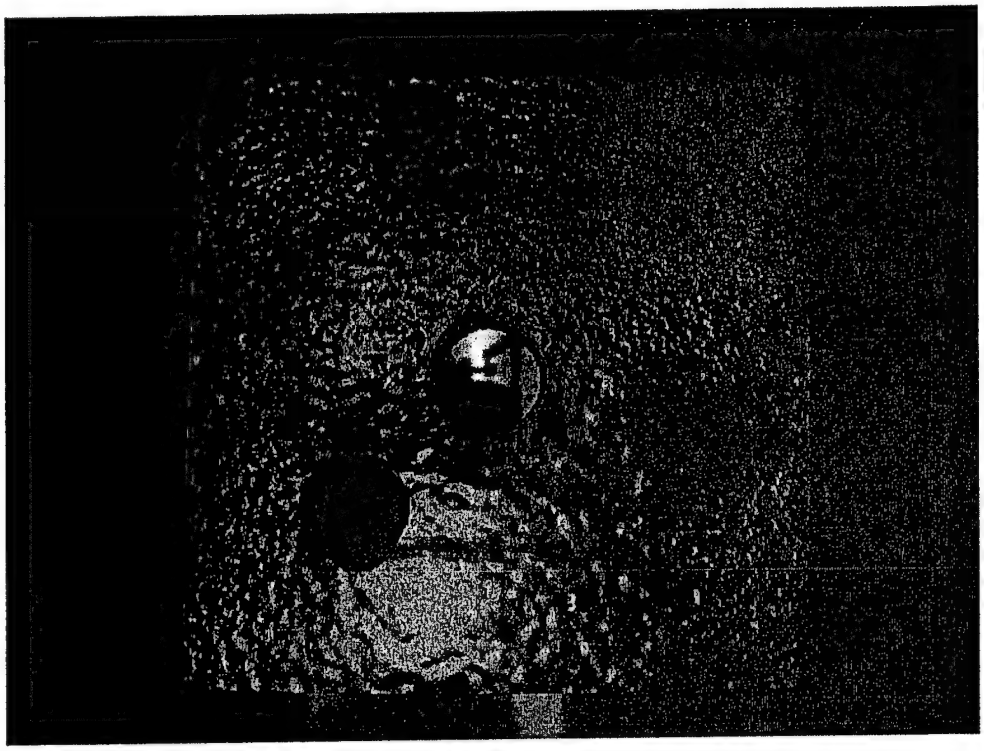

FIG. 251. Gas Gun Test 1, Specimen Five

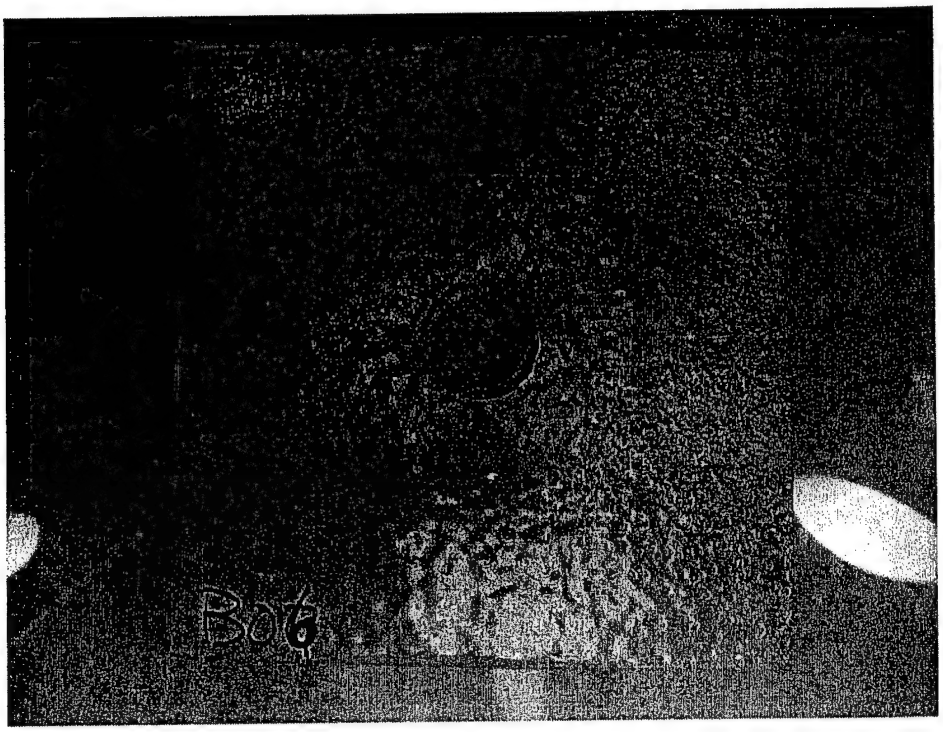

FIG. 252. Gas Gun Test 1, Specimen Six Top View

FIG. 253. Gas Gun Test 1, Specimen Six Bottom View

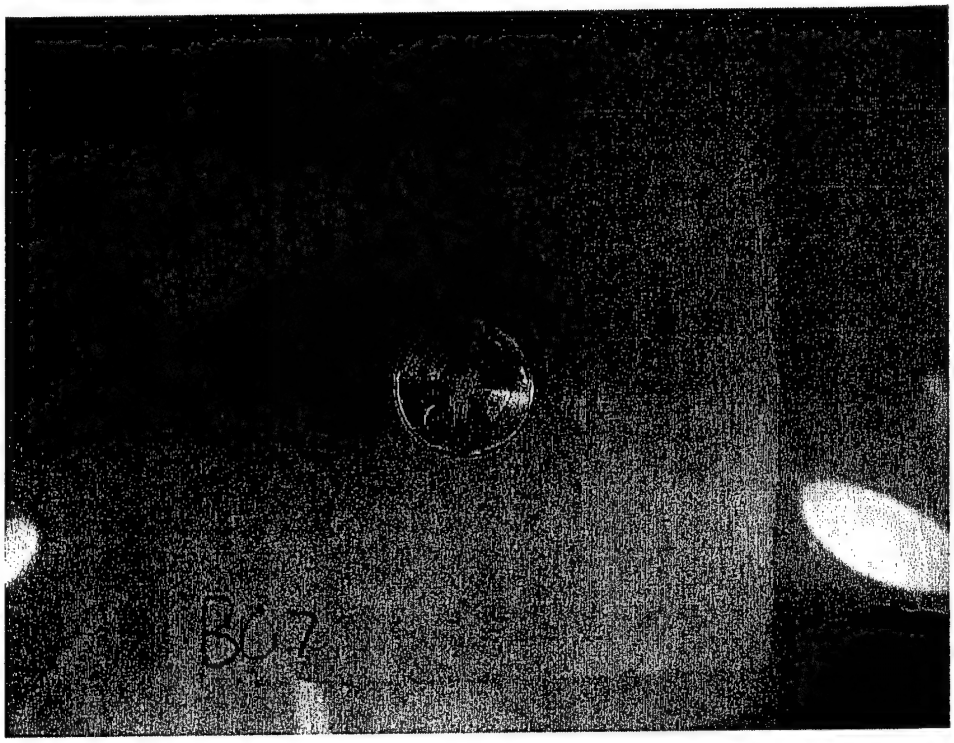

FIG. 254. Gas Gun Test 1, Specimen Seven Top View

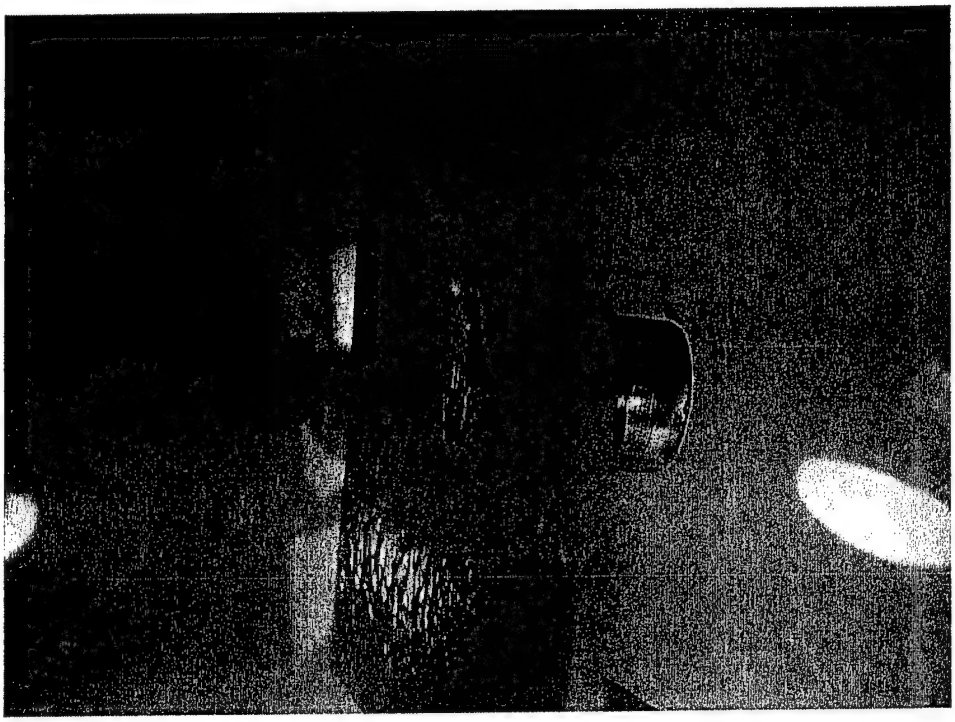

FIG. 255. Gas Gun Test 1, Specimen Seven Left Side View

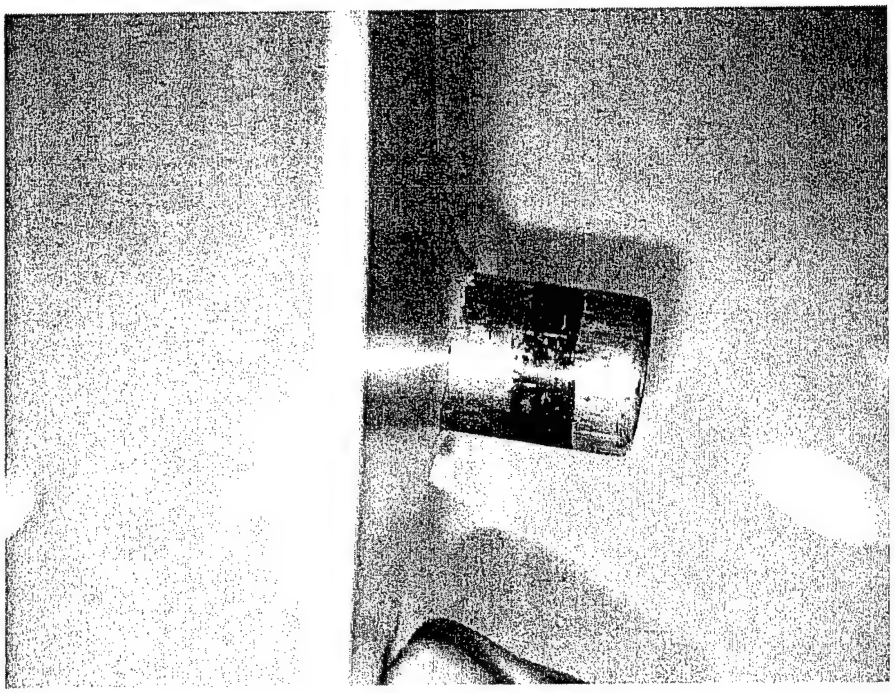

FIG. 256. Gas Gun Test 1, Specimen Seven Right Side View

After BO7 was tested, the aluminum projectile was replaced with a white ultra-high molecular weight polyethylene (UHMWPE). This projectile was used for two tests, BO8 and BO14. It was cylindrical in shape, but its mass was much lower at 0.13 lb. The velocity of this projectile just before hitting specimen eight (BO8) was measured at 505 ft/sec. The projectile ruptured the specimen but did not reach the ballistic limit. BO8 was thicker than the seven previous specimens.

The last specimen tested was BO14. Because the projectile was deformed in the testing of BO8, it was filed to restore the cylindrical shape, slightly decreasing the mass. A pressure of 49.25 psig was applied. However, the velocity gauge was not properly set, so no data was returned. The specimen did not puncture upon impact.

4.4.3 Gas Gun Test 1 Results

The energy that a material absorbs is equal to the kinetic energy at entrance minus the kinetic energy at exit ($E = \frac{1}{2} m_1 v_1^2 - \frac{1}{2} m_2 v_2^2$). The chronographs, however, will not read velocities if they are less than 49 ft/sec. The chronographs could also mistake a flying piece coming off the back of the material from the actual exiting projectile. For these reasons, residual velocities are difficult to measure. An alternate way to quantify the energy a material can absorb is to calculate the ballistic limit by applying just enough pressure that the projectile enters but does not exit the material. By altering the conditions of the test, the maximum energy can be found. Data from the test, including the calculated energies, are shown in Table 36.

Table 36. Gas Gun Test 1 Results

Specimen #	Projectile	Weight of Projectile (lb)	Pressure (psi)	Entrance Velocity (ft/sec)	Energy Absorbed (ft*lb)
BO1	Aluminum	0.35	35	290	460
BO2	Aluminum	0.35	27	253	350
BO3	Aluminum	0.35	13	Gauge Failure	-
BO4	Aluminum	0.35	25	234	300
BO5	Aluminum	0.35	27	Gauge Failure	-
BO6	Aluminum	0.35	24	240	316
BO7	Aluminum	0.35	25	243	326
BO8	UHMWPE	0.13	47	505	511
BO14	UHMWPE	0.13	49	Gauge Failure	-

4.4.4 Gas Gun Test 2 Methodology

Using concrete masonry blocks in the gas gun apparatus is not feasible. Therefore, concrete pavers were used to represent the concrete blocks. These pavers were notched with a concrete saw along the center to represent the connection of two blocks at the mortar joint.

The concrete pavers used in Gas Gun Test 2 were 16 in. x 8 in. x 1 in. However, the gas gun could only hold objects 12.5 inches in height. The block size was reduced to 12 in. to allow them to fit into the apparatus. Then they were notched in the center along their width to encourage failure along the center. The width of the notch was the same for every block. However, the depth of the notches varied. The width and depths of each sample are listed in Table 37. A notched block is shown in Fig. 257.

Five polymer-coated blocks were used in this test. The polymer was the same as that used in full-scale testing. Because the material is applied by hand spraying, thicknesses of the blocks were not consistent. The general thickness was 1/8 in.

TABLE 37. Gas Gun Test 2, Notch Data

Specimen	Width of Notch (in.)	Depth of Notch (in.)
1	0.11	1.00
2	0.11	0.96
3	0.11	0.97
4	0.11	1.00
5	0.11	0.96

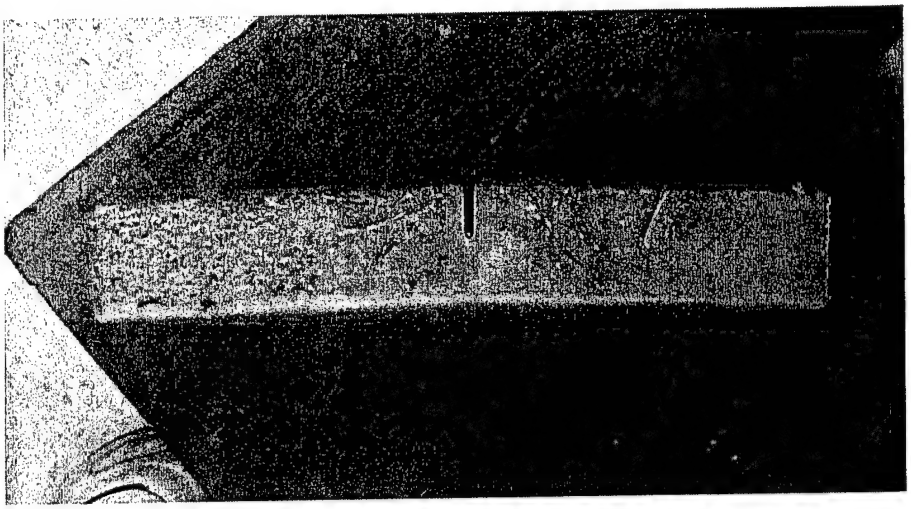

FIG. 257. Gas Gun Test 2, Notched Block

The specimens were placed in the gas gun. There was a small angle at the bottom that kept the block from translating. A small wedge was placed at the top to tighten the gap between the block and the top of the gas gun frame. The support conditions used in the test simulated simply supported conditions, with connections 12 in. apart. An image of a block positioned in the gas gun is shown in Fig. 258.

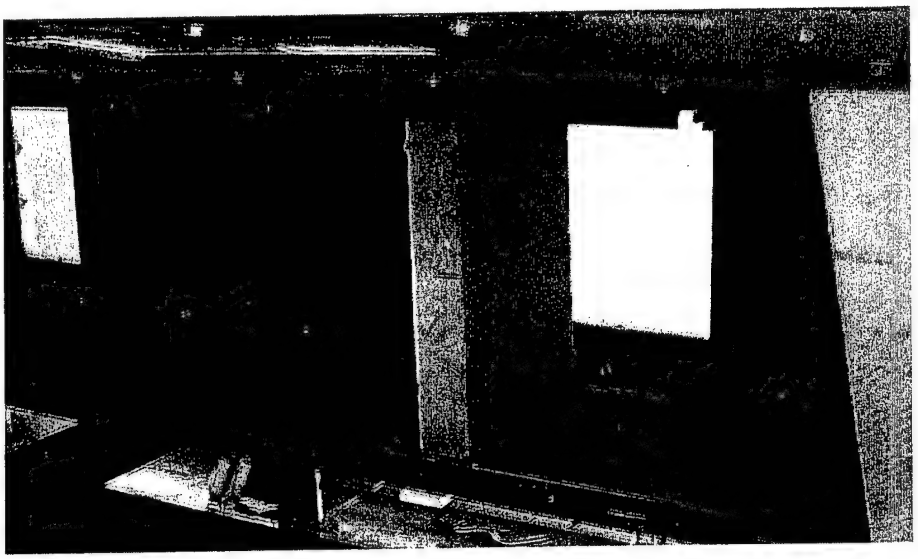

FIG. 258. Gas Gun Test 2, Standing Block

A 6061 T6 aluminum cylinder weighing 0.35 lb was selected to impact the polymer-coated pavers. For Sample 1, the pressure of 90.6 used to launch the projectile was too high and the concrete fragmented. The polymer on the back separated from the concrete. The interface between the polymer and the block absorbed most of the energy involved in the impact. This indicates that the polymer did not fail, but the concrete failed in tension. Even with the failure, the membrane was successful in stopping the projectile, as the projectile was found on the right side of the block. The side view of Sample 1 is shown in Fig. 259. It is shown in Fig. 260 after being removed from the Gas Gun.

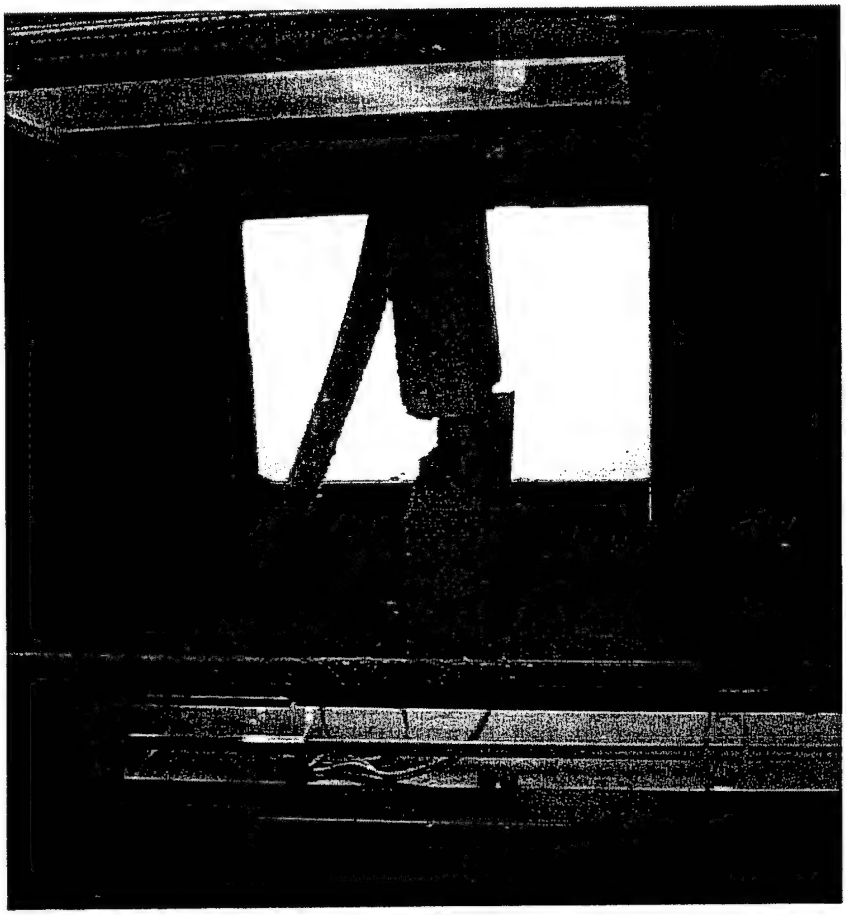

FIG. 259. Gas Gun Test 2, Sample 1 Side View

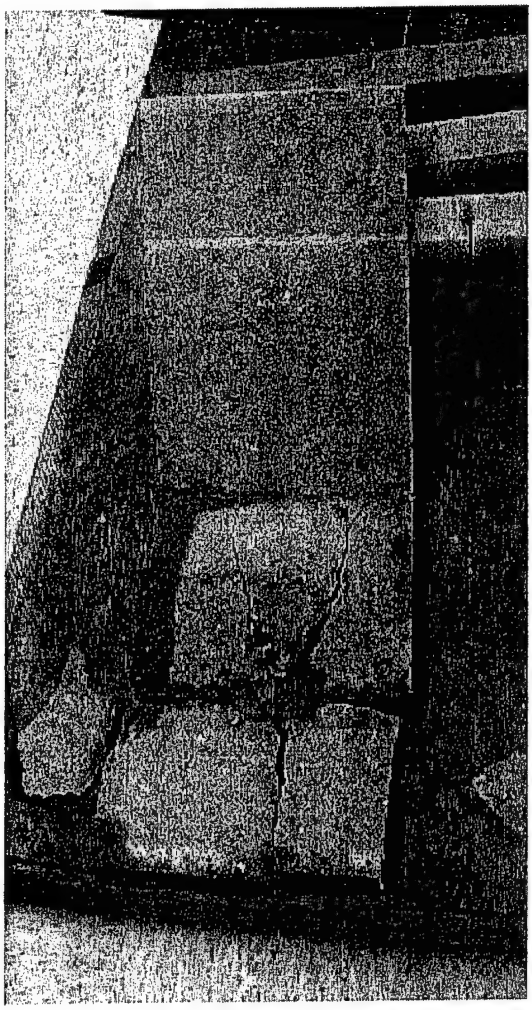

FIG. 260. Gas Gun Test 2, Sample 1

The pressure was reduced to 40.12 psi for Sample 2. The concrete failed, but the polymer did not. An image of the block immediately after the impact is shown in Fig. 261. This block experienced local failure. The projectile was stopped by the polymer. A side view of the block is shown in Fig. 262. This image shows the damage done to the concrete, as well as the strength of the bond of the polymer to the concrete. Fig. 263 shows the polymer side of this sample after impact. There were no tears in the polymer.

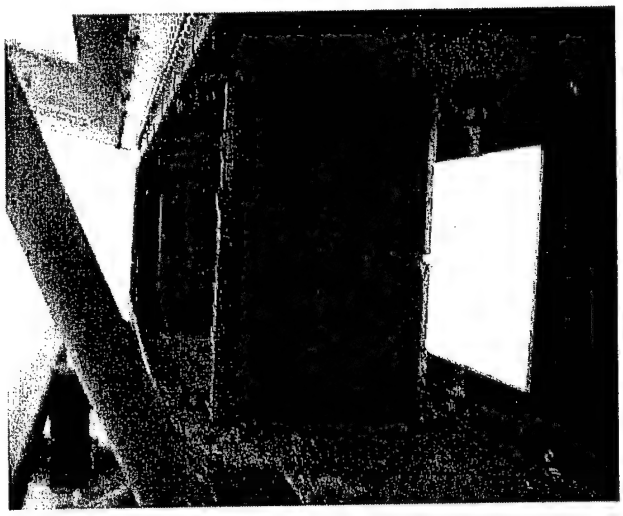

FIG. 261. Gas Gun Test 2, Sample 2

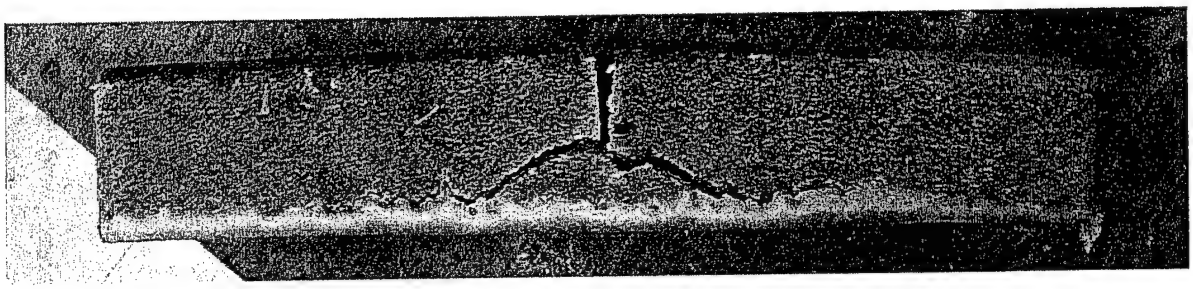

FIG. 262. Gas Gun Test 2, Sample 2 Side View

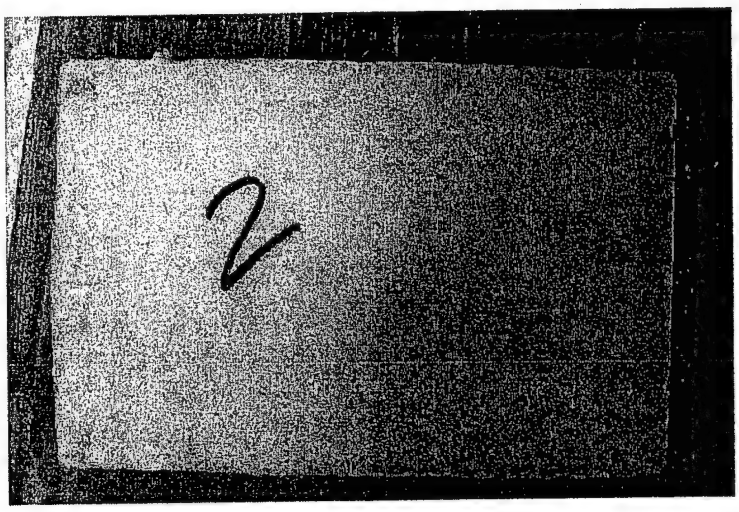

FIG. 263. Gas Gun Test 2, Sample 2

The pressure used for Sample 2 was too low. A pressure somewhere in the middle was required. To reach the ballistic limit, the projectile needed to be stopped in the concrete with polymer. Sample 3 was impacted by a projectile launched from 69.7 psi of nitrogen in the gas chamber.

Upon impact, the concrete shattered. The large pieces were pieced back together to be photographed and are shown in Fig. 264. The polymer completely separated from the block. Despite this, the projectile did not pass to the other side of the concrete.

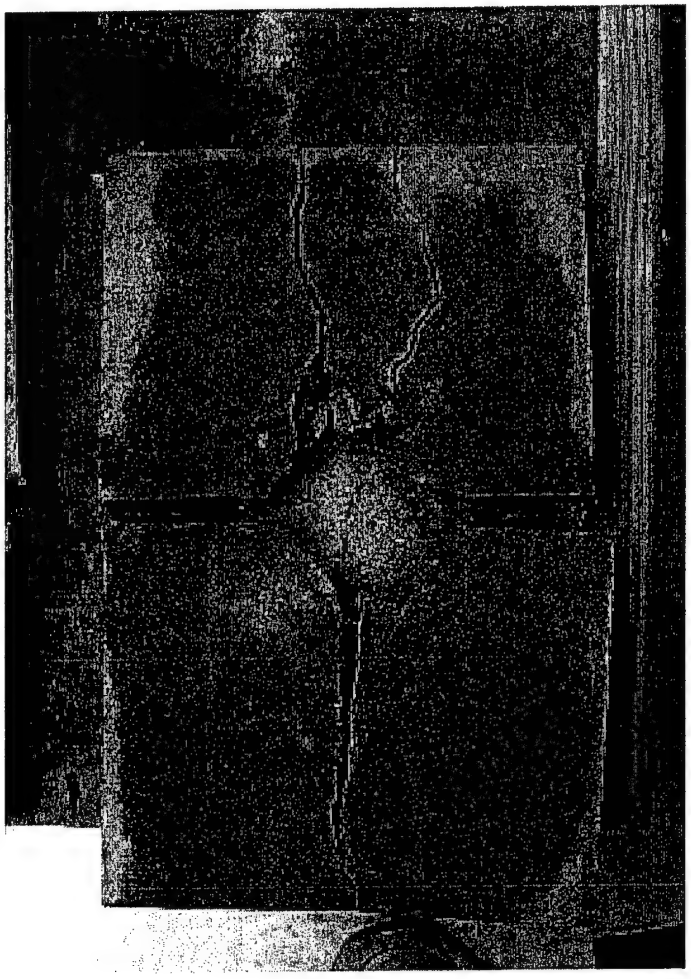

FIG. 264. Gas Gun Test 2, Sample 3

Due to the total fragmentation of Sample 3, the pressure was reduced to 50.7 psi for Sample 4 and polymer stopped the projectile. It did not debond or result in significant permanent strain. The projectile rebounded without passing through. Sample 4 is shown in Fig. 265.

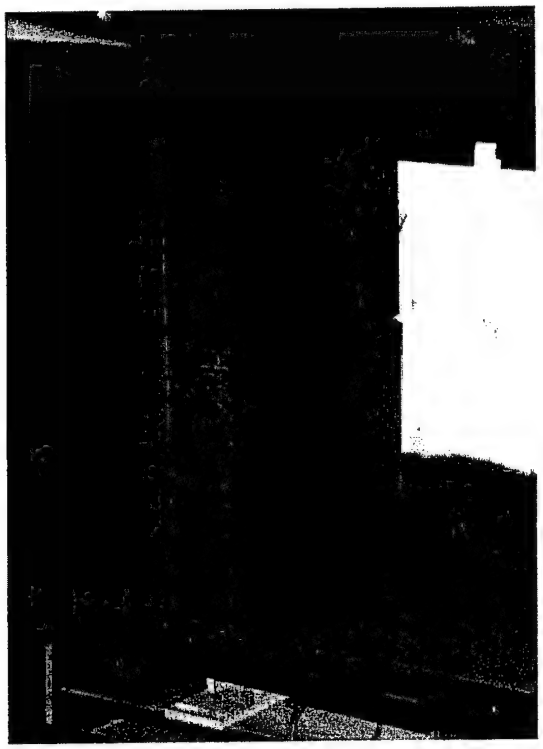

FIG. 265. Gas Gun Test 2, Sample 4

For the last sample, it was desirable to distribute the energy across the block, as previous samples had failed locally. To do this, a bar was propped on a piece of cardboard. The projectile impacted the bar, which then distributed the load across the block. An image of this setup is shown in Fig. 266. The impacted paver is shown in Fig. 267.

FIG. 266. Gas Gun Test 2, Sample 5 Setup

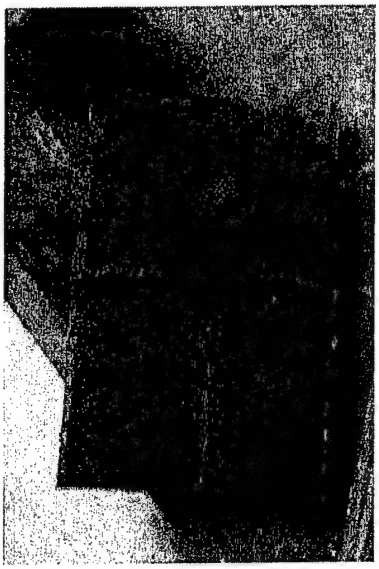

FIG. 267. Gas Gun Test 2, Sample 5

The pressure was increased for Sample 5, as the load would be distributed across the block. 90.7 psi was reached in the gas gun chamber. The projectile was launched. The test setup was successful in distributing the load across the block. The concrete did fail, but the polymer remained completely intact, and once again, prevented the projectile from penetrating the block.

4.4.5 Gas Gun Test 2 Results

Like Gas Gun Test 1, the energy absorbed is equal to the energy capacity only if the ballistic limit is reached. However, for testing two-inch thick concrete, it is not likely that a ballistic limit would be reached. In Gas Gun Test 2, no projectiles were stuck in the concrete/polymer in this manner. However, none of the projectiles exited through the material. In this test, the energy capacity can be obtained by finding the highest mass and velocity that can be projected without penetrating the material. Data from the five samples is shown in Table 38. Included in the table is the pressure used to launch the projectiles and the entrance velocity of each.

TABLE 38. Gas Gun Test 2 Results

Specimen	Pressure (psi)	Entrance Velocity (ft/sec)	Energy Absorbed (ft*lb)
1	90.6	494	1344
2	40.1	315	546
3	69.7	444	1083
4	50.7	375	774
5	90.7	496	1353

4.4.6 Conclusions

The gas gun test yields insight into a material's ability to absorb energy. Gas Gun Test 1 demonstrated the energy absorption potential of the neat polymer membrane and the fracture mechanism in a dynamic shear environment. Gas Gun Test 2 offers insight into fracture mechanisms of the reinforcement/substrate system in a dynamic load

environment. With further development and study, both of these tests may prove valuable towards evaluating a potential blast reinforcement concept.

4.5 MTS TENSILE TESTS

4.5.1 Introduction

Application of highly ductile, resilient polymer materials to wall systems can protect buildings and their occupants from flying debris caused by external explosions. Guidelines are needed for the selection of blast reinforcing materials. Full-scale explosive tests are just one of the many tests that may be conducted to establish the potential effectiveness of a polymeric reinforcement.

As the success of the AFRL retrofit program has become more widely known, companies have submitted numerous material specimens as possible retrofit material to be applied to the walls in the full-scale tests. However, full-scale explosive tests are expensive and time consuming. Additional methods are being sought to determine the value of a material as a polymer retrofit. An MTS testing machine was used to conduct uniaxial tensile tests to aid in selecting and/or eliminating materials as blast reinforcement candidates. The purpose of the tensile test was to characterize the mechanical properties of a material in terms of the relationship between tensile stress and strain, toughness, secant modulus, and percent elongation.

4.5.2 Test Methodology

The Standard Test Method for Tensile Properties of Plastics "covers the determination of the tensile properties of unreinforced and reinforced plastics in the form

of standard dumbbell-shaped test specimens when tested under defined conditions of the pretreatment, temperature, humidity, and testing machine speed" (ASTM 2000b). It is used to produce tensile property data that in turn yields static mechanical characterization used for research and development.

The uniaxial tension test requires measuring the width and thickness of the test specimens at several points along their narrow sections to the nearest thousandth of an inch. The specimens were then placed in the grips of the testing machine with the long axis of the specimen aligned with the grips. The grips were tightened evenly and firmly to prevent slippage of the specimen during the test. An extensometer was used to record elongation data. A stroke rate of 20 in./min was used to pull the specimens, and load and grip separation were recorded throughout the test. Using this and pre-test dimensions for area and length, the stress vs. strain relationship was calculated.

Percent Elongation: Percent elongation is the fracture strain of a specimen expressed as a percent. It quantifies ductility and is related to strain energy absorption. As applicable to the blast reinforcement purpose, significant elongation ability of a material is required to allow blast energy to be transformed into strain energy and be redistributed throughout the wall system. Percent elongation was calculated by taking the change in gauge length at the highest load, dividing that length by the original length, and multiplied by 100. Maximum elongation for each specimen was recorded, as well as the percent elongation at the maximum tensile stress, which often is not the same. Percent elongation is plotted in the graphs and recorded in the tables provided in the Appendix.

Tensile Stress: Tensile stress is the amount of stress in a specimen undergoing tensile loading. Tensile stress was calculated by taking the load at any given time and

dividing it by the original, preloaded area of the specimen. Tensile stress vs. strain is shown in the graphs and maximum stress is provided in the tables of the Appendix.

Secant Modulus: The secant modulus is usually employed in place of modulus of elasticity in the case of materials whose stress-strain diagram does not demonstrate proportionality of stress to strain (ASTM 2000b). It is defined as the ratio of nominal stress to corresponding strain at any particular point on the stress-strain curve. The secant modulus provides an indication of a material's stiffness. The stiffness of a polymeric material used as blast reinforcement is important for controlling the maximum displacement of a wall structure. Numerical values for secant modulus were calculated by first finding 10% and 60% of the maximum stress. The corresponding elongations were found for the 10% and 60% stress levels. The difference in stress divided by the difference in elongation yielded the secant modulus.

Toughness: Modulus of toughness is the measure of the ability of a material to absorb energy prior to fracture (Boresi and Schmidt 2003). Its numerical value is calculated as the area under the stress-strain curve up to rupture. A higher modulus of toughness reflects a greater ability to absorb strain energy without fracturing. Toughness is a way to combine stiffness, tensile stress, and percent elongation into one parameter. It does not, however, account for resistance to deflection, a key element in the blast reinforcement application. In this test, toughness was calculated by keeping a cumulative total of average stress and multiplying it by the incremental strain for each sampling point acquired.

Test Specimens: All specimens used in the test were cut with a razor blade from the same sheet of material. Thicknesses of the materials were generally very uniform.

Six dimensions from each specimen were recorded (thickness three places; width three places). 53 materials were considered in the test, and three samples, usually A, B, and C, were cut from each material.

4.5.3 Results

The results of the tensile tests are shown in the Appendix. The manufacturers of the materials are not disclosed but are named in the tables and figures below simply as a "material number." Tables in the Appendix quantify the tensile stress, percent elongation, secant modulus, and toughness of each material. Figures show the stress-strain relationship for each material.

All graphs have been smoothed from their original forms. Graphs may vary slightly from the tabular results. In addition, some materials had a sample that varied significantly from the other two and was not included in averaging the data. The samples that were removed from averages have been highlighted in the tables. Ideally, about ten samples of each material would be required for thorough testing.

4.5.4 Conclusions

The uniaxial tensile test was valuable in producing fundamental static mechanical property data that can aid in initial down-select of materials for blast reinforcement. The data for each material is shown in the Appendix, and a summary is provided here to conclude and summarize. Table 39 shows the averages of the maximum tensile stress, elongation at maximum tensile stress, maximum elongation, secant modulus, and toughness for the three samples tested for each material. The material that has been used

for full-scale testing is highlighted. This provides insight into the mechanical properties of a material that has been proven for blast reinforcement.

Maximum tensile stresses ranged from 298 psi to 22,600 psi. The lowest maximum tensile stress of 298 psi (Material 32) did not have a very high elongation or toughness. The maximum tensile stress of all the materials was 22,600 psi (Material 15). However, this material had one of the lowest elongations of all the materials. High tensile stress capacity does not necessarily make a material a good blast reinforcement candidate.

It is believed that the elongation capability is important in the success of a blast reinforcement material. Elongation at maximum tensile stress for these materials varied from 3.11% (Material 9) to 326% (Material 39). Although the elongation for Material 9 is relatively low, its maximum tensile stress was high. Its secant modulus was also very high. 3.11% elongation may not be high enough to allow attenuation and effective distribution of blast energy.

Material 39 yielded high elongation at the maximum tensile stress, and its maximum tensile stress was not low. In fact, the maximum tensile stress was approximately two hundred psi lower than that of the material that was used in full-scale testing, and its elongation far exceeded that of the material that had been tested. This material might qualify as a good candidate given its elongation ability, but its low stiffness would likely result in excess deflection and collapse. A balance between elongation ability and stiffness is necessary.

Values for secant modulus ranged from 571 psi (Material 38) to 647,000 psi (Material 9). The Material 38 secant modulus is significantly lower than that of the

polymer that has been used in full-scale testing. Material 9, as mentioned before, has a relatively high maximum tensile stress, but its high tensile stress would probably not make up for its very low elongation. The secant modulus of Material 9 is high but its low percent elongation would likely exclude it as a blast reinforcement.

Values for toughness fall between 46 psi*in./in. and 7230 psi*in./in. The weakest material in terms of toughness is Material 2, which also has the lowest maximum tensile stress. Material 1, with the largest toughness, looks superior in all areas. It has an above-average tensile stress, above-average elongation, and average secant modulus. Material 37 may be a good candidate. It has values that are better in every category than those of the polymer used in the blast tests.

It has been observed, though not fully supported by defendable research, that the order of importance for material selection for blast retrofitting is percent elongation, secant modulus, and maximum tensile stress. The most desirable materials, given the data from this test alone, appear to be Materials 1, 4, 37, and 53. Materials 16, 20, and 45 might also be of interest. The materials that would be least likely to work would be Materials 10, 11, 40, 41, 42, and 43. The same manufacturer makes Materials 10 and 11. A different manufacturer makes materials 40 through 43. Material 9 has the lowest elongation, but more testing is needed to determine what impact of the extremely high tensile stress and secant modulus.

4.6 Exploratory Testing Conclusions

Selecting advanced materials for the blast reinforcement purpose is difficult, as many behave well in two of the categories but poorly in the others. To further complicate

matters, other conditions besides the properties listed must be satisfied before a material can be deemed a "good candidate." It is worth noting that the primary material used in the full-scale wall tests, as described previously in this document, does not qualify as a "best" or "worst" candidate.

There is one important part of this test that needs to be noted. All of the samples were cut using razor blades, not a die cut as recommended in ASTM D638. All of the samples failed at the transition point. This could possibly put the validity of the test into question. However, all the samples were cut the same way. This allowed materials to be compared to the other materials in this particular test. Hopefully this test will provide insight on which materials may be good candidates and should be tested further.

Many factors outside the scope of these laboratory tests must be considered in retrofit selection, including cost and availability of the material, ease of application, and toxicity. A material that is advantageous in strength and elongation would not be acceptable if, when the building caught on fire, smoke toxicity resulted in death of occupants. This illustrates why the material selection process is so complicated. Materials 48 through 51 in the MTS Tensile Test are different variations of the materials that have been tested in the full-scale wall tests. This material was chosen as a "medium" candidate. It was advantageous because it was cost effective and relatively easy to apply. So far, this material has been very effective in reducing fragmentation of masonry walls. The materials labeled as "best" may have problems in other areas that challenge their candidacy.

Table 39. Uniaxial Tension Test, Material Averages

Sample Name	Maximum Tensile Stress (psi)	Elongation at Maximum Tensile Stress (%)	Maximum Elongation (%)	Secant Modulus (psi)	Toughness (psi*in/in)
1	5,760	147	149	61,800	7,230
2	6,200	9.6	103	111,000	5,650
3	1,760	6.5	90	42,800	1,230
4	1,780	214	235	34,600	3,210
5	1,690	191	211	1,710	2,520
6	1,580	17	32	28,200	242
7	2,220	92	95	5,600	1,510
8	1,100	87	90	2,510	679
9	18,500	3.1	3.2	647,000	344
10	9,420	5.9	21	205,000	1,460
11	8,830	5.7	21	200,000	1,470
12	1,970	248	252	13,900	3,730
13	1,630	188	203	12,000	2,710
14	20,800	3.8	3.8	552,000	445
15	22,600	4.9	5.1	430,000	562
16	2,090	151	153	10,974	2,524
17	1,160	90	101	4,420	887
18	1,610	24	26	8,630	262
19	2,540	34	35	9,590	563
20	2,410	299	300	8,390	5,090
21	2,700	258	258	2,650	4,440
22	2,370	299	299	1,570	5,040
23	1,130	298	300	2,170	2,370
24	1,300	298	300	1,110	2,540
25	1,130	297	300	669	2,370
26	1,540	266	267	2,020	3,040
27	2,340	41	41	8,550	628
28	3,070	47	47	8,800	926
29	3,350	49	49	8,810	1,020
30	760	93	94	1,040	450
31	1,570	100	108	3,340	1,210
32	298	21	25	1,010	46
33	1,360	95	103	6,880	1,100
34	831	69	75	1,650	406
35	896	85	87	1,620	517
36	1,410	264	267	2,730	2,800

Table 39. Uniaxial Tension Test, Material Averages (Continued)

37	3,280	188	189	19,600	4,710
38	925	166	176	571	964
39	1,380	326	335	730	3,130
40	9,330	6.2	14	201,500	865
41	9,220	6.2	27	200,000	1,830
42	7,700	5.8	25	169,000	1,410
43	7,760	5.8	24	173,000	1,370
44	1,740	52	57	20,300	833
45	2,030	151	181	5,250	2,870
46	1,620	98	109	9,380	1,380
47	1,780	108	113	9,570	1,560
48	1,980	82	89	23,100	1,490
49	976	52	79	12,400	682
50	1,650	110	159	19,800	1,570
51	1,980	82	89	23,100	1,490
52	1,670	50	75	27,300	1,100
53	3,620	153	155	24,200	4,380
Average	3,780	114	125	63,800	1,940

CHAPTER 5

CONCLUSIONS

5.1 Summary and Conclusions

An elastomeric polymer was evaluated as an external reinforcement for concrete masonry walls subjected to blast. Seven full-scale explosive tests of polymer-reinforced walls were conducted by the AFRL at Tyndall AFB, Florida. The polymer was found to be effective at reducing wall deflection, preventing collapse, and preventing flying debris from entering occupant space. The full-scale blast tests indicated that polymer-reinforced masonry walls can withstand blast pressures that exceed 60 psi without collapse or significant breaching, compared to a collapse pressure of less than 5 psi for unreinforced masonry walls.

Because the explosive tests indicated a high level of effectiveness, there is much interest in developing new and improved materials for blast reinforcement. With hundreds or even thousands of possible materials, however, it is challenging to choose candidates with a high likelihood of effectiveness. Full-scale explosive tests cannot be performed for every possible blast mitigant material. Therefore, there is a need to develop non-explosive laboratory methodology and minimum performance criteria that establish a material as a blast reinforcement candidate worthy of full-scale testing, and to relate results of laboratory tests to blast resistance effectiveness.

An objective of this work was to identify laboratory tests that would characterize material specimens as good or poor candidates for blast reinforcement. Several

laboratory tests were explored using resources at the University of Alabama at Birmingham. A static flexural test was performed on several polymeric materials bonded to concrete blocks. This test examined the strength of the material as well as the bond between the material and the block. The blocks were notched in the center to induce failure similar to that seen at the mortar joint in the full-scale wall tests. Tensile strength, elongation, and bond strength of materials in conjunction with their bonding agents were determined in the static flexural test when the materials remained bonded. For materials that debonded, the test was useful in identifying bond failure mechanisms. Three out of four of the tested materials debonded before material failure was reached.

The second laboratory test performed was the high-speed puncture test using the drop tower equipment at UAB. This test provided a method of ranking the dynamic energy absorption effectiveness and observing shear failure mechanisms of potential blast reinforcement materials. Impact energy, total energy, strain energy absorption capacity, and maximum load were determined from the mass and velocity of the impact. The drop tower test provided insight into failure modes of materials in the dynamic punching shear environment.

The third laboratory test explored was the gas gun test. The velocities of the projectiles used in the gas gun test can approach 1000 ft/sec. Samples of the elastomeric polymer were placed in the gas gun and impacted with projectiles. The ballistic limit of several candidate materials was achieved for several of the specimens, and the total energy absorbed was calculated for each of these specimens. The gas gun facility was also used to test polymer-coated concrete blocks. The energy capacity of each was

calculated from data provided by the testing apparatus. The polymer coating did not experience local punching and did not fail during testing.

Uniaxial tension tests were performed by the AFRL at Tyndall AFB. Tests were performed on 53 materials submitted for blast reinforcement consideration. The tests quantified stress-strain properties of each material through rupture. Mechanical properties determined for each material included tensile stress, elongation, secant modulus, and toughness. The uniaxial tension test allowed static properties of various reinforcement materials to be easily compared. The 53 materials tested in the uniaxial tension test exhibited a wide range of properties. The AFRL will use the results from this test to choose potential candidates for later phases of blast reinforcement research.

5.2 Recommendations and Suggested Research

The full-scale explosive tests show that reinforcing masonry walls with elastomeric coatings can significantly increase survival and reduce injuries in blasts. The success of the project could encourage owners of buildings, especially buildings that would be considered at a higher threat level, to retrofit walls.

Research should be concentrated on optimizing blast reinforcement materials and application processes. The blast tests conducted by AFRL focused on a single, off-the-shelf coating material that was developed for other purposes. Other materials may prove to be more effective. Furthermore, stiffer and stronger materials will be required for other types of wall structures. Laboratory tests need to be designed to help identify good material candidates for blast reinforcement.

Another important area of research is the development of techniques for connecting other polymeric or composite materials to walls. The material used in the explosive tests was a spray-on material that resulted in an excellent bond. Easy bonding is an appealing characteristic. Although applying the material is relatively easy, cumbersome protective gear and clothing is required as the fumes are hazardous during application. The polymer coating considered in the blast tests also requires large equipment. Methods of bonding and connecting must be developed that can be done easily at a construction site.

There has been much thought of using a material as a "catcher system," where the material would not be bonded directly to the wall but would instead "catch" the wall debris as it fractured from effects of the blast. However, methods that connect membrane materials at the top and bottom so they would not shear during the blast have not yet been devised. An ultimate goal is to develop reinforcement into a "wallpaper" form that could be quickly applied.

Materials with fiber reinforcement may also have advantages for retrofit. Research is required on the strength of fiber-reinforced materials and how they could be bonded to the walls. Research is also needed to show how these materials would behave in blast load environments.

LIST OF REFERENCES

ASTM. (2000a). "Standard test method for high speed puncture properties of plastics using load and displacement sensors." D 3763-00, West Conshohocken, Pa.

ASTM. (2000b). "Standard test method for tensile properties of plastics." D 638-00, West Conshohocken, Pa.

"Attack on the USS Cole." (2004). *Yemen Gateway*. <www.al-bab.com/yemen/cole1>

Boresi, A.P., and Schmidt, R.J. (2003). *Advanced mechanics of materials.* 6th Edition. John Wiley and Sons, New York.

Clark, G. (1997). "Two university researchers keep masonry walls from tumbling down." *Arizona Summer Wildcat*. University of Arizona.

Committee on Feasibility of Applying Blast-Mitigating Technologies and Design Methodologies from Military Facilities to Civilian Buildings. Board on Infrastructure and the Constructed Environment; Commission on Engineering and Technical Systems; National Research Council. (1995). *Protecting buildings from damage: transfer of blast-effects mitigation technologies from military to civilian applications*. National Academy Press, Washington, D.C.

Connell, J. D. (2002). "Evaluation of elastomeric polymers for retrofit of unreinforced masonry walls subjected to blast." Masters Thesis, University of Alabama at Birmingham, Alabama.

Crawford, J. E., Bogosian, D. D., and Wesevich, J. W. (1997). "Evaluation of the effects of explosive loads on masonry walls and an assessment of retrofit techniques for increasing their strength." *Proc., 8th International Symposium on Interaction of the Effects of Munitions with Structures,* McLean, Virginia.

Crawford, J. E., Malvar, L. J., Wesevich, J. W., Valancius, J., and Reynolds, A. D. (1997). "Retrofit of reinforced concrete structures to resist blast effects." Technical paper, *Title No. 94-S34, ACI Structural Journal*, 94(4), 371-377.

Duan, Y., Saigal, A., and Greif, R., and Zimmerman, M.A. (2003). Impact behavior and modeling of engineering polymers. *Polymer Engineering and Science*, 43(1), 112-124.

Englekirk, R. E., and Hart, G. C. (1982). *Earthquake design of concrete masonry buildings: response spectra analysis and general earthquake modeling Considerations.* Volume 1. The Concrete Masonry Association of California and Nevada. Prentice Hall, Inc. Englewood Cliffs, NJ.

Futura Coatings, Inc., Technical Data. (2002a). "Futura-Bond 415." Futura Coatings, Inc., St. Louis, Mont.

Futura Coatings, Inc., Technical Data. (2002b). "Geothane 520." Futura Coatings, Inc., St. Louis, Mont.

Knox, K.J., Hammons, M.I., Lewis, T.T., and Porter J.R. (2000). "Polymer materials for structural retrofit." Force Protection Branch, Air Expeditionary Forces Technology Division, Air Force Research Laboratory, Tyndall AFB, Florida.

Laursen, P.T., Seible, F., and Hegemeir, G.A. (1995). "Seismic retrofit and repair of reinforced concrete with carbon overlays." *Rep. No SSRP-95/01*, Structural Systems Research Project, University of California, San Diego, California.

MacGregor, J. G., and Luse, I., eds. (1978). *Structural Design of Tall Concrete and Masonry Buildings.* Council on Tall Buildings and Urban Habitat. American Society of Civil Engineers.

McLaughlin, Marin. (1998). "Questions Mount in Kenya, Tanzania Bombings." *World Socialist Web Site*. <www.wsws.org/news/1998/aug1998/bomb-a13>

"The Oklahoma City Bombing." (1996). *CNN Interactive*. <http://www.cnn.com/US/OKC/bombing.html>

Purcell, M.R., Muszynski, L.C., and Taun, C.Y. (1995). "Explosive field tests to evaluate composite reinforcement of concrete and masonry walls." Applied Research Associates, Inc., Gulf Coast Division, Tyndall AFB, Florida.

Ross, C.A., Jerome, D.M., and Hughes, M.L. (1994). "Hardening and rehabilitation of concrete structures using carbon fiber reinforced plastics (CFRP)." *Rep. No. WL-TR-94-7100*, Wright Laboratory Armament Directorate, Eglin AFB, Florida.

Seible, F., and Karbhari V.M. (1996). "Seismic retrofit of bridge colums using advanced composite materials." Division of Structural Engineering, University of California, San Diego, La Jolla, California.

Schoeppner, G.A., and Abrate, S. (2000). "Delamination threshold loads for low velocity impact on composite laminates." *Composites Part A: Applied Science and Manufacturing*, 31(9), 903-915.

"Terrorism Through America's History." (2004). *American History*. <http://americanhistory.about.com/library/fastfacts/blffterrorism.htm>

Wall response to airblast loads: the wall analysis code (WAC). (1995). U.S. Army Engineer Waterways Experiment Station, Vicksburg, Misissippi.

Weeks, J., Seible, F., Hegemeir, G., and Priestly, M.J.N. (1994). "The U.S.-TCCMAR full-scale five-story masonry research building test: part V – repair and retest." *Rep. No. SSRP-94/05*, Structural Systems Research Project, University of California, San Diego.

Whiting, W.D., and Coltharp, D.R. (1996). "Retrofit measures for conventional concrete masonry unit building subject to terrorist threat." U.S. Army Engineer Waterways Experiment Station, Vicksburg, Mississippi.

Wilkens, William. (2000). "World Trade Center Bombing." <www.nycop.com/Stories/Dec_00/World_Trade_Center_Bombing/body_world_trade_center_bombing>

Williams, Dave. (1998). "The Bombing of the World Trade Center in New York City." *Interpol*. <http://www.interpol.int/Public/Publications/ICPR/ICPR469_3.asp>

APPENDIX

UNIAXIAL TENSION TEST MATERIAL DATA

Table A1. Uniaxial Tension Test, Material 1

Sample Name	Maximum Tensile Stress (psi)	Elongation at Maximum Tensile Stress (%)	Maximum Elongation (%)	Secant Modulus (psi)	Toughness (psi*in/in)
A	5,760	150	152	61,000	7,310
B	5,730	145	148	61,600	7,180
C	5,780	146	147	62,900	7,200
Mean	5,760	147	149	61,800	7,230

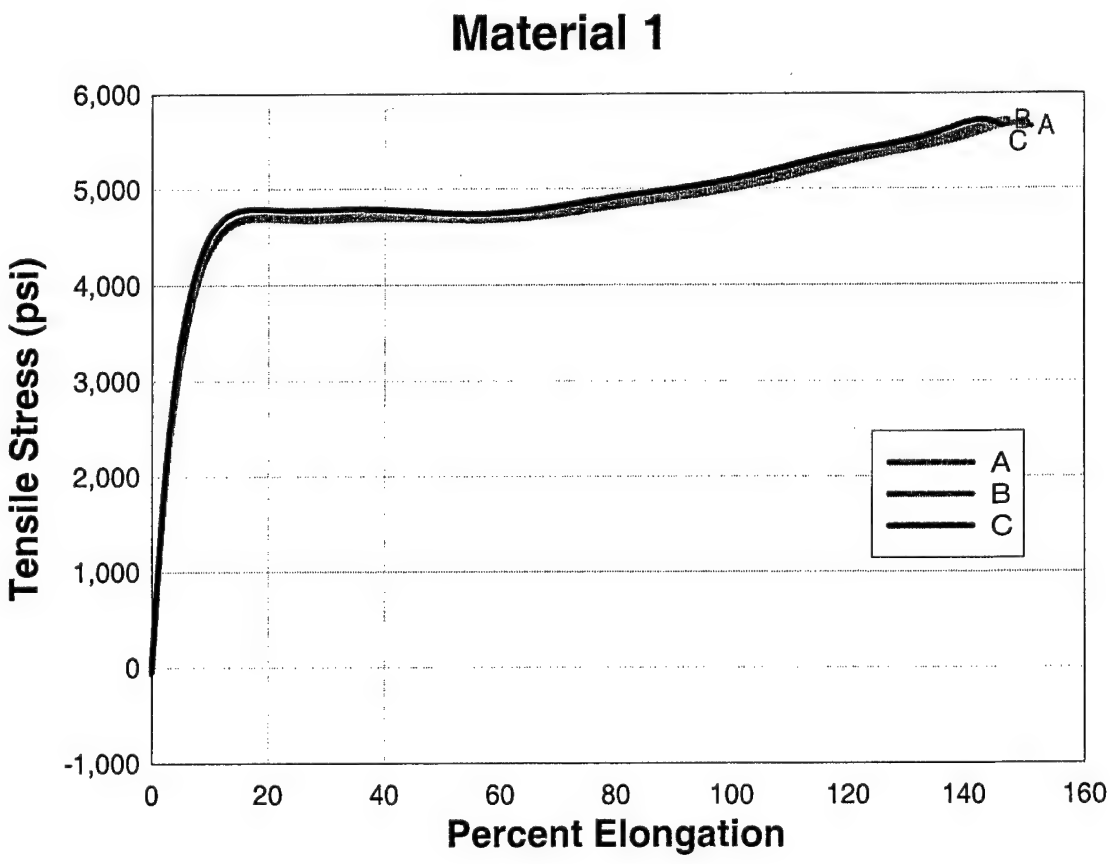

FIG. A1. Uniaxial Tension Test, Material 1

TABLE A2. Uniaxial Tension Test, Material 2

Sample Name	Maximum Tensile Stress (psi)	Elongation at Maximum Tensile Stress (%)	Maximum Elongation (%)	Secant Modulus (psi)	Toughness (psi*in/in)
A	6,300	117	123	108,000	6,960
B	6,200	9.2	103	112,000	5,600
C	6,100	9.9	104	109,000	5,700
Mean	6,200	9.6	103	111,000	5,650

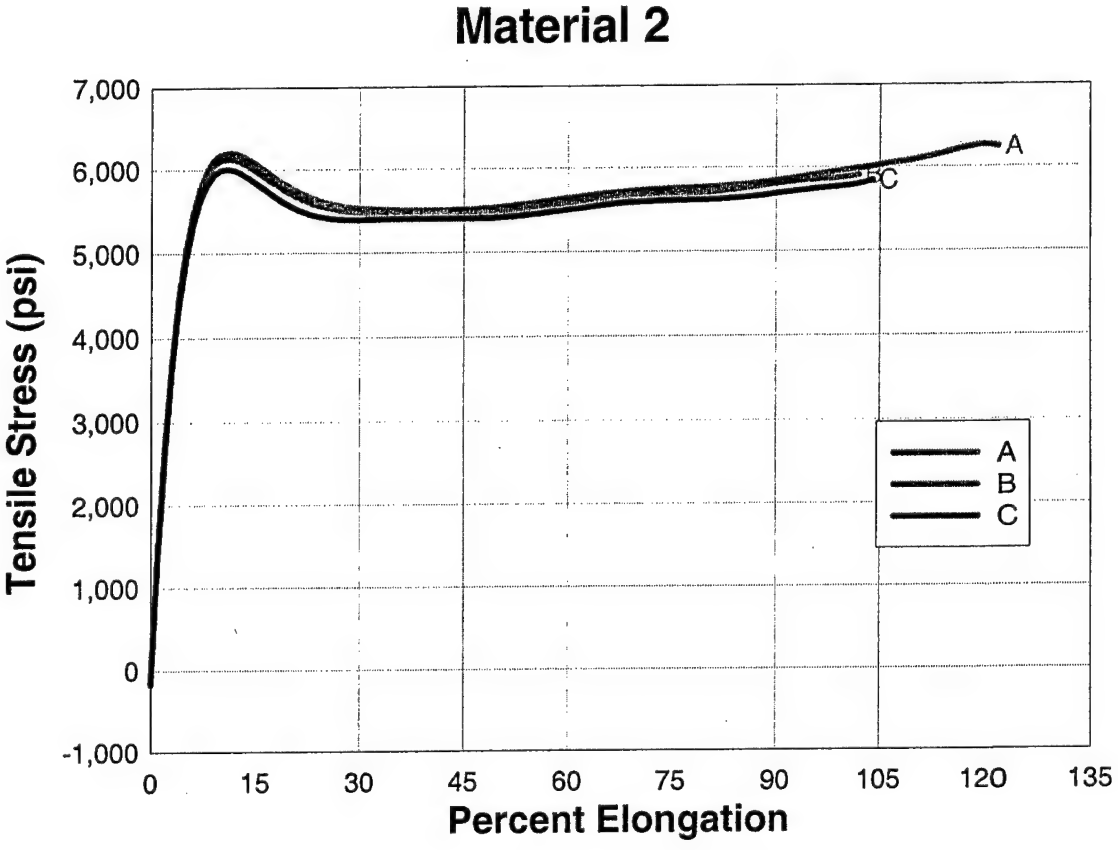

FIG A2. Uniaxial Tension Test, Material 2

TABLE A3. Uniaxial Tension Test, Material 3

Sample Name	Maximum Tensile Stress (psi)	Elongation at Maximum Tensile Stress (%)	Maximum Elongation (%)	Secant Modulus (psi)	Toughness (psi*in/in)
A	1,860	5.9	77	39,000	1,160
B	2,170	258	259	43,800	4,070
C	1,660	7.1	104	46,500	1,300
Mean	1,760	6.5	90	42,800	1,230

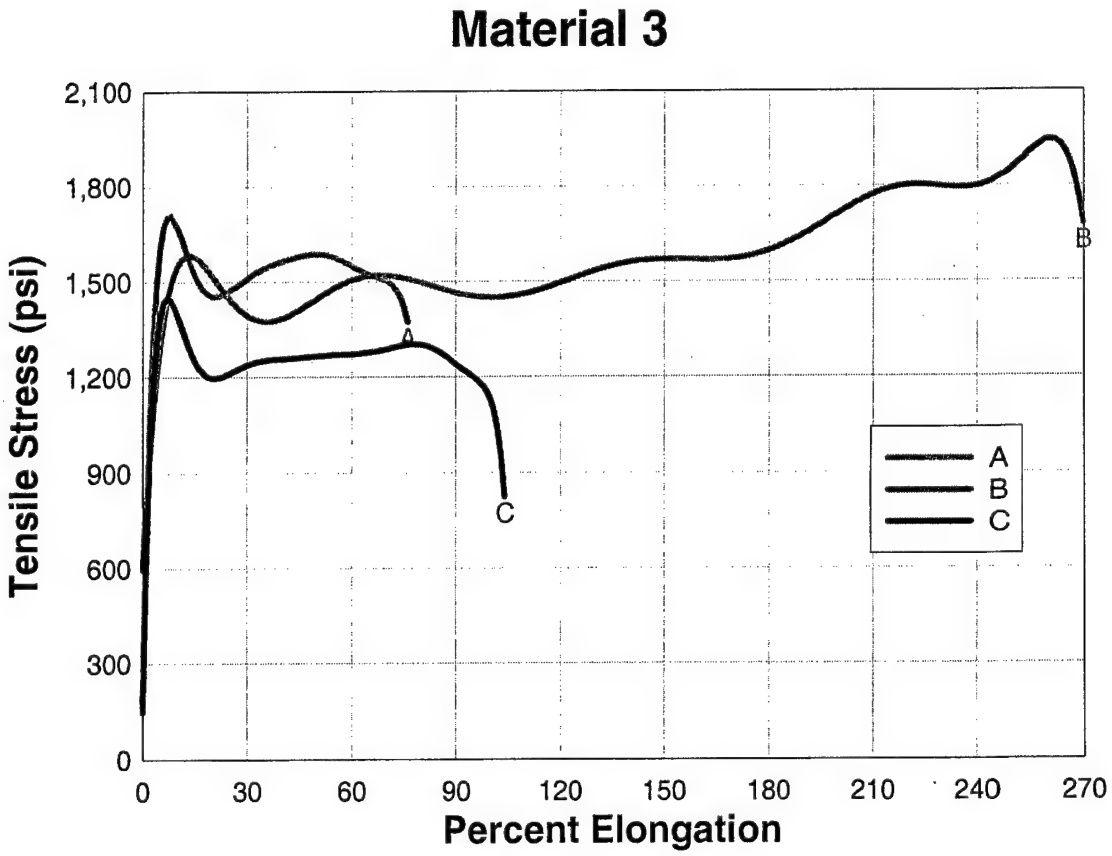

FIG. A3. Uniaxial Tension Test, Material 3

TABLE A4. Uniaxial Tension Test, Material 4

Sample Name	Maximum Tensile Stress (psi)	Elongation at Maximum Tensile Stress (%)	Maximum Elongation (%)	Secant Modulus (psi)	Toughness (psi*in/in)
A	1,780	243	265	32,800	3,630
B	1,770	186	205	36,300	2,790
Mean	1,780	214	235	34,600	3,210

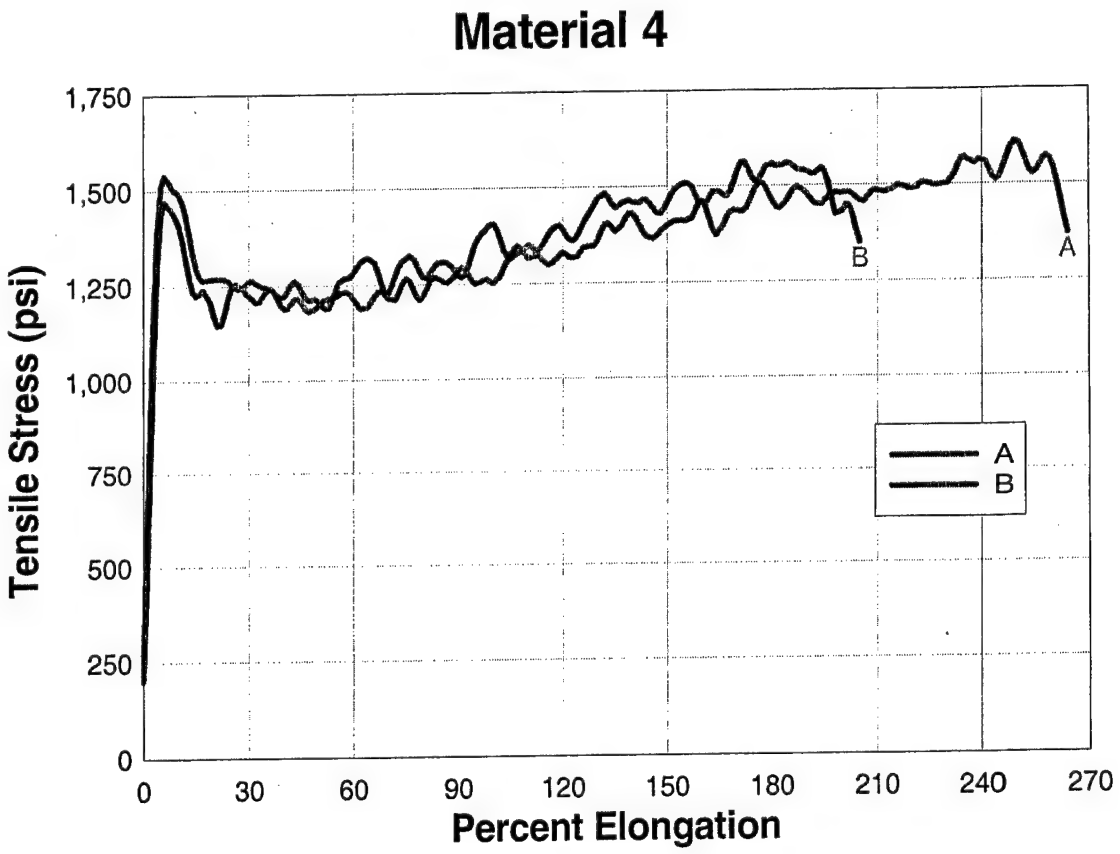

FIG A4 Uniaxial Tension Test, Material 4

TABLE A5. Uniaxial Tension Test, Material 5

Sample Name	Maximum Tensile Stress (psi)	Elongation at Maximum Tensile Stress (%)	Maximum Elongation (%)	Secant Modulus (psi)	Toughness (psi*in/in)
A	1,800	184	203	2,130	2,620
B	1,430	167	195	1,780	1,920
C	1,840	221	235	1,200	3,030
Mean	1,690	191	211	1,710	2,520

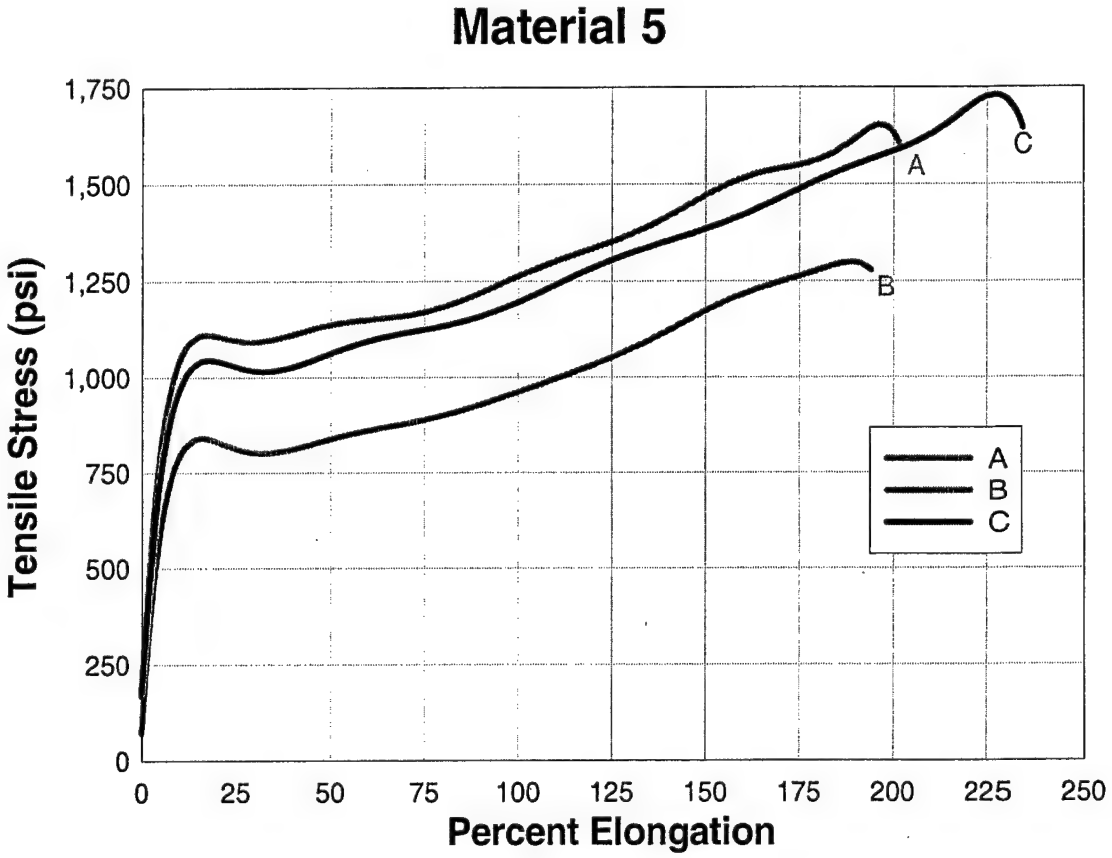

FIG A5. Uniaxial Tension Test, Material 5

TABLE A6. Uniaxial Tension Test, Material 6

Sample Name	Maximum Tensile Stress (psi)	Elongation at Maximum Tensile Stress (%)	Maximum Elongation (%)	Secant Modulus (psi)	Toughness (psi*in/in)
A	1,580	17	32	28,200	242
B	1,580	17	32	28,200	242
C	1,580	17	32	28,200	242
Mean	1,580	17	32	28,200	242

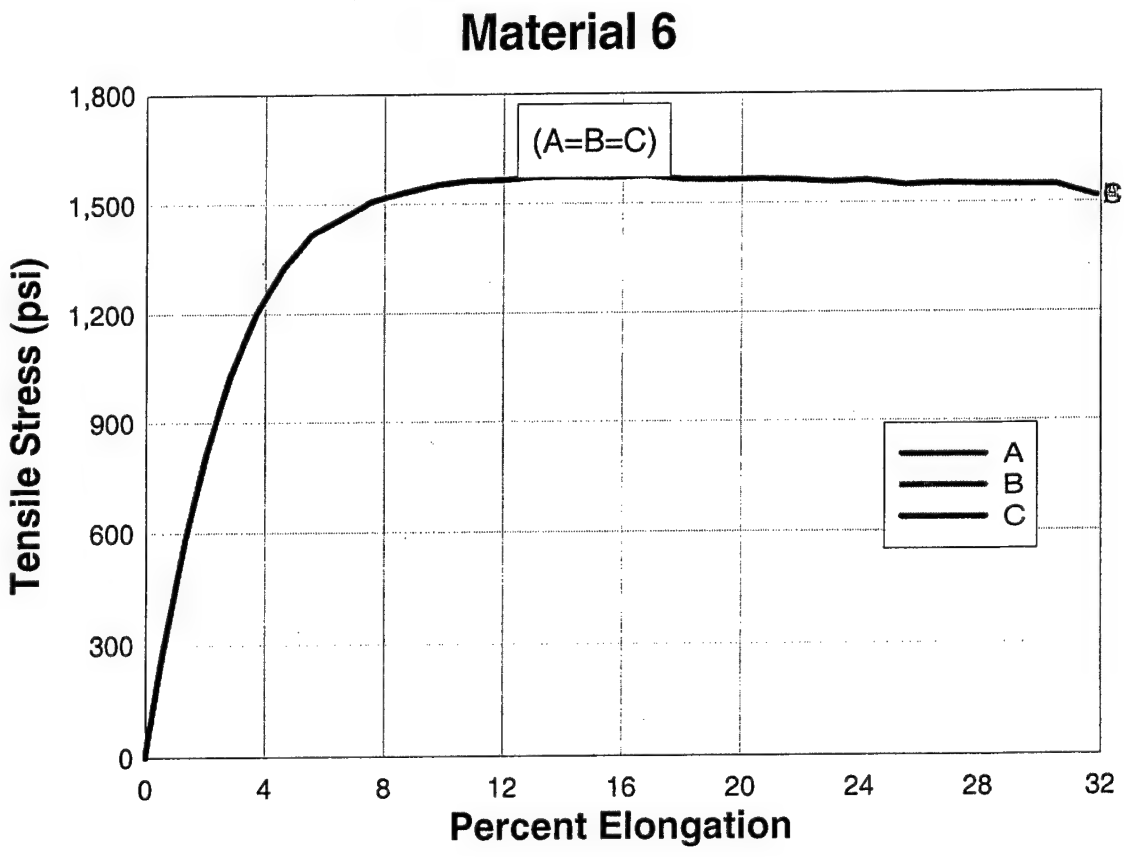

FIGA6. Uniaxial Tension Test, Material 6

TABLE A7. Uniaxial Tension Test, Material 7

Sample Name	Maximum Tensile Stress (psi)	Elongation at Maximum Tensile Stress (%)	Maximum Elongation (%)	Secant Modulus (psi)	Toughness (psi*in/in)
A	2,290	95	97	5,270	1,590
B	2,270	92	96	5,540	1,560
C	2,110	89	90	5,990	1,390
Mean	2,220	92	95	5,600	1,510

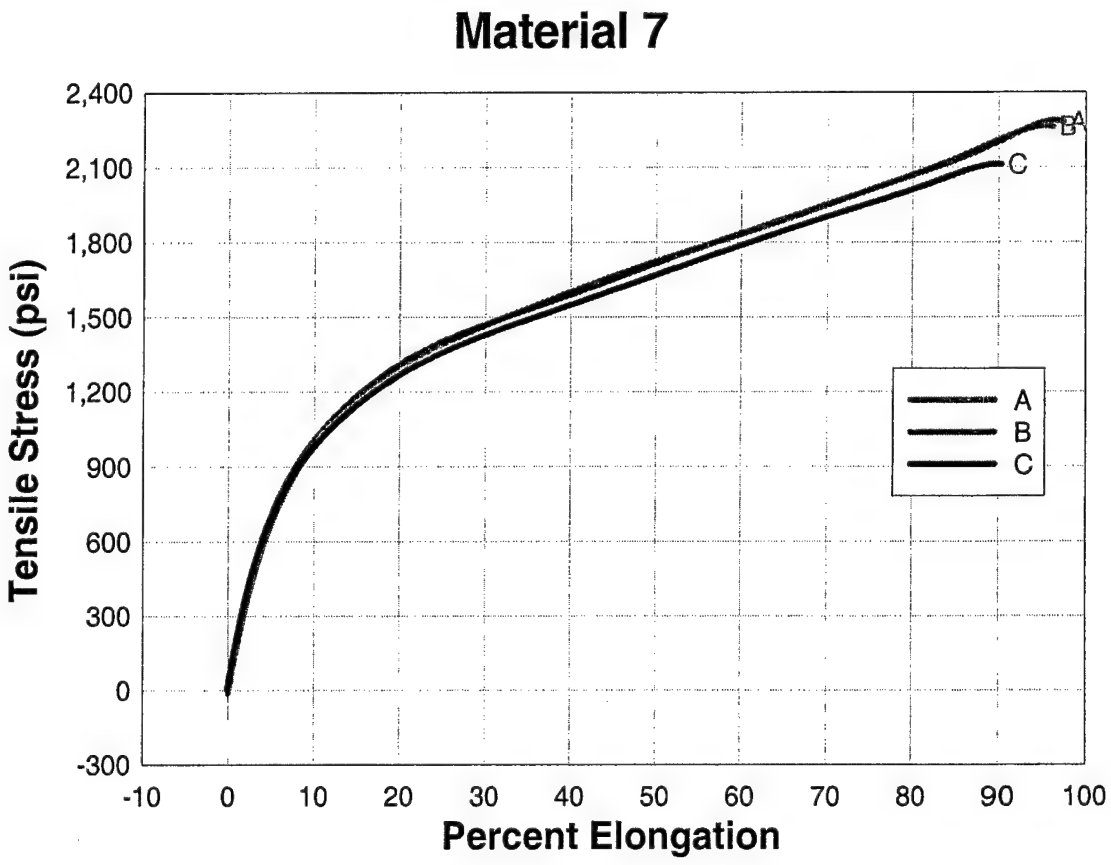

FIG. A7. Uniaxial Tension Test, Material 7

TABLE A8. Uniaxial Tension Test, Material 8

Sample Name	Maximum Tensile Stress (psi)	Elongation at Maximum Tensile Stress (%)	Maximum Elongation (%)	Secant Modulus (psi)	Toughness (psi*in/in)
A	1,100	77	79	3,190	606
B	1,090	97	102	1,840	752
Mean	1,100	87	90	2,510	679

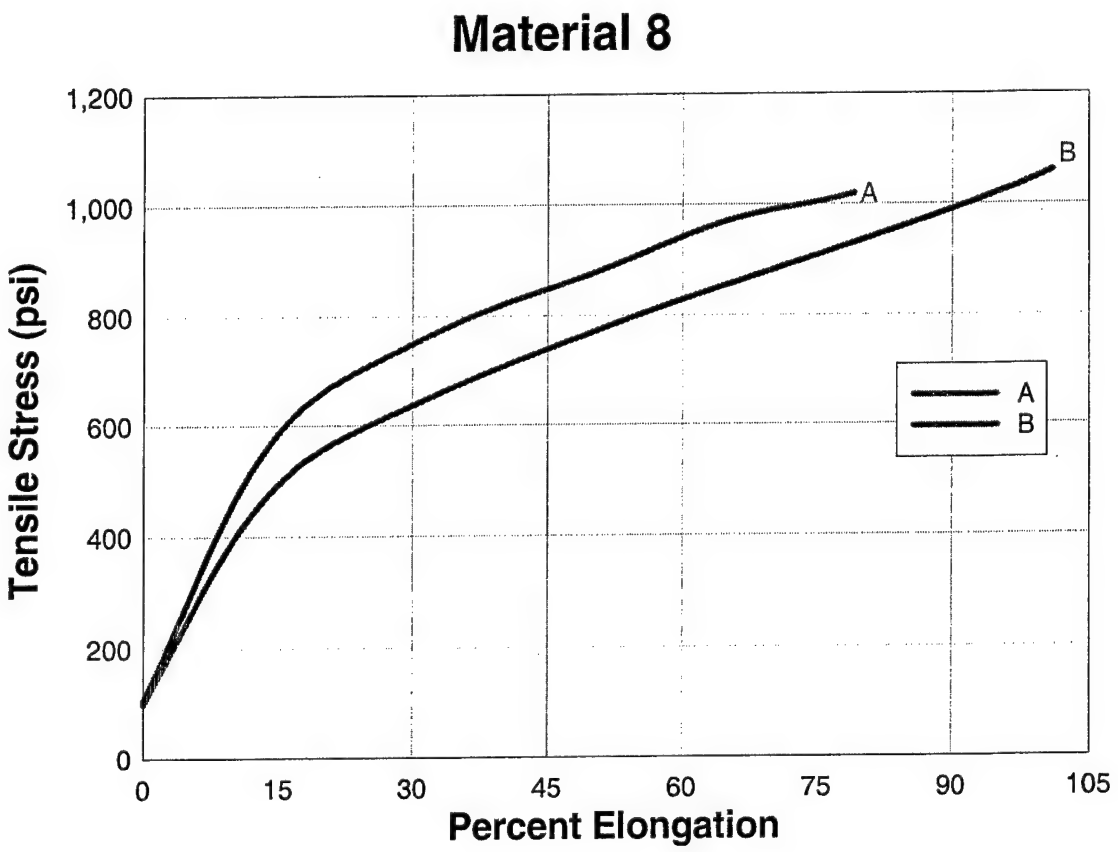

FIG A8. Uniaxial Tension Test, Material 8

TABLE A9. Uniaxial Tension Test, Material 9

Sample Name	Maximum Tensile Stress (psi)	Elongation at Maximum Tensile Stress (%)	Maximum Elongation (%)	Secant Modulus (psi)	Toughness (psi*in/in)
A	18,900	3.5	3.6	584,000	395
B	22,400	3.2	3.2	774,000	410
C	14,200	2.7	2.7	583,000	226
Mean	18,500	3.1	3.2	647,000	344

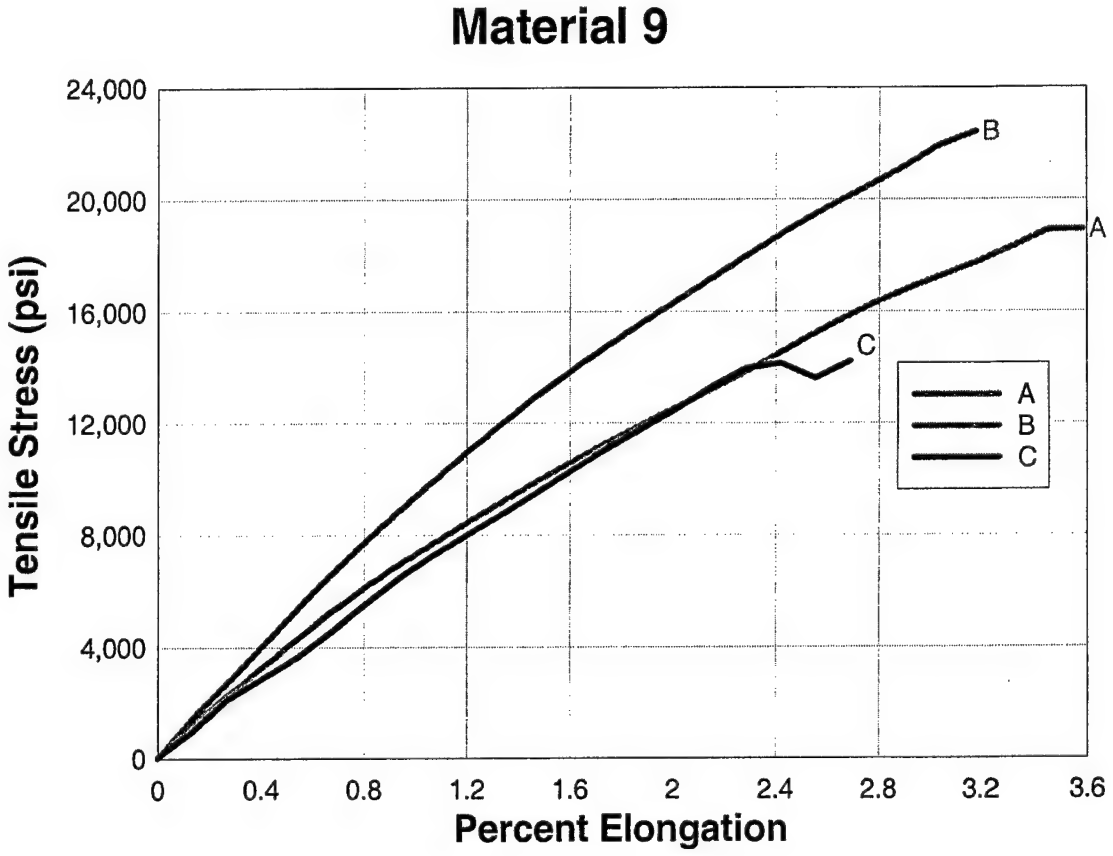

FIG. A9. Uniaxial Tension Test, Material 9

TABLE A10. Uniaxial Tension Test, Material 10

Sample Name	Maximum Tensile Stress (psi)	Elongation at Maximum Tensile Stress (%)	Maximum Elongation (%)	Secant Modulus (psi)	Toughness (psi*in/in)
A	9,450	6.0	21	205,000	1,470
B	9,470	5.8	20	204,000	1,390
C	9,350	5.9	22	205,000	1,520
Mean	9,420	5.9	21	205,000	1,460

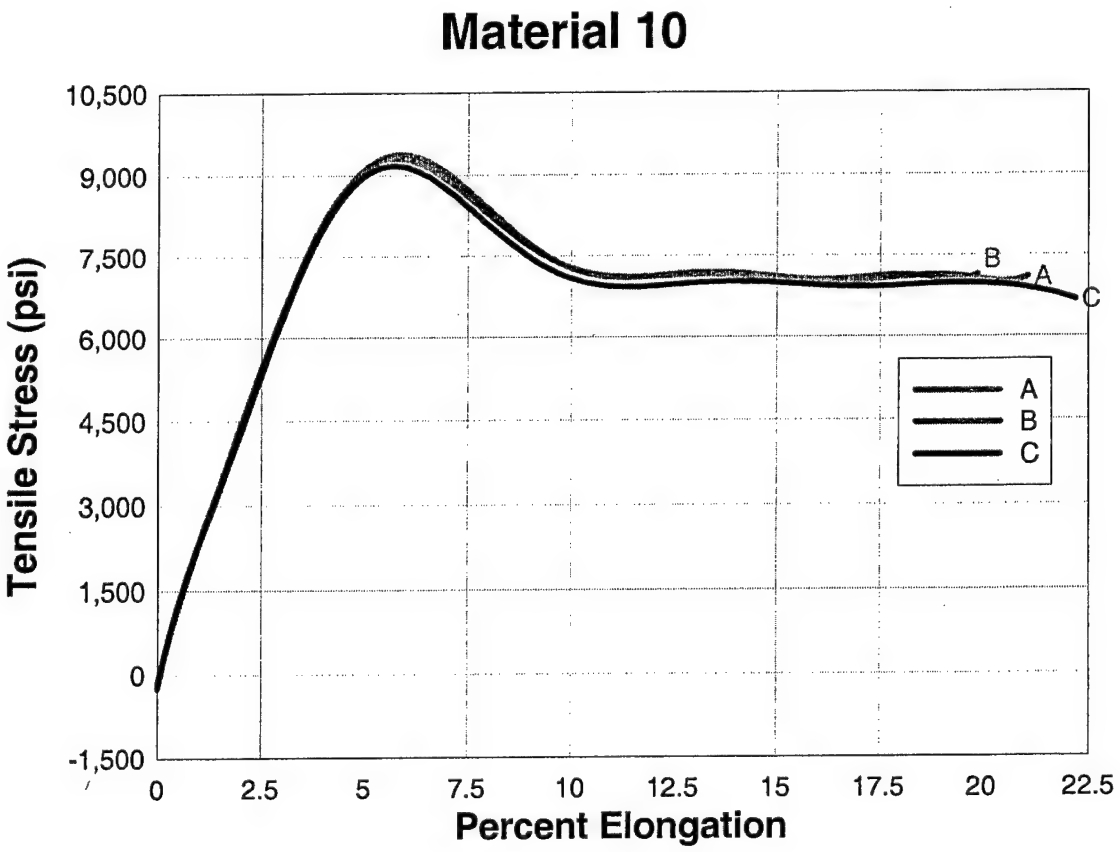

FIG. A10. Uniaxial Tension Test, Material 10

TABLE A11. Uniaxial Tension Test, Material 11

Sample Name	Maximum Tensile Stress (psi)	Elongation at Maximum Tensile Stress (%)	Maximum Elongation (%)	Secant Modulus (psi)	Toughness (psi*in/in)
A	8,860	5.7	13	200,000	804
B	8,930	5.8	21	201,000	1,470
C	8,730	5.6	22	198,000	1,460
Mean	8,830	5.7	21	200,000	1,470

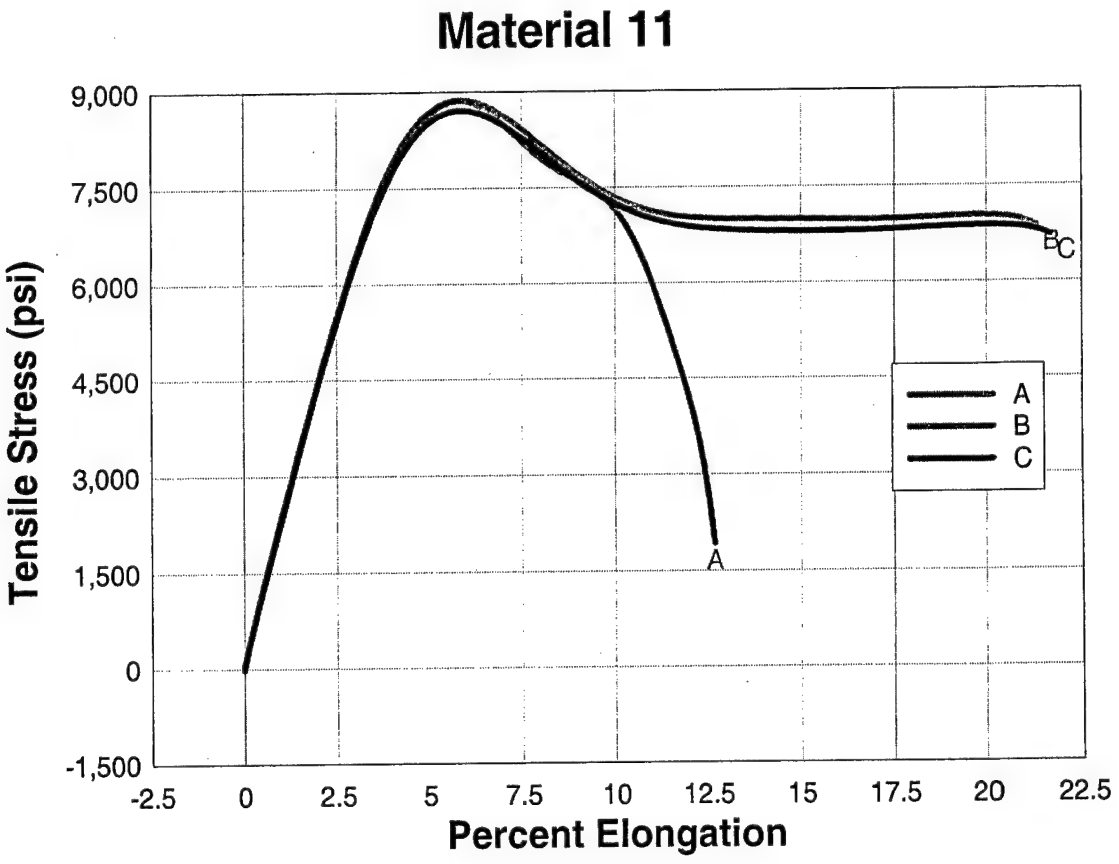

FIG. A11. Uniaxial Tension Test, Material 11

TABLE A12. Uniaxial Tension Test, Material 12

Sample Name	Maximum Tensile Stress (psi)	Elongation at Maximum Tensile Stress (%)	Maximum Elongation (%)	Secant Modulus (psi)	Toughness (psi*in/in)
A	2,010	250	251	14,500	3,740
B	1,930	246	253	13,200	3,720
C	1,600	160	202	12,900	2,730
Mean	1,970	248	252	13,900	3,730

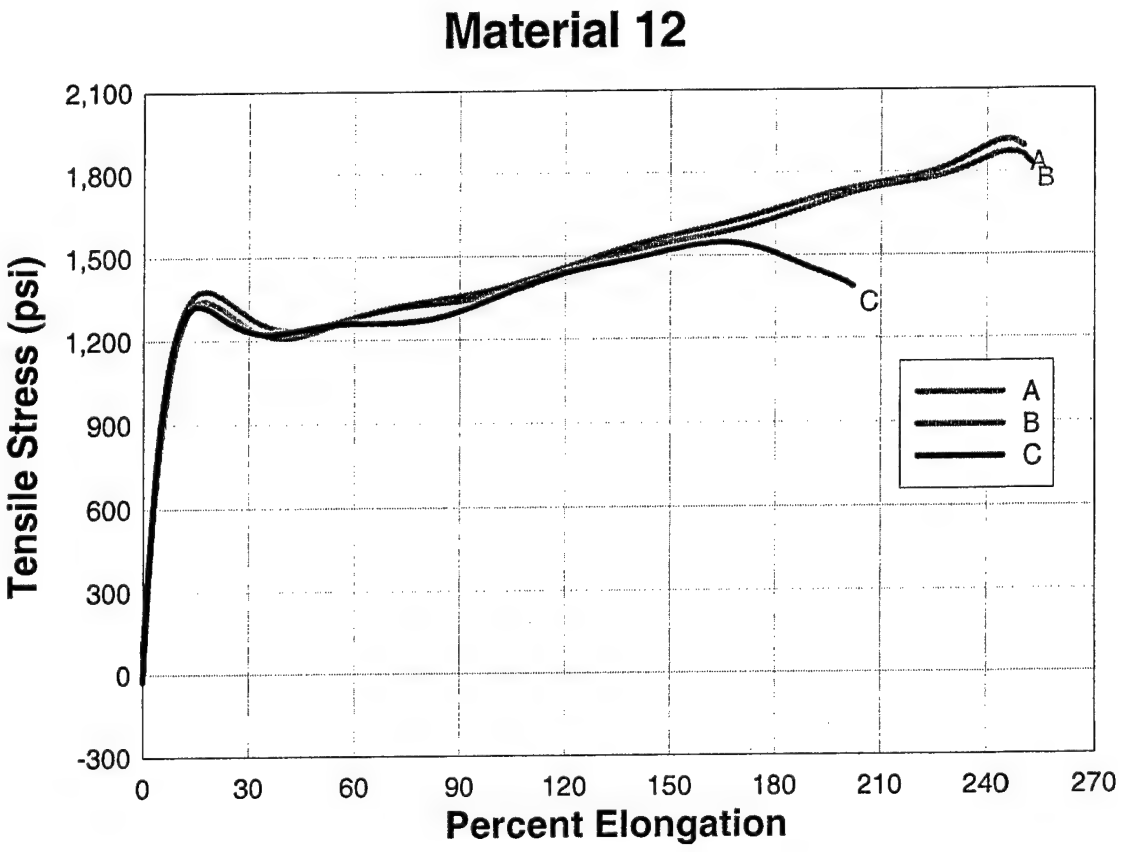

FIG. A12. Uniaxial Tension Test, Material 12

TABLE A13. Uniaxial Tension Test, Material 13

Sample Name	Maximum Tensile Stress (psi)	Elongation at Maximum Tensile Stress (%)	Maximum Elongation (%)	Secant Modulus (psi)	Toughness (psi*in/in)
A	1,560	185	194	12,600	2,480
B	1,490	175	194	9,810	2,390
C	1,830	204	221	13,600	3,270
Mean	1,630	188	203	12,000	2,710

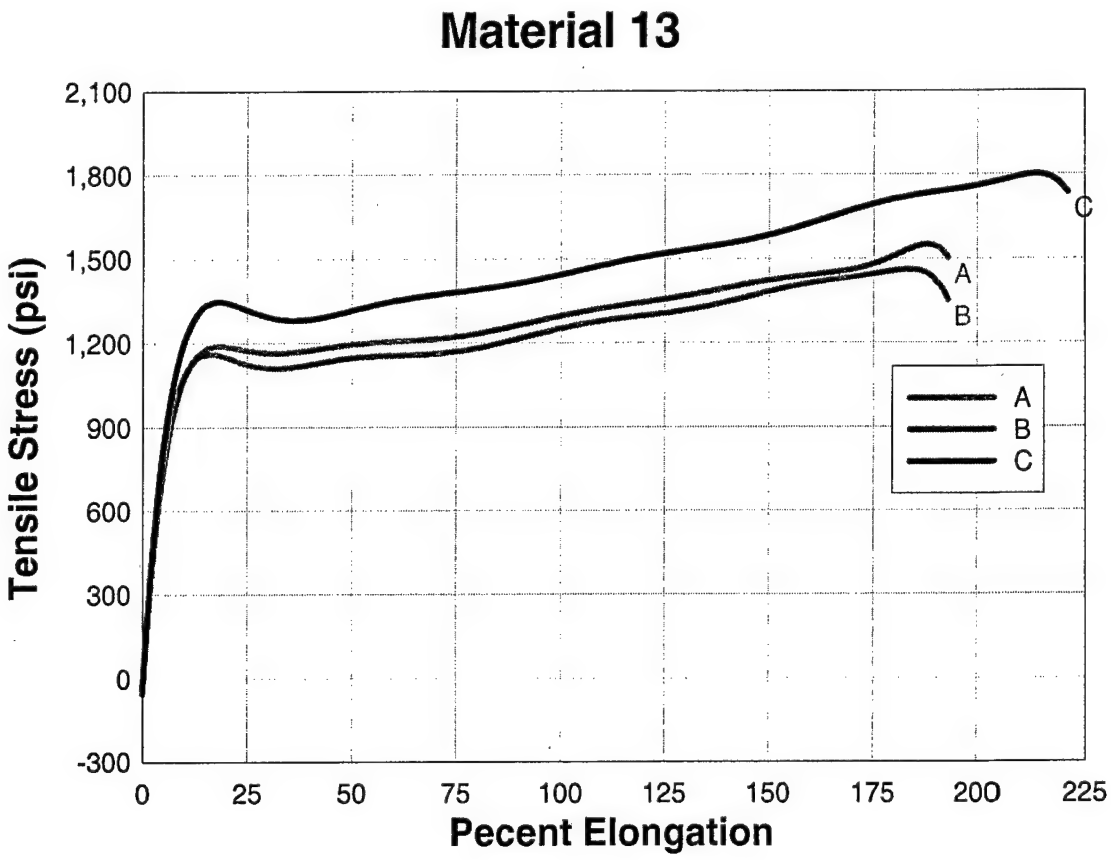

FIG. A13. Uniaxial Tension Test, Material 13

TABLE A14. Uniaxial Tension Test, Material 14

Sample Name	Maximum Tensile Stress (psi)	Elongation at Maximum Tensile Stress (%)	Maximum Elongation (%)	Secant Modulus (psi)	Toughness (psi*in/in)
A	21,400	3.9	3.9	581,000	460
B	23,800	4.2	4.2	572,000	569
C	17,300	3.3	3.3	503,000	308
Mean	20,800	3.8	3.8	552,000	445

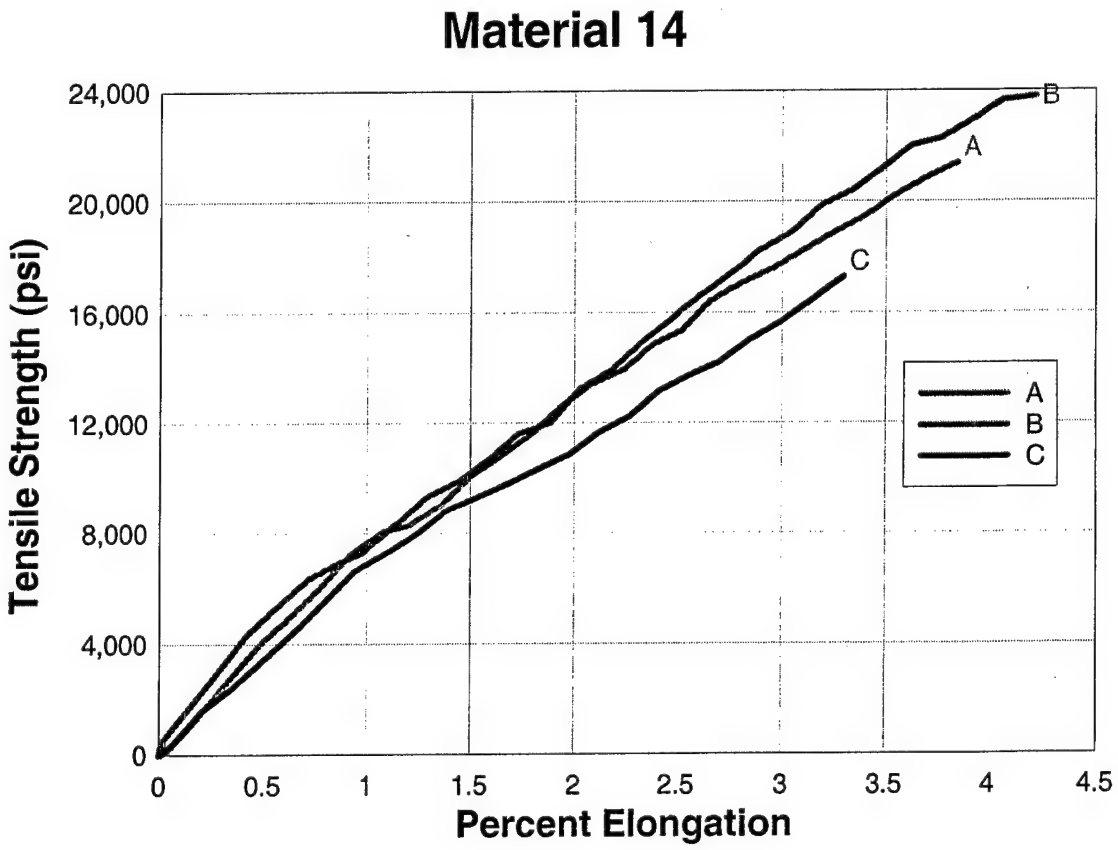

FIG. A14. Uniaxial Tension Test, Material 14

TABLE A15. Uniaxial Tension Test, Material 15

Sample Name	Maximum Tensile Stress (psi)	Elongation at Maximum Tensile Stress (%)	Maximum Elongation (%)	Secant Modulus (psi)	Toughness (psi*in/in)
A	26,500	5.3	5.3	419,000	612
B	20,000	5.1	5.1	385,000	511
C	21,200	4.4	5.0	487,000	562
Mean	22,600	4.9	5.1	430,000	562

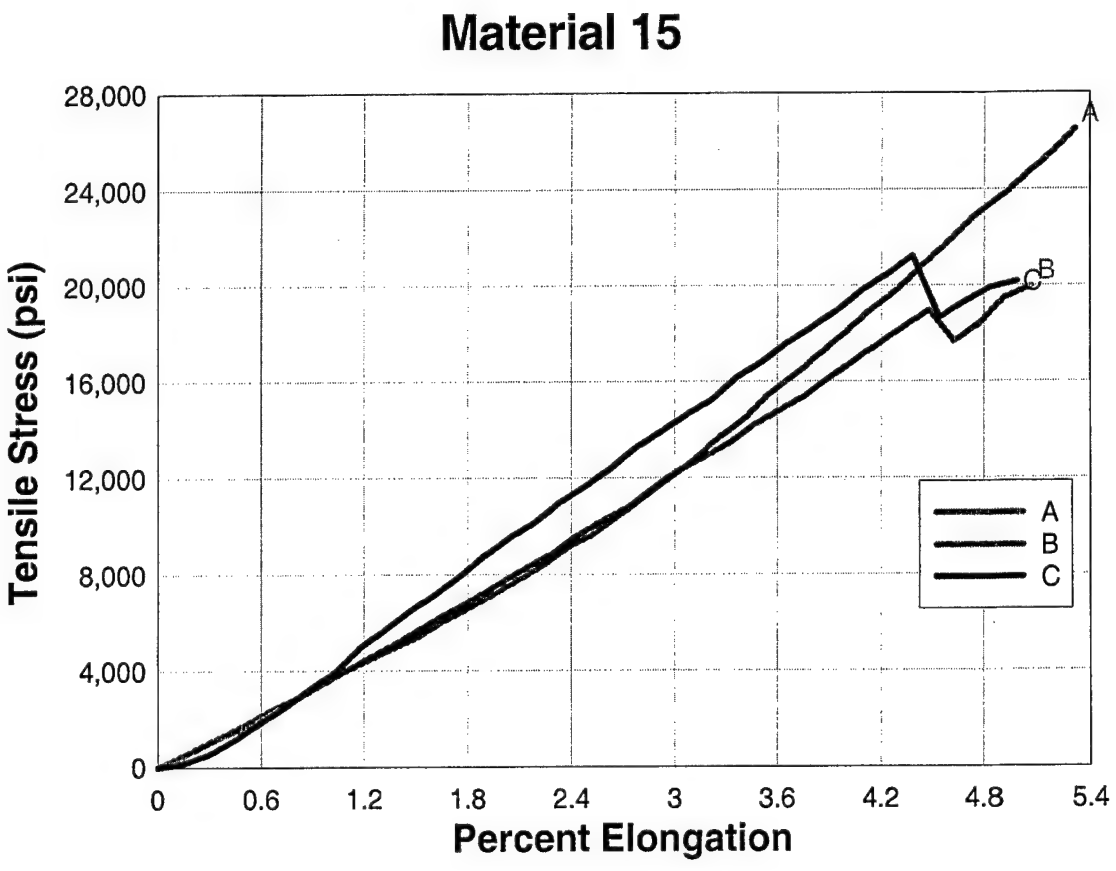

FIG. A15. Uniaxial Tension Test, Material 15

TABLE A16. Uniaxial Tension Test, Material 16

Sample Name	Maximum Tensile Stress (psi)	Elongation at Maximum Tensile Stress (%)	Maximum Elongation (%)	Secant Modulus (psi)	Toughness (psi*in/in)
A	2,130	153	157	11,300	2,620
B	2,130	159	160	10,600	2,680
C	2,010	142	144	11,100	2,280
Mean	2,090	151	153	11,000	2,530

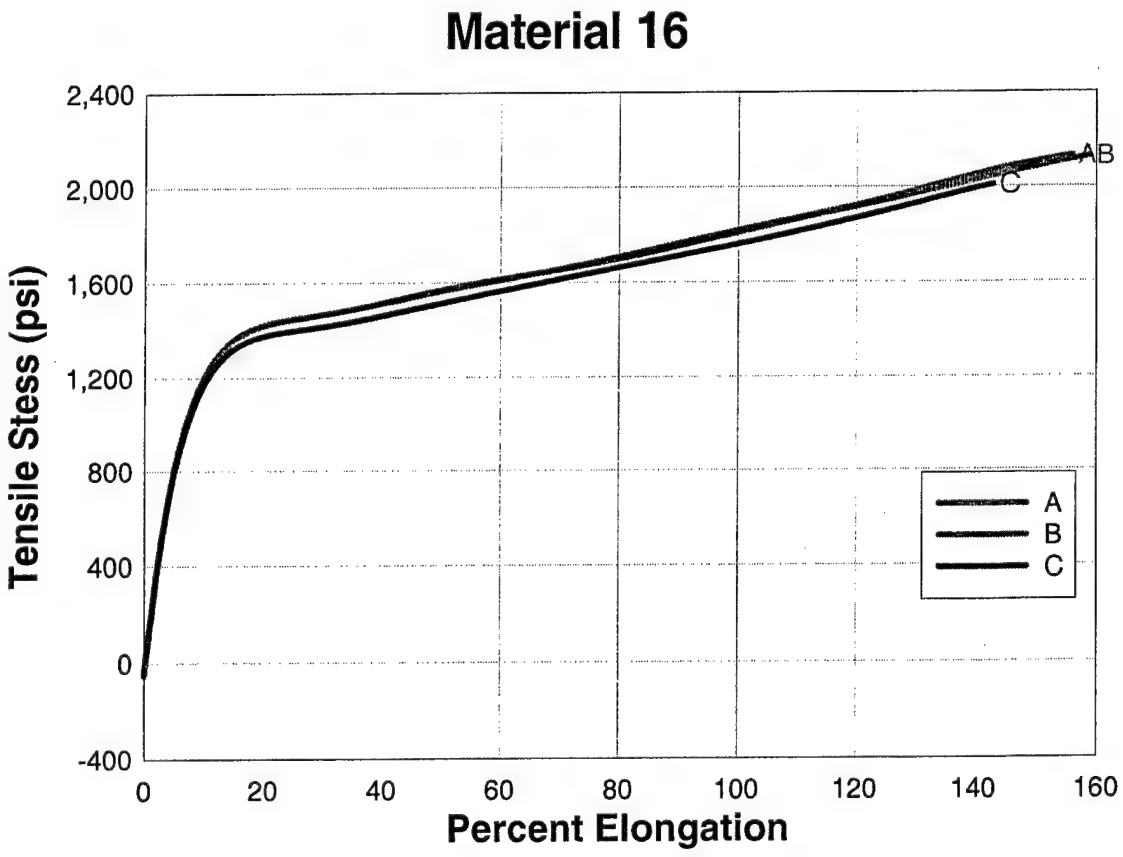

FIG. A16. Uniaxial Tension Test, Material 16

TABLE A17. Uniaxial Tension Test, Material 17

Sample Name	Maximum Tensile Stress (psi)	Elongation at Maximum Tensile Stress (%)	Maximum Elongation (%)	Secant Modulus (psi)	Toughness (psi*in/in)
A	1,170	86	106	4,110	945
B	1,160	81	92	4,460	818
C	1,150	102	105	4,690	898
Mean	1,160	90	101	4,420	887

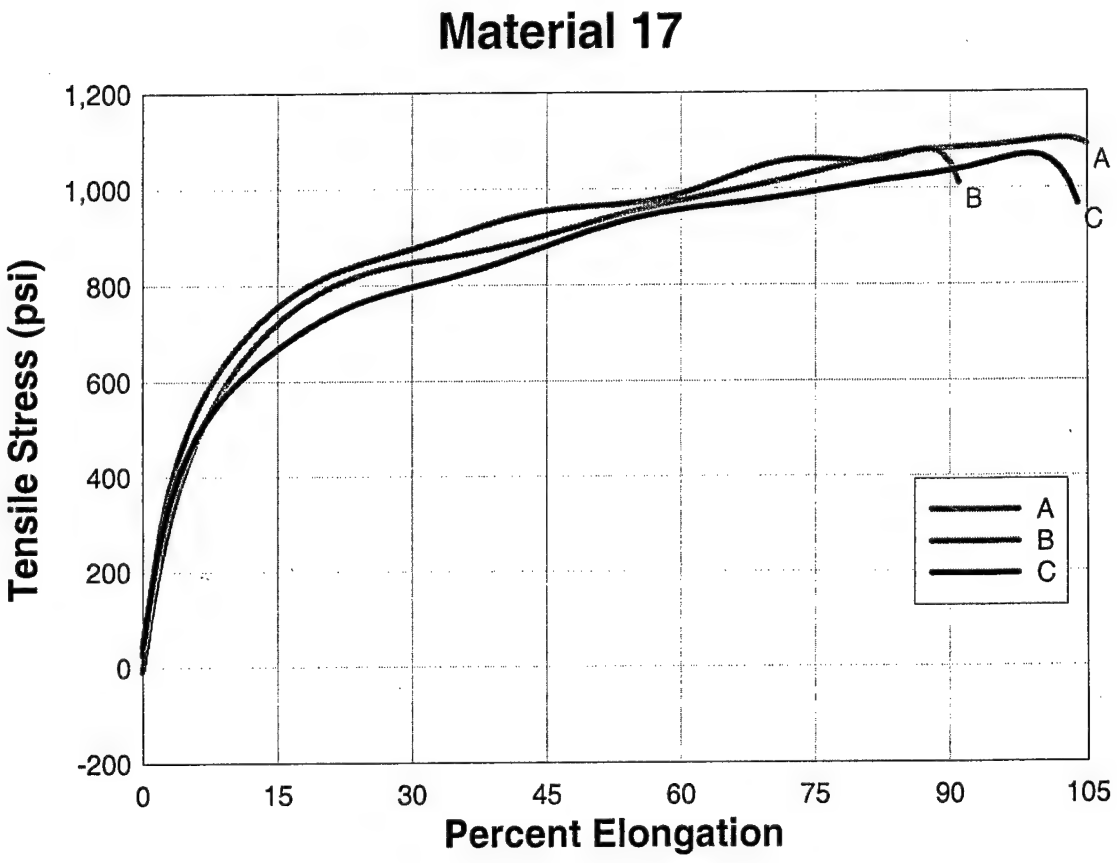

FIG. A17. Uniaxial Tension Test, Material 17

TABLE A18. Uniaxial Tension Test, Material 18

Sample Name	Maximum Tensile Stress (psi)	Elongation at Maximum Tensile Stress (%)	Maximum Elongation (%)	Secant Modulus (psi)	Toughness (psi*in/in)
A	2,250	35	35	9,300	505
B	1,530	22	23	8,880	228
C	1,690	26	28	8,370	296
Mean	1,610	24	26	8,630	262

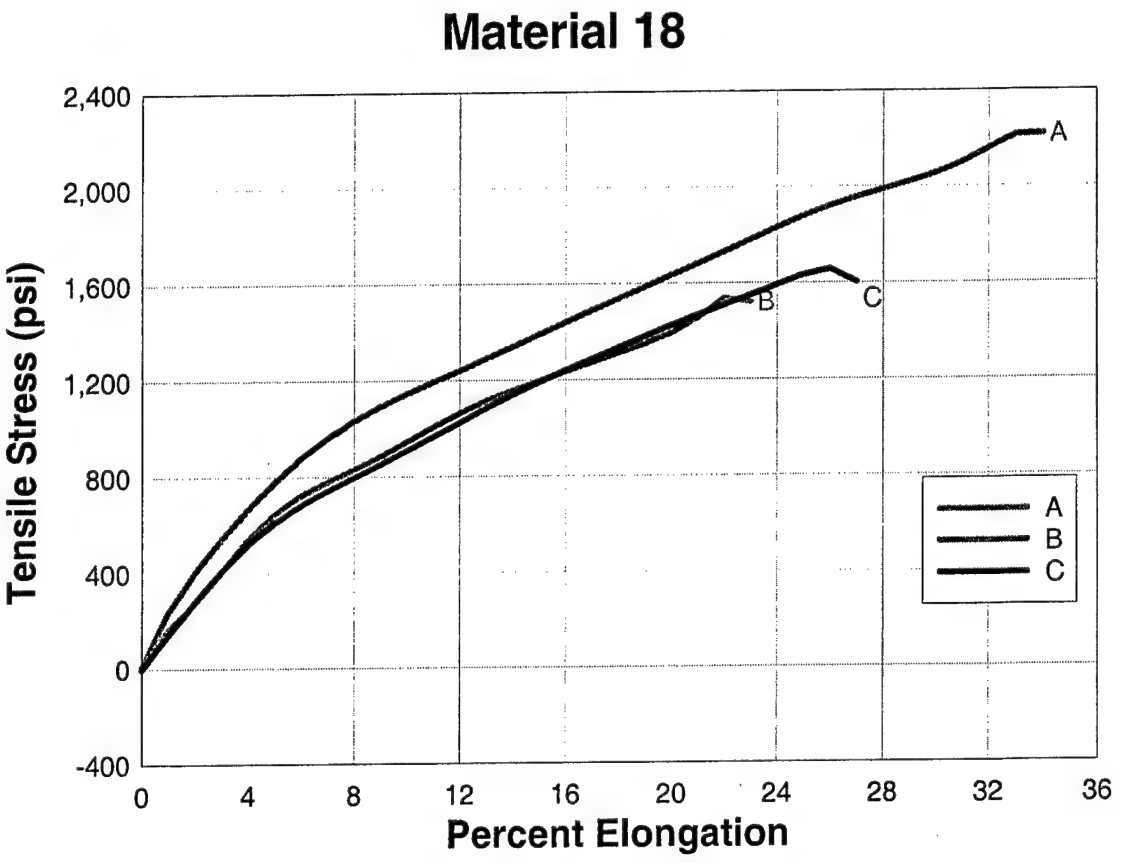

FIG. A18. Uniaxial Tension Test, Material 18

TABLE A19. Uniaxial Tension Test, Material 19

Sample Name	Maximum Tensile Stress (psi)	Elongation at Maximum Tensile Stress (%)	Maximum Elongation (%)	Secant Modulus (psi)	Toughness (psi*in/in)
A	2,730	38	38	9,300	632
B	2,700	34	35	10,100	607
C	2,200	31	32	9,370	450
Mean	2,540	34	35	9,590	563

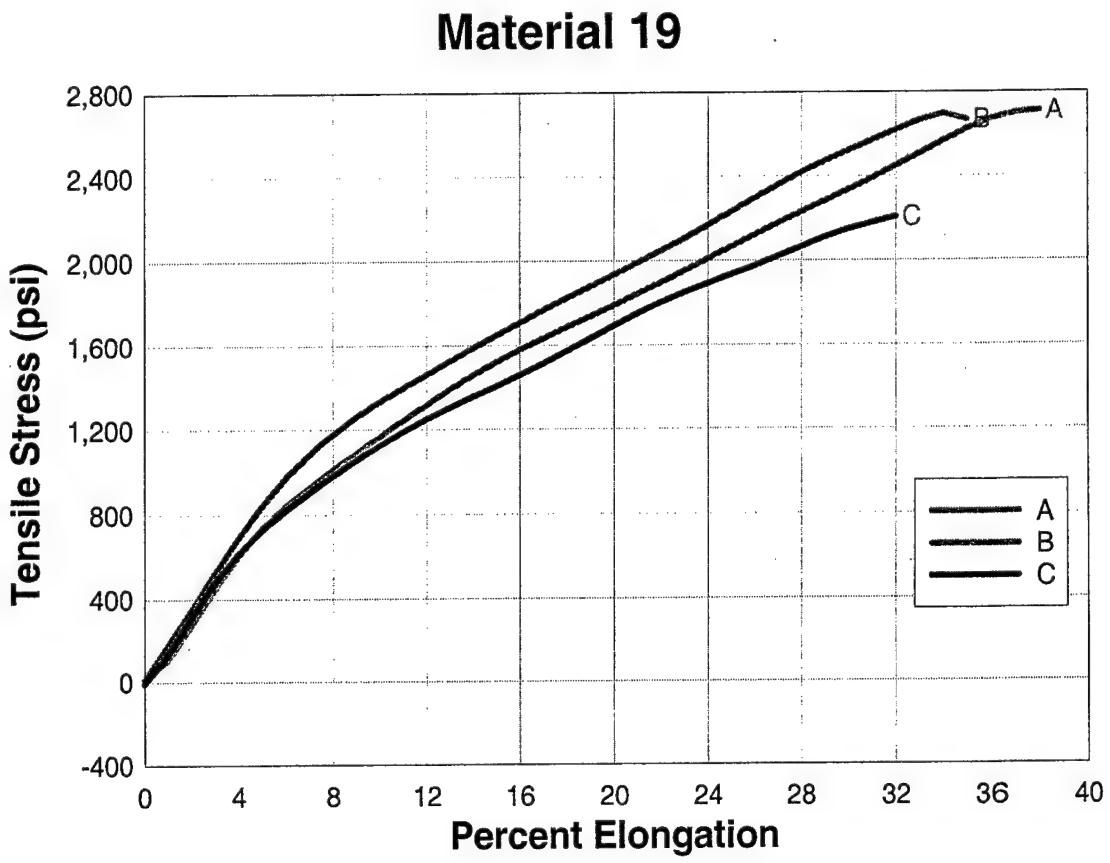

FIG. A19. Uniaxial Tension Test, Material 19

TABLE A20. Uniaxial Tension Test, Material 20

Sample Name	Maximum Tensile Stress (psi)	Elongation at Maximum Tensile Stress (%)	Maximum Elongation (%)	Secant Modulus (psi)	Toughness (psi*in/in)
A	2,500	300	300	8,320	5,210
B	2,390	298	300	8,750	5,100
C	2,340	299	299	8,090	4,970
Mean	2,410	299	300	8,390	5,090

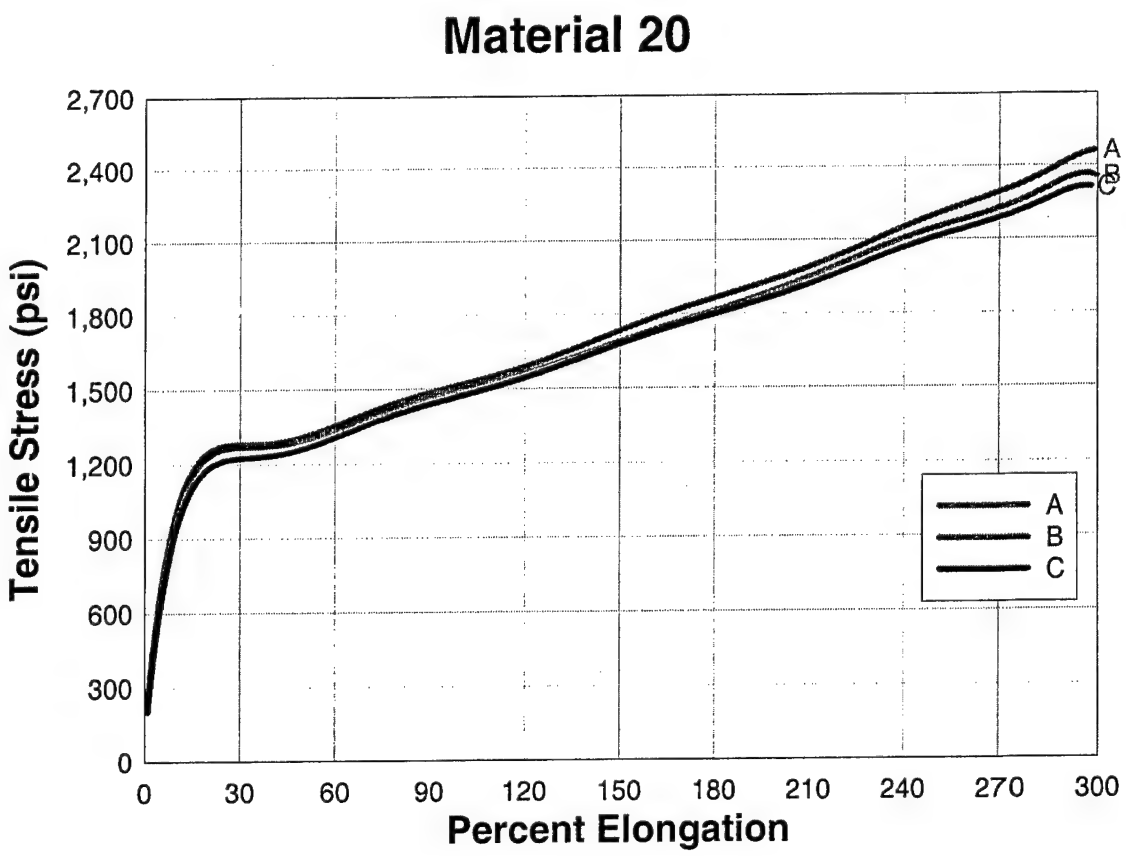

FIG. A20. Uniaxial Tension Test, Material 20

TABLE A21. Uniaxial Tension Test, Material 21

Sample Name	Maximum Tensile Stress (psi)	Elongation at Maximum Tensile Stress (%)	Maximum Elongation (%)	Secant Modulus (psi)	Toughness (psi*in/in)
A	2,680	268	268	2,240	4,500
B	3,150	292	294	2,060	5,660
C	2,270	213	213	3,660	3,170
Mean	2,700	258	258	2,650	4,440

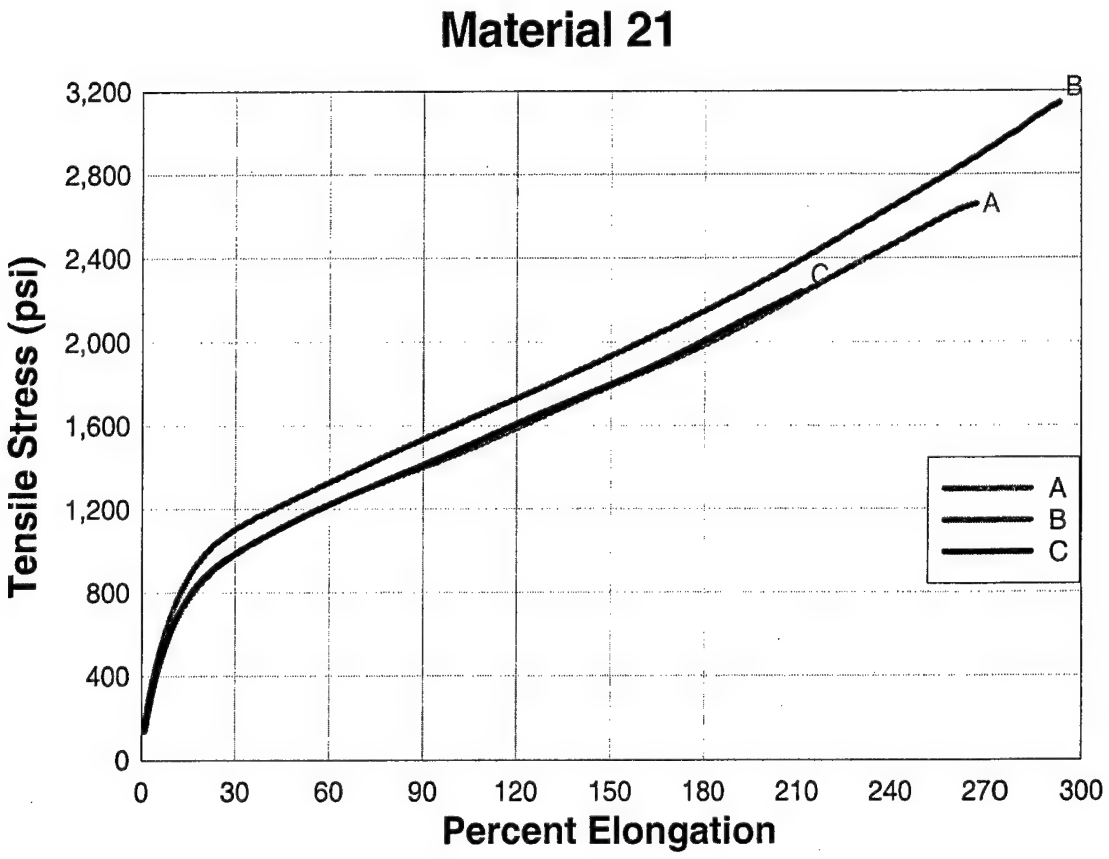

FIG. A21. Uniaxial Tension Test, Material 21

TABLE A22. Uniaxial Tension Test, Material 22

Sample Name	Maximum Tensile Stress (psi)	Elongation at Maximum Tensile Stress (%)	Maximum Elongation (%)	Secant Modulus (psi)	Toughness (psi*in/in)
A	2,680	268	268	1,150	4,500
B	2,390	298	300	1,520	5,100
C	2,340	299	298	1,620	4,970
Mean	2,370	299	299	1,570	5,040

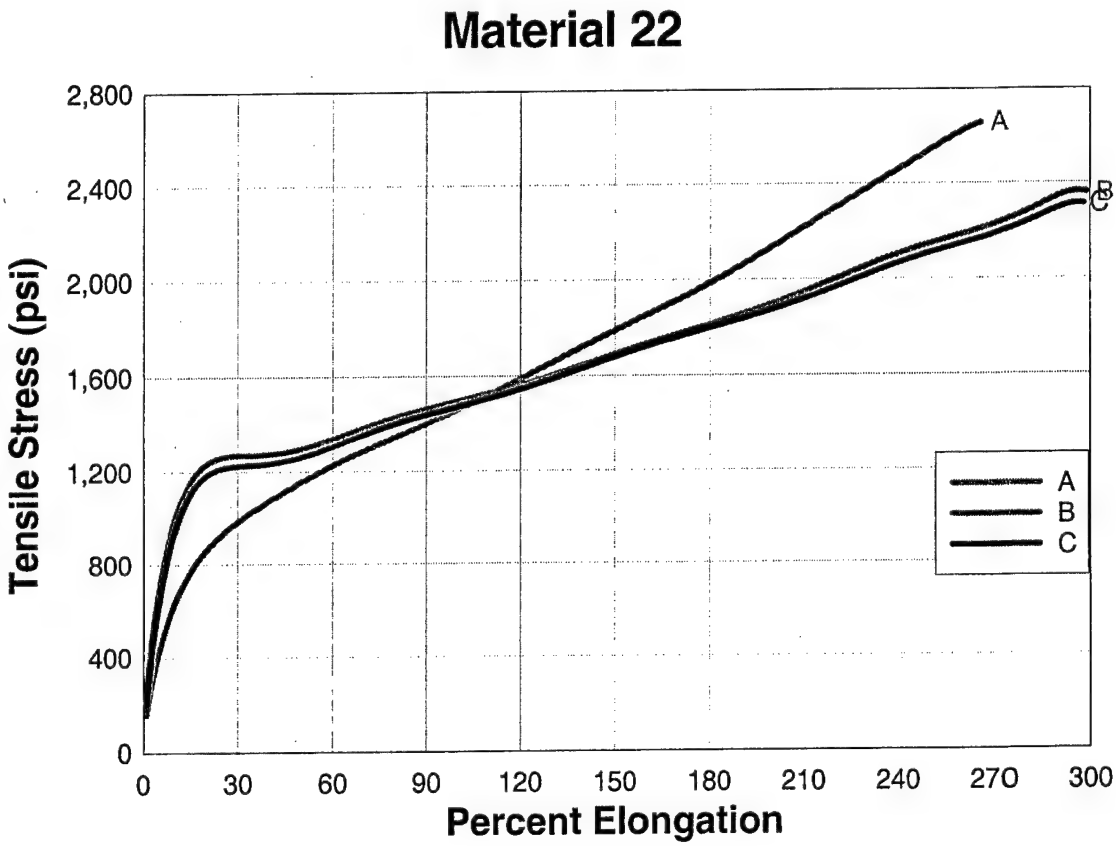

FIG. A22. Uniaxial Tension Test, Material 22

TABLE A23. Uniaxial Tension Test, Material 23

Sample Name	Maximum Tensile Stress (psi)	Elongation at Maximum Tensile Stress (%)	Maximum Elongation (%)	Secant Modulus (psi)	Toughness (psi*in/in)
A	1,130	300	300	2,280	2,370
B	1,120	295	300	2,280	2,370
C	1,130	299	300	1,940	2,360
Mean	1,130	298	300	2,170	2,370

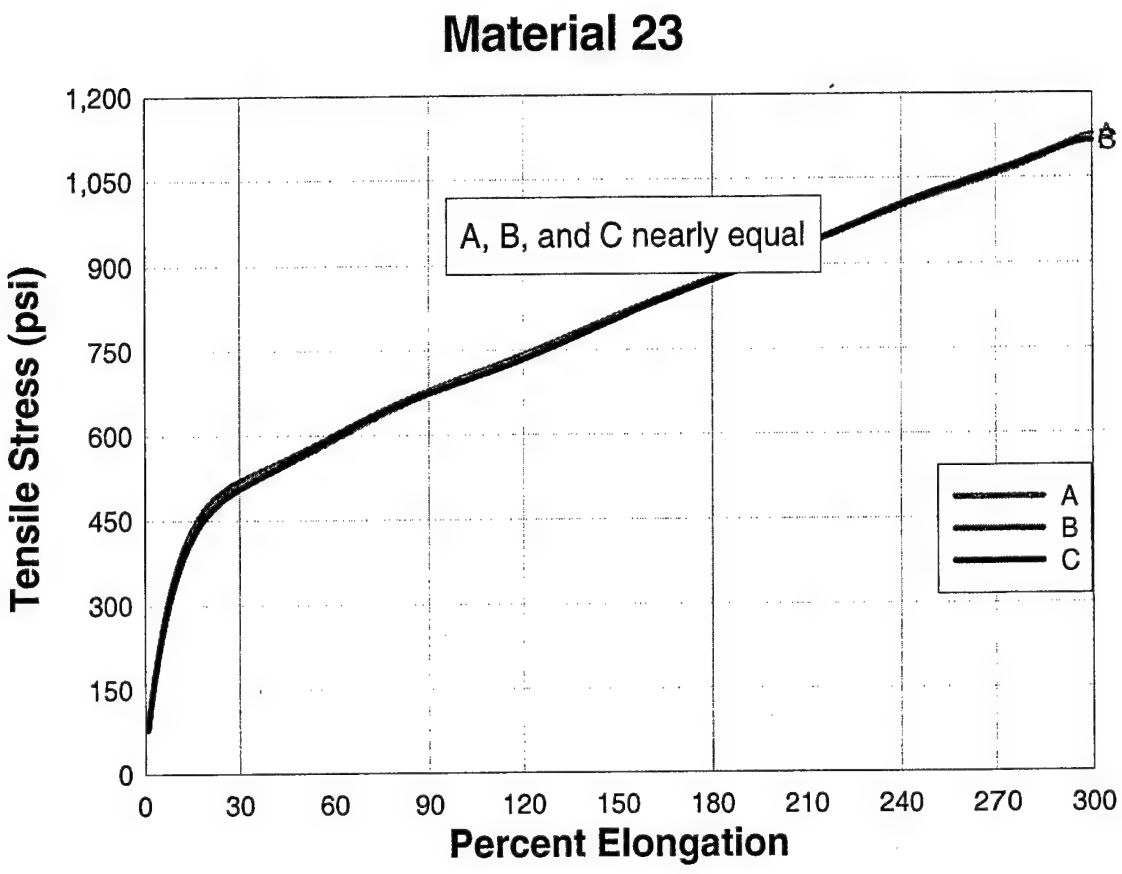

FIG. A23. Uniaxial Tension Test, Material 23

TABLE A24. Uniaxial Tension Test, Material 24

Sample Name	Maximum Tensile Stress (psi)	Elongation at Maximum Tensile Stress (%)	Maximum Elongation (%)	Secant Modulus (psi)	Toughness (psi*in/in)
A	1,250	296	300	1,100	2,450
B	1,320	298	300	1,120	2,600
C	1,330	298	300	1,110	2,570
Mean	1,300	298	300	1,110	2,540

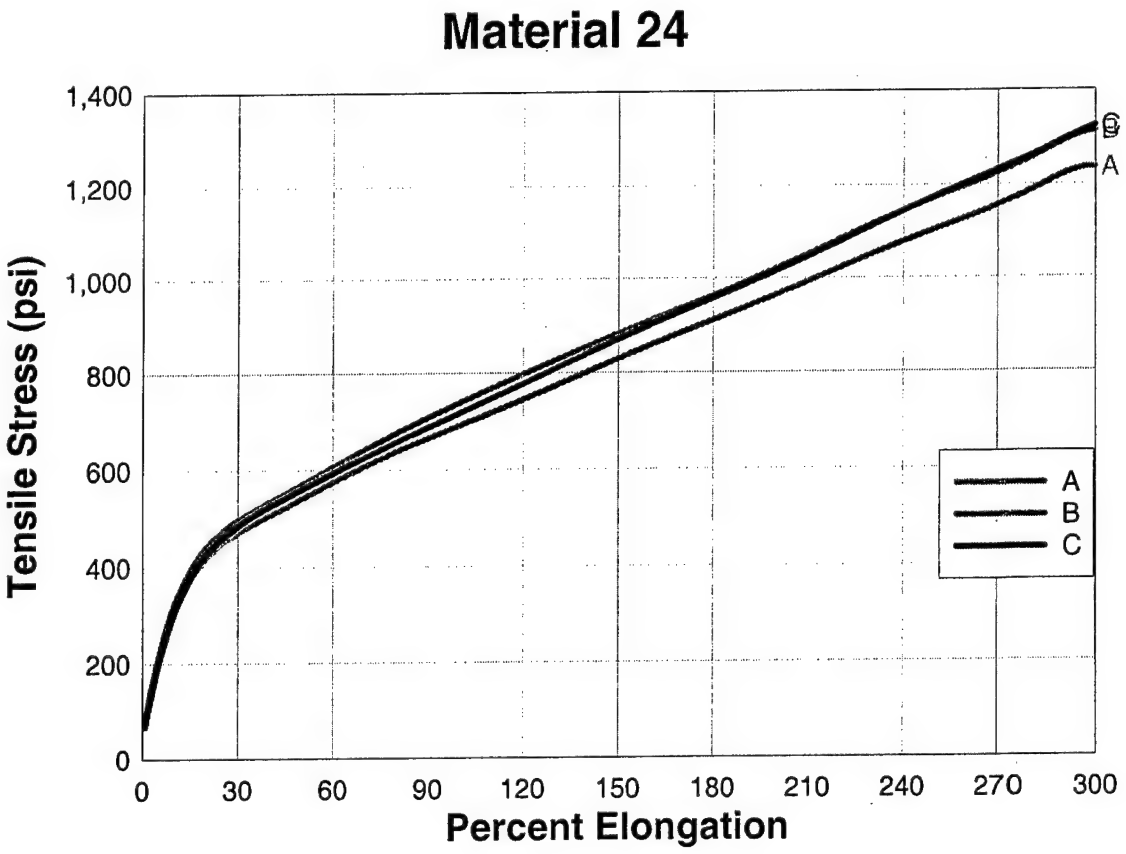

FIG. A24. Uniaxial Tension Test, Material 24

TABLE A25. Uniaxial Tension Test, Material 25

Sample Name	Maximum Tensile Stress (psi)	Elongation at Maximum Tensile Stress (%)	Maximum Elongation (%)	Secant Modulus (psi)	Toughness (psi*in/in)
A	2,500	300	300	1,370	5,210
B	1,120	295	300	670	2,370
C	1,130	299	300	668	2,360
Mean	1,130	297	300	669	2,370

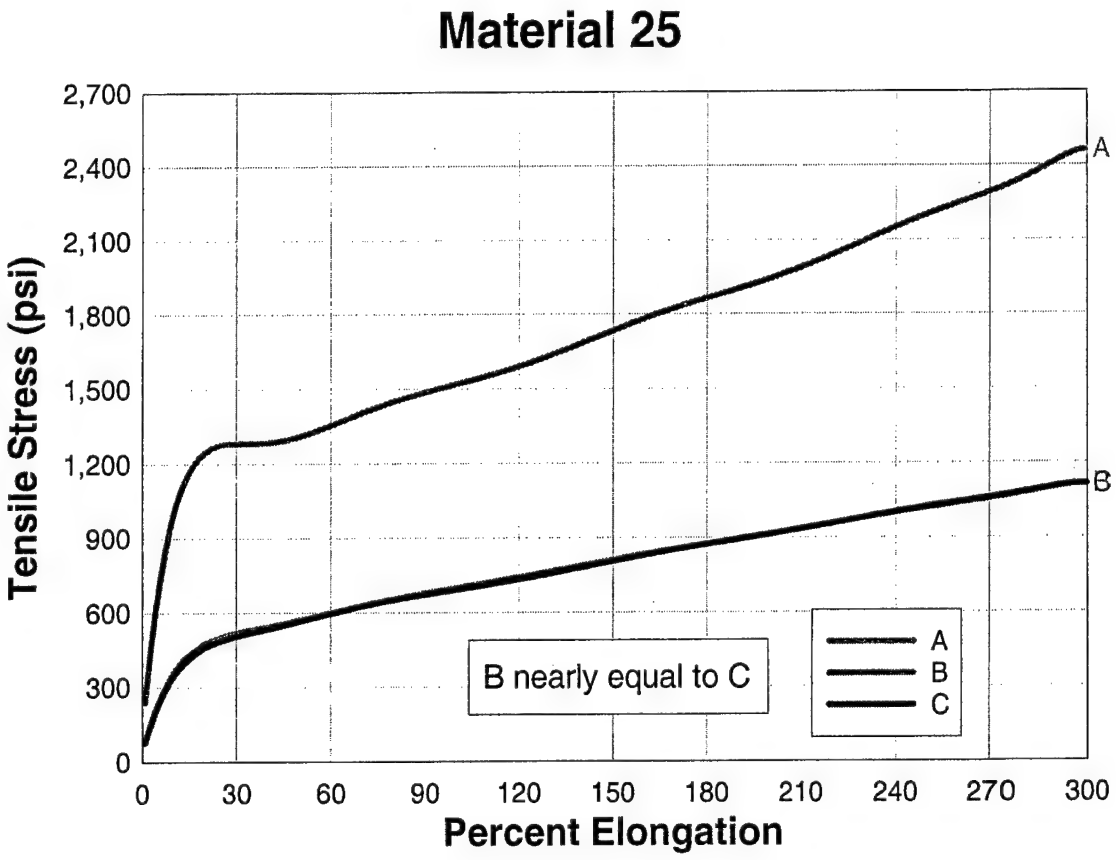

FIG. A25. Uniaxial Tension Test, Material 25

TABLE A26. Uniaxial Tension Test, Material 26

Sample Name	Maximum Tensile Stress (psi)	Elongation at Maximum Tensile Stress (%)	Maximum Elongation (%)	Secant Modulus (psi)	Toughness (psi*in/in)
A	1,540	266	267	1,660	3,020
B	1,520	267	267	2,220	3,010
C	1,560	266	267	2,170	3,100
Mean	1,540	266	267	2,020	3,040

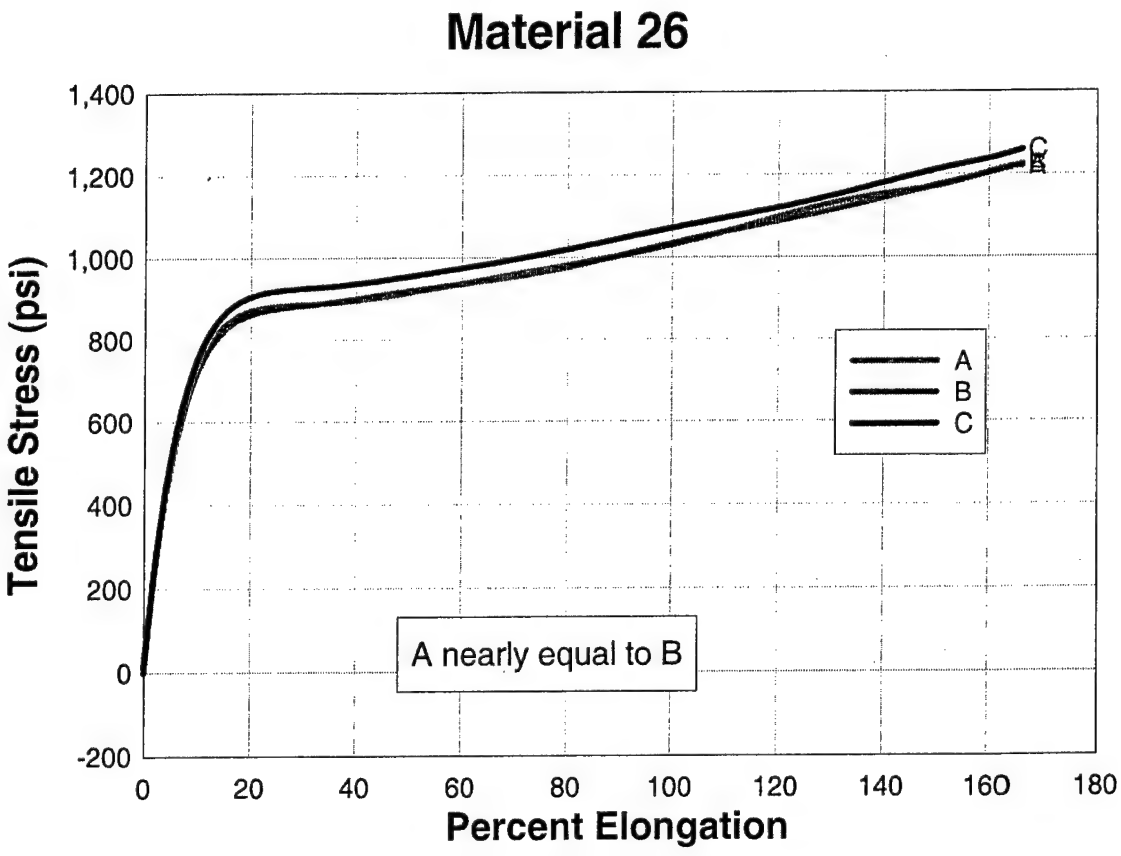

FIG. A26. Uniaxial Tension Test, Material 26

TABLE A27. Uniaxial Tension Test, Material 27

Sample Name	Maximum Tensile Stress (psi)	Elongation at Maximum Tensile Stress (%)	Maximum Elongation (%)	Secant Modulus (psi)	Toughness (psi*in/in)
A	2,570	44	44	8,750	727
B	2,000	32	32	9,040	429
C	2,450	47	47	7,860	729
Mean	2,340	41	41	8,550	628

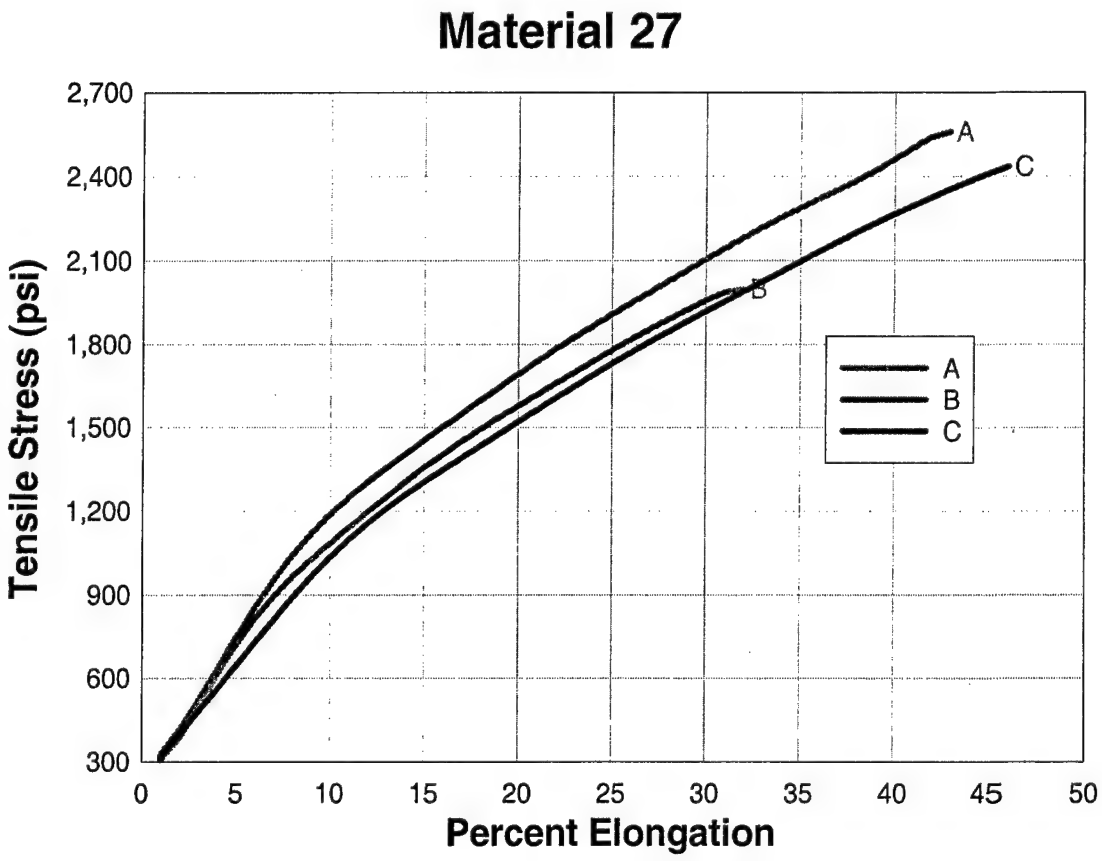

FIG. A27. Uniaxial Tension Test, Material 27

TABLE A28. Uniaxial Tension Test, Material 28

Sample Name	Maximum Tensile Stress (psi)	Elongation at Maximum Tensile Stress (%)	Maximum Elongation (%)	Secant Modulus (psi)	Toughness (psi*in/in)
A	2,570	44	44	8,750	727
B	3,470	51	52	8,800	1,100
C	3,160	48	48	8,850	950
Mean	3,070	47	47	8,800	926

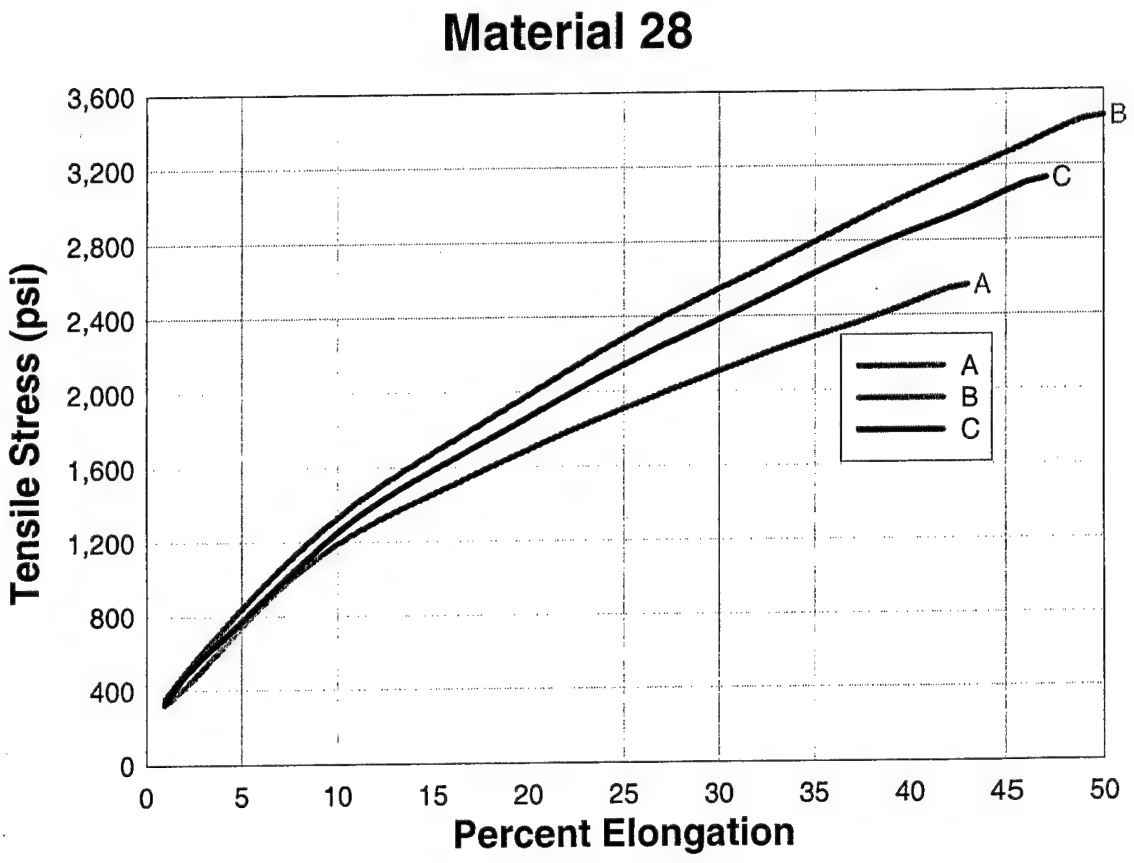

FIG. A28. Uniaxial Tension Test, Material 28

TABLE A29. Uniaxial Tension Test, Material 29

Sample Name	Maximum Tensile Stress (psi)	Elongation at Maximum Tensile Stress (%)	Maximum Elongation (%)	Secant Modulus (psi)	Toughness (psi*in/in)
A	3,410	47	47	8,760	1,010
B	3,470	52	51	8,800	1,100
C	3,170	48	48	8,850	950
Mean	3,350	49	49	8,810	1,020

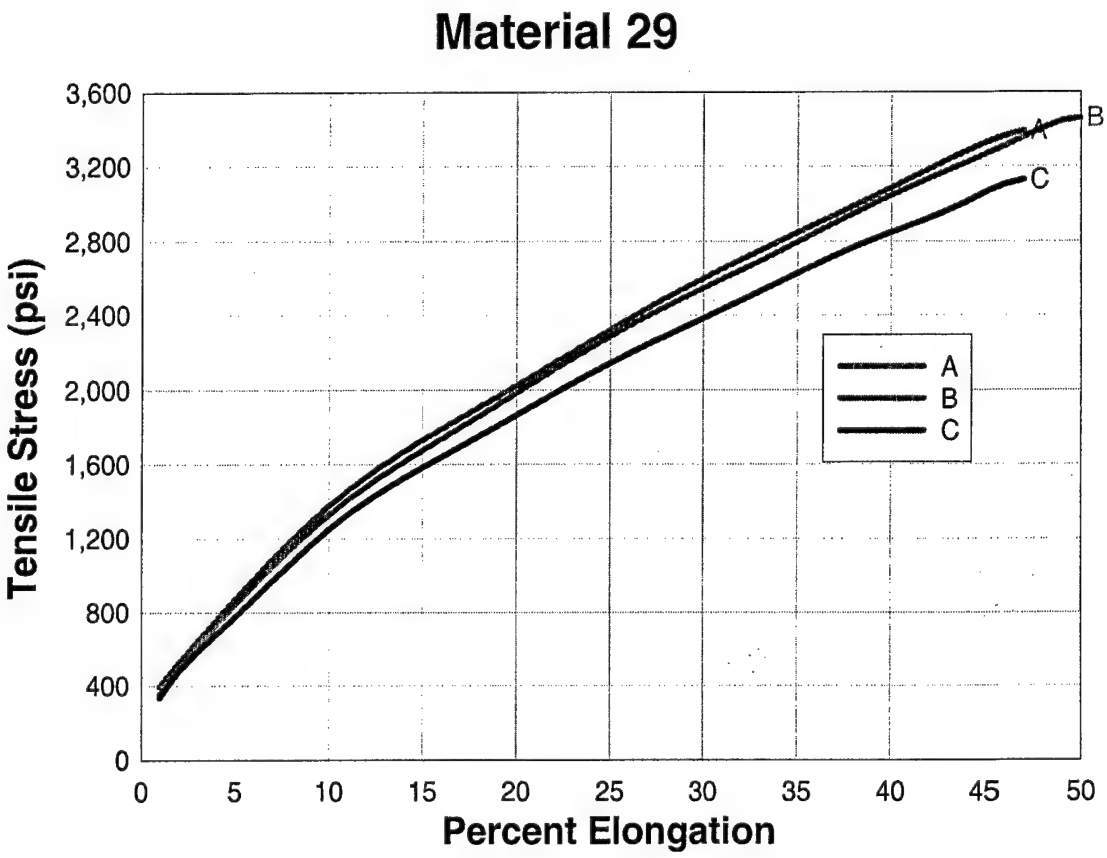

FIG. A29. Uniaxial Tension Test, Material 29

TABLE A30. Uniaxial Tension Test, Material 30

Sample Name	Maximum Tensile Stress (psi)	Elongation at Maximum Tensile Stress (%)	Maximum Elongation (%)	Secant Modulus (psi)	Toughness (psi*in/in)
A	742	93	93	1,010	436
B	900	103	104	1,230	596
C	639	83	84	885	317
Mean	760	93	94	1,040	450

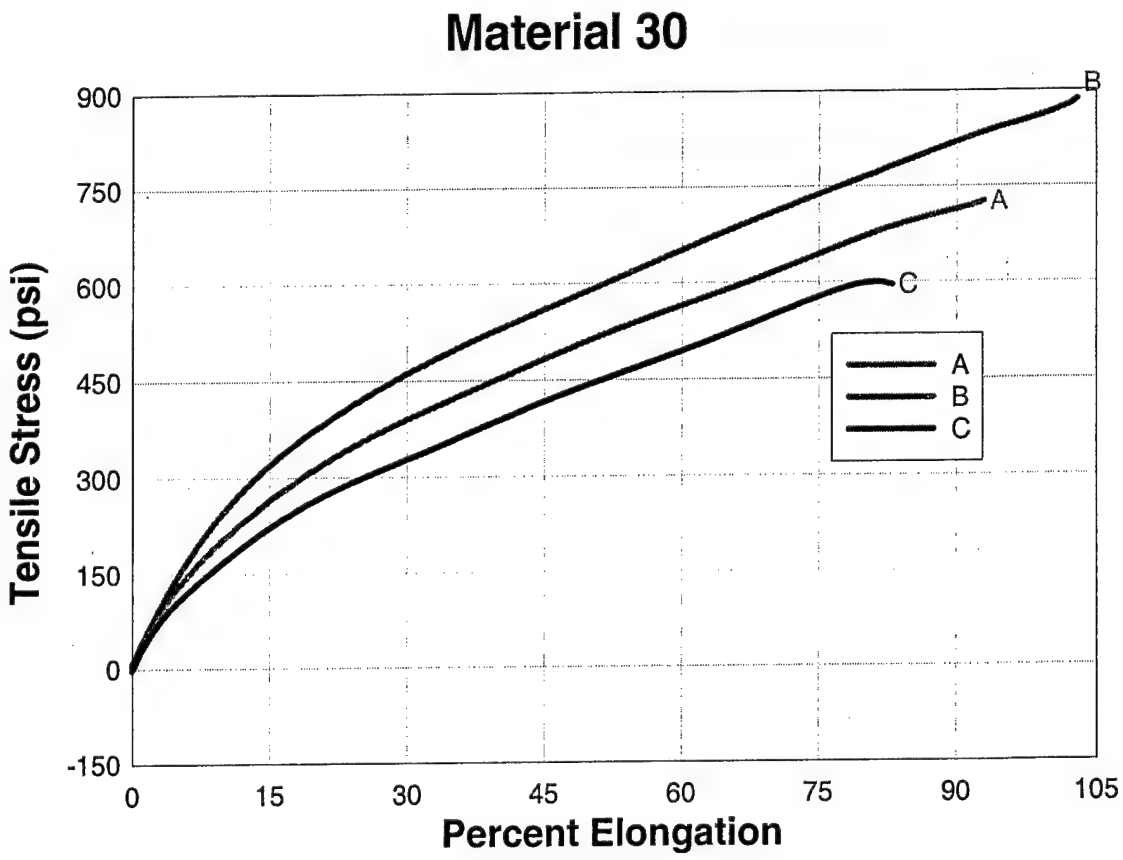

FIG. A30. Uniaxial Tension Test, Material 30

TABLE A31. Uniaxial Tension Test, Material 31

Sample Name	Maximum Tensile Stress (psi)	Elongation at Maximum Tensile Stress (%)	Maximum Elongation (%)	Secant Modulus (psi)	Toughness (psi*in/in)
A	1,500	88	105	3,210	1,120
B	1,550	100	109	3,390	1,200
C	1,650	111	112	3,430	1,310
Mean	1,570	100	108	3,340	1,210

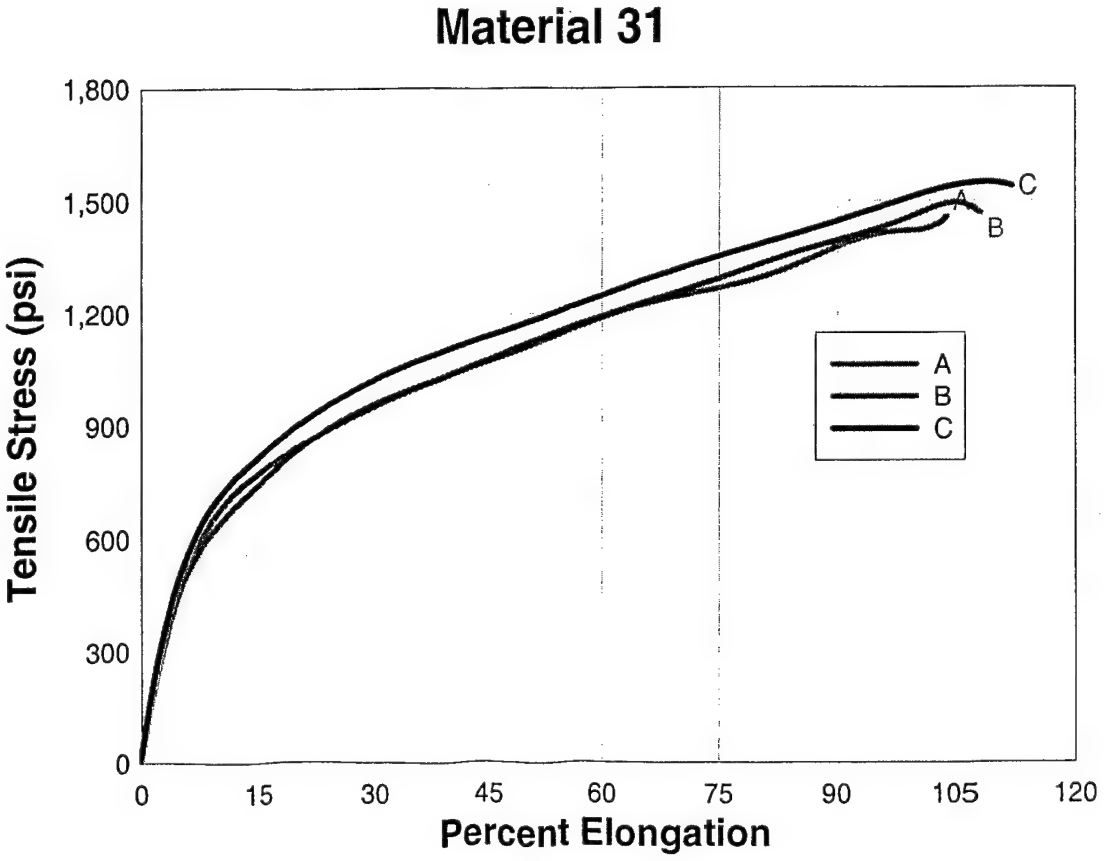

FIG. A31. Uniaxial Tension Test, Material 31

TABLE A32. Uniaxial Tension Test, Material 32

Sample Name	Maximum Tensile Stress (psi)	Elongation at Maximum Tensile Stress (%)	Maximum Elongation (%)	Secant Modulus (psi)	Toughness (psi*in/in)
A	310	21	27	1,440	54
B	287	21	24	582	39
Mean	298	21	25	1,010	46

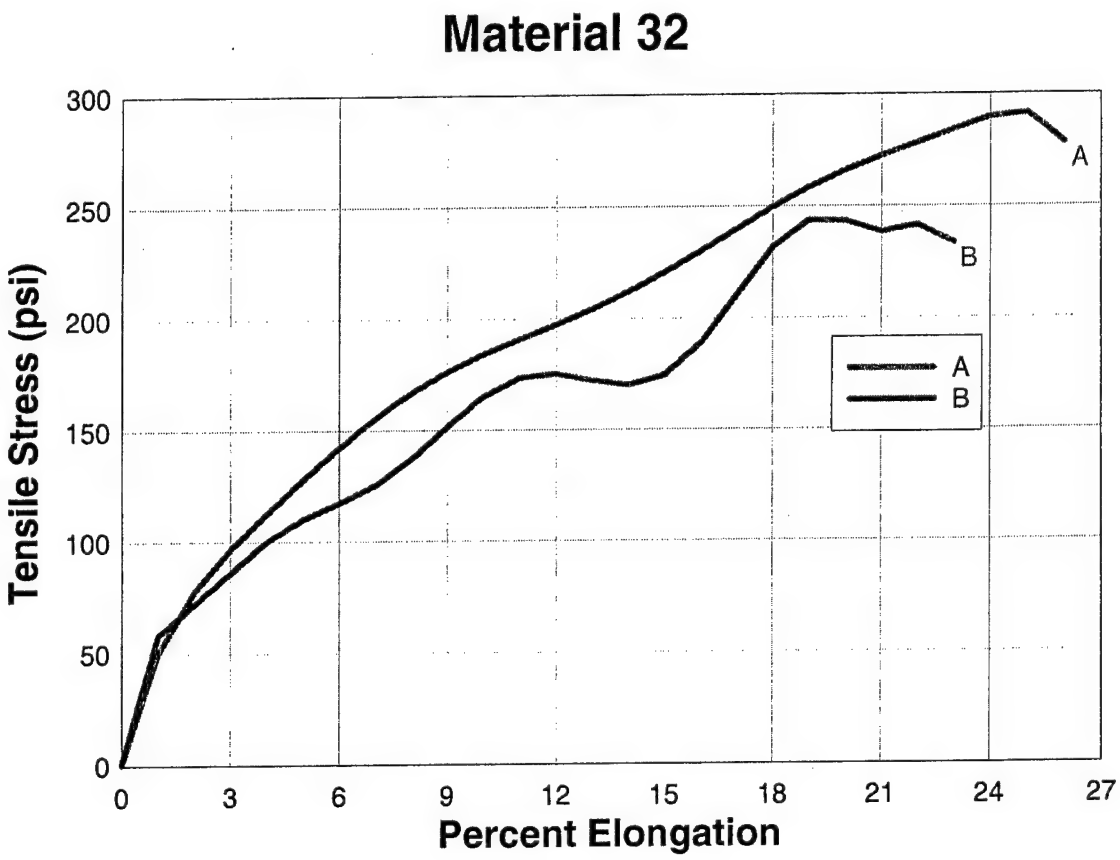

FIG. A32. Uniaxial Tension Test, Material 32

TABLE A33. Uniaxial Tension Test, Material 33

Sample Name	Maximum Tensile Stress (psi)	Elongation at Maximum Tensile Stress (%)	Maximum Elongation (%)	Secant Modulus (psi)	Toughness (psi*in/in)
A	1,340	95	102	6,930	1,060
B	1,370	96	104	6,820	1,140
Mean	1,360	95	103	6,880	1,100

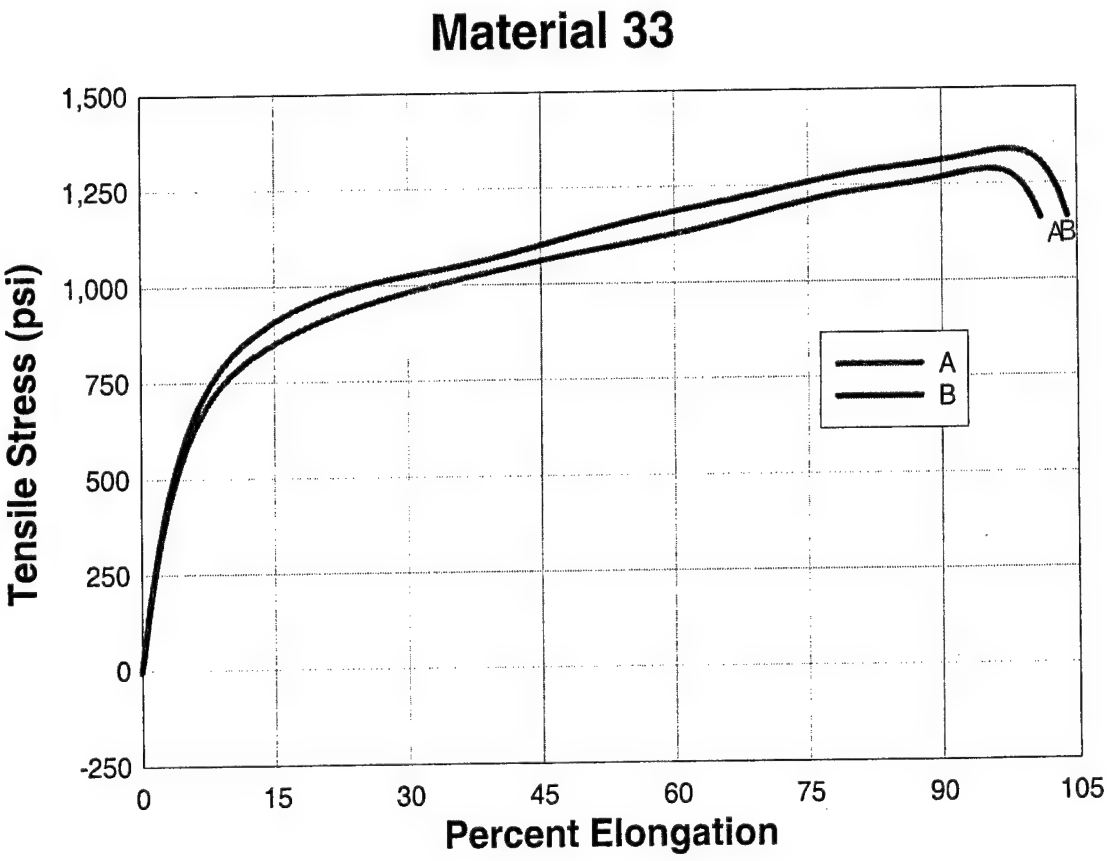

FIG. A33. Uniaxial Tension Test, Material 33

TABLE A34. Uniaxial Tension Test, Material 34

Sample Name	Maximum Tensile Stress (psi)	Elongation at Maximum Tensile Stress (%)	Maximum Elongation (%)	Secant Modulus (psi)	Toughness (psi*in/in)
A	794	60	64	1,720	328
B	869	74	84	1,670	478
C	830	74	76	1,560	412
Mean	831	69	75	1,650	406

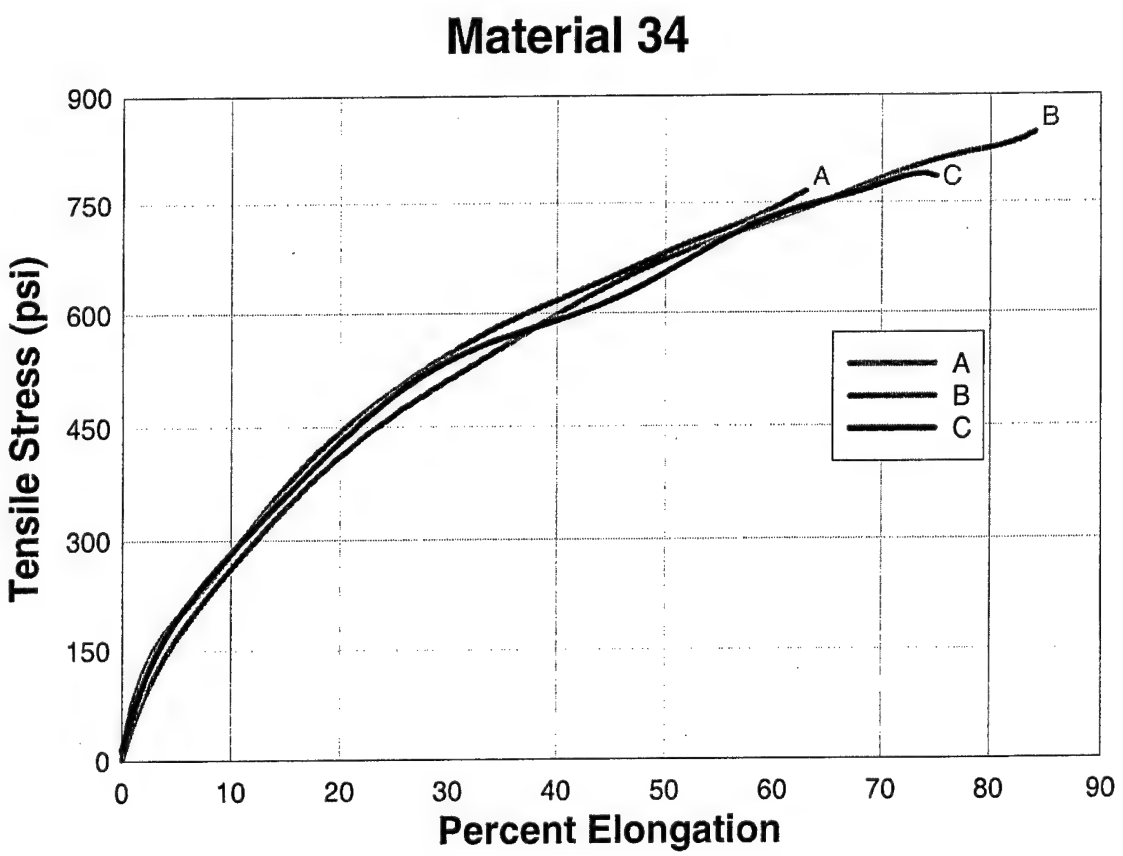

FIG. A34. Uniaxial Tension Test, Material 34

TABLE A35. Uniaxial Tension Test, Material 35

Sample Name	Maximum Tensile Stress (psi)	Elongation at Maximum Tensile Stress (%)	Maximum Elongation (%)	Secant Modulus (psi)	Toughness (psi*in/in)
A	918	84	86	1,780	507
B	802	68	71	1,660	377
C	970	103	103	1,410	667
Mean	896	85	87	1,620	517

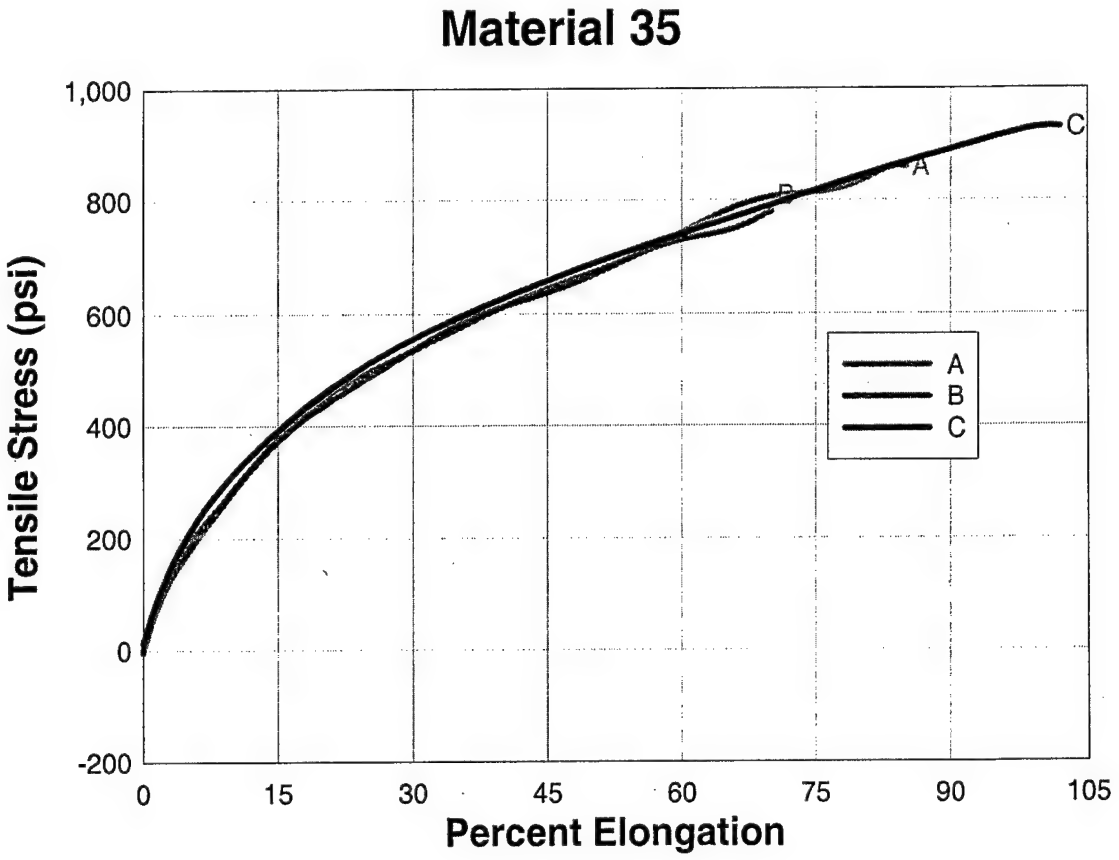

FIG. A35. Uniaxial Tension Test, Material 35

TABLE A36. Uniaxial Tension Test, Material 36

Sample Name	Maximum Tensile Stress (psi)	Elongation at Maximum Tensile Stress (%)	Maximum Elongation (%)	Secant Modulus (psi)	Toughness (psi*in/in)
A	2,120	400	400	25,150	5,500
B	1,350	262	267	2,090	2,700
C	1,470	266	267	3,370	2,900
Mean	1,410	264	267	2,730	2,800

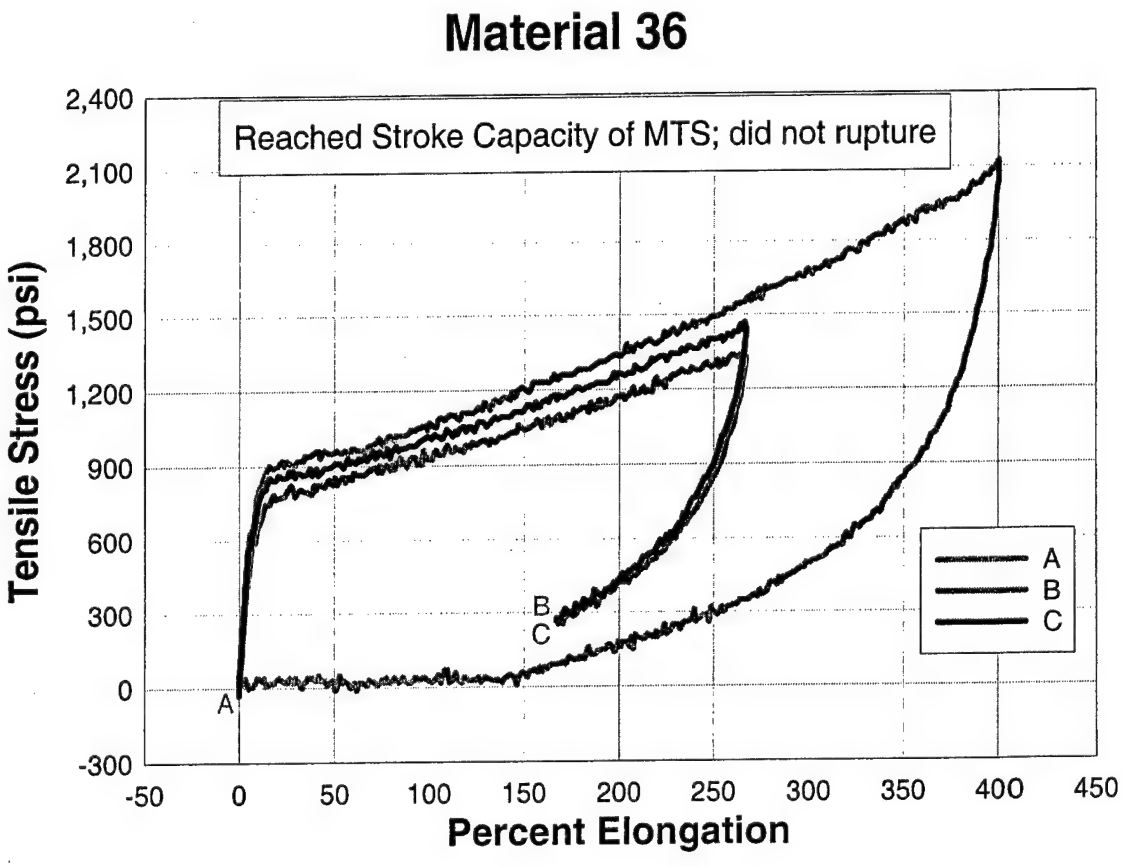

FIG. A36. Uniaxial Tension Test, Material 36

TABLE A37. Uniaxial Tension Test, Material 37

Sample Name	Maximum Tensile Stress (psi)	Elongation at Maximum Tensile Stress (%)	Maximum Elongation (%)	Secant Modulus (psi)	Toughness (psi*in/in)
A	3,310	193	195	20,000	4,870
B	3,460	206	206	17,400	5,230
C	3,070	165	167	21,500	4,030
Mean	3,280	188	189	19,600	4,710

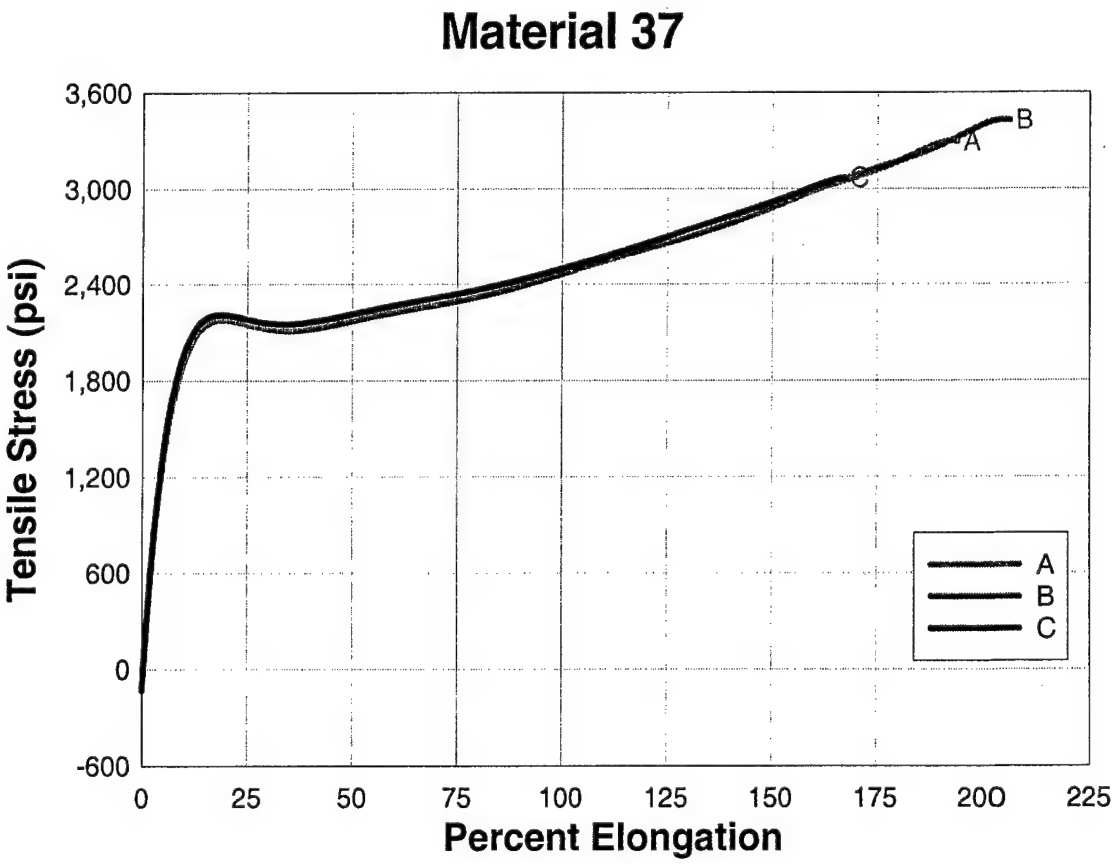

FIG. A37. Uniaxial Tension Test, Material 37

TABLE A38. Uniaxial Tension Test, Material 38

Sample Name	Maximum Tensile Stress (psi)	Elongation at Maximum Tensile Stress (%)	Maximum Elongation (%)	Secant Modulus (psi)	Toughness (psi*in/in)
A	787	141	151	560	712
B	1,010	177	191	584	1,110
C	979	179	188	569	1,070
Mean	925	166	176	571	964

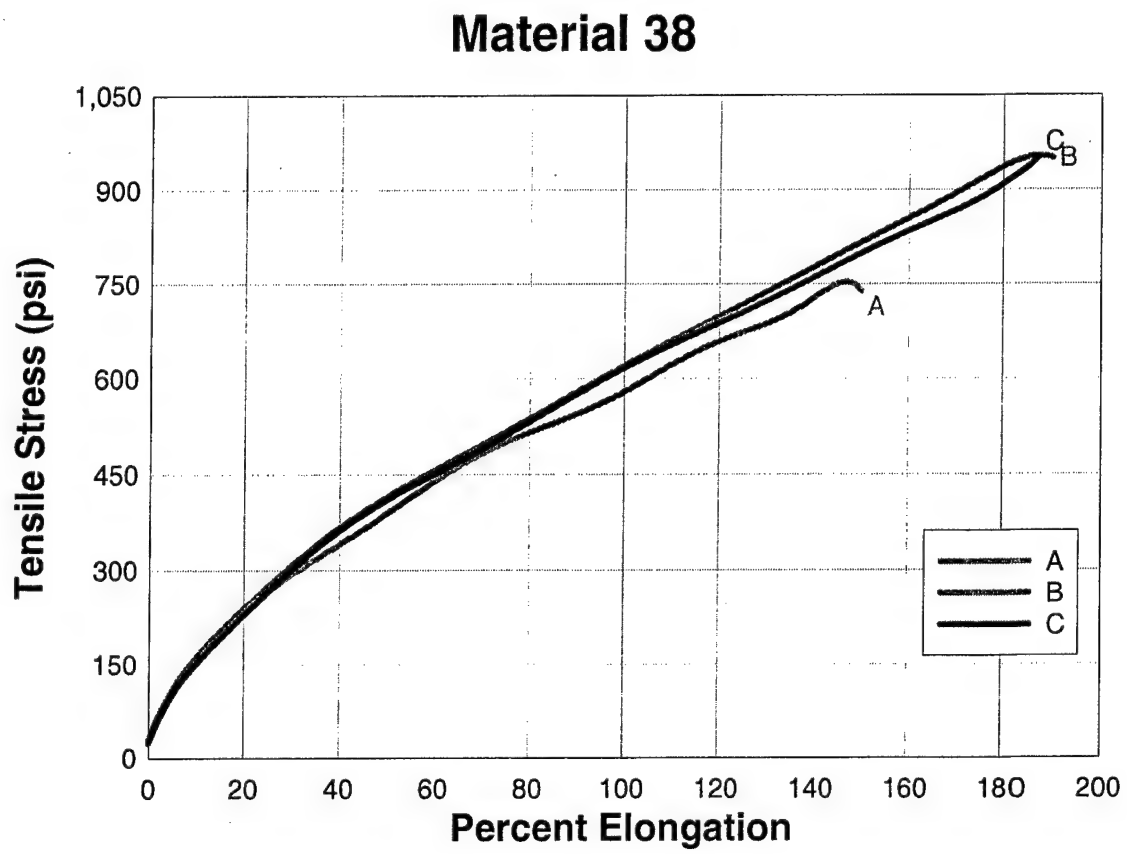

FIG. A38. Uniaxial Tension Test, Material 38

TABLE A39. Uniaxial Tension Test, Material 39

Sample Name	Maximum Tensile Stress (psi)	Elongation at Maximum Tensile Stress (%)	Maximum Elongation (%)	Secant Modulus (psi)	Toughness (psi*in/in)
A	1,200	308	316.	575	2,520
B	1,470	353	369	693	3,620
C	1,470	317	320	923	3,260
Mean	1,380	326	335	730	3,130

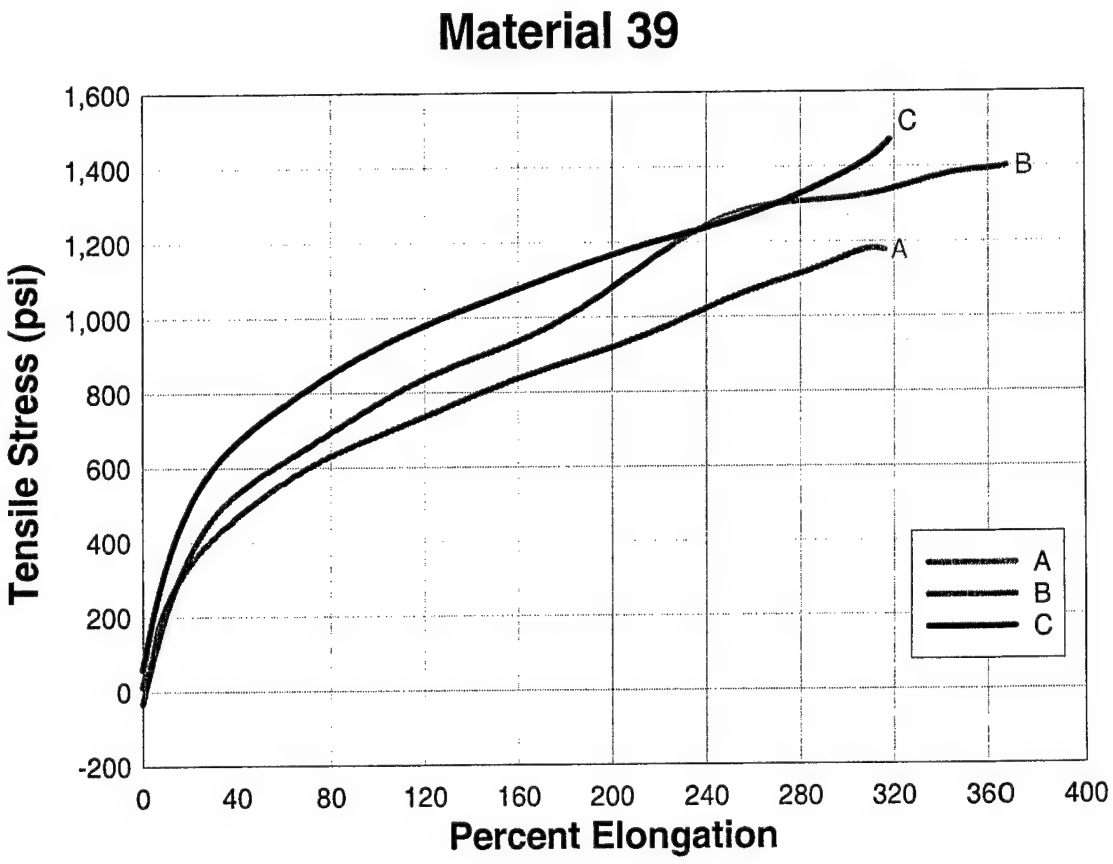

FIG. A39. Uniaxial Tension Test, Material 39

TABLE A40. Uniaxial Tension Test, Material 40

Sample Name	Maximum Tensile Stress (psi)	Elongation at Maximum Tensile Stress (%)	Maximum Elongation (%)	Secant Modulus (psi)	Toughness (psi*in/in)
A	9,420	6.2	12	206,000	771
B	9,270	6.3	23	202,000	686
C	9,240	6.2	15	197,000	958
Mean	9,330	6.2	14	201,500	865

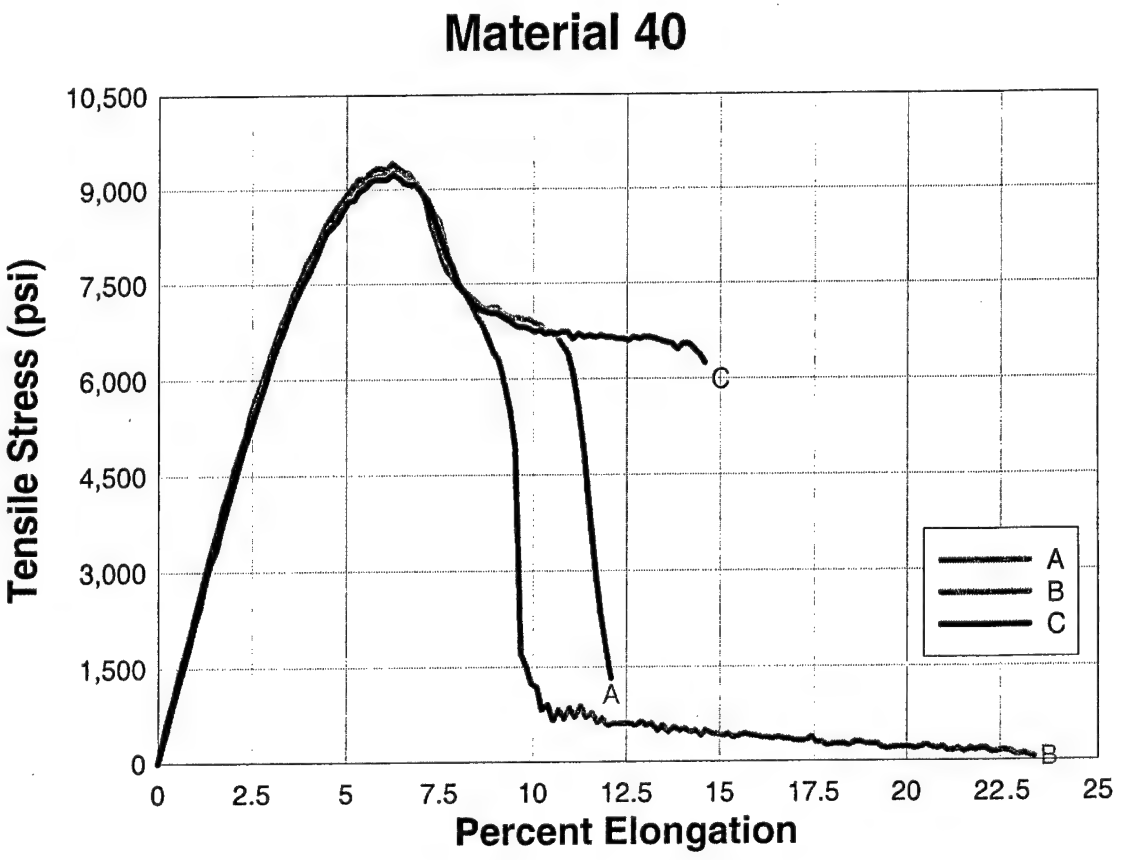

FIG. A40. Uniaxial Tension Test, Material 40

TABLE A41. Uniaxial Tension Test, Material 41

Sample Name	Maximum Tensile Stress (psi)	Elongation at Maximum Tensile Stress (%)	Maximum Elongation (%)	Secant Modulus (psi)	Toughness (psi*in/in)
A	9,130	6.1	29	196,000	1,950
B	9,090	6.3	31	201,000	2,070
C	9,430	6.3	21	204,000	1,480
Mean	9,220	6.2	27	200,000	1,830

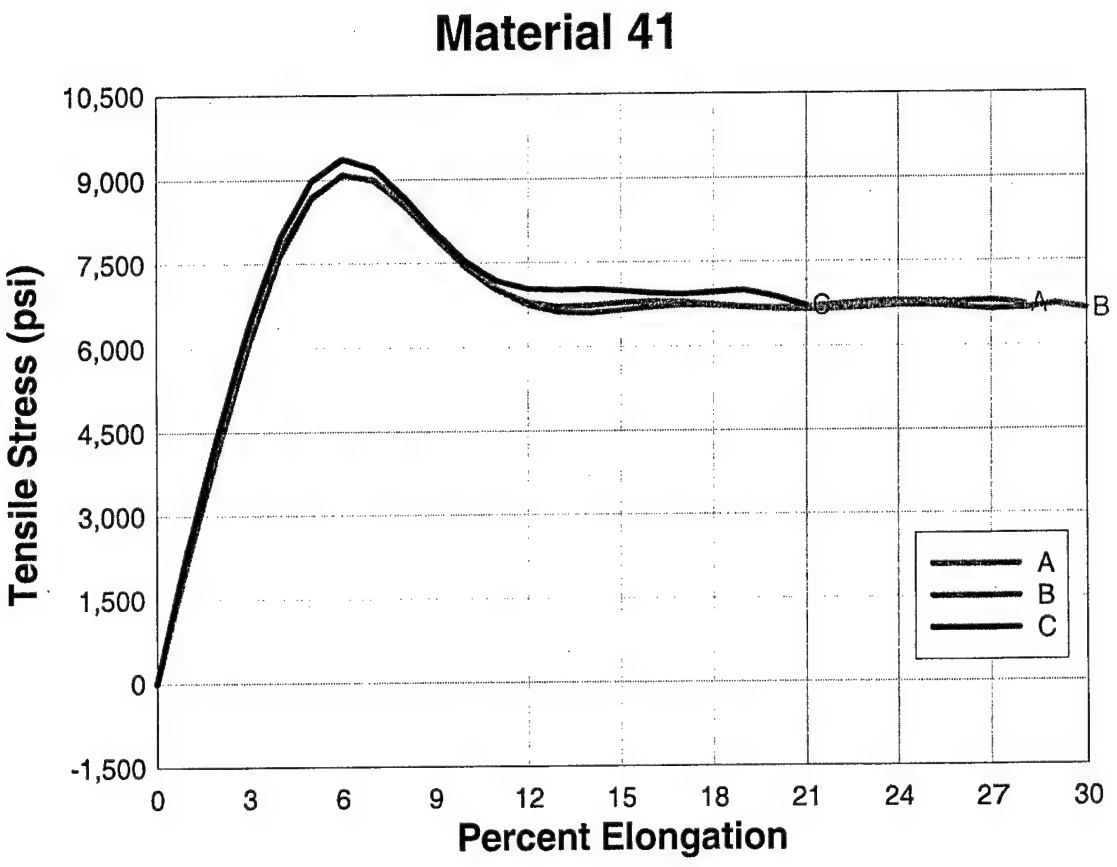

FIG. A41. Uniaxial Tension Test, Material 41

TABLE A42. Uniaxial Tension Test, Material 42

Sample Name	Maximum Tensile Stress (psi)	Elongation at Maximum Tensile Stress (%)	Maximum Elongation (%)	Secant Modulus (psi)	Toughness (psi*in/in)
A	7,730	5.8	23	172,000	1,320
B	7,620	5.8	23	165,000	1,320
C	7,740	5.9	28	171,000	1,590
Mean	7,700	5.8	25	169,000	1,410

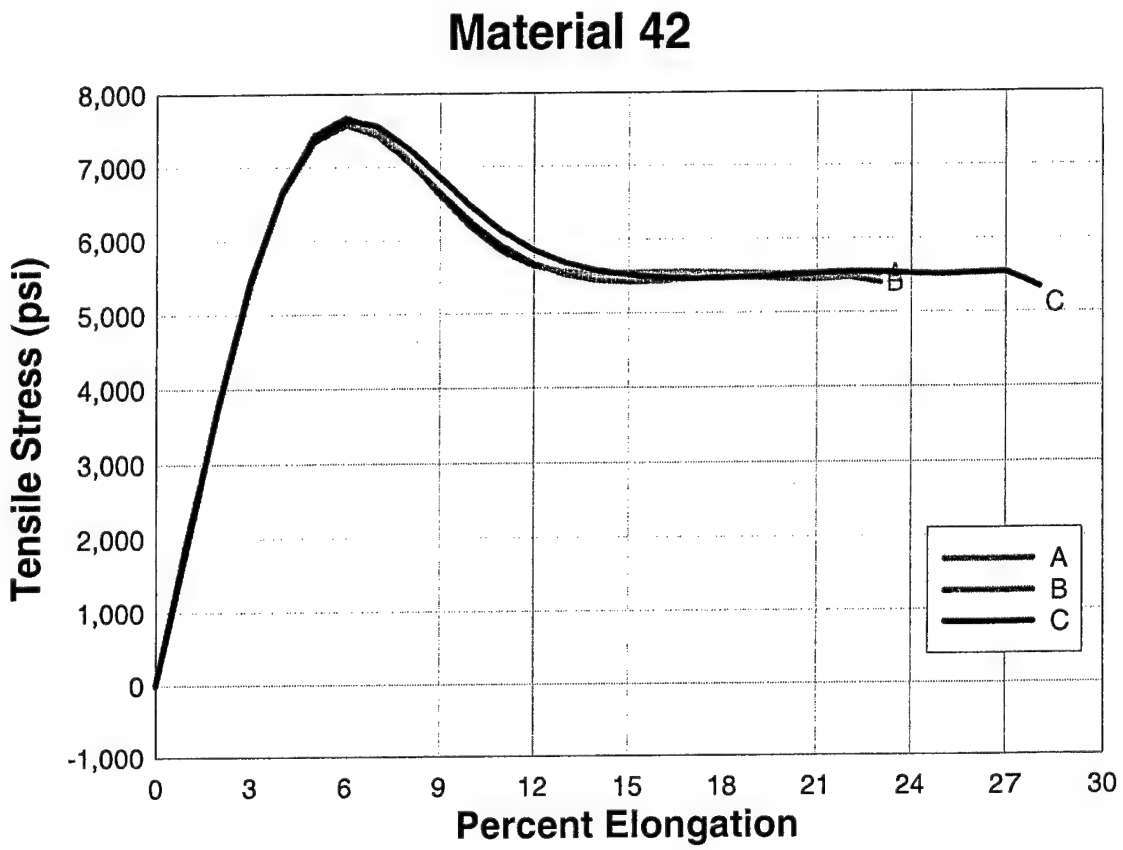

FIG. A42. Uniaxial Tension Test, Material 42

TABLE A43. Uniaxial Tension Test, Material 43

Sample Name	Maximum Tensile Stress (psi)	Elongation at Maximum Tensile Stress (%)	Maximum Elongation (%)	Secant Modulus (psi)	Toughness (psi*in/in)
A	7,720	5.8	23	172,000	1,320
B	7,800	5.9	25	174,000	1,410
Mean	7,760	5.8	24	173,000	1,370

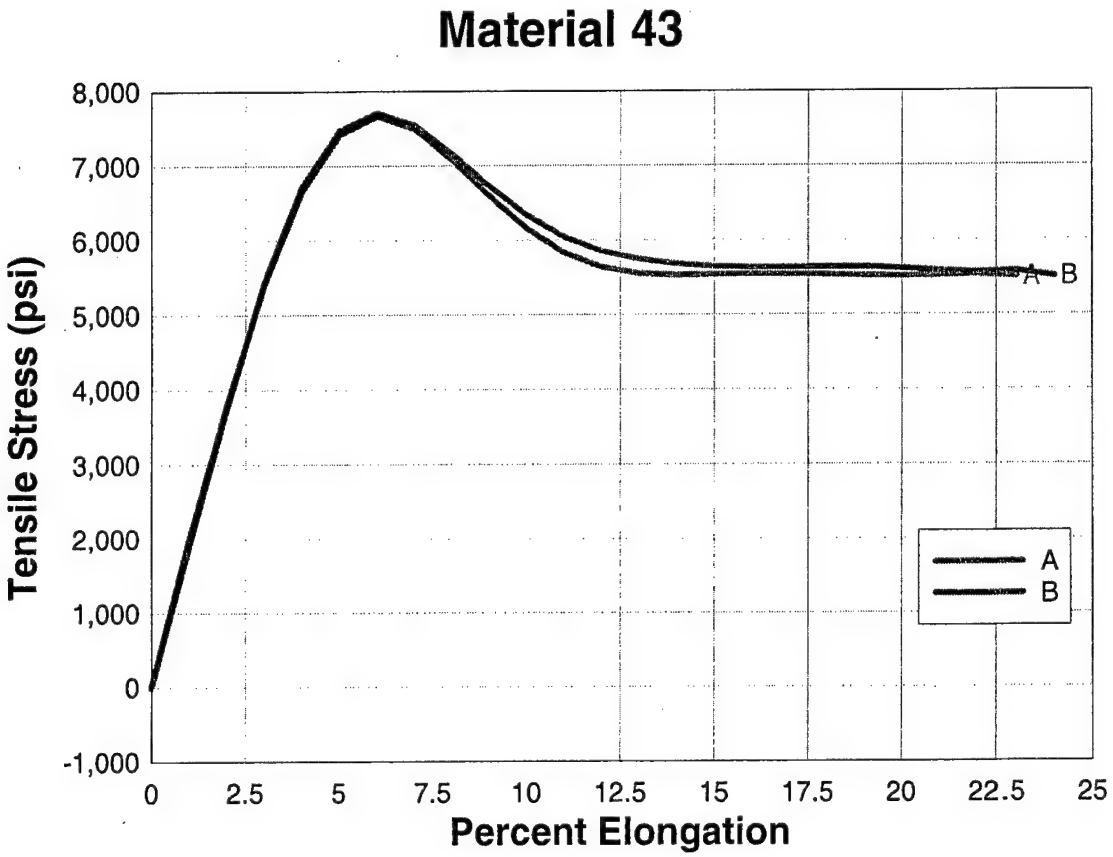

FIG. A43. Uniaxial Tension Test, Material 43

TABLE A44. Uniaxial Tension Test, Material 44

Sample Name	Maximum Tensile Stress (psi)	Elongation at Maximum Tensile Stress (%)	Maximum Elongation (%)	Secant Modulus (psi)	Toughness (psi*in/in)
A	1,700	51	59	20,700	848
B	1,780	50	53	21,100	787
C	1,730	56	60	19,200	863
Mean	1,740	52	57	20,300	833

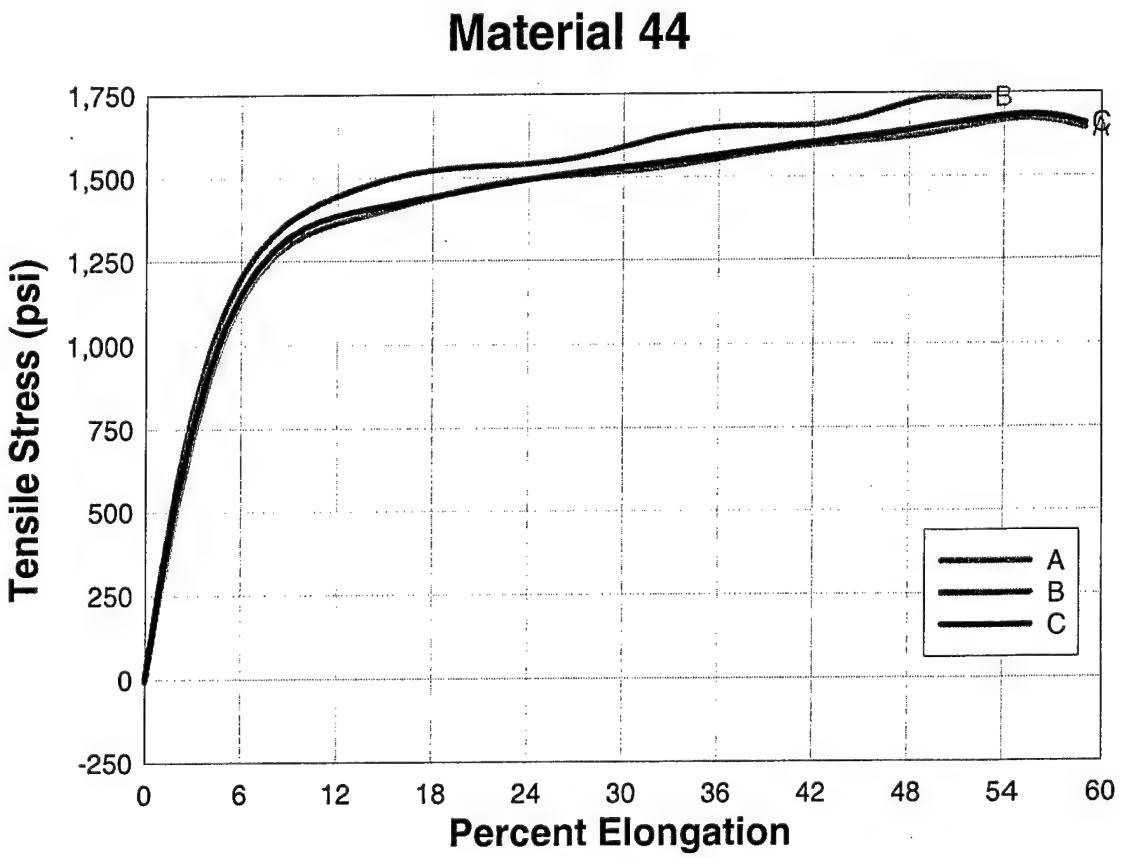

FIG. A44. Uniaxial Tension Test, Material 44

TABLE A45. Uniaxial Tension Test, Material 45

Sample Name	Maximum Tensile Stress (psi)	Elongation at Maximum Tensile Stress (%)	Maximum Elongation (%)	Secant Modulus (psi)	Toughness (psi*in/in)
A	2,000	168	174	5,930	2,750
B	2,000	101	183	4,960	2,850
C	2,080	186	187	4,850	3,010
Mean	2,030	151	181	5,250	2,870

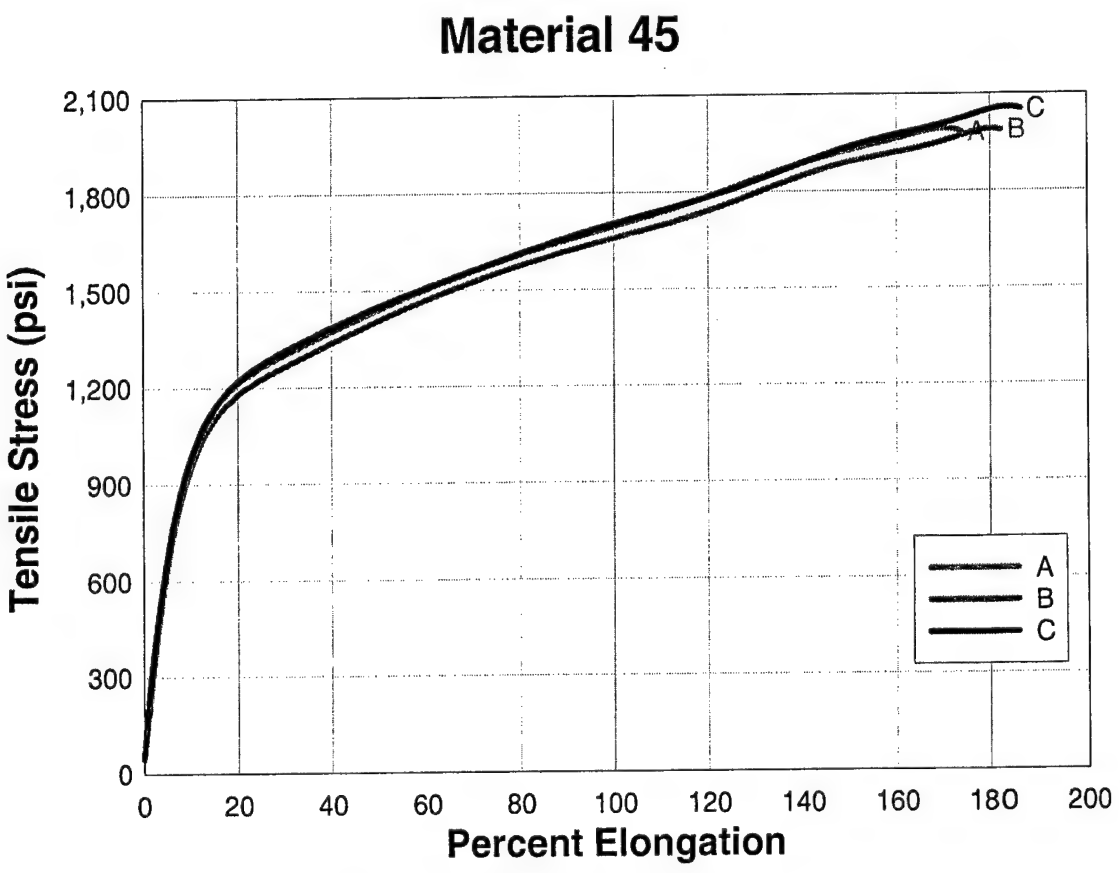

FIG. A45. Uniaxial Tension Test, Material 45

TABLE A46. Uniaxial Tension Test, Material 46

Sample Name	Maximum Tensile Stress (psi)	Elongation at Maximum Tensile Stress (%)	Maximum Elongation (%)	Secant Modulus (psi)	Toughness (psi*in/in)
A	1,770	115	124	8,380	1,690
B	1,600	84	96	10,500	1,200
C	1,490	95	107	9,260	1,240
Mean	1,620	98	109	9,380	1,380

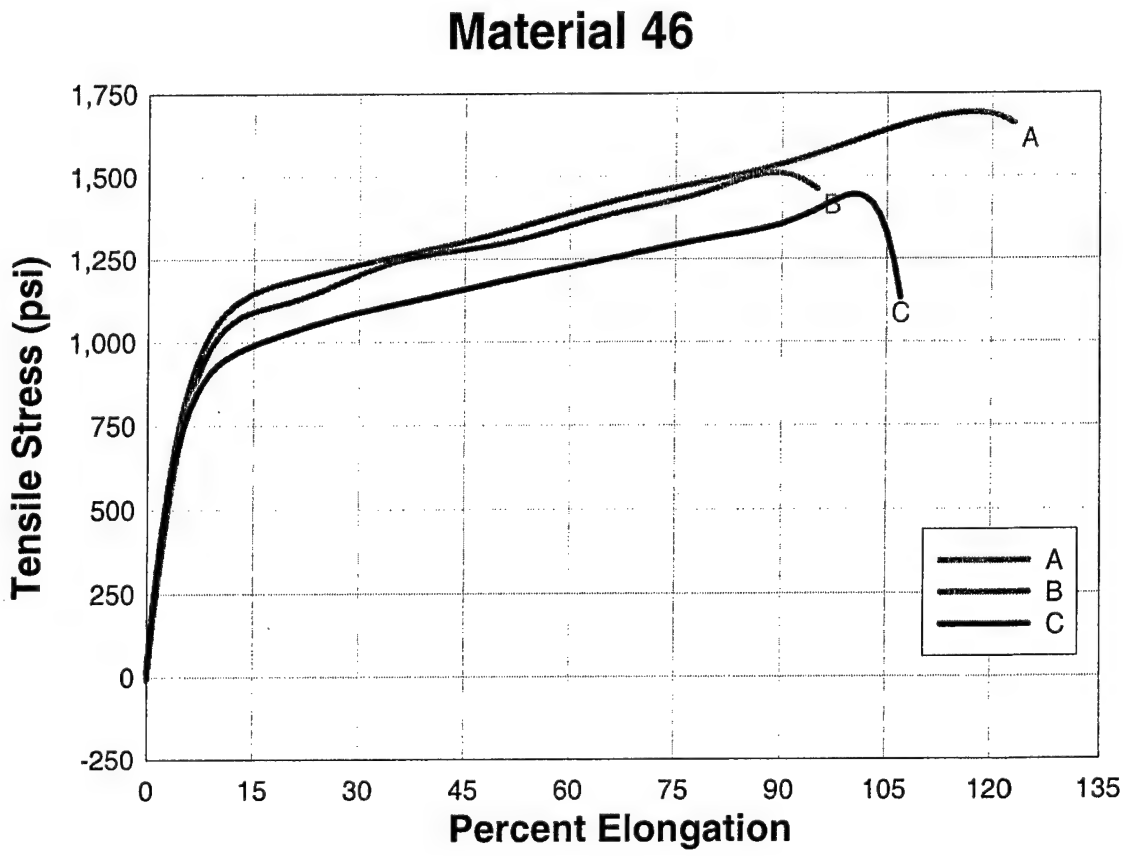

FIG. A46. Uniaxial Tension Test, Material 46

TABLE A47. Uniaxial Tension Test, Material 47

Sample Name	Maximum Tensile Stress (psi)	Elongation at Maximum Tensile Stress (%)	Maximum Elongation (%)	Secant Modulus (psi)	Toughness (psi*in/in)
A	1,870	123	123	7,710	1,750
B	1,670	88	93	12,500	1,260
C	1,800	113	122	8,500	1,680
Mean	1,780	108	113	9,570	1,560

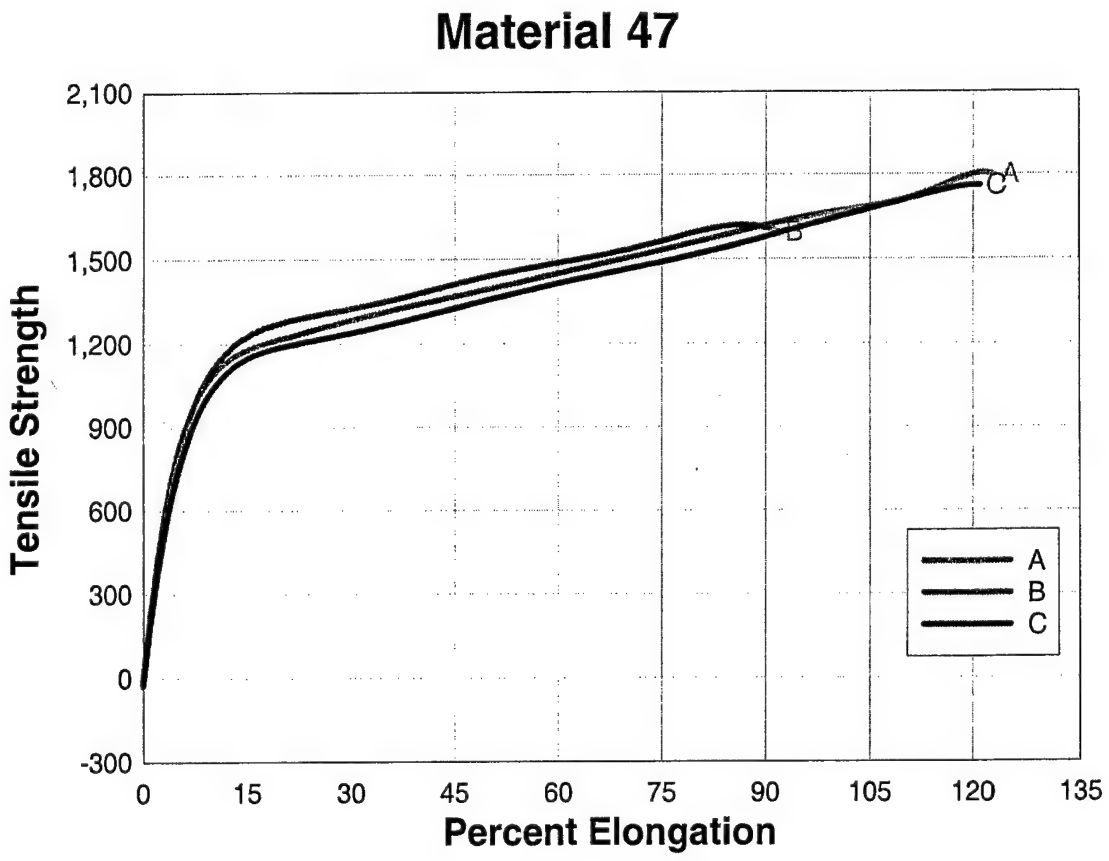

FIG. A47. Uniaxial Tension Test, Material 47

TABLE A48. Uniaxial Tension Test, Material 48

Sample Name	Maximum Tensile Stress (psi)	Elongation at Maximum Tensile Stress (%)	Maximum Elongation (%)	Secant Modulus (psi)	Toughness (psi*in/in)
A	1,840	46	54	26,100	846
B	2,040	74	83	24,200	1,460
C	1,920	89	94	22,000	1,520
Mean	1,980	82	89	23,100	1,490

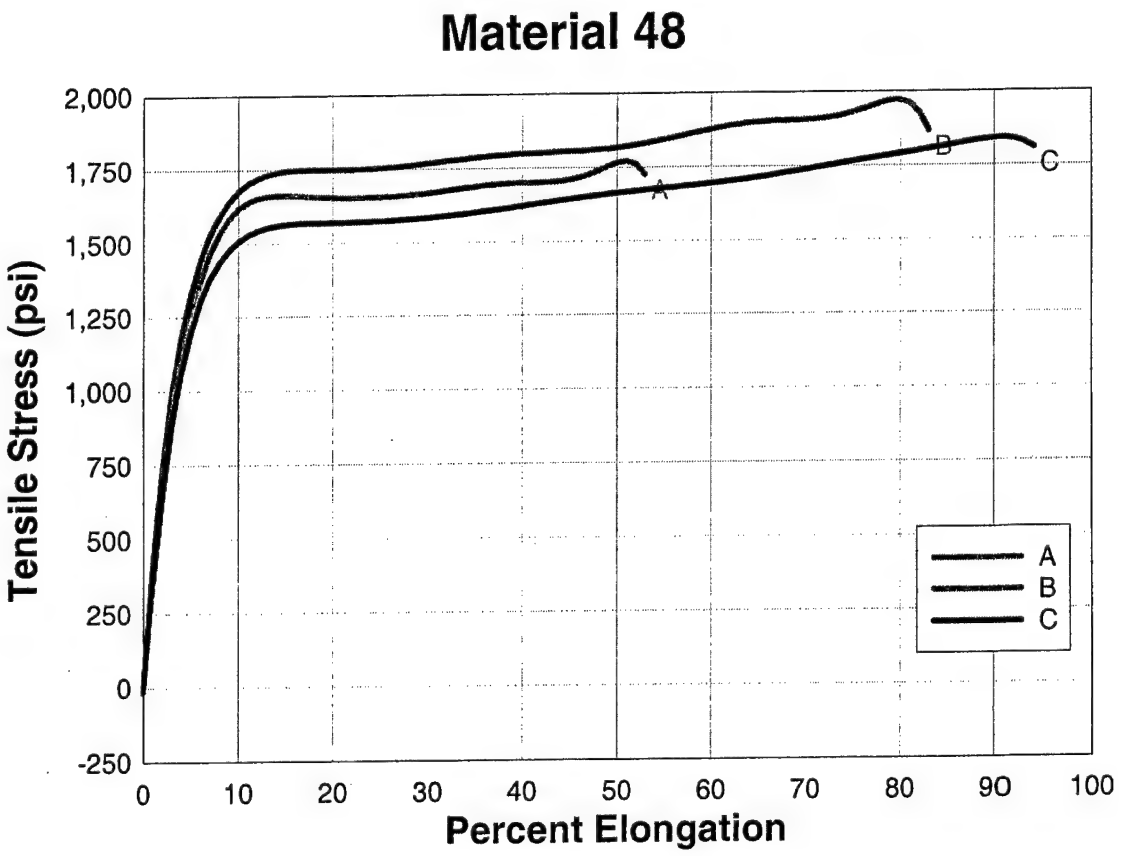

FIG. A48. Uniaxial Tension Test, Material 48

TABLE A49. Uniaxial Tension Test, Material 49

Sample Name	Maximum Tensile Stress (psi)	Elongation at Maximum Tensile Stress (%)	Maximum Elongation (%)	Secant Modulus (psi)	Toughness (psi*in/in)
A	982	34	66	12,300	559
B	947	51	85	13,000	701
C	1,000	71	88	11,800	787
Mean	976	52	79	12,400	682

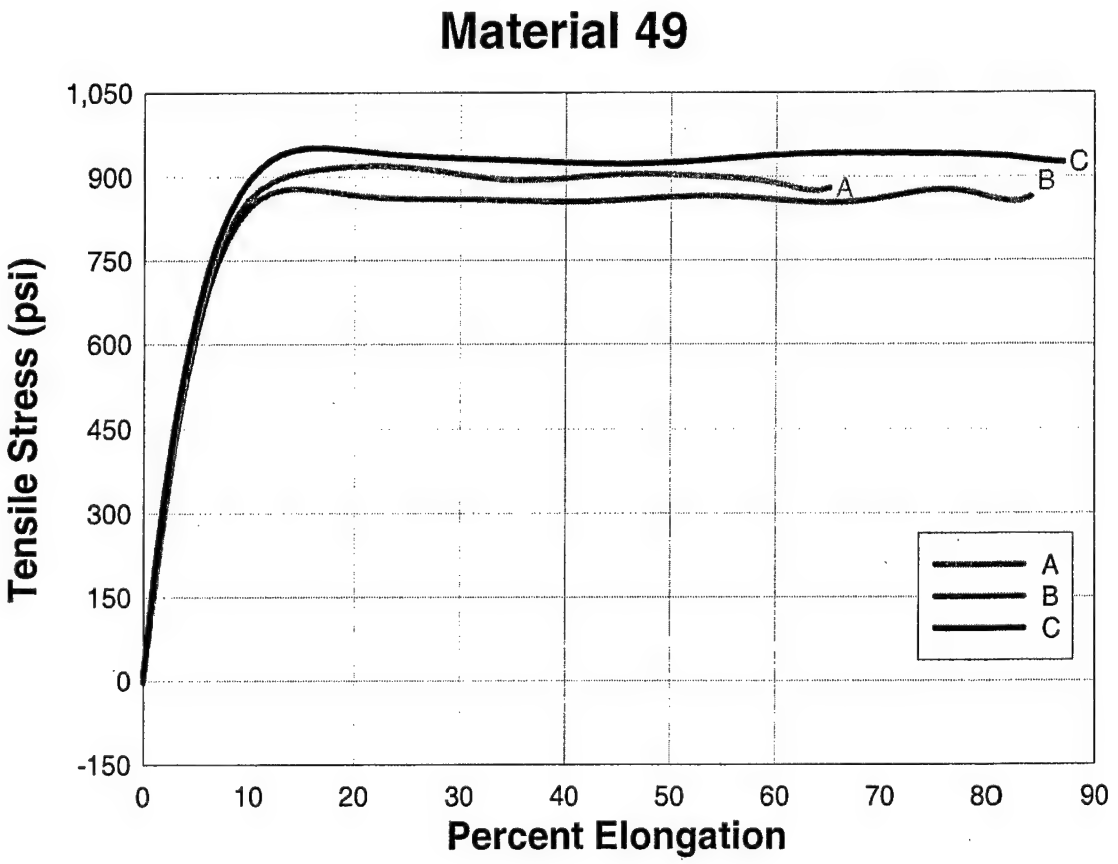

FIG. A49. Uniaxial Tension Test, Material 49

TABLE A50. Uniaxial Tension Test, Material 50

Sample Name	Maximum Tensile Stress (psi)	Elongation at Maximum Tensile Stress (%)	Maximum Elongation (%)	Secant Modulus (psi)	Toughness (psi*in/in)
A	1,610	111	156	20,200	1,530
B	1,650	106	163	19,800	1,570
C	1,700	113	159	19,300	1,620
Mean	1,650	110	159	19,800	1,570

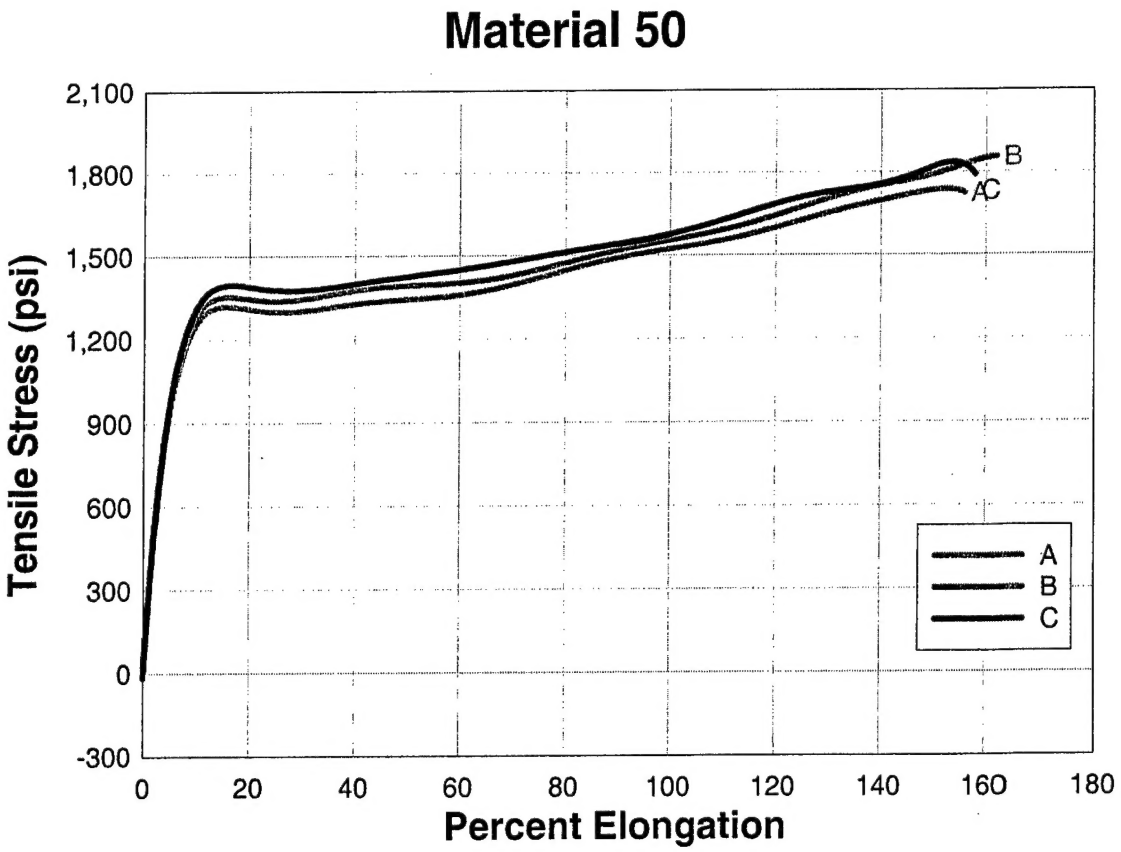

FIG. A50. Uniaxial Tension Test, Material 50

TABLE A51. Uniaxial Tension Test, Material 51

Sample Name	Maximum Tensile Stress (psi)	Elongation at Maximum Tensile Stress (%)	Maximum Elongation (%)	Secant Modulus (psi)	Toughness (psi*in/in)
A	1,840	46	54	26,100	846
B	2,040	74	83	24,200	1,460
C	1,920	89	94	22,000	1,520
Mean	1,980	82	89	23,100	1,490

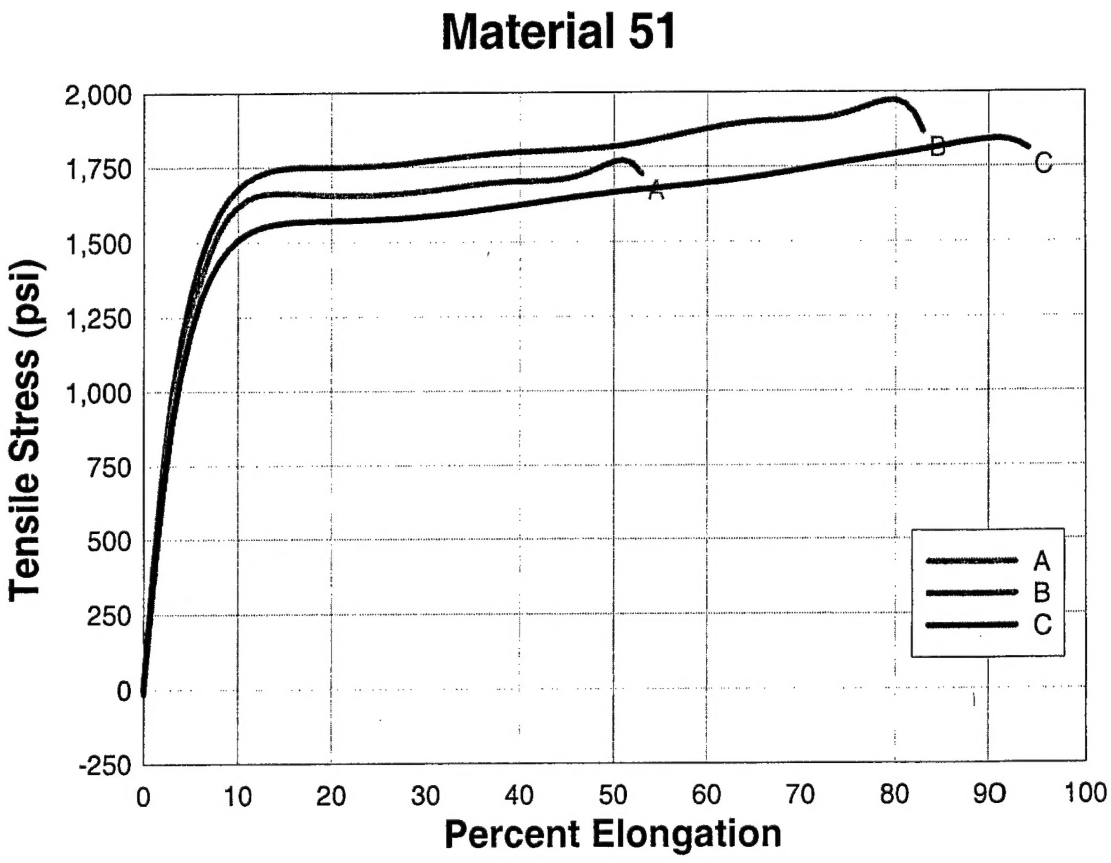

FIG. A51. Uniaxial Tension Test, Material 51

TABLE A52. Uniaxial Tension Test, Material 52

Sample Name	Maximum Tensile Stress (psi)	Elongation at Maximum Tensile Stress (%)	Maximum Elongation (%)	Secant Modulus (psi)	Toughness (psi*in/in)
A	1,880	578	80	30,500	1,360
B	1,680	48	81	27,100	1,240
C	1,650	51	68	27,500	1,010
Mean	1,670	50	75	27,300	1,100

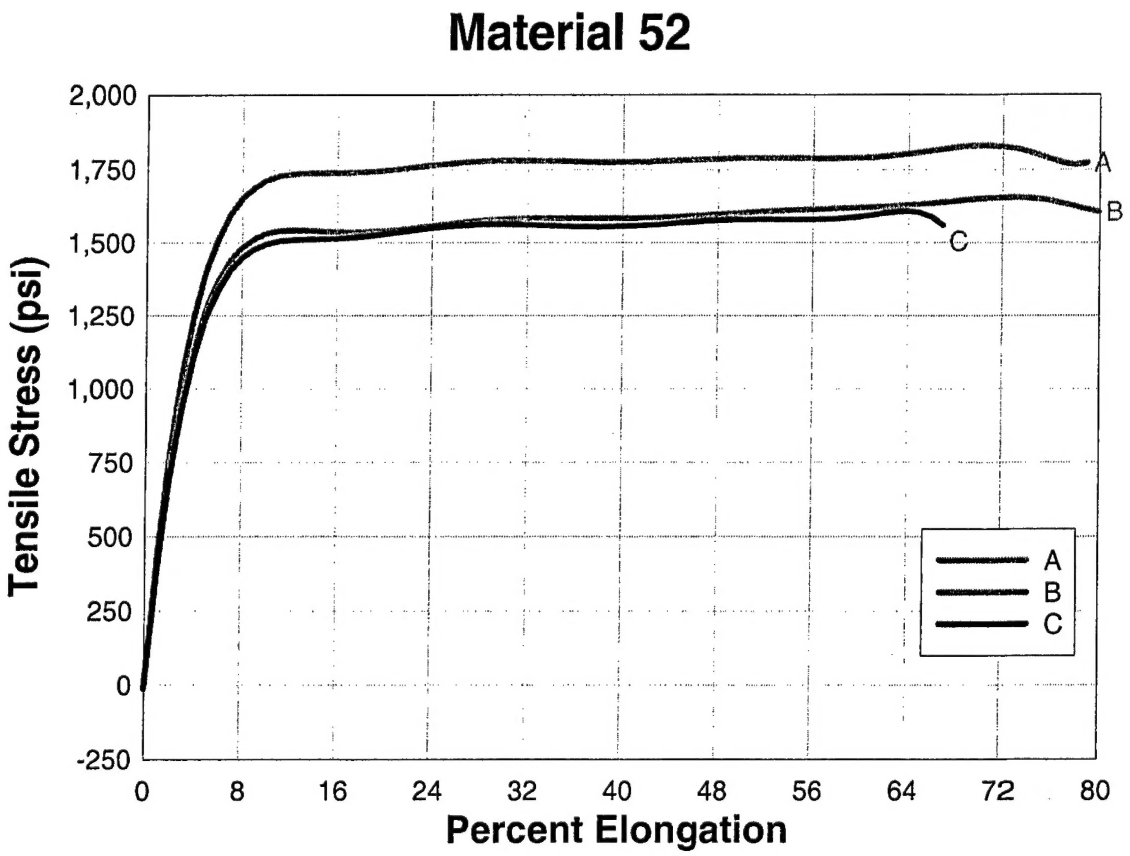

FIG. A52. Uniaxial Tension Test, Material 52

TABLE A53. Uniaxial Tension Test, Material 53

Sample Name	Maximum Tensile Stress (psi)	Elongation at Maximum Tensile Stress (%)	Maximum Elongation (%)	Secant Modulus (psi)	Toughness (psi*in/in)
A	3,410	139	141	25,000	3,790
B	3,620	152	153	24,900	4,330
C	3,830	169	171	22,600	5,010
Mean	3,620	153	155	24,200	4,380

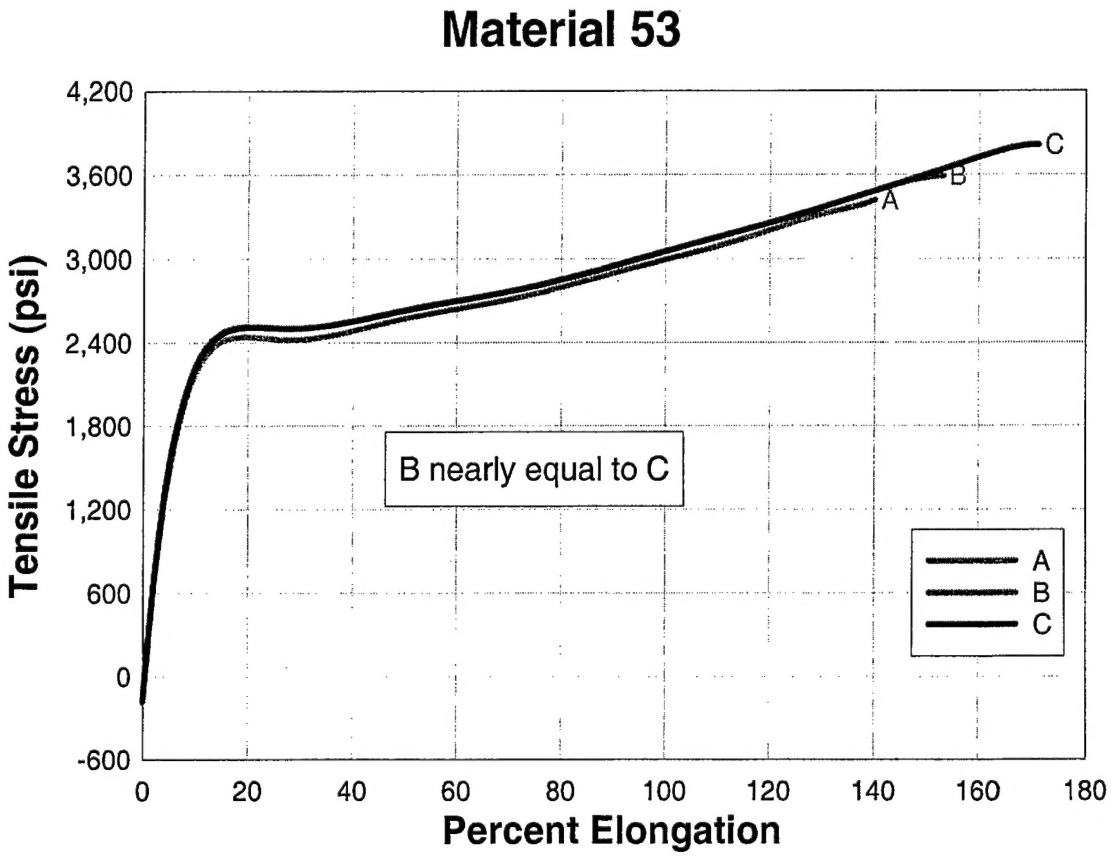

FIG. A53. Uniaxial Tension Test, Material 53